

UNCLASSIFIED

AD NUMBER	
AD384924	
CLASSIFICATION CHANGES	
TO:	UNCLASSIFIED
FROM:	CONFIDENTIAL
LIMITATION CHANGES	
TO: Approved for public release; distribution is unlimited.	
FROM: Distribution authorized to U.S. Gov't. agencies only; Administrative/Operational Use; AUG 1967. Other requests shall be referred to U.S. Army Aviation Materiel Laboratories, Fort Eustis, VA.	
AUTHORITY	
USAAML Notice dtd 17 Oct 1968; USAAML ltr dtd 12 Feb 1971	

THIS PAGE IS UNCLASSIFIED

UNCLASSIFIED

AD 384924

USAAVLABS TECHNICAL REPORT 67-30
ELEMENT DESIGN AND DEVELOPMENT
OF
SMALL CENTRIFUGAL COMPRESSOR (U)
VOLUME II

By
A. D. Welliver
J. Acurio

August 1967

U. S. ARMY AVIATION MATERIEL LABORATORIES
FORT EUSTIS, VIRGINIA

CONTRACT DA 44-177-AMC-173(T)
THE BOEING COMPANY
SEATTLE, WASHINGTON

This material contains information affecting
the national defense of the United States
within the meaning of the Espionage Laws
Title 18, U.S.C. Sec. 793 and 794, the transmission

Downgraded from CONFIDENTIAL to UNCLASSIFIED
and will appear in TAB 69-5 dated
1 March 1969 (cited in letter from DDC-TS
dated 23 January 1969)

In addition to security requirements which
apply to this document and must be met, each
transmittal outside the agencies of the US
Government must have prior approval of US
Army Aviation Materiel Laboratories, Fort
Eustis, Virginia 23604.

Fred J. Galante
Fred J. Galante PFS

24 January 1969



UNCLASSIFIED

y 10 of 96 Copies

Disclaimers

When Government drawings, specifications, or other data are used for any purpose other than in connection with a definitely related Government procurement operation, the United States Government thereby incurs no responsibility nor any obligation whatsoever; and the fact that the Government may have formulated, furnished, or in any way supplied the said drawings, specifications, or other data is not to be regarded by implication or otherwise as in any manner licensing the holder or any other person or corporation, or conveying any rights or permission, to manufacture, use, or sell any patented invention that may in any way be related thereto.

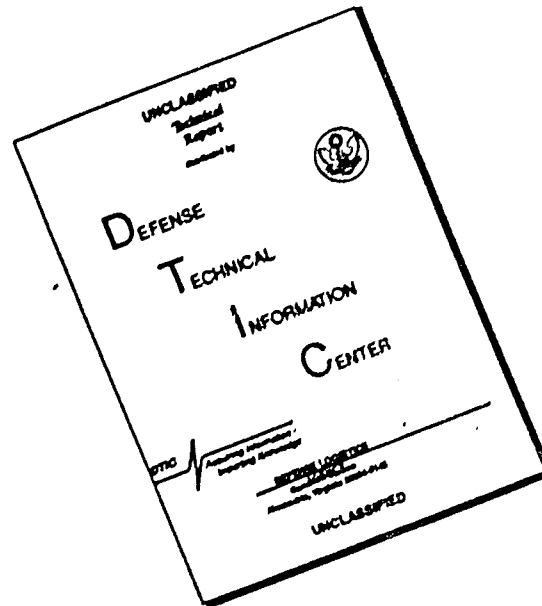
Trade names cited in this report do not constitute an official endorsement or approval of the use of such commercial hardware or software.

Disposition Instructions

When this report is no longer needed, Department of the Army organizations will destroy it in accordance with the procedures given in AR 380-5.

3

DISCLAIMER NOTICE



THIS DOCUMENT IS BEST QUALITY AVAILABLE. THE COPY FURNISHED TO DTIC CONTAINED A SIGNIFICANT NUMBER OF PAGES WHICH DO NOT REPRODUCE LEGIBLY.

UNCLASSIFIED



DEPARTMENT OF THE ARMY
U. S. ARMY AVIATION MATERIEL LABORATORIES
FORT EUSTIS, VIRGINIA 23604

(U) This Command has reviewed this report and concurs with the conclusions contained herein. The findings and recommendations as outlined in this report will be further considered and defined in a subsequent research report entitled "Design and Development of Small, Single-Stage Centrifugal Compressor."

MISSING PAGE NUMBERS ARE BLANK

UNCLASSIFIED

UNCLASSIFIED

1M121401D14413

15 DA-44-177-AMC-173(T)

18 USAAVLABS Technical Report 67-30

11 August 1967

19 TR-67-30-Vol-2

12 500 p.

6 ELEMENT DESIGN AND DEVELOPMENT
OF
SMALL CENTRIFUGAL COMPRESSOR, (U).
VOLUME II

9 - initial rept.
14 D4-3434-Vol-2

10 A. D. Welliver and
J. Acurio,

Prepared by

The Boeing Company
Seattle, Washington 657 600

This material contains information affecting
the national defense of the United States
within the meaning of the Espionage Laws
(18 U. S. C. 793 and 794), the transmission
or revelation of which in any manner to an
unauthorized person is prohibited by law.

for

U. S. ARMY AVIATION MATERIEL LABORATORIES
FORT EUSTIS, VIRGINIA

In addition to security requirements which
apply to this document and must be met, each
transmittal outside the agencies of the US
Government must have prior approval of US
Army Aviation Materiel Laboratories, Fort
Eustis, Virginia 23604.

UNCLASSIFIED

UNCLASSIFIED

UNCLASSIFIED

Individual pages of Appendixes I and X are unclassified; however, when compiled in complete appendixes, such material is classified as confidential.

UNCLASSIFIED

UNCLASSIFIED

(U) CONTENTS

<u>Appendix</u>	<u>Page</u>
I IMPELLER RADIAL-EQUILIBRIUM DESIGN.	1
1.0 General Information	2
1.1 Purpose	2
1.2 Assumptions	2
1.3 Limitations	2
2.0 Procedure	3
2.1 Nomenclature	3
2.2 Method	12
2.3 Results	37
3.0 Input Preparation and Output Description	38
3.1 Input-Data Preparation.	38
3.2 Output Description.	44
3.3 Sample Case	45
4.0 Operating Information	45
4.1 Program and Data Setup	45
4.2 Run Information	62
5.0 Programming Information.	64
5.1 Flow Diagrams	64
5.2 Program Routines	78
5.3 Program Listing	80

CONTENTS (Continued)

<u>Appendix</u>	<u>Page</u>
II IMPELLER STRESS AND VIBRATION ANALYSIS.	125
1.0 Discussion	130
2.0 MF-1 Impeller Analysis	134
3.0 MF-2 Impeller Analysis	144
4.0 MF-3 Impeller Analysis	156
5.0 RF-1 Impeller Analysis	168
6.0 Workhorse Impeller Analysis	178
III TEST-RIG DEVELOPMENT	187
1.0 Introduction	190
2.0 Diffuser Test Sections	190
2.1 Bearing System	190
2.2 Rotor Dynamics Analysis	195
2.3 Modifications	200
2.4 Conclusions	202
3.0 Impeller Test Sections	202
3.1 Bearing System	202
3.2 Rotor Dynamics Analyses	206
3.3 Modifications	209
3.4 Conclusions	216

CONTENTS (Continued)

<u>Appendix</u>		<u>Page</u>
IV	SPIN-PIT TESTING	219
	1.0 Background and Introduction	220
	2.0 Boeing Spin-Pit Facility	220
	3.0 Impeller Spin Tests	221
	4.0 Discussion	223
	4.1 Residual Imbalance	223
	4.2 Impeller-To-Shaft Fit	224
	4.3 Axial Clamping Load	224
	4.4 Extraneous Excitations	224
	5.0 Conclusions and Recommendations	233
V	MODAL BALANCE	235
	1.0 General Information	237
	2.0 Instrumentation	238
	3.0 Procedure	238
	3.1 Trial and Error Method	238
	3.2 Analytical Method	244
VI	VIBRATORY-STRESS TEST OF WORKHORSE IMPELLER.	247
	1.0 Summary	249
	2.0 Discussion	249

CONTENTS (Continued)

<u>Appendix</u>	<u>Page</u>
2.1 Rig Components and Instrumentation Equipment	249
2.2 Procedure	250
2.3 Results	260
3.0 Conclusions	263
 VII WAKE INTERACTION EFFECTS AND PERFORMANCE CHARACTERISTICS OF STAGNATION-TYPE THERMOCOUPLE .	 267
1.0 Summary, Conclusions, and Outline of Analysis	271
1.1 Summary	271
1.2 Recommendations and Conclusions	271
1.3 Outline of Analysis	271
2.0 Steady-State Probe Behavior	272
2.1 Conclusions	281
2.2 Recommendations	281
3.0 Equilibrium Temperature of an Isolated Probe in a High- Frequency Intermittent Flow	 282
3.1 The Effect of High-Frequency Fluctuations	282
3.2 The Low-Velocity Heat-Transfer Problem — Energy- Balance Relations	 285
3.3 Estimate of the Jet- and Wake-Flow Conditions Affecting the Temperature-Measuring Problem	 289
3.4 The Effect of Velocity Fluctuations on the Heat-Transfer Coefficient	 289

CONTENTS (Continued)

<u>Appendix</u>	<u>Page</u>
3.5 The Effect of Fluctuations in the Angle of Incidence of the Stream	290
3.6 The High-Velocity Heat-Transfer Problem	290
3.7 Simplifications Based on $h_1 = h_2$ and $\rho_1 V_1 = \rho_2 V_2$	292
4.0 The Effect of Wake Fluid Entrainment and Probe Position	292
 VIII INSTRUMENTATION RESEARCH	 299
1.0 Introduction	301
1.1 Objective	301
1.2 Scope	301
2.0 Measurement of Blade-to-Shroud Running Clearance	301
2.1 Goals	301
2.2 Research and Development Effort	301
3.0 Measurement of Total Pressure in the Presence of Unsteady Flow.	311
3.1 Goals	311
3.2 Research Effort	311
4.0 Measurement of Torque at Rotational Speeds to 60,000 RPM.	319
4.1 Research Effort	319
4.2 Conclusions	321
5.0 Accurate Measurement of Total Temperature in Compressor Diffuser Passages	322
5.1 Research Effort	322
5.2 Conclusions	330

CONTENTS (Continued)

<u>Appendix</u>	<u>Page</u>
IX COMPUTER PRINTOUT OF DIFFUSER DATA — STATIC PRESSURES	335
 X SCHLIEREN PHOTOGRAPHS	379
1.0 Objectives	380
2.0 Method	380
3.0 Results	384
 XI INLET-MACH-NUMBER EFFECTS ON SUBSONIC DIFFUSER PERFORMANCE	417
1.0 Literature Surveys of Subsonic Diffusers	419
2.0 Evaluation of Inlet-Mach-Number Effects	419
2.1 Effect of Inlet Mach Number on Group A Diffusers	423
2.2 Effect of Inlet Mach Number on Group B Diffusers	423
2.3 Effect of Inlet Mach Number on Group C Diffusers	426
3.0 Summary	426
 XII STRAIGHT DIFFUSER PERFORMANCE AT HIGH INLET MACH NUMBERS	429
1.0 Introduction	432
2.0 Experimental Procedure	436
2.1 Geometrical Parameters	437
2.2 Flow Parameters	443

CONTENTS (Continued)

<u>Appendix</u>	<u>Page</u>
2.3 Flow Measurements	444
2.4 Flow Unsteadiness	452
3.0 Results and Discussion	452
3.1 C_p Versus Inlet Mach Number	453
3.2 C_p Supercritical Flow Conditions	463
3.3 Comparison of Present Data with Low Mach Number Data of Roneau — C_p Versus 2θ	463
3.4 C_p Versus B and Aspect Ratio at High Inlet Mach Numbers	467
4.0 Recommendations	472
4.1 High Mach Number Diffuser Map	472
4.2 Low Mach Number Data	472
4.3 Resolving Unsteady Character of Mass Flow Rate	473
4.4 Inlet Boundary-Layer Velocity Profile	473
5.0 Uncertainty Analysis	473
6.0 Conclusions	477

(U) LIST OF ILLUSTRATIONS

<u>Figure</u>		<u>Page</u>
<u>APPENDIX I</u>		
1	Impeller Meridional View	13
2	Angle Sign Conventions	14
<u>APPENDIX II</u>		
3	Blade and Disk Metal Temperature Calculations	131
4	Goodman Diagram	133
5	Disk and Blade Profile of MF-1	135
6	Temperature Distribution of MF-1	135
7	Natural Frequencies of MF-1 Blades	136
8	Campbell Diagram for MF-1	137
9	Blade Stress Calculations for MF-1	138
10	MF-1 Impeller-Blade Force, Weight, and Inertia	139
11	Blade-Root Stress, Temperature, and Safety Factor for MF-1	140
12	Impeller Flow Area of MF-1	141
13	Disk Calculations for MF-1	143
14	Disk and Blade Profile of MF-2	145
15	Temperature Distribution of MF-2	145
16	Natural Frequencies of MF-2 Blades	146
17	Revised Natural Frequencies of MF-2 Blades	147
18	Campbell Diagram for MF-2	148
19	Blade Stress Calculations for MF-2	149

LIST OF ILLUSTRATIONS (Continued)

<u>Figure</u>		<u>Page</u>
20	MF-2 Impeller-Blade Force, Weight, and Inertia	150
21	Blade-Root Stress, Temperature, and Safety Factor for MF-2 .	151
22	Impeller Flow Area of MF-2	153
23	Disk Calculations for MF-2	155
24	Disk and Blade Profile of MF-3	157
25	Temperature Distribution of MF-3	157
26	Natural Frequencies of MF-3 Blades	158
27	Natural Frequencies of Modified MF-3 Blades	159
28	Campbell Diagram for MF-3	160
29	Blade Stress Calculations for MF-3	161
30	MF-3 Impeller-Blade Force, Weight, and Inertia	162
31	Blade-Root Stress, Temperature, and Safety Factor for MF-3 .	163
32	Impeller Flow Area of MF-3	165
33	Disk Calculations for MF-3	167
34	Disk and Blade Profile of RF-1	169
35	Temperature Distribution of RF-1	169
36	Natural Frequencies of RF-1 Blades	170
37	Campbell Diagram for RF-1	171
38	Blade Stress Calculations of RF-1	172
39	RF-1 Impeller-Blade Force, Weight, and Inertia	173
40	Blade-Root Stress, Temperature, and Safety Factor for RF-1 .	174

LIST OF ILLUSTRATIONS (Continued)

<u>Figure</u>		<u>Page</u>
41	Impeller Flow Area of RF-1	175
42	Disk Calculations for RF-1	177
43	Disk and Blade Profile of Workhorse Impeller	179
44	Temperature Distribution of Workhorse Impeller	180
45	Natural Frequencies of Workhorse Impeller Blades	181
46	Campbell Diagram for Workhorse Impeller	182
47	Blade Stress Calculations for Workhorse Impeller	183
48	Workhorse Impeller-Blade Force, Weight, and Inertia	184
49	Blade-Root Stress, Temperature, and Safety Factor for Workhorse Impeller	185
50	Disk Calculations for Workhorse Impeller	186

APPENDIX III

51	Variation of Speed Ratio with Sommerfeld Number for Full-Floating Journal Bearing	194
52	Bearing Stiffness Versus Rotor Speed	198
53	Shaft Mode Shapes	199
54	Diffuser Rig Rotor System	201
55	Impeller Shaft Arrangements	203
56	MF-1 Rotor Force Diagram	205
57	MF-2 Rotor Force Diagram	207
58	Critical Speed Versus Bearing Stiffness	208
59	MF-1 Vibration Levels	210

LIST OF ILLUSTRATIONS (Continued)

<u>Figure</u>		<u>Page</u>
60	MF-1 Clearance Changes	212
61	Effects of Viscous Damping	213

APPENDIX IV

62	Spin-Pit Facility	220
63	MF-2 Impeller (Spin-Pit Installation)	222
64	MF-2 Impeller (Spin-Pit Speed Record)	225
65	Spin-Pit Drive Quill Shaft After Attempted Proof Spin of Impeller MF-2	226
66	Spin-Pit Drive Turbine Lower Bearing After Attempted Proof Spin of Impeller MF-2	227
67	Impeller MF-2 After Attempted Proof Spin	229
68	Upper (Rear) Face of Impeller MF-2 After Attempted Proof Spin	230
69	Broken Arbor at the Upper End of Impeller MF-2 After Attempted Proof Spin	231
70	Broken Arbor at the Lower End of Impeller MF-2 After Attempted Proof Spin	232

APPENDIX V

71	Shaft-Bending Schematic	238
72	Proximity Probe	239
73	Proximity-Probe Installation	240
74	Amplitude-Phase Relationship	241
75	Typical Modal-Balance Weights	242

LIST OF ILLUSTRATIONS (Continued)

<u>Figure</u>		<u>Page</u>
76	Impeller With Modal-Balance Weight	243
77	Shaft-Displacement Sketch	245
78	Phase Angle Versus Rotational Speed	245
79	Shaft-Displacement Diagram	245

APPENDIX VI

80	Bench-Test Strain-Gage Locations	253
81	Campbell Diagram	256
82	Maximum Vibratory-Stress Points	257
83	Rig-Test Strain-Gage Locations	258
84	Test Equipment Instrumentation	259
85	Data Reduction Method	261
86	Expanded Oscillograph Trace	262
87	Campbell Diagram	264
88	Compressor Map	265

APPENDIX VII

89	Sketch of Temperature Probe	272
90	Variation in Overall Probe-Recovery Factor	278
91	Annular-Control Volume (Jet and Wake)	295

LIST OF ILLUSTRATIONS (Continued)

<u>Figure</u>		<u>Page</u>
APPENDIX VIII		
92	Gated-Beam Proximity Detection System (Schematic Diagram)	303
93	Detail of Water-Cooled Sensor Adapter	305
94	Eddy-Current Clearance-Probe Data	309
95	Actuated Rub Sensor Data and Eddy-Current Clearance- Probe Data	310
96	Rectangular-Wave Pressure Pulsation	312
97	Effect of Pressure Pulse Shape on Root-Mean Balance Pressure	314
98	Pressure Probes Tested	316
99	Supersonic Duct (Temperature-Recovery Calibration Facility)	323
100	Temperature Recovery Data	325
101	Temperature Probes	326
102	Slotted-Shield Total-Temperature-Probe Data	327
103	Miniature Total-Temperature-Probe Data	328
104	Total-Temperature-Probe Mounting Tower	329
APPENDIX IX		
105	Test Points	336
106	Diffuser Static-Pressure Instrumentation, DI-1	341
107	Diffuser Static-Pressure Instrumentation, DI-1	345
108	Diffuser Static-Pressure Instrumentation, DI-1	349

LIST OF ILLUSTRATIONS (Continued)

<u>Figure</u>		<u>Page</u>
109	Diffuser Static-Pressure Instrumentation, DI-1-2 . . .	353
110	Diffuser Static-Pressure Instrumentation, DI-1-3 . . .	357
111	Diffuser Static-Pressure Instrumentation, DI-2 . . .	363
112	Diffuser Static-Pressure Instrumentation, DI-X1 . . .	367
113	Diffuser Static-Pressure Instrumentation, DI-X1-2 and DI-X1-3	373
114	Diffuser Static-Pressure Instrumentation, DI-2-2 . . .	377

APPENDIX X

115	Impeller-Blade Positions for Schlieren Photographs . . .	381
116	Time-Delay Calibration	382
117	Test Points	384
118	Schlieren Photograph of DI-2 (Test Number 3312, Impeller Position = 16 Degrees, Impeller Speed = 46,000 rpm, Data Point 5)	386
119	Schlieren Photograph of DI-2 (Test Number 3312, Impeller Position = 12 Degrees, Impeller Speed = 46,000 rpm, Data Point 5)	387
120	Schlieren Photograph of DI-2 (Test Number 3312, Impeller Position = 8 Degrees, Impeller Speed = 46,000 rpm, Data Point 5)	388
121	Schlieren Photograph of DI-2 (Test Number 3312, Impeller Position = 4 Degrees, Impeller Speed = 46,000 rpm, Data Point 5)	389
122	Schlieren Photograph of DI-2 (Test Number 3312, Impeller Position = 0 Degrees, Impeller Speed = 46,000 rpm, Data Point 5)	390

LIST OF ILLUSTRATIONS (Continued)

<u>Figure</u>		<u>Page</u>
123	Schlieren Photograph of DI-2 (Test Number 3312, Impeller Speed = 46,000 rpm, Data Point 3)	391
124	Schlieren Photograph of DI-2 (Test Number 3312, Impeller Speed = 46,000 rpm, Data Point 7)	392
125	Schlieren Photograph of DI-1 (Test Number 3311, Impeller Speed = 15,000 rpm, Data Point 5)	393
126	Schlieren Photograph of DI-1 (Test Number 3311, Impeller Speed = 20,000 rpm, Data Point 5)	394
127	Schlieren Photograph of DI-1 (Test Number 3311, Impeller Speed = 25,000 rpm, Data Point 5)	395
128	Schlieren Photograph of DI-1 (Test Number 3311, Impeller Speed = 30,000 rpm, Data Point 5)	396
129	Schlieren Photograph of DI-1 (Test Number 3311, Impeller Speed = 35,000 rpm, Data Point 5)	397
130	Schlieren Photograph of DI-1 (Test Number 3311, Impeller Speed = 46,000 rpm, Data Point 5)	398
131	Schlieren Photograph of DI-1 (Test Number 3317, Impeller Speed = 50,000 rpm, Data Point 5)	399
132	Schlieren Photograph of DI-2 (Test Number 3312, Impeller Speed = 20,000 rpm, Data Point 5)	400
133	Schlieren Photograph of DI-2 (Test Number 3312, Impeller Speed = 25,000 rpm, Data Point 5)	401
134	Schlieren Photograph of DI-2 (Test Number 3312, Impeller Speed = 30,000 rpm, Data Point 5)	402
135	Schlieren Photograph of DI-2 (Test Number 3312, Impeller Speed = 35,000 rpm, Data Point 5)	403
136	Schlieren Photograph of DI-2 (Test Number 3312, Impeller Speed = 39,000 rpm, Data Point 5)	404

LIST OF ILLUSTRATIONS (Continued)

<u>Figure</u>		<u>Page</u>
137	Schlieren Photograph of DI-2 (Test Number 3313, Impeller Speed = 46,000 rpm, Data Point 5)	405
138	Schlieren Photograph of DI-3 (Test Number 3314, Impeller Speed = 25,000 rpm)	406
139	Schlieren Photograph of DI-3 (Test Number 3314, Impeller Speed = 46,000 rpm, Data Point 2)	407
140	Schlieren Photograph of DI-3 (Test Number 3314, Impeller Speed = 46,000 rpm, Data Point 3)	408
141	Schlieren Photograph of DI-3 (Test Number 3314, Impeller Speed = 46,000 rpm, Data Point 5)	409
142	Schlieren Photograph of DI-3 (Test Number 3314, Impeller Speed = 46,000 rpm, Data Point 7)	410
143	Schlieren Photograph of DI-1-2 (Test Number 3319, Impeller Speed = 50,000 rpm, Data Point 5)	411
144	Schlieren Photograph of DI-X1 (Test Number 3315, Impeller Speed = 50,000 rpm, Data Point 5)	412
145	Schlieren Photograph of DI-X1-2 (Test Number 3318, Impeller Speed = 50,000 rpm, Data Point 5)	413
146	Schlieren Unit	414
147	Schlieren Schematic Diagram	415

APPENDIX XI

148	Typical Variation of Pressure-Recovery Coefficient Versus Inlet Mach Number.	421
149	Velocity Profiles of Normal and Separating Boundary Layers	421
150	Flow-Regime Map	422

LIST OF ILLUSTRATIONS (Continued)

<u>Figure</u>		<u>Page</u>
151	Locus of Maximum Pressure Recovery Versus System Geometry	424
152	Critical Inlet Mach Number Versus Inlet Blockage Ratio	425
APPENDIX XII		
153	Characteristic Grouping of Diffuser Data (C_p Versus Inlet Mach Number at Fixed Geometry)	433
154	Flow-Regime Map, Inlet Mach Number Group Classification	434
155	Critical Inlet Mach Number Versus Blockage Ratio	435
156	Flow Arrangement and Measurement Techniques	438
157	Diffuser Test Section (5.7 Aspect Ratio).	439
158	Nozzle and Diffuser Block Dimensions (5.7 Aspect Ratio)	440
159	Diffuser Test Section (0.25 Aspect Ratio)	441
160	Nozzle and Diffuser Block Geometry (0.25 Aspect Ratio Tests, $L/W = 15$)	442
161	Centerline Stagnation Pressure Change (3.5-Inch-Long Throat).	446
162	Straight Diffuser Performance (Pressure Ratio Versus Axial Distance for Various Backpressures, 0.25 Aspect Ratio, $2\theta = 6^\circ$, $L_{throat} = 0.125$ Inch)	447
163	Straight Diffuser Performance (Pressure Ratio Versus Axial Distance For Various Backpressures, 0.25 Aspect Ratio, $2\theta = 6^\circ$, $L_{throat} = 1.625$ Inch).	448
164	Straight Diffuser Performance (Pressure Ratio Versus Axial Distance For Various Backpressures, 0.25 Aspect Ratio, $2\theta = 6^\circ$, $L_{throat} = 3.5$ Inches)	450

LIST OF ILLUSTRATIONS (Continued)

<u>Figure</u>		<u>Page</u>
165	Straight Diffuser Performance (C_p Versus Mach Number)	454
166	Straight Diffuser Performance (C_p Versus Mach Number)	455
167	Straight Diffuser Performance (C_p Versus Mach Number)	456
168	Straight Diffuser Performance (C_p Versus Mach Number)	457
169	Straight Diffuser Performance (C_p Versus Mach Number)	458
170	Straight Diffuser Performance (C_p Versus Mach Number)	459
171	Straight Diffuser Performance (C_p Versus Mach Number)	460
172	Straight Diffuser Performance (C_p Versus Mach Number)	461
173	Straight Diffuser Performance (C_p Versus Mach Number)	462
174	Straight Diffuser Performance (Pressure Recovery Versus Divergence Angle, $L/W = 10$)	464
175	Straight Diffuser Performance (Pressure Recovery Versus Divergence Angle, $L/W = 15$)	465
176	Straight Diffuser Performance (Pressure Recovery Versus Divergence Angle, $L/W = 15$)	466
177	Straight Diffuser Performance (Blockage Versus Divergence Angle With Pressure Recovery as Parameter)	469

LIST OF ILLUSTRATIONS (Continued)

<u>Figure</u>		<u>Page</u>
178	Straight Diffuser Performance (Blockage Versus Divergence Angle With Pressure Recovery as Parameter)	470
179	Straight Diffuser Performance	471

(U) TABLES

<u>Table</u>		<u>Page</u>
APPENDIX III		
I	Compressor Critical Speeds	215
APPENDIX VII		
II	Compressor Data for the General Test Case of the Workhorse Impeller Supplied by the Contractor	284
APPENDIX X		
III	Time Delay in Microseconds	383
APPENDIX XI		
XI	Reference Data and Symbols	420

UNCLASSIFIED

(C) APPENDIX I (U)

IMPELLER RADIAL-EQUILIBRIUM DESIGN (U)

ABSTRACT (U)

This program is used to perform a two-dimensional axisymmetrical design analysis of the fluid flow in radial rotors. Given inlet, geometry, recovery and flow-angle information, the program can be used to solve for radial equilibrium at stations normal to the meridional streamlines of a compressor. Temperatures, pressures, and vector diagrams are program outputs.

UNCLASSIFIED

The program is written in FORTRAN IV for use on the SRU 1107 computer.

1.1 PURPOSE

The purpose of this program is to facilitate the radial equilibrium analysis of the fluid flow in radial- and mixed-flow impellers for given design conditions. The radial-equilibrium equation is solved at stations normal to the meridional streamlines of an impeller.

The total inlet conditions, exit-flow-angle distribution, recovery distribution, and the impeller geometry are inputs to the program. The design results printed out consist of temperatures, pressures, velocities, and angles determined at equilibrium streamlines for the inlet and downstream normal stations. The equilibrium results are used to compute blade surface velocities, which are also program outputs.

1.2 ASSUMPTIONS

- 1) The fluid is nonviscous but compressible.
- 2) Flow is axisymmetrical.
- 3) The meridional angle, γ' , is constant along any normal streamline, and $0^\circ < \gamma' < 90^\circ$.
- 4) Real fluid losses are accounted for by using relative, total-pressure-recovery factors.
- 5) The impeller blades are composed of radial blade elements.

1.3 LIMITATIONS

- 1) The blade and flow angles are the same inside the channel, up to the station at which slip begins.
- 2) Boundary-layer blockage is constant at any normal station, but variable metal blockage is used.
- 3) The meridional distance is constant along any streamline and is measured along the mean line.
- 4) Relative velocities inside the impeller are subsonic.
- 5) There is a maximum of 20 stations, including the inlet and exit stations.

UNCLASSIFIED

2.0 PROCEDURE

2.1 NOMENCLATURE

The A-, C-, and V-arrays are used in routine IMPEL, which computes conditions at the normal stations. The nomenclature for these arrays is given below. When different from those used in the program, the units correspond to the dimensions used for input and output data.

<u>Program Symbol</u>	<u>Math Symbol</u>	<u>Units</u>	<u>Description</u>
A			IMPEL storage array
AC	A_c	in.^2	Actual area check
ACCEL	A_{ccel}	ft/sec^2	Acceleration due to first two terms of dp/dn equation
AK	γ		Specific heat ratio
ALPHA, A (121-125)	α	deg	Absolute fluid-flow angle
AMASS, C (21-25)	W_a	lbm/sec	Mass flow rate, input
AREA, A (1-5)	A	in.^2	Actual annulus area
A8256-260), V (11-15)	A_{ann}	in.^2	Blocked annulus area
A (236-240)	A'_{ann}	in.^2	Adjusted A_{ann}
A (219)	$A_{\text{ann}, T}$	in.^2	Total A_{ann}
A(218)	$A'_{\text{ann}, T}$	in.^2	Total A'_{ann}
A (66-70)	$(A/A^*)_3$		Relative isentropic area ratio

UNCLASSIFIED

CONFIDENTIAL

<u>Program Symbol</u>	<u>Math Symbol</u>	<u>Units</u>	<u>Description</u>
A (146-150)	$(A/A^*)_4$		Absolute isentropic area ratio
	$(A/A^*)'_3$		Adjusted $(A/A^*)_3$
	α''	deg	Wrap angle
BETA, A (56-60)	β	deg	Relative fluid-flow angle
BLADES, V (23)	B		Number impeller blades
BLF, V (8)	BLF		Total blockage factor
BLFOUT	BLF_{exit}		Exit blockage factor
	BLF_{BL}		Boundary-layer factor
	BLF_m		Metal-blockage factor
C			IMPEL storage array
CF			Indicates if curvature will be used at inlet
DDMARG	$(\frac{2\pi}{B} R - t) V_{t4}$	in. fps	Angular momentum of blade-surface velocities
DERIV1	dR/dZ		First derivative of radius with respect to axial distance
DERIV2	d^2R/dZ^2	in. ⁻¹	Second derivative of radius with respect to axial distance
DGR	0.01745329	rad/deg	Geometric conversion factor
DPDN, A (191-195)	dP_3/dn	m. Hg/in.	First derivative of static pressure with respect to normal distance

CONFIDENTIAL

<u>Program Symbol</u>	<u>Math Symbol</u>	<u>Units</u>	<u>Description</u>
A (46-50)	$d\alpha''/dZ$	deg/in.	First derivative of wrap angle with respect to axial distance
A (451-500)	$d\alpha''/dZ$	deg/in.	$d\alpha''/dZ$ table
	dV_T/dm	ft/in. -sec	First derivative of tangential velocity with respect to meridional distance
A (176-180)	F_N	ft/sec ²	Component of blade force per unit mass in normal direction
GAMMA, A (204), V (4)	γ'	deg	Meridional fluid-flow angle, measured from axis of rotation
GC	g	$\frac{\text{lbm-ft}}{\text{lbf-sec}}^2$	Gravitational constant, 32.17
GIVM	W_{aT}	lbm/sec	Total given mass flow rate
GRID			Storage array for TALL14 plots
HGPSI	2.03593	in. Hg/psi	Pressure conversion factor
HJ	J	ft-lbf/Btu	Work conversion factor, 778.2
HS	h_s	Btu/lbm	Static enthalpy
HRT, A (21-25)	h_T	Btu/lbm	Relative total enthalpy
HT, A (161-165)	h_T	Btu/lmb	Absolute total enthalpy
	H	in.	Normal blade height
KSLIP	k_{slip}		Slip station

CONFIDENTIAL

<u>Program Symbol</u>	<u>Math Symbol</u>	<u>Units</u>	<u>Description</u>
K2	k		Station number, one at inlet
A (241-245)	M'_3		Adjusted M_3
NOMODE			Storage array for TALL14 plots
NORMLS	norm		Number of normals past inlet
NPLOT			Plot logical indicator
NS, V (10)			Number of stations, NORMLS + 1
NSLIP	n_{slip}		Slip station, if input
NTITLE			Title storage array
NXY			Number of points in input curve
A (213)	ω	rad/sec	Rotational speed
PHI	ϕ	deg	Blade angle
PI	π		Geometric constant, 3.14159
PLOTDX		in.	X-axis plot interpolation, x
PS, A (86-90)	p_s	in. Hg	Static pressure
PRT, C (6-10) A (36-40)	P_T	in. Hg	Relative total pressure
PT, A (151-155)	P_T	in. Hg	Absolute total pressure
A (196-200)	P'_{S3}	in. Hg	Present adjusted relative static pressure

CONFIDENTIAL

CONFIDENTIAL

<u>Program Symbol</u>	<u>Math Symbol</u>	<u>Units</u>	<u>Description</u>
A (261-265)	$P'_{S3, \text{ previous}}$	in. Hg	Previous P'_{S3}
A (31-25)	P_{r3}		Relative pressure function
A (166-170)	P_{r4}		Absolute pressure function
Q			Equivalent to V-array
QMASS	\dot{M}	lbm/sec	Computed mass flow rate
R	R	$\frac{\text{ft-lbf}}{\text{lbm-}^\circ\text{R}}$	Gas constant for air, 53.35
RAD		rad/deg	Same as DGR
RADIUS, A (11-15), C (1-5)	R	in.	Radial distance from axis, streamlines are rms of tubes
RCURV A (181-185)	R_c	in.	Radius of curvature
REC, V (16-20)	R_{ec}		Relative pressure recovery
	R_{ec_i}		Inducer recovery
	δR_{ec}		Recovery correction factor
RHO	ρ_T	lbm/in. ³	Total mass density
RIN	R	in.	Inlet mean radius
RPM, C (26)	N	rpm	Rotational speed
A (186-190)	ρ	lbm/in. ³	Static mass density
SLIP, V (9)			Slip logic indicator

CONFIDENTIAL

CONFIDENTIAL

<u>Program Symbol</u>	<u>Math Symbol</u>	<u>Units</u>	<u>Description</u>
SLIPFC	K_{slip}		Velocity slip factor input, usually about 1.4
	t_{hub}	in.	Blade thickness at hub measured in plane normal to axis of rotation
	t_{tip}	in.	Blade thickness at tip measured in plane normal to axis of rotation
TABLE, TAB 2	$\hat{f} ()$		Indicates a table interpola- tion of degree one, except for geometry (third degree) table look-ups
TS, A (91-95)	T_s	°R	Static temperature
TRT, A (26-30), C (16-20)	T_T	°R	Relative total temperature
TT, A (156-160)	T_T	°R	Absolute total temperature
U, A (16-20)	U	fps	Wheel speed
V			IMPEL storage array
V, A (126-130)	V	fps	Absolute total velocity
VCR	V_{cr}	fps	Critical velocity
VP	V_P	fps	Pressure blade surface velocity
VPW	$V_P/V_{2, \text{mean}}$		Normalized pressure velocity
VR	V_r	fps	Absolute radial velocity
VS	V_s	fps	Suction blade-surface velocity

CONFIDENTIAL

<u>Program Symbol</u>	<u>Math Symbol</u>	<u>Units</u>	<u>Description</u>
VSND, A (96-100)	a	fps	Sonic velocity
VSW	$V_s/V_{2, \text{mean}}$	fps	Normalized suction velocity
VTW	$V_s/V_{2, \text{mean}}$		Normalized total relative velocity
VU, A (116-120)	V_T	fps	Absolute tangential velocity
VVSND, A (131-135)	M		Absolute Mach number
VX	V_x	fps	Absolute axial velocity
W, A (101-105)	V	fps	Relative total velocity
WM, A (106-110)	V_m	fps	Relative meridional velocity
WR	V_r	fps	Relative radial velocity
WU, C (11-15), A (111-115)	V_T	fps	Relative tangential velocity
XBLF		in.	Independent array of n for $BLF = f(n)$ and $\alpha_3 = f(n)$
XL ϕ C (1, K2)	Z_{hub}	in.	Axial distance to normal intersection with hub
XL ϕ C, V (6), A (41-45)	Z	in.	Axial distance
XMD, V (21)	m	in.	Meridional distance from inlet along mean line
XND, A (61-65)	n	in.	Normal distance from hub
XRC		in.	Independent array of n for $R_c = f(n)$

CONFIDENTIAL

CONFIDENTIAL

<u>Program Symbol</u>	<u>Math Symbol</u>	<u>Units</u>	<u>Description</u>
XVAL			Independent variable array for input tables
YAL		rad	Dependent array of α_3 for $\alpha_3 = f(n)$
YBLF			Dependent array of BLF for BLF = f(n)
YRC		in.	Dependent array of R_c for $R_c = f(n)$
YVAL			Dependent variable array for input tables
ZTIPG	$z_{\text{tip, guess}}$	in.	First guess of axial distance to normal intersection with the tip
XLØC (4, K2), A (401, 450)	Z_{mean}	in.	Axial distance to normal intersection with mean line
X	$\alpha'3$	rad	Relative fluid-flow angle based on ϕ

<u>Subscripts</u>	<u>Description</u>
1	Inlet absolute
2	Inlet relative (to moving blade row)
3	Exit (or normal) relative
4	Exit (or normal) absolute
exit	Exit station (or last normal)
hub	Impeller hub
inlet	Inlet station
j	Streamline (or streamtube), j = 1 for hub streamtube

CONFIDENTIAL

<u>Subscripts</u>	<u>Description</u> (Continued)
k	Station, k = 1 for inlet station, k = 20 for discharge station
m	Meridional direction, or mean line
mean	Mean line, that curve dividing the total annulus area in half
r	Radial direction
S	Static
slip	Slip station (where slip begins)
T	Total, or tangential direction
tip	Impeller tip
x	Axial direction
1	Hub streamtube
2	Second streamtube
.	.
.	.
.	.
5	Tip streamtube
1	Inlet station
2	Second station (first normal station)
.	.
.	.
.	.
20	Twentieth station

CONFIDENTIAL

2.2 METHOD

The 5-streamtube approach is used, and the method of analysis for radial equilibrium downstream from the inlet is that developed in NACA Report 1082.* Radial equilibrium at the impeller inlet is established for the given inlet flow rates by using the methods of Swan.** Geometric dependent calculations are made for each normal station. The resulting inlet relative conditions and geometry are used, together with given recovery and fluid angle information, to solve the radial-equilibrium equation at each station along a streamline normal to the meridional plane.

See Figures 1 and 2 for the definitions of geometry and sign conventions. The functional notation, $y = f(x)$, indicates that x and y are in tabular form; the degree of interpolation is noted for $f(\)$ in Section 2.1 of this appendix. The streamtube subscript is j , where $j = 1$ at the hub streamtube; k is the station subscript, where $k = 1$ at the inducer inlet. For clarity, the equations do not have the unit conversion factors, such as DGR and HGPSI, included. The last normal station downstream from the inlet is considered to be the exit.

2.2.1 INLET CALCULATIONS

Five streamtubes of equal area are assumed initially. The velocity profile is varied until a total mass flow balance is attained. If streamtube continuity is not satisfied, the streamtube areas are adjusted, and a total mass balance is again attained. This process and the velocity equation ensure radial equilibrium. The given information at the inlet is:

- 1) Mass-flow rate per streamtube, $W_{a,j}$;
- 2) Total-temperature schedule, $T_{T1} = f(R)$;
- 3) Total-pressure schedule, $P_{T1} = f(R)$;
- 4) Absolute-fluid-flow-angle schedule, $\alpha_1 = f(R)$;
- 5) Total-blockage schedule, $BLF_1 = f(R)$;

*J. T. Hamrick, A. Ginsberg, and W.M. Osborn, Method of Analysis for Compressible Flow Through Mixed-Flow Centrifugal Impellers of Arbitrary Design, NACA Report 1082 (Supersedes NACA TN 2165), 1952.

**W. C. Swan, A Practical Engineering Solution of the Three Dimensional Flow in Transonic Type Axial Flow Compressors, WADC TR 58-57, 1959.

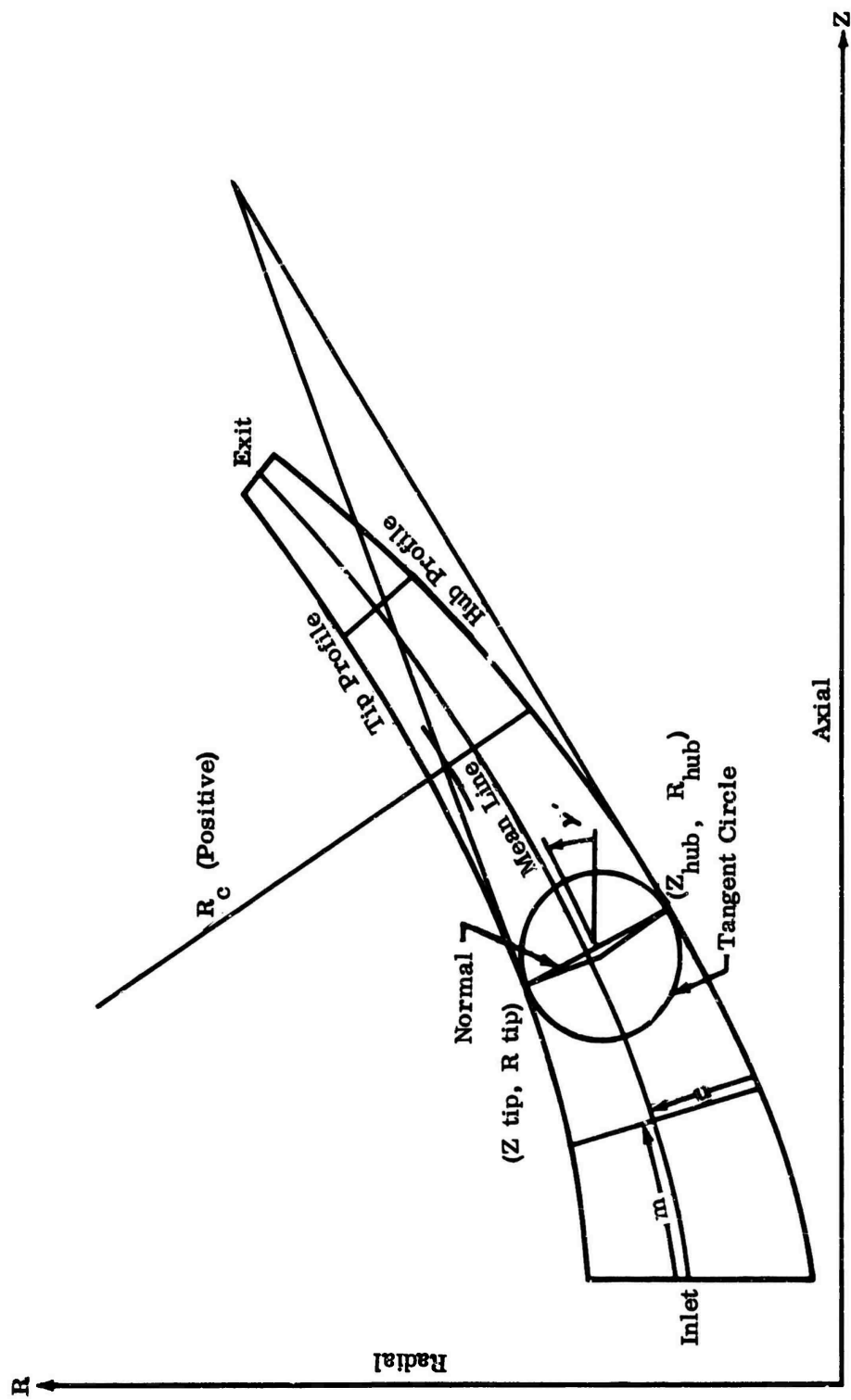


Figure 1. Impeller Meridional View.

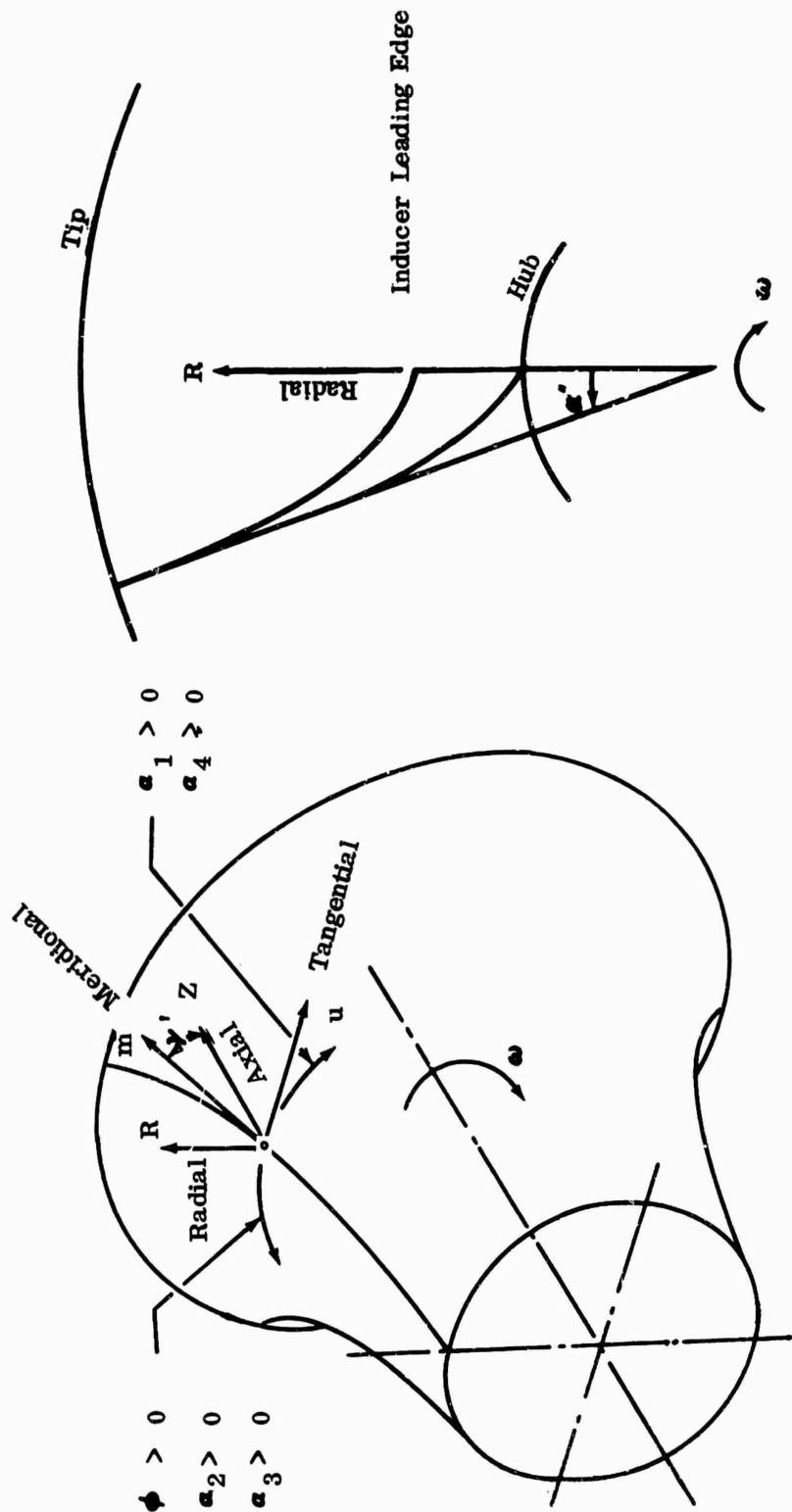


Figure 2. Angle Sign Conventions.

CONFIDENTIAL

- 6) Hub- and tip-radius schedules, $R = f(z)$;
- 7) Station location, Z_1 ;
- 8) Rotational speed, N ;
- 9) Thermodynamic tables, $h = f(T)$ and $\gamma = f(T)$.

Equal-Area Streamtubes

$$R_{\text{hub}} = f(Z_1) \quad (1)$$

$$R_{\text{tip}} = f(Z_1) \quad (2)$$

$$A_T = \pi (R_{\text{tip}}^2 - R_{\text{hub}}^2) \quad (3)$$

$$A_j = A_T/5 \quad (4)$$

$$R_{\text{hub}, 1} = R_{\text{hub}} \quad (5)$$

$$R_{\text{tip}, j} = \sqrt{A_j/\pi + R_{\text{hub}, j}^2} \quad (6)$$

$$R_j = \sqrt{(R_{\text{tip}, j}^2 + R_{\text{hub}, j}^2)/2} \quad (7)$$

$$R_{\text{hub}, j+1} = R_{\text{tip}, j} \quad \text{for } j = 1, 2, 3, 4, 5. \quad (8)$$

Radial Derivatives

$R_j +$ and $R_j -$ are determined as above at stations downstream and upstream, respectively, from the inducer inlet.

CONFIDENTIAL

$$\left(\frac{dR}{dz} \right)_j = \left(\frac{R^+ - R^-}{2 \Delta X} \right)_j \quad \Delta X = 0.1 \text{ inch} \quad (9)$$

$$\left(\frac{d^2 R}{dz^2} \right)_j = \left(\frac{R^+ - 2R + R^-}{\Delta X^2} \right)_j \quad (10)$$

Scheduled Input

$$T_{T1,j} = f(z_1) \quad (11)$$

$$P_{T1,j} = f(z_1) \quad (12)$$

$$\alpha_{1,j} = f(z_1) \quad (13)$$

$$BLF_{1,j} = f(z_1) \quad (14)$$

Velocity Profile

$V_{X1, \text{hub}}$ is assumed to be initially 600 fps when the bisection and Newton methods are used.

$$V_{T1,j} = V_{X1} \cos \alpha_{1,j} \quad (15)$$

$$\gamma = f \left\{ \left(T_{T1,j+1} - T_{T1,j} \right) \right\} / 2 \quad (16)$$

$$c_j = 2 \gamma R / J(\gamma - 1) \quad (17)$$

$$\Delta R_j = R_{j+1} - R_j \quad (18)$$

CONFIDENTIAL

$$a_j = g_c J(T_{T1,j+1} + T_{T1,j}) \quad (19)$$

$$b_j = \frac{R}{J} \ln \left\{ \frac{(T_{T1,j+1}/T_{T1,j})^{\frac{\gamma}{\gamma+1}}}{P_{T1,j+1}/P_{T1,j}} \right\} \quad (20)$$

$$h_{T1,j} = f(T_{T1,j}) \quad (21)$$

$$C1 = V_{X1,j}^2 \left\{ 1 + \frac{b}{c} \left[1 + \left(\frac{dR}{dZ} \right)^2 \right] + \frac{d^2 R}{dZ^2} \Delta R \right\}_j - a_j b_j \quad (22)$$

$$C2 = 2 g_c J(h_{T1,j+1} - h_{T1,j}) \quad (23)$$

$$C3 = V_{T1,j+1}^2 \left\{ \left(\frac{b}{c} \right)_{j+1} - 2 + \frac{R_j}{R_{j+1}} \right\} + V_{T1,j}^2 \left\{ \left(\frac{b}{c} \right)_j + 2 - \frac{R_{j+1}}{R_j} \right\} \quad (24)$$

$$C4 = 1 - \left(\frac{b}{c} \right)_j \left\{ 1 + \left(\frac{dR}{dZ} \right)_{j+1}^2 \right\} - 9 \left(\frac{d^2 R}{dZ^2} \right)_{j+1} \Delta R_j \quad (25)$$

$$V_{X1,j+1}^2 = \frac{C1 + C2 + C3}{C4} \quad \text{for } j = 1, 2, 3, 4. \quad (26)$$

Total Mass Balance

$$M_j = \left(BLF_1 \frac{\rho V_{X1}}{\rho_T V_{crl}} - \rho_T V_{crl} A \right)_j \quad (27)$$

CONFIDENTIAL

$$\dot{M}_T = \sum_{j=1}^5 \dot{M}_j \quad (28)$$

$$\frac{\rho V_{X1}}{\rho_T V_{crl}} = \left(\frac{V_{X1}}{V_{crl}} \right)_j \left\{ 1 - \frac{\gamma-1}{\gamma+1} \left(\frac{V_{X1}}{V_{crl}} \right)^2 \left[1 + \tan^2 \alpha_1 + \left(\frac{dR}{dZ} \right)^2 \right] \right\}^{\frac{1}{\gamma-1}} \quad (29)$$

$$\gamma = f(T_{T1,j}) \quad (30)$$

$$V_{crl,j} = \sqrt{\gamma g R \frac{2T_{T1,i}}{\gamma-1}} \quad (31)$$

$$\rho_{T,j} = \left(\frac{P_{TL}}{R T_{T1}} \right)_j \quad (32)$$

$$W_{aT} = \sum_{j=1}^5 W_{a,j} \quad (33)$$

If $\left| \dot{M}_T - W_{aT} \right| < 0.005$, a total mass balance has been achieved and a check on streamtube continuity is made; otherwise, a new velocity profile is computed based on a new $V_{X1, hub}$ (see Velocity Profile section of this appendix).

Streamtube Mass Balance

$$A_{c,j} = A_j W_{a,j} / M_j \quad (34)$$

CONFIDENTIAL

If $|A_{c, j} - A_j| < 0.01$ for $j = 1, 2, 3, 4, 5$, complete radial equilibrium has been attained; otherwise, a streamline shift is made as shown below and the process is repeated beginning with the steps in the Scheduled Input section.

$$R_{hub, 1} = R_{hub} \quad (5)$$

$$R_{tip, j} = \sqrt{(A_c / \pi + R_{hub}^2)_j} \quad (35)$$

$$\delta R_j = (R_{tip} - R_{hub})_j \quad (36)$$

$$R_{hub, j+1} = R_{tip, j} \text{ for } j = 1, 2, 3, 4, 5 \quad (8)$$

$$\Delta R_T = R_{tip} - R_{hub} \quad (37)$$

$$\delta R_T = \sum_{j=1}^5 \delta R_j \quad (38)$$

$$\Delta R_j = \delta R_j \frac{\Delta R_T}{\delta R_T} \quad (39)$$

$$R_j = \sqrt{R_{hub}^2 + (R_{hub} + \Delta R)^2}_j / 2 \quad (40)$$

$$A_j = \pi \left\{ (R_{hub} + \Delta R)^2 - R_{hub}^2 \right\}_j \quad (41)$$

$$R_{hub, j+1} = R_{tip, j} \text{ for } j = 1, 2, 3, 4, 5. \quad (8)$$

Return to the steps in the Scheduled Input section.

CONFIDENTIAL

Additional Calculations

After complete equilibrium is established, the following inlet calculations are made:

$$T_{S1,j} = T_{T1,j} \left\{ 1 - \frac{\gamma - 1}{\gamma + 1} \left(\frac{V_1}{V_{cr1}} \right)^2 \right\} = \gamma_r + (T_{T1,j}) \quad (42)$$

$$V_{r1,j} = \left(\frac{dR}{dz} \right)_j V_{X1,j} \quad (43)$$

$$V_{1,j} = \sqrt{(V_{r1}^2 + V_{X1}^2 + V_{T1}^2)_j} \quad (44)$$

$$P_{S1,j} = P_{T1,j} \left\{ \left(\frac{T_{S1}}{T_{T1}} \right)^{\frac{\gamma}{\gamma - 1}} \right\}, \gamma = f \left\{ (T_{S1} + T_{T1})_j^{1/2} \right\} \quad (45)$$

$$a_{1,j} = \sqrt{\gamma g_c R T_{S1,j}} \quad \gamma = f(T_{S1,j}) \quad (46)$$

$$M_{1,j} = \left(\frac{V_1}{a_1} \right)_j \quad (47)$$

$$U_{1,j} = \pi R_j N/360 \quad (48)$$

$$V_{T2,j} = (U_1 - V_{T1})_j \quad (49)$$

$$V_{X2,j} = V_{X1,j} \quad (50)$$

$$V_{r2,j} = V_{r1,j} \quad (51)$$

CONFIDENTIAL

$$V_{2,j} = \sqrt{\left(V_{r2}^2 + V_{X2}^2 + V_{r2}^2\right)}_j \quad (52)$$

$$M_{2,j} = \left(\frac{V_2}{a_1}\right)_j \quad (53)$$

$$\alpha_{2,j} = \tan^{-1} \left(\frac{V_{T2}}{V_{X2}}\right)_j \quad (54)$$

$$V_{M2,j} = \sqrt{\left(V_{X2}^2 + V_{r2}^2\right)}_j \quad (55)$$

$$h_{s1,j} = f(T_{s,j}) \quad (56)$$

$$h_{T2,j} = \left(h_{s1} + V_2/2 g_c J\right)_j \quad (57)$$

$$T_{T2,j} = f(h_{T2,j}) \quad (58)$$

$$P_{T2,j} = \left(\frac{T_{T2}}{T_{S1}}\right)^{\frac{\gamma}{\gamma-1}} P_{T1,j}, \quad \gamma = f\left\{(T_{r2} + T_{S1})/2\right\} \quad (59)$$

$$R_{c,j} = \frac{\left\{1 + \left(\frac{dR}{dz}\right)_j^2\right\}^{1.5}}{\left(\frac{d^2R}{dz^2}\right)_j} \quad (60)$$

CONFIDENTIAL

CONFIDENTIAL

2.2.2 GEOMETRIC CALCULATIONS

At each station downstream from the inlet, the intersections of the normal stations with the hub and tip profiles in the meridional plane are determined first. The initial streamtube areas, the meridional angle, the mean line, and meridional distances, and the radius of curvature schedules can then be calculated. Schedules for the relative pressure recoveries and blockage factors are next developed at each normal station. The above preliminary information is used, together with input information, to solve the radial equilibrium equation at each station, as described in Section 2.2.3 of this appendix. The given information relevant to calculations in this section is listed below:

- 1) Hub profile, $R_{\text{hub}} = f(z)$;
- 2) Tip profile, $R_{\text{tip}} = f(z)$;
- 3) Exit total blockage, BLF;
- 4) Inducer streamtube recovery schedules, $R_{\text{eci}, j} = f(M_2)$;
- 5) Recovery correction schedule, $\delta R_{\text{ec}} = f(H)$;
- 6) Axial distance to stations at the hub, $Z_{\text{hub}, k}$;
- 7) Axial distance (approximate) to stations at the tip, $Z_{\text{tip guess}, k}$;
- 8) Number of impeller blades, B ;
- 9) Blade thickness schedules, $t_{\text{hub}} = f(z)$ and $t_{\text{tip}} = f(z)$;
- 10) Radius of curvature schedules, $R_{\text{Chub}} = f(Z)$ and $R_{\text{Ctip}} = f(Z)$.

Normal Determination

Refer to the reference* for a detailed development of the equations. The normal station passing through a known point ($Z_{\text{hub}}, R_{\text{hub}}$) is found, which satisfies the tangent circle criterion (see Figure 1). The iterative algorithm uses a third-degree exact polynomial fit to determine profile slopes. The tip point ($Z_{\text{tip guess}}, R_{\text{tip}}$) provides a starting point in the iteration. After the stations normal to the streamlines have been determined, the following information is known:

*See second footnote, page 12.

CONFIDENTIAL

$$(Z_{\text{hub}}, R_{\text{hub}})_k$$

$$(Z_{\text{tip}}, R_{\text{tip}})_k$$

$$\gamma'_k = \tan^{-1} \left(\frac{Z_{\text{hub}} - Z_{\text{tip}}}{R_{\text{tip}} - R_{\text{hub}}} \right)_k \quad (61)$$

where: k = station number (at inlet $k = 1$).

Station Geometry

$$A_T = \pi(R_{\text{tip}}^2 - R_{\text{hub}}^2)/\cos \gamma' \quad (62)$$

$$A_j = A_T/5 \quad (4)$$

$$R_{\text{hub}, 1} = R_{\text{hub}} \quad (5)$$

$$R_{\text{tip}, j} = \sqrt{(\cos \gamma' / \pi + P_{\text{hub}}^2)_j} \quad (63)$$

$$R_j = \sqrt{(R_{\text{tip}}^2 + R_{\text{hub}}^2)_j} / 2 \quad (7)$$

$$n_j = (R_j - R_{\text{hub}})/\cos \gamma' \quad (64)$$

$$R_{\text{hub}, j+1} = R_{\text{tip}, j} \text{ for } j = 1, 2, 3, 4, 5 \quad (8)$$

$$Z_j = Z_{\text{tip}} + \tan \gamma' (R_{\text{tip}} - R_j) \quad (65)$$

CONFIDENTIAL

$$R_m = R_3 \quad (66)$$

$$Z_m = Z_3 \quad (67)$$

$$n_m = n_3 \quad (68)$$

The R_c versus n schedule at each station is constructed by computing R_c at the hub and tip.

$$R_{C_{hub}} = f(Z_{hub}) \quad (69)$$

$$R_{C_{tip}} = f(Z_{tip}) \quad (70)$$

With the hub and tip radii of curvature being used, the streamline R_c values are obtained by linear interpolation of normal distance. After the above geometric calculations have been made, the meridional distance, m , from the inlet to each station is determined by linear (station-to-station) integration along the mean-line points (Z_m, R_m).

Station Recovery and Blockage Schedules

$$BLF_{metal} = \frac{A - (H \cdot \bar{t} \cdot B)}{A} = 1 - \frac{\bar{t} \cdot B}{2 \bar{R}} \quad (71)$$

$$\bar{R} = (R_{hub} + R_{tip})/2 \quad (72)$$

$$\bar{t} = (t_{hub} + t_{tip})/2 \quad (73)$$

$$BLF_{BL, exit} = \frac{BLF_{exit}}{BLF_{metal, exit, mean}} \quad (74)$$

CONFIDENTIAL

CONFIDENTIAL

$$BLF_{BL, in.} = \frac{BLF_{i, mean}}{BLF_{metal, in., mean}} \quad (75)$$

BLF_{BL} at each station is determined by linear interpolation of meridional distance and is assessed in a one-dimensional analysis.

$$BLF_{BL, K} = \frac{BLF_{BL, exit} - BLF_{BL, in.}}{m_{exit}} m_k + BLF_{BL, in.} \quad (76)$$

BLF_{metal} is determined for streamtubes at each station, and a total blockage schedule, $BLF = f(n)$, is computed for each station.

$$BLF_{k, j} = \left(BLF_{metal, k, j} \right) \left(BLF_{BL, k} \right) \quad (77)$$

k = station number

j = streamline number (1, 2, 3, 4, 5)

$$A_{ann, k, j} = A_{k, j} BLF_{k, j} \quad (78)$$

$$\delta R_{ec_j} = f\left(\frac{n_j}{n_{tip}} 100\right)_{exit} \quad (79)$$

$$R_{ec_{i, j}} = f(M_{2, j}) \quad (80)$$

$$R_{ec_{exit, j}} = R_{ec_{i, j}} \delta R_{ec_j} \quad (81)$$

The streamtube recovery distributions are calculated by linear interpolation from a recovery of one at the inlet to the respective streamtube recovery at the exit as a function of meridional distance.

CONFIDENTIAL

CONFIDENTIAL

$$R_{ec_{k,j}} = - \frac{R_{ec_{exit,j}}^{m_{exit} - 1}}{m_{exit}} m_k + 1 \quad (82)$$

2.2.3 IMPELLER NORMAL CALCULATIONS

In general, the methods developed by Hamrick, et al* are followed. The radial-equilibrium equation to be solved is:

$$\frac{dP_3}{dn} = \rho \left(\frac{12V_{T4}^2}{R} \cos \gamma' - \frac{12V_{M4}^2}{R_c} - F_N \right) \quad (83)$$

The static-pressure change in the direction normal to the mean line and in the meridional plane is equated to the force per unit volume due to rotation about the impeller axis, plus the centrifugal force per unit volume due to the curvilinear paths of the fluid particles, plus the component of the blade surface force per unit volume normal to the meridional streamline.

The general outline of the iterative method of solution is now described. An initial area distribution is assumed, and solution is obtained for the vector triangles (Vectors 3 and 4) at the station of interest. This gives a schedule of static pressure versus normal distance. The radial equilibrium is used to adjust the static-pressure schedule about the mean-line static-pressure value. If the static-pressure values do not agree with those calculated, area distribution is adjusted and the calculations are repeated.

The blade-surface velocities are computed at each station after the radial equilibrium for all stations has been established. The method proposed by Stanitz and Prian** is used.

The information given for the impeller normal station calculations is computed as shown in Sections 2.2.1 or 2.2.2, or is used as data input as follows:

- 1) Metal blade angle schedule, $\phi = f(z_m)$;
- 2) Station number, n_{slip} , at which $\alpha_3 = 0$ and slip begins, and which may be downstream from the last normal if no slip is expected;

*(See footnote, page 12)

**J.D. Stanitz, and V.D. Prian, A Rapid Approximate Method for Determining Velocity Distribution on Impeller Blades of Centrifugal Compressors, NACA TN 2421, July 1951.

- 3) If n_{slip} is not specified, a constant K_{slip} (approximately 1.4) is used as input data, which the program compares with $(V_2/V_3)_{mean}$ to determine where slip begins;
- 4) Thermodynamic table, $P_r = f(T)$;
- 5) Exit relative fluid-flow angle schedule, $\alpha_{3, exit} = f(\%H)$, required if slip is expected upstream from the last normal station (impeller exit).

Vector Diagrams

$$A_{ann, T} = \sum_{j=1}^5 A_{ann, j} \quad (84)$$

After the first iteration, the blockage factor becomes $BLF_m = f(n_j)$:

$$A_j = A_{ann, j} / BLF_j \quad (85)$$

$$R_{tip, 1} = \sqrt{\cos \gamma' A_1 / \pi + R_{hub}^2} \quad (86)$$

$$R_{tip, j} = \sqrt{\cos \gamma' A_j / \pi + R_{tip, j-1}^2}, \quad j = 2, 3, 4, 5 \quad (87)$$

$$R_1 = \sqrt{(R_{hub}^2 + R_{tip, 1}^2) / 2} \quad (88)$$

$$R_j = \sqrt{(R_{tip, j-1}^2 + R_{tip, j}^2) / 2} \quad (89)$$

$$n_j = (R_j - R_{hub}) / 12 \cos \gamma', \quad U_{4, j} = \pi N R_j / 360 \quad (90)$$

$$h_{T3, j} = h_{T2, j} + (U_{4, j} / 223.77)^2 \cdot \left\{ 1 - \left(\frac{R_{inlet, j}}{R_j} \right)^2 \right\} \quad (91)$$

CONFIDENTIAL

$$T_{T3,j} = f(h_{T3,j}) \quad (92)$$

$$P_{r3,j} = f(T_{T3,j}) \quad (93)$$

$$P_{T3,j} = P_{T2,j} R_{ec,j} P_{r3,j} / P_{r2,j} \quad (94)$$

$$Z_i = Z_{hub} - (R_j - R_{hub}) \tan \gamma' \quad (95)$$

The following steps were used in calculating impeller slip.

Step a) α_3 Before Slip — A schedule of $\left(\frac{d\alpha''}{dz}\right)_m = f(z_m)$ is constructed.

$$\left(\frac{d\alpha''}{dz}\right)_{k,m} = \frac{\tan \phi_k}{R_{k,m} \cos \gamma'_k} \quad (96)$$

$$\phi_k = f(z_{k,m}) \quad (97)$$

$k = 1, 2, \dots, \text{norm} + 1$

m means one-dimensional

$$\left(\frac{d\alpha''}{dz}\right)_j = f(z_j) \quad (98)$$

$$\alpha_{3,j} = \tan^{-1} \left\{ R_j \left(\frac{d\alpha''}{dz}\right)_j \cos \gamma'_j \right\} \quad (99)$$

$\alpha_{3,j} = \alpha_{3,j}$ and is always computed.

CONFIDENTIAL

Step b) α_3 at Slip — If n_{slip} is specified, α_3 at that station is zero; $\alpha_{3,j} = \text{zero}$.

Step c) α_3 After Slip — If K_{slip} is specified, the program defines the station at

which slip begins to become $\left(\frac{V_2}{V_3}\right)_{\text{mean}} \geq K_{\text{slip}}$. After slip, α_3 is computed by

linear interpolation of $\alpha_{3,\text{exit}}$ as a function of meridional distance from the point of the slip.

$$\alpha_{3,\text{exit},j} = f\left(\frac{n_j}{n_{\text{tip}}} 100\right)_{\text{exit}} \quad (100)$$

$$\alpha_{3,k,j} = \frac{(\alpha_{3,\text{exit}} - \alpha_{3,\text{slip},j})}{(m_{\text{exit}} - m_{\text{slip}})} (M_k - M_{\text{slip}}) + \alpha_{3,\text{slip},j} \quad (101)$$

where:

k = present station number.

If n_{slip} is specified, $\alpha_{3,\text{slip},j} = 0$; otherwise, the $\alpha_{3,\text{slip},j}$ values are as computed in Step a) above.

Relative Mach Number Calculation

Step a) — $(A/A^*)_{3,j} = \frac{K P_{T3,j} A_{\text{ann},j} \cos \alpha_{3,j}}{W_{a,j} \sqrt{T_{T3,j}}} \quad (102)$

$$K = .49118 \left[\frac{\gamma g}{R} \left(\frac{2}{\gamma + 1} \right)^{\frac{\gamma + 1}{\gamma - 1}} \right]^{1/2}, \quad \gamma = f(T_{T1})_{\text{mean}} \quad (103)$$

CONFIDENTIAL

CONFIDENTIAL

On the first d P_{s3}/dn iteration, the $(A/A^*)_{3,j}$ values are compared to 1. If all the $(A/A^*)_{3,j}$ values are greater than or equal to 1, skip to Step c) below. If the average is less than 1, the input is considered to be invalid, a message is printed, and the calculations for the present normal are terminated. If the average $(A/A^*)_3$, which is represented by $(A/A^*)_3$, is equal to or greater than 1, the assumed streamtube-area distribution is adjusted as follows:

Step b) —
$$A'_{ann,j} = A_{ann,j} \frac{\overline{(A/A^*)_3}}{(A/A^*)_{3,j}} \quad (104)$$

$$A'_{ann,T} = \sum_{j=1}^5 A'_{ann,j} \quad (105)$$

$$A_{ann,j} = A'_{ann,j} \frac{A_{ann,T}}{A'_{ann,T}} \quad (106)$$

Calculations begin again with the steps in the Vector Diagrams section.

Step c) — Iterate to solve the equations in Step d) for $M_{3,j}$ and γ ; solve for $M_{3,j}$ by using bisection and by assuming $\gamma = 1.4$ initially.

Step d) —
$$\left(\frac{A}{A^*}\right)_{3,j} = \frac{1}{M_{3,j}} \left\{ \frac{2}{\gamma+1} \left[1 + \frac{\gamma-1}{2} M_{3,j}^2 \right] \right\}^{\frac{\gamma+1}{2(\gamma-1)}} \quad (107)$$

$$\left(\frac{T_S}{T_{T3,j}}\right) = \left(1 + \frac{\gamma-1}{2} M_{3,j}^2\right)^{-1} \quad (108)$$

$$T_{S3,j} = \left(\frac{T_S}{T_{T3,j}}\right) T_{T3,j} \quad (109)$$

$$\gamma'' = f(T_{S3,j}) \quad (110)$$

CONFIDENTIAL

If $|\gamma'' - \gamma| < 0.0005$, check $\left(\frac{A}{A^*}\right)'_{3,j}$; otherwise, let $\gamma = \gamma''$ and return to Step d)

above. If $\left|\left(\frac{A}{A^*}\right)_{3,j} - \left(\frac{A}{A^*}\right)'_{3,j}\right| < 0.0005$, compute $\left(\frac{P_S}{P_T}\right)_{3,j}$; otherwise, adjust $M_{3,j}$ by using bisection and reuse Step d).

$$\left(\frac{P_S}{P_T}\right)_{3,j} = \left\{ \left[1 + \frac{\gamma-1}{2} M_{3,j}^2 \right]^{\frac{\gamma}{\gamma-1}} \right\}^{-1} \quad (111)$$

$$P_{S3,j} = P_{T3,j} \left(\frac{P_S}{P_T}\right)_{3,j} \quad (112)$$

$$a_{3,j} = \sqrt{\gamma g R T_{S3,j}}, \quad \gamma = 1.4 \quad (113)$$

$$V_{3,j} = M_{3,j} a_{3,j} \quad (114)$$

$$V_{M3,j} = V_{3,j} \cos \alpha_{3,j} \quad (115)$$

$$V_{T3,j} = V_{3,j} \sin \alpha_{3,j} \quad (116)$$

$$V_{T4,j} = U_{3,j} - V_{T3,j} \quad (117)$$

$$\alpha_{4,j} = \tan^{-1} \left(\frac{V_{T4}}{V_{M3}} \right)_j \quad (118)$$

CONFIDENTIAL

$$V_{4,j} = V_{M3,j} / \cos \alpha_{4,j} \quad (119)$$

$$M_{4,j} = V_{4,j} / a_{3,j} \quad (120)$$

$$T_{S4,j} = T_{S3,j} \quad (121)$$

Step e) — Solve the equations in Step e) for $(A/A^*)_{4,j}$ and γ . Four successive replacement iterations are used to solve for γ , assuming that $\gamma = 1.4$ initially.

$$\left(\frac{A}{A^*}\right)_{4,j} = \frac{1}{M_{4,j}} \left\{ \frac{1}{\gamma+1} \left(\frac{T_T}{T_S} \right)_{4,j} \right\}^{\frac{\gamma+1}{2(\gamma-1)}} \quad (122)$$

where:

$$\left(\frac{T_S}{T_T}\right)_{4,j} = \left(1 + \frac{\gamma-1}{2} M_{4,j}^2 \right) \quad (123)$$

$$T_{T4,j} = T_{S4,j} / \left(\frac{T_S}{T_T}\right)_{4,j} \quad (124)$$

$$\gamma = f(T_{T4})_{\text{mean}} \quad (125)$$

Return to Step e) if this is not the fourth iteration; otherwise, compute $(P_S/P_T)_{4,j}$.

$$\left(\frac{P_S}{P_T}\right)_{4,j} = \left\{ \left(\frac{T_T}{T_S}\right)_{4,j} \right\}^{\frac{\gamma}{\gamma-1} - 1} \quad (126)$$

CONFIDENTIAL

$$P_{S4,j} = P_{S3,j} \quad (127)$$

$$P_{T4,j} = P_{S4,j} \left/ \left(\frac{P_S}{P_I} \right)_{4,j} \right. \quad (128)$$

$$h_{T4,j} = f(T_{T4,j}) \quad (129)$$

$$P_{r4,j} = f(T_{T4,j}) \quad (130)$$

Radial-Equilibrium Equation

The equations used in the radial-equilibrium calculations are:

$$\omega = 2 \pi N/60 \quad (131)$$

and at the first normal station, $k = 2$, and,

$$\left(\frac{d V_T}{dm} \right)_j = \left(\frac{V_{T2} - V_{T3,k}}{M_k - M_{k-1}} \right)_j^{12} \quad (132)$$

otherwise,

$$\left(\frac{d V_T}{dm} \right)_j = \left(\frac{V_{T3,k-1} - V_{T3,k}}{M_k - M_{k-1}} \right)_j^{12} \quad (133)$$

$$F_{N,j} = V_{3,j} \sin \alpha'_{3,j} \sin \gamma' \tan \gamma' \left\{ 2 \omega + \left(\frac{d V_T}{dm} \right)_j \frac{1}{\sin \gamma'} - \frac{V_{3,j}^{12}}{R_j} \sin \alpha'_{3,j} \right\} \quad (134)$$

$$R_{c,j} = f(n_j) \quad (135)$$

CONFIDENTIAL

$$\rho_j = \frac{P_{S,3}}{R T_{S,3}} \quad (136)$$

The radial-equilibrium equation is:

$$\left(\frac{dP_3}{dn}\right)_j = \rho_j \left[\frac{-12 V_{m3,j}^2}{R_{c,j}} + \frac{12 V_{T3,j}^2}{R_j} \cos^2 \theta - F_{N,j} \right] \quad (137)$$

The solution of the exit vectors has given 5 points on the curve, $P_{S3} = f(n)$. The slopes, $\frac{dP_S}{dn}$, found by using the radial-equilibrium equation are used to adjust the P_{S3} curve about the point $(n_{\text{mean}}, P_{S3, \text{mean}})$. The static-pressure values at n_j from the adjusted curve are $P'_{S3,j}$ where:

$$P'_{S3,3} = P_{S3,3} \quad (138)$$

$$P'_{S3,2} = P'_{S3,3} - \frac{(n_3 - n_2)}{2} \left[\left(\frac{dP_3}{dn}\right)_3 + \left(\frac{dP_3}{dn}\right)_3 \right] \quad (139)$$

$$P'_{S3,1} = P'_{S3,2} - \frac{(n_2 - n_1)}{2} \left[\left(\frac{dP_3}{dn}\right)_2 + \left(\frac{dP_3}{dn}\right)_1 \right] \quad (140)$$

$$P'_{S3,4} = P'_{S3,3} + \frac{(n_4 - n_3)}{2} \left[\left(\frac{dP_3}{dn}\right)_4 + \left(\frac{dP_3}{dn}\right)_3 \right] \quad (141)$$

$$P'_{S3,5} = P'_{S3,4} + \frac{(n_5 - n_4)}{2} \left[\left(\frac{dP_3}{dn}\right)_5 + \left(\frac{dP_3}{dn}\right)_4 \right] \quad (142)$$

CONFIDENTIAL

If this is the first iteration, continue to Step a) below; otherwise, compare the P'_{S3} values with the P_{S3} values. If

$$\left| P'_{S3} - P_{S3} \right|_j / P_{S3} \leq 0.002 \quad (143)$$

the radial-equilibrium iteration is considered converged, and the logic proceeds to Step c) below. Otherwise, the following area adjustments are made in Step a) below.

Step a)—If $\left(\frac{P_{T3}}{P'_{S3}} \right)_j \leq 1$ for any streamline, j , decrease all $P'_{S3,j}$ by 0.5 continually until the inequality is satisfied: $\gamma = f(T_{T4})_{\text{mean}}$.

$$M'_{3,j} = \left\{ \left[\left(\frac{P_{T3}}{P'_{S3}} \right)^{\frac{\gamma-1}{\gamma}} - 1 \right] \frac{2}{\gamma-1} \right\}^{1/2} \quad (144)$$

$$(A/A^*)'_{3,j} = \frac{1}{M'_{3,j}} \left\{ \frac{2}{\gamma+1} \left[1 + \frac{\gamma-1}{2} (M'_{3,j})^2 \right] \right\}^{\frac{\gamma+1}{2(\gamma-1)}} \quad (145)$$

$$A'_{\text{ann},j} = (A/A^*)'_{3,j} A_{\text{ann},j} / (A/A^*)_{3,j} \quad (146)$$

$$A'_{\text{ann},T} = \sum_{j=1}^5 A'_{\text{ann},j} \quad (147)$$

If $\left| A'_{\text{ann},T} - A_{\text{ann},T} \right| / A_{\text{ann},T} \leq 0.003$, continue to Step b); otherwise, make the following adjustments:

CONFIDENTIAL

$$\text{Const} = -0.02 P'_{S3, \text{mean}} \frac{A'_{\text{ann}, T} - A_{\text{ann}, T}}{A_{\text{ann}, T}} \quad (148)$$

$$P'_{S3, j} = P'_{S3, j} + \text{Const.} \quad (149)$$

The logic now returns to Step a).

Step b) —

$$A_{\text{ann}, j} = A'_{\text{ann}, j} \left(\frac{A_{\text{ann}, T}}{A'_{\text{ann}, T}} \right) \quad (150)$$

This ends one radial-equilibrium iteration; return to the calculations in the Vector Diagrams section of this appendix.

Step c) — The acceleration is computed:

$$A_{\text{ccel}, j} = \left(\frac{12V_{T4}^2}{R} \cos \gamma' - \frac{12V_{M3}^2}{R_C} \right)_j \quad (151)$$

Blade-Surface Velocities

The blade-surface velocities are calculated after radial equilibrium has been found for each station. The metal blade angle of the blade pressure surface at any station is assumed to be equal to that of the blade suction surface.*

$$\Delta V_r = \frac{1}{2} \cos \alpha_3 \frac{d}{m} \left[\left(\frac{2\pi R}{B} - t \right) V_{T4} \right] \quad (152)$$

After vector diagrams have been found that satisfy radial equilibrium at each normal station downstream from the inlet, the following relationship is known:

*See second footnote, page 26.

CONFIDENTIAL

$$\left(\frac{2 \pi R}{B} - t \right) V_{T4} = f(m) \quad (153)$$

The blade-surface velocities are calculated at each station as follows:

$$\left[\left(\frac{2 \pi R}{B} - t \right) V_{T4,j} \right]^- = f(m_j - \Delta m), \quad \Delta m = 0.02 \quad (154)$$

$$\left[\left(\frac{2 \pi R}{B} - t \right) V_{T4,j} \right]^+ = f(m_j + \Delta m) \quad (155)$$

$$\frac{d}{dm} \left[\left(\frac{2 \pi R}{B} - t \right) V_{T4,j} \right] = \left[\frac{f(m_j + \Delta m) - f(m_j - \Delta m)}{2 \Delta m} \right] \quad (156)$$

$$V_{S,j} = V_{3,j} + \Delta V_{r,j} \quad (157)$$

$$V_{P,j} = V_{3,j} - \Delta V_{r,j} \quad (158)$$

$$(V_S/V_2)_j = V_{S,j}/V_{2, \text{mean}} \quad (159)$$

$$(V_P/V_2)_j = V_{P,j}/V_{2, \text{mean}} \quad (160)$$

$$(V/V_2)_j = V_{3,j}/V_{2, \text{mean}} \quad (161)$$

2.3 RESULTS

The inlet calculations were checked against hand calculations; the geometry calculations were checked graphically.

CONFIDENTIAL

3.0 INPUT PREPARATION AND OUTPUT DESCRIPTION

3.1 INPUT-DATA PREPARATION

Input data are regulated by alphabetic control cards. The data for each control card must follow a specified sequence. However, a control card and associated data need not appear in any particular sequence, except for the CONSTANTS data, which must appear before the Z(HUB) and Z(TIP GUESS) data, and the BEGIN COMPUTE card, which must be the last card for any set of data that defines the impeller. Multiple impellers or cases can be run by altering only the changed data, followed by a BEGIN COMPUTE card. The program uses a seven-digit or character field. All data are read in 10E7.0 format, and all control cards and the title card are read in 16A5 format. All input data are on punched cards. The following control cards are valid:

TITLE;
CONSTANTS;
MASS FLOW RATES;
Z(HUB) AT NORMALS;
Z(TIP GUESS) AT NORMALS;
TABLE;
GEOMETRY PLOT;
BEGIN COMPUTE;
END PLOT.

All numerical input data must have decimal points. A complete explanation of the input data format is presented on the following pages.

<u>Card No.</u>	<u>Field No.</u>	<u>Symbol</u>	<u>Description</u>
1	1	TITLE	Control card indicating that a title card follows.
2	1-11		Comment: This information will be printed as a heading in each output page.
1	1-2	CONSTANTS	Control card indicating that constant data follow.
	3-11		Comment: This will be printed with input data for identification.

CONFIDENTIAL

<u>Card No.</u>	<u>Field No.</u>	<u>Symbol</u>	<u>Description</u>
2	1	N	Shaft speed, rpm.
	2	B	No. impeller blades.
	3	norm	No. stations downstream from the inlet, $1 \leq \text{norm} \leq 19$; at least one required.
	4	CF	= 0 for using radial derivations at inlet; = 1 for setting these to zero.
	5	Z_{inlet}	Axial distance to inlet, in.
	6	BLF_{exit}	Exit total blockage, where last normal is considered the exit.
	7	n_{slip}	Station no. at which slip begins, where inlet station no. is 1. If $n_{\text{slip}} = 0$, the program will use k_{slip} to determine the slip station. If $n_{\text{slip}} > \text{norm} + 1$, slip- page will not occur.
	8	k_{slip}	Factor program used to determine sta- tion at which slip begins (see <u>Vector</u> <u>Diagrams</u> section of this appendix).
1	1-3	MASS FLOW RATES	Control card indicating that mass flow rates follow.
	4-11		Comment.
2	1	W_{a1}	Mass flow rate, lbm/sec, for hub streamtube.
	2	W_{a2}	Mass flow rate, lbm/sec, for Stream- tube 2.
	3	W_{a3}	Mass flow rate, lbm/sec, for Stream- tube 3.
	4	W_{a4}	Mass flow rate, lbm/sec, for Stream- tube 4.

CONFIDENTIAL

<u>Card No.</u>	<u>Field No.</u>	<u>Symbol</u>	<u>Description</u>
	5	W_{a5}	Mass flow rate, lbm/sec, for tip streamtube.
1	1-3	Z(HUB)AT NORMALS	Control card indicating Z_{hub} values follow.
	4-11		Comment.
2	1	$Z_{hub, 1}$	Axial distance, in., to intersection of hub profile and first normal downstream from inlet.
	2	$Z_{hub, 2}$	Axial distance, in., to intersection of hub profile and second normal.
		$Z_{hub, norm}$	Axial distance, in., to intersection of hub profile and exit normal.

NOTE: The last normal is considered the exit. At least one Z_{hub} is required. These two cards must follow CONSTANTS card.

1	1-4	Z(TIP GUESS) AT NORMALS	Control card indicating that $Z_{tip\ guess}$ values follow.
	5-11		Comment.
2	1	$Z_{tip\ guess, 1}$	First estimate of axial distance, in., to intersection of tip profile and first normal (see <u>Normal Determination</u> section).
	2	$Z_{tip\ guess, 2}$	First estimate of axial distance, in., to intersection of tip profile and second normal.
		$Z_{tip\ guess, norm}$	First estimate of axial distance, in., to intersection of tip profile and exit normal.

NOTE: These two cards must follow CONSTANTS cards.

1	1	TABLE	Control card indicating that table data follow.
---	---	-------	---

CONFIDENTIAL

<u>Card No.</u>	<u>Field No.</u>	<u>Symbol</u>	<u>Description</u>
	2-11		Comment.
2	1	n_{tab}	Table no., $1 \leq n_{\text{tab}} \leq 20$.
	2	n_{pts}	No. points in this table, $2 \leq n_{\text{pts}} \leq 50$, except for input tables 4 and 5, then $4 \leq n_{\text{pts}} \leq 50$.
3	1	X_1	Independent argument.
	2	Y_1	Dependent argument corresponding to X_1 .
		$X_{n_{\text{tab}}}$	
		$Y_{n_{\text{tab}}}$	
1	1-2	GEOMETRY PLOT	Control card indicating that geometry plot is desired (see Section 3.2 of this appendix).
	3-11		Comment.
2	1	X_{grid}	Length, in., of Z plot scale; $1 \leq X_{\text{grid}} \leq 50$.
	2	Y_{grid}	Length, in., of R plot scale, $1 \leq Y_{\text{grid}} \leq 9.5$.
	3	ΔX	Axial increment, in., used for profile interpolations.
1	1-2	BEGIN COMPUTE	Control card indicating that all data for 1 case have been given and computation is beginning.
1	1-2	END PLOT	Control card indicating that the plotting generated by the previous GEOMETRY PLOT card is ended; the END PLOT card must follow a BEGIN COMPUTE card and cause the program to rewind and sign off the plot tape.

CONFIDENTIAL

1	2	3	4	5	6	7	8	9	10	11	12	13	14	15	16	17	18	19	20	21	22	23	24	25	26	27	28	29	30	31	32	33	34	35	36	37	38	39	40	41	42	43	44	45	46	47	48	49	50	51	52	53	54	55	56	57	58	59	60	61	62	63	64	65	66	67	68	69	70	71	72	73	74	75	76	77	78	79	80	81	82	83	84	85	86	87	88	89	90	91	92	93	94	95	96	97	98	99	100	IDENT	PAGE	OF
TITLE																																																																																																						
(comment)																																																																																																						
CONSTANTS																																																																																																						
N																																																																																																						
B																																																																																																						
norm																																																																																																						
CF																																																																																																						
Z_inlet																																																																																																						
BLF_exit																																																																																																						
n_slip																																																																																																						
k_slip																																																																																																						
MASS FLOW RATES																																																																																																						
W_a1																																																																																																						
W_a2																																																																																																						
W_a3																																																																																																						
W_a4																																																																																																						
W_a5																																																																																																						
Z(HUB) AT NORMALS																																																																																																						
Z_hub1																																																																																																						
Z_hub2																																																																																																						
Z_hub3																																																																																																						
Z_hub4																																																																																																						
Z_hub5																																																																																																						
Z(TIP GUESS) AT NORMALS																																																																																																						
Z_tip_guess1																																																																																																						
Z_tip_guess2																																																																																																						
Z_tip_guess3																																																																																																						
Z_tip_guess4																																																																																																						
Z_tip_guess5																																																																																																						
Z_tip_guess6																																																																																																						
Z_tip_guess7																																																																																																						
Z_tip_guess8																																																																																																						
Z_tip_guess9																																																																																																						
Z_tip_guess10																																																																																																						
Z_tip_guess11																																																																																																						
Z_tip_guess12																																																																																																						
Z_tip_guess13																																																																																																						
Z_tip_guess14																																																																																																						
Z_tip_guess15																																																																																																						
Z_tip_guess16																																																																																																						
Z_tip_guess17																																																																																																						
Z_tip_guess18																																																																																																						
Z_tip_guess19																																																																																																						
Z_tip_guess20																																																																																																						
Z_tip_guess21																																																																																																						
Z_tip_guess22																																																																																																						
Z_tip_guess23																																																																																																						
Z_tip_guess24																																																																																																						
Z_tip_guess25																																																																																																						
Z_tip_guess26																																																																																																						
Z_tip_guess27																																																																																																						
Z_tip_guess28																																																																																																						
Z_tip_guess29																																																																																																						
Z_tip_guess30																																																																																																						
Z_tip_guess31																																																																																																						
Z_tip_guess32																																																																																																						
Z_tip_guess33																																																																																																						
Z_tip_guess34																																																																																																						
Z_tip_guess35																																																																																																						
Z_tip_guess36																																																																																																						
Z_tip_guess37																																																																																																						
Z_tip_guess38																																																																																																						
Z_tip_guess39																																																																																																						
Z_tip_guess40																																																																																																						
Z_tip_guess41																																																																																																						
Z_tip_guess42																																																																																																						
Z_tip_guess43																																																																																																						
Z_tip_guess44																																																																																																						
Z_tip_guess45																																																																																																						
Z_tip_guess46																																																																																																						
Z_tip_guess47																																																																																																						
Z_tip_guess48																																																																																																						
Z_tip_guess49																																																																																																						
Z_tip_guess50																																																																																																						
Z_tip_guess51																																																																																																						
Z_tip_guess52																																																																																																						
Z_tip_guess53																																																																																																						
Z_tip_guess54																																																																																																						
Z_tip_guess55																																																																																																						
Z_tip_guess56																																																																																																						
Z_tip_guess57																																																																																																						
Z_tip_guess58																																																																																																						
Z_tip_guess59																																																																																																						
Z_tip_guess60																																																																																																						
Z_tip_guess61																																																																																																						
Z_tip_guess62																																																																																																						
Z_tip_guess63																																																																																																						
Z_tip_guess64																																																																																																						
Z_tip_guess65																																																																																																						
Z_tip_guess66																																																																																																						
Z_tip_guess67																																																																																																						
Z_tip_guess68																																																																																																						
Z_tip_guess69																																																																																																						
Z_tip_guess70																																																																																																						
Z_tip_guess71																																																																																																						
Z_tip_guess72																																																																																																						
Z_tip_guess73																																																																																																						
Z_tip_guess74																																																																																																						
Z_tip_guess75																																																																																																						
Z_tip_guess76																																																																																																						
Z_tip_guess77																																																																																																						
Z_tip_guess78																																																																																																						
Z_tip_guess79																																																																																																						
Z_tip_guess80																																																																																																						
Z_tip_guess81																																																																																																						
Z_tip_guess82																																																																																																						
Z_tip_guess83																																																																																																						
Z_tip_guess84																																																																																																						
Z_tip_guess85																																																																																																						
Z_tip_guess86																																																																																																						
Z_tip_guess87																																																																																																						
Z_tip_guess88																																																																																																						
Z_tip_guess89																																																																																																						
Z_tip_guess90																																																																																																						
Z_tip_guess91																																																																																																						
Z_tip_guess92																																																																																																						
Z_tip_guess93																																																																																																						
Z_tip_guess94																																																																																																						
Z_tip_guess95																																																																																																						
Z_tip_guess96																																																																																																						
Z_tip_guess97																																																																																																						
Z_tip_guess98																																																																																																						
Z_tip_guess99																																																																																																						
Z_tip_guess100																																																																																																						
Z_tip_guess101																																																																																																						
Z_tip_guess102																																																																																																						
Z_tip_guess103																																																																																																						
Z_tip_guess104																																																																																																						
Z_tip_guess105																																																																																																						
Z_tip_guess106																																																																																																						
Z_tip_guess107																																																																																																						
Z_tip_guess108																																																																																																						
Z_tip_guess109																																																																																																						
Z_tip_guess110																																																																																																						
Z_tip_guess111																																																																																																						
Z_tip_guess112																																																																																																						
Z_tip_guess113																																																																																																						
Z_tip_guess114																																																																																																						
Z_tip_g																																																																																																						

CONFIDENTIAL

A list of the tables needed for the program is given below. Independent variables must be input data in either increasing or decreasing order.

<u>Table</u>	<u>Dependent Variable</u>	<u>Independent Variable</u>	<u>Comment</u>
1	$h(\text{lbm})$	$T(^{\circ}\text{R})$	For air at low pressure
2	P_r	$T(^{\circ}\text{R})$	For air at low pressure
3		$T(^{\circ}\text{R})$	For air at low pressure
4	$R_{\text{hub}}(\text{in.})$	$Z(\text{in.})$	Hub profile (minimum four points)
5	$R_{\text{tip}}(\text{in.})$	$Z(\text{in.})$	Tip profile (minimum four points)
6	$T_{T1}(\text{in. Hg})$	$R(\text{in.})$	Inlet pressure
7	$T_{T1}(^{\circ}\text{R})$	$R(\text{in.})$	Inlet temperature
8	BLF_1	$R(\text{in.})$	Inlet total blockage
9	$\alpha_1(\text{deg})$	$R(\text{in.})$	Inlet absolute flow angle
10	$t_{\text{hub}}(\text{in.})$	$Z(\text{in.})$	Hub blade thickness must include inlet t_{hub} measured in plane normal to axis of rotation
11	$t_{\text{tip}}(\text{in.})$	$Z(\text{in.})$	Tip blade thickness must include inlet t_{tip} measured in plane normal to axis of rotation
12	$\phi(\text{deg})$	$Z_m(\text{in.})$	Blade angle, from inlet to exit
13	$\alpha_{3, \text{exit}}(\text{deg})$	% H(from hub)	Exit relative flow angle: input if slip is to occur upstream from exit normal
14	δR_{ec}	% H (from hub)	Recovery correction factor vs % H at exit

CONFIDENTIAL

CONFIDENTIAL

<u>Table</u>	<u>Dependent Variable</u>	<u>Independent Variable</u>	<u>Comment</u>
15	$R_{ec_{i1}}$	M_2	Inducer recovery for hub tube
16	$R_{ec_{i2}}$	M_2	Inducer recovery for second tube
17	$R_{ec_{i3}}$	M_2	Inducer recovery for third tube
18	$R_{ec_{i4}}$	M_2	Inducer recovery for fourth tube
19	$R_{ec_{i5}}$	M_2	Inducer recovery for tip tube
20	$R_{c, hub}^{(in.)}$	$Z^{(in.)}$	Radius of curvature for hub profile
21	$R_{c, tip}^{(in.)}$	$Z^{(in.)}$	Radius of curvature for tip profile

All tables must have at least 2 points, and Tables 4 and 5 must have at least 4 points. Except for Tables 4 and 5, all table look-ups are accomplished by using linear interpolation across small segments. Third-degree polynomial interpolation is used for the hub and tip profiles (see Tables 4 and 5).

Third-degree interpolation involves finding the third-degree polynomial passing through the 4 points nearest the value of interest. This method is used to calculate numerically the derivatives dR/dZ and d^2R/dZ^2 in the normal finding and to determine the radius of curvature at the inlet. The interpolated curve will pass through the input points, but care must be taken in defining the profiles so that the interpolated curves observed on the plot have the desired smoothness and curvature. To ensure a straight-line segment, 4 points should be inserted as input data. Smooth curves should be represented with points that are spaced about evenly with points closer together where the curvature is greatest. Several points should be given to define the curves upstream from the inlet and downstream from the exit normal.

3.2 OUTPUT DESCRIPTION

Input data are printed out as they are read. Computed results for each station are output data, with 1 page of output data per station. The case title, station number, and streamtube numbers are printed, as are the data labels and units.

CONFIDENTIAL

CONFIDENTIAL

When a Tally plot is specified, the program generates a labeled plot of points for the following 9 curves: hub profile, tip profile, interpolated (third-degree) hub profile, interpolated (third-degree) tip profile, and 5 streamlines. The plot is titled and the axes are labeled.

3.3 SAMPLE CASE

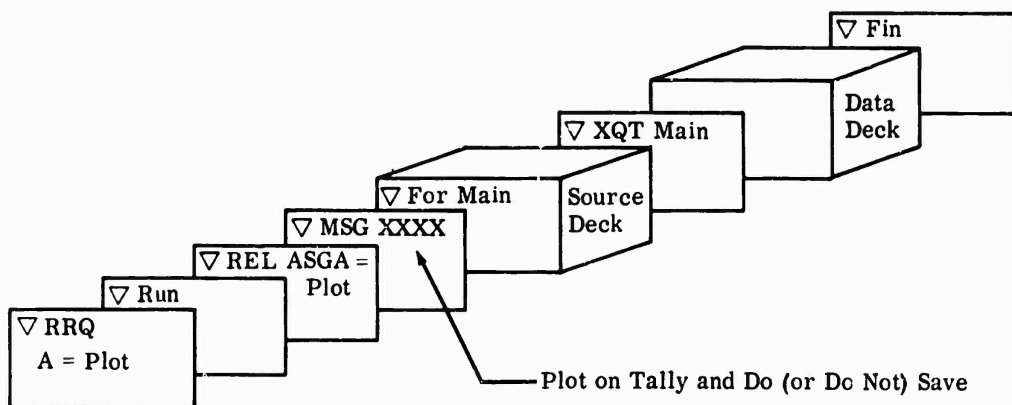
The following 3 pages list the input data deck, and are followed by the corresponding program output data.

4.0 OPERATING INFORMATION

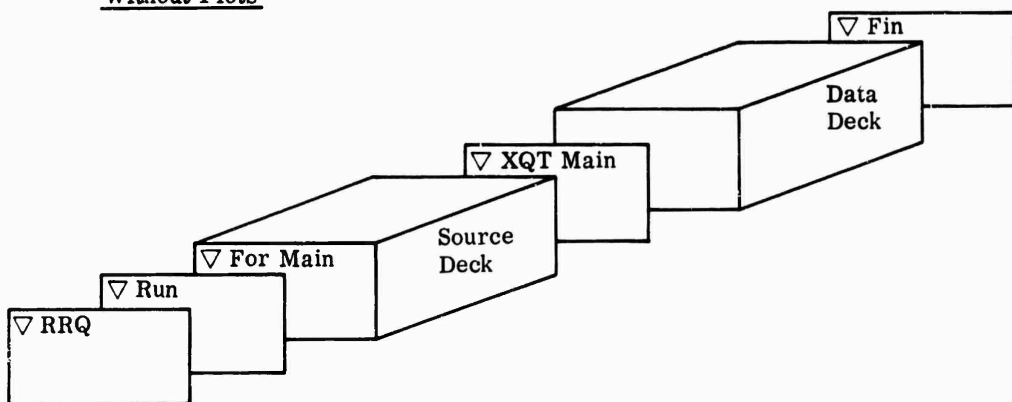
4.1 PROGRAM AND DATA SETUP

The deck setups for the SRU 1107 computer are shown below. If more than 1 plot is needed, the plot tape should be saved.

With Tally Plots



Without Plots



CONFIDENTIAL

- XOT MAIN

TITLE

AS 2496 TEST CASE

CONSTANTS

57000. 22. 7. 0. 0. .88 5. 0.

MASS FLOW RATES

.4 .4 .4 .4 .4

Z(HUB) AT NORMALS

.83 1.685 2.485 3.08 3.442 3.55 3.653

Z(TIP) GUESS) AT NORMALS

.8 1.5 2.2 2.7 3.2 3.3 3.5

TABLE 1 H=F(T) FOR AIR

1.	50.								
100.	23.74	125.	29.72	150.	35.71	175.	41.69	200.	47.67
225.	53.66	250.	59.64	275.	65.62	300.	71.61	325.	77.59
350.	83.57	375.	89.55	400.	95.53	425.	101.52	450.	107.50
475.	113.50	500.	119.48	525.	125.47	550.	131.46	575.	137.47
600.	143.47	650.	155.50	700.	167.56	750.	179.66	800.	191.81
850.	204.01	900.	216.26	950.	228.58	1000.	240.98	1050.	253.45
1100.	265.99	1150.	278.61	1200.	291.30	1250.	304.08	1300.	316.94
1350.	329.88	1400.	342.90	1450.	356.00	1500.	369.17	1550.	382.42
1600.	395.74	1700.	422.59	1800.	449.71	1900.	477.09	2000.	504.71
3000.	790.68	4000.	1088.26	5000.	1392.87	6000.	1702.99	6500.	1858.44

TABLE 2 PR=F(T) FOR AIR

2.	44.								
420.	.5760	440.	.6776	460.	.7923	480.	.9182	500.	1.059
520.	1.2147	540.	1.386	560.	1.5742	580.	1.78	600.	2.005
620.	2.249	640.	2.514	660.	2.801	680.	3.111	700.	3.446
720.	3.806	740.	4.193	760.	4.607	780.	5.051	800.	5.526
820.	6.033	840.	6.573	860.	7.149	880.	7.761	900.	8.411
920.	9.102	940.	9.834	960.	10.61	980.	11.43	1000.	12.298
1020.	13.215	1040.	14.182	1060.	15.203	1080.	16.278	1100.	17.413
1120.	18.604	1140.	19.858	1160.	21.18	1180.	22.56	1200.	24.01
1220.	25.53	1240.	27.13	1260.	28.80	1280.	30.55		

TABLE 3 K=F(T) FOR AIR

3.	35.								
300.	1.4024	350.	1.4023	400.	1.4020	450.	1.4016	500.	1.4010
550.	1.4000	600.	1.3989	650.	1.3975	700.	1.3960	750.	1.3941
800.	1.3920	850.	1.3897	900.	1.3870	950.	1.3842	1000.	1.3810
1050.	1.3776	1100.	1.3741	1150.	1.3710	1200.	1.3679	1250.	1.3649
1300.	1.3620	1350.	1.3590	1400.	1.356	1450.	1.3536	1500.	1.3504
1550.	1.3477	1600.	1.3453	1650.	1.3429	1700.	1.3405	1750.	1.3381
1800.	1.3361	1850.	1.3341	1900.	1.3320	1950.	1.3301	2000.	1.3282

TABLE 4 R(HUB)=F(Z)

4.	9.								
-.4	1.176	.41	1.187	1.26	1.285	2.105	1.56	2.825	2.097
3.292	2.839	3.5	3.439	3.653	4.01	3.75	4.373		

TABLE 5 R(TIP)=F(Z)

5.	9.								
-.4	1.964	.384	1.977	1.136	2.046	1.854	2.22	2.461	2.510
2.996	3.008	3.256	3.512	3.471	4.068	3.6	4.403		

TABLE 6 PT1=F(R)

6.	2.								
1.	29.62	2.	29.62						

CONFIDENTIAL

CONFIDENTIAL

TABLE 7 $TT1=F(R)$

7. 2.
1. 519.7 2. 519.7

TABLE 8 $BLF1=F(R)$

8. 2.
1. .9 2. .9

TABLE 9 $ALPHA1=F(R)$

9. 2.
1. 0. 2. 0.

TABLE 10 $T(HUB)=F(Z)$

10.	15.								
0.	.046	.2	.079	.41	.100	.833	.110	1.26	.120
1.69	.130	2.102	.130	2.484	.125	2.824	.124	3.083	.116
3.292	.103	3.441	.093	3.5	.083	3.55	.078	3.653	.048

TABLE 11 $T(TIP)=F(Z)$

11.	15.								
0.	.046	.193	.043	.084	.038	.768	.035	1.138	.032
1.508	.03	1.954	.028	2.162	.026	2.462	.026	2.743	.025
2.996	.025	3.184	.025	3.256	.025	3.325	.025	3.471	.025

TABLE 12 $PHI=F(Z-MID)$

12.	7.								
0.	50.	.4	44.7	.8	37.9	1.96	19.7	2.913	1.5
3.148	0.	3.562	0.						

TABLE 13 $ALPHA(EXIT)=F(PERCENT\ BLADE\ HEIGHT)$

13.	12.								
10.	42.5	28.	32.5	34.	30.	38.	29.4	44.	29.
50.	29.	56.	29.1	60.	29.2	64.	29.6	68.	30.5
80.	37.5	100.	49.5						

TABLE 14 $REC\ CORR\ FACTOR=F(PERCENT\ BLADE\ HEIGHT)$

14.	2.								
0.	.95	100.	.95						

TABLE 15 $INDUCER\ REC1=F(M2)$

15.	6.								
.35	.98	.45	.979	.55	.973	.65	.964	.75	.951
.85	.936								

TABLE 16 $INDUCER\ REC2=F(M2)$

16.	6.								
.4	.99	.5	.99	.6	.986	.7	.98	.8	.972
.9	.962								

TABLE 17 $INDUCER\ REC3=F(M2)$

17.	6.								
.45	.996	.55	.995	.65	.991	.75	.986	.85	.98
.95	.974								

TABLE 18 $INDUCER\ REC4=F(M2)$

18.	6.								
.5	.987	.6	.982	.7	.974	.8	.964	.9	.953
1.	.940								

TABLE 19 $INDUCER\ REC5=F(M2)$

19.	6.								
.55	.965	.65	.952	.75	.936	.85	.917	.95	.896
1.05	.874								

TABLE 20 $HUB\ RC=F(X)$

20.	7.								
.83	5.55	1.7	2.85	2.5	1.75	3.1	2.15	3.4	7.5

CONFIDENTIAL

3.55 21.25 3.65 100.
TABLE 21 TIP RC=F(X)
21. 7.
.75 6.65 1.5 3.8 2.15 2.25 2.75 1.5 3.2 4.65
3.3 13.2 3.5 70.
GEOMETRY PLOT
12.4 9.50 .0050
BEGIN COMPUTE
END PLOT
- FIN

000118

CONFIDENTIAL

IMPELLER RADIAL EQUILIBRIUM DESIGN PROGRAM INPUT

TITLE

AS 2496 TEST CASE

CONSTANTS

57000.0 22. 7. 8. .0000 .0000 5. .0000

MASS FLOW RATES

.0000 .0000 .0000 .0000

Z(MU) AT NORMALS

.8300 1.0050 2.0050 3.0040 3.0500 3.6530

Z(TIP GUESS) AT NORMALS

.0000 1.5000 2.2000 2.7000 3.2000 3.5000

TABLE 1 REF(T) FOR AIR

PRINT

100.0000	25.7400	125.0000	29.7200	150.0000	35.7100	175.0000	91.6900	200.0000	97.6700
225.0000	53.6600	250.0000	59.6400	275.0000	65.6200	300.0000	71.6100	325.0000	77.5900
350.0000	83.5700	375.0000	89.5500	400.0000	95.5300	425.0000	101.5200	450.0000	107.5000
475.0000	113.5000	500.0000	119.4800	525.0000	125.4700	550.0000	131.4600	575.0000	137.4700
600.0000	143.4700	650.0000	155.5000	700.0000	167.5600	750.0000	179.6600	800.0000	191.8100
850.0000	204.9100	900.0000	216.2600	950.0000	228.5800	1000.0000	240.9800	1050.0000	253.4500
1100.0000	265.9900	1149.9999	276.6100	1200.0000	291.3000	1250.0000	304.0800	1300.0000	316.9400
1350.0000	329.0800	1399.9999	342.9000	1450.0000	356.0000	1500.0000	369.1700	1549.9999	382.4200
1600.0000	395.7400	1699.9999	422.5900	1800.0000	449.7100	1900.0000	477.0900	2000.0000	504.7100
3000.0000	790.0000	4000.0000	1080.2400	5000.0000	1322.6699	5999.9999	1702.9099	6500.0000	1850.4400

TABLE 2 REF(T) FOR AIR

PRINT

420.0000	.5760	440.0000	.6776	460.0000	.7923	480.0000	.9182	500.0000	1.0590
520.0000	1.2147	540.0000	1.3860	560.0000	1.5742	580.0000	1.7800	600.0000	2.0050
620.0000	2.2490	640.0000	2.5120	660.0000	2.8010	680.0000	3.1110	700.0000	3.4460
720.0000	3.8060	740.0000	4.1930	760.0000	4.6070	780.0000	5.0510	800.0000	5.5260
820.0000	4.8330	840.0000	5.3730	860.0000	5.9400	880.0000	6.5360	900.0000	7.1610
920.0000	5.1020	940.0000	5.6540	960.0000	6.2300	980.0000	6.8300	1000.0000	7.4500
1020.0000	13.2150	1039.9999	14.1820	1060.0000	15.2030	1080.0000	16.2780	1100.0000	17.4130
1120.0000	18.6040	1140.0000	19.6583	1160.0000	21.1800	1179.9999	22.5400	1200.0000	24.0190
1219.9999	25.3300	1240.0000	27.1300	1259.9999	28.6000	1280.0000	30.5500		

TABLE 3 REF(T) FOR AIR

PRINT

300.0000	1.4024	350.0000	1.4023	400.0000	1.4020	450.0000	1.4016	500.0000	1.4010
550.0000	1.3980	600.0000	1.3989	650.0000	1.3975	700.0000	1.3960	750.0000	1.3941
800.0000	1.3920	850.0000	1.3897	900.0000	1.3870	950.0000	1.3842	1000.0000	1.3810
1050.0000	1.3776	1100.0000	1.3751	1150.0000	1.3718	1200.0000	1.3678	1250.0000	1.3638

1300.0000	1.3420	1350.0000	1.3590	1399.9999	1.3500	1450.0000	1.3534	1500.0000	1.3544
1349.9999	1.3477	1400.0000	1.3453	1450.0000	1.3429	1499.9999	1.3405	1550.0000	1.3401
1400.0000	1.3361	1449.9999	1.3341	1500.0000	1.3320	1550.0000	1.3301	1600.0000	1.3283
TABLE 4 R(HUB)=F(Z)									
9									
1.0000	1.1760	.9100	1.1870	1.2400	1.2550	2.1050	1.5400	2.0250	2.0970
3.2920	2.8390	3.5000	3.5390	3.6530	4.0100	3.7500	4.3730		
TABLE 5 R(TIP)=F(Z)									
9									
1.0000	1.9450	.3040	1.9770	1.1340	2.0440	1.0340	2.2200	2.4610	2.5100
2.9960	3.0000	3.2560	3.5120	3.0710	4.0400	3.4000	4.4030		
TABLE 6 PTI=F(R)									
6									
1.0000	29.6200	2.0000	29.6200						
TABLE 7 TTI=F(R)									
7									
1.0000	519.7000	2.0000	519.7000						
TABLE 8 RUF=F(R)									
8									
1.0000	.9000	2.0000	.9000						
TABLE 9 ALPHA=F(R)									
9									
1.0000	.0000	2.0000	.0000						
TABLE 10 T(HUB)=F(Z)									
10									
1.0000	.0440	.2000	.0790	.9100	.1000	.0330	.1100	1.2600	.1200
1.6900	.1300	2.1020	.1300	2.4040	.1250	2.0240	.1240	3.0830	.1160
3.2920	.1950	3.4410	.0930	3.5000	.0630	3.5500	.0760	3.6530	.0400
TABLE 11 T(TIP)=F(Z)									
11									
1.0000	.0440	.1930	.0430	.3040	.0300	.7600	.0330	1.1300	.0320
1.5000	.0300	1.0540	.0280	2.1620	.0260	2.4420	.0260	2.7430	.0250
2.9960	.0250	3.1040	.0250	3.4750	.0250	3.3350	.0250	3.9710	.0250
TABLE 12 PHI=F(Z-MID)									
12									
1.0000	26.0000	.4000	44.7000	.0000	37.9000	1.9000	19.7000	2.9130	1.5000
3.1400	.0000	3.5620	.0000						
TABLE 13 ALPHA(XIT)=F(PERCENT BLADE HEIGHT)									

TABLE 10 REC CORR FACTOR=F(PERCENT BLADE HEIGHT)											
13.	12.										
10.0000	42.5000	28.0000	32.5000	34.0000	30.0000	30.0000	30.0000	29.0000	29.0000	29.0000	29.0000
50.0000	29.0000	56.0000	29.1000	64.0000	29.2000	64.0000	64.0000	64.0000	64.0000	64.0000	64.0000
80.0000	37.5000	100.0000	49.5000								
TABLE 15 INDUCER REC1=F(M2)											
14.	2.										
.0000	.9500	100.0000	.9500								
15.	6.										
.3500	.9000	.9500	.9700	.9500	.9700	.9500	.9700	.9500	.9700	.9500	.9500
.0500	.9300										
TABLE 16 INDUCER REC2=F(M2)											
16.	6.										
.0000	.9000	.9000	.9000	.6000	.9000	.7000	.9000	.8000	.9000	.8000	.9720
.0000	.9420										
TABLE 17 INDUCER REC3=F(M2)											
17.	6.										
.0500	.9000	.3500	.9700	.6500	.9910	.7500	.9000	.8500	.9000	.8500	.9400
.9500	.9700										
TABLE 18 INDUCER REC4=F(M2)											
18.	6.										
.5000	.9070	.0000	.9020	.7000	.9700	.8000	.9000	.9000	.9000	.9000	.9500
1.0000	.9400										
TABLE 19 INDUCER REC5=F(M2)											
19.	6.										
.5500	.9050	.0500	.9520	.7500	.9300	.8500	.9170	.9500	.9500	.9500	.8000
1.0500	.8700										
TABLE 20 HUB REC=F(X)											
20.	7.										
.0300	9.5300	1.7000	2.6500	2.3000	1.7500	3.1000	2.1500	3.0000	3.0000	7.5000	
3.3500	21.2300	3.0500	100.0000								
TABLE 21 TIP REC=F(X)											
21.	7.										
.7500	6.6300	1.5000	3.0000	2.1500	2.2500	2.7500	1.3000	3.2000	3.2000	.6000	
3.3000	13.2000	3.5000	70.0000								
GEOMETRY PLOT											
12.00	9.50	.0050									
HUB IN COMPUTE											

IMPELLER RADIAL EQUILIBRIUM DESIGN RESULTS FOR STATION 1						
AS 2496 TEST CASE						
	1	2	3	4	5	TIP
DISTANCES(INCHES)						
AXIAL	.000	.000	.000	.000	.000	.000
RADIAL	1.177	1.462	1.623	1.769	1.904	1.967
MERIDIONAL						
RADIUS OF CURVATURE	16.97	19.48	20.61	21.47	22.11	22.38
ACTUAL AREA(50 IN)						
BLOCKAGE FACTOR	1.579	1.569	1.561	1.554	1.548	1.540
TEMPERATURES(°R)						
TOTAL	519.7	519.7	519.7	519.7	519.7	519.7
STATIC	486.2	485.5	485.0	484.5	484.1	483.7
RELATIVE TOTAL	553.5	563.8	574.8	584.2	594.4	604.6
PRESSURES(IN HG)						
TOTAL	29.62	29.62	29.62	29.62	29.62	29.62
STATIC	23.97	23.36	23.26	23.18	23.11	23.04
RELATIVE TOTAL	36.91	39.38	41.94	44.61	47.39	50.17
MACH NUMBERS						
ABSOLUTE	.546	.592	.598	.602	.606	.607
RELATIVE	.831	.897	.957	1.014	1.067	1.106
ANGLES(DEGREES)						
MERIDIONAL			.61			
ABSOLUTE FLUID	.00	.00	.00	.00	.00	.00
RELATIVE FLUID	45.10	48.64	51.36	53.56	55.37	56.80
ABS VELOCITIES(FT/SEC)						
TOTAL	634.0	648.2	645.4	649.9	653.9	657.9
TANGENTIAL						
SOUND	1081.3	1080.6	1080.8	1079.4	1078.9	1078.5
WHEEL	636.1	727.1	697.4	680.0	666.9	654.5
REL VELOCITIES(FT/SEC)						
TOTAL	690.1	968.7	1033.6	1094.0	1150.8	1207.6
MERIDIONAL	634.0	648.2	645.4	649.9	653.9	657.9
TANGENTIAL	536.1	727.1	697.4	680.0	666.9	654.5

IMPELLER RADIAL EQUILIBRIUM DESIGN RESULTS FOR STATION 2

AS 2496 TEST CASE

	1	2	3	4	5	TIP
DISTANCES(INCHES)						
AXIAL	.830	.817	.794	.781	.769	.754
RADIAL	-1.219	1.353	1.564	1.716	1.881	2.000
NORMAL	.0000	.1353	.3465	.6493	.9446	.7852
PERIDONAL				.789		
RADIUS OF CURVATURE	5.55	5.74	6.03	6.24	6.41	6.63
ACTUAL AREA(50 IN)						
BLOCKAGE FACTOR	2.107	1.644	1.464	1.341	1.278	1.898
TEMPERATURES(DEG R)			.816	.661	.692	.916
TOTAL						
STATIC	543.4	570.5	575.0	578.7	582.5	
RELATIVE TOTAL	533.9	534.9	535.5	536.3	536.1	
PRESSURES(IN HG)	557.5	578.1	580.1	589.5	596.0	
TOTAL						
STATIC	30.57	40.49	41.44	42.41	42.48	
RELATIVE TOTAL	31.95	32.31	32.44	32.49	32.49	
MACH NUMBERS	32.16	32.31	32.44	32.49	32.49	
ABSOLUTE	.526	.577	.608	.629	.642	
RELATIVE	.478	.574	.647	.794	.754	
ANGLES(DEGREES)						
MERIDIONAL			5.44			
BLADE			38.10			
ABSOLUTE FLUID	48.99	36.04	34.39	32.04	32.19	
RELATIVE FLUID	38.21	36.59	39.21	41.40	43.22	
ABS VELOCITIES(FT/SEC)						
TOTAL	595.3	654.8	649.3	713.5	730.2	
TANGENTIAL	349.7	392.1	349.4	387.2	369.0	
WHEEL	1132.2	1133.2	1133.9	1134.8	1136.7	
REL VELOCITIES(FT/SEC)	606.3	777.8	853.4	915.6	949.8	994.9
TOTAL						
MERIDIONAL	531.0	650.2	734.1	799.0	840.1	
TANGENTIAL	458.8	523.4	548.9	599.3	618.0	
RELATIVE	283.5	385.7	444.1	528.4	580.8	
SURFACE VEL(FT/SEC)						
SUCTION	844.4	716.6	808.2	879.6	934.8	
PRESSURE	479.3	503.8	646.1	718.4	751.3	
SUCTION/V2 MEAN						
PRESSURE/V2 MEAN	.945	.893	.742	.651	.604	
REL TOTAL/V2 MEAN	.945	.845	.639	.495	.437	
REL TOTAL/V2 MEAN	.915	.849	.718	.573	.529	
ACCEL(FT/SEC S)						
RECOVERY	.9167+06	.6287+06	.4329+06	.3084+06	.2289+06	
DP/ON(IN HG/FT)	.9821	.9856	.9876	.9876	.9876	
	25.81	13.98	8.45	-0.78	-4.83	

IMPELLER RADIAL EQUILIBRIUM DESIGN RESULTS FOR STATION 3

AS 2496 TEST CASE

	HUB	1	2	3	4	5	TIP
DISTANCES (INCHES)							
AXIAL	1.685	1.689	1.592	1.554	1.524	1.498	1.464
RADIAL	1.388	1.523	1.727	1.863	1.970	2.058	2.113
NORMAL	.8000	1.005	.9528	.9930	.9660	.7054	.7519
MERIDIONAL		1.587					
RADIUS OF CURVATURE	2.90	3.00	3.34	3.52	3.67	3.79	3.85
ACTUAL AREA (SQ IN)		2.549	1.751	1.429	1.295	1.227	1.268
BLOCKAGE FACTOR		.782	.807	.853	.885	.911	
TEMPERATURES (DEG F)							
TOTAL		597.4	612.0	620.9	629.3	637.7	
STATIC		555.0	559.7	562.0	564.0	571.1	
RELATIVE TOTAL		567.5	581.2	591.2	599.8	607.8	
PRESSURES (IN HG)							
TOTAL		46.55	51.02	53.91	55.00	57.21	
STATIC		35.93	37.27	38.00	38.97	39.85	
RELATIVE TOTAL		36.85	42.52	45.36	47.17	48.29	
MACH NUMBERS							
ABSOLUTE		.620	.685	.725	.749	.765	
RELATIVE		.434	.438	.509	.546	.566	
ANGLES (DEGREES)							
MERIDIONAL				15.39			
BLADE				25.73			
ABSOLUTE FLUID		59.62	54.49	51.29	50.35	50.03	
RELATIVE FLUID		21.18	24.69	27.06	28.96	30.63	
ABS VELOCITIES (FT/SEC)							
TOTAL		715.6	794.6	842.5	873.3	895.9	
TANGENTIAL		617.3	646.8	637.5	672.4	690.6	
SOUND		1154.3	1159.2	1161.7	1165.8	1171.0	
WHEEL	699.2	757.6	859.8	926.6	988.8	1028.5	1030.8
REL VELOCITIES (FT/SEC)							
TOTAL		348.1	508.8	591.6	637.0	663.3	
MERIDIONAL		361.8	461.5	526.8	557.3	570.7	
TANGENTIAL		148.2	212.2	269.1	308.4	337.9	
SURFACE VEL (FT/SEC)							
SUCTION		445.8	597.9	649.2	742.4	777.7	
PRESSURE		318.3	918.1	894.0	931.5	948.8	
SUCTION/V2 MEAN		.451	.578	.667	.718	.752	
PRESSURE/V2 MEAN		.348	.404	.478	.514	.531	
REL TOTAL/V2 MEAN		.573	.691	.872	.916	.932	
ACCEL (FT/SEC SQ)		.8344+07	.2036+07	.1739+07	.1637+07	.1638+07	
RECOVERY		.9498	.9218	.9258	.9638	.9423	
DP/DN (IN HG/FT)		82.56	66.84	52.04	44.69	41.68	

CONFIDENTIAL

IMPELLER RADIAL EQUILIBRIUM DESIGN RESULTS FOR STATION A

AS 2496 TEST CASE

	1	2	3	4	5	TIP
DISTANCES(INCHES)						
AXIAL	2.427	2.236	2.276	2.224	2.176	2.151
RADIAL	1.873	2.026	2.129	2.215	2.295	2.335
NORMAL	.0000	.2922	.6125	.5120	.6055	.6525
PERIODICAL			2.378			
RADIUS OF CURVATURE	1.77	1.98	2.67	2.14	2.21	2.35
ACTUAL AREA(SQ IN)	2.618	1.240	1.402	1.313	1.337	1.425
BLOCKAGE FACTOR	.764	.824	.860	.907	.910	
TEMPERATURES(DEG R)						
TOTAL	153.8	673.4	684.9	696.2	708.9	
STATIC	590.2	590.0	593.6	599.7	608.6	
RELATIVE TOTAL	991.9	644.2	613.9	620.7	628.1	
PRESSURES(IN HG)						
TOTAL	63.44	78.45	75.17	78.18	80.53	
STATIC	42.22	44.21	45.36	46.23	47.11	
RELATIVE TOTAL	34.28	34.24	30.85	32.14	32.56	
RACH NUMBERS						
ABSOLUTE	.786	.845	.882	.901	.911	
RELATIVE	.257	.317	.407	.418	.399	
ANGLES(DEGREES)						
PERIODICAL			38.78			
BLADE			13.85			
ABSOLUTE FLUID	71.1	66.29	63.39	63.42	65.25	
RELATIVE FLUID	9.45	12.16	18.03	15.57	17.07	
ABS VELOCITIES(FT/SEC)						
TOTAL	931.3	1085.3	1052.7	1091.1	1101.2	
TANGENTIAL	881.6	920.5	941.2	946.6	1000.0	
WHEEL	1184.8	1190.2	1193.6	1200.0	1209.0	
REL VELOCITIES(FT/SEC)	882.6	1007.5	1059.8	1101.6	1141.6	1161.7
TOTAL	304.8	913.5	946.1	902.1	982.3	
PERIODICAL	308.4	404.2	471.6	483.7	461.1	
TANGENTIAL	84.5	87.1	117.8	134.8	161.6	
SURFACE VEL(FT/SEC)						
SUCTION	872.3	579.5	855.8	678.7	641.7	
PRESSURE	157.3	247.5	317.2	329.6	302.9	
SUCTION/V2 MEAN	.457	.941	.634	.853	.640	
PRESSURE/V2 MEAN	.133	.239	.307	.319	.293	
REL TOTAL/V2 MEAN	.285	.808	.478	.586	.467	
ACCEL(FT/SEC SQ)	.3478+87	.3427+87	.3084+87	.3045+87	.3342+87	
RECOVERY	.942	.9573	.9426	.9459	.9138	
DP/DN(IN HG/FT)	146.36	127.78	108.68	166.58	117.57	

CONFIDENTIAL

IMPELLER RADIAL EQUILIBRIUM DESIGN RESULTS FOR STATION 5

AS 2490 TEST CASE

	1	2	3	4	5	TIP
DISTANCES (INCHES)						
STRAIGHT	2.494	2.491	2.492	2.492	2.776	2.729
AXIAL	2.494	2.491	2.492	2.492	2.776	2.729
RADIAL	2.494	2.491	2.492	2.492	2.776	2.729
PERIODICAL	2.494	2.491	2.492	2.492	2.776	2.729
RADIIUS OF CURVATURE						
2.10	2.494	2.491	2.492	2.492	2.776	2.729
ACTUAL AREA (SQ IN)						
2.10	2.494	2.491	2.492	2.492	2.776	2.729
TEMPERATURES (DEG F)						
TOTAL	2.494	2.491	2.492	2.492	2.776	2.729
STATIC	2.494	2.491	2.492	2.492	2.776	2.729
RELATIVE TOTAL	2.494	2.491	2.492	2.492	2.776	2.729
PRESSURES (IN HG)						
TOTAL	2.494	2.491	2.492	2.492	2.776	2.729
RELATIVE TOTAL	2.494	2.491	2.492	2.492	2.776	2.729
MACH						
RELATIVE	2.494	2.491	2.492	2.492	2.776	2.729
RELATIVE	2.494	2.491	2.492	2.492	2.776	2.729
ANGLES (DEGREES)						
PERIODICAL	2.494	2.491	2.492	2.492	2.776	2.729
BLADE	2.494	2.491	2.492	2.492	2.776	2.729
ABSOLUTE FLUID						
RELATIVE FLUID	2.494	2.491	2.492	2.492	2.776	2.729
ABS VELOCITIES (FT/SEC)						
TOTAL	2.494	2.491	2.492	2.492	2.776	2.729
RELATIVE TOTAL	2.494	2.491	2.492	2.492	2.776	2.729
REL VELOCITIES (FT/SEC)						
TOTAL	2.494	2.491	2.492	2.492	2.776	2.729
RELATIVE TOTAL	2.494	2.491	2.492	2.492	2.776	2.729
Suction/12 MEAN						
RELATIVE TOTAL	2.494	2.491	2.492	2.492	2.776	2.729
Suction/12 MEAN						
RELATIVE TOTAL	2.494	2.491	2.492	2.492	2.776	2.729
ACCEL (FT/SEC SQ)						
RELATIVE TOTAL	2.494	2.491	2.492	2.492	2.776	2.729
RECOVERY						
RELATIVE TOTAL	2.494	2.491	2.492	2.492	2.776	2.729
OP/OM (IN MM/FT)						
RELATIVE TOTAL	2.494	2.491	2.492	2.492	2.776	2.729

CONFIDENTIAL

IMPELLER RADIAL EQUILIBRIUM DESIGN RESULTS FOR STATION 6

AS 20% TEST CASE

	1	2	3	4	5	TIP
STRAIGHTNESS						
DISTANCES (INCHES)						
AXIAL	3.317	3.371	3.331	3.291	3.227	3.169
RADIAL	3.262	3.241	3.296	3.312	3.338	3.355
NORMAL	.5273	.0748	.1192	.1425	.2320	.2780
MERIDIONAL			3.991			
RADIUS OF CURVATURE	10.40	9.97	8.43	7.37	5.46	4.53
ACTUAL AREA(SQ IN)	1.117	.916	.837	.762	1.931	3.771
RESCAPE FACTOR	.839	.851	.861	.872	.888	
TEMPERATURE(°C)						
TOTAL	907.8	916.9	921.4	930.8	948.7	
STATIC	721.3	721.3	721.3	726.6	743.3	
RELATIVE TOTAL	738.2	740.6	740.7	748.9	765.4	
PRESSURES (IN HG)						
TOTAL	199.26	205.16	211.41	212.42	213.73	
STATIC	89.99	94.60	97.47	98.15	99.37	
RELATIVE TOTAL	92.99	99.31	97.20	95.31	91.14	
MACH NUMBERS						
ABSOLUTE	1.199	1.194	1.202	1.199	1.193	
RELATIVE	.320	.349	.392	.336	.168	
ANGLES (DEGREES)						
MERIDIONAL			68.26			
BLADE			.90			
ABSOLUTE FLUID	78.07	72.71	71.70	74.39	82.44	
RELATIVE FLUID	22.83	17.24	15.63	15.70	20.82	
ABS VELOCITIES (FT/SEC)						
TOTAL	1519.4	1550.6	1580.8	1586.2	1599.4	
TANGENTIAL	1042.3	1060.1	1000.8	1027.3	1081.5	
SOUND	1316.0	1316.0	1315.6	1322.7	1321.8	
TIME	1622.7	1631.9	1639.7	1647.7	1640.5	
REL VELOCITIES (FT/SEC)						1640.9
TOTAL	621.5	649.1	615.5	644.8	624.2	
MERIDIONAL	390.2	443.3	496.5	428.2	209.8	
TANGENTIAL	199.5	165.8	138.9	120.4	79.0	
SURFACE VEL (FT/SEC)						
SUCTION	726.9	790.7	814.4	751.6	554.2	
PRESSURE	118.2	176.6	214.7	138.1	-105.7	
SUCTION/V2 MEAN	.703	.765	.790	.727	.536	
PRESSURE/V2 MEAN	.412	.474	.408	.346	-.102	
REL TOTAL/V2 MEAN	.446	.609	.499	.430	.217	
ACCEL (FT/SEC SQ)						
RECOVERY	.2744-07	.2728-07	.2686-07	.2831-07	.3237-07	
DP/DX (IN HG/FT)	.9096	.9182	.9371	.9090	.8450	
	190.05	191.23	189.82	199.26	225.73	

CONFIDENTIAL

IMPELLER RADIAL EQUILIBRIUM DESIGN RESULTS FOR STATION 7

AS 2496 TEST CASE

	1	2	3	4	5	YIP
DISTANCES (INCHES)						
AXIAL	3.330	3.494	3.443	3.432	3.372	3.329
RADIAL	3.427	3.439	3.443	3.439	3.476	3.493
PERIPHERAL	.0012	.0012	.0015	.0017	.0016	.0026
RADIUS OF CURVATURE	21.25	21.26	21.27	21.27	21.29	21.29
ACTUAL AREA (SQ IN)	.967	.772	.793	.821	2.076	5.330
BLOCKAGE FACTOR	.082	.046	.046	.073	.046	
TEMPERATURES (DEG R)						
TOTAL	97.4	964.4	972.2	1004.0	1034.1	1034.1
STATIC	772.1	744.2	744.0	776.0	776.0	776.0
RELATIVE TOTAL	769.5	791.1	792.5	794.1	797.0	797.0
PRESSURES (IN HG)						
TOTAL	252.33	444.26	274.98	279.37	289.81	289.81
STATIC	187.57	188.25	188.78	189.31	190.33	190.33
RELATIVE TOTAL	115.62	119.54	71.50	110.00	112.05	112.05
MACH	1.182	1.016	1.037	1.043	1.044	1.044
RELATIVE	.029	.046	.003	.041	.040	.040
ANGLES (DEGREES)						
PERIPHERAL	71.75	71.75	71.75	71.75	71.75	71.75
BLADE	76.26	73.45	72.55	75.33	80.42	80.42
ABSOLUTE FLUID	32.32	25.67	22.87	22.17	20.36	20.36
RELATIVE FLUID						
ABS VELOCITIES (FT/SEC)						
TANGENTIAL	1699.5	1693.2	1679.8	1700.2	1744.8	1744.8
SOUND	1944.2	1504.4	1602.4	1646.7	1737.6	1737.6
REL	1342.2	1396.0	1356.0	1385.3	1385.7	1385.7
REL VELOCITIES (FT/SEC)	1699.1	1610.0	1619.0	1629.2	1635.0	1635.0
REL TOTAL	808.4	510.3	507.0	445.0	193.2	193.2
PERIPHERAL	376.1	45.3	50.0	430.0	165.7	165.7
TANGENTIAL	239.3	233.6	212.6	175.5	23.4	23.4
SURFACE VELOCITY (FT/SEC)						
REL	773.9	699.2	694.5	699.0	591.2	591.2
REL TOTAL	123.4	17.3	197.6	160.8	207.3	207.3
PRESSURE						
SUCTION/V2 MEAN	.799	.827	.847	.802	.873	.873
PRESSURE/V2 MEAN	.119	.172	.191	.097	.199	.199
REL TOTAL/V2 MEAN	.036	.099	.029	.050	.107	.107
ACCEL (FT/SEC SQ)	.2494+07	.2477+07	.2502+07	.2074+07	.3068+07	.3068+07
RECOVERY	.9011	.9215	.9312	.9005	.9016	.9016
DP/ON (IN HG/FT)	190.28	282.86	288.21	219.21	248.74	248.74

IMPELLER RADIAL EQUILIBRIUM DESIGN RESULTS FOR STATION 0

AS 2000 TEST CASE

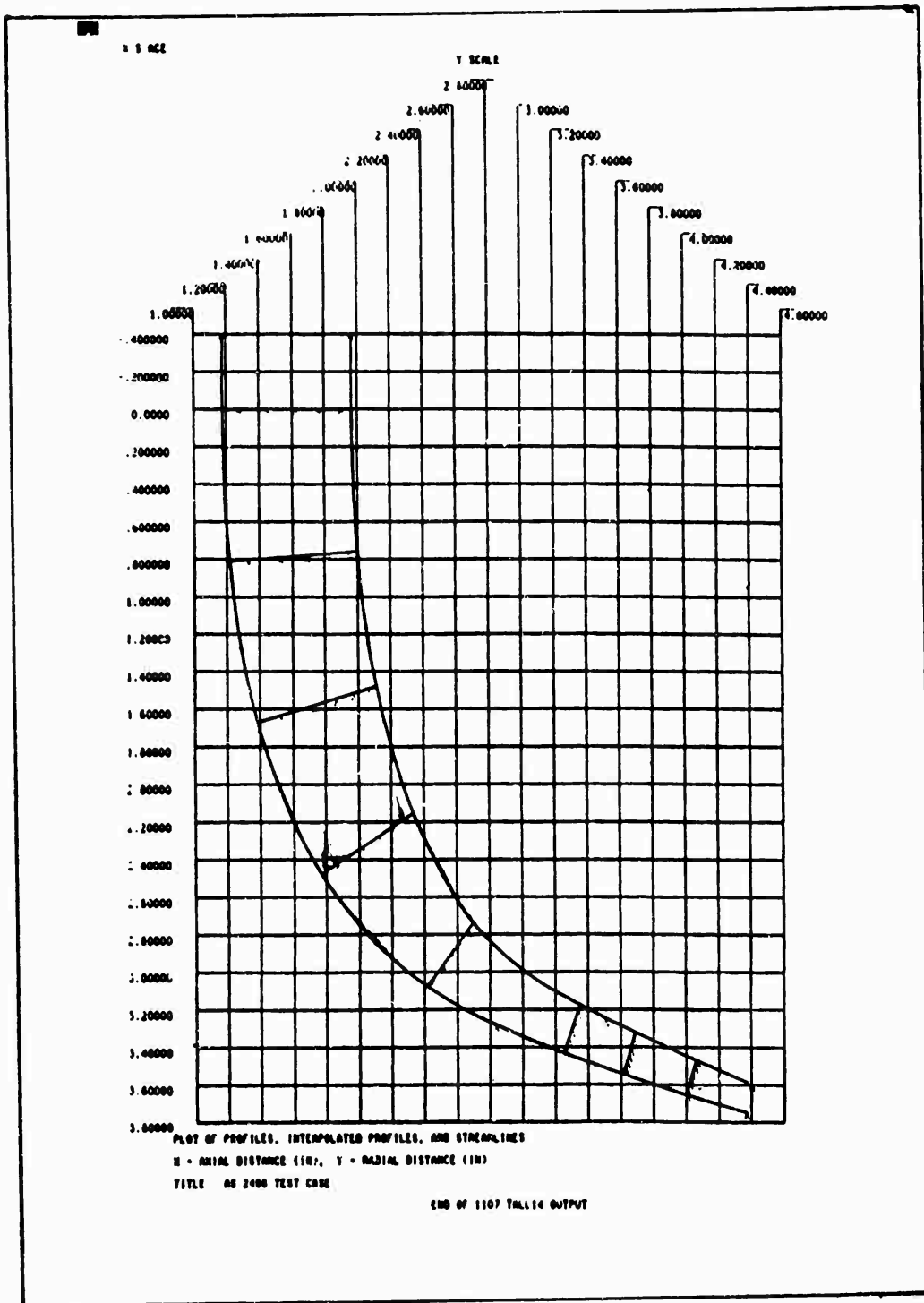
	1	2	3	4	5	TIP
DISTANCES(INCHES)						
AXIAL	3.437	3.408	3.385	3.342	3.309	3.471
RADIAL	4.015	4.024	4.022	4.039	4.056	4.064
WALL	.0000	.0000	.0000	.0000	.0000	.0000
WALL	.0000	.0000	.0000	.0000	.0000	.0000
RADIUS OF CURVATURE	94.77	92.94	87.34	82.09	78.51	81.01
ACTUAL AREA(SB IN)	.057	.051	.076	.083	2.103	4.072
BLOCKAGE FACTOR	.078	.075	.077	.080	.085	
TEMPERATURES(DEG R)						
TOTAL	1056.1	1063.8	1074.9	1093.0	1101.2	
STATIC	836.0	826.1	824.0	833.4	833.5	
RELATIVE TOTAL	809.4	850.9	852.1	853.3	856.1	
PRESSURES(M)						
TOTAL	332.72	321.26	346.94	375.57	400.89	
STATIC	237.57	237.57	237.57	237.57	237.57	
RELATIVE TOTAL	148.99	153.72	159.37	138.00	163.32	
MACH NUMBER	1.207	1.252	1.273	1.288	1.329	
ABSOLUTE	.341	.392	.417	.430	.453	
RELATIVE						
ANGLES(DEGREES)						
WALL	76.12	76.91	78.89	76.24	85.76	
ABSOLUTE FLUID	43.14	34.49	29.94	29.00	36.08	
RELATIVE FLUID						
ABS VELOCITIES(FT/SEC)						
TOTAL	1704.0	1704.2	1770.3	1821.3	1817.2	
STATIC	1644.4	1680.8	1713.9	1769.1	1812.0	
TANGENTIAL	1412.2	1408.3	1408.6	1414.6	1431.3	
SOUND	1597.2	1601.7	1605.4	1609.2	1617.3	
REL VELOCITIES(FT/SEC)						
TOTAL	681.0	552.5	507.2	495.2	474.7	
STATIC	351.0	310.9	310.9	333.1	341.6	
WALL	320.0	312.9	289.5	240.1	185.5	
TANGENTIAL						
SURFACE VEL(FT/SEC)						
SUCTION	701.0	803.7	943.0	943.7	948.0	
PRESSURE	100.0	221.6	230.7	126.7	-215.4	
SUCTION/V2 MEAN	.750	.085	.913	.036	.850	
PRESSURE/V2 MEAN	.175	.214	.223	.123	-.200	
REL TOTAL/V2 MEAN	.065	.535	.868	.079	.171	
ACCEL(FT/SEC SB)	.2510+07	.2511+07	.2610+07	.0802+07	.3207+07	
RECOVERY	.810	.812	.820	.813	.808	
DP/DN(IN HG/FT)	243.34	250.58	250.00	272.36	310.95	

2023.7

1994.6

PLOT INDICATOR = 0 (ZERO FOR SUCCESS)			
IMPELLER RADIAL EQUILIBRIUM DESIGN PROGRAM INPUT			
END PLOT			
EXECUTION TERMINATED BY AN ATTEMPT TO READ THRU AN END OF FILE			

CONFIDENTIAL



CONFIDENTIAL

CONFIDENTIAL

4.2 RUN INFORMATION

A normal run is ended by attempting to read another case and by reading the end of file. The program may terminate the execution of a station and may print out the accumulated results and a diagnostic routine. The program diagnostic routine and originating routines are listed below.

MAIN

"THE FOLLOWING CONTROL CARD IS IN ERROR XXXX." This is caused by an incorrect control card or by a misplaced control card. Execution is attempted.

"PLOT INDICATOR = XX (ZERO FOR SUCCESS)." This is printed after an attempt to plot. If the number is zero, the plot was a success.

IMPEL

"THE TABLE LOOK-UP ON DA/DZ HAS FAILED FOR STATION XX." This refers to the computation of α_3 from $\frac{d\alpha}{dz} - f(Z_m)$ in the Vector Diagrams section of this appendix and is caused by an error in input, probably in Table 12, reference page 43. The A-array is also printed, and execution for station XX is terminated.

"AT STREAMLINE X, STATION XX, A/A STAR FAILED TO CONVERGE." This refers to the M_3 bisection iteration of the Vector Diagrams section; it is printed after 20 iterations and is caused by bad inputs. It also refers to the adjustment of the initial area distribution in the Vector Diagrams section; it is printed after 10 adjustments, or, if the average $A/A^* < 1$, it is caused by bad inputs. The A-array is dumped, and execution for station XX is terminated.

"K FAILED TO CONVERGE AT STATION XX." This refers to the iteration on γ included in the M_3 solution of the Vector Diagrams section; it is printed after 10^3 iterations and is caused by bad input. The A-array is dumped, and execution is continued.

"AT STATION XX PS3 PRIME FAILED TO CONVERGE." This refers to the radial-equilibrium iteration in the Radial-Equilibrium Equation section of this appendix; it is printed after 20 iterations and it is caused by extreme inputs. The A-array is dumped, and execution is continued using the non-equilibrium results.

"PS3 PRIME ADJUSTMENT OF A ANN PRIME FAILED TO CONVERGE AT STATION XX." This is printed if the number of P'_{S3} adjustments in the Radial-Equilibrium Equation section have reached 300 during one dP_{S3}/dn iteration. The

CONFIDENTIAL

A-array is printed, and execution is continued; the non-equilibrium results are used.

INLET

"THE AXIAL VELOCITY SQUARED IS XXX, AT STATION XX, STREAMLINE X, WHEN THE HUB VELOCITY EQUALS XXX." This indicates difficulty in the total mass balance iteration of the Velocity Profile section, which is caused by extreme inlet conditions. The program makes automatic adjustments and attempts a solution.

"THE PROGRAM WAS UNABLE TO OBTAIN A VELOCITY PROFILE THAT WOULD GIVE A MASS BALANCE AT STATION XX, EPS M = XX COMPUTED M = XX GIVEN M = XXX." This is caused by bad inputs associated with the inlet in the Total Mass Balance section, and the execution of this case is terminated.

"THE PROGRAM WAS UNABLE TO OBTAIN A CORRECT SET OF STREAMLINE POSITIONS AT STATION XX NO. INCORRECT X." This is caused by extreme inputs for the inlet (see Streamtube Mass Balance section), but remaining calculations are attempted.

CHORD

"THE NUMBER OF ITERATIONS ON SLOPES HAS EXCEEDED 100 AND THE ITERATION IS DISCONTINUED: XHUB YHUB HSLOPE XTIP YTIP TSLOPE ANG C XXX XXX XXX XXX XXX XXX XXX XXX."

"AFTER 25 ITERATIONS CANNOT CONVERGE ON MIDSLOPE: X-GUESS Y-GUESS Y-PP X-HUB YHUB HSLOPE XTIP YTIP TSLOPE XXX XXX XXX XXX XXX XXX XXX XXX." These are caused by irregular hub or tip profiles, or a bad Z_{tip} guess. The results may still be usable and execution is attempted.

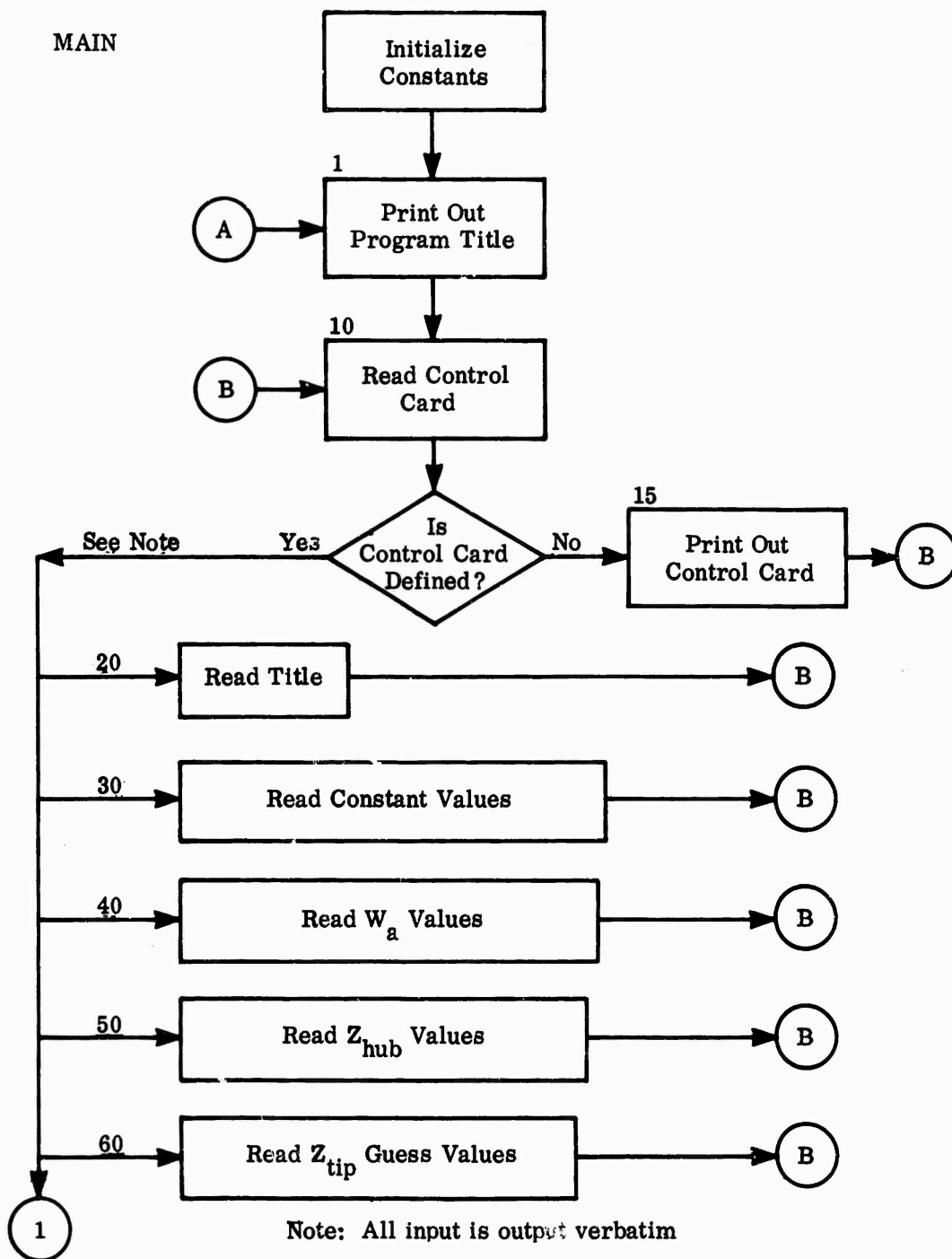
Average run time for a geometric plot of 15 stations is 2:00 minutes; it is 1:30 minutes without a plot. About 0:30 minute of this time is used for compilation, and this amount of time can be saved by placing the program complex file on magnetic tape or drum.

CONFIDENTIAL

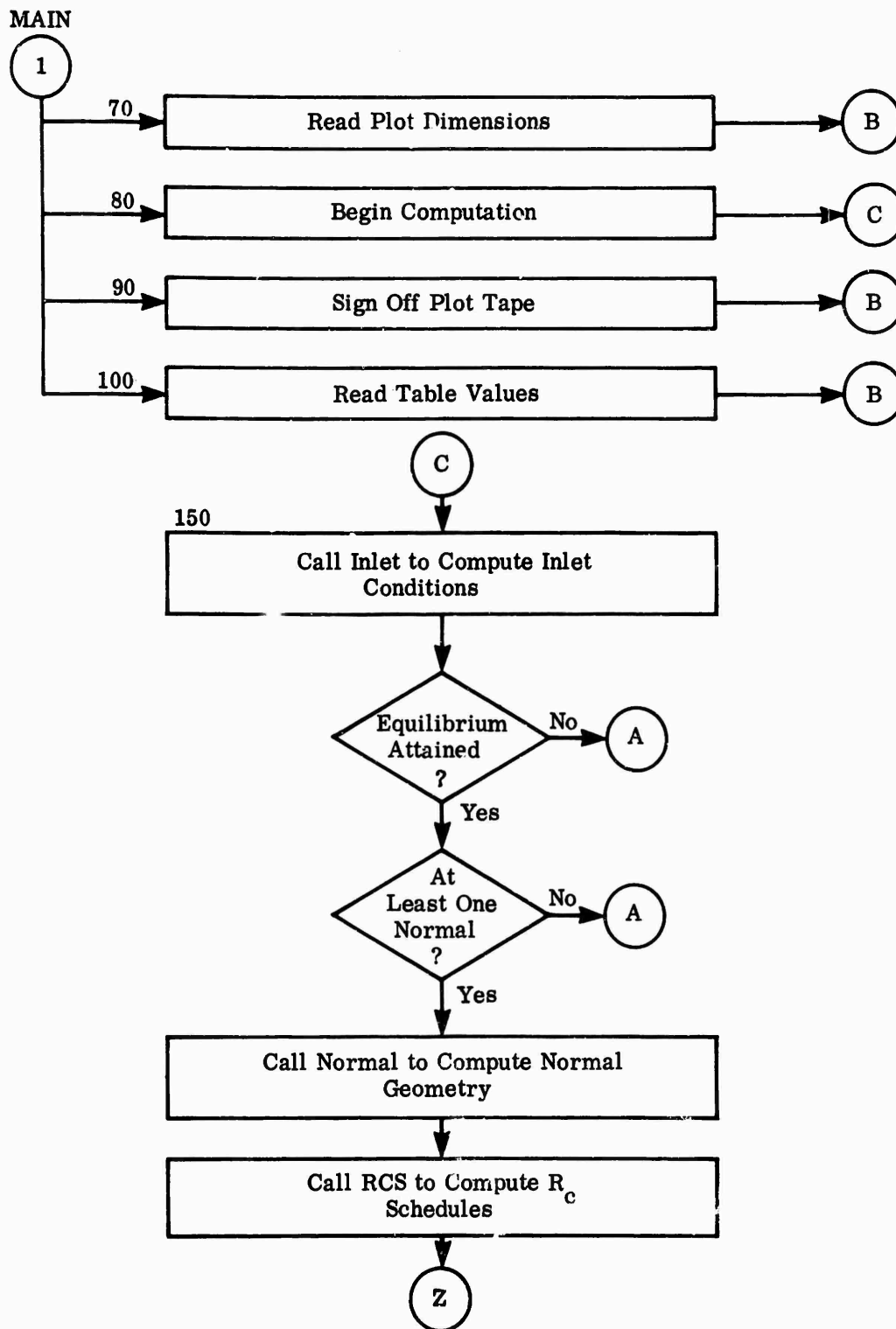
CONFIDENTIAL

5.0 PROGRAMMING INFORMATION

5.1 FLOW DIAGRAMS



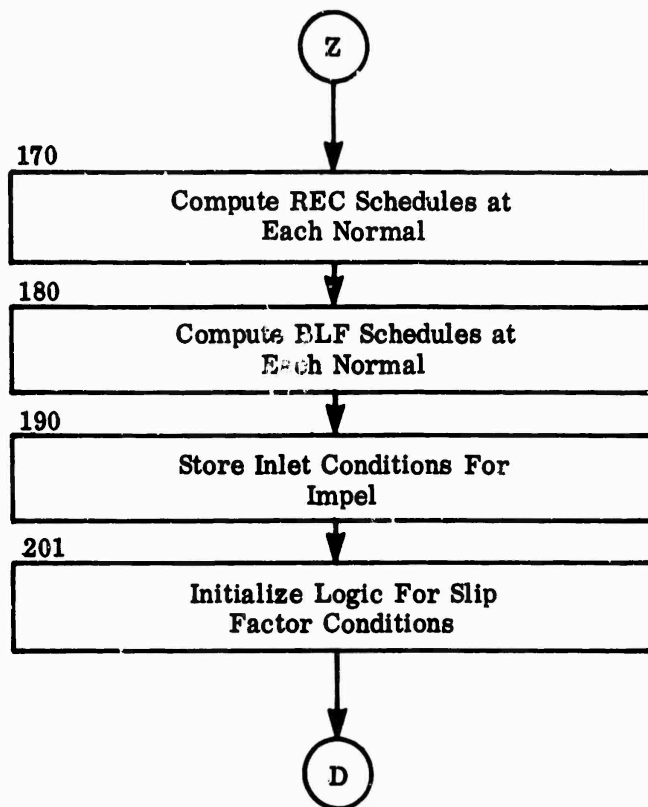
CONFIDENTIAL



CONFIDENTIAL

CONFIDENTIAL

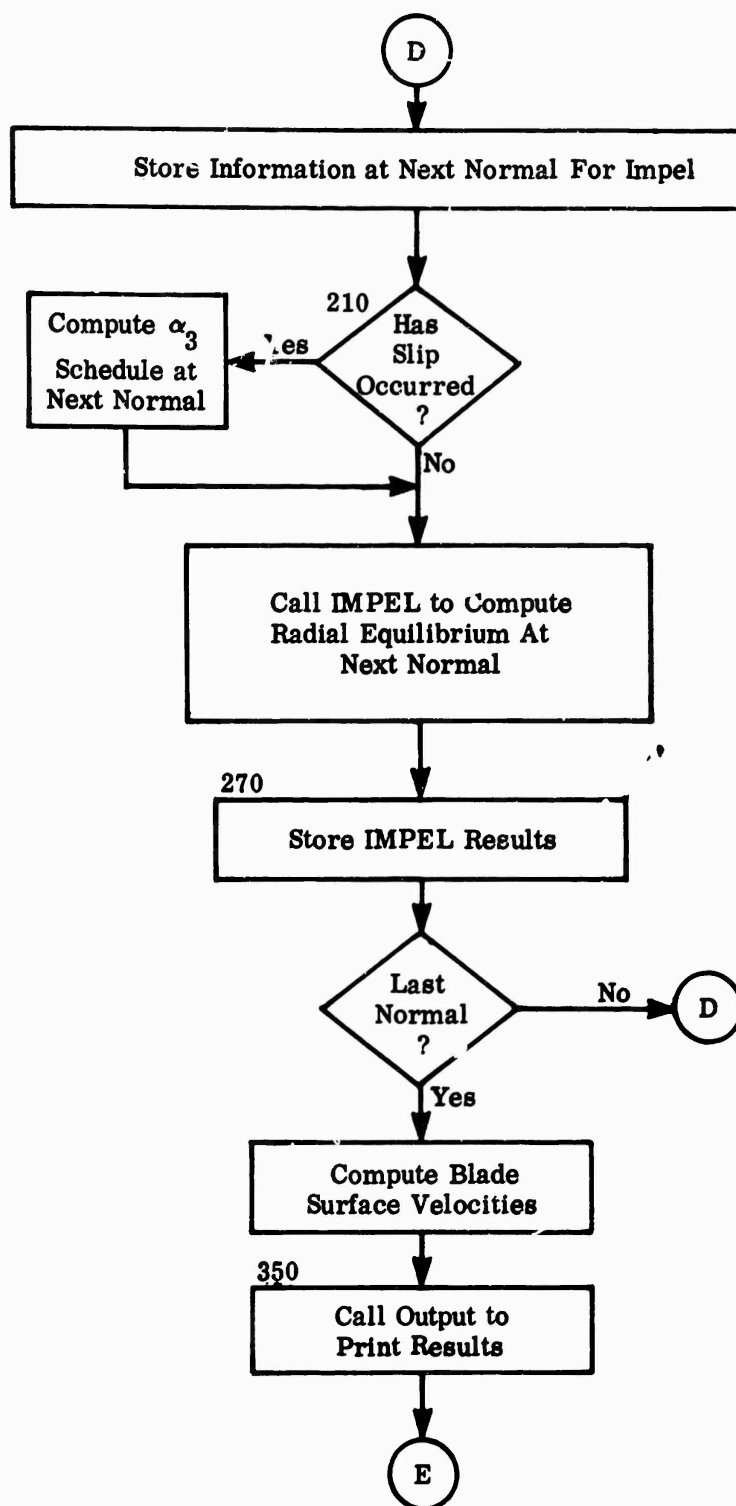
MAIN



CONFIDENTIAL

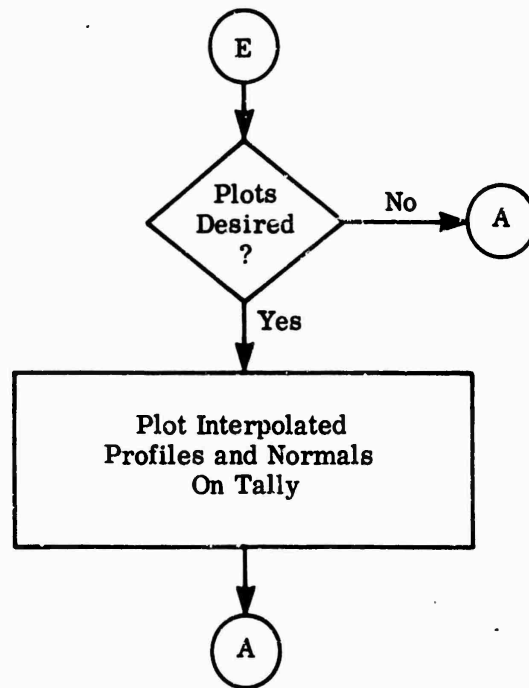
CONFIDENTIAL

MAIN

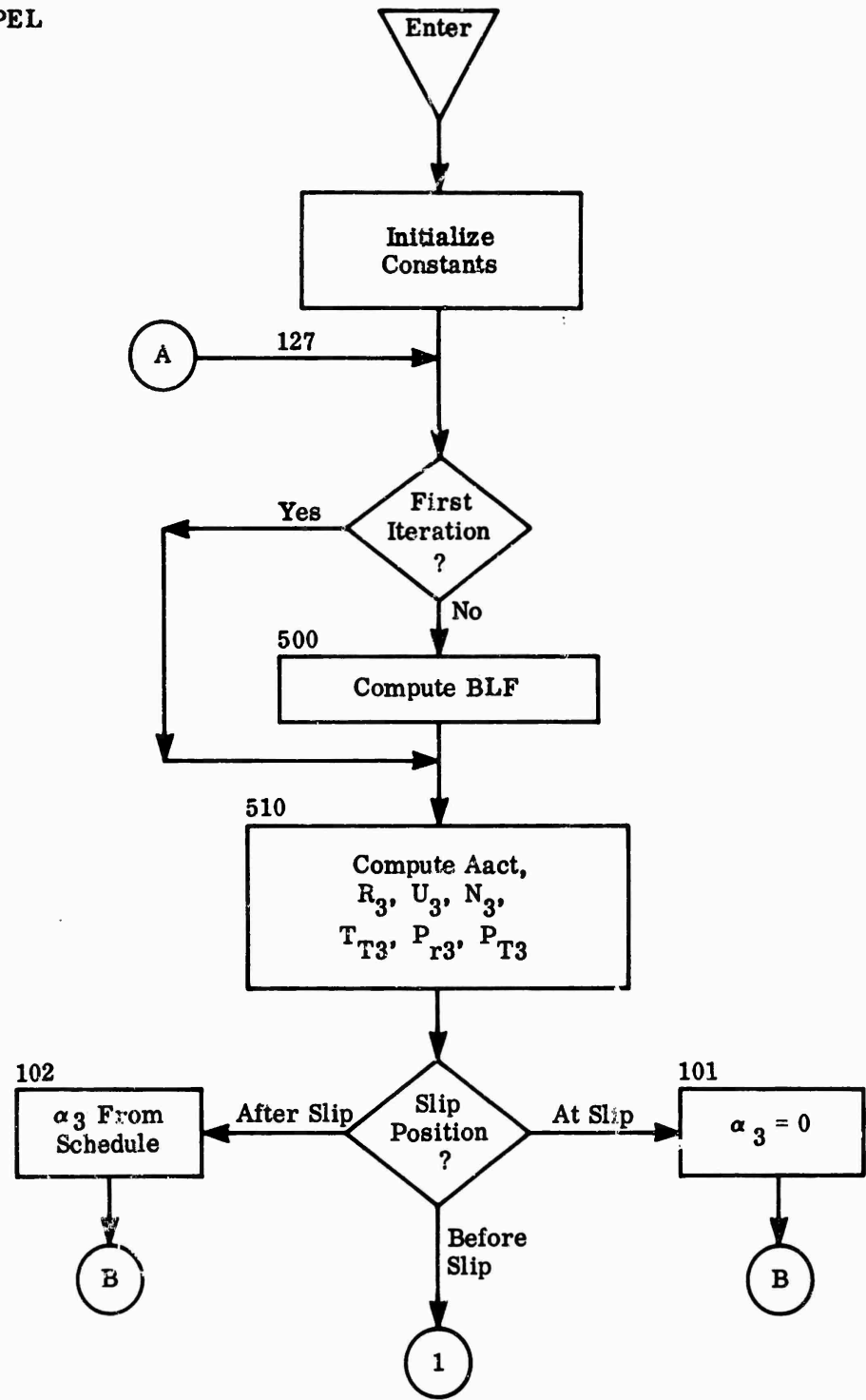


CONFIDENTIAL

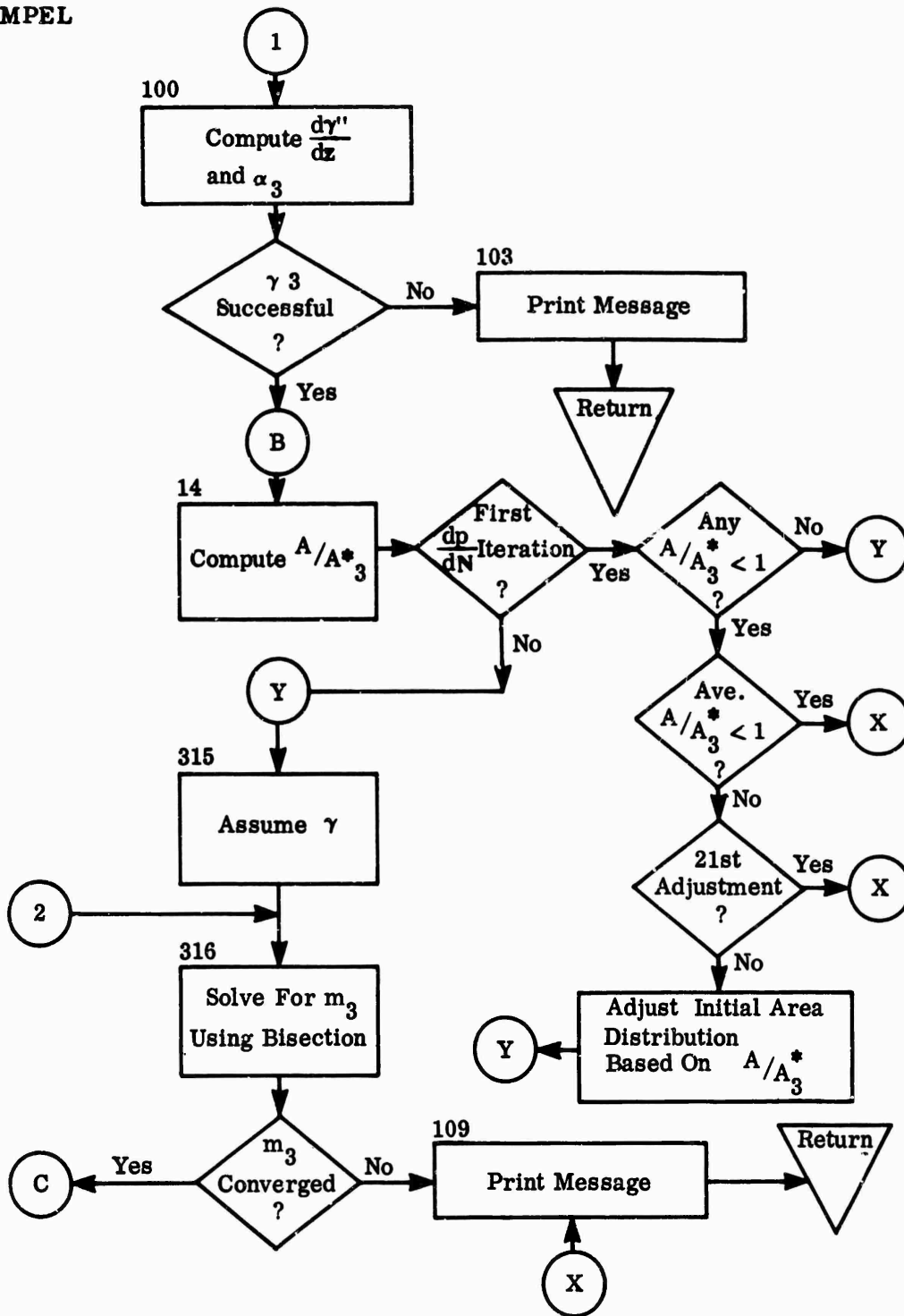
MAIN



IMPEL

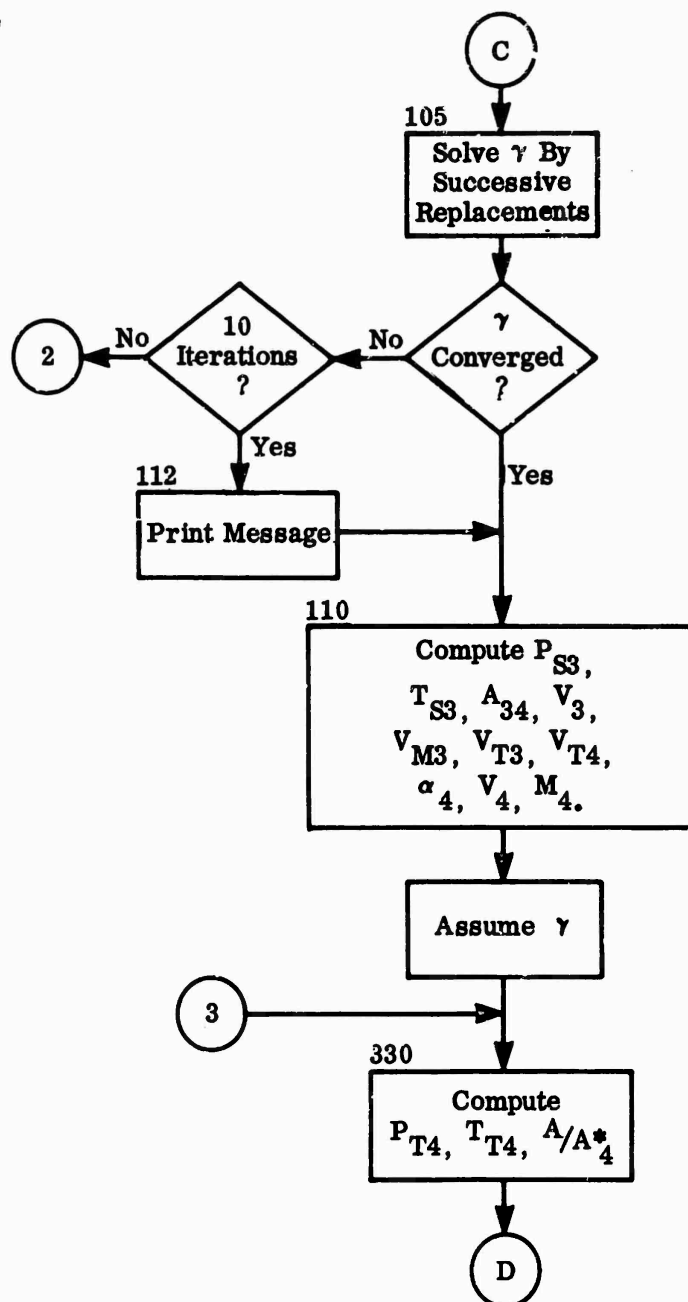


IMPEL



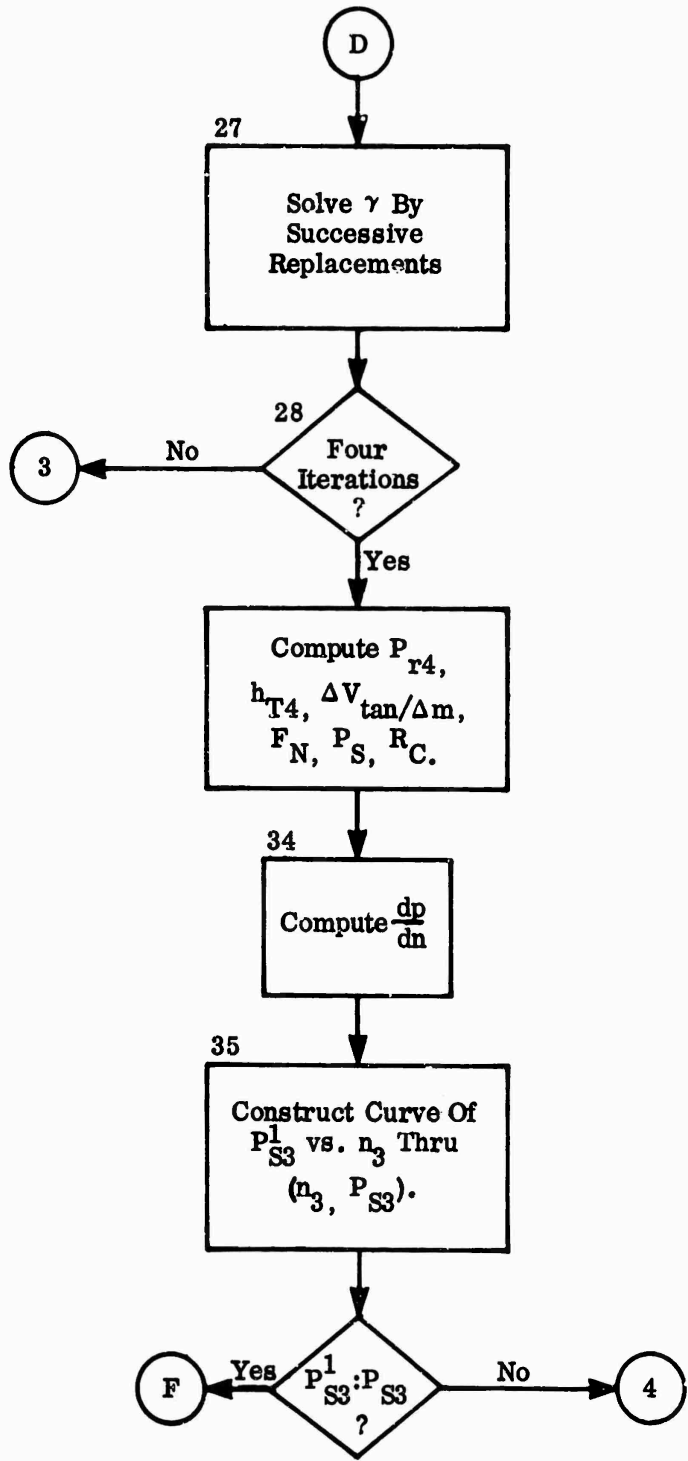
CONFIDENTIAL

IMPEL

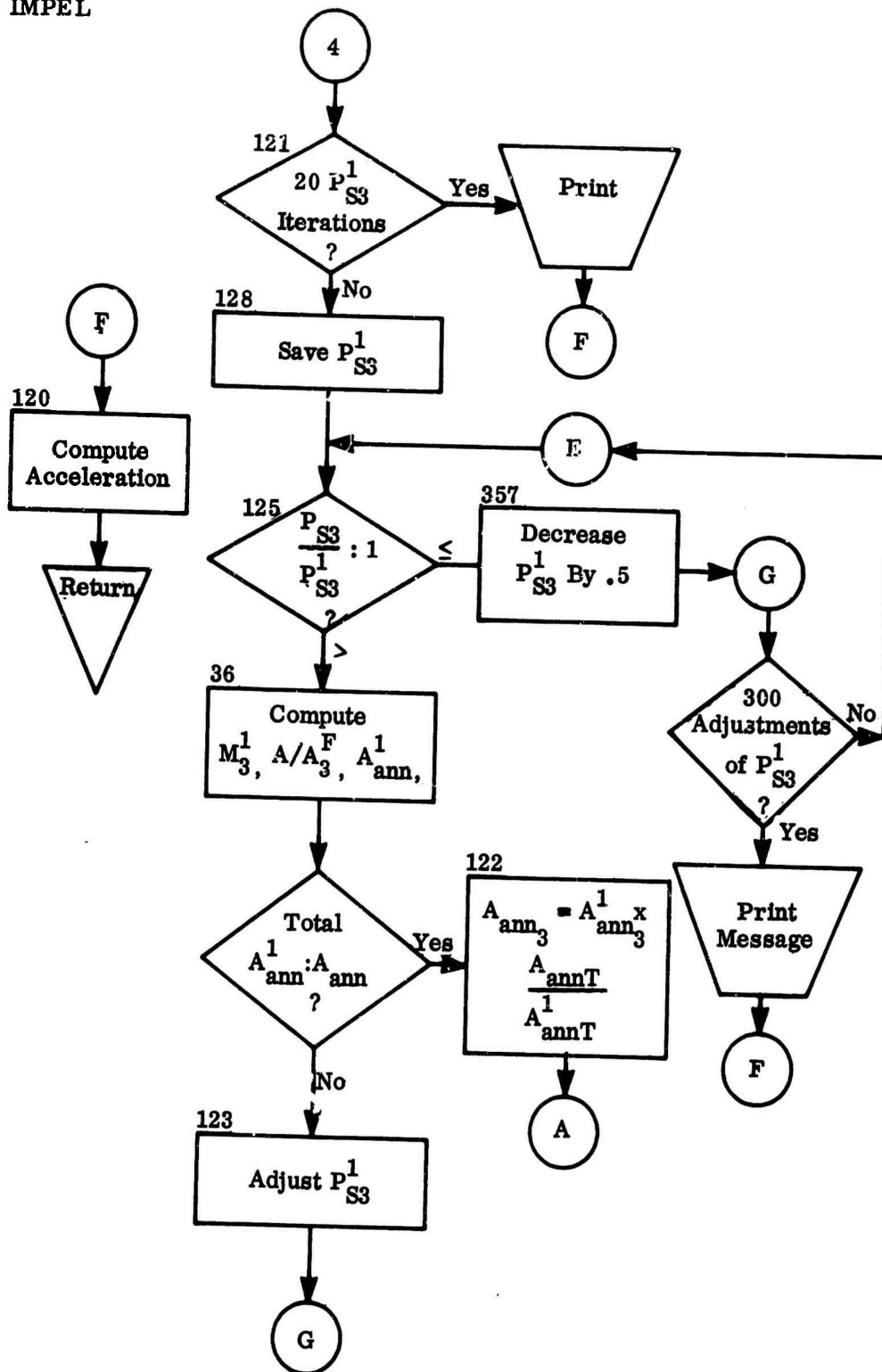


CONFIDENTIAL

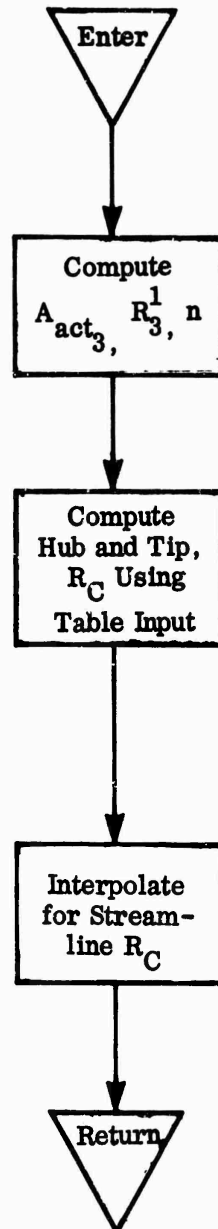
IMPEL



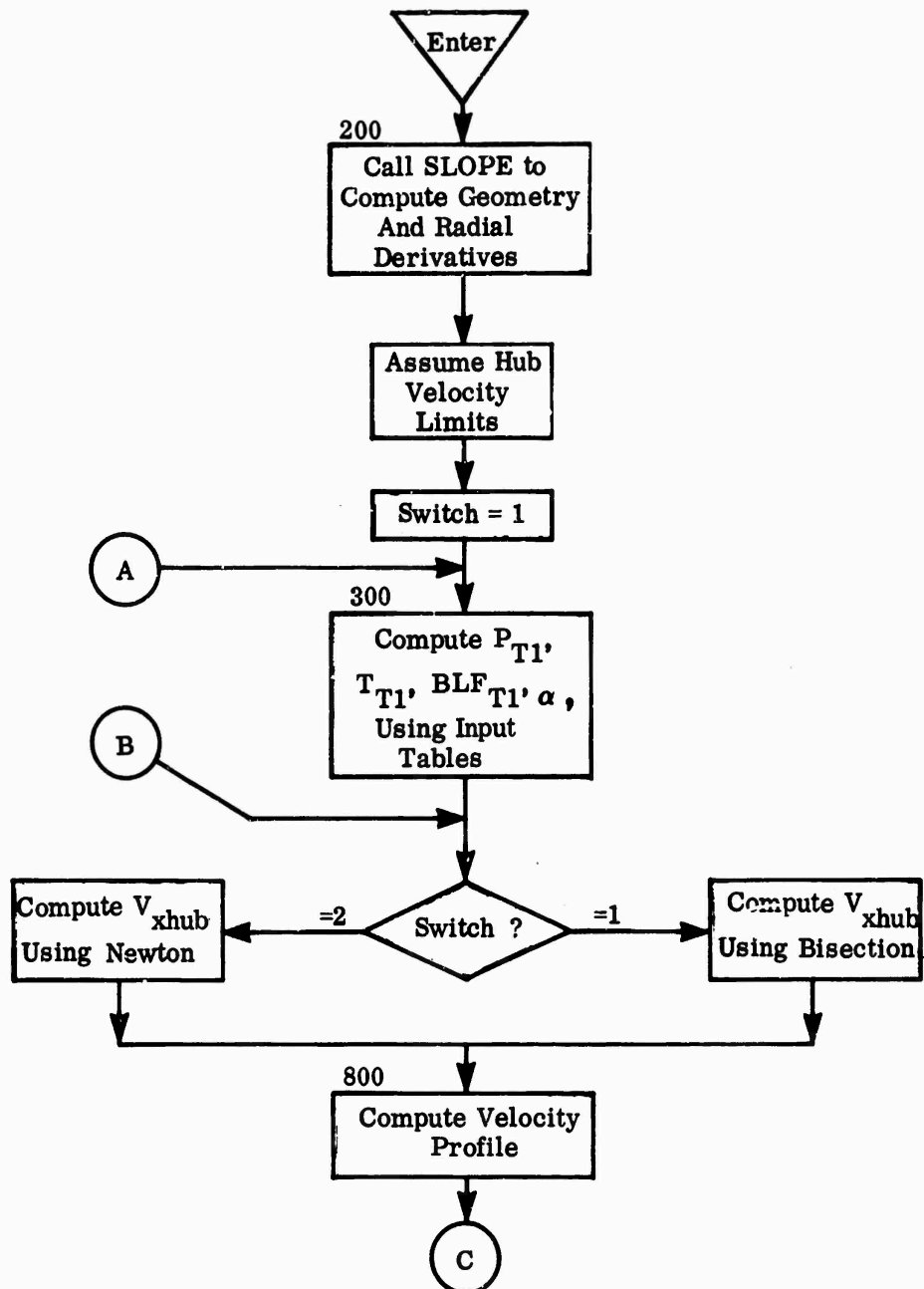
IMPEL



RCS

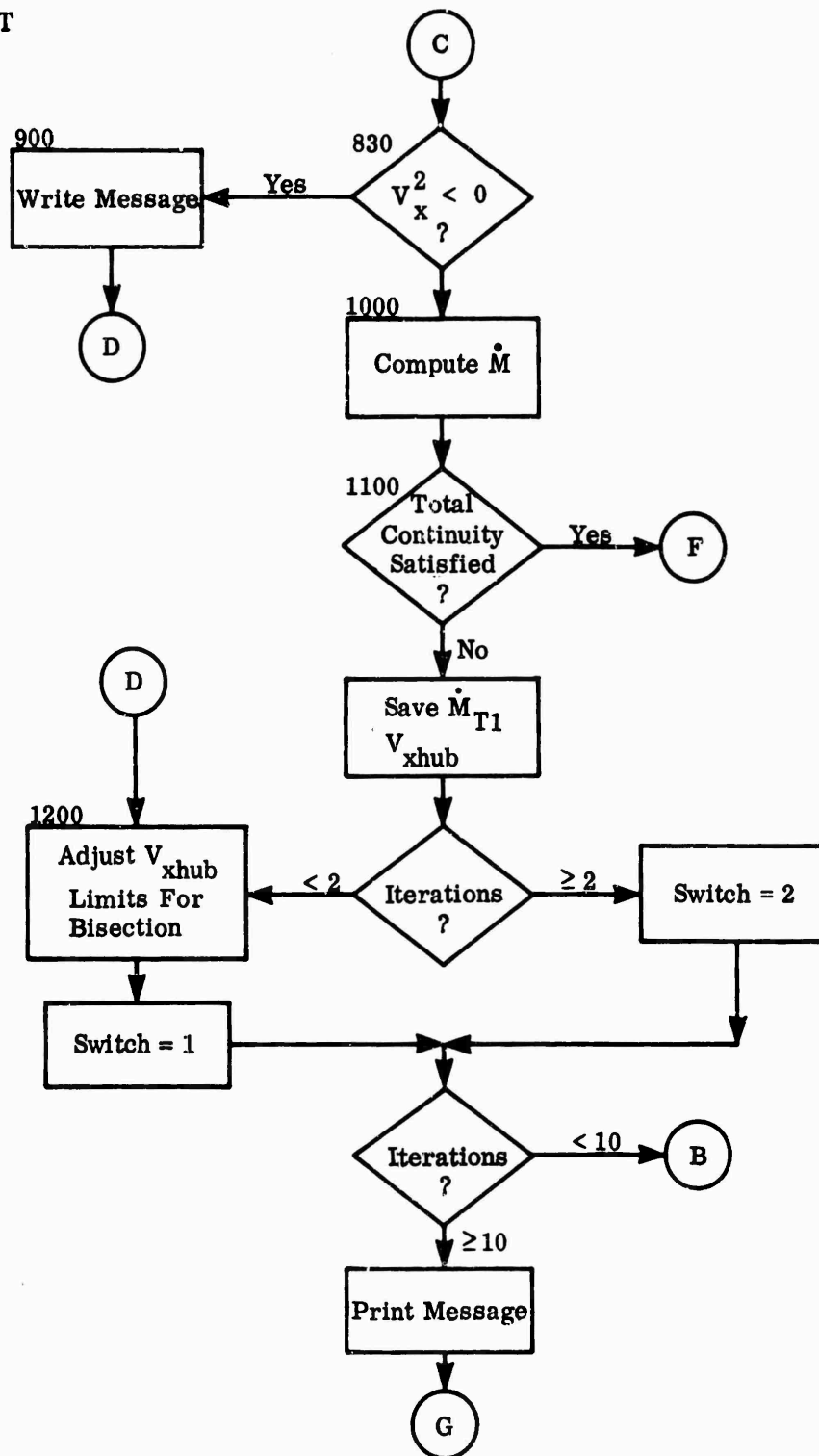


INLET



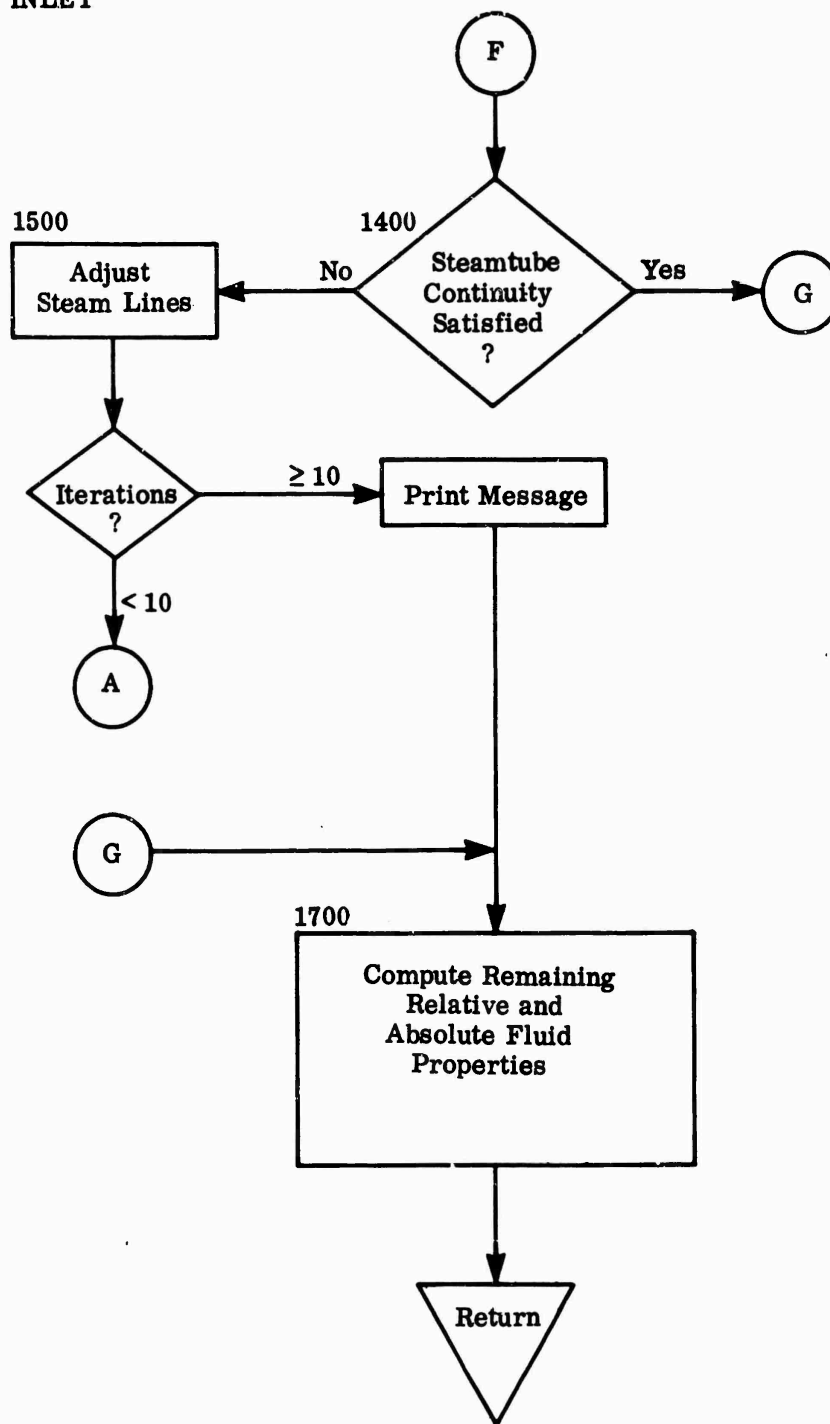
CONFIDENTIAL

INLET



CONFIDENTIAL

INLET



CONFIDENTIAL

5.2 PROGRAM ROUTINES

This section describes the functions of each routine, its calling sequence, and the routines used in this computer program.

MAIN

MAIN accomplishes input, control, and some intermediate calculations. MAIN references INLET, CHORD, RCS, IMPEL, OUTPUT, TALL14, TALLZZ, TABLE, TAB2, SQRT, ATAN, and COS.

IMPEL (K2)

IMPEL computes the impeller-station conditions that satisfy radial equilibrium in the meridional plane along the normal. IMPEL references TABLE, TAB2, SQRT, SIN, COS, TAN, ATAN, and ATAN2.

K2 = Station number.

INLET (K2)

INLET computes the inducer-inlet relative conditions along a radial line in the meridional plane to verify that the conditions satisfy radial equilibrium. INLET references SLOPE, TABLE, TAB2, SORT, SQRT, ATAN, ATAN2, TAN, and ALOG.

K2 = Station number.

RCS (K2, XLOC, RADIUS, GAMMA, DX, AREA, XND, and BLF)

RCS computes streamtubes of equal area and the radius of curvature schedule along a normal. RCS refers NORMAL, TABLE, COS, SQRT, and TAN.

K2	=	station number
XLOC	=	radial distance
GAMMA	=	meridional angle
DX	=	change in axial distance used for derivatives
AREA	=	actual annulus area
XND	=	normal distance
RADIUS	=	average streamtube radius
BLF	=	blockage factor

CONFIDENTIAL

SLOPE (XHUB, DX, RADIUS, AREA, CF, DERIV1, DERIV2)

SLOPE computes streamtubes of equal area along a radial line and the first and second radial derivatives of the streamlines. SLOPE references TABLE and SQRT.

XHUB = axial distance to a radial station
DX = change in axial distance used for derivatives
RADIUS = radial distance
AREA = actual annulus area
CF = 0 if derivatives are to be computed
CF = 1 if not
DERIV1 = first radial derivative
DERIV2 = second radial derivative

OUTPUT

OUTPUT prints out the calculated streamtube results at each station.

CHORD (XHUB, TIPG, HX, HY, TX, TY, NH, NT, K, XTIP, RTIP, and SLOPE)

CHORD computes the normal in an annulus cross section of a duct that satisfies the tangent circle criterion. CHORD references TAB2, ATAN, TAN, and SQRT.

XHUB = station-hub axial distance
XTIPG = guess as to station-tip axial distance
XTIP = station-tip axial distance
RTIP = station-tip radial distance
HX = array of hub Z-values
HY = array of hub R-values
TX = array of tip Z-values
TY = array of tip R-values
NH = number of hub points

CONFIDENTIAL

NT = number of tip points
SLOPE = the angle that the normal angle makes with Z-axis

SORT (TX, TY, and NT)

SORT sorts a single table by increasing values of the independent variable.

TX = independent variable array
TY = dependent variable array
NT = number of points to be sorted

TABLE (NT and ARG)

TABLE performs a single table look-up and references TAB2.

NT = table number
ARG = argument

TAB2 (X, Y, NX, NDEG, ARG, and IE)

TAB2 performs a multidegree interpolation of a single table using Aitkins exact polynomial fit algorithm.

X = independent variable array
Y = dependent variable array
NX = number of points in table
NDEG = degree of interpolation
ARG = independent argument
IE = 1 for success
IE = 2 for overflow
IE = 3 for failure

5.3 PROGRAM LISTING

FOR MAIN 2496A002
COMPIATION BY UNIVAC 1100 FORTRAN-IV DATED NOV. 23, 1965 F4008
TIME, COMPIATION WAS DONE ON 19 AUG 66 AT 17:37:00

MAIN PROGRAM ENTRY POINT 000000
STORAGE USED (BLOCK, NAME, LENGTH)

0001 *CODE 002324
0000 *DATA 010422
0002 *BLANK 004735
0003 RC 000170
0004 IMPELR 002335
0005 BLOCK 010757

EXTERNAL REFERENCES (BLOCK, NAME)

0006 TALLZZ
0007 INLET
0010 CHORD
0011 TABLE
0012 RCS
0013 SORT
0014 IMPEL
0015 TAB2
0016 COS
0017 OUTPUT
0020 TALL14
0021 NWDUS
0022 NI02\$
0023 NR0US
0024 NI01\$
0025 NERR2\$
0026 NEXP6\$
0027 NSTOP\$

STORAGE ASSIGNMENT FOR VARIABLES (BLOCK, TYPE, RELATIVE LOCATION, NAME)

0001	000014	IL	0001	00020	10L	0001	00450	100L	0000	010226	1000F	0000	010240	1001F
0000	010241	1002F	0000	010243	1003F	0000	010245	1004F	0000	010255	1005F	0000	010264	1006F
0000	010267	1007F	0000	010272	1008F	0000	010275	1009F	0001	002155	1016G	0001	002172	1024G
0001	002217	1036G	0001	002304	1047G	0001	000025	135G	0001	000033	142G	0001	000555	150L
0001	000072	154G	0001	000624	156L	0001	000104	164\$	0001	000115	172\$	0001	000077	20L
0001	000126	200G	0001	01274	201L	0001	001313	202L	0000	010302	2020F	0000	010334	2030E
0001	001315	205L	0001	001350	208L	0001	000140	210G	0001	001415	210L	0001	001426	211L
0001	001433	213L	0001	001457	220L	0001	001467	221L	0001	000207	227G	0001	001521	230L
0001	000220	235G	0001	00032	245G	0001	001556	250L	0001	000243	253G	0001	001565	260L
0001	000254	261G	0001	001575	261L	0001	001612	270L	0001	000271	271G	0001	000302	277G
0001	000133	30L	0001	000313	305G	0001	000330	315G	0001	000341	323G	0001	000352	331G
0001	000400	347G	0001	000424	346G	0001	000436	374G	0001	002065	375L	0001	000225	40L
0001	002102	400L	0001	000515	415G	0001	000530	424G	0001	000546	434G	0001	000573	451G
0001	000615	463G	0001	000441	477G	0001	000261	50L	0001	000743	513G	0001	001014	526G
0001	001016	525G	0001	001122	542G	0001	001143	547G	0001	001175	562G	0001	000220	60L

0001	001326	6176	0001	001360	6256	0001	001452	6456	0001	001513	6566	0001	001531	6666
0001	000357	70L	0001	001846	7216	0001	001774	7606	0001	001776	7636	0001	000417	80L
0001	000431	90L	0001	002317	900L	0004	R 000000	A	0005	R 000000	ACCEL	0000	R 010174	AK
0005	R 000214	ALPHA	0005	R 000430	AMASE	0005	R 000644	AREA	0005	R 010154	BETA	0000	R 010172	BIT
0000	R 010152	BLADES	0004	R 000764	BLF	0000	R 010171	BLFM	0000	R 010154	BLFOOT	0000	R 010173	BOU
0004	R 001200	C	0005	R 001274	CF	0000	R 01017C	CONST	0016	R 000000	COS	0000	R 000202	DATA
0000	R 000000	DMARG	0005	001275	DERIV1	0005	001511	DERIV2	0005	R 001725	DGR	0005	R 001726	DPDN
0000	R 010205	DV	0004	R 001262	GAHMA	0005	R 003142	GC	0005	002143	GIW4	0000	R 010120	GRID
0005	R 002144	HPSI	0005	R 002145	HJ	0000	I 010150	I	0000	I 010213	JAMP	0000	I 010203	IE
0000	I 010147	J	0000	I 010206	JHUB	0000	I 010207	JTIP	0000	I 010175	JUMP	0000	I 010175	JUMPL
0000	I 010177	JUMP2	0000	I 010212	K	0000	I 010201	KSLIP	0000	I 010154	K2	0000	I 000144	LIRAY
0000	I 010162	N	0000	I 010210	NHUB	0000	I 010113	NOMODE	0000	I 010153	NORMLS	0000	I 010151	NPIOT
0005	I 002146	NS	0000	I 010155	NSLIP	0000	I 010211	NTIP	0005	I 002147	NTITLE	0000	I 000156	NWGRD
0000	I 010163	NX	0002	I 000000	NY	0005	R 002173	PHI	0005	R 002217	PI	0000	R 010157	PLATDX
0005	R 002220	PRT	0005	R 002434	PS	0005	R 003650	PT	0004	R 001522	Q	0005	R 003064	R
0004	R 002220	PRT	0005	R 003065	RCURV	0005	R 003301	REC	0005	R 003515	RIN	0000	R 010165	RLA51
0004	R 001306	RADIUS	0000	R 010156	SLIPFC	0000	R 010167	SLOPE	0013	R 000000	SHORT	0011	R 000000	TABLE
0005	R 003516	RPM	0000	R 000000	TAB2	0005	R 003517	TRI	0005	R 003733	TS	0005	R 004147	TT
0000	R 010160	TABNO	0005	R 004407	TY	0005	R 004433	U	0005	R 004647	V	0005	R 005063	VP
0005	R 004363	TX	0005	005513	VR	0005	R 005727	V5	0005	R 006143	V5NO	0005	R 006357	VSM
0004	R 000000	VW	0005	R 006573	VU	0005	R 007007	VVSND	0005	R 007223	VX	0005	R 007937	X
0005	R 007653	WM	0005	R 010303	WU	0005	R 010067	WVSND	0000	R 000240	X	0004	R 001604	XULF
0004	R 001750	XLOC	0005	R 010317	XMO	0000	R 010161	XN	0005	R 010543	XND	0003	R 000000	XRC
0002	R 000051	XVAL	0000	R 010200	XZ	0000	R 010214	X10	0000	R 010216	X11	0000	R 010220	X12
0000	R 010222	X13	0000	R 010224	X14	0000	R 004160	Y	0004	R 002164	YAL	0000	R 010217	Y11
0003	R 000074	YRC	0002	R 002373	YVAL	0000	R 010202	Y1	0000	R 010215	Y10	0000	R 010217	Y11
0000	R 010221	Y12	0000	R 010223	Y13	0000	R 010225	Y14	0000	R 010204	Y2	0000	R 000214	ZTIPG
0000	R 010166	ZZZZ												

00100	1.	C	00100	2.	C	00100	3.	C	00100	4.	C	00100	5.	C	00100	6.	C	00100	7.	C	00100	8.	C	00100	9.	C	00100	10.	C	00100	11.	C	00100	12.	C	00100	13.	C	00100	14.	C	00100	15.	C	00100	16.	C	00100	17.	C	00100	18.	C	00100	19.	C	00100	20.	C	00100	21.	C	00100	22.	C	00100	23.	C	00100	24.	C	00100	25.	C	00100	26.	C
00100	1.	C	00100	2.	C	00100	3.	C	00100	4.	C	00100	5.	C	00100	6.	C	00100	7.	C	00100	8.	C	00100	9.	C	00100	10.	C	00100	11.	C	00100	12.	C	00100	13.	C	00100	14.	C	00100	15.	C	00100	16.	C	00100	17.	C	00100	18.	C	00100	19.	C	00100	20.	C	00100	21.	C	00100	22.	C	00100	23.	C	00100	24.	C	00100	25.	C	00100	26.	C
00100	1.	C	00100	2.	C	00100	3.	C	00100	4.	C	00100	5.	C	00100	6.	C	00100	7.	C	00100	8.	C	00100	9.	C	00100	10.	C	00100	11.	C	00100	12.	C	00100	13.	C	00100	14.	C	00100	15.	C	00100	16.	C	00100	17.	C	00100	18.	C	00100	19.	C	00100	20.	C	00100	21.	C	00100	22.	C	00100	23.	C	00100	24.	C	00100	25.	C	00100	26.	C
00100	1.	C	00100	2.	C	00100	3.	C	00100	4.	C	00100	5.	C	00100	6.	C	00100	7.	C	00100	8.	C	00100	9.	C	00100	10.	C	00100	11.	C	00100	12.	C	00100	13.	C	00100	14.	C	00100	15.	C	00100	16.	C	00100	17.	C	00100	18.	C	00100	19.	C	00100	20.	C	00100	21.	C	00100	22.	C	00100	23.	C	00100	24.	C	00100	25.	C	00100	26.	C
00100	1.	C	00100	2.	C	00100	3.	C	00100	4.	C	00100	5.	C	00100	6.	C	00100	7.	C	00100	8.	C	00100	9.	C	00100	10.	C	00100	11.	C	00100	12.	C	00100	13.	C	00100	14.	C	00100	15.	C	00100	16.	C	00100	17.	C	00100	18.	C	00100	19.	C	00100	20.	C	00100	21.	C	00100	22.	C	00100	23.	C	00100	24.	C	00100	25.	C	00100	26.	C
00100	1.	C	00100	2.	C	00100	3.	C	00100	4.	C	00100	5.	C	00100	6.	C	00100	7.	C	00100	8.	C	00100	9.	C	00100	10.	C	00100	11.	C	00100	12.	C	00100	13.	C	00100	14.	C	00100	15.	C	00100	16.	C	00100	17.	C	00100	18.	C	00100	19.	C	00100	20.	C	00100	21.	C	00100	22.	C	00100	23.	C	00100	24.	C	00100	25.	C	00100	26.	C
00100	1.	C	00100	2.	C	00100	3.	C	00100	4.	C	00100	5.	C	00100	6.	C	00100	7.	C	00100	8.	C	00100	9.	C	00100	10.	C	00100	11.	C	00100	12.	C	00100	13.	C	00100	14.	C	00100	15.	C	00100	16.	C	00100	17.	C	00100	18.	C	00100	19.	C	00100	20.	C	00100	21.	C	00100	22.	C	00100	23.	C	00100	24.	C	00100	25.	C	00100	26.	C
00100	1.	C	00100	2.	C	00100	3.	C	00100	4.	C	00100	5.	C	00100	6.	C	00100	7.	C	00100	8.	C	00100	9.	C	00100	10.	C	00100	11.	C	00100	12.	C	00100	13.	C	00100	14.	C	00100	15.	C	00100	16.	C	00100	17.	C	00100	18.	C	00100	19.	C	00100	20.	C	00100	21.	C	00100	22.	C	00100	23.	C	00100	24.	C	00100	25.	C	00100	26.	C
00100	1.	C	00100	2.	C	00100	3.	C	00100	4.	C	00100	5.	C	00100	6.	C	00100	7.	C	00100	8.	C	00100	9.	C	00100	10.	C	00100	11.	C	00100	12.	C	00100	13.	C	00100	14.	C	00100	15.	C	00100	16.	C	00100	17.	C	00100	18.	C	00100	19.	C	00100	20.	C	00100	21.	C	00100	22.	C	00100	23.	C	00100	24.	C	00100	25.	C	00100	26.	C
00100	1.	C	00100	2.	C	00100	3.	C	00100	4.	C	00100	5.	C	00100	6.	C	00100	7.	C	00100	8.	C	00100	9.	C	00100	10.	C	00100	11.	C	00100	12.	C	00100	13.	C	00100	14.	C	00100	15.	C	00100	16.	C	00100	17.	C	00100	18.	C	00100	19.	C	00100	20.	C	00100	21.	C	00100	22.	C	00100	23.	C	00100	24.	C	00100	25.	C	00100	26.	C
00100	1.	C	00100	2.	C	00100	3.	C	00100	4.	C	00100	5.	C	00100	6.	C	00100	7.	C	00100	8.	C	00100	9.	C	00100	10.	C	00100	11.	C	00100	12.	C	00100	13.	C	00100	14.	C	00100	15.	C	00100	16.	C	00100	17.	C	00100	18.	C	00100	19.	C	00100	20.	C	00100	21.	C	00100	22.	C	00100	23.	C	00100	24.	C	00100	25.	C	00100	26.	C
00100	1.	C	00100	2.	C	00100	3.	C	00100	4.	C	00100	5.	C	00100	6.	C	00100	7.	C	00100	8.	C	00100	9.	C	00100	10.	C	00100	11.	C	00100	12.	C	00100	13.	C	00100	14.	C	00100	15.	C	00100	16.	C	00100	17.	C	00100	18.	C	00100	19.	C	00100	20.	C	00100	21.	C	00100	22.	C	00100	23.	C	00100	24.	C	00100	25.	C	00100	26.	C
00100	1.	C	00100	2.	C	00100	3.	C	00100	4.	C	00100	5.	C	00100	6.	C	00100	7.	C	00100	8.	C	00100	9.	C	00100	10.	C	00100	11.	C	00100	12.	C	00100	13.	C	00100	14.	C	00100	15.	C	00100	16.	C	00100	17.	C	00100	18.	C	00100	19.	C	00100	20.	C	00100	21.	C	00100	22.	C	00100	23.	C	00100	24.	C	00100	25.	C	00100	26.	C
00100	1.	C	00100	2.	C	00100	3.	C	00100	4.	C	00100	5.	C	00100	6.	C	00100	7.	C	00100	8.	C	00100	9.	C	00100	10.	C	00100	11.	C	00100	12.	C	00100	13.	C	00100	14.	C	00100	15.	C	00100	16.	C	00100	17.	C	00100	18.	C	00100	19.	C	00100	20.	C	00100	21.	C	00100	22.	C	00100	23.	C	00100	24.	C	00100	25.	C	00100	26.	C
00100	1.	C	00100	2.	C	00100	3.	C	00100	4.	C	00100	5.	C	00100	6.	C	00100	7.	C	00100	8.	C	00100	9.	C	00100	10.	C																																																

00115	27.		DATA (LIBRARY(I),I=1,9)ZSHITLE,SHCONST,SHMASS,SHZ(UUB,SHZLIP,	2496A056
00115	28.		*SHYABLE,SHGEONE,SHBEGIN,SHEND P/	2496A058
00117	29.		DATA NPL0T/1/	2496A060
00117	30.	C		2496A062
00117	31.	C	INITIALIZE CONSTANTS	2496A064
00121	32.		GC=32.17	2496A066
00122	33.		MJ=778.2	2496A068
00123	34.		R=53.35	2496A070
00124	35.		PI=3.14159	2496A072
00125	36.		DGR=.01745329	2496A074
00126	37.		HGPSI=2.03593	2496A076
00127	38.	1	CONTINUE	2496A078
00130	39.		WRITE(6,1000)	2496A080
00130	40.	C		2496A082
00130	41.	C	READ IN A CONTROL WORD	2496A084
00132	42.	10	CONTINUE	2496A086
00133	43.		READ(5,1001)(NWORD(I),I=1,16)	2496A088
00133	44.	C		2496A090
00133	45.	C	DETERMINE IF THE WORD IS DEFINED IN THE LIBRARY	2496A092
00141	46.		DO 15 I=1,9	2496A094
00144	47.		IF(NWORD(I).EQ.LIBRARY(I)) GO TO (20,30,40,50,60,100,70,80,90),I	2496A096
00146	48.	15	CONTINUE	2496A098
00146	49.	C		2496A100
00146	50.	C	PRINT OUT ILLEGAL DATA CONTROL CARD	2496A102
00150	51.		WRITE(6,1004)	2496A104
00152	52.		WRITE(6,1003)(NWORD(I),I=1,16)	2496A106
00160	53.		GO TO 10	2496A108
00160	54.	C		2496A110
00160	55.	C	READ IN TITLE CARD	2496A112
00161	56.	20	CONTINUE	2496A114
00162	57.		READ(5,1001)(NTITLE(I),I=1,16)	2496A116
00170	58.		WRITE(6,1003)(NWORD(I),I=1,16)	2496A118
00176	59.		WRITE(6,1003)(NTITLE(I),I=1,16)	2496A120
00204	60.		GO TO 10	2496A122
00204	61.	C		2496A124
00204	62.	C	READ IN CONSTANTS	2496A126
00205	63.	30	CONTINUE	2496A128
00206	64.		READ(5,1002)(DATA(I),I=1,8)	2496A130
00214	65.		RPM=DATA(1)	2496A132
00215	66.		BLADES=DATA(2)	2496A134
00216	67.		NORMLS=DATA(3)	2496A136
00217	68.		CF=DATA(4)	2496A138
00220	69.		XL0C(1,1)=DATA(5)	2496A140
00221	70.		BLFOU=DATA(6)	2496A142
00222	71.		NSLIP=DATA(7)	2496A144
00223	72.		SLIPFC=DATA(8)	2496A146
00224	73.		NS=NORMLS*1	2496A148
00225	74.		WRITE(6,1003)(NWORD(I),I=1,16)	2496A150
00233	75.		WRITE(6,1005)(DATA(I),I=1,8)	2496A152
00241	76.		GO TO 10	2496A154
00241	77.	C		2496A156
00241	78.	C	READ IN MASS FLOW RATES	2496A158
00242	79.		CONTINUE	2496A160
00243	80.	40	READ(5,1002)(AMASS(I),I=1,5)	2496A162
00251	81.		WRITE(6,1003)(NWORD(I),I=1,16)	2496A164
00257	82.		WRITE(6,1006)(AMASS(I),I=1,5)	2496A166
00265	83.		GO TO 10	2496A168
00265	84.	C		2496A170

00265	65.	C	READ IN Z(HUB) VALUES	2496A172
00266	66.	50	CONTINUE	2496A174
00267	67.		READ(5,1002)(XLOC(I,1),I=2,NS)	2496A176
00275	68.		WRITE(6,1003)(NWORD(I),I=1,16)	2496A178
00303	69.		WRITE(6,1006)(XLOC(I,1),I=2,NS)	2496A180
00311	90.		GO TO 10	2496A182
00311	91.	C		2496A184
00311	92.	C	READ IN Z(TIP GUESS) VALUES	2496A186
00312	93.	60	CONTINUE	2496A188
00313	94.		READ(5,1002)(ZTIPG(I),I=1,NORMLS)	2496A190
00321	95.		WRITE(6,1003)(NWORD(I),I=1,16)	2496A192
00327	96.		WRITE(6,1006)(ZTIPG(I),I=1,NORMLS)	2496A194
00335	97.		GO TO 10	2496A196
00335	98.	C		2496A198
00335	99.	C	READ IN PLOT DIMENSIONS	2496A200
00336	100.	70	CONTINUE	2496A202
00337	101.		READ(5,1002)GRID(3),GRID(5),PLOTDX	2496A204
00344	102.		NPLOT=2	2496A206
00345	103.		WRITE(6,1003)(NWORD(I),I=1,16)	2496A208
00353	104.		WRITE(6,1007)GRID(3),GRID(5),PLOTDX	2496A210
00360	105.		GO TO 10	2496A212
00360	106.	C		2496A214
00360	107.	C	BEGIN COMPUTATION	2496A216
00361	108.	80	CONTINUE	2496A218
00362	109.		WRITE(6,1003)(NWORD(I),I=1,16)	2496A220
00370	110.		GO TO 150	2496A222
00370	111.	C		2496A224
00370	112.	C	SIGN OFF GEOMETRY PLOT TAPE	2496A226
00371	113.	90	CONTINUE	2496A228
00372	114.		WRITE(6,1008)(NWORD(I),I=1,16)	2496A230
00400	115.		NPLOT=1	2496A232
00401	116.		CALL TALLZZ(1)	2496A234
00402	117.		GO TO 10	2496A236
00402	118.	C		2496A238
00402	119.	C	READ IN TABLE DATA	2496A240
00403	120.	100	CONTINUE	2496A242
00404	21.		READ(5,1002)TABNO,XN	2496A244
00410	122.		N=TABNO	2496A246
00411	123.		NX=XN	2496A248
00412	124.		NXY(N)=NX	2496A250
00413	125.		READ(5,1002)(XVAL(I,N),YVAL(I,N),I=1,NX)	2496A252
00422	126.		WRITE(6,1003)(NWORD(I),I=1,16)	2496A254
00430	127.		WRITE(6,1009)TABNO,XM,XVAL(I,N),YVAL(I,N),I=1,NX)	2496A256
00441	128.		GO TO 10	2496A258
00441	129.	C		2496A260
00441	130.	C	COMPUTE INLET CONDITIONS	2496A262
00442	131.	150	CONTINUE	2496A264
00443	132.		K2=1	2496A266
00444	133.		CALL INLET(K2)	2496A268
00445	134.		XMD(1)=0.	2496A270
00446	135.		RLAST=RLN	2496A272
00447	136.		XMD(1)=0.	2496A274
00450	137.		DO 155 J=1,5	2496A276
00453	138.		PT(1,J)=PT(1,J)+HGPSI	2496A278
00454	139.		PS(1,J)=PS(1,J)+HGPSI	2496A280
00455	140.		PR(1,J)=PR(1,J)+HGPSI	2496A282
00456	141.		ALPHA(1,J)=ALPHA(1,J)/DGR	2496A284
00457	142.		BETA(1,J)=BETA(1,J)/DGR	2496A286

```
00460 143. 155 CONTINUE 2496A288
00462 144. DO 156 J=1,7 2496A290
00465 145. IF (ABS(RCURV(1,J)).GT.0.1) GO TO 156 2496A292
00467 146. RCURV(1,J)=10000. 2496A294
00470 147. CONTINUE 2496A296
00472 148. IF (K2.LT.1) GO TO 900 2496A298
00474 149. IF (NS.EQ.1) GO TO 900 2496A300
00476 150. C 2496A302
00478 151. C 2496A304
00480 152. DO 160 J=2,NS 2496A306
00482 153. ZZZZ=ZTIPG(J-1) 2496A308
00484 154. CALL CHORD(XLOC(J,1),Z,XYZ(1,4),YVAL(1,4),XVAL(1,4), 2496A310
00486 155. *YVAL(1,5),NXY(4),NXY(5),3,XLOC(J,7),RADIUS(J,7),SLOPE) 2496A312
00488 156. GAMMA(J)=(SLOPE-90.)*DGR 2496A314
00490 157. RADIUS(J,1)=TABLE(4,XLOC(J,1)) 2496A316
00492 158. CALL RCS(J,XLOC,RADIUS,GAMMA,0.05,AREA,XND,BLF) 2496A318
00494 159. XMD(J)=SORT((XLOC(J,4)-XLOC(J-1,4))*2+(RADIUS(J,4)-RLAST)**2) 2496A320
00496 160. *XMD(J-1) 2496A322
00498 161. RLAST=RADIUS(J,4) 2496A324
00500 162. CONTINUE 2496A326
00502 163. C 2496A328
00504 164. C 2496A330
00506 165. DO 170 J=1,5 2496A332
00508 166. REC(NS,J)=TABLE(J+14,NVND(1,J))*TABLE(14,XND(NS,J+1)/ 2496A334
00510 167. *XND(NS,7)+100.) 2496A336
00512 168. TX(J)=(REC(NS,J)-1.)/XMD(NS) 2496A338
00514 169. CONTINUE 2496A340
00516 170. DO 180 K2=2,NS 2496A342
00518 171. REC(K2,J)=TX(J)*XMD(K2)+1. 2496A344
00520 172. CONTINUE 2496A346
00522 173. C 2496A348
00524 174. C 2496A350
00526 175. C 2496A352
00528 176. C 2496A354
00530 177. C 2496A356
00532 178. C 2496A358
00534 179. C 2496A360
00536 180. C 2496A362
00538 181. C 2496A364
00540 182. C 2496A366
00542 183. C 2496A368
00544 184. C 2496A370
00546 185. C 2496A372
00548 186. C 2496A374
00550 187. C 2496A376
00552 188. C 2496A378
00554 189. C 2496A380
00556 190. C 2496A382
00558 191. C 2496A384
00560 192. C 2496A386
00562 193. C 2496A388
00564 194. C 2496A390
00566 195. C 2496A392
00568 196. C 2496A394
00570 197. C 2496A396
00572 198. C 2496A398
00574 199. C 2496A400
00576 200. C 2496A402
```

00570	201.	200	CONTINUE	2496A404
00572	202.		C(26)=RPM	2496A406
00573	203.		AK=TABLE(3,TT(1,3))	2496A408
00574	204.		C(27)=SORT(AK*GC/H*(2,/(AK+2)))*((AK+1,)))*.49118	2496A410
00574	205.	C		2496A412
00574	206.	C	Q ARRAY IS V ARRAY IN IMPEL	2496A414
00575	207.		Q(22)=V(1,3)	2496A416
00576	208.		Q(23)=BLADES	2496A418
00577	209.		Q(10)=FLOAT(NS)	2496A420
00577	210.	C		2496A422
00600	211.		JUMP=1	2496A424
00601	212.		IF(NSLIP,LT,1)JUMP=2	2496A426
02603	213.		GO TO (201,202),JUMP	2496A428
00604	214.	201	JUMP1=1	2496A430
00605	215.		IF(NSLIP,EO,2)JUMP1=2	2496A432
00607	216.		IF(NSLIP,EG,1)JUMP1=3	2496A434
00611	217.		GO TO 205	2496A436
00612	218.	202	JUMP2=1	2496A438
00613	219.	205	Q(9)=1.	2496A440
00614	220.		IF(NSLIP,GT,NS) GO TO 208	2496A442
00616	221.		DO 206 J=1,5	2496A444
00621	222.	206	BETA(NS,J)=TABLE(13,XND(NS,J+1)/XND(NS,7)*100.)	2496A446
00623	223.	208	CONTINUE	2496A448
00623	224.	C		2496A450
00623	225.			2496A452
00624	226.		DO 300 K2=2,NS	2496A454
00627	227.		Q(1)=RADIUS(K2,1)	2496A456
00630	228.		Q(2)=RADIUS(K2,7)	2496A458
00631	229.		Q(3)=FLOAT(K2-1)	2496A460
00632	230.		Q(4)=GAMMA(K2)/DGR	2496A462
00633	231.		Q(5)=FLOAT(K2)	2496A464
00634	232.		Q(6)=XLOC(K2,1)	2496A466
00634	233.	C		2496A468
00634	234.	C		2496A470
00635	235.		DETERMINE RELATIVE SLIP POSITION	2496A472
00636	236.	213	GO TO (210,220),JUMP	2496A474
00637	237.	211	GO TO (230,211,213),JUMP1	2496A476
00640	238.		Q(9)=2.	2496A478
00641	239.		JUMP1=3	2496A480
00642	240.	213	GO TO 230	2496A482
00643	241.		Q(9)=3.	2496A484
00644	242.		XYZ=(XMD(K2)-XMD(NSLIP))/(XMD(NS)-XMD(NSLIP))	2496A486
00647	243.	214	DO 214 J=1,5	2496A488
00651	244.		YAL(J)=XYZ*BETA(NS,J)	2496A490
00652	245.	220	GO TO (236,221),JUMP2	2496A492
00653	246.	221	Q(9)=3.	2496A494
00654	247.		XYZ=(XMD(K2)-XMD(KSLIP))/(XMD(NS)-XMD(KSLIP))	2496A496
00655	248.		DO 222 J=1,5	2496A498
00660	249.	222	YAL(J)=(XYZ*(BETA(NS,J)-BETA(KSLIP,J))+BETA(KSLIP,J))	2496A500
00662	250.	230	CONTINUE	2496A502
00663	251.		Q(7)=(XMD(K2)-XMD(K2-1))/12.	2496A504
00664	252.		Q(8)=BLF(K2,3)	2496A506
00665	253.		DO 240 J=.5	2496A508
00670	254.		C(J+10)=XU(K2-1,J)	2496A510
00671	255.		Q(J+10)=AREA(K2,J)*BLF(K2,J)	2496A512
00672	256.	240	Q(J+15)=REC(K2,J)	2496A514
00674	257.		Q(21)=XMD(K2)	2496A516
00675	258.		CALL IMPEL(K2)	2496A518

	GO TO (250,260),JUMP		2496A520
00676	IF(K2+1).EQ.NSLIP) JUMP1=2	250	2496A522
00677	GO TO 270		2496A524
00678	GO TO (261,270),JUMP2	260	2496A526
00702	IF(W(1,3)/A(103)).LT.SLIPFC) GO TO 270	261	2496A528
00703	KSLIP=K2		2496A530
00705	JUMP2=2		2496A532
00706	GO TO 270		2496A534
00707	CONTINUE	270	2496A536
00710	RURV(K2,1)=YRC(1,K2)		2496A538
00711	RCURV(K2,7)=YRC(3,K2)		2496A540
00712	U(K2,1)=PI*RPW*RADIUS(K2,1)/360.		2496A542
00713	U(K2,7)=PI*RPW*RADIUS(K2,7)/360.		2496A544
00714	GAMMA(K2)=GAMMA(K2)*DGR		2496A546
00715	PHI(K2)=TABLE(12,XLOC(K2,4))		2496A548
00716	TX(K2)=XND(K2)		2496A550
00717	DO 350 JE1,5		2496A552
00720	AREA(K2,J)=A(J)		2496A554
00723	RADIUS(K2,J+1)=A(J+10)		2496A556
00724	U(K2,J+1)=A(J+5)		2496A558
00725	TRI(K2,J)=A(J+23)		2496A560
00726	PRT(K2,J)=A(J+35)		2496A562
00727	XLOC(K2,J+1)=A(J+90)		2496A564
00730	BETA(K2,J)=A(J+55)		2496A566
00731	XPD(K2,J+1)=A(J+60)+12.		2496A568
00732	MVSND(K2,J)=A(J+70)		2496A570
00733	PS(K2,J)=A(J+85)		2496A572
00734	TS(K2,J)=A(J+90)		2496A574
00735	VNSD(K2,J)=A(J+95)		2496A576
00736	M(K2,J)=A(J+100)		2496A578
00737	NM(K2,J)=A(J+105)		2496A580
00740	VOUK2,J)=A(J+110)		2496A582
00741	VI(K2,J)=A(J+115)		2496A584
00742	ALPHA(K2,J)=A(J+120)		2496A586
00743	V(K2,J)=A(J+125)		2496A588
00744	VNSD(K2,J)=A(J+130)		2496A590
00745	PT(K2,J)=A(J+150)		2496A592
00746	T(K2,J)=A(J+155)		2496A594
00747	RCURV(K2,J+1)=A(J+180)*12.		2496A596
00750	DPDN(K2,J)=A(J+190)		2496A598
00751	ACCEL(K2,J)=A(J+315)		2496A600
00752	DHARG(K2,J)=VUI(K2,J)*(RADIUS(K2,J+1)*CONET-(XND(K2,J+1)*TABLE(11,2496A602		2496A602
00753	*XLOC(K2,7))+TABLE(10,XLOC(K2,1))*XND(K2,1))*XND(K2,2)+1)))XND(K2,7)+2496A604		2496A604
00753	C	300	2496A606
00754	CONTINUE		2496A608
00754	COMPUTE THE SURFACE VELOCITIES		2496A610
00754	DO 350 K2=2,MS		2496A612
00757	DO 350 JE1,5		2496A614
00762	Y1=TABLE(TX,DHARG(1,J),NS,I,XMD(K2)-0.02 ,IE)		2496A616
00765	Y2=TABLE(TX,DHARG(1,J),NS,I,XMD(K2)+0.02 ,IE)		2496A618
00766	DV= 12.5*COS(BFTA(K2,J)*DGR)*LYZ-YY		2496A620
00767	VS(K2,J)=W(K2,J)*DV		2496A622
00770	VPI(K2,J)=W(K2,J)-OV		2496A624
00771	VSM(K2,J)=VS(K2,J)/W(1,3)		2496A626
00772	VPM(K2,J)=VPI(K2,J)/W(1,3)		2496A628
00773	VTW(K2,J)=W(K2,J)/W(1,3)		2496A630
00774	CONTINUE		2496A632
00775	DO 350	350	2496A634


```

00775 317. C PRINT OUT RESULTS 2496A636
00776 318. C CONTINUE 2496A638
01000 319. 375 CALL OUTPUT 2496A640
01001 320. NS=NORMLS+1 2496A642
01002 321. GO TO (1,400),NPL0T 2496A644
01003 322. C 2496A646
01004 323. C PLOT OUT GEOMETRY 2496A648
01005 324. C CONTINUE 2496A650
01006 325. 400 JHUB=N*Y(4) 2496A652
01007 326. JHUB=N*Y(5) 2496A654
01008 327. NHUB=(XVAL(JHUB,4)-XVAL(1,4))/PLOTDX+2. 2496A656
01009 328. NTIP=(XVAL(JTIP,5)-XVAL(1,5))/PLOTDX+2. 2496A658
01010 329. X(1,1)=XVAL(1,4) 2496A660
01011 330. X(1,2)=XVAL(1,5) 2496A662
01012 331. Y(1,1)=YVAL(1,4) 2496A664
01013 332. Y(1,2)=YVAL(1,5) 2496A666
01014 333. DO 410 J=2,NHUB 2496A668
01015 334. X(J,1)=X(J-1,1)+PLOTDX 2496A670
01016 335. Y(J,1)=Y(J-1,1)+PLOTDX 2496A672
01017 336. 410 Y(J,1)=Y(J,1)+X(J,1) 2496A674
01018 337. DO 420 J=2,NTIP 2496A676
01019 338. X(J,2)=X(J-1,2)+PLOTDX 2496A678
01020 339. Y(J,2)=Y(J-1,2)+PLOTDX 2496A680
01021 340. NOMODE(1)=NHUB 2496A682
01022 341. NOMODE(3)=NTIP 2496A684
01023 342. NOMODE(5)=NXY(4) 2496A686
01024 343. NOMODE(7)=NXY(5) 2496A688
01025 344. DO 460 J=1,5 2496A690
01026 345. K=2,J+7 2496A692
01027 346. 460 NOMODE(K)=NS 2496A694
01028 347. IBAD=-1 2496A696
01029 348. CALL TALL14(GRID,NOMODE,1,IBAD,4,X(1,1),Y(1,1),X(1,2),Y(1,2), 2496A698
01030 349. *XVAL(1,4),YVAL(1,4),XVAL(1,5),YVAL(1,5),XLOC(1,2), 2496A700
01031 350. *RADIUS(1,2),XLOC(1,3),RADIUS(1,3),XLOC(1,4),RADIUS(1,4), 2496A702
01032 351. *XLOC(1,5),RADIUS(1,5),XLOC(1,6),RADIUS(1,6),X10,Y10,X11,Y11, 2496A704
01033 352. *X12,Y12,X13,Y13,X14,Y14,60) 2496A706
01034 353. WRITE(1,2020)(NTITLE(K),K=1,16) 2496A708
01035 354. 2020 WRITE(6,2030) IBAD 2496A710
01036 355. GO TO 1 2496A712
01037 356. CONTINUE 2496A714
01038 357. NS=1 2496A716
01039 358. GO TO 375 2496A718
01040 359. 1000 FORMAT(1H120X,40HIMPELLER RADIAL EQUILIBRIUM DESIGN PROGRAM INPUT) 2496A720
01041 360. 1001 FORMAT(16A5) 2496A722
01042 361. 1002 FORMAT(10F7.0) 2496A724
01043 362. 1003 FORMAT(//6X,16A5) 2496A726
01044 363. 1004 FORMAT(//39H THE FOLLOWING CONTROL CARD IS IN ERROR ) 2496A728
01045 364. 1005 FORMAT(10X,F11.1,3F11.0,2F11.4,F11.0,F11.4) 2496A730
01046 365. 1006 FORMAT(10X,10F11.4) 2496A732
01047 366. 1007 FORMAT(10X,2F11.2,F11.4) 2496A734
01048 367. 1008 FORMAT(1H1,5X,16A5) 2496A736
01049 368. 1009 FORMAT(10X,2F11.0/(10X,10F11.4)) 2496A738
01050 369. 2020 FORMAT(10X,57HPLOT OF PROFILES, INTERPOLATED PROFILES, AND STREAML 2496A740
01051 370. *INES /1H /10X,53HX = AXIAL DISTANCE (IN), Y = RADIAL DISTANCE 2496A742
01052 371. *N) /1H /10X,8HTITLE ,16A5) 2496A744
01053 372. 2030 FORMAT(1H1,16HPLOT INDICATOR = ,12,20H (ZERO FOR SUCCESS) ) 2496A746
01054 373. END 2496A748

```

END OF LISTING. 0 DIAGNOSTIC MESSAGE(S).

FOR INLET
24968002
COMPILATION BY UNIVAC 1108 FORTRAN-IV DATED NOV..23,1965 F4008
THIS COMPILATION WAS DONE ON 19 AUG 66 AT 17:37:05

SUBROUTINE INLET ENTRY POINT 001354

STORAGE USED (BLOCK, NAME, LENGTH)

0001 *CODE 001401
0000 *DATA 000234
0002 *BLANK 004735
0003 RC 000170
0004 IMPELR 002335
0005 BLOCK 010757

EXTERNAL REFERENCES (BLOCK, NAME)

0006 SLOPE
0007 ATAN
0010 TABLE
0011 TAB2
0012 TAN
0013 ALOG
0014 SORT
0015 SORT
0016 ATAN2
0017 NEXP6\$
0020 NWOUS
0021 NIO1\$
0022 NIO2\$

STORAGE ASSIGNMENT FOR VARIABLES (BLOCK, TYPE, RELATIVE LOCATION, NAME)

0001 000407 1000L 0001 000563 1200L 0001 000570 1210L 0001 000015 1220L 0001 000575 1220L
0001 000601 1299L 0000 000201 1310F 0001 000622 1400L 0001 000643 1410L 0001 000661 1446
0001 000605 150G 0000 000235 1610F 0001 000140 164G 0001 000754 1700L 0001 000165 177G
0001 000202 205G 0001 000415 247G 0001 000631 332G 0001 000710 356G 0001 000763 400G
0001 000152 610L 0001 000163 615L 0001 000367 900L 0000 000154 910F 0004 R 000000 A
0000 R 000000 AC 0005 000000 ACCEL 0000 R 000127 AK 0000 R 000130 AK1 0013 R 000000 ALOG
0005 R 000430 AMASS 0005 R 000644 AREA 0007 R 000000 ATAN 0016 R 000000 ATAN2
0000 R 000131 B 0005 R 001060 BETA 0004 R 000764 BLF 0000 R 001200 C 0005 R 001274 CF
0000 R 000133 C1 0000 R 000134 C2 0000 R 000135 C3 0000 R 00136 C4 0000 R 000137 DEN
0005 R 001275 DERIV1 0005 R 001511 DERIV2 0005 R 001725 DGR 0005 R 001726 DFDN 0005 R 000132 DR
0000 R 000104 EPSM 0004 R 001252 GAMMA 0005 R 002142 GC 0005 R 002143 GIVM 0005 R 002144 HGPS1
0005 R 002145 HJ 0000 R 000126 IE 0000 R 000152 HS 0000 R 000056 HT 0000 R 000122 IA
0000 I 000125 IB 0000 I 000126 J 0000 I 000127 JND 0000 I 000124 ITRAT 0000 I 000111 J
0000 I 000112 J80 0000 I 000141 JPI 0000 I 000105 K1 0000 I 000123 MGO 0000 I 000107 NM1
0005 R 002146 NS 0005 R 002147 NTITLE 0000 I 000106 NTUDES 0002 000000 NXY 0005 002173 FY1
0005 R 002217 PI 0005 R 002220 PRI 0005 R 002434 PS 0005 R 002650 PT 0004 001522 Q
0000 R 000075 QMASS 0005 R 003064 R 0004 R 001306 RADIVS 0000 R 000150 RC 0005 R 003065 RCURV
0000 R 003301 REC 0000 R 000143 RHO 0000 R 000113 RHUB 0000 R 000115 RHUB1 0005 R 003515 RIN
0005 R 003516 RPM 0000 R 000114 RTIP 0000 R 000116 RTIP1 0000 R 000146 RVRVCR 0014 R 000000 SQR
0000 R 000110 STUBES 0010 R 000000 TAB2 0011 R 000000 TAB2 0012 R 000000 TAN 0000 R 000117 JDR

```

0000 R 000151 TORC      0000 R 000142 THASS      0005 R 003517 TRT      0005 R 003733 TS      0005 R 004147 TT
0005 004363 TX          0005 00407 TY          0005 R 004433 U          0005 R 001444 VCR
0000 R 000121 VLL        0005 005063 VP          0005 R 005277 V1          0005 R 005513 VR          0005 005727 VS
0005 R 005143 VSN0       0000 R 000140 V50        0005 006357 VSM          0005 R 005273 VU          0000 R 000120 VUL
0005 R 007007 VSN0       0005 R 007223 VX          0000 R 000145 VXCR          0005 R 007437 W          0005 R 007653 WM
0005 R 005513 WM         0005 R 010303 WU          0005 R 010667 WVSND          0004 001604 XBLF          0004 R 001750 XLOC
0005 010517 XMD         0005 010543 XND          0000 000000 XRC          0000 R 000007 XTMASS      0002 000031 XVAL
0000 R 000033 XWX        0004 002164 XAL          0004 002171 YBLF          0003 000075 YRC          0002 002373 YVAL
0000 R 000057 ZOR

```

```

00101 1. C
00101 2. C
00101 3. C
00101 4. C
00103 5. C
00104 6. C
00105 7. C
00105 8. C
00105 9. C
00106 10. C
00106 11. C
00106 12. C
00106 13. C
00106 14. C
00106 15. C
00106 16. C
00106 17. C
00106 18. C
00106 19. C
00106 20. C
00107 21. C
00110 22. C
00111 23. C
00112 24. C
00112 25. C
00112 26. C
00112 27. C
00120 28. C
00121 29. C
00124 30. C
00125 31. C
00125 32. C
00125 33. C
00127 34. C
00127 35. C
00127 36. C
00130 37. C
00131 38. C
00132 39. C
00133 40. C
00134 41. C
00135 42. C
00136 43. C
00137 44. C
00140 45. C

SUBROUTINE INLET(K2)
THIS ROUTINE COMPUTES THE INLET CONDITIONS
COMMON/RC/XRC(13,20),YRC(13,20)
COMMON NXY(125),XVAL(50,25),YVAL(50,25)
COMMON/IMP/ELR/A(500)
*GAMMA(20) ,YAL(5)
*XLOC(20,7) ,RADIUS(20,7) ,BLF(20,7) ,C(50)
COMMON/BLOCK/ ACCEL(20,7) ,YBLF(5,20) ,XBLF(5,20)
*AREA(20,7) ,BETA(20,7) ,CF
*DERIV2(20,7) ,DGR ,DPEN(20,7) ,AMASS(20,7)
*HGRS1,HJ,NS ,NTITLE(20) ,PHI(20) ,PI ,GC ,GIVM
*PSI(20,7) ,PT(20,7) ,R ,RPH ,RCURV(20,7)
*REC(20,7) ,RIN ,RPM ,RT(20,7) ,TS(20,7)
*TI(20,7) ,TX(20) ,TY(20) ,U(20,7)
*VI(20,7) ,VPI(20,7) ,VPM(20,7) ,VR(20,7)
*VSI(20,7) ,VSN0(20,7) ,VSM(20,7) ,VUI(20,7)
*VVSND(20,7) ,VX(20,7) ,XMD(20,7) ,XND(20,7)
*VVSND(20,7) ,WU(20,7) ,XMD(20)
DIMENSION AC(7),WR(20,7),XTMASS(20),XWX(20),ZDRL(7),H(17)
EQUIVALENCE (VR,WR)
DATA EPSM/.005/,K1/1/,NTUBES/5/,NML/4/,STUBES/3./
DO 100 J=1,5
GIVN=0
GIVN=GIVN+AMASS(1,J)
CONTINUE
100 CONTINUE
JGO=0 AND 1 FOR NORMAL AND ERROR RETURNS
JGO=0
JGO=0
C***ASSUME STREAMLINES BASED ON EQUAL AREAS AND COMPUTE DERIVATIVES
200 CONTINUE
CALL SLOPE(XLOC(1,1),0.05,RADIUS,AREA,CF,DERIV1,DERIV2)
R1=RADIUS(1,1)
RHUR=RADIUS(1,1)
RTIP=RADIUS(1,7)
RHUR1=RHUR
RTIP1=RTIP
TDERTIP=RHUR
GAMMA(1)=ATAN(DERIV1(1,4))

```

```
00140 46. C
00141 47. C**ASSUME LIMITS FOR HUB VELOCITY
00142 48. VLL=1200.
00143 49. VLL=2.
00144 50. C
00145 51. DO 1599 JA=1,10
00146 52. C**COMPUTE INLET TOTAL PRESSURE FROM INPUT OF P=F(R)
00147 53. 300 CO*TIME
00148 54. DO 399 JE=1,NTUBES
00149 55. PT(1,J)=TABLE(6,RADIUS(1,J+1)/HGPSI
00150 56. TT(1,J)=TABLE(7,RADIUS(1,J+1))
00151 57. BU(1,J)=TABLE(8,RADIUS(1,J+1))
00152 58. ALP(1,J)=TABLE(9,RADIUS(1,J+1))*OGK
00153 59. HT(J)=TABLE(1,TT(1,J))
00154 60. 399 CO*TIME
00155 61. C
00156 62. MGC=1
00157 63. ITPAT=0
00158 64. C
00159 65. DO 1299 IB=1,10
00160 66. C
00161 67. C**COMPUTE HUB VELOCITY BASED ON ASSOCIATED LIMITS
00162 68. 600 CO*TIME
00163 69. IF(1GO,EQ,2) GO TO 610
00164 70. VX(K2,1)=(VUL+VLL)/2.0
00165 71. GO TO 615
00166 72. 610 CO*TIME
00167 73. VX(K2,1)=TAB2(XTMASS,XWX,ITPAT,1,GIVM,IE)
00168 74. 615 CO*TIME
00169 75. DO 800 JE=1,5
00170 76. VU(1,J)=TAN(ALPHA(1,J))*VX(1,J)
00171 77. 800 CONTINUE
00172 78. C
00173 79. C**COMPUTE THE VELOCITY PROFILE
00174 80. DO 899 JE=1,NM1
00175 81. A=GC*HJ*(TT(K2,J+1)+TT(K2,J))
00176 82. AK=TABLE(3,(TT(1,J+1)+TT(1,J))/2.)
00177 83. AK1=AK/(AK-1.0)
00178 84. B=R/HJ*ALC3((TT(K2,J+1)+TT(K2,J))*AK1/(PT(K2,J+1)+PT(K2,J)))
00179 85. C=2.0*R*AK/(HJ*(AK-1.0))
00180 86. D=R/RADIUS(1,J+2)-RADIUS(1,J+1)
00181 87. C1=VX(1,J)*2*(1.0+G/C*(1.0+DERIV1(1,J+1)*2)+DERIV2(1,J+1)*DR)-A*B
00182 88. C2=2.0*GC*HJ*(HT(J+1)-HT(J))
00183 89. C3=VU(1,J+1)*2*(B/C-2)+RADIUS(1,J+1)/RADIUS(1,J+2)+VU(1,J)*2
00184 90. C4=1.0-B/C*(1.0+DERIV1(1,J+2)*2)
00185 91. C5=1.0-B/C*(1.0+DERIV1(1,J+2)*2)
00186 92. DEN=C4-DERIV2(1,J+2)*DR
00187 93. VSO=(C1+C2+C3)/DEN
00188 94. C
00189 95. C**IS THE VELOCITY SQUARED NEGATIVE
00190 96. 830 CO*TIME
00191 97. IF(VSO,LT,0) GO TO 900
00192 98. VX(K2,J+1)=SQRT(VSO)
00193 99. 899 CONTINUE
00194 100. GO TO 1000
00195 101. C
00196 102. C**PRINT DIAGNOSTIC MESSAGE
00197 103. C
```

```

00231 104. C
00232 105. 900 CONTINUE
00233 106. JPI=J+1
00234 107. WRITE(6,910)VS0,K1,JPI,VX(K2,1)
00242 108. FORMAT(//31H THE AXIAL VELOCITY SQUARED IS ,E11.4,12H AT STATION24968218
00243 109. 1 ,12,12H, STREAMLINE ,12,31H, WHEN THE HUB VELOCITY EQUALS ,F8.24968220
00244 110. 22)
00245 111. GO TO 1210
00246 112. C
00247 113. C***COMPUTE MASS FLOW RATE BASED ON VELOCITY PROFILE
00248 114. 1000 CONTINUE
00249 115. TMASS = 0.0
00250 116. DO 1099 J=1,NTUBES
00251 117. AK=1/ABLE(3,IT(1,J))
00252 118. RHO=PT(K2,J)/R/TT(K2,J)
00253 119. VCR=SQRT(AK*GC*R*2.0*TT(K2,J)/(AK+1.0))
00254 120. VXVCR=VX(K2,J)/VCR
00255 121. AK1=(AK-1.0)/(AK+1.0)
00256 122. RVRVCR=VXVCR*(1.0-AK1+VXVCR**2*(1.0+TAN(ALPHA(K2,J))**2+DERIV1(K2,J)
00257 123. *J+1)**2))**0.5/(AK-1.0)
00258 124. QMASS(J)=BLF(1,J)*RVRVCR*RHO*VCR*AREA(1,J)
00259 125. TMASS=TMASS+QMASS(J)
00260 126. AC(J)=AMASS(1,J)/BLF(K2,J)/RVRVCR/RHO/VCR
00261 127. 1099 CONTINUE
00262 128. C
00263 129. C***IS OVERALL CONTINUITY SATISFIED
00264 130. 1100 CONTINUE
00265 131. IF(ABS(TMASS-GIVM),LT, EPSM) GO TO 1400
00266 132. ITRAT=ITRAT+1
00267 133. XMX(ITRAT)=VX(K2,1)
00270 134. XTMASS(ITRAT)=TMASS
00271 135. IF(ITRAT,LT,2) GO TO 1200
00272 136. CALL SORT(X*MASS,XMX,ITRAT)
00273 137. NGO=2
00274 138. GO TO 1299
00275 139. C
00276 140. C***ADJUST THE HUB VELOCITY LIMITS
00277 141. 1200 CONTINUE
00278 142. IF(TMASS,GT,GIVM) GO TO 1220
00279 143. C
00280 144. C INCREASE HUB VELOCITY
00281 145. 1210 CONTINUE
00282 146. VLL=VX(K2,1)
00283 147. NGO=1
00284 148. GO TO 1299
00285 149. C
00286 150. C DECREASE HUB VELOCITY
00287 151. 1220 CONTINUE
00288 152. VUL=VX(K2,1)
00289 153. NGO=1
00290 154. 1299 CONTINUE
00291 155. C
00292 156. C***PRINT DIAGNOSTIC MESSAGE
00293 157. 1300 CONTINUE
00294 158. WRITE(6,1310) K1,EPSM,TMASS,GIVM
00295 159. FORMAT(//1X,94H THE PROGRAM WAS UNABLE TO OBTAIN A VELOCITY PROFILE24968218
00296 160. 1 THAT WOULD GIVE A MASS BALANCE AT STATION 12 /6X,THEPS M = F7.24968222
00297 161. 24,3X,12HCOMPUTED M = F7.4,3X19H GIVEN M = F7.4,1

```

```
00323 162. J60=1 24968326
00324 163. GO TO 1700 24968328
00325 164. C 24968330
00326 165. C**IS STREAMLINE CONTINUITY SATISFIED 24968332
00327 166. 1400 CONTINUE 24968334
00328 167. IND=0 24968336
00329 168. RHUB=RHUB1 24968338
00330 169. TDR=0 24968340
00331 170. DO 1499 J=1,NTUBES 24968342
00332 171. IF (ABS(IAC(J)-AREA(K2,J)) .LT. 0.010) GO TO 1410 24968344
00333 172. IND=IND+1 24968346
00334 173. 1410 CONTINUE 24968348
00335 174. RC=SORT(AC(J)/PI+RHUB**2) 24968350
00336 175. ZDR(J)=RC-RHUB 24968352
00337 176. TDR = TDR+ZDR(J) 24968354
00338 177. RHUB=RC 24968356
00339 178. 1499 CONTINUE 24968358
00340 179. C 24968360
00341 180. IF (IND.EQ.0) GO TO 1700 24968362
00342 181. C 24968364
00343 182. C**ADJUST STREAMLINES BASED ON VELOCITY PROFILE 24968366
00344 183. 1500 CONTINUE 24968368
00345 184. VUL=VX(K2,1)+200. 24968370
00346 185. VLL=VX(K2,1)-200. 24968372
00347 186. TDR=RTIP1-RHUB1 24968374
00348 187. RHUB=RHUB1 24968376
00349 188. DO 1599 J=1,NTUBES 24968378
00350 189. ZDR(J)=ZDR(J)+TDR 24968380
00351 190. RADIUS(1,J+1)=SORT((RHUB**2+(RHUB+ZDR(J))**2)/2.) 24968382
00352 191. AREA(K2,J)=PI*((RHUB+ZDR(J))**2-RHUB**2) 24968384
00353 192. RHUB=RHUB+ZDR(J) 24968386
00354 193. 1599 CONTINUE 24968388
00355 194. C 24968390
00356 195. C**PRINT DIAGNOSTIC MESSAGE 24968392
00357 196. 1600 CONTINUE 24968394
00358 197. WRITE(6,1610) K1,IND 24968396
00359 198. 1610 FORMAT(/,3H THE PROGRAM WAS UNABLE TO OBTAIN A CORRECT SET OF STR 24968398
00360 199. LEANLINE POSITIONS AT STATION 12. /6X,13HNO. INCORRECT IN ) 24968400
00361 200. C 24968402
00362 201. C**COMPUTE REMAINING INLET FLUID PROPERTIES 24968404
00363 202. 1700 CONTINUE 24968406
00364 203. AREA(1,6)=0. 24968408
00365 204. DO 1799 J=1,NTUBES 24968410
00366 205. AREA(1,6)=AREA(1,6)+AREA(1,J) 24968412
00367 206. XLOC(1,J+1)=XLOC(1,1) 24968414
00368 207. RCURV(1,J+1)=(1.+DERIV1(1,J+1)**2)**1./DERIV2(1,J+1) 24968416
00369 208. AK=TABLE(3,TT(K2,J)) 24968418
00370 209. AK1 = (AK-1.0)/(AK+1.0) 24968420
00371 210. VR(1,J)=VX(1,J)*DERIV1(1,J+1) 24968422
00372 211. V(K2,J) = SORT(VX(K2,J)**2+VR(K2,J)**2+VR(K2,J)**2) 24968424
00373 212. VCR = SORT(AK*GC*VR**2.0+TT(K2,J)/(AK+1.0)) 24968426
00374 213. TS(1,J)=TT(1,J)*(1.-AK1*(V(1,J)/VCR)**2) 24968428
00375 214. AK=TABLE(3,TS(1,J)) 24968430
00376 215. VVND(K2,J)=SGRT(AK*GC*TS(K2,J)) 24968432
00377 216. VVND(K2,J)=V(K2,J)/VVND(K2,J) 24968434
00378 217. AK=TABLE(3,(TT(1,J)+TS(1,J))/2.) 24968436
00379 218. PS(K2,J)=PT(K2,J)*(TS(K2,J)/TT(K2,J))**((AK/(AK-1.)) 24968438
00380 219. U(1,J+1)=PI*RADIUS(1,J+1)*RPM/360. 24968440
```

00421	220.	WU(1,J)=U(1,J+1)-WU(1,J)	24968442
00422	221.	W(K2,J)=SORT(VX(K2,J)*2,WU(K2,J)*2+WR(K2,J)*2)	24968444
00423	222.	WVND(K2,J)=W(K2,J)/VSNQ(K2,J)	24968446
00424	223.	WM(1,J)=SORT(VX(1,J)*2+WR(1,J)*2)	24968448
00425	224.	BETA(K2,J)=ATAN2(WU(K2,J),VX(K2,J))	24968450
00426	225.	HS=TABLE(1,TS(1,J))	24968452
00427	226.	HRT=HS+W(1,J)*2/2./GC/HJ	24968454
00430	227.	TRT(1,J)=TABLE(-1,HRT)	24968456
00431	228.	AK=TABLE(3,TT(1,J)+TRT(1,J)/2.)	24968458
00432	229.	PRT(1,J)=(TRT(1,J)/TT(1,J))*AK/(AK-1.)*PT(1,J)	24968460
00433	230.	CONTINUE	24968462
00435	231.	C	24968464
00436	232.	J=NTUBES+1	24968466
00437	233.	XLOC(1,J+1)=XLOC(1,1)	24968468
00440	234.	RCURV(1,J+1)=(1.+DERIV1(1,J+1)*2)*1.5/DERIV2(1,J+1)	24968470
00441	235.	U(1,J+1)=PI*RADIUS(1,J+1)*RPH/360.	24968472
00442	236.	J=0	24968474
00443	237.	RCURV(1,J+1)=(1.+DERIV1(1,J+1)*2)*1.5/DERIV2(1,J+1)	24968476
00444	238.	U(1,J+1)=PI*RADIUS(1,J+1)*RPH/360.	24968478
00445	239.	CONTINUE	24968480
00447	240.	C	24968482
00448	241.	IF(JGO.EQ.1)K2=-1	24968484
00449	242.	RETURN	24968486
00450	243.	END	24968488

END OF LISTING. 0 *DIAGNOSTIC* MESSAGE(S).

FOR SLOPE
 COMPILATION BY UNIVAC 1108 TRAN-IV DATED NOV. 23, 1965 F4008 2496B490
 THIS COMPILATION DONE ON AUG 66 AT 17:37:09

SUBROUTINE SLOPE ENTRY POINT 000206

STORAGE USED (BLOCK, NAME, LENGTH)

0001 *CODE 000257
 0000 *DATA 000130
 0002 *BLANK 000000

EXTERNAL REFERENCES (BLOCK, NAME)

0003 TABLE
 0004 SORT

STORAGE ASSIGNMENT FOR VARIABLES (BLOCK, TYPE, RELATIVE LOCATION, NAME)

0001 000023 1173 0001 000111 1406 0001 000113 1436 0001 000163 350L 0001 000165 395L
 0000 R 000023 A 0000 I 000072 I 0000 I 000071 J 0000 I 000065 K2 0000 I 000057 L
 0000 I 000066 M 0000 I 000063 NTUBES 0000 R 000062 PI 0000 R 000000 RH 0000 R 000050 RS
 0000 R 000012 RT 0004 R 000000 SORT 0000 R 000064 STUBES 0003 R 000000 TABLE 0000 R 000070 X
 0000 R 000000 Z

00101 1. SUBROUTINE SLOPE(XHUB,DX,RADIUS,AREA,CE,DERIV1,DERIV2) 2496B492
 00101 2. C 2496B494
 00101 3. C SLOPE COMPUTES FIRST AND SECOND RADIAL DERIVATIVES OF STREAMLINES 2496B496
 00101 4. C OF STREAMTUBES OF EQUAL AREA 2496B498
 00101 5. C 2496B500
 00103 6. DIMENSION N(10),RT(10),Z(10),A(10),RS(10) 2496B502
 00104 7. DIMENSION RADIUS(20,7),AREA(20,7),CE(1),DERIV1(20,7),DERIV2(20,7) 2496B504
 00105 8. DATA PI/3.14159,NTUBES/5,STUBES/5,1.0/1,M/S/1.2/ 2496B506
 00105 9. C 2496B508
 00105 10. C SET UP HUB AND TIP POINTS 2496B510
 00114 11. 100 CONTINUE 2496B512
 00114 12. C 2496B514
 00115 13. X=XHUB-DX 2496B516
 00116 14. DO 199 JE1,M 2496B518
 00121 15. Z(J)=X 2496B520
 00122 16. RH(J)=TABLE(4,X) 2496B522
 00123 17. RT(J)=TABLE(5,X) 2496B524
 00124 18. X=X+DX 2496B526
 00125 19. A(J)=(RT(J)**2-RH(J)**2)/STUBES 2496B528
 00126 20. CONTINUE 2496B530
 00130 21. RADIUS(1,1)=RH(1) 2496B532
 00131 22. RADIUS(1,7)=RT(1) 2496B534
 00132 23. DERIV1(1,1)=(RH(3)-RH(1))/2./DX 2496B536
 00133 24. DERIV1(1,7)=(RT(3)-RT(1))/2./DX 2496B538
 00134 25. DERIV2(1,1)=(RH(3)-2.*RH(2)+RH(1))/DX**2 2496B540

00135	26.		DERIV2(1,7)=(RT(3)-2.*RT(2)+RT(1))/DX**2	24968542
00135	27.	C		24968544
00135	28.	C	SET UP STREAMLINE POINTS BASED ON EQUAL AREAS	24968546
00136	29.	200	CONTINUE	24968548
00137	30.		DO 399 J=1,NTUBES	24968550
00142	31.		DO 299 I=1,M	24968552
00145	32.		RT(I)=SORT(A(I)+RH(I)**2)	24968554
00146	33.		RS(I)=SORT((RT(I)**2+RH(I)**2)/2.)	24968556
00147	34.		RH(I)=RT(I)	24968558
00150	35.	299	CONTINUE	24968560
00152	36.		RADIUS(1,J*1)=RS(L)	24968562
00153	37.		AREA(K2,J)=A(L)*PI	24968564
00154	38.		IF(CF(K2).GT.0.) GO TO 350	24968566
00154	39.	C		24968568
00154	40.	C	COMPUTE THE RADIAL DERIVATIVE	24968570
00156	41.	300	CONTINUE	24968572
00157	42.		DERIV1(1,J*1)=(RS(3)-RS(1))/2./DX	24968574
00160	43.		DERIV2(1,J*1)=(RS(3)-2.*RS(2)+RS(1))/DX**2	24968576
00161	44.		GO TO 399	24968578
00162	45.	350	CONTINUE	24968580
00163	46.		DERIV1(1,J*1)=0.	24968582
00164	47.		DERIV2(1,J*1)=0.	24968584
00165	48.	399	CONTINUE	24968586
00167	49.		RETURN	24968588
00170	50.		END	24968590

END OF LISTING. 0 *DIAGNOSTIC* MESSAGE(S).

24968592

FOR SORT
 COMPILE BY UNIVAC 1100 FORTRAN-IV DATED NOV. 23-1965 F4008
 THIS COMPILE WAS DONE ON 19 AUG 66 AT 17:37:11

SUBROUTINE SORT ENTRY POINT 000065

STORAGE USED (BLOCK, NAME, LENGTH)

0001 *CODE 000114
 0000 *DATA 000022
 0002 *BLANK 000000

STORAGE ASSIGNMENT FOR VARIABLES (BLOCK, TYPE, RELATIVE LOCATION, NAME)

0001 000013 1106 0001 000022 1156 0001 000014 1314 0001 000052 139L 0000 I 000001 JJ1
 0000 I 000003 JJ2 0000 I 000004 JJ3 0000 I 000002 NT1 0000 I 000000 NT2 0000 R 000005 TEMP1
 0000 R 000006 TEMP2

00101 1. C SUBROUTINE SORT(TX, TY, NT)
 00101 2. C
 00101 3. C SORT SORTS THE TX ARRAY IN INCREASING ORDER AND THE
 00101 4. C TY ARRAY CORRESPONDINGLY
 00101 5. C
 00101 6. C NT IS THE NUMBER OF POINTS TO BE SORTED
 00101 7. C
 00103 8. DIMENSION TX(1), TY(1)
 00104 9. IF (NT.LT.2) RETURN
 00106 10. NT2=NT-1
 00107 11. DO 139 JJ1=1, NT2
 00112 12. CONTINUE
 00113 13. NT1=NT-JJ1
 00114 14. DO 139 JJ2=1, NT1
 00117 15. JJ3=JJ1+JJ2
 00120 *DIAGNOSTIC* THE TEST FOR EQUALITY BETWEEN NON-INTEGERS MAY NOT BE MEANINGFUL.
 00120 16. IF (TX(JJ1).LE.TX(JJ3)) GO TO 139
 00122 17. TEMP1=TX(JJ1)
 00123 18. TEMP2=TX(JJ3)
 00124 19. TX(JJ1)=TX(JJ3)
 00125 20. TX(JJ3)=TEMP1
 00126 21. TX(JJ3)=TEMP2
 00127 22. TY(JJ3)=TEMP2
 00130 23. GO TO 136
 00131 24. CONTINUE
 00134 25. RETURN
 00135 26. END

END OF LISTING. 1 *DIAGNOSTIC* MESSAGE(S).

0001	002171	1000L	0000	000035	1001F	0000	000007	1002F	0000	00004	1003F	0000	000074	1004F
0001	002172	1001F	0000	000036	1002F	0000	000071	1001F	0000	00013	1001F	0001	000075	1005F
0001	002173	1002F	0000	000037	1003F	0000	000072	1002F	0000	00014	1002F	0001	000076	1006F
0001	002174	1003F	0000	000038	1004F	0000	000073	1003F	0000	00015	1003F	0001	000077	1007F
0001	002175	1004F	0000	000039	1005F	0000	000074	1004F	0000	00016	1004F	0001	000078	1008F
0001	002176	1005F	0000	000040	1006F	0000	000075	1005F	0000	00017	1005F	0001	000079	1009F
0001	002177	1006F	0000	000041	1007F	0000	000076	1006F	0000	00018	1006F	0001	000080	1010F
0001	002178	1007F	0000	000042	1008F	0000	000077	1007F	0000	00019	1007F	0001	000081	1011F
0001	002179	1008F	0000	000043	1009F	0000	000078	1008F	0000	00020	1008F	0001	000082	1012F
0001	002180	1009F	0000	000044	1010F	0000	000079	1009F	0000	00021	1009F	0001	000083	1013F
0001	002181	1010F	0000	000045	1011F	0000	000080	1010F	0000	00022	1010F	0001	000084	1014F
0001	002182	1011F	0000	000046	1012F	0000	000081	1011F	0000	00023	1011F	0001	000085	1015F
0001	002183	1012F	0000	000047	1013F	0000	000082	1012F	0000	00024	1012F	0001	000086	1016F
0001	002184	1013F	0000	000048	1014F	0000	000083	1013F	0000	00025	1013F	0001	000087	1017F
0001	002185	1014F	0000	000049	1015F	0000	000084	1014F	0000	00026	1014F	0001	000088	1018F
0001	002186	1015F	0000	000050	1016F	0000	000085	1015F	0000	00027	1015F	0001	000089	1019F
0001	002187	1016F	0000	000051	1017F	0000	000086	1016F	0000	00028	1016F	0001	000090	1020F
0001	002188	1017F	0000	000052	1018F	0000	000087	1017F	0000	00029	1017F	0001	000091	1021F
0001	002189	1018F	0000	000053	1019F	0000	000088	1018F	0000	00030	1018F	0001	000092	1022F
0001	002190	1019F	0000	000054	1020F	0000	000089	1019F	0000	00031	1019F	0001	000093	1023F
0001	002191	1020F	0000	000055	1021F	0000	000090	1020F	0000	00032	1020F	0001	000094	1024F
0001	002192	1021F	0000	000056	1022F	0000	000091	1021F	0000	00033	1021F	0001	000095	1025F
0001	002193	1022F	0000	000057	1023F	0000	000092	1022F	0000	00034	1022F	0001	000096	1026F
0001	002194	1023F	0000	000058	1024F	0000	000093	1023F	0000	00035	1023F	0001	000097	1027F
0001	002195	1024F	0000	000059	1025F	0000	000094	1024F	0000	00036	1024F	0001	000098	1028F
0001	002196	1025F	0000	000060	1026F	0000	000095	1025F	0000	00037	1025F	0001	000099	1029F
0001	002197	1026F	0000	000061	1027F	0000	000096	10						

0000 I 000017 JUST
0000 I 000034 CD
0000 R 000000 SORT
0000 R 000005 X
0000 R 000017 TBLF

0000 I 000015 K
0000 R 000010 RAD
0010 R 000000 TBLF
0000 R 000000 TBLF
0000 R 000000 TBLF

0000 I 000015 K
0000 R 000010 RAD
0010 R 000000 TBLF
0000 R 000000 TBLF
0000 R 000000 TBLF

0000 I 000017 JUST
0000 I 000034 CD
0000 R 000000 SORT
0000 R 000005 X
0000 R 000017 TBLF

0000 I 000017 JUST
0000 I 000034 CD
0000 R 000000 SORT
0000 R 000005 X
0000 R 000017 TBLF

0000 I 000017 JUST
0000 I 000034 CD
0000 R 000000 SORT
0000 R 000005 X
0000 R 000017 TBLF

0000 I 000017 JUST
0000 I 000034 CD
0000 R 000000 SORT
0000 R 000005 X
0000 R 000017 TBLF

0000 I 000017 JUST
0000 I 000034 CD
0000 R 000000 SORT
0000 R 000005 X
0000 R 000017 TBLF

00101 1. SUBROUTINE IMPEL(R2)
00102 2. IMPEL COMPUTES THE VELOCITY VECTORS SATISFYING RADIAL
00103 3. EQUILIBRIUM ALONG AN IMPELLER NORMAL STATION
00104 4. C
00105 5. C
00106 6. C
00107 7. C
00108 8. C
00109 9. C
00110 10. C
00111 11. C
00112 12. C
00113 13. C
00114 14. C
00115 15. C
00116 16. C
00117 17. C
00118 18. C
00119 19. C
00120 20. C
00121 21. C
00122 22. C
00123 23. C
00124 24. C
00125 25. C
00126 26. C
00127 27. C
00128 28. C
00129 29. C
00130 30. C
00131 31. C
00132 32. C
00133 33. C
00134 34. C
00135 35. C
00136 36. C
00137 37. C
00138 38. C
00139 39. C
00140 40. C
00141 41. C
00142 42. C
00143 43. C
00144 44. C
00145 45. C
00146 46. C
00147 47. C
00148 48. C
00149 49. C
00150 50. C

00151 51. C
00152 52. C
00153 53. C
00154 54. C
00155 55. C
00156 56. C
00157 57. C
00158 58. C
00159 59. C
00160 60. C
00161 61. C
00162 62. C
00163 63. C
00164 64. C
00165 65. C
00166 66. C
00167 67. C
00168 68. C
00169 69. C
00170 70. C
00171 71. C
00172 72. C
00173 73. C
00174 74. C
00175 75. C
00176 76. C
00177 77. C
00178 78. C
00179 79. C
00180 80. C
00181 81. C
00182 82. C
00183 83. C
00184 84. C
00185 85. C
00186 86. C
00187 87. C
00188 88. C
00189 89. C
00190 90. C
00191 91. C
00192 92. C
00193 93. C
00194 94. C
00195 95. C
00196 96. C
00197 97. C
00198 98. C
00199 99. C
00200 100. C

```

00157 A(12)=SORT((A(16)+2+A(17)+2)/2.0)
00160 A(13)=SORT((A(17)+2+A(18)+2)/2.0)
00163 A(14)=SORT((A(18)+2+A(19)+2)/2.0)
00166 A(15)=SORT((A(19)+2+A(20)+2)/2.0)
00169 U 3
00172 A(20)=3.14159*(20)/360.
00175 DO 5 K=1,20
00178 A(K)=A(20)+A(K-5)
00181 CONTINUE
00184 K3
00187 DO 13 K=1,65
00190 A(K)=A(K-50)+V(11)/COS(V(4)+.01743295)/15.0
00193 CONTINUE
00196 M Y 3
00199 DO 3 K=1,25
00202 A(203)=TABLE(1,C(K-5))
00205 A(K)=A(203)+A(K-5)/223.77+2*(1.0-(C(K-20)/A(K-10))**2)
00208 CONTINUE
00211 T Y 3 AND P R 3
00214 DO 6 K=1,30
00217 A(K)=A(203)+A(K-5)
00220 A(K)=TABLE(2,A(K))
00223 CONTINUE
00226 P Y 3
00229 DO 5 K=30,60
00232 A(K)=A(K-20)+V(2-2)*A(K-5)/TABLE(8+C(K-20))
00235 CONTINUE
00238 Z
00241 DO 6 K=1,65
00244 A(K)=V(6)-(A(K-30)-V(11))*TAN(V(4)+.01743295)
00247 CONTINUE
00250 SLIP DETERMINATION
00253 V(4)=1 BEFORE SLIP =2 AT SLIP =3 AFTER SLIP
00256 SLIP=V(5)
00259 CONTINUE
00262 BUILD GA/DZ TABLES
00265 J=FIX(V(10))+900
00268 IF(K2-67.2) 80 TO 801
00271 DO 7 K=801,J
00274 A(K)=LOC(K-900.5)
00277 A(K)=50)*TAN(TABLE(12+A(K))*RAD)/RADIUS(K-900.5)/
00280 *COS(8*PI*(K-900))
00283 CONTINUE
00286 CONTINUE
00289 D ALPHA/DZ
00292 DO 9 K=84,90
00295 A(K)=TAN(1401)*A(951)+J-900.3*A(K-5),1E)
00298
00251 50.
00252 51.
00253 52.
00254 53.
00255 54.
00256 55.
00257 56.
00258 57.
00259 58.
00260 59.
00261 60.
00262 61.
00263 62.
00264 63.
00265 64.
00266 65.
00267 66.
00268 67.
00269 68.
00270 69.
00271 70.
00272 71.
00273 72.
00274 73.
00275 74.
00276 75.
00277 76.
00278 77.
00279 78.
00280 79.
00281 80.
00282 81.
00283 82.
00284 83.
00285 84.
00286 85.
00287 86.
00288 87.
00289 88.
00290 89.
00291 90.
00292 91.
00293 92.
00294 93.
00295 94.
00296 95.
00297 96.
00298 97.
00299 98.
00300 99.
00301 100.
00302 101.
00303 102.
00304 103.
00305 104.
00306 105.
00307 106.
00308 107.

```

2496C102
2496C104
2496C106
2496C108
2496C110
2496C112
2496C114
2496C116
2496C118
2496C120
2496C122
2496C124
2496C126
2496C128
2496C130
2496C132
2496C134
2496C136
2496C138
2496C140
2496C142
2496C144
2496C146
2496C148
2496C150
2496C152
2496C154
2496C156
2496C158
2496C160
2496C162
2496C164
2496C166
2496C168
2496C170
2496C172
2496C174
2496C176
2496C178
2496C180
2496C182
2496C184
2496C186
2496C188
2496C190
2496C192
2496C194
2496C196
2496C198
2496C200
2496C202
2496C204
2496C206
2496C208
2496C210
2496C212
2496C214
2496C216
2496C218

```

00233 109.  GO TO (0.103,103),1E
00234 109.  CONTINUE
00235 110.  WRITE(6,1001)M2
00236 111.  WRITE(6,1001)(A(10),10E1,999)
00237 112.  RETURN
00238 113.  CONTINUE
00239 114.  C
00240 115.  TAN BETA
00241 116.  DO 9 K=5,99
00242 117.  A(K)=A(K-49)*A(K-9)
00243 118.  CONTINUE
00244 119.  C
00245 120.  ALPHA 3
00246 121.  DO 10 K=50,60
00247 122.  A(K)=A(K-5)*COS(V(41)*.017453293)/.017453293
00248 123.  A(K-55)=A(K)
00249 124.  CONTINUE
00250 125.  10
00251 126.  GO TO (104,101,102),SLIP
00252 127.  C
00253 128.  AT SLIP
00254 129.  ALPHA 3
00255 130.  CONTINUE
00256 131.  DO 11 K=50,60
00257 132.  A(K)=0.
00258 133.  CONTINUE
00259 134.  11
00260 135.  GO TO 104
00261 136.  C
00262 137.  AFTER SLIP
00263 138.  ALPHA 3
00264 139.  CONTINUE
00265 140.  IF(I(1)IV(101),E0,X3) GO TO 4002
00266 141.  DO 12 K=50,60
00267 142.  A(K)=A(K-5)*VAL(9.1*(K-5)*12.,*1E)
00268 143.  CONTINUE
00269 144.  12
00270 145.  GO TO 104
00271 146.  C
00272 147.  CONTINUE
00273 148.  DO 1003 K=50,60
00274 149.  A(K)=A(K-5)*1200./XRC(13,E2)
00275 150.  CONTINUE
00276 151.  1003
00277 152.  C
00278 153.  A(K)=0
00279 154.  DO 14 K=50,70
00280 155.  A(K)=A(K-30)*A(K-150)*COS(A(K-10)*.017453293)/(C(K-45)*S(45))
00281 156.  CONTINUE
00282 157.  14
00283 158.  C
00284 159.  INVOY2
00285 160.  DO 1610 K=50,70
00286 161.  IF(A(K).LT.1.5001) INVOY2
00287 162.  CONTINUE
00288 163.  IF(INVOY.LT.1) GO TO 318
00289 164.  IF(JUST-8E,20) GO TO 3000
00290 165.  IF(JUST-8E,11) TIME=TIME+1
00291 166.  IF(ABS(A(101)/A(17)*A(180)/A(169)*A(170))/5.
00292 167.  IF(ABS(A(101)/A(17)*A(180)/A(169)*A(170))/5.
00293 168.  DO 2010 17,21,23
00294 169.  2010

```

103


```
00510 225. 18 CONTINUEZ 2996C450
00511 226. C V3 2996C452
00512 227. C DO 19 K=101,105 2996C454
00513 228. A(K)=A(K-5)*A(K-5) 2996C456
00514 229. CONTINUE 2996C458
00515 230. C 2996C460
00516 231. C V3 2996C462
00517 232. DO 20 K=106,110 2996C464
00518 233. A(K)=A(K-5)*COS(A(K-5)*.017453293) 2996C466
00519 234. CONTINUE 2996C468
00520 235. C 2996C470
00521 236. C V3 2996C472
00522 237. DO 21 K=111,115 2996C474
00523 238. A(K)=A(K-5)*SIN(A(K-5)*.017453293) 2996C476
00524 239. CONTINUE 2996C478
00525 240. C 2996C480
00526 241. C V3 2996C482
00527 242. DO 22 K=116,120 2996C484
00528 243. A(K)=A(K-10)*A(K-5) 2996C486
00529 244. CONTINUE 2996C488
00530 245. C 2996C490
00531 246. C ALPHA 2996C492
00532 247. DO 23 K=121,125 2996C494
00533 248. A(K)=ATAN2(A(K-5),A(K-15))/(.017453293) 2996C496
00534 249. CONTINUE 2996C498
00535 250. C 2996C500
00536 251. C V4 2996C502
00537 252. DO 24 K=126,130 2996C504
00538 253. A(K)=A(K-20)/COS(A(K-5)*.017453293) 2996C506
00539 254. CONTINUE 2996C508
00540 255. C 2996C510
00541 256. C V4 2996C512
00542 257. DO 25 K=131,135 2996C514
00543 258. A(K)=A(K-5)/A(K-35) 2996C516
00544 259. CONTINUE 2996C518
00545 260. C 2996C520
00546 261. C ASSUME K 2996C522
00547 262. A(12)=1.4 2996C524
00548 263. DO 26 K=136,140 2996C526
00549 264. TT/TS 2996C528
00550 265. C 2996C530
00551 266. C A(K)=1.0*(A(12)-1.0)/(2.0*A(K-5)*.2 2996C532
00552 267. C 2996C534
00553 268. C A(K)=A(K)*A(K)*A(12)/(A(12)-1.0) 2996C536
00554 269. C 2996C538
00555 270. C A(K)=1.0*(1.0/A(K-5))*((2.0/(A(12)+1.0))*A(K))*((A(12)+1.0)/(2.0 2996C540
00556 271. C 2996C542
00557 272. C 2996C544
00558 273. C 2996C546
00559 274. C 2996C548
00560 275. C 2996C550
00561 276. C 2996C552
00562 277. C 2996C554
00563 278. C 2996C556
00564 279. C 2996C558
00565 280. C 2996C560
00566 281. C 2996C562
00567 282. C 2996C564
```

```
00610 282. C      XTA PRK
00611 283. C      DO 29 K=161,165
00612 284. C      A(K)=TABLE(1,A(K-5))
00613 285. C      A(K+5)=TABLE(2,A(K-5))
00614 286. C      CONTINUE
00615 287. C      29
00616 288. C
00617 289. C      DELTA VT
00618 290. C
00619 291. C      DO 30 K=171, 175
00620 292. C      A(K)=C*(K-160)-A(K-60)
00621 293. C      CONTINUE
00622 294. C      30
00623 295. C
00624 296. C      FN
00625 297. C      DO 32 K=176, 180
00626 298. C      A(K) = A(K-75)*SIN(X(K-175)*RAD)+TAN(Y(K)*RAD)* SIN(V(K)*RAD)*
00627 299. C      1/(2*A(213)-12*A(K-75)*SIN(X(K-175)*RAD)/A(K-165)) +
00628 300. C      2A(K-5)/V(7)/SIN(V(K)*RAD))
00629 301. C      CONTINUE
00630 302. C      32
00631 303. C      RADIUS OF CURVATURE
00632 304. C      DO 33 K=181, 185
00633 305. C      A(K)=(YRC(3,K2)-YRC(1,K2))/(XRC(3,K2)-XRC(1,K2))*(A(K-120)*12,
00634 306. C      *-XRC(1,K2))*YRC(1,K2))/12.
00635 307. C      CONTINUE
00636 308. C      33
00637 309. C      RHO 5
00638 310. C      DO 34 K=186, 190
00639 311. C      A(K) = A(K-100)/(32.2*53.342*A(K-95))
00640 312. C      CONTINUE
00641 313. C      34
00642 314. C      CP/DN
00643 315. C      DO 35 K=191, 195
00644 316. C      A(K) = A(K-5)*A(K-75)*2*OS(V(K)*.017453293)*12.0*(A(K-180)-A(K-
00645 317. C      15)*2/A(K-10)-A(K-15))
00646 318. C      CONTINUE
00647 319. C      35
00648 320. C      P 5 3 PRIME
00649 321. C      A(198) = A(88)
00650 322. C      A(197) = A(88)-(A(63)-A(62))*A(193)/A(192)/2.0
00651 323. C      A(196) = A(197)-(A(62)-A(61))*A(192)/A(191)/2.0
00652 324. C      A(195) = A(60)*(A(63)-A(62))*A(193)/A(194)/2.0
00653 325. C      A(200) = A(199)*(A(65)-A(64))*A(195)/A(194)/2.0
00654 326. C      DO 39 K=196, 200
00655 327. C      IF(ABS(A(K)-A(K-110)))/A(K-110)*.002139,39,121
00656 328. C      CONTINUE
00657 329. C      39
00658 330. C
00659 331. C      GO TO 120
00660 332. C
00661 333. C      121
00662 334. C      CONTINUE
00663 335. C      A(220)=A(220)+1.0
00664 336. C      IF(A(220)-20.0) 128,128,129
00665 337. C      129
00666 338. C      CONTINUE
00667 339. C      WRITE(6,1004)(A(10),10=1,500)
00668 340. C
00669 341. C
00670 342. C
00671 343. C
00672 344. C
00673 345. C
00674 346. C
00675 347. C
00676 348. C
00677 349. C
00678 350. C
00679 351. C
00680 352. C
00681 353. C
00682 354. C
00683 355. C
00684 356. C
00685 357. C
00686 358. C
00687 359. C
00688 360. C
00689 361. C
00690 362. C
00691 363. C
00692 364. C
00693 365. C
00694 366. C
00695 367. C
00696 368. C
00697 369. C
00698 370. C
00699 371. C
00700 372. C
00701 373. C
00702 374. C
00703 375. C
00704 376. C
00705 377. C
00706 378. C
00707 379. C
00708 380. C
00709 381. C
00710 382. C
00711 383. C
00712 384. C
00713 385. C
00714 386. C
00715 387. C
00716 388. C
00717 389. C
00718 390. C
00719 391. C
00720 392. C
00721 393. C
00722 394. C
00723 395. C
00724 396. C
00725 397. C
00726 398. C
00727 399. C
00728 400. C
00729 401. C
00730 402. C
00731 403. C
00732 404. C
00733 405. C
00734 406. C
00735 407. C
00736 408. C
00737 409. C
00738 410. C
00739 411. C
00740 412. C
00741 413. C
00742 414. C
00743 415. C
00744 416. C
00745 417. C
00746 418. C
00747 419. C
00748 420. C
00749 421. C
00750 422. C
00751 423. C
00752 424. C
00753 425. C
00754 426. C
00755 427. C
00756 428. C
00757 429. C
00758 430. C
00759 431. C
00760 432. C
00761 433. C
00762 434. C
00763 435. C
00764 436. C
00765 437. C
00766 438. C
00767 439. C
00768 440. C
00769 441. C
00770 442. C
00771 443. C
00772 444. C
00773 445. C
00774 446. C
00775 447. C
00776 448. C
00777 449. C
00778 450. C
00779 451. C
00780 452. C
00781 453. C
00782 454. C
00783 455. C
00784 456. C
00785 457. C
00786 458. C
00787 459. C
00788 460. C
00789 461. C
00790 462. C
00791 463. C
00792 464. C
00793 465. C
00794 466. C
00795 467. C
00796 468. C
00797 469. C
00798 470. C
00799 471. C
00800 472. C
00801 473. C
00802 474. C
00803 475. C
00804 476. C
00805 477. C
00806 478. C
00807 479. C
00808 480. C
00809 481. C
00810 482. C
00811 483. C
00812 484. C
00813 485. C
00814 486. C
00815 487. C
00816 488. C
00817 489. C
00818 490. C
00819 491. C
00820 492. C
00821 493. C
00822 494. C
00823 495. C
00824 496. C
00825 497. C
00826 498. C
00827 499. C
00828 500. C
00829 501. C
00830 502. C
00831 503. C
00832 504. C
00833 505. C
00834 506. C
00835 507. C
00836 508. C
00837 509. C
00838 510. C
00839 511. C
00840 512. C
00841 513. C
00842 514. C
00843 515. C
00844 516. C
00845 517. C
00846 518. C
00847 519. C
00848 520. C
00849 521. C
00850 522. C
00851 523. C
00852 524. C
00853 525. C
00854 526. C
00855 527. C
00856 528. C
00857 529. C
00858 530. C
00859 531. C
00860 532. C
00861 533. C
00862 534. C
00863 535. C
00864 536. C
00865 537. C
00866 538. C
00867 539. C
00868 540. C
00869 541. C
00870 542. C
00871 543. C
00872 544. C
00873 545. C
00874 546. C
00875 547. C
00876 548. C
00877 549. C
00878 550. C
00879 551. C
00880 552. C
00881 553. C
00882 554. C
00883 555. C
00884 556. C
00885 557. C
00886 558. C
00887 559. C
00888 560. C
00889 561. C
00890 562. C
00891 563. C
00892 564. C
00893 565. C
00894 566. C
00895 567. C
00896 568. C
00897 569. C
00898 570. C
00899 571. C
00900 572. C
00901 573. C
00902 574. C
00903 575. C
00904 576. C
00905 577. C
00906 578. C
00907 579. C
00908 580. C
00909 581. C
00910 582. C
00911 583. C
00912 584. C
00913 585. C
00914 586. C
00915 587. C
00916 588. C
00917 589. C
00918 590. C
00919 591. C
00920 592. C
00921 593. C
00922 594. C
00923 595. C
00924 596. C
00925 597. C
00926 598. C
00927 599. C
00928 600. C
00929 601. C
00930 602. C
00931 603. C
00932 604. C
00933 605. C
00934 606. C
00935 607. C
00936 608. C
00937 609. C
00938 610. C
00939 611. C
00940 612. C
00941 613. C
00942 614. C
00943 615. C
00944 616. C
00945 617. C
00946 618. C
00947 619. C
00948 620. C
00949 621. C
00950 622. C
00951 623. C
00952 624. C
00953 625. C
00954 626. C
00955 627. C
00956 628. C
00957 629. C
00958 630. C
00959 631. C
00960 632. C
00961 633. C
00962 634. C
00963 635. C
00964 636. C
00965 637. C
00966 638. C
00967 639. C
00968 640. C
00969 641. C
00970 642. C
00971 643. C
00972 644. C
00973 645. C
00974 646. C
00975 647. C
00976 648. C
00977 649. C
00978 650. C
00979 651. C
00980 652. C
00981 653. C
00982 654. C
00983 655. C
00984 656. C
00985 657. C
00986 658. C
00987 659. C
00988 660. C
00989 661. C
00990 662. C
00991 663. C
00992 664. C
00993 665. C
00994 666. C
00995 667. C
00996 668. C
00997 669. C
00998 670. C
00999 671. C
01000 672. C
01001 673. C
01002 674. C
01003 675. C
01004 676. C
01005 677. C
01006 678. C
01007 679. C
01008 680. C
01009 681. C
01010 682. C
01011 683. C
01012 684. C
01013 685. C
01014 686. C
01015 687. C
01016 688. C
01017 689. C
01018 690. C
01019 691. C
01020 692. C
01021 693. C
01022 694. C
01023 695. C
01024 696. C
01025 697. C
01026 698. C
01027 699. C
01028 700. C
01029 701. C
01030 702. C
01031 703. C
01032 704. C
01033 705. C
01034 706. C
01035 707. C
01036 708. C
01037 709. C
01038 710. C
01039 711. C
01040 712. C
01041 713. C
01042 714. C
01043 715. C
01044 716. C
01045 717. C
01046 718. C
01047 719. C
01048 720. C
01049 721. C
01050 722. C
01051 723. C
01052 724. C
01053 725. C
01054 726. C
01055 727. C
01056 728. C
01057 729. C
01058 730. C
01059 731. C
01060 732. C
01061 733. C
01062 734. C
01063 735. C
01064 736. C
01065 737. C
01066 738. C
01067 739. C
01068 740. C
01069 741. C
01070 742. C
01071 743. C
01072 744. C
01073 745. C
01074 746. C
01075 747. C
01076 748. C
01077 749. C
01078 750. C
01079 751. C
01080 752. C
01081 753. C
01082 754. C
01083 755. C
01084 756. C
01085 757. C
01086 758. C
01087 759. C
01088 760. C
01089 761. C
01090 762. C
01091 763. C
01092 764. C
01093 765. C
01094 766. C
01095 767. C
01096 768. C
01097 769. C
01098 770. C
01099 771. C
01100 772. C
01101 773. C
01102 774. C
01103 775. C
01104 776. C
01105 777. C
01106 778. C
01107 779. C
01108 780. C
01109 781. C
01110 782. C
01111 783. C
01112 784. C
01113 785. C
01114 786. C
01115 787. C
01116 788. C
01117 789. C
01118 790. C
01119 791. C
01120 792. C
01121 793. C
01122 794. C
01123 795. C
01124 796. C
01125 797. C
01126 798. C
01127 799. C
01128 800. C
01129 801. C
01130 802. C
01131 803. C
01132 804. C
01133 805. C
01134 806. C
01135 807. C
01136 808. C
01137 809. C
01138 810. C
01139 811. C
01140 812. C
01141 813. C
01142 814. C
01143 815. C
01144 816. C
01145 817. C
01146 818. C
01147 819. C
01148 820. C
01149 821. C
01150 822. C
01151 823. C
01152 824. C
01153 825. C
01154 826. C
01155 827. C
01156 828. C
01157 829. C
01158 830. C
01159 831. C
01160 832. C
01161 833. C
01162 834. C
01163 835. C
01164 836. C
01165 837. C
01166 838. C
01167 839. C
01168 840. C
01169 841. C
01170 842. C
01171 843. C
01172 844. C
01173 845. C
01174 846. C
01175 847. C
01176 848. C
01177 849. C
01178 850. C
01179 851. C
01180 852. C
01181 853. C
01182 854. C
01183 855. C
01184 856. C
01185 857. C
01186 858. C
01187 859. C
01188 860. C
01189 861. C
01190 862. C
01191 863. C
01192 864. C
01193 865. C
01194 866. C
01195 867. C
01196 868. C
01197 869. C
01198 870. C
01199 871. C
01200 872. C
01201 873. C
01202 874. C
01203 875. C
01204 876. C
01205 877. C
01206 878. C
01207 879. C
01208 880. C
01209 881. C
01210 882. C
01211 883. C
01212 884. C
01213 885. C
01214 886. C
01215 887. C
01216 888. C
01217 889. C
01218 890. C
01219 891. C
01220 892. C
01221 893. C
01222 894. C
01223 895. C
01224 896. C
01225 897. C
01226 898. C
01227 899. C
01228 900. C
01229 901. C
01230 902. C
01231 903. C
01232 904. C
01233 905. C
01234 906. C
01235 907. C
01236 908. C
01237 909. C
01238 910. C
01239 911. C
01240 912. C
01241 913. C
01242 914. C
01243 915. C
01244 916. C
01245 917. C
01246 918. C
01247 919. C
01248 920. C
01249 921. C
01250 922. C
01251 923. C
01252 924. C
01253 925. C
01254 926. C
01255 927. C
01256 928. C
01257 929. C
01258 930. C
01259 931. C
01260 932. C
01261 933. C
01262 934. C
01263 935. C
01264 936. C
01265 937. C
01266 938. C
01267 939. C
01268 940. C
01269 941. C
01270 942. C
01271 943. C
01272 944. C
01273 945. C
01274 946. C
01275 947. C
01276 948. C
01277 949. C
01278 950. C
01279 951. C
01280 952. C
01281 953. C
01282 954. C
01283 955. C
01284 956. C
01285 957. C
01286 958. C
01287 959. C
01288 960. C
01289 961. C
01290 962. C
01291 963. C
01292 964. C
01293 965. C
01294 966. C
01295 967. C
01296 968. C
01297 969. C
01298 970. C
01299 971. C
01300 972. C
01301 973. C
01302 974. C
01303 975. C
01304 976. C
01305 977. C
01306 978. C
01307 979. C
01308 980. C
01309 981. C
01310 982. C
01311 983. C
01312 984. C
01313 985. C
01314 986. C
01315 987. C
01316 988. C
01317 989. C
01318 990. C
01319 991. C
01320 992. C
01321 993. C
01322 994. C
01323 995. C
01324 996. C
01325 997. C
01326 998. C
01327 999. C
01328 1000. C
01329 1001. C
01330 1002. C
01331 1003. C
01332 1004. C
01333 1005. C
01334 1006. C
01335 1007. C
01336 1008. C
01337 1009. C
01338 1010. C
01339 1011. C
01340 1012. C
01341 1013. C
01342 1014. C
01343 1015. C
01344 1016. C
01345 1017. C
01346 1018. C
01347 1019. C
01348 1020. C
01349 1021. C
01350 1022. C
01351 1023. C
01352 1024. C
01353 1025. C
01354 1026. C
01355 1027. C
01356 1028. C
01357 1029. C
01358 1030. C
01359 1031. C
01360 1032. C
01361 1033. C
01362 1034. C
01363 1035. C
01364 1036. C
01365 1037. C
01366 1038. C
01367 1039. C
01368 1040. C
01369 1041. C
01370 1042. C
01371 1043. C
01372 1044. C
01373 1045. C
01374 1046. C
01375 1047. C
01376 1048. C
01377 1049. C
01378 1050. C
01379 1051. C
01380 1052. C
01381 1053. C
01382 1054. C
01383 1055. C
01384 1056. C
01385 1057. C
01386 1058. C
01387 1059. C
01388 1060. C
01389 1061. C
01390 1062. C
01391 1063. C
01392 1064. C
01393 1065. C
01394 1066. C
01395 1067. C
01396 1068. C
01397 1069. C
01398 1070. C
01399 1071. C
01400 1072. C
01401 1073. C
01402 1074. C
01403 1075. C
01404 1076. C
01405 1077. C
01406 1078. C
01407 1079. C
01408 1080. C
01409 1081. C
01410 1082. C
01411 1083. C
01412 1084. C
01413 1085. C
01414 1086. C
01415 1087. C
01416 1088. C
01417 1089. C
01418 1090. C
01419 1091. C
01420 1092. C
01421 1093. C
01422 1094. C
01423 1095. C
01424 1096. C
01425 1097. C
01426 1098. C
01427 1099. C
01428 1100. C
01429 1101. C
01430 1102. C
01431 1103. C
01432 1104. C
01433 1105. C
01434 1106. C
01435 1107. C
01436 1108. C
01437 1109. C
01438 1110. C
01439 1111. C
01440 1112. C
01441 1113. C
01442 1114. C
01443 1115. C
01444 1116. C
01445 1117. C
01446 1118. C
01447 1119. C
01448 1120. C
01449 1121. C
01450 1122. C
01451 1123. C
01452 1124. C
01453 1125. C
01454 1126. C
01455 1127. C
01456 1128. C
01457 1129. C
01458 1130. C
01459 1131. C
01460 1132. C
01461 1133. C
01462 1134. C
01463 1135. C
01464 1136. C
01465 1137. C
01466 1138. C
01467 1139. C
01468 1140. C
01469 1141. C
01470 1142. C
01471 1143. C
01472 1144. C
01473 1145. C
01474 1146. C
01475 1147. C
01476 1148. C
01477 1149. C
01478 1150. C
01479 1151. C
01480 1152. C
01481 1153. C
01482 1154. C
01483 1155. C
01484 1156. C
01485 1157. C
01486 1158. C
01487 1159. C
01488 1160. C
01489 1161. C
01490 1162. C
01491 1163. C
01492 1164. C
01493 1165. C
01494 1166. C
01495 1167. C
01496 1168. C
01497 1169. C
01498 1170. C
01499 1171. C
01500 1172. C
01501 1173. C
01502 1174. C
01503 1175. C
01504 1176. C
01505 1177. C
01506 1178. C
01507 1179. C
01508 1180. C
01509 1181. C
01510 1182. C
01511 1183. C
01512 1184. C
01513 1185. C
01514 1186. C
01515 1187. C
01516 1188. C
01517 1189. C
01518 1190. C
01519 1191. C
01520 1192. C
01521 1193. C
01522 1194. C
01523 1195. C
01524 1196. C
01525 1197. C
01526 1198. C
01527 1199. C
01528 1200. C
01529 1201. C
01530 1202. C
01531 1203. C
01532 1204. C
01533 1205. C
01534 1206. C
01535 1207. C
01536 1208. C
01537 1209. C
01538 1210. C
01539 1211. C
01540 1212. C
01541 1213. C
01542 1214. C
01543 1215. C
01544 1216. C
01545 1217. C
01546 1218. C
01547 1219. C
01548 1220. C
01549 1221. C
01550 1222. C
01551 1223. C
01552 1224. C
01553 12
```

```

00714 380. 11TIME=-1
00715 381. 60 TO 120
00716 382. 12R CONTINUE
00717 383. C
00718 384. C PT3/PS3 PRIVE
00719 385. C
00720 386. 125 CONTINUE
00721 387. JG60=0
00722 388. JG60=JG60+1
00723 389. IF JG60.EQ.300)60 TO 1000
00724 390. DO 36 K=226, 230
00725 391. AIK) = AIK-190/A(K-30)
00726 392. IF (AIK)-1.) 357, 357, 36
00727 393. 357 DO 359 J=196, 200
00728 394. AIJ) = AIJ) -.5
00729 395. 359 CONTINUE
00730 396. 80 TO 125
00731 397. 36 CONTINUE
00732 398. C
00733 399. DO 37 K=231, 235
00734 400. P PRIME = SQR((AIK-5)+((A(212)-1.0)/A(212))-.2-.6)/(A(212)-1.0))
00735 401. A(210) = SQR((AIK-5)+((A(212)-1.0)/A(212))-.2-.6)/(A(212)-1.0))
00736 402. A/ASTAR PRIME (K+10.1))+(2.0/(A(212)+1.0)+1.0/(A(212)-1.0)).2.0*
00737 403. 1/(K+1.1)+.2)*((A(212)+1.0)/2.0/(A(212)-1.0))
00738 404. 37 CONTINUE
00739 405. C
00740 406. C ANN PRIME
00741 407. DO 38 K=236, 240
00742 408. AIK) = AIK-5/A(K-170)*A(K+20)
00743 409. 38 CONTINUE
00744 410. AI(218) = A(236)*A(237)+A(238)+A(239)+A(240)
00745 411. C
00746 412. C ANNULUS AREA COMPARISON
00747 413. IF (ABS(A(218)-A(219)))/A(219)=-.003)122,122,123
00748 414. 123 CONTINUE
00749 415. CONST = -.020*(190)/A(218)-A(219)/A(219)
00750 416. DO 41 K=196, 200
00751 417. AIK)=AIK)+CONST
00752 418. 41 CONTINUE
00753 419. 80 TO 125
00754 420. C
00755 421. 122 DO 43 K=1, 5
00756 422. AIK+255) = A(K+235)*A(219)/A(218)
00757 423. 43 CONTINUE
00758 424. C
00759 425. DO 46 K=261, 265
00760 426. AIK) = AIK-65
00761 427. 46 CONTINUE
00762 428. 80 TO 127
00763 429. C
00764 430. 120 CONTINUE
00765 431. IF (IFIX(A(201).EQ.11TIME) 60 TO 125
00766 432. ACCELERATION=A N,TOT
00767 433. DO 131 K=318,320
00768 434. AIK)=12.*AIK-200)*.02+COS(V(N)*RAD)/(A(K-305)-AIK-210)*.02/A(K-135)
00769 435. 131 CONTINUE
00770 436. C
00771 437. 200 RETURN
00772 438.
00773 439.
00774 440.
00775 441.
00776 442.
00777 443.
00778 444.
00779 445.
00780 446.
00781 447.
00782 448.
00783 449.
00784 450.
00785 451.
00786 452.
00787 453.
00788 454.
00789 455.
00790 456.
00791 457.
00792 458.
00793 459.
00794 460.
00795 461.
00796 462.
00797 463.
00798 464.
00799 465.
00800 466.
00801 467.
00802 468.
00803 469.
00804 470.
00805 471.
00806 472.
00807 473.
00808 474.
00809 475.
00810 476.
00811 477.
00812 478.
00813 479.
00814 480.
00815 481.
00816 482.
00817 483.
00818 484.
00819 485.
00820 486.
00821 487.
00822 488.
00823 489.
00824 490.
00825 491.
00826 492.
00827 493.
00828 494.
00829 495.
00830 496.
00831 497.
00832 498.
00833 499.
00834 500.
00835 501.
00836 502.
00837 503.
00838 504.
00839 505.
00840 506.
00841 507.
00842 508.
00843 509.
00844 510.
00845 511.
00846 512.
00847 513.
00848 514.
00849 515.
00850 516.
00851 517.
00852 518.
00853 519.
00854 520.
00855 521.
00856 522.
00857 523.
00858 524.
00859 525.
00860 526.
00861 527.
00862 528.
00863 529.
00864 530.
00865 531.
00866 532.
00867 533.
00868 534.
00869 535.
00870 536.
00871 537.
00872 538.
00873 539.
00874 540.
00875 541.
00876 542.
00877 543.
00878 544.
00879 545.
00880 546.
00881 547.
00882 548.
00883 549.
00884 550.
00885 551.
00886 552.
00887 553.
00888 554.
00889 555.
00890 556.
00891 557.
00892 558.
00893 559.
00894 560.
00895 561.
00896 562.
00897 563.
00898 564.
00899 565.
00900 566.
00901 567.
00902 568.
00903 569.
00904 570.
00905 571.
00906 572.
00907 573.
00908 574.
00909 575.
00910 576.
00911 577.
00912 578.
00913 579.
00914 580.
00915 581.
00916 582.
00917 583.
00918 584.
00919 585.
00920 586.
00921 587.
00922 588.
00923 589.
00924 590.
00925 591.
00926 592.
00927 593.
00928 594.
00929 595.
00930 596.
00931 597.
00932 598.
00933 599.
00934 600.
00935 601.
00936 602.
00937 603.
00938 604.
00939 605.
00940 606.
00941 607.
00942 608.
00943 609.
00944 610.
00945 611.
00946 612.
00947 613.
00948 614.
00949 615.
00950 616.
00951 617.
00952 618.
00953 619.
00954 620.
00955 621.
00956 622.
00957 623.
00958 624.
00959 625.
00960 626.
00961 627.
00962 628.
00963 629.
00964 630.
00965 631.
00966 632.
00967 633.
00968 634.
00969 635.
00970 636.
00971 637.
00972 638.
00973 639.
00974 640.
00975 641.
00976 642.
00977 643.
00978 644.
00979 645.
00980 646.
00981 647.
00982 648.
00983 649.
00984 650.
00985 651.
00986 652.
00987 653.
00988 654.
00989 655.
00990 656.
00991 657.
00992 658.
00993 659.
00994 660.
00995 661.
00996 662.
00997 663.
00998 664.
00999 665.

```

```
01025 398. 1000 CONTINUE 2496C748
01026 399. WRITE(6,1005)K2 2496C800
01031 400. WRITE(6,1004)(A(IQ),IC=1,500) 2496C802
01037 401. GO TO 120 2496C804
01040 402. 3000 CONTINUE 2496C806
01041 403. KD=K-70 2496C808
01042 404. WRITE(6,1002)KD,K2 2496C810
01046 405. WRITE(6,1004)(A(IQ),IC=1,500) 2496C812
01054 406. RETURN 2496C814
01054 407. C 2496C816
01055 408. 1001 FORMAT(10H,8HTHE TABLE LOOKUP ON 04/07 HAS FAILED FOR STATION,13) 2496C818
01056 409. 1002 FORMAT(10H,8HTAT STREAMLINE,13,9H, STATION,13,29H, A/A STAR FAILED FOR STATION,13,29H, 2496C820
01057 410. * TO CONVERGE 2496C822
01057 411. 1003 FORMAT(10H,31HK FAILED TO CONVERGE AT STATION,13) 2496C824
01057 412. 1004 FORMAT(15H,THE A APPRY IS,16X,10E11,41) 2496C826
01061 413. 1005 FORMAT(17H,PS3 PRIME ADJUSTMENT OF A ANN PRIME TOTAL FAILED TO CON 2496C828
01061 414. *VERSE AT STATION,13) 2496C830
01062 415. 1088 FORMAT(10H,10HAT STATION,13,29H PS3 PRIME FAILED TO CONVERGE) 2496C832
01063 416. ENQ 2496C834
```

END OF LISTING. 0 *DIAGNOSTIC* MESSAGE(S),
IMPEL CODE RELOCATABLE

10 AUG 66 00:13:31 1 00053674 36 1 (DELETED)
14 139 0 00053740 14 139

9 FOR CHORD 24690002
COMPILATION BY UNIVAC 1108 FORTRAN-IV DATED NOV. 23, 1965 F4008
THIS COMPILATION WAS DONE ON 19 AUG 66 AT 17:37:17

SUBROUTINE CHORD ENTRY POINT 000731

STORAGE USED (BLOCK, NAME, LENGTH)

0001 *CODE 001073
0000 *DATA 000165
0002 *BLANK 000000

EXTERNAL REFERENCES (BLOCK, NAME)

0003 TAB2
0004 SGR1
0005 ATAN
0006 TAN
0007 NWDUS
0010 NI01\$
0011 NI02\$

STORAGE ASSIGNMENT FOR VARIABLES (BLOCK, TYPE, RELATIVE LOCATION, NAME)

0000 000047 1000F 0000 000110 1001F 0001 000160 15L 0001 000621 2000L 0001 000272 25L
0001 000332 35L 0001 000334 40L 0001 000372 45L 0001 000403 50L 0001 000434 55L
0001 000571 60L 0001 000611 65L 0001 000632 66L 0001 000667 67L 0001 000680 68L
0000 R 000035 ANG 0000 R 000036 ANG 0005 R 000030 ATAN 0000 R 000032 CTAN 0001 R 000033 ANOC
0000 R 000034 GTAN 0000 R 000005 GUESS 0000 R 000010 GUESS 0000 R 000020 HSLOPE 0000 I 000011 IA
0000 I 000015 IB 0000 I 000017 IC 0000 I 000024 ID 0000 I 000026 IE 0000 I 000031 IF
0000 I 000043 IH 0000 I 000044 II 0000 I 000045 IJ 0000 I 000046 IK 0000 I 000006 INOX
0000 I 000007 JNOX 0000 R 000000 RDN 0000 R 000021 XMT 0003 R 000000 TAB2 0000 R 000000 TAN
0000 R 000027 TSLOPE 0000 R 000012 XMH 0000 R 000040 XO 0000 R 000013 XPH
0000 R 000022 XPT 0000 R 000037 XSLOPE 0000 R 000001 X1 0000 R 000003 X2 0000 R 000030 YHUB
0000 R 000014 YMH 0000 R 000023 YMT 0000 R 000041 YQ 0000 R 000016 YPH 0000 R 000042 YPP
0000 R 000025 YPT 0000 R 000002 Y1 0000 R 000004 Y2

00100 1. C HX(I) INDEPENDENT VARIABLE - HUB ARRAY -24690004
00100 2. C HY(I) INDEPENDENT VARIABLE - HUB ARRAY -24690006
00100 3. C TX(I) INDEPENDENT VARIABLE - TIP ARRAY -24690008
00100 4. C TY(I) INDEPENDENT VARIABLE - TIP ARRAY -24690010
00100 5. C XMH CURRENT HUB X-VALUE MINUS INCREMENT -24690012
00100 6. C XPH CURRENT HUB X-VALUE PLUS INCREMENT -24690014
00100 7. C YMH CURRENT HUB Y-VALUE MINUS INCREMENT -24690016
00100 8. C YPH CURRENT HUB Y-VALUE PLUS INCREMENT -24690018
00100 9. C NH NUMBER OF INDEPENDENT VARIABLES IN HUB ARRAY -24690020
00100 10. C NT NUMBER OF INDEPENDENT VARIABLES IN TIP ARRAY -24690022
00100 11. C XMT CURRENT TIP X-VALUE MINUS INCREMENT -24690024
00100 12. C XPT CURRENT TIP X-VALUE PLUS INCREMENT -24690026
00100 13. C YMT CURRENT TIP Y-VALUE MINUS INCREMENT -24690028

00100	14.	C	YPT	CURRENT TIP Y-VALUE PLUS INCREMENT	-24690030
00100	15.	C	GUESS	AN ESTIMATE OF THE X-TIP VALUE CORRESPONDING TO THE	-24690032
00100	16.	C		FIRST TABLE VALUE FOR X-HUB	-24690034
00100	17.	C	CTAN	TANGENT OF TANGENT LINE COMPUTED BY FORMULA	-24690036
00100	18.	C	TSLOPE	SLOPE OF TANGENT LINE AT A POINT ON TIP PROFILE	-24690038
00100	19.	C	HSLOPE	SLOPE OF TANGENT LINE AT A POINT ON HUB PROFILE	-24690040
00100	20.	C	GTAN	TANGENT OF ANGLE OF DESIRED LINE FROM POINTS	-24690042
00100	21.	C	ANGC	ARCTANGENT(CTAN)	-24690044
00100	22.	C	ANGG	ARCTANGENT(GTAN)	-24690046
00101	23.			SUBROUTINE CHORD(XHUB,GUESS,HX,HY,IX,IY,NH,NI,K,XTIP,YTIP,ANGANS)	24690048
00103	24.			DIMENSION HX(1),HY(1),TX(1),TY(1)	24690050
00104	25.			DATA RDN/57.29578/	24690052
00106	26.			DYDX(X1,Y1,X2,Y2)=(Y2-Y1)/(X2-X1)	24690054
00107	27.			GUESSX=GUESS	24690056
00110	28.			INDX=0	24690058
00111	29.			JNDX=0	24690060
00112	30.			GUESSY=TAB2(TX(1),TY(1),NT,K,GU/55,2.4)	24690062
00113	31.			XMH=XHUB-0.05	24690064
00114	32.			XPH=XHUB+0.05	24690066
00115	33.			YMH=TAB2(HX(1),HY(1),NH,K,XMH,IB)	24690068
00116	34.			YPH=TAB2(HX(1),HY(1),NH,K,XPH,IC)	24690070
00117	35.			HFSLOPE=DYDX(XMH,YMH,XPH,YPH)	24690072
00120	36.			IF (ABS(YMH-YPH),LT,1.0E-04)HSLOPE=0.0	24690074
00122	37.			XMT=GUESS-0.05	24690076
00123	38.			XPT=GUESS+0.05	24690078
00124	39.			YMT=TAB2(TX(1),TY(1),NT,K,XMT,ID)	24690080
00125	40.			YPT=TAB2(TX(1),TY(1),NT,K,XPT,IE)	24690082
00126	41.			TSLOPE=DYDX(XMT,YMT,XPT,IPT)	24690084
00127	42.			IF (ABS(YMT-YPT),LT,1.0E-04)TSLOPE=0.0	24690086
00131	43.			YHUB=TAB2(HX(1),HY(1),NH,K,XHUB,IG)	24690088
00132	44.			IF (ABS(TSLOPE)+ABS(HSLOPE),LT,0.001)GO TO 35	24690090
00134	45.			THE TEST FOR EQUALITY BETWEEN NON-INTEGERS MAY NOT BE MEANINGFUL.	24690092
00136	46.			IF (HSLOPE,GE,0.0.AND,TSLOPE,GE,0.0.OR,HSLOPE,LE,0.0.AND,TSLOPE,LE,	24690094
00140	47.			-0.0)GO TO 25	24690096
00140	48.			-30 CTANE=SQRT((1.0+HSLOPE**2)*(1.0+TSLOPE**2))-1.0+HSLOPE*TSLOPE)/(HS	24690098
00140	49.			-LOPE*TSLOPE)	24690100
00141	50.			ANGC=ATAN(CTAN)*RON	24690102
00142	51.			IF (CTAN,LT,0.0)ANGC=ANGC+180.0	24690104
00144	52.			GO TO 40	24690106
00145	53.			25 CTANE=SQRT((1.0+HSLOPE**2)*(1.0+TSLOPE**2))+1.0-HSLOPE*TSLOPE)/(H	24690108
00145	54.			-SLOPE*TSLOPE)	24690110
00146	55.			ANGC=ATAN(CTAN)*RON	24690112
00147	56.			IF (CTAN,LT,0.0)ANGC=ANGC+180.0	24690114
00151	57.			GO TO 40	24690116
00152	58.			35 ANGC=90.0	24690118
00153	59.			40 IF (ABS(XHUB-GUESS),LT,0.001)GO TO 45	24690120
00155	60.			GTAN=DYDX(XHUB,YHUB,GUESS,GUESSY)	24690122
00156	61.			ANGG=ATAN(GTAN)*RON	24690124
00157	62.			IF (GTAN,LT,0.0)ANGG=ANGG+180.0	24690126
00161	63.			GO TO 50	24690128
00162	64.			45 IF (ABS(ANGC-90.0),LT,1.0E-2)GO TO 60	24690130
00164	65.			ANGG=90.0	24690132
00165	66.			50 IF (ABS(ANGG-ANGC),LT,1.0E-1)GO TO 65	24690134
00167	67.			INDX=INDX+1	24690136
00170	68.			IF (INDX,GT,100)GO TO 66	24690138
00172	69.			ANGX=0.5*(ANGC+ANGG)	24690140
00173	70.			XSLOPE=TAN(ANGX/RON)	24690142

00174	71.	55	XO=(XSLOPE*XHUB-TSLOPE+GUESS-YHUB+GUESS)/(XSLOPE-TSLOPE)	24690144
00175	72.		YO=(XSLOPE+GUESS-TSLOPE+GUESS-YHUB+XSLOPE*TSLOPE*(XHUB-GUESS))/	24690146
00176	73.		YPP=TSLOPE	24690148
00177	74.		YPP=TSLOPE	24690150
00178	75.		YPP=TSLOPE	24690152
00179	76.		YPP=TSLOPE	24690154
00180	77.		YPP=TSLOPE	24690156
00181	78.		YPP=TSLOPE	24690158
00182	79.		YPP=TSLOPE	24690160
00183	80.		YPP=TSLOPE	24690162
00184	81.		YPP=TSLOPE	24690164
00185	82.		YPP=TSLOPE	24690166
00186	83.		YPP=TSLOPE	24690168
00187	84.		YPP=TSLOPE	24690170
00188	85.		YPP=TSLOPE	24690172
00189	86.		YPP=TSLOPE	24690174
00190	87.	60	YPP=TSLOPE	24690176
00191	88.		YPP=TSLOPE	24690178
00192	89.		YPP=TSLOPE	24690180
00193	90.		YPP=TSLOPE	24690182
00194	91.		YPP=TSLOPE	24690184
00195	92.	65	YPP=TSLOPE	24690186
00196	93.		YPP=TSLOPE	24690188
00197	94.		YPP=TSLOPE	24690190
00198	95.		YPP=TSLOPE	24690192
00199	96.	2000	YPP=TSLOPE	24690194
00200	97.		YPP=TSLOPE	24690196
00201	98.		YPP=TSLOPE	24690198
00202	99.		YPP=TSLOPE	24690200
00203	100.		YPP=TSLOPE	24690202
00204	101.		YPP=TSLOPE	24690204
00205	102.	66	YPP=TSLOPE	24690206
00206	103.		YPP=TSLOPE	24690208
00207	104.		YPP=TSLOPE	24690210
00208	105.		YPP=TSLOPE	24690212
00209	106.		YPP=TSLOPE	24690214
00210	107.		YPP=TSLOPE	24690216
00211	108.	1000	YPP=TSLOPE	24690218
00212	109.		YPP=TSLOPE	24690220
00213	110.		YPP=TSLOPE	24690222
00214	111.		YPP=TSLOPE	24690224
00215	112.		YPP=TSLOPE	24690226
00216	113.	67	YPP=TSLOPE	24690228
00217	114.		YPP=TSLOPE	24690230
00218	115.		YPP=TSLOPE	24690232
00219	116.		YPP=TSLOPE	24690234
00220	117.		YPP=TSLOPE	24690236
00221	118.		YPP=TSLOPE	24690238
00222	119.	1001	YPP=TSLOPE	24690240
00223	120.		YPP=TSLOPE	24690242
00224	121.		YPP=TSLOPE	24690244
00225	122.		YPP=TSLOPE	24690246
00301	123.		END	24690248

END OF LISTING. 1 *DIAGNOSTIC* MESSAGE(S).

9 FOR RCS 2469D250
COMPILATION BY UNIVAC 1108 FORTAN-IV DATED NOV. 23, 1965 F4008
THIS COMPILATION WAS DONE ON 19 AUG 66 AT 17:37:20

SUBROUTINE RCS ENTRY POINT 000165

STORAGE USED (BLOCK, NAME, LENGTH)

0001 *CODE 000251
0000 *DATA 000027
0002 *BLANK 000000
0003 RC 000170

EXTERNAL REFERENCES (BLOCK, NAME)

0004 COS
0005 SORT
0006 TAN
0007 TADLE

STORAGE ASSIGNMENT FOR VARIABLES (BLOCK, TYPE, RELATIVE LOCATION, NAME)

0001 000043 116G 0001 000122 134G 0000 R C30001 A 0000 R 000002 AJ 0004 R 000000 COS
0000 R 000006 COSG 0000 I 000004 J 0000 R 000000 PI 0000 R 000003 RHUB 0000 R 000005 RTIP
0005 R 000000 SORT 0007 R 000000 TABLE 0006 R 000000 TAN 0003 R 000003 XRC 0003 R 000074 YRC

00101 1. SUBROUTINE RCS(K2,XLOC,RADIUS,GAMMA,DX,AREA,XND,BLF) 2469D252
00101 2. C 2469D254
00101 3. C RCS COMPUTES STREAMTUBES OF EQUAL AREA ALONG A NORMAL 2469D256
00101 4. C AND RC=F(N) 2469D258
00101 5. C 2469D260
00103 6. COMMON/RC/XRC(13,20),YRC(13,20) 2469D262
00104 7. DIMENSION XLOC(20,7),RADIUS(20,7),GAMMA(20),AREA(20,7),XND(20,7) 2469D264
00105 8. DIMENSION BLF(20,7) 2469D266
00105 9. C 2469D268
00106 10. DATA PI/3.14159/ 2469D270
00106 11. C AREAS AND RADII 2469D272
00110 12. A=(RADIUS(K2,7)**2-RADIUS(K2,1)**2) 2469D274
00111 13. AREA(K2,6)=PI*A/COS(GAMMA(K2)) 2469D276
00112 14. AJ=AREA(K2,6)/5. 2469D278
00113 15. A=AJ/5. 2469D280
00114 16. RHUB=RADIUS(K2,1) 2469D282
00115 17. DO 100 J=1,5 2469D284
00120 18. AREA(K2,J)=AJ 2469D286
00121 19. RTIP=SQRT(A+RHUB**2) 2469D288
00122 20. RADIUS(K2,J+1)=SQRT((RHUB**2+RTIP**2)/2.) 2469D290
00123 21. BLF(K2,J)=(RHUB+RTIP)/2. 2469D292
00124 22. RHUB=RTIP 2469D294
00125 23. XLOC(K2,J+1)=XLOC(K2,7)+TAN(GAMMA(K2))*RADIUS(K2,7)-RADIUS(K2,J+1)*2469D296
00125 24. 1) 2469D298

END OF LISTING. 0 *DIAGNOSTIC* MESSAGE(S).

2569D332

FOR OUTPUT
COMPILATION BY UNIVAC 1108 FORTRAN-IV DATED NOV. 23, 1965 F4008
THIS COMPILATION WAS DONE ON 19 AUG 66 AT 17:37:22

SUBROUTINE OUTPUT ENTRY POINT 000757

STORAGE USED (BLOCK, NAME, LENGTH)

0001 *CODE 000776
0001 *DATA 000517
0002 *BLANK 000000
0003 IMPELR 002335
0004 BLOCK 010757

EXTERNAL REFERENCES (BLOCK, NAME)

0005 WNDUS
0006 NI01\$
0007 NI02\$
0010 NERR2\$

STORAGE ASSIGNMENT FOR VARIABLES (BLOCK, TYPE, RELATIVE LOCATION, NAME)

0001	000122	1L	0000	000003	10F	0001	000036	1116	0000	000017	12F	0001	000356	1206
0001	000076	1326	0000	000022	14F	0001	000106	1406	0001	000030	150G	0000	000040	16F
0001	000147	1626	0001	000157	1706	0001	000167	1762	0000	000044	18F	0001	000134	2L
0000	000052	20F	0001	000203	2066	0001	000213	2146	0000	000060	22F	0001	000223	2226
0001	000237	2326	0000	000066	24F	0001	000251	2406	0001	000263	246G	0001	000301	2566
0000	000075	26F	0001	000313	2646	0000	000103	2806	0001	000343	3L	0000	000312	30F
0001	000356	3056	0001	000370	3136	0000	000121	3256	0001	000406	336G	0001	000420	331E
0001	000432	3376	0000	000126	34F	0001	000444	3456	0001	000462	355G	0000	000135	36F
0001	000474	3636	0001	000506	3716	0000	000146	38F	0001	000352	4L	0000	000153	40F
0001	000536	4036	0001	000550	4116	0001	000562	4176	0000	000357	42F	0001	000574	4256
0001	000606	4336	0000	000166	44F	0001	000620	4416	0001	000632	447G	0001	000644	4556
0000	000175	46F	0000	000204	48F	0001	000524	5L	0000	000207	50F	0000	000216	52F
0000	000225	54F	0000	000231	56F	0000	000240	58F	0000	000247	60F	0000	000256	62F
0000	000265	64F	0000	000272	66F	0000	000301	68F	0001	000650	7L	0000	000310	70F
0000	000317	72F	0000	000325	74F	0000	000332	76F	0000	000341	78F	0000	000350	80F
0000	000357	82F	0000	000364	84F	0000	000373	86F	0000	000402	88F	0000	000411	90F
0000	000427	91F	0000	000420	92F	0000	000436	94F	0000	000445	96F	0003	000000	A
0004	R 000000	ACCEL	0004	R 000214	ALPHA	0004	000436	ANASS	0004	R 000644	AREA	0004	R 001060	BETA
0003	R 000764	BLF	0003	001200	C	0004	001274	CF	0004	001275	DERIV1	0004	001511	DERIV2
0004	001725	DGR	0004	R 001726	DPDN	0003	R 001262	GAMMA	0004	002142	6C	0004	002143	G1VH
0004	002144	HGPSI	0004	002145	HJ	0000	I 000002	I	0000	I 000001	J	0000	I 000001	JGO
0004	I 002146	NS	0004	I 002147	NTITLE	0004	R 002173	PHI	0004	002217	P1	0004	R 002220	FAT
0004	R 002434	PS	0004	R 002650	PT	0003	001522	G	0004	003064	R	0003	R 001356	NAUTUS
0004	R 003065	RCURV	0004	R 003301	REC	0004	003515	RIN	0004	003516	RPM	0004	R 003517	TRI
0004	R 003733	TS	0004	R 004147	TY	0004	004363	TX	0004	004407	TY	0004	R 004433	U
0004	R 004647	V	0004	R 005065	VP	0004	R 005277	VPM	0004	005313	VR	0004	R 005727	VS
0004	R 006143	VSND	0004	R 006357	VSH	0003	R 000000	VTM	0004	R 006573	YU	0004	R 007007	VYSND
0004	007223	VX	0004	R 007437	W	0004	R 007653	WM	0004	R 010303	WU	0004	R 010067	WVSND
0003	001604	XBLF	0003	R 001750	XLOC	0004	R 010517	XMD	0004	R 010543	XNO	0003	R 002164	YAL
0003	002171	YBLF												

00101	1.	SUBROUTINE OUTPUT					24690334
00103	2.	COMMON/IMPELR/A(500)					24690336
00103	3.	*GAMMA(20)					24690338
00103	4.	*XLOC(20,7)					24690340
00104	5.	COMMON/BLOCK/ ACCEL(20,7)					24690342
00104	6.	*AREA(20,7)					24690344
00104	7.	*DERIV2(20,7)					24690346
00104	8.	*HGPS1(J,NS)					24690348
00104	9.	*PS(20,7)					24690350
00104	10.	*REC(20,7)					24690352
00104	11.	*TT(20,7)					24690354
00104	12.	*VP(20,7)					24690356
00104	13.	*VS(20,7)					24690358
00104	14.	*VVSND(20,7)					24690360
00104	15.	*VVSND(20,7)					24690362
00105	16.	DIMENSION VTM(20,5)					24690364
00106	17.	EQUIVALENCE (VTM(1,1),A(1))					24690366
00107	18.	J60=2					24690368
00110	19.	DO 8 J=1,NS					24690370
00113	20.	WRITE(6,10)J					24690372
00116	21.	WRITE(6,12)(NTITLE(I),I=1,16)					24690374
00124	22.	WRITE(6,14)					24690376
00126	23.	WRITE(6,16)					24690378
00130	24.	WRITE(6,18)(XLOC(J,1),I=1,7)					24690380
00136	25.	WRITE(6,20)(RADIUS(J,1),I=1,7)					24690382
00144	26.	GO TO (1,2),J60					24690384
00145	27.	CONTINUE					24690386
00146	28.	WRITE(6,22)(XND(J,1),I=1,7)					24690388
00154	29.	CONTINUE					24690390
00155	30.	WRITE(6,24)XND(J)					24690392
00160	31.	WRITE(6,26)(RCURV(J,1),I=1,7)					24690394
00166	32.	WRITE(6,28)(AREA(J,1),I=1,6)					24690396
00174	33.	WRITE(6,30)(BLF(J,1),I=1,5)					24690398
00202	34.	WRITE(6,32)					24690400
00204	35.	WRITE(6,34)(TT(J,1),I=1,5)					24690402
00212	36.	WRITE(6,36)(TS(J,1),I=1,5)					24690404
00220	37.	WRITE(6,38)(TRT(J,1),I=1,5)					24690406
00226	38.	WRITE(6,40)					24690408
00230	39.	WRITE(6,42)(PT(J,1),I=1,5)					24690410
00236	40.	WRITE(6,44)(PS(J,1),I=1,5)					24690412
00244	41.	WRITE(6,46)(PRT(J,1),I=1,5)					24690414
00252	42.	WRITE(6,48)					24690416
00254	43.	WRITE(6,50)(VVSND(J,1),I=1,5)					24690418
00262	44.	WRITE(6,52)(VVSND(J,1),I=1,5)					24690420
00270	45.	WRITE(6,54)					24690422
00272	46.	WRITE(6,56)GAMMA(J)					24690424
00275	47.	GO TO (3,4),J60					24690426
00276	48.	CONTINUE					24690428
00277	49.	WRITE(6,58) PHI(J)					24690430
00302	50.	CONTINUE					24690432
00303	51.	WRITE(6,60)(ALPHA(J,1),I=1,5)					24690434
00311	52.	WRITE(6,62)(BETA(J,1),I=1,5)					24690436
00317	53.	WRITE(6,64)					24690438
00321	54.	WRITE(6,66)(V(J,1),I=1,5)					24690440
00327	55.	WRITE(6,68)(VU(J,1),I=1,5)					24690442
00335	56.	WRITE(6,70)(VVSND(J,1),I=1,5)					24690444
00343	57.	WRITE(6,72)(UI(J,1),I=1,7)					24690446

00351	58.	WRITE(6,74)	2469D448
00353	59.	WRITE(6,763)(W(J,I),I=1,5)	2469D450
00361	60.	WRITE(6,78)(WM(J,I),I=1,5)	2469D452
00367	61.	WRITE(6,80)(WU(J,I),I=1,5)	2469D454
00375	62.	GO TO (5,7),JGO	2469D456
00376	63.	CONTINUE	2469D458
00377	64.	WRITE(6,82)	2469D460
00401	65.	WRITE(6,84)(VS(J,I),I=1,5)	2469D462
00407	66.	WRITE(6,86)(VP(J,I),I=1,5)	2469D464
00415	67.	WRITE(6,88)(VSW(J,I),I=1,5)	2469D466
00423	68.	WRITE(6,90)(VPM(J,I),I=1,5)	2469D468
00431	69.	WRITE(6,91)(VTW(J,I),I=1,5)	2469D470
00437	70.	WRITE(6,92)(ACCL(J,I),I=1,5)	2469D472
00445	71.	WRITE(6,94)(REC(J,I),I=1,5)	2469D474
00453	72.	WRITE(6,96)(OPDN(J,I),I=1,5)	2469D476
00461	73.	CONTINUE	2469D478
00462	74.	JGO=1	2469D480
00463	75.	CONTINUE	2469D482
00465	76.	RETURN	2469D484
00466	77.	FORMAT(1H1,29X,56HIMPELLER RADIAL EQUILIBRIUM DESIGN RESULTS FOR S2469D486	2469D488
00467	78.	*TATTON ,12)	2469D490
00467	79.	FORMAT(1H0,23X,12A5)	2469D492
00470	80.	FORMAT(1H0,14X,10HSTREAMTUBE,8X,3HHUB,10X,1H1,11X,1H2,11X,1H3,11X,1H4,11X,1H5,10X,3HTIP)	2469D494
00471	81.	*1H4,11X,1H5,10X,3HTIP)	2469D496
00471	82.	FORMAT(18H DISTANCES(INCHES))	2469D498
00472	83.	FORMAT(6X,20HAXIAL-----	2469D500
00473	84.	FORMAT(6X,20HRADIAL-----	2469D502
00474	85.	FORMAT(6X,20HNORMAL-----	2469D504
00475	86.	FORMAT(6X,20HMERIDIONAL-----	2469D506
00476	87.	FORMAT(6X,20HRADIUS OF CURVATURE-----	2469D508
00477	88.	FORMAT(6X,20HACTUAL AREA(SQ IN)-----	2469D510
00500	89.	FORMAT(6X,20HBLOCKAGE FACTOR-----	2469D512
00501	90.	FORMAT(20H TEMPERATURES(DEG R))	2469D514
00502	91.	FORMAT(6X,20HTOTAL-----	2469D516
00503	92.	FORMAT(6X,20HSTATIC-----	2469D518
00504	93.	FORMAT(6X,20HRELATIVE TOTAL-----	2469D520
00505	94.	FORMAT(17H PRESSURES(IN HG))	2469D522
00506	95.	FORMAT(6X,20HTOTAL-----	2469D524
00507	96.	FORMAT(6X,20HSTATIC-----	2469D526
00510	97.	FORMAT(6X,20HRELATIVE TOTAL-----	2469D528
00511	98.	FORMAT(13H MACH NUMBERS)	2469D530
00512	99.	FORMAT(6X,20HABSOLUTE-----	2469D532
00513	100.	FORMAT(6X,20HRELATIVE-----	2469D534
00514	101.	FORMAT(16H ANGLES(DEGREES))	2469D536
00515	102.	FORMAT(6X,20HMERIDIONAL-----	2469D538
00516	103.	FORMAT(6X,20HBLADE-----	2469D540
00517	104.	FORMAT(6X,20HABSOLUTE FLUID-----	2469D542
00520	105.	FORMAT(6X,20HRELATIVE FLUID-----	2469D544
00521	106.	FORMAT(23H ABS VELOCITIES(FT/SEC))	2469D546
00522	107.	FORMAT(6X,20HTOTAL-----	2469D548
00523	108.	FORMAT(6X,20HTANGENTIAL-----	2469D550
00524	109.	FORMAT(6X,20HSOUND-----	2469D552
00525	110.	FORMAT(6X,20HWHEEL-----	2469D554
00526	111.	FORMAT(23H REL VELOCITIES(FT/SEC))	2469D556
00527	112.	FORMAT(6X,20HTOTAL-----	2469D558
00530	113.	FORMAT(6X,20HMERIDIONAL-----	2469D560
00531	114.	FORMAT(6X,20HTANGENTIAL-----	2469D562
00532	115.	FORMAT(20H SURFACE VEL(FT/SEC))	

00533	116.	84	FORMAT(6X,20HSUCTION----	,12X,6F12.1)	24690564
00534	117.	86	FORMAT(6X,20HPRESSURE----	,12X,6F12.1)	24690566
00535	118.	88	FORMAT(/6X,20HSUCTION/V2 MEAN----	,12X,6F12.3)	24690568
00536	119.	90	FORMAT(6X,20HPRESSURE/V2 MEAN----	,12X,6F12.3)	24690570
00537	120.	92	FORMAT(/6X,20HACCEL(FT/SEC 50)----	,12X,6E12.4)	24690572
00540	121.	91	FORMAT(6X,20HREL TOTAL/V2 MEAN----	,12X,6F12.3)	24690574
00541	122.	94	FORMAT(6X,20HRECOVERY-----	,12X,6F12.8)	24690576
00542	123.	96	FORMAT(6X,20HDP/DN(IN HG/FT)-----	,12X,6F12.2)	24690578
00543	124.		END		24690580

END OF LISTING. 0 *DIAGNOSTIC* MESSAGE(S).

0 FOR TABLE		2469D562	
COMPILATION BY UNIVAC 1108 FORTRAN-IV DATED NOV. 23, 1965 F4008			
THIS COMPILATION WAS DONE ON 19 AUG 66 AT 17:37:24			
FUNCTION TABLE		ENTRY POINT 000065	
STORAGE USED (BLOCK, NAME, LENGTH)			
0001	*CODE 000077		
0000	*DATA 000043		
0002	*BLANK 004735		
EXTERNAL REFERENCES (BLOCK, NAME)			
0003	TAB2		
STORAGE ASSIGNMENT FOR VARIABLES (BLOCK, TYPE, RELATIVE LOCATION, NAME)			
0001	000032 10L	0000 1 000032 I	0000 1 000033 IE
0002	000000 NXY	0000 R 000000 TAB2	0002 R 000031 XVAL
			0000 1 000001 NDEG
			0002 R 002373 YVAL
00101	1. FUNCTION TABLE (NT, ARG)		2469D584
00103	2. COMMON NXY(25), XVAL(50, 25), YVAL(50, 25)		2469D586
00104	3. DIMENSION NDEG(25)		2469D588
00105	4. DATA (NDEG(1), I=1, 25)/3*1, 3, 20, 1/		2469D590
00107	5. IF (NT .LT. 0) GO TO 10		2469D592
00111	6. TABLE= TAB2(XVAL(1, NT), YVAL(1, NT), NXY(NT), NDEG(NT), ARG, IE)		2469D594
00112	7. RETURN		2469D596
00113	8. 16 KT=NT		2469D598
00114	9. TABLE= TAB2(YVAL(1, KT), XVAL(1, KT), NXY(KT), NDEG(KT), ARG, IE)		2469D600
00115	10. RETURN		2469D602
00116	11. END		2469D604
END OF LISTING. 0 *DIAGNOSTIC* MESSAGE(S).			

P FOR TAB2
COMPILATION BY UNIVAC 1108 FORTRAN-IV DATED NOV. 23, 1965 F4008 2469D606
THIS COMPILATION WAS DONE ON 19 AUG 66 AT 17:37:26

FUNCTION TAB2 ENTRY POINT 000263

STORAGE USED (BLOCK, NAME, LENGTH)

0001 *CODE 000324
0000 *DATA 000050
0002 *BLANK 000000

EXTERNAL REFERENCES (BLOCK, NAME)

0003 OVERFL

STORAGE ASSIGNMENT FOR VARIABLES (BLOCK, TYPE, RELATIVE LOCATION, NAME)

0001 000211 100L 0001 000243 110L 0001 000054 1236 0001 000131 1419 0001 000145 1506
0001 000154 1546 0001 000225 1756 0001 000072 20L 0001 000121 24L 0001 000124 30L
0001 000206 40L 0001 000247 94L 0001 000251 94L 0000 I 000024 I 0000 I 000021 J
0000 I 000022 K 0000 I 000023 LAST 0000 I 000030 M 0000 I 000025 N 0000 I 000017 NO2
0000 I 000027 NW 0000 I 000016 NP1 0000 I 000020 NP102 0000 I 000015 NXM1 0000 I 000026 NY
0000 R 000000 TAB2 0000 R 000001 XX 0000 R 000007 YY

FUNCTION TAB2(X,Y,NX,NDEG,ARG,IE)

SINGLE INTERPOLATION ROUTINE

DIMENSION XX(6), YY(6), X(1), Y(1)

X---INDEPENDENT VARIABLE ARRAY STORED IN CONSECUTIVE LOCATIONS

Y---DEPENDENT VARIABLE ARRAY STORED IN CONSECUTIVE LOCATIONS

NX---NUMBER OF X OR Y-VALUES IN THE TABLE

NDEG---THE DEGREE OF INTERPOLATION DESIRED

ARG---THE ARGUMENT FOR WHICH A CORRESPONDING VALUE OF Y WILL BE

IE---=1 FOR SUCCESS,=2 FOR OVERFLOW,=3 FOR INCORRECT CALLING

IF(NXM1-NDEG)98,110,2

NP1=NDEG+1

DETERMINE IF IT IS POSSIBLE TO GIVE THE DEGREE REQUESTED

IF(NXM1-NDEG)98,110,2

NP1=NDEG+1

NP102=NP1/2

J=NP102+2

K=J

LAST = NX-NP102

00101 1. C 2469D608
00101 2. C 2469D610
00101 3. C 2469D612
00101 4. C 2469D614
00101 5. C 2469D616
00101 6. C 2469D618
00101 7. C 2469D620
00101 8. C 2469D622
00101 9. C 2469D624
00101 10. C 2469D626
00101 11. C 2469D628
00101 12. C 2469D630
00101 13. C 2469D632
00101 14. C 2469D634
00101 15. C 2469D636
00101 16. C 2469D638
00101 17. C 2469D640
00101 18. C 2469D642
00101 19. C 2469D644
00101 20. 2 2469D646
00112 21. NP102=NP1/2 2469D648
00113 22. J=NP102+2 2469D650
00114 23. K=J 2469D652
00115 24. LAST = NX-NP102 2469D654
00115 25. C 2469D656

```

00115 26. C IS THE ARRAY IN INCREASING ORDER
00116 27. C IF (X(1).GT.X(2)) GO TO 100
00116 28. C
00116 29. C THE ARRAY IS IN INCREASING ORDER
00116 30. C
00116 31. C CHECK FOR EXTRAPOLATION
00120 *DIAGNOSTIC* THE TEST FOR EQUALITY BETWEEN NON-INTEGERS MAY NOT BE MEANINGFUL
00120 32. C IF (X(J-1).GE.ARG) GO TO 110
00120 33. C
00120 34. C DETERMINE WHAT POINTS THE ARGUMENT LIES BETWEEN
00120 35. C
00122 36. C DO 12 I=K, LAST
00125 *DIAGNOSTIC* THE TEST FOR EQUALITY BETWEEN NON-INTEGERS MAY NOT BE MEANINGFUL
00125 37. C IF (X(1).GE.ARG) GO TO 20
00127 38. C 12 J=J+1
00127 39. C
00127 40. C EXTRAPOLATE ON FAR SIDE OF CURVE
00127 41. C
00127 42. C J=NX
00132 43. C GO TO 30
00132 44. C
00132 45. C IS THE DEGREE OF INTERPOLATION ODD OR EVEN
00133 46. C 20 IF (2*ND2.NE.NDEG) GO TO 24
00133 47. C
00133 48. C THE DEGREE OF INTERPOLATION IS EVEN
00133 49. C
00135 50. C IF (ABS(X(J-1)-ARG).LT.ABS(X(J)-ARG)) J=J-1
00137 51. C 24 J=J+ND2
00137 52. C
00140 53. C DO 32 N=1,NP1
00143 54. C XX(N)=ARG-X(J)
00144 55. C YY(N)=Y(J)
00145 56. C 32 J=J-1
00145 57. C
00147 58. C DO 36 N=1,NDEG
00152 59. C N1=N+1
00152 60. C
00153 61. C DO 36 N=N1,NP1
00156 62. C YY(NN)=YY(N)+XX(NN)-YY(NN)+XX(NN)/(XX(NN)-XX(N))
00157 63. C CALL OVERFL(M)
00160 64. C IF (M.EQ.1) GO TO 40
00162 65. C 36 CONTINUE
00162 66. C
00162 67. C INTERPOLATION WAS SUCCESSFUL RETURN
00165 68. C IE=1
00166 69. C TAB2=YY(NP1)
00167 70. C RETURN
00167 71. C
00170 72. C 40 IE=2
00171 73. C GO TO 99
00171 74. C
00171 75. C THE ARRAY IS IN DECREASING ORDER
00171 76. C
00171 77. C
00172 *DIAGNOSTIC* CHECK FOR EXTRAPOLATION
00172 78. C 100 THE TEST FOR EQUALITY BETWEEN NON-INTEGERS MAY NOT BE MEANINGFUL
00172 79. C IF (ARG.GE.X(J-1)) GO TO 110
00172 80. C
00174 80. C DO 104 I=K, LAST

```

24690658
24690660
24690662
24690664
24690666
24690668
24690670
24690672
24690674
24690676
24690678
24690680
24690682
24690684
24690686
24690688
24690690
24690692
24690694
24690696
24690698
24690700
24690702
24690704
24690706
24690708
24690710
24690712
24690714
24690716
24690718
24690720
24690722
24690724
24690726
24690728
24690730
24690732
24690734
24690736
24690738
24690740
24690742
24690744
24690746
24690748
24690750
24690752
24690754
24690756
24690758
24690760
24690762
24690764
24690766

00177	*DIAGNOSTIC*	THE TEST FOR EQUALITY BETWEEN NON-INTEGERS MAY NOT BE MEANINGFUL.	24690768
00177	21.	IF(ARG.GE.X(1)) GO TO 20	24690770
00201	82.	J = J+1	24690772
00201	83.	104 C	24690774
00203	84.	J=NX	24690776
00204	85.	GO TO 30	24690778
00204	86.	C	24690780
00205	87.	J=DEG*1	24690782
00206	88.	GO TO 30	24690784
00206	89.	C	24690786
00207	90.	IE=3	24690788
00210	91.	TAD2 = ARG	24690790
00211	92.	RETURN	24690792
00212	93.	END	
END OF LISTING. *DIAGNOSTIC* MESSAGE (5).			

0 NOT MAIN

BLANK COMMON 163043 167777
STARTING ADDRESS 014000
CORE LIMITS 014000 047237 100000 134271

MAIN /CODE
0 10000-110421
1 014000-016323
WPAUS /CODE
1 016324-016371
MEXPLS /CODE
1 016372-016626
2 110422-110431
EXP /CODE
1 016627-016671
2 110432-110451
ALON /CODE
1 016672-016736
2 110452-110504
NEPRA /CODE
1 016737-017182
2 110505-110505
CHAREY /CODE
0 110506-110506
MIMPTs /CODE
1 017183-020061
2 110507-110563
MTABs /CODE
2 110564-112500
NFTVg /CODE
1 020062-020105

MENTS /CODE
1 020106-021011
2 112501-112614
MLISTS/CODE
1 021012-021183
2 112615-112616
MOUTS /CODE
1 021184-022313
2 112617-112743
TALL2 /CODE
0 112744-113711
1 022314-030654
LIFTS /CODE
1 030655-030741
TALL3 /CODE
0 113712-114107
1 030742-032424
TAM /CODE
1 032425-032450
2 114110-114115
AYAM /CODE
1 032451-032535
2 114116-114157
OUTPUT/CODE
0 114158-114676
1 032536-033533
SIMCOS/CODE
1 033534-033624
2 114677-114716
TAB2 /CODE
0 114717-114766
1 033625-034150
IMPEL /CODE
0 114767-115250
1 034151-036437
SERT /CODE
1 036438-036502
2 115251-115256
RCS /CODE
0 115257-115305
1 036503-036753
TABL2 /CODE
0 115306-115350
1 036754-037052

CHORD /CODE
0 115331-115339
1 037053-040104
INLET /CODE
0 115335-116070
1 040105-041505
SORT /CODE
0 116071-116112
1 041506-041621
SLOPE /CODE
0 116113-116242
1 041622-042100
TALL /CODE
0 116243-117561
1 042101-045655
MRLNDS /CODE
1 045656-045722
THRU /CODE
0 117562-117665
TYPE /CODE
0 117666-117702
EDATES /CODE
1 045723-046013
NTRAN /CODE
1 046014-047237
2 117703-120029
YSCRS /CODE
0 120029-120263
YSWAPS /CODE
0 120264-120363
TIMTLE /CODE
0 120364-120471
RC /CODE
0 120472-120661
IMPEL /CODE
0 120662-123216
BLOCK /CODE
0 123217-134175
TALLCP /CODE
0 134176-134271

CONFIDENTIAL

END OF ALLOCATION

124

CONFIDENTIAL

IMPELLER STRESS AND VIBRATION ANALYSIS

ABSTRACT

A discussion of the procedure and the results of the stress and vibration analyses are presented for the MF-1, MF-2, MF-3, RF-1, and workhorse impellers. The temperature distribution, Campbell diagram, natural-frequency calculations, and stress calculations are included for each impeller.

SYMBOLS

A	true flow area (in. ²), $A = A^1 \cos \phi$
A'	total geometric area less area blocked by blades (in. ²), $A' = A_T - A_B$
A_B	area blocked by blades (in. ²), $A_B = \frac{N}{2} h' (t_t + t_r)$
A_T	total geometric area (in. ²), $A_T = \pi h (r_1 + r_2)$
A_{td}	cross-sectional area of impeller disk (in. ²)
E	modulus of elasticity (psi)
F', F_r'	blade radial force per inch of axial length (lb/in.)
F_{fu}	failure force based on ultimate stress (lb)
F_{fy}	failure force based on yield stress (lb)
F_{sr}	calculated blade pull (lb)
T_{td}	total disk force (lb)
F_{ts}	total blade force (lb)
F_{tw}	total wheel force (lb)
g	gravitational constant (32.17 ft/sec ²)
h	flow-passage height normal to mean flow path, includes clearance (in.)
h'	blade height normal to mean flow path (in.)

SYMBOLS (Continued)

I'	blade mass moment of inertia per inch of axial length (lb-in. - sec ² /in.)
I_{td}	total disk mass moment of inertia (lb-in.-sec ²)
I_{ts}	total blade mass moment of inertia (lb-in.-sec ²)
I_{tw}	total wheel mass moment of inertia (lb-in.-sec ²)
L_r	total meridional length along blade root (in.)
L_t	total meridional length along shroud (in.)
ℓ_r	meridional distance to point along blade root (in.)
ℓ_t	meridional distance to point along blade tip (in.)
N	rotational speed (rpm) or number of impeller blades
r	radius (in.)
r_r	root radius (in.)
r_t	tip radius (in.)
r_1	disk bore radius (in.)
r_2	impeller-hub radius at the inlet (in.)
r_3	impeller-tip radius at the exit (in.)
S_{as}	allowable stress (psi)
S_c	calculated blade-root stress (psi)

SYMBOLS (Continued)

S_f failure stress (psi)

S_{root} local blade-root stress (psi)

S_{tan} average tangential disk stress (psi)

T metal temperature ($^{\circ}\text{F}$)

T_a bore temperature at forward pilot ($^{\circ}\text{F}$),

$$T_a = \frac{T_o + T_i}{2}$$

T_b bore temperature at rear pilot ($^{\circ}\text{F}$)

T_d downstream disk-face temperature ($^{\circ}\text{F}$),

$$T_d = T_b + \left(\frac{T_e - T_b}{r_3 - r_1} \right) r$$

T_e relative exit total temperature ($^{\circ}\text{F}$)

T_i relative inlet total temperature ($^{\circ}\text{F}$)

T_o ambient air inlet temperature ($^{\circ}\text{F}$)

T_r metal temperature along the blade root ($^{\circ}\text{F}$),

$$T_r = T_i + \left(\frac{T_e - T_i}{L_r} \right) \ell_r$$

T_t metal temperature along the blade tip ($^{\circ}\text{F}$),

$$T_t = T_i + \left(\frac{T_e - T_i}{L_t} \right) \ell_t$$

T_u upstream disk-face temperature ($^{\circ}\text{F}$),

$$T_u = T_a + \left(\frac{T_i - T_a}{r_2 - r_1} \right) r$$

SYMBOLS (Continued)

t	axial length of disk element (in.)
t_r	blade thickness at the root (in.)
t_t	blade thickness at the tip (in.)
W'	weight of blade per inch of axial length (lb/in.)
W_{td}	total disk weight (lb)
W_{ts}	total blade weight (lb)
W_{tw}	total wheel weight (lb)
Z	axial distance (in.)
α	inclination of blade cross section (degrees)
γ	material density (lb/in. ³)
η_s	safety factor based on allowable stress
η_u	safety factor based on ultimate stress
η_y	safety factor based on yield stress
ϕ	angle between blade and meridional plane (degrees)
ω	angle velocity (radians/sec)

1.0 DISCUSSION

Impeller stress and vibration analyses were conducted through use of a series of computer programs developed during company-sponsored research. For initial stress checks, a preliminary scaled layout of the disk, blade, and shroud profile was prepared for each aerodynamic design. Blade-root and blade-tip dimensions, wrap angles, and inlet- and exit-gas temperatures were also provided. Temperature distribution for the blade and disk was then estimated from the aerodynamic design data. The procedures used were developed empirically for previous impeller designs.

The blade metal temperatures were assumed to vary linearly as functions of meridional length along the shroud and disk profiles as shown on Figure 3. For the blade tip along the shroud,

$$T_t = T_i + \left(\frac{T_e - T_i}{L_t} \right) \ell_t \quad (162)$$

and along the blade root,

$$T_r = T_i + \left(\frac{T_e - T_i}{L_r} \right) \ell_r \quad (163)$$

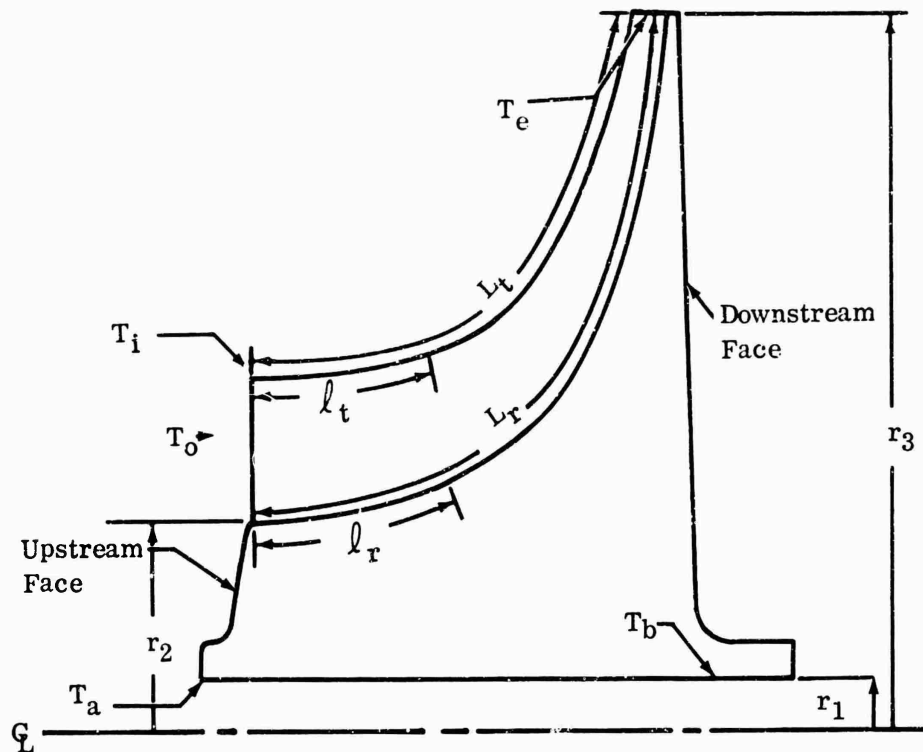
Similarly, the upstream and downstream disk-face temperatures were assumed to be linear functions of radius; thus,

$$T_u = T_a + \left(\frac{T_i - T_a}{r_2 - r_1} \right) r \quad (164)$$

and

$$T_d = T_b + \left(\frac{T_e - T_b}{r_3 - r_1} \right) r \quad (165)$$

The symbols used are described in Figure 3.



- L_r = total meridional length along blade root (in.)
 L_t = total meridional length along shroud (in.)
 T_a = bore temperature at forward pilot, $\frac{T_o + T_i}{2}$
 T_o = ambient air inlet temperature ($^{\circ}\text{F}$)
 T_i = relative inlet total temperature at shroud ($^{\circ}\text{F}$)
 T_e = relative exit total temperature ($^{\circ}\text{F}$)
 T_b = bore temperature at rear pilot (200 $^{\circ}\text{F}$ assumed for journal bearing application; 300 $^{\circ}\text{F}$ for oil-mist-lubricated ball bearing)
 l_r = distance to point along blade root (in.)
 l_t = distance to point along blade tip (in.)
 r = radius (in.)

Figure 3. Blade and Disk Metal Temperature Calculations.

Blade natural frequencies were determined through a contractor-developed computer program with inputs from blade drawing tabulations of root and tip thickness, wrap angle, and axial location. Blade root and tip thickness were taken in a plane normal to the axis of the disk. The first 5 natural frequencies were calculated, and the results were plotted on a Campbell diagram. A Campbell diagram shows blade frequency versus shaft speed, and the orders are excitation caused by wakes or obstructions in the flow path. Each time the blade passes a wake the blade encounters a sharp change in pressure which causes the blade to deflect slightly. Because the number of wakes that the blade encounters is a linear function of shaft speed, the orders appear on the Campbell diagram as straight lines, fanning out from the origin. For example, if 4 inlet struts were used, each blade would feel the disturbance 4 times per revolution of the shaft; the order number, therefore, would be 4. Other potentially critical orders are caused by the inlet guide vanes and the diffuser passages. If the shaft speed and order frequency were to coincide with a blade natural frequency, the blade might vibrate and fail in a short time. Consequently, it is necessary to design a blade so that an order line and a natural-frequency line do not intersect at the design speed.

The blade radial force (F'_r), weight (W'_t), mass moment of inertia (I'), and root stress (S_c) were computed with the same design data as the blade-frequency calculation. Several representative stations along the blade, including a station at the exit tip, were chosen; independent plates or strips were assumed to exist at these points.

The thickness and height of the plates were the same as those of the blade at that station, and the length was assumed to be unity. The resulting calculated radial force, weight, and polar mass moment of inertia were plotted versus axial position of the calculation station. Integration of these plots yielded blade pull, F_{sr} (pounds-force), blade weight, W_{ts} (pounds-weight), and blade polar mass moment of inertia, I_{ts} (lb-in.-sec²).

The calculated blade-root stress (s_c), blade-root temperature (T_r), allowable stress (s_{as}), and safety factor (η_s) to allowable stress were plotted versus axial length. The blade-root temperature was taken from the temperature distribution estimate, and the allowable stress was obtained from the material strength versus temperature curve. The material strength versus temperature curve has a built-in vibratory-stress margin, which is determined by discounting the yield or rupture curve by using a Goodman diagram (see Figure 4).

Two such material strength curves were used, 1 with a discount corresponding to $\pm 20,000$ psi vibratory stress and one with a discount corresponding to $\pm 12,000$ psi vibratory stress. The $\pm 20,000$ psi vibratory stress is the maximum which can be allowed and still maintain design integrity in the inducer section of the impeller. Based on the contractor's experience with aluminum impellers, the maximum allowable vibratory stress must be reduced by 40 percent in the radial

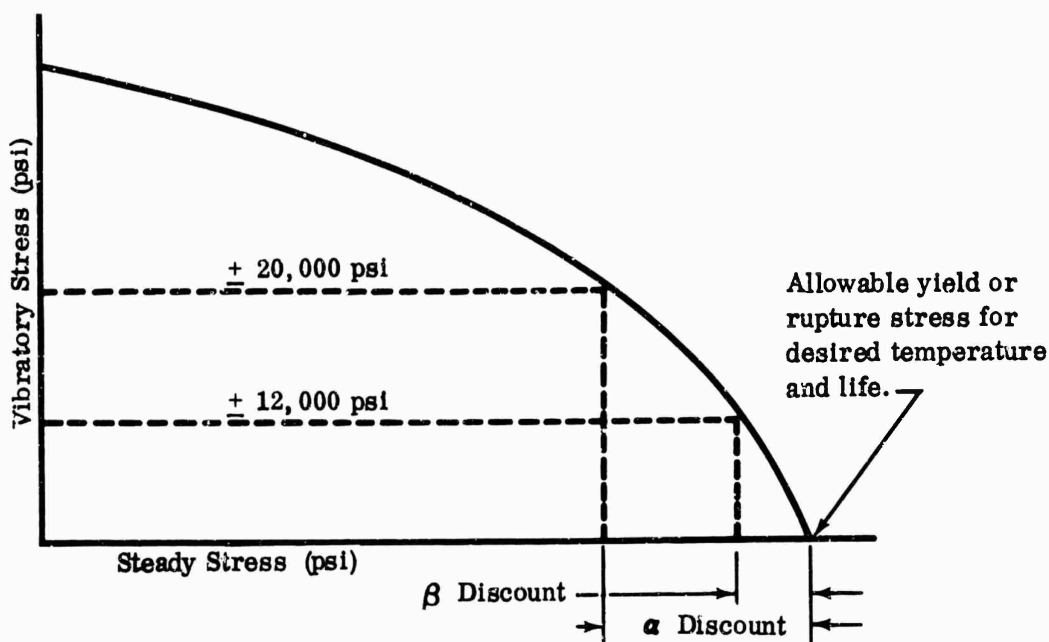


Figure 4. Goodman Diagram.

portion of the impeller. Even though the vibration characteristics of titanium are better than those of aluminum, the 40-percent reduction was used to provide a conservative design because of lack of titanium test data. Region α , defined as the first 25 percent of the blade root meridional length, is the impeller blade section with the allowable $\pm 20,000$ psi vibratory stress. Region β is the remainder of the blade with an allowable vibratory stress of $\pm 12,000$ psi. The aerodynamic blade load was assumed to be a negligible percentage of the total blade stress. Because the calculation of the blade-root stress does not consider shear stress between adjacent plates, which would distribute the stress more evenly along the blade root, the stress analysis of the blade is conservative.

The disk tangential force, cross-sectional area, weight, and polar mass moment of inertia were computed. The failure load was divided by the tangential force to determine a safety factor to failure. Failure was defined as minimum yield or minimum rupture stress. However, failure was not meant to be a disk burst. For steady-state operation, this safety factor must be at least 1.25 to minimum yield stress or to minimum rupture stress, whichever is least. For momentary overspeed conditions, the safety factor may be reduced to 1.10 to minimum yield stress or 1.25 to minimum ultimate stress, whichever is least.

2.0 MF-1 IMPELLER ANALYSIS

The life of the MF-1 impeller is not limited for operation at 62,700 rpm and 60° F inlet temperature if the vibratory stresses do not exceed $\pm 20,000$ psi and $\pm 12,000$ psi in the α and β regions of the blade, respectively. Figure 8 indicates that blade resonant conditions may exist at 35,700 and 47,000 rpm. If continuous operation is expected in these regions, an experimental vibration survey should be conducted to determine modifications that may be required.

The calculated minimum safety factors for steady-state operation at 62,700 rpm and an impeller inlet temperature of 60° F are as follows:

- 1) Blade safety factor is 3.42 to minimum 0.2-percent yield stress including $\pm 12,000$ psi vibratory stress.
- 2) Disk safety factors are 1.44 to minimum 0.2-percent yield stress and 1.62 to minimum ultimate stress.

The calculated minimum safety factors for momentary operation at 71,500 rpm and an impeller inlet temperature of 60° F are as follows:

- 1) Blade safety factor is 2.66 to minimum 0.2-percent yield stress.
- 2) Disk safety factors are 1.10 to minimum 0.2-percent yield stress and 1.25 to minimum ultimate stress.

The weight of the impeller is 7.67 pounds, and the mass moment of inertia is 0.0899 lb-in.-sec².

Figures 5 through 13 present the results of stress and vibration analyses for the MF-1 impeller.

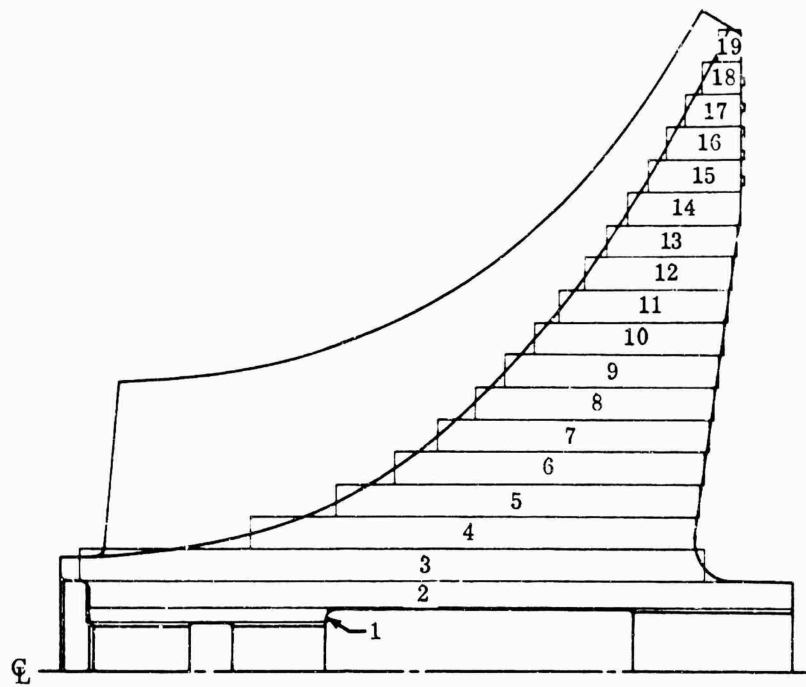


Figure 5. Disk and Blade Profile of MF-1.

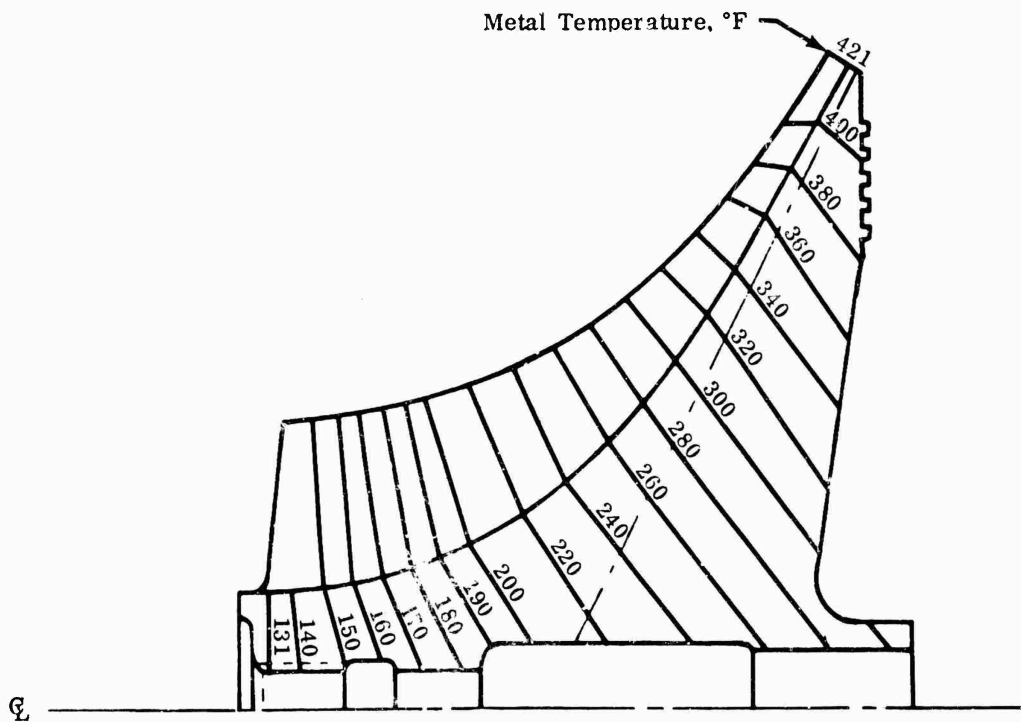


Figure 6. Temperature Distribution of MF-1.

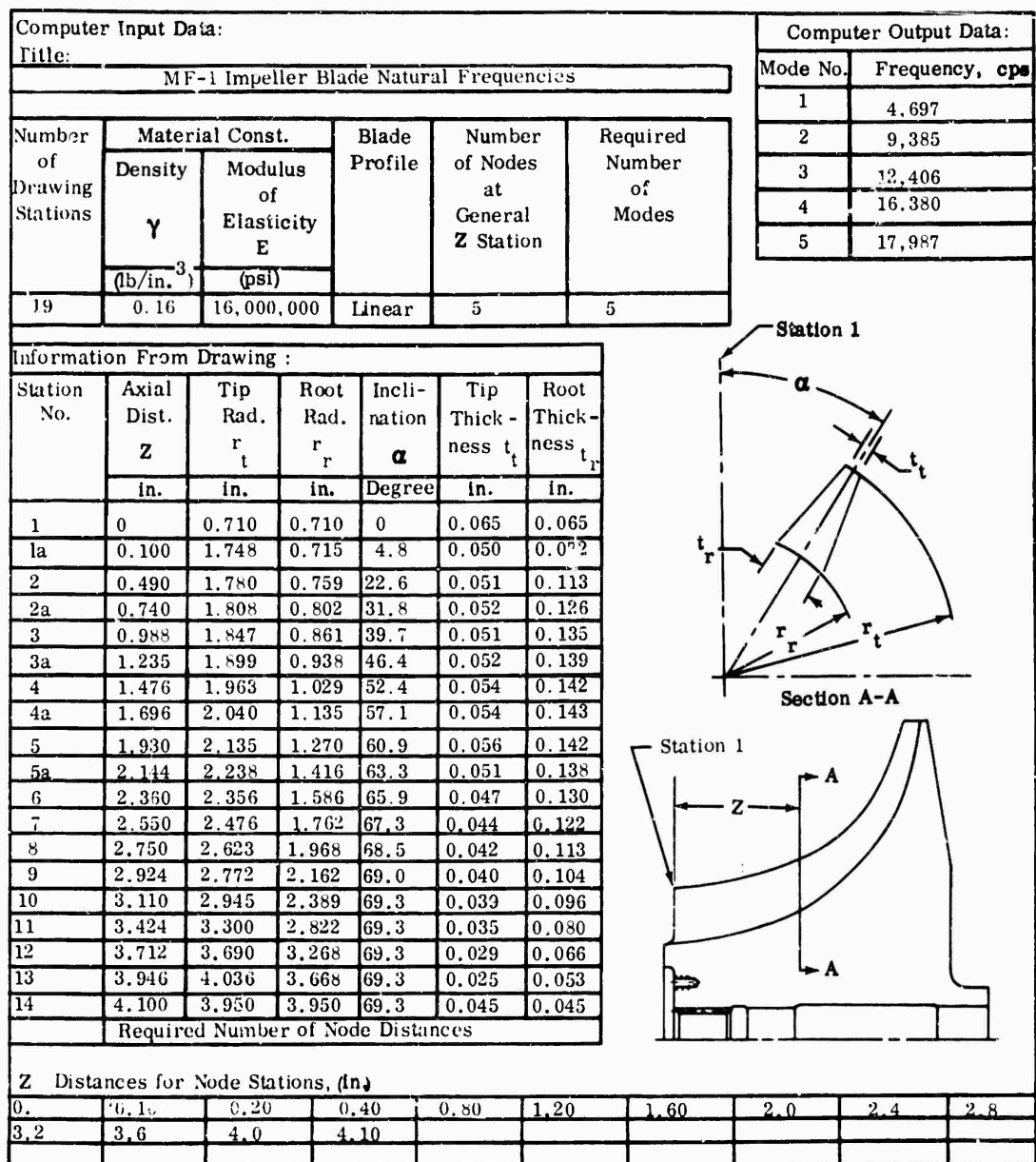


Figure 7. Natural Frequencies of MF-1 Blades.

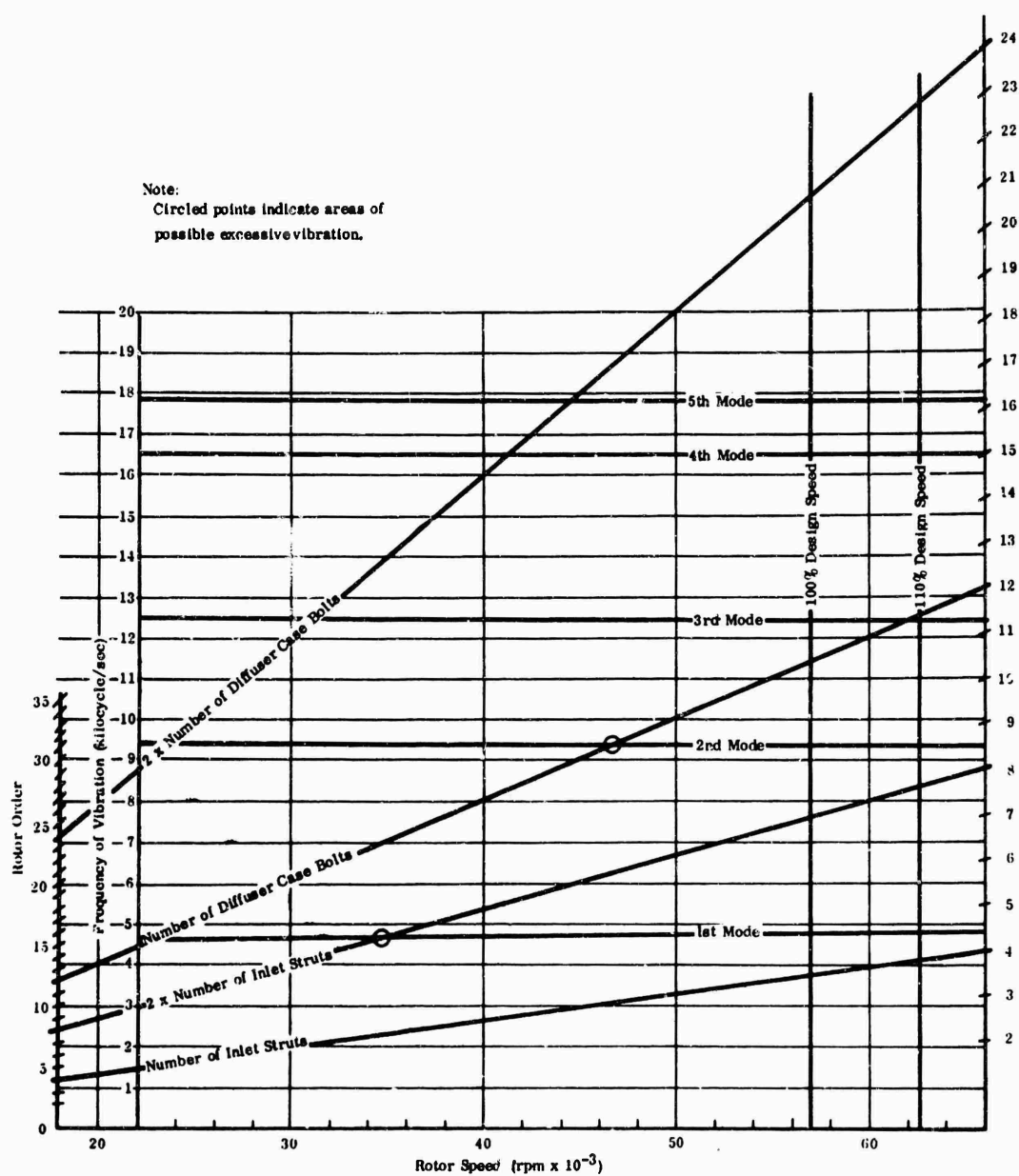


Figure 8. Campbell Diagram for MF-1.

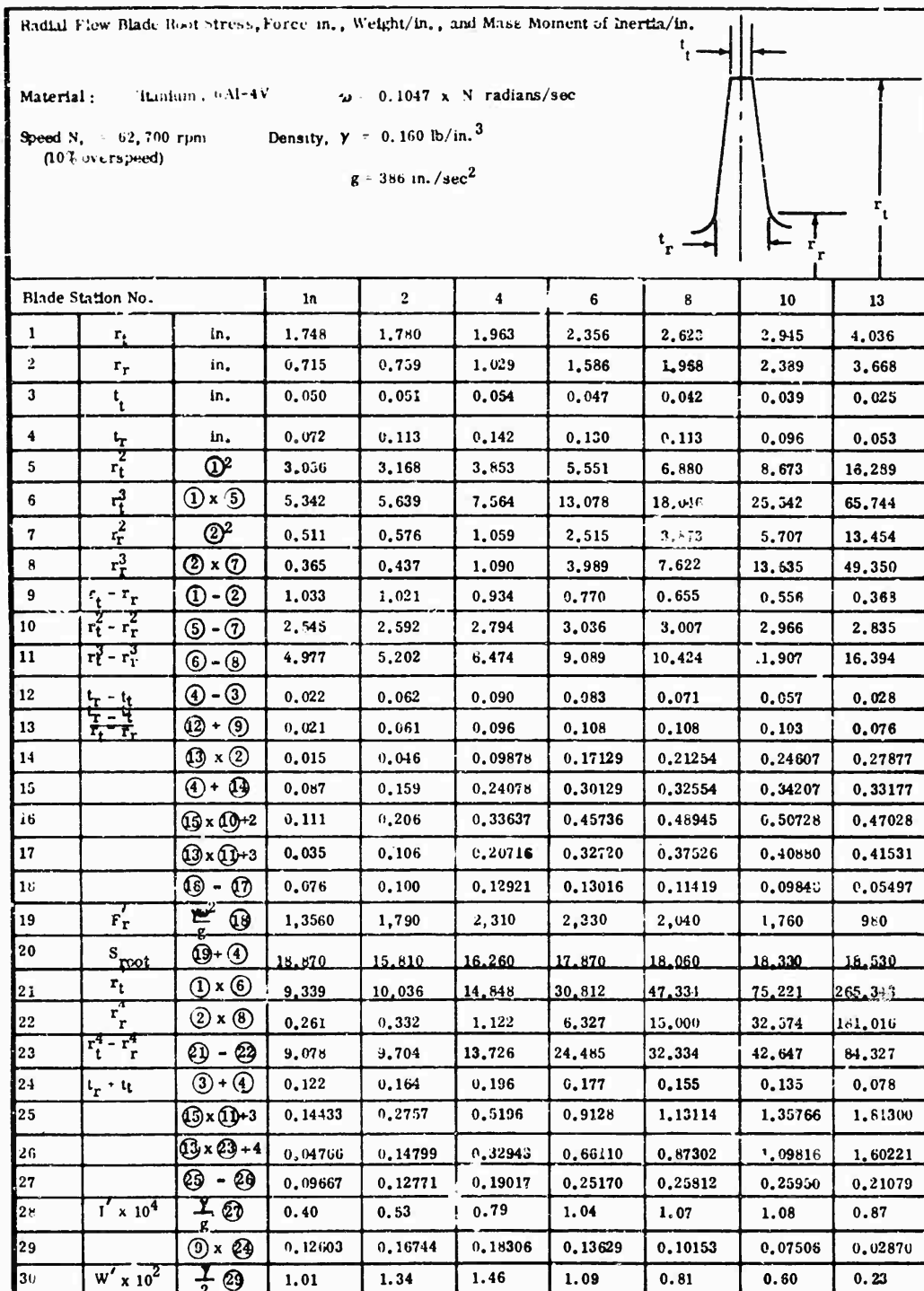


Figure 9. Blade Stress Calculations for MF-1.

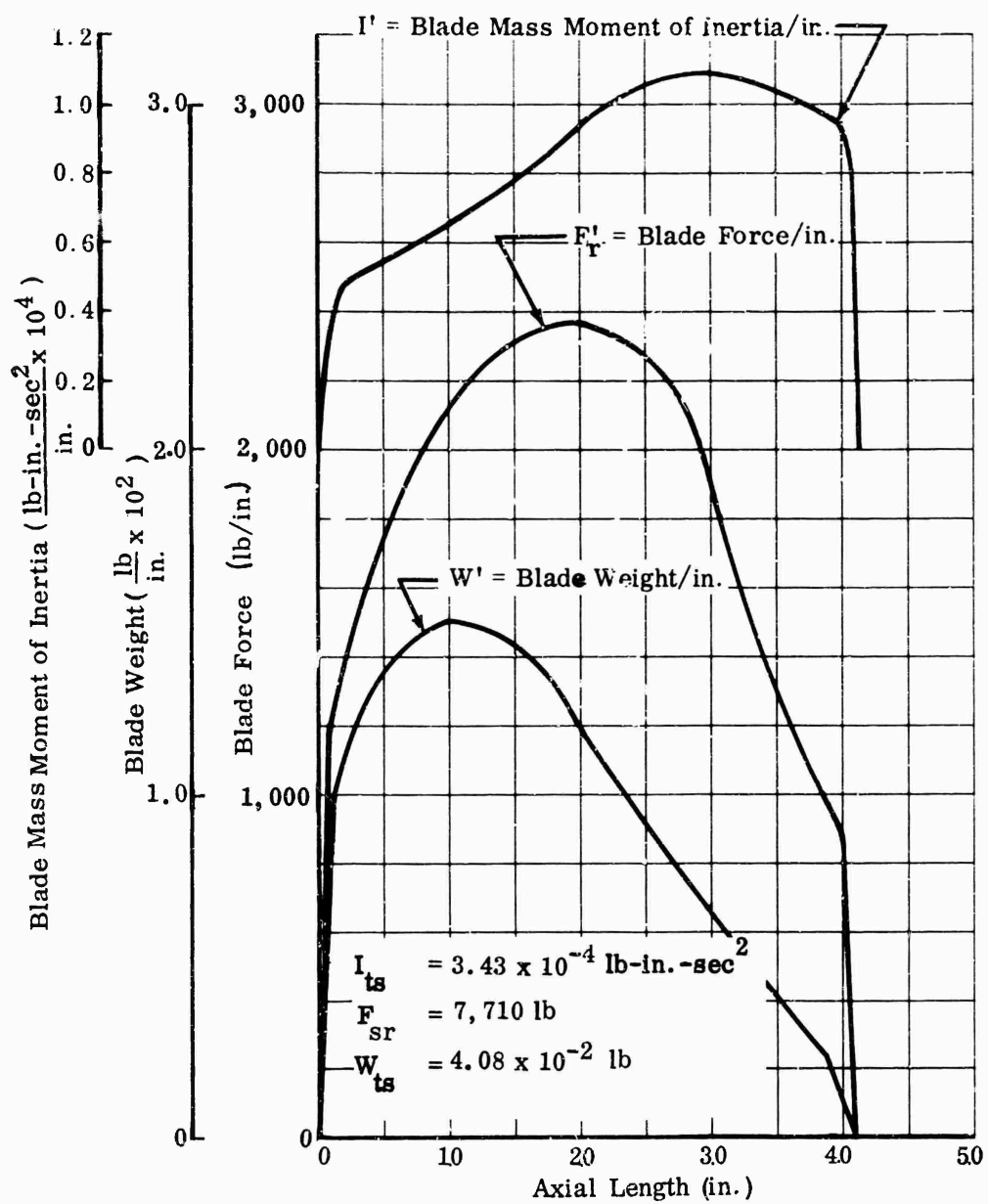


Figure 10. MF-1 Impeller-Blade Force, Weight, and Inertia.

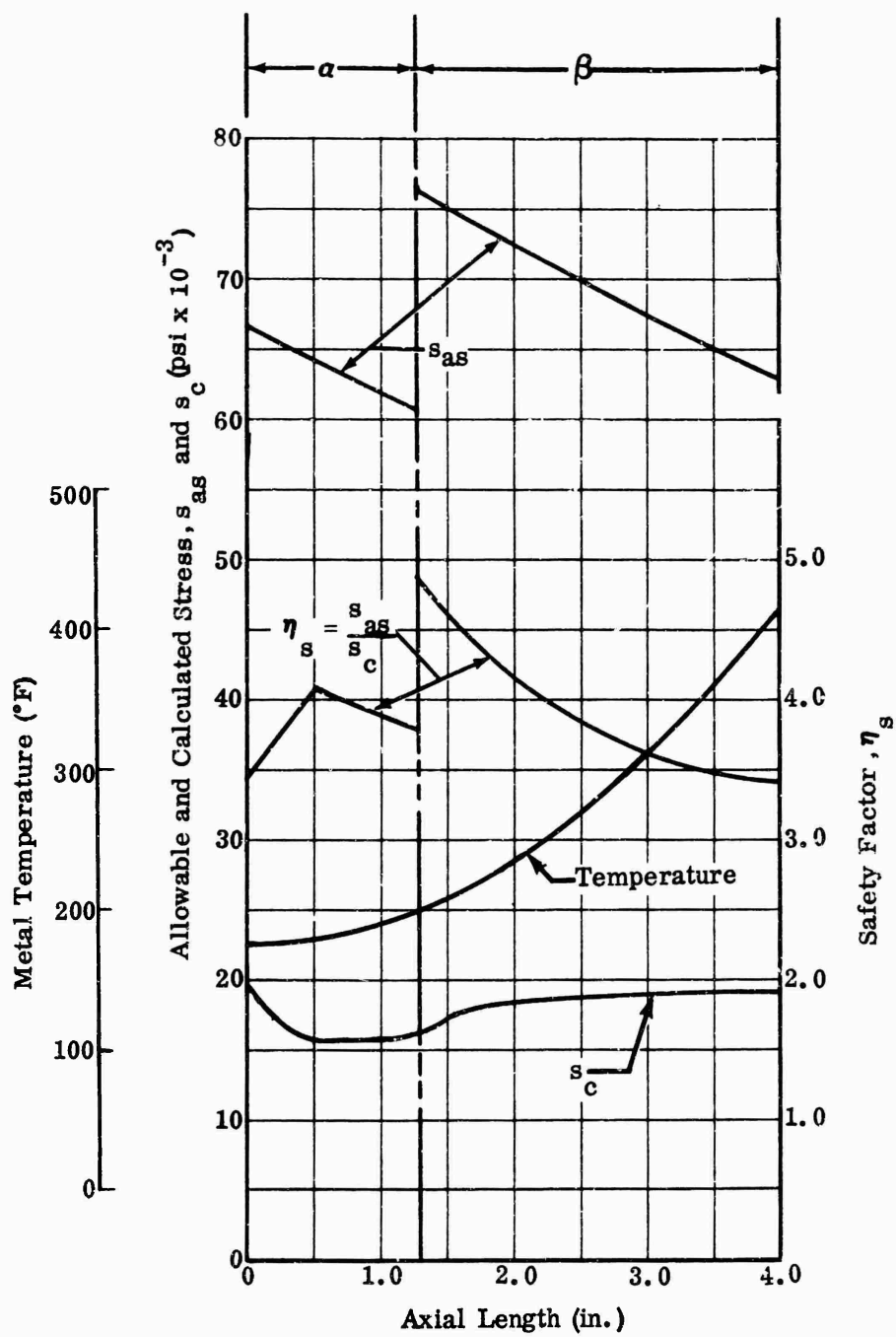


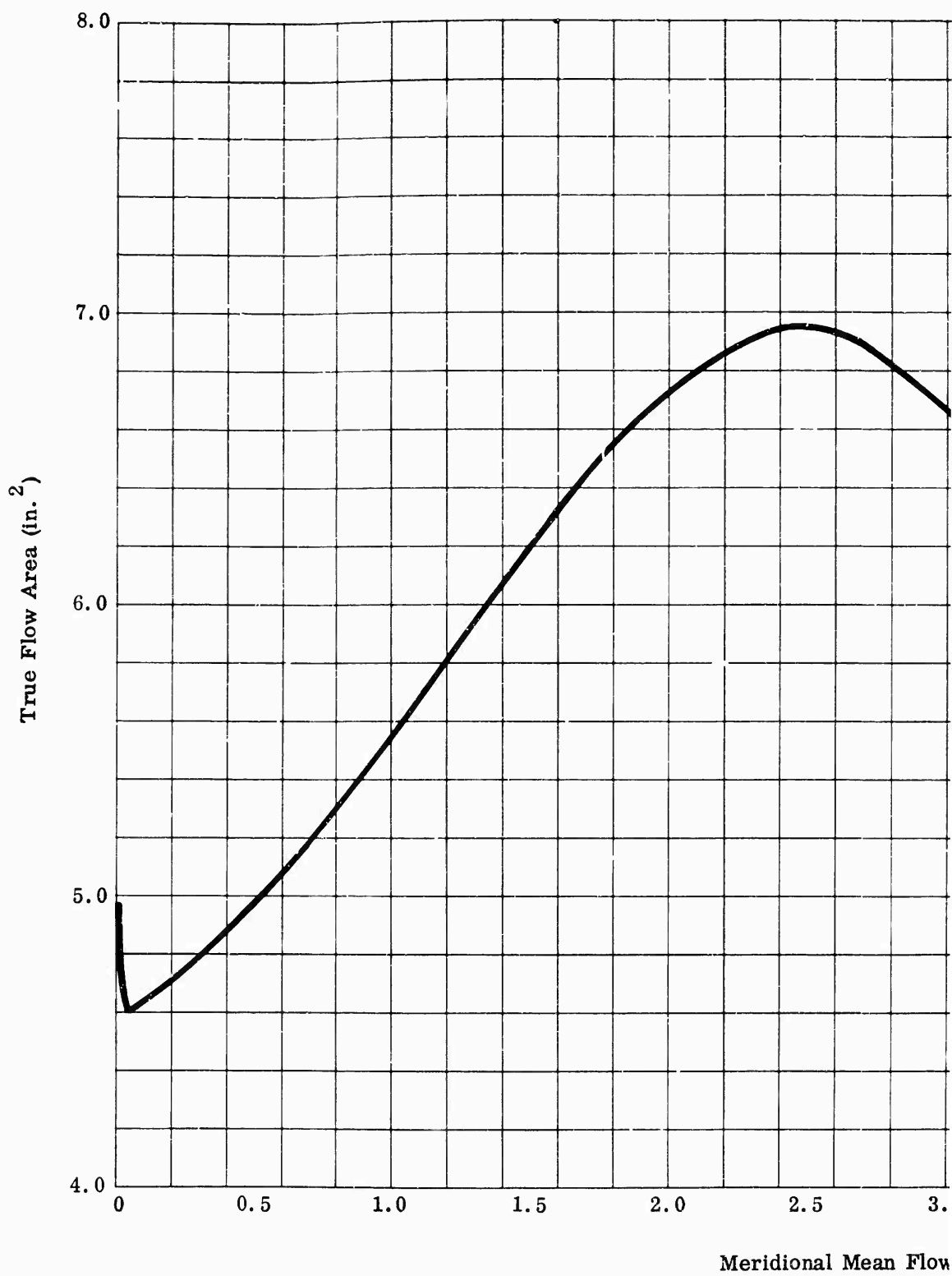
Figure 11. Blade-Root Stress, Temperature, and Safety Factor for MF-1.

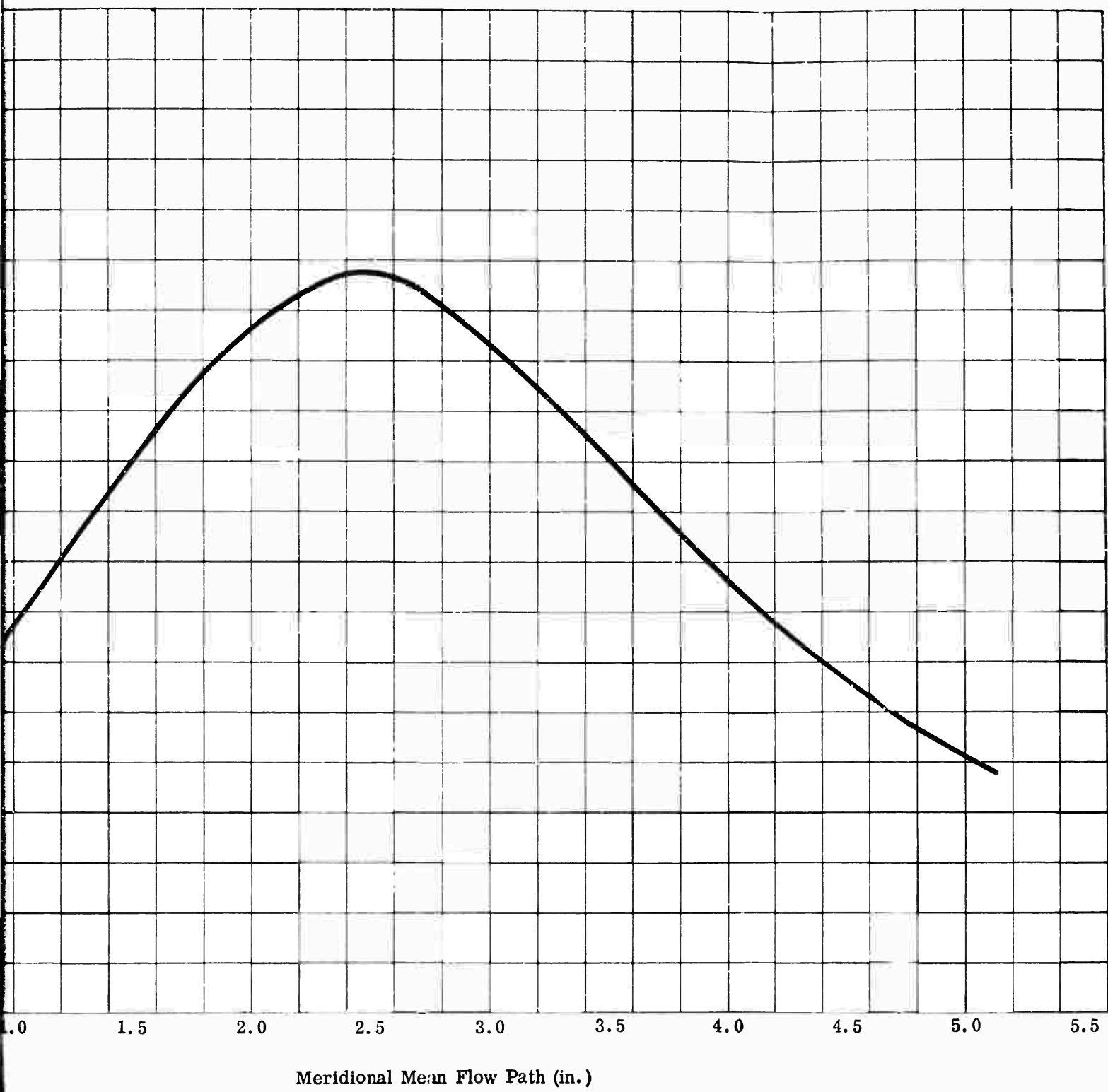
Flow Area Calculation											
Sec.	h	r ₁	r ₂	A _T $\pi h (r_1 + r_2)$	h'	t _t	t _r	A _B $\frac{N}{2} h' (t_t + t_r)$	A' (A _T - A _B)	φ	C
A	1.057	1.765	0.710	8.219	1.037			0.0	8.219	50.84	0
B	1.056	1.772	0.718	8.261	1.036	0.050	0.077	1.184	7.077	49.40	0
C	1.034	1.795	0.770	8.331	1.014	0.051	0.115	1.515	6.816	43.60	0
D	0.978	1.847	0.895	8.423	0.960	0.052	0.136	1.624	6.799	36.30	0
E	0.898	1.941	1.100	8.579	0.876	0.054	0.142	1.545	7.034	28.90	0
F	0.780	2.080	1.400	8.526	0.757	0.056	0.140	1.335	7.191	21.50	0
G	0.640	2.280	1.757	8.118	0.617	0.050	0.121	0.950	7.168	14.30	0
H	0.500	2.528	2.155	7.357	0.478	0.043	0.105	0.637	6.720	7.00	0
I	0.388	2.843	2.574	6.603	0.366	0.038	0.087	0.412	6.191	0.20	0
J	0.308	3.190	3.002	5.994	0.283	0.036	0.075	0.283	5.711	0	1
K	0.250	3.582	3.440	5.512	0.226	0.031	0.061	0.187	5.325	0	1
L	0.212	3.950	3.832	5.183	0.186	0.027	0.048	0.126	5.057	0	1

Figure 12. Impeller Flow Area of MF-1.

1

$\cos \phi$	$\frac{A}{A' \cos \phi}$
0.6315	5.190
0.6508	4.606
0.7242	4.936
0.8059	5.479
0.8755	6.158
0.9304	6.691
0.9690	6.946
0.9926	6.670
0.9999	6.190
1.0	5.711
1.0	5.325
1.0	5.057





**Disk Tangential Stress, Mass Section Properties, Weight
Mass Moment of Inertia, and Failure Load**

Material: Titanium
6Al-4V

$$I_{ts} = 3.43 \times 10^{-4} \text{ lb-in.-sec}^2$$

$$\omega = 0.1047 \text{ N radians/sec}$$

Speed, $N = 62,760 \text{ rpm}$
(10% overspeed)

$$v = 7.7 \times 10^5 \text{ lb}$$

$$\text{Density, } \gamma = 0.160 \text{ lb/in.}^3$$

Number of Blades, $n = 18$

$$W_{ts} = 4.08 \times 10^{-2} \text{ lb}$$

$$g = 386 \text{ in./sec}^2$$

Sg- in.-in. No.	①	②	③	④	⑤	⑥	⑦	Failure Stress 0.2% Yield			Failure Stress Ultimate				
	r	Δr	t	② x ③	① x ④	① x ⑤	① x ⑥	1	S _t	T	④ x ⑨	5	S _t	T	④ x ⑨
	in.	in.	in.	in. ²	in. ³	in. ⁴	in. ⁵	in.	psi	lb	psi	lb	psi	lb	psi
1	0.3425	0.0850	1.570	0.1335	0.04572	0.01566	0.005	156	101,500	13,550	150	111,000	14,818		
2	0.46875	0.1675	4.010	0.7722	0.36196	0.16967	0.079	211	95,500	73,745	211	106,000	81,111		
3	0.6525	0.2000	4.120	0.8240	0.53766	0.35082	0.229	222	94,500	71,068	222	105,500	79,362		
4	0.8525		2.925	0.7850	0.4971	0.42615	0.2	232	93,500	68,950	232	105,000	61,425		
5	1.0525		2.390	0.4780	0.50310	0.82961	0.557	243	92,500	44,215	243	104,000	49,712		
6	1.2525		2.040	0.4080	0.51102	0.88005	0.822	255	91,500	37,332	255	103,500	42,228		
7	1.4525		1.790	0.3580	0.52000	0.75536	1.097	268	90,500	32,398	268	102,500	36,695		
8	1.6525		1.575	0.3150	0.52754	0.68019	1.421	279	90,000	28,350	279	102,000	32,130		
9	1.8525		1.405	0.2810	0.52953	0.60432	1.786	291	89,000	25,009	291	101,500	28,722		
10	2.0525		1.245	0.2490	0.51167	1.04897	2.133	303	88,000	21,912	303	100,500	25,025		
11	2.2525		1.105	0.2230	0.49780	1.12129	2.526	316	87,500	19,588	316	100,000	22,100		
12	2.4525		0.975	0.1950	0.47824	1.17288	2.876	328	86,500	16,868	328	99,500	19,403		
13	2.6525		0.855	0.1710	0.45358	1.23312	3.191	341	86,000	14,706	341	98,500	16,844		
14	2.8525		0.740	0.1480	0.42217	1.20424	3.435	353	85,000	12,580	353	98,000	14,504		
15	3.0525		0.625	0.1240	0.37831	1.15540	3.527	366	84,500	10,478	366	97,500	12,090		
16	3.2525		0.500	0.1000	0.32525	1.05788	3.441	378	83,500	8,350	378	97,000			
17	3.4525		0.375	0.0740	0.25349	0.92626	3.045	390	83,000	6,142	390	96,000	7,104		
18	3.6525		0.255	0.0510	0.18028	0.68039	2.485	403	82,500	4,208	403	95,500	4,871		
19	3.8525		0.140	0.0260	0.09264	0.33375	1.515	414	82,000	2,181	414	95,000	2,327		

$A_{td} = 2 \Sigma ④$	11.03	in. ²
$t_d = [(2\gamma\omega^2 + \kappa) \Sigma ⑥]$	522,900	lb
$F_{ts} = F_{sr} x n + \pi$	44,199	lb
$I_{tw} = I_{td} / t_s$	567,099	lb
$I_{tu} = [(2\gamma\omega^2 + \kappa) \Sigma ⑦]$	0.8992	lb-in-sec ²
$I_{tw} = I_{td} / n I_{ts}$	0.0961	lb-in-sec ²
$W_d = 2\gamma \Sigma ⑤$	7.67	lb
$W_w = W_d / n I_{ts}$	8.40	lb
$\eta = F_{fy} / W_d$	1.44	-
$\eta_u = F_{fy} / F_{tw}$	1.62	-
$S_{tan} = F_{tw} / A_{td}$	51,400	psi

S_{tan} = Average Tangential Disk Stress

$$F_{fy} = 1.62 \times \Sigma ⑩ = 816,597 \quad F_{fy} = 1.62 \times \Sigma ⑩ = 920,942$$

S_t Failure Stress at Temperature, T

Figure 13. Disk Calculations for MF-1.

3.0 MF-2 IMPELLER ANALYSIS

This impeller is limited to 77,000 rpm for steady-state operation for the blade profile defined in Figure 16 due to the possibility of high vibratory stress at the 80,300 rpm design speed. By cutting the leading edge back in a straight line from the root at station no. 1 to the tip at station no. 3, as dimensioned in Figure 17, the maximum steady-state speed is increased to 80,300 rpm.

The calculated minimum safety factors for steady-state operation at 80,300 rpm and for an impeller inlet temperature of 60°F are as follows:

- 1) Blade safety factor is 1.95 to minimum 0.2-percent yield stress including $\pm 20,000$ psi vibratory stress.
- 2) Disk safety factors are 1.34 to minimum 0.2-percent yield stress and 1.53 to minimum ultimate stress.

The calculated minimum safety factors for momentary operation at 88,600 rpm and for an impeller inlet temperature of 60°F are as follows:

- 1) Blade safety factor is 2.50 to minimum 0.2-percent yield stress.
- 2) Disk safety factors are 1.10 to minimum 0.2-percent yield stress and 1.25 to minimum ultimate stress.

The weight of the impeller is 5.24 pounds, and the mass moment of inertia is 0.0347 lb-in.-sec².

Figures 14 through 23 present the results of stress and vibration analyses for the MF-2 impeller.

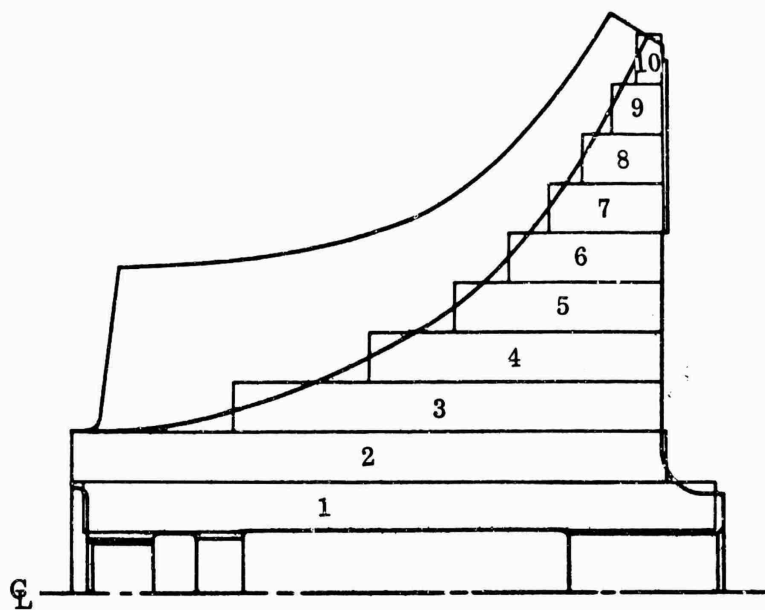


Figure 14. Disk and Blade Profile of MF-2.

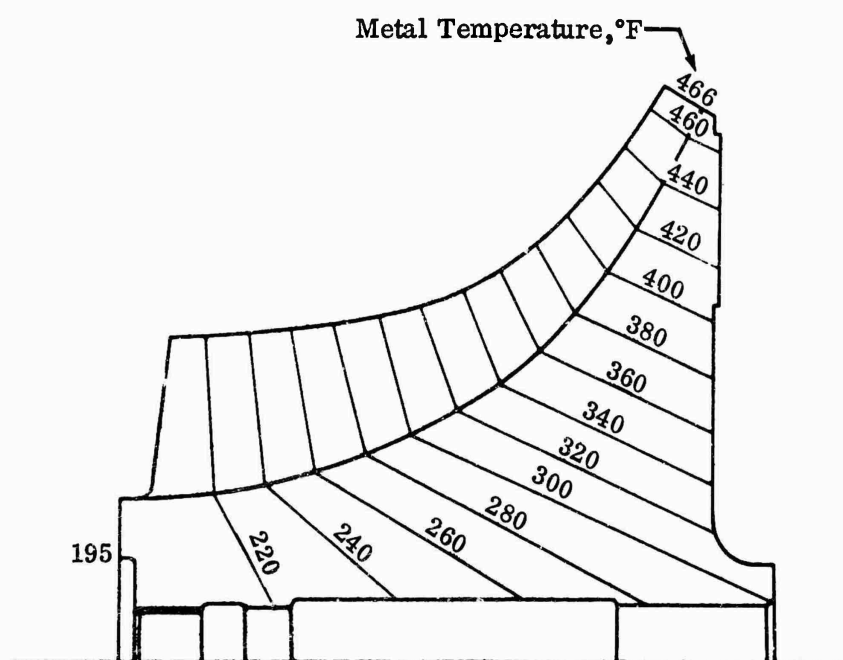


Figure 15. Temperature Distribution of MF-2.

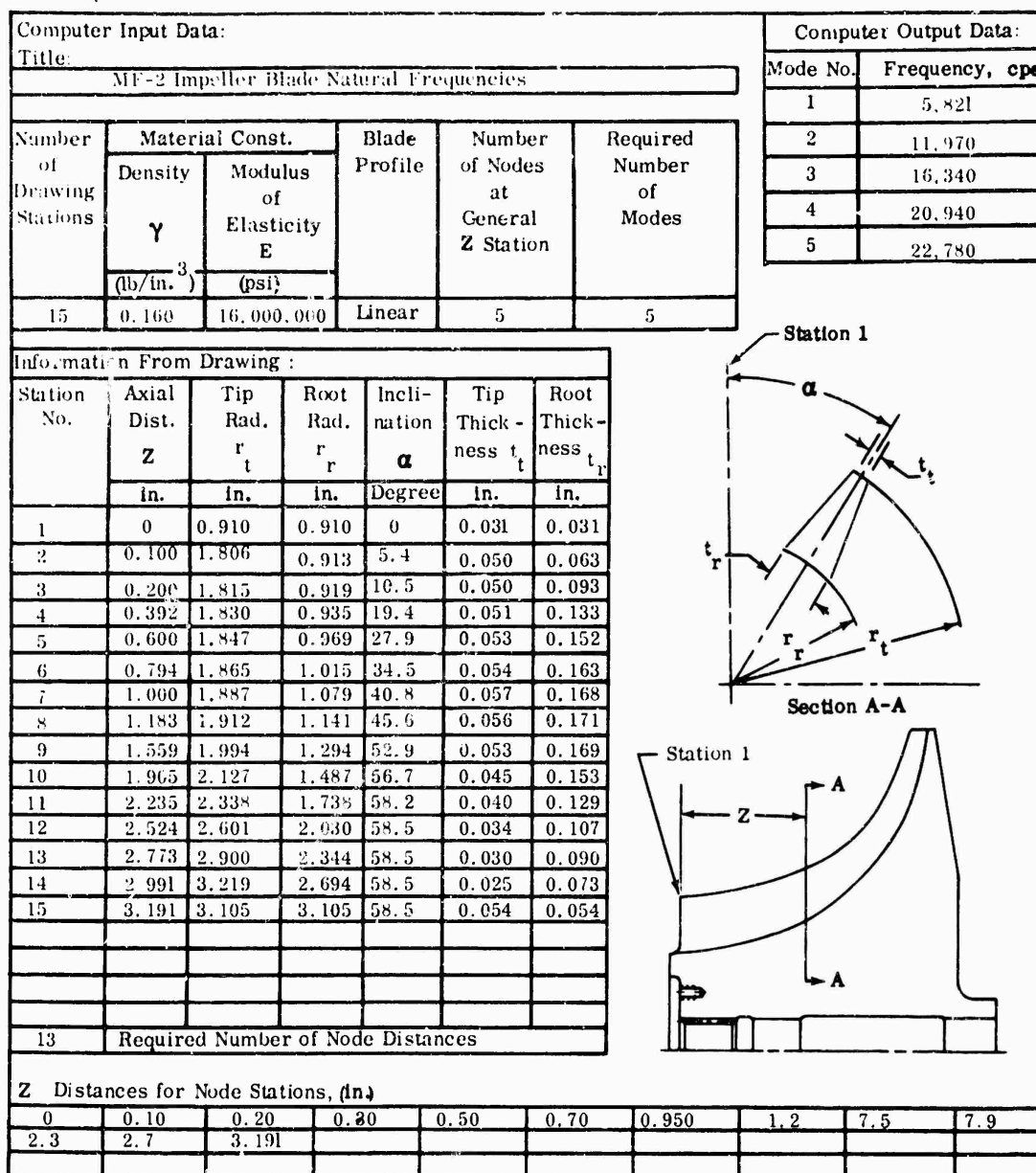


Figure 16. Natural Frequencies of MF-2 Blades.

Computer Input Data:

Title: MF-2 Impeller - Modified Blade Natural Frequencies

Number of Drawing Stations	Material Const.		Blade Profile	Number of Nodes at General Z Station	Required Number of Modes
	Density	Modulus of Elasticity			
	γ	E			
	(lb/in. ³)	(psi)			
15	0.160	16,000,000	Linear	5	5

Information From Drawing :

Station No.	Axial Dist. Z	Tip Rad. r _t	Root Rad. r _r	Inclination α	Tip Thick-ness t _t	Root Thick-ness t _r
	in.	in.	in.	Degree	in.	in.
1	0	0.910	0.910	0	0.031	0.031
2	0.100	1.361	0.913	5.4	.041	0.063
3	0.200	1.815	0.919	10.5	0.050	0.093
4	0.392	1.830	0.935	19.4	0.051	0.133
5	0.600	1.847	0.969	27.9	0.053	0.152
6	0.794	1.865	1.015	34.5	0.054	0.163
7	1.000	1.887	1.079	40.8	0.057	0.168
8	1.183	1.912	1.141	45.6	0.056	0.171
9	1.559	1.994	1.294	52.9	0.053	0.169
10	1.905	2.127	1.487	56.7	0.045	0.153
11	2.235	2.338	1.738	58.2	0.040	0.129
12	2.524	2.601	2.030	58.5	0.034	0.107
13	2.773	2.900	2.344	58.5	0.030	0.090
14	2.991	3.219	2.694	58.5	0.025	0.073
15	3.191	3.105	3.195	58.5	0.054	0.054
13	Required Number of Node Distances					

Z Distances for Node Stations, (in.)

0	0.10	0.20	0.30	0.50	0.70	0.95	1.20	1.50	1.90
2.30	2.70	3.191							

Computer Output Data:

Mode No.	Frequency, cps
1	5.970
2	11.760
3	16.240
4	19.260
5	21.870

Station 1

Section A-A

Figure 17. Revised Natural Frequencies of MF-2 Blades.

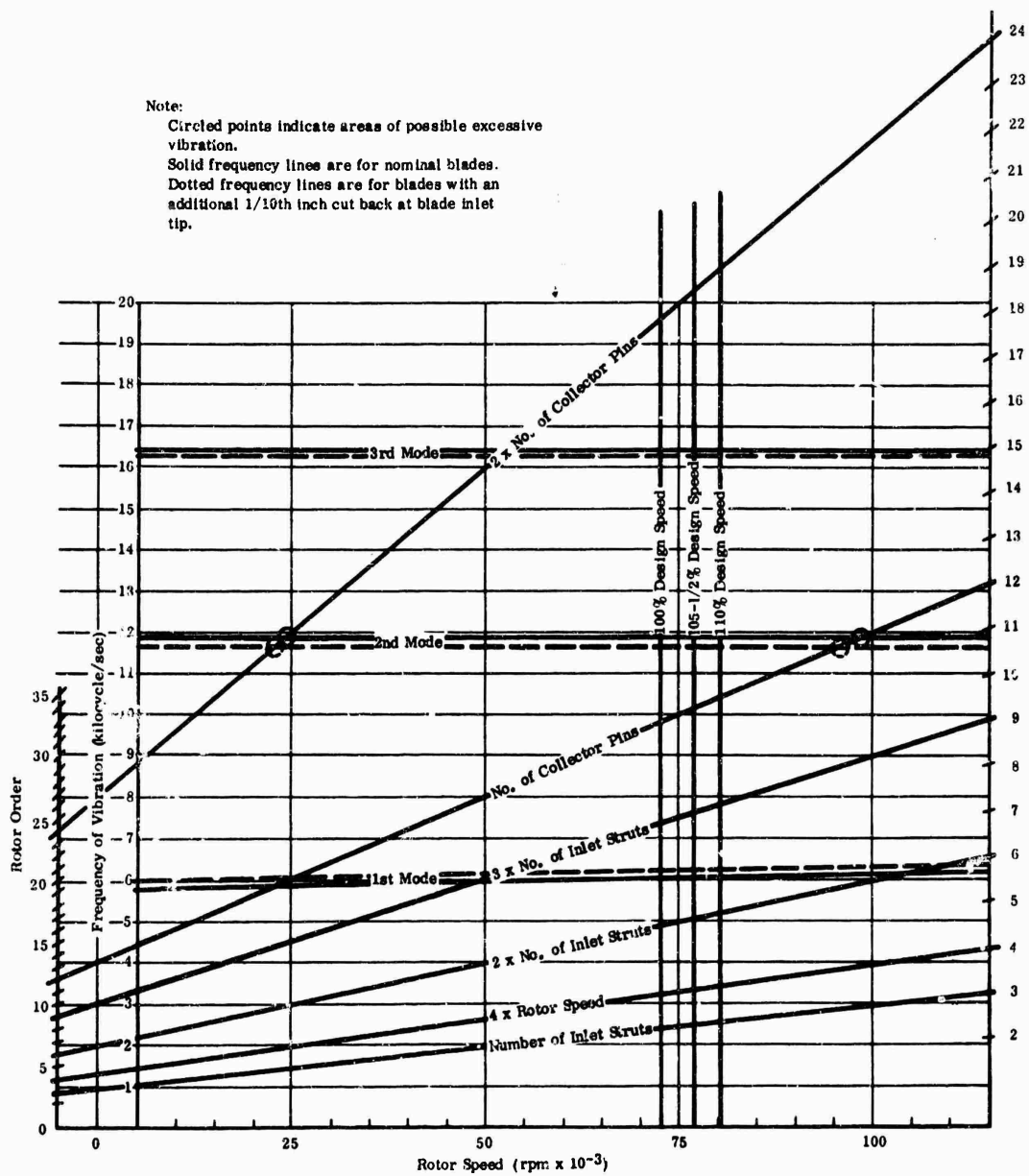


Figure 18. Campbell Diagram for MF-2.

Radial Flow Blade Root Stress, Force/in., Weight/in., and Mass Moment of Inertia/in.

Material: Titanium, 6Al-4V

$\omega = 0.1047 \times N \text{ radians/sec}^2$

Speed, $N = 80,300 \text{ rpm}$
(10% overspeed)

Density, $\gamma = 0.160 \text{ lb/in.}^3$

$g = 386 \text{ in./sec}^2$

Blade Station No.			2	3	5	9	10	12	14
1	r_t	in.	1.807	1.816	1.848	1.995	2.127	2.601	3.219
2	r_r	in.	0.913	0.918	0.969	1.295	1.488	2.030	2.694
3	t_t	in.	0.050	0.050	0.053	0.053	0.045	0.034	0.025
4	t_r	in.	0.063	0.093	0.152	0.169	0.153	0.107	0.073
5	r_t^2	① ²	3.2652	3.2979	3.4151	3.9800	4.5241	6.7652	10.3620
6	r_r^2	① x ⑤	5.9003	5.9849	6.3111	7.9401	9.6328	17.5963	33.3553
7	r_t^3	② ³	0.8336	0.8427	0.8390	1.6770	2.2141	4.1209	7.2876
8	r_r^3	② x ⑦	0.7610	0.7736	0.9099	2.1717	3.2946	8.3654	19.5521
9	$r_t - r_r$	① - ②	0.8940	0.898	0.879	0.700	0.639	0.571	0.525
10	$r_t^2 - r_r^2$	⑤ - ⑦	2.4916	2.4552	2.4761	2.303	2.310	2.6443	3.1044
11	$r_t^3 - r_r^3$	⑥ - ⑧	5.1393	5.2153	5.4012	5.7684	6.3282	8.2309	13.8032
12	$t_t - t_r$	④ - ③	0.013	0.043	0.099	0.116	0.108	0.0730	0.048
13	$r_t^2 - t_t^2$	⑤ - ④	0.0145	0.0479	0.1126	0.1657	0.1690	0.1278	0.0914
14		③ x ②	0.0132	0.0440	0.1091	0.2146	0.2515	0.2594	0.2462
15		④ + ③	0.0762	0.1370	0.2611	0.3836	0.4045	0.3664	0.3192
16		⑤ x ⑩ + 2	0.0926	0.1681	0.3233	0.4417	0.4672	0.4844	0.4955
17		③ x ⑩ + 3	0.0248	0.0835	0.2027	0.3186	0.3565	0.3932	0.4205
18		⑥ - ⑦	0.0678	0.0848	0.1206	0.1231	0.1107	0.0912	0.0750
19	F_r	$\frac{\gamma \omega^2}{g}$ ⑬	1,990	2,480	3,530	3,610	3,240	2,670	2,200
20	S_{root}	⑬ + ④	31,530	26,720	23,250	21,340	21,200	24,970	30,100
21	r_t^4	① x ⑥	10.6616	10.8758	11.6629	15.8405	20.4677	45.7680	107.3717
22	r_r^4	② x ⑧	0.6948	0.7102	0.8808	2.8124	4.9024	16.9818	52.6734
23	$r_t^4 - r_r^4$	②1 - ②2	9.9670	10.1656	10.7821	13.0281	15.5653	28.7862	54.6973
24	$t_t^4 - t_r^4$	③ + ④	0.113	0.143	0.205	0.222	0.198	0.141	0.098
25		③ x ⑩ + 3	0.1305	0.2382	0.4701	0.7376	0.8533	1.1274	1.4687
26		③ x ⑩ + 4	0.0361	0.1217	0.3035	0.5397	0.6576	0.9197	1.2498
27		⑤ - ⑥	0.0944	0.1165	0.1666	0.1979	0.1957	0.2077	0.2189
28	$I' \times 10^4$	$\frac{\gamma}{g}$ ②7	0.39	0.48	0.69	0.83	0.81	0.86	0.91
29		⑨ x ④	0.1010	0.1284	0.1802	0.314	0.1265	0.0805	0.0515
30	$W' \times 10^3$	$\frac{\gamma}{g}$ ②9	0.81	1.03	1.44	1.24	1.01	0.84	0.41

Figure 19. Blade Stress Calculations for MF-2.

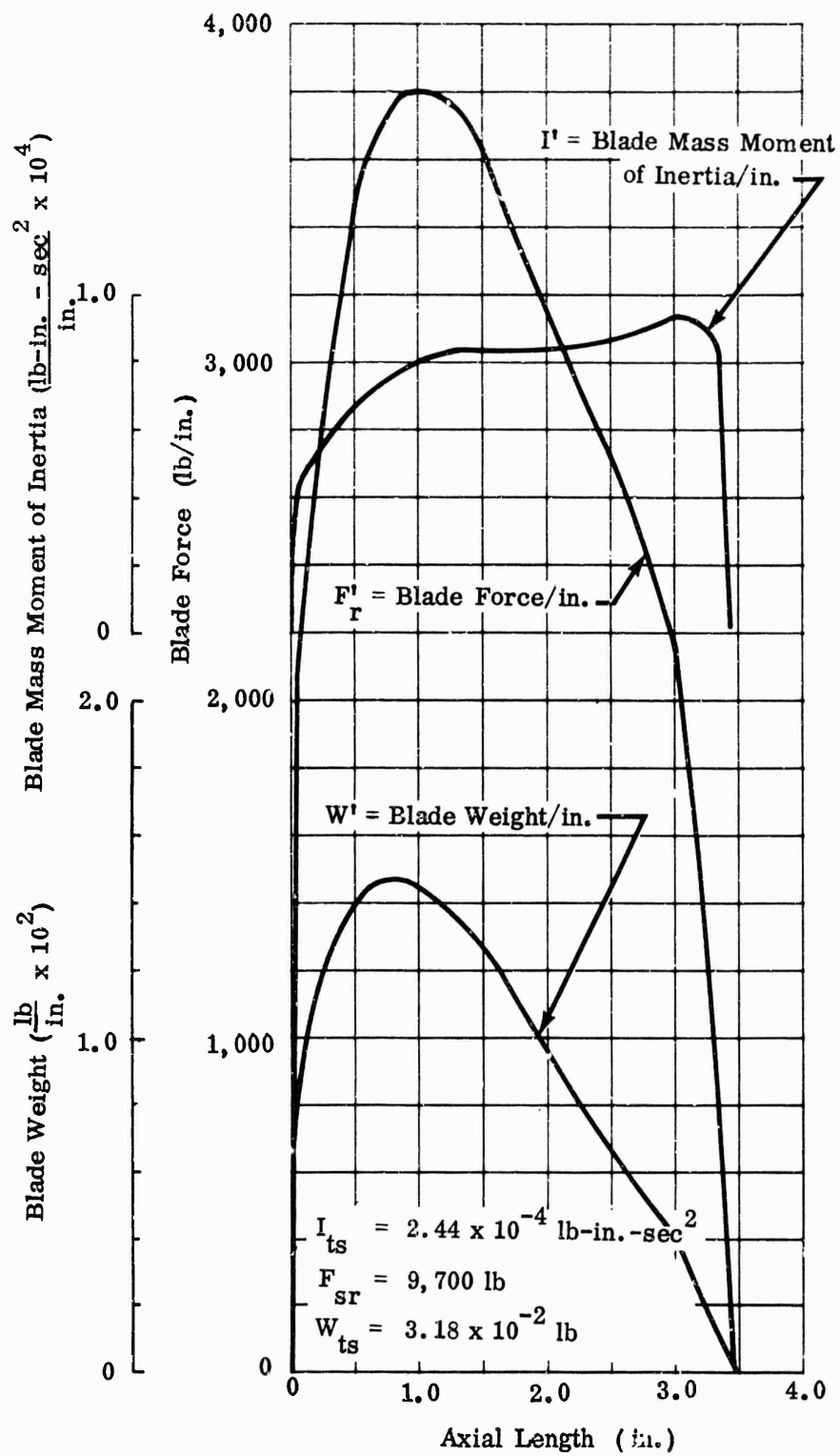


Figure 20. MF-2 Impeller-Blade Force, Weight, and Inertia.

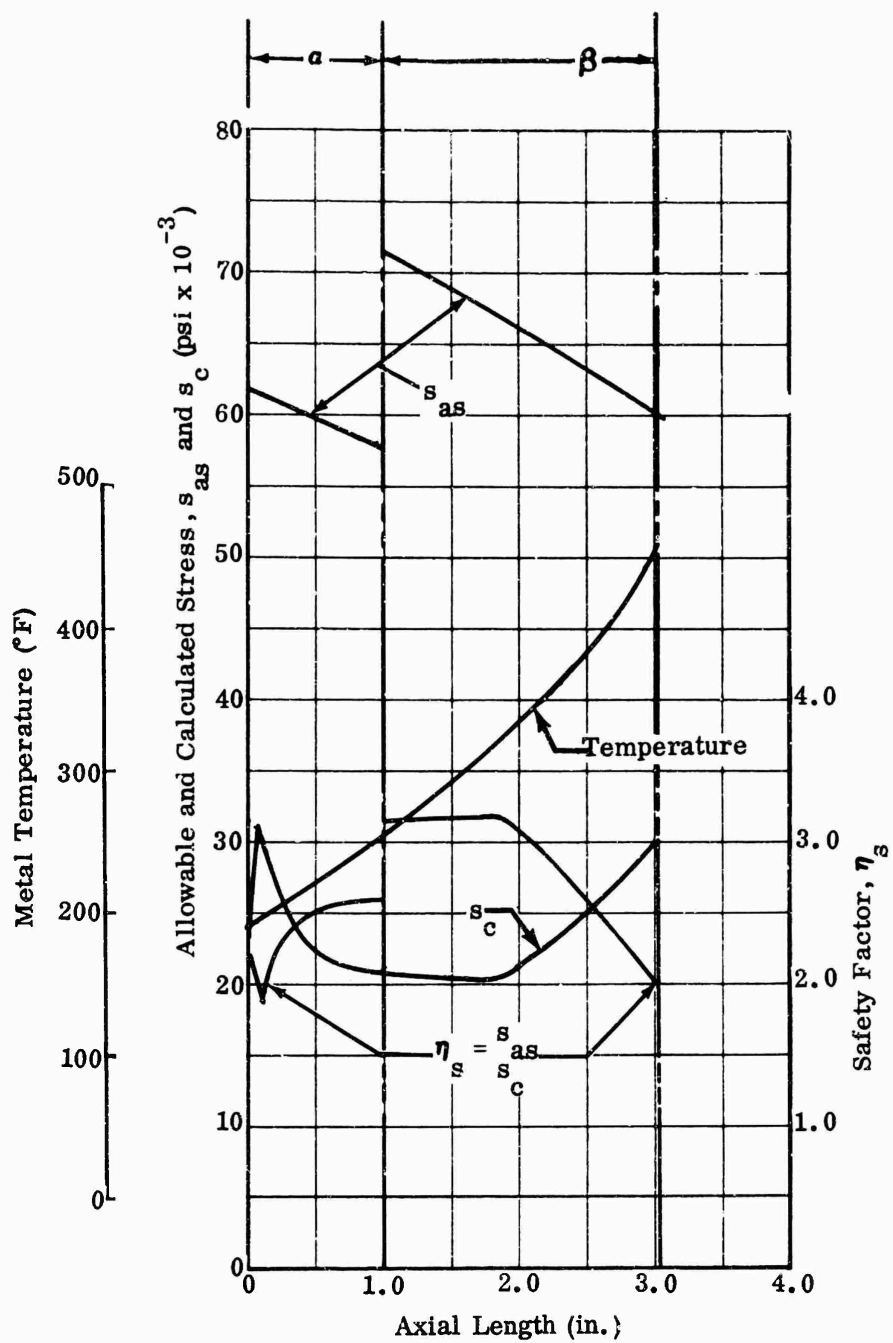
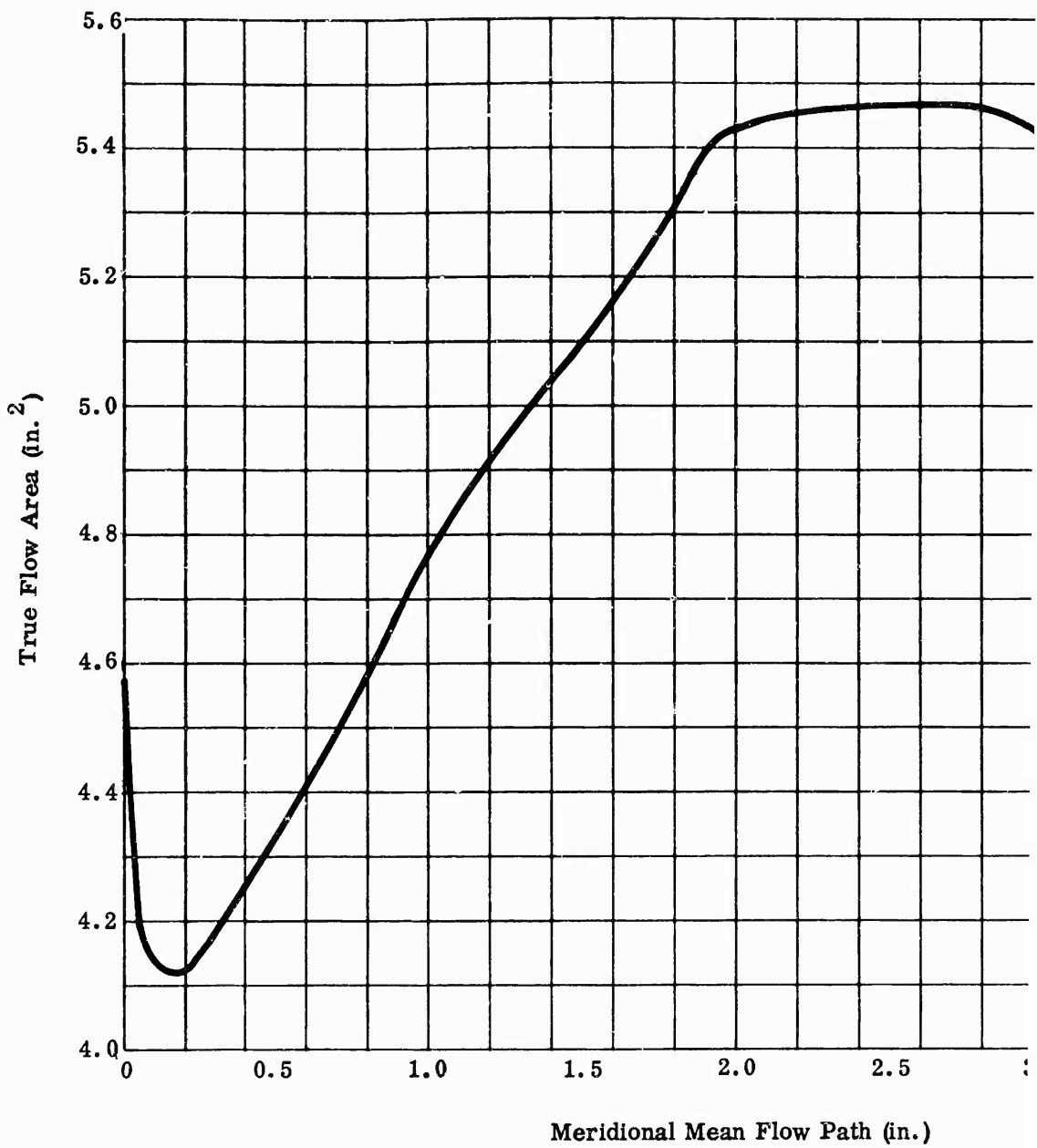


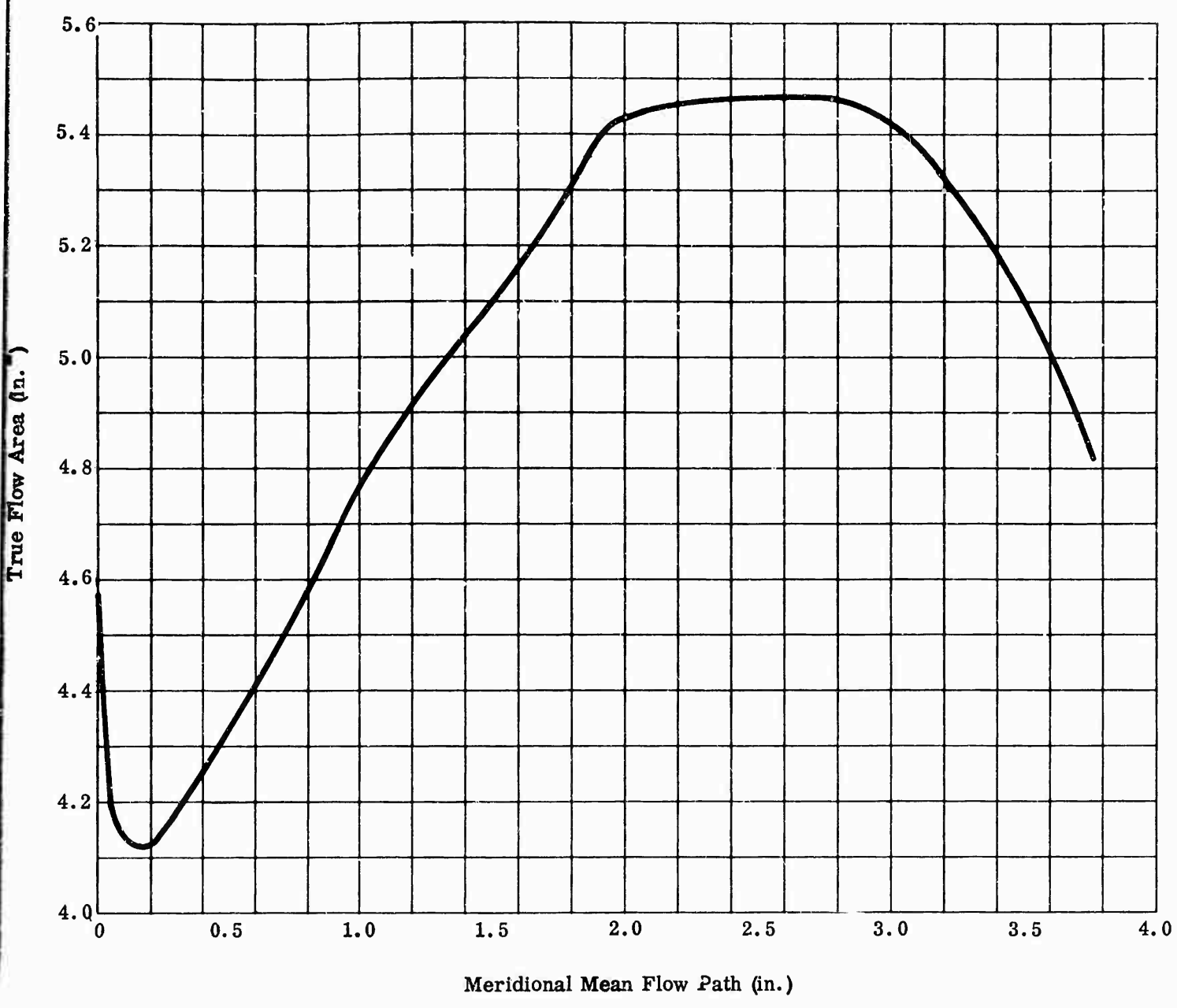
Figure 21. Blade-Root Stress, Temperature, and Safety Factor for MF-2.

Flow Area Calculation											
Sec.	h	r ₁	r ₂	$\frac{A_T}{\pi h (r_1 + r_2)}$	h'	t _t	t _r	$\frac{N}{2} \frac{A_B}{h' (t_t + t_r)}$	$A' (A_T - A_B)$	Φ	C
A	0.909	1.819	0.910	7.793					7.793	54.00	0.
B	0.911	1.826	0.914	7.842	0.782	0.051	0.073	0.970	6.872	53.00	0.
C	0.915	1.834	0.920	7.917	0.894	0.050	0.100	1.341	6.576	51.20	0.
D	0.911	1.849	0.942	7.988	0.891	0.050	0.138	1.675	6.313	47.70	0.
E	0.852	1.880	1.038	7.810	0.832	0.053	0.165	1.814	5.996	40.20	0.
F	0.763	1.921	1.177	7.426	0.743	0.057	0.172	1.702	5.724	32.50	0.
G	0.670	1.987	1.356	7.037	0.650	0.054	0.165	1.424	5.613	23.65	0.
H	0.570	2.089	1.591	6.590	0.550	0.048	0.143	1.051	5.539	12.35	0.
I	0.475	2.257	1.889	6.1869	0.455	0.041	0.117	0.719	5.468	4.30	0.
J	0.404	2.489	2.218	5.974	0.384	0.037	0.097	0.515	5.459	0	1
K	0.340	2.767	2.562	5.692	0.320	0.032	0.079	0.355	5.337	0	1
L	0.294	2.993	2.831	5.379	0.274	0.029	0.066	0.260	5.119	0	1
M	0.279	3.075	2.933	5.266	0.259	0.028	0.061	0.230	5.036	0	1
N	0.265	3.153	3.020	5.139	0.245	0.027	0.058	0.208	4.931	0	1
O	0.251	3.230	3.105	5.000	0.231	0.025	0.054	0.182	4.813	0	1

Figure 22. Impeller Flow Area of MF-2.

$\cos \phi$	$A' \cos \phi$
0.58779	4.581
0.60182	4.136
0.62660	4.121
0.67301	4.249
0.76380	4.580
0.84339	4.828
0.91601	5.142
0.97686	5.411
0.99719	5.453
1.0000	5.459
1.0000	5.337
1.0000	5.119
1.0000	5.036
1.0000	4.931
1.0000	4.813





4.0 MF-3 IMPELLER ANALYSIS

The impeller is satisfactory for steady-state operation. Analysis of the configuration defined in Figure 26 indicated that excessive blade vibration might be encountered. The leading edge of the impeller blade was modified as defined in Figure 27. Frequency calculations were made for both configurations to serve as a guide for leading edge modifications. The circled points on Figure 28 indicate the regions of concern.

The blade stress analysis was based on dimensions of the preliminary design. These dimensions differ from those used in the blade frequency analyses (Figures 26 and 27) because the blade dimensions were modified slightly to change the frequencies to the proper range. The blade stresses were not recalculated for the new blade configurations because a check of the most highly stressed station showed that the revised dimensions produced lower stresses.

The minimum safety factors for steady-state operation at 65,000 rpm and for an impeller inlet temperature of 60°F are as follows:

- 1) Blade safety factor is 3.07 to minimum 0.2-percent yield stress including $\pm 20,000$ psi vibratory stress.
- 2) Disk safety factors are 1.80 to minimum 0.2-percent yield stress and 2.02 to minimum ultimate stress.

The minimum safety factors for momentary operation at 82,600 rpm and an impeller inlet temperature of 60°F are as follows:

- 1) Blade safety factor is 2.68 to minimum 0.2-percent yield stress.
- 2) Disk safety factors are 1.11 to minimum 0.2-percent yield stress and 1.25 to minimum ultimate stress.

The weight of the impeller is 5.30 pounds, and the mass moment of inertia is 0.0450 lb-in.-sec².

Figures 24 through 33 present the results of stress and vibration analyses for the MF-3 impeller.

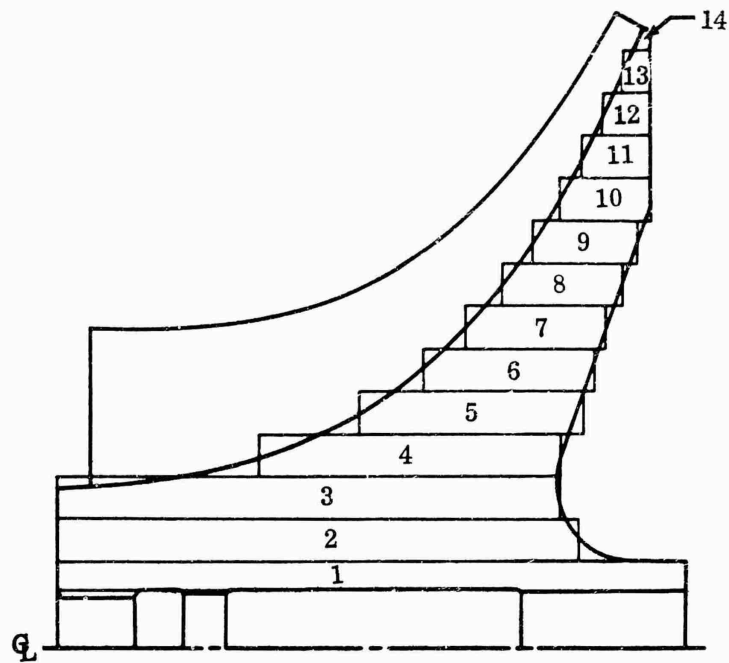


Figure 24. Disk and Blade Profile of MF-3.

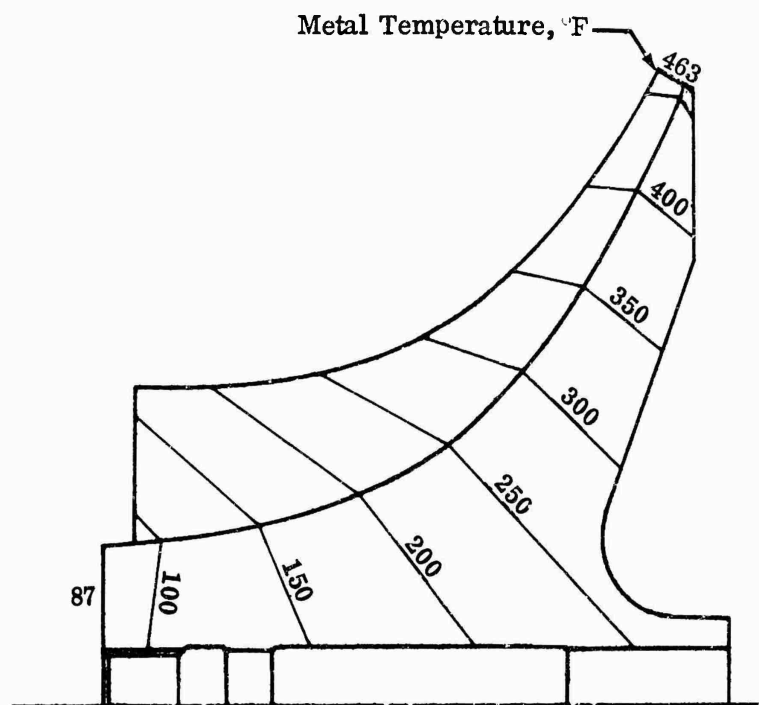
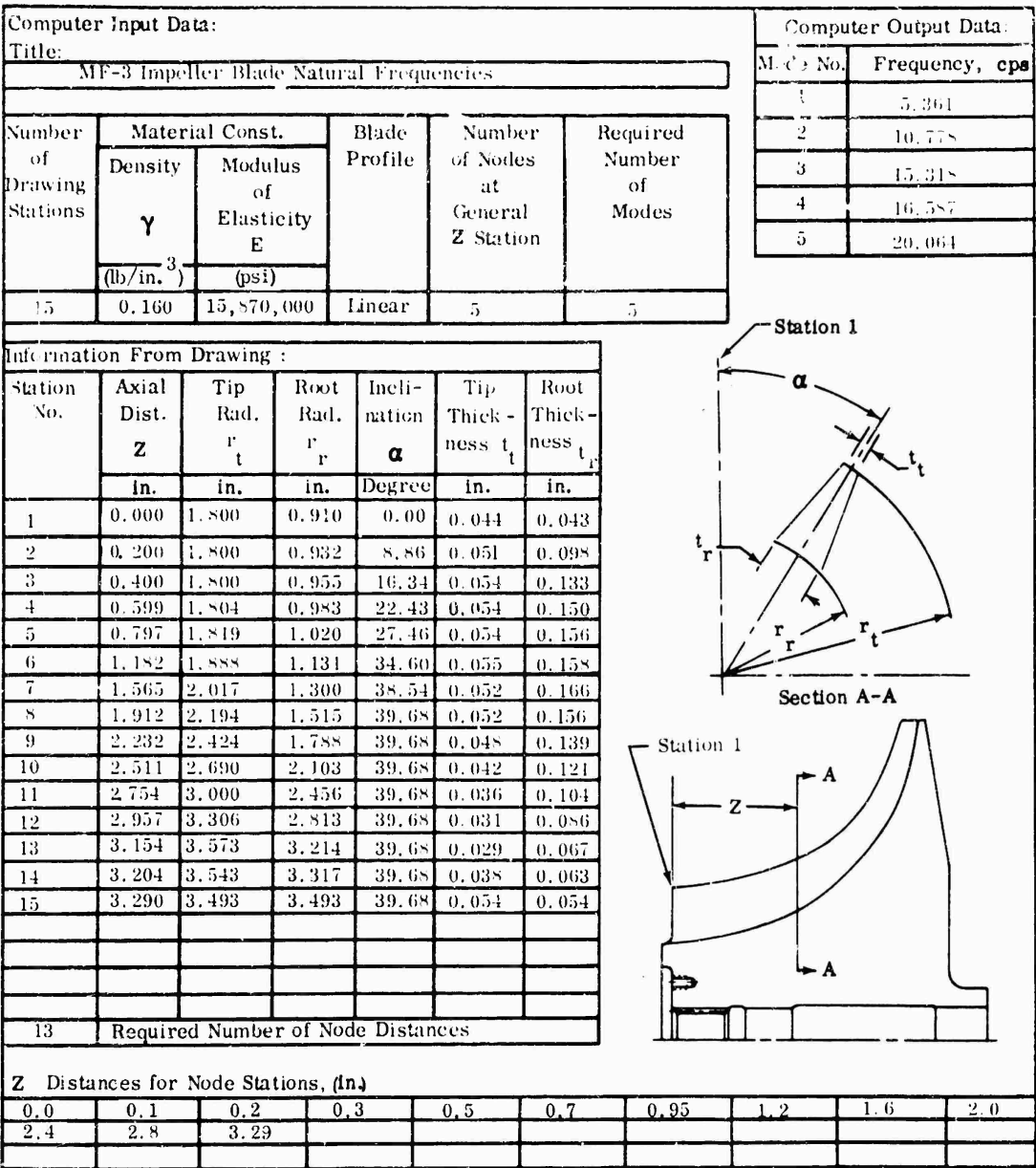


Figure 25. Temperature Distribution of MF-3.



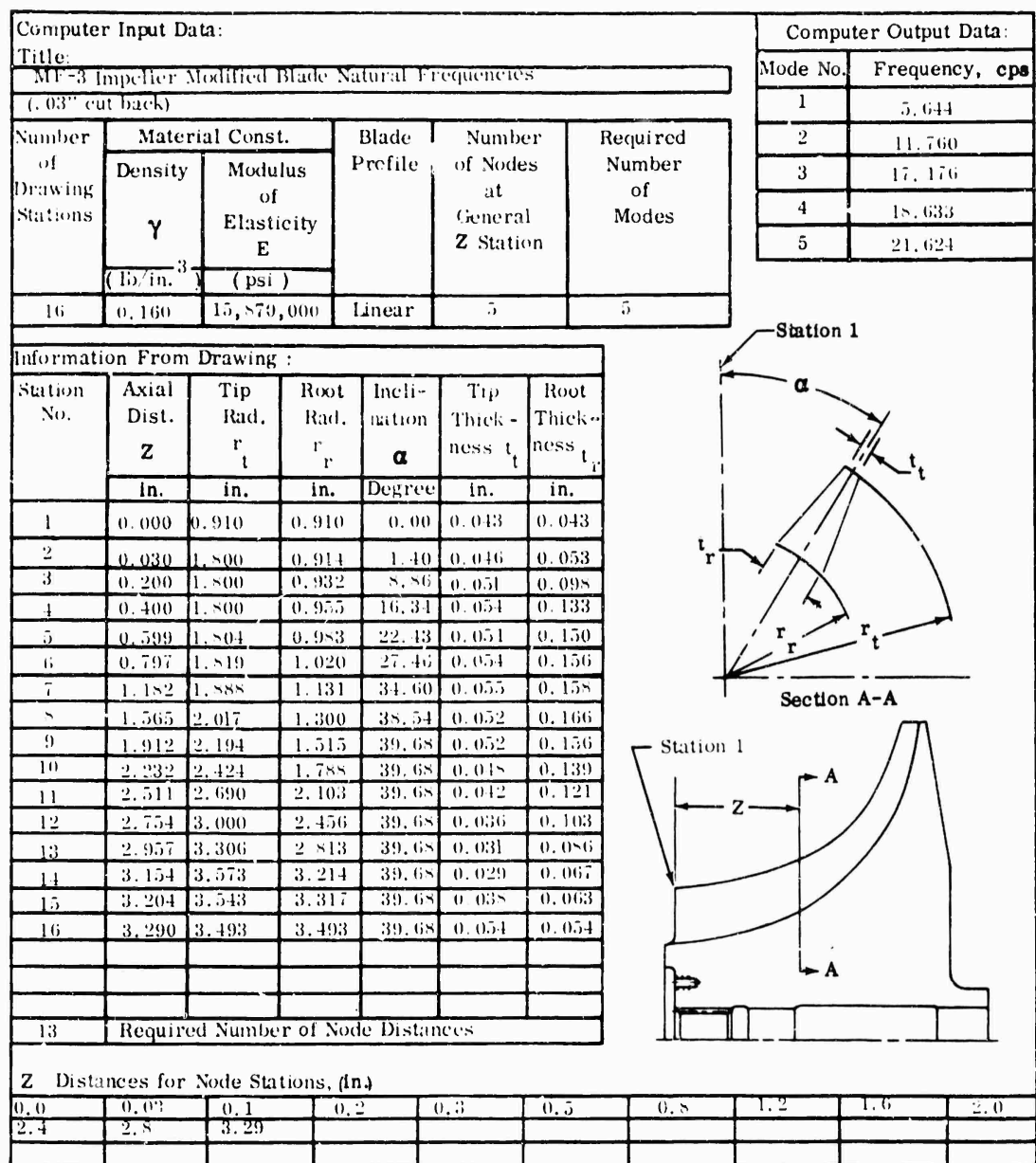


Figure 27. Natural Frequencies of Modified MF-3 Blades.

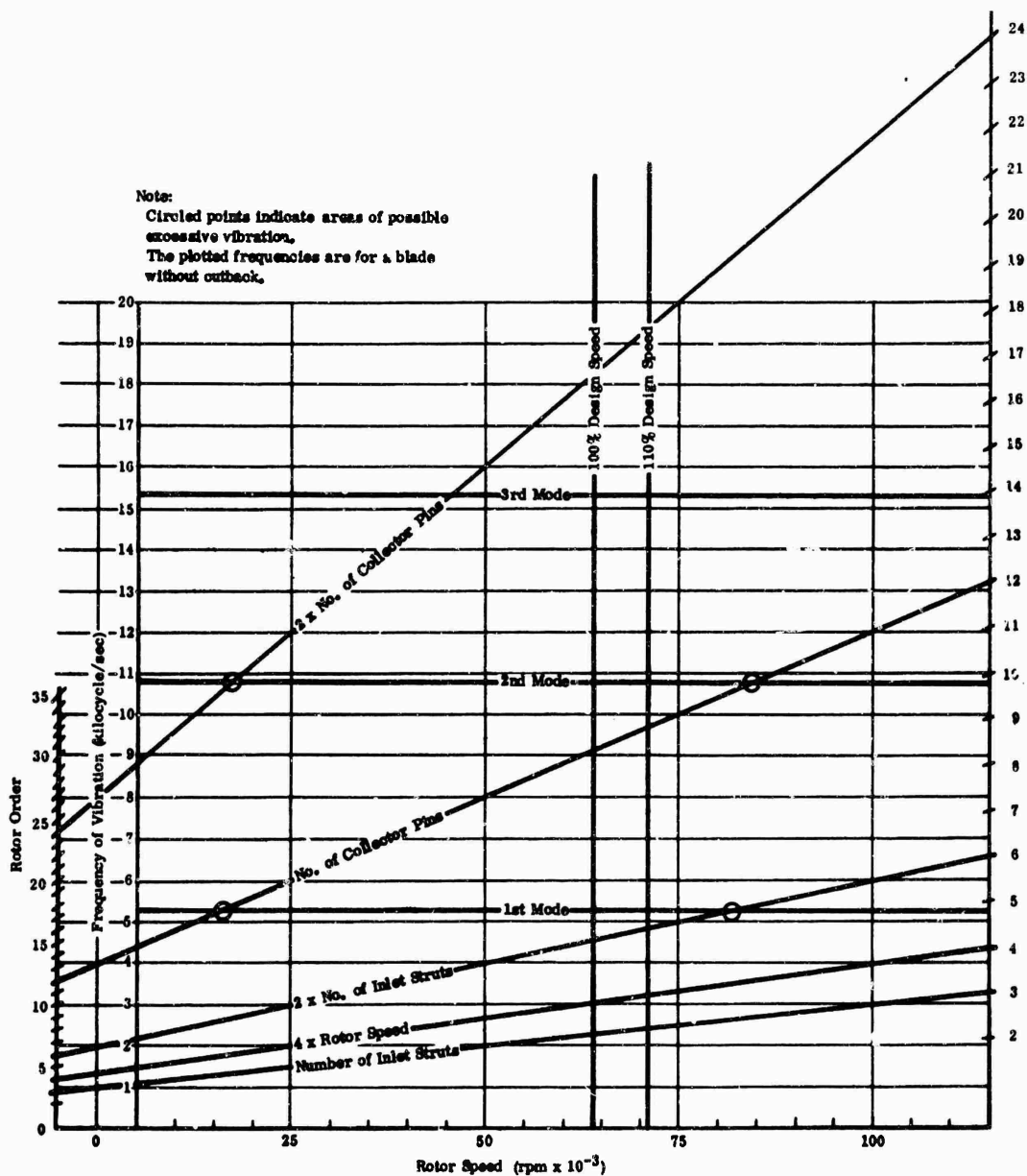


Figure 28. Campbell Diagram for MF-3.

Density, $\gamma = 0.160 \text{ lb/in.}^3$

[illegible]

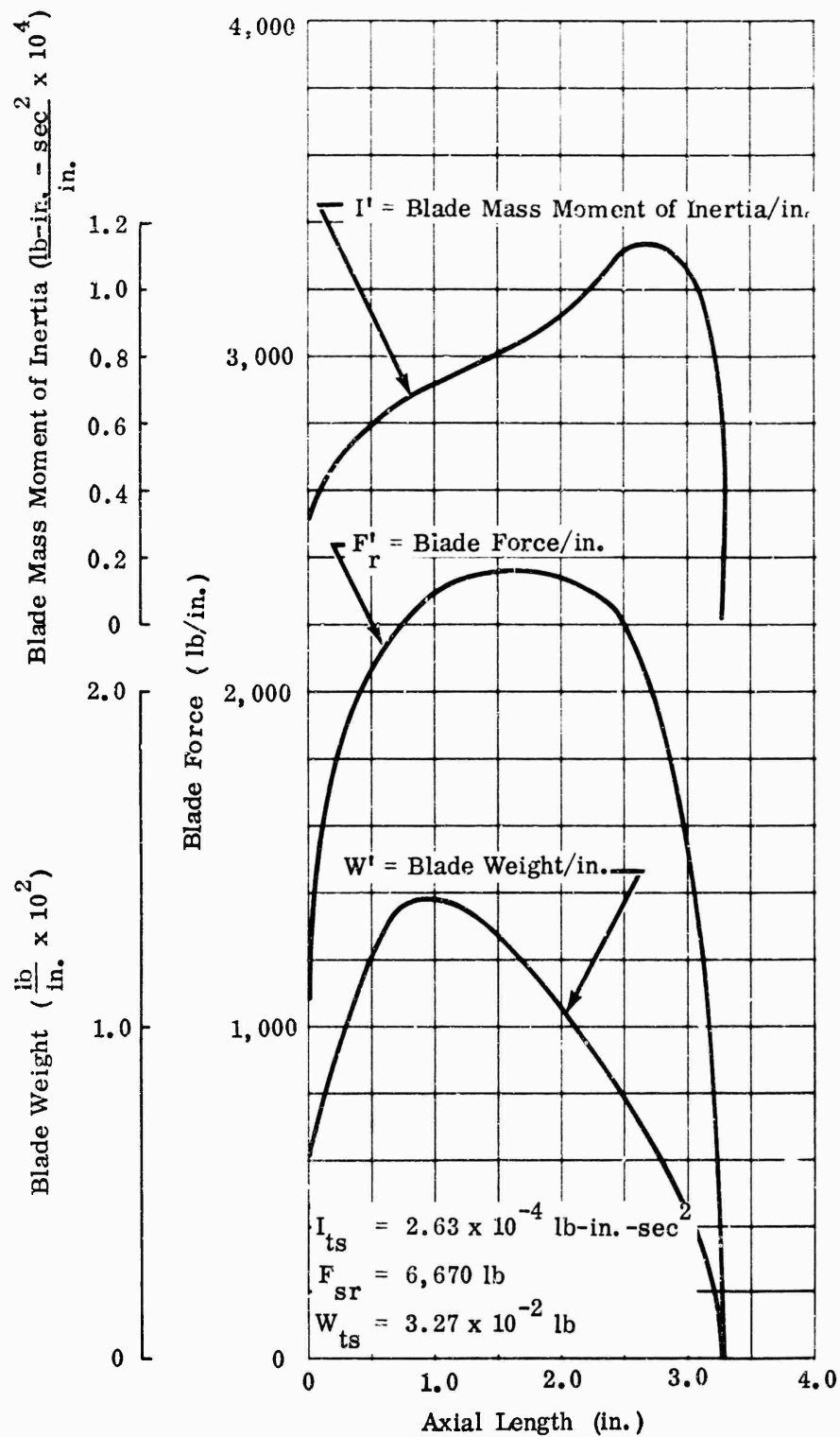


Figure 30. MF-3 Impeller-Blade Force, Weight, and Inertia.

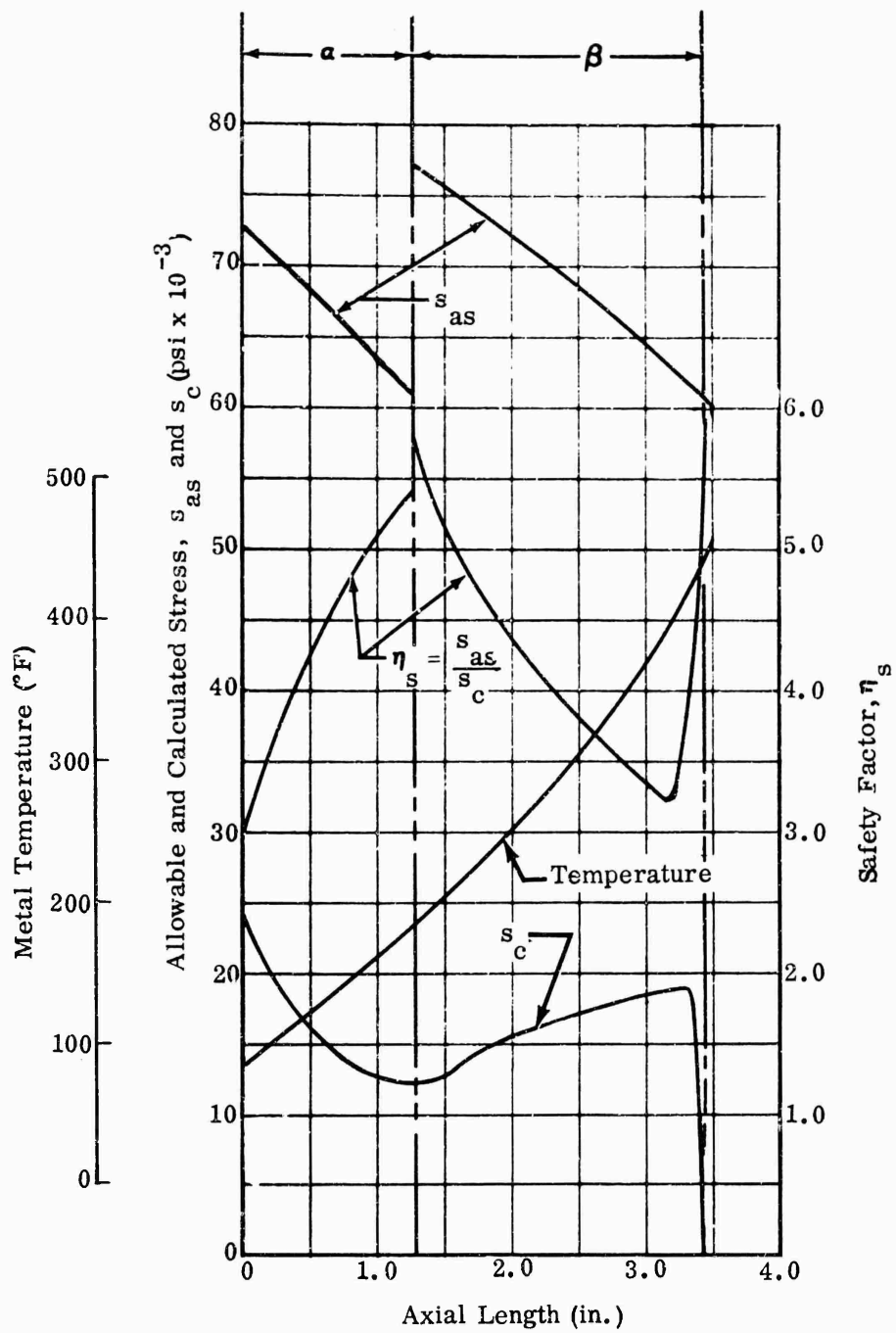
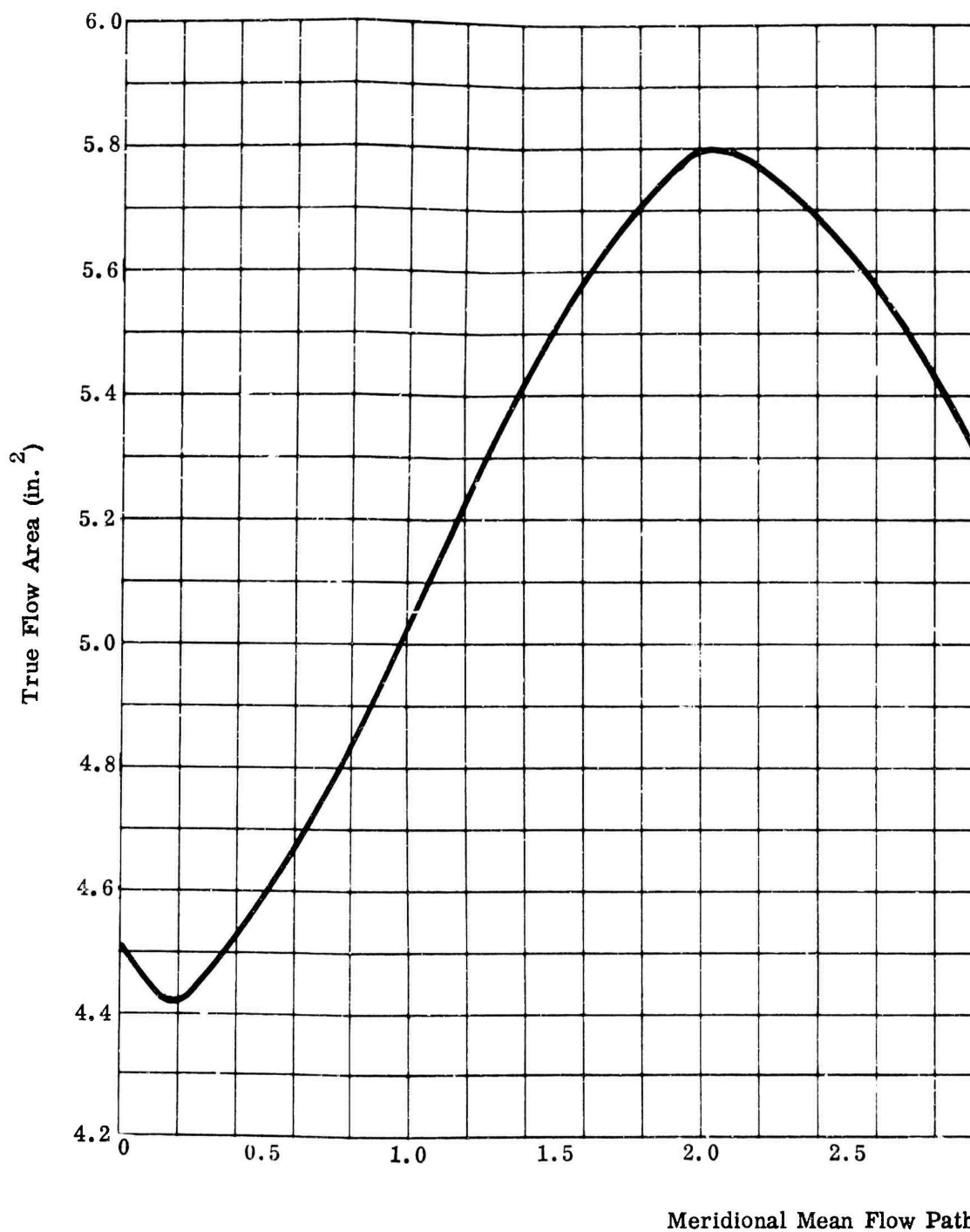


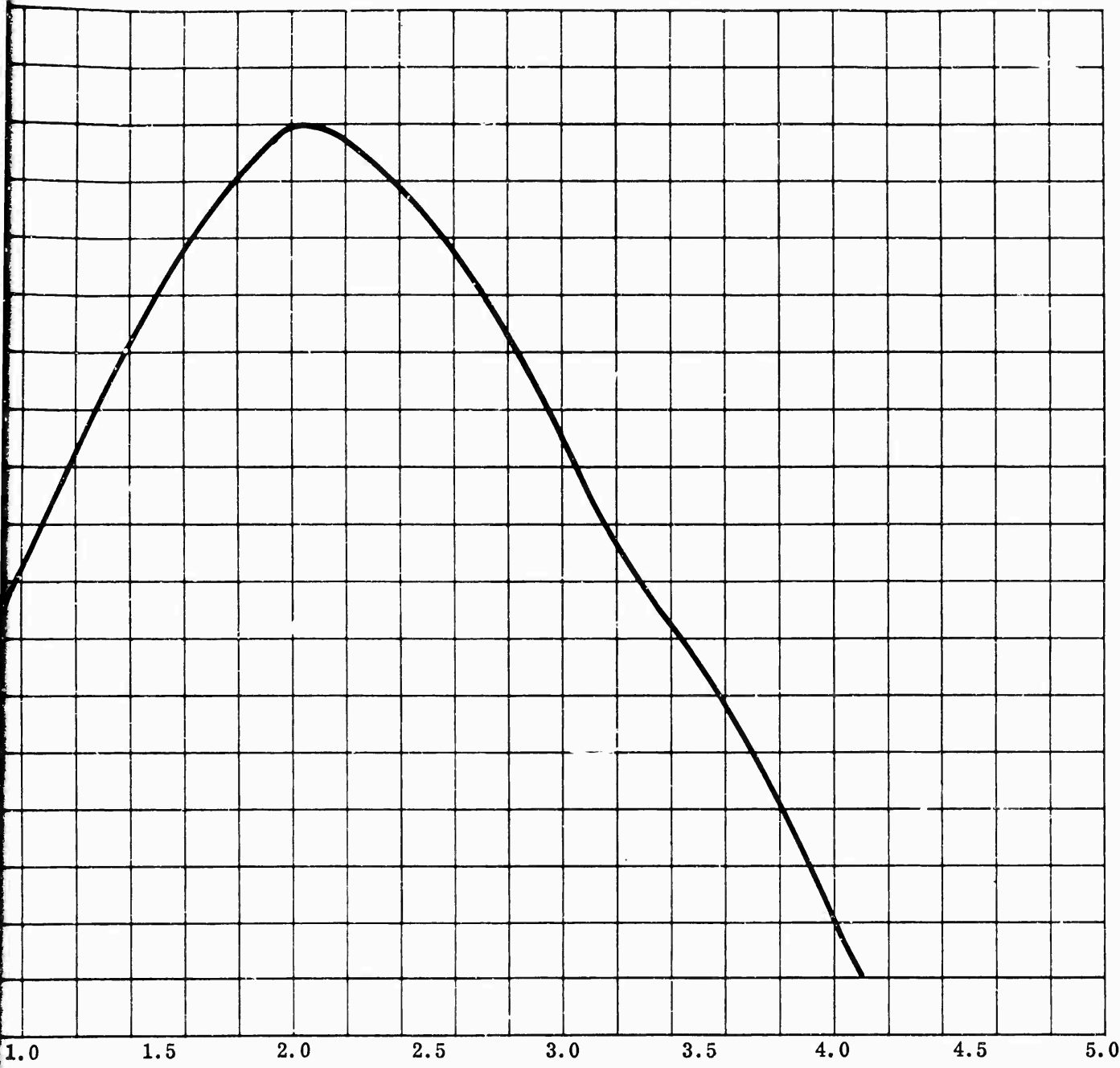
Figure 31. Blade-Root Stress, Temperature, and Safety Factor for MF-3.

Flow Area Calculation											
Sec.	h	r ₁	r ₂	$\frac{A_T}{\pi h (r_1 + r_2)}$	h'	t _t	t _r	$\frac{A_B}{\frac{N}{2} h' (t_t + t_r)}$	A' (A _T - A _B)	Φ	
A	0.910	1.820	0.910	7.805	0.890	0.044	0.043	0.774	7.031	50.0	0.
B	0.888	1.820	0.932	7.677	0.868	0.049	0.101	1.302	6.375	46.1	0.
C	0.863	1.820	0.958	7.530	0.843	0.053	0.135	1.585	5.945	40.4	0.
D	0.835	1.821	0.991	7.380	0.815	0.054	0.152	1.679	5.701	35.1	0.
E	0.805	1.830	1.037	7.251	0.785	0.054	0.156	1.649	5.602	30.6	0.
F	0.739	1.883	1.181	7.110	0.719	0.055	0.162	1.560	5.550	20.0	0.
G	0.664	1.985	1.391	7.045	0.644	0.052	0.164	1.391	5.654	10.0	0.
H	0.580	2.130	1.655	6.900	0.560	0.051	0.147	1.109	5.791	0	1.
I	0.482	2.326	1.973	6.510	0.462	0.050	0.128	0.822	5.688	0	1.
J	0.391	2.568	2.318	6.000	0.371	0.045	0.109	0.571	5.429	0	1.
K	0.313	2.855	2.680	5.445	0.293	0.039	0.091	0.381	5.064	0	1.
L	0.257	3.181	3.051	5.032	0.237	0.033	0.074	0.254	4.778	0	1.
M	0.210	3.509	3.402	4.560	0.190	0.028	0.059	0.165	4.395	0	1.
N	0.200	3.593	3.493	4.450	0.180	0.026	0.054	0.144	4.306	0	1.

Figure 32. Impeller Flow Area of MF-3.

	$\cos \phi$	$\frac{A}{A' \cos \phi}$
	0.64279	4.519
	0.69340	4.420
	0.76154	4.527
	0.81815	4.664
	0.86074	4.822
	0.93969	5.215
	0.98491	5.568
	1.0000	5.791
	1.0000	5.688
	1.0000	5.429
	1.0000	5.064
	1.0000	4.778
	1.0000	4.395
	1.0000	4.306





Meridional Mean Flow Path (in.)

5.0 RF-1 IMPELLER ANALYSIS

The Campbell diagram, Figure 37, indicates that this impeller is satisfactory for steady-state operation to 60,000 rpm and for short intervals of operation to 62,700 rpm. Accurate natural frequencies should be determined by test. The impeller is safe for steady-state operation to 62,700 rpm if the natural frequencies are slightly higher or if the amplitudes are small enough to produce vibratory stresses within the design limits.

The calculated minimum safety factors for steady-state operation at 62,700 rpm and for an impeller inlet temperature of 60°F are as follows:

- 1) Blade safety factor is 2.20 to minimum 0.2-percent yield stress including $\pm 20,000$ psi vibratory stress.
- 2) Disk safety factors are 1.74 to minimum 0.2-percent yield stress and 1.99 to minimum ultimate stress.

The calculated minimum safety factors for momentary operation at 68,970 rpm and for an impeller inlet temperature of 60°F are as follows:

- 1) Blade safety factor is 1.82 to minimum 0.2-percent yield stress.
- 2) Disk safety factors are 1.44 to minimum 0.2-percent yield stress and 1.64 to minimum ultimate stress.

The weight of the impeller is 7.20 pounds, and the mass moment of inertia is 0.0699 lb-in.-sec².

Figures 34 through 42 present the results of stress and vibration analyses for the RF-1 impeller.

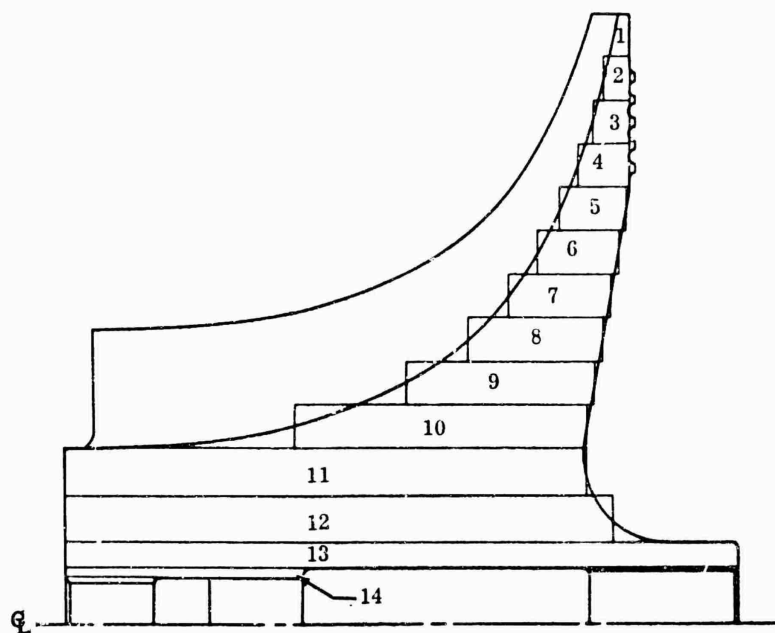


Figure 34. Disk and Blade Profile of RF 1.

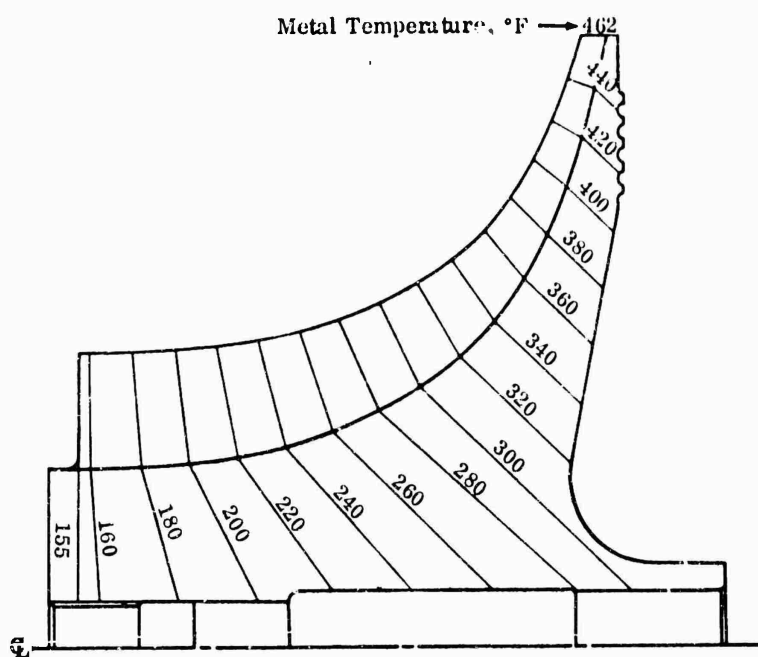


Figure 35. Temperature Distribution of RF-1.

Computer Input Data						Computer Output Data	
Title						Mode No.	Frequency, cps
Blade Impeller Blade Natural Frequencies						1	1,892
						2	9,785
						3	12,755
						4	15,496
						5	16,360

Number of Drawing Stations	Material Const.		Blade Profile	Number of Nodes at General Z Station	Required Number of Modes
	Density	Modulus of Elasticity			
	γ (lb./in. ³)	E (psi)			
1	0.160	16,000,000	Linear	5	5

Information From Drawing :						
Station No.	Axial Dist. Z	Tip Rad. r_t	Root Rad. r_r	Inclination α	Tip Thickness t_t	Root Thickness t_r
	in.	in.	in.	Degree	in.	in.
1	0	1.918	1.179	0	0.045	0.051
2	0.200	1.951	1.181	8.15	0.043	0.077
3	0.400	1.957	1.187	15.5	0.039	0.110
4	0.800	1.984	1.215	27.73	0.035	0.145
5	1.196	2.031	1.272	37.25	0.031	0.157
6	1.583	2.120	1.361	44.40	0.029	0.165
7	1.960	2.211	1.500	49.55	0.027	0.165
8	2.315	2.111	1.676	52.95	0.026	0.155
9	2.638	2.623	1.909	51.88	0.026	0.136
10	2.913	2.868	2.197	55.61	0.025	0.118
11	3.118	3.197	2.550	55.71	0.025	0.113
12	3.320	3.588	2.888	55.71	0.025	0.161
13	3.385	3.768	3.040	55.71	0.025	0.100
14	3.443	3.936	3.216	55.71	0.025	0.094
15	3.476	4.010	3.317	55.71	0.025	0.090
16	3.562	4.010	3.655	55.71	0.034	0.075
17	3.662	4.010	4.010	55.71	0.045	0.045
13	Required Number of Node Distances					

Z Distances for Node Stations, (in.)									
0	0.1	0.2	0.3	0.5	0.7	1.0	1.4	1.8	2.2
2.6	3.0	3.662							

Section A-A

Figure 36. Natural Frequencies of RF-1 Blades.

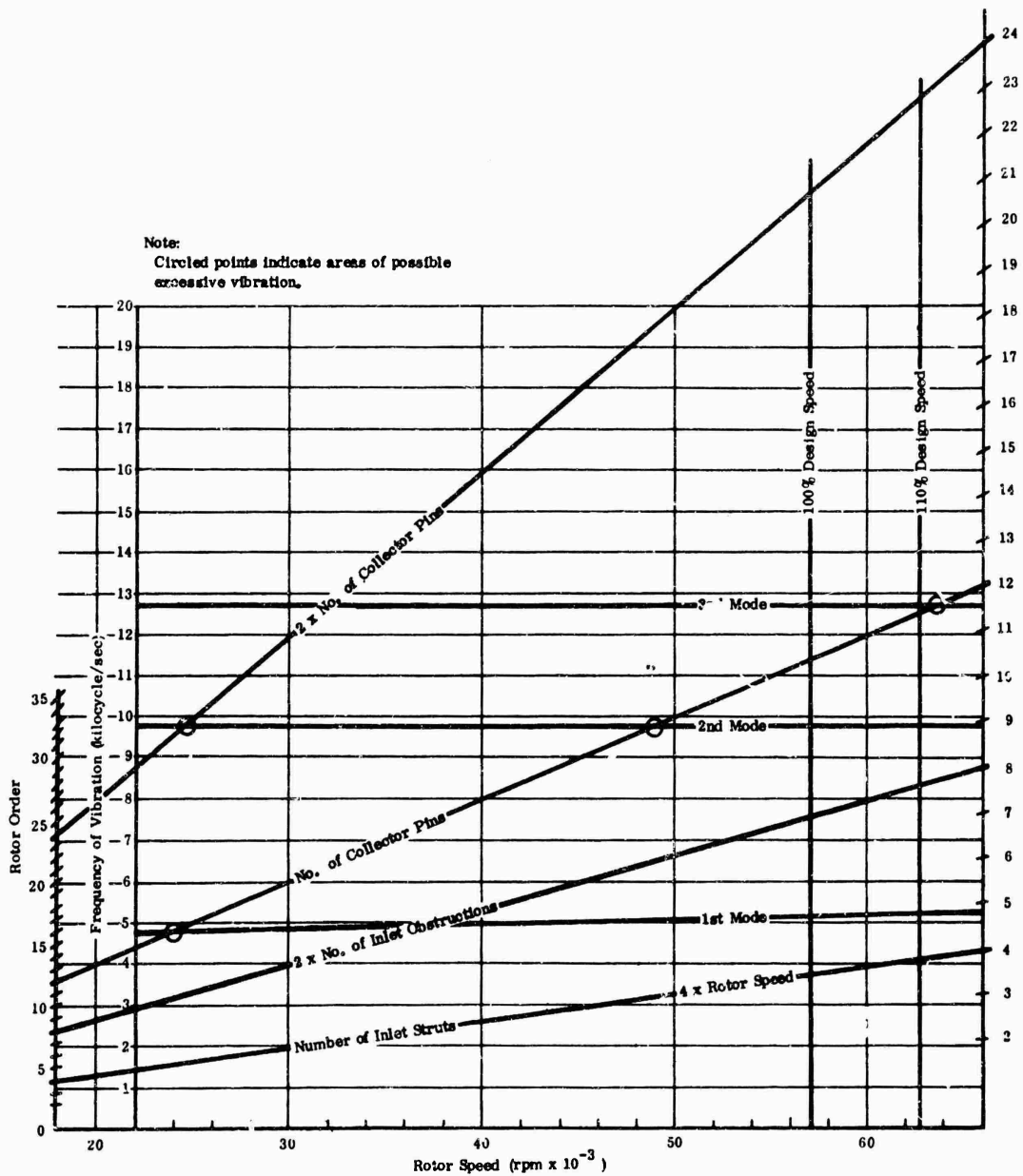


Figure 37. Campbell Diagram for RF-1.

172

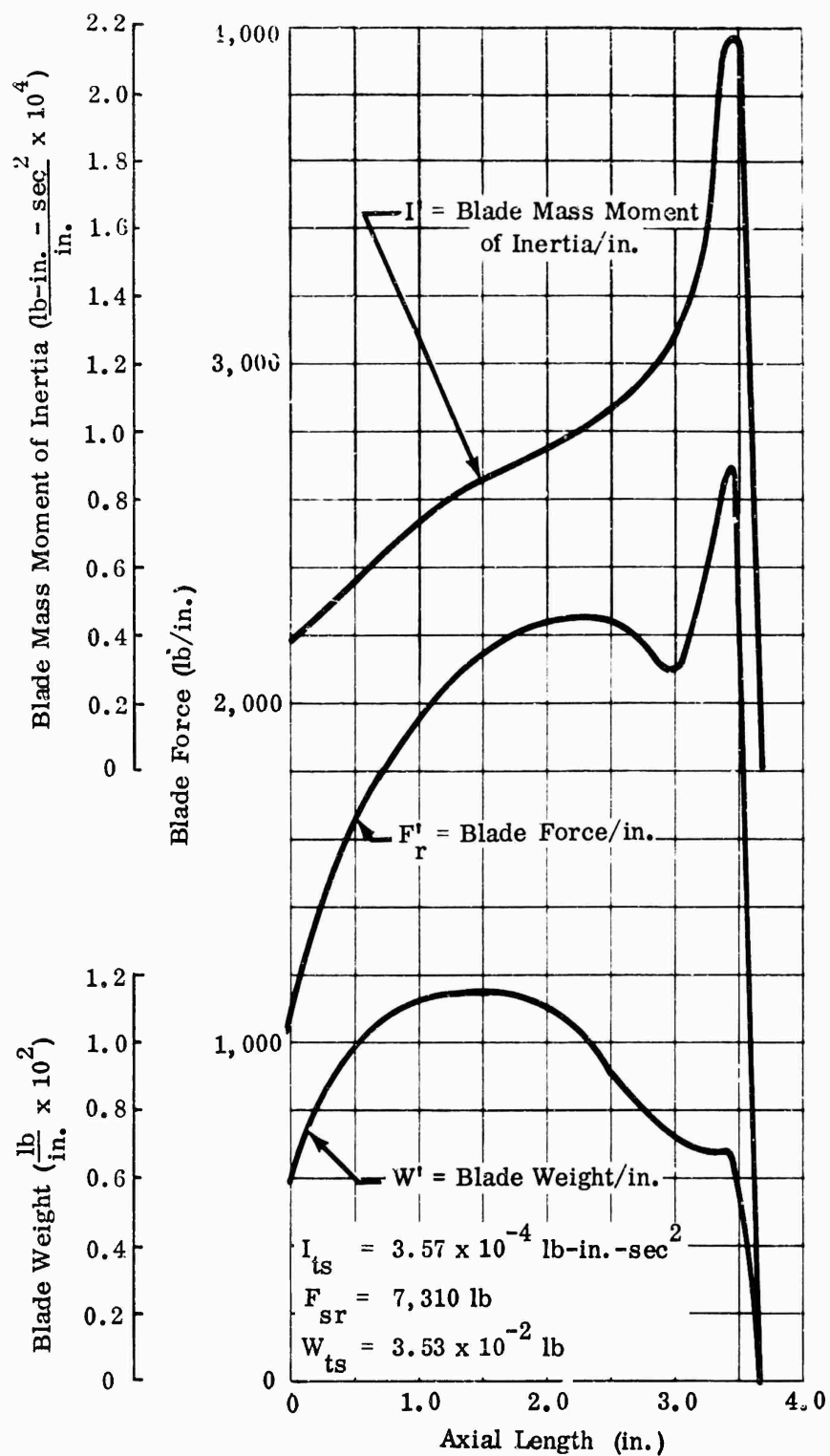


Figure 39. RF-1 Impeller-Blade Force, Weight, and Inertia.

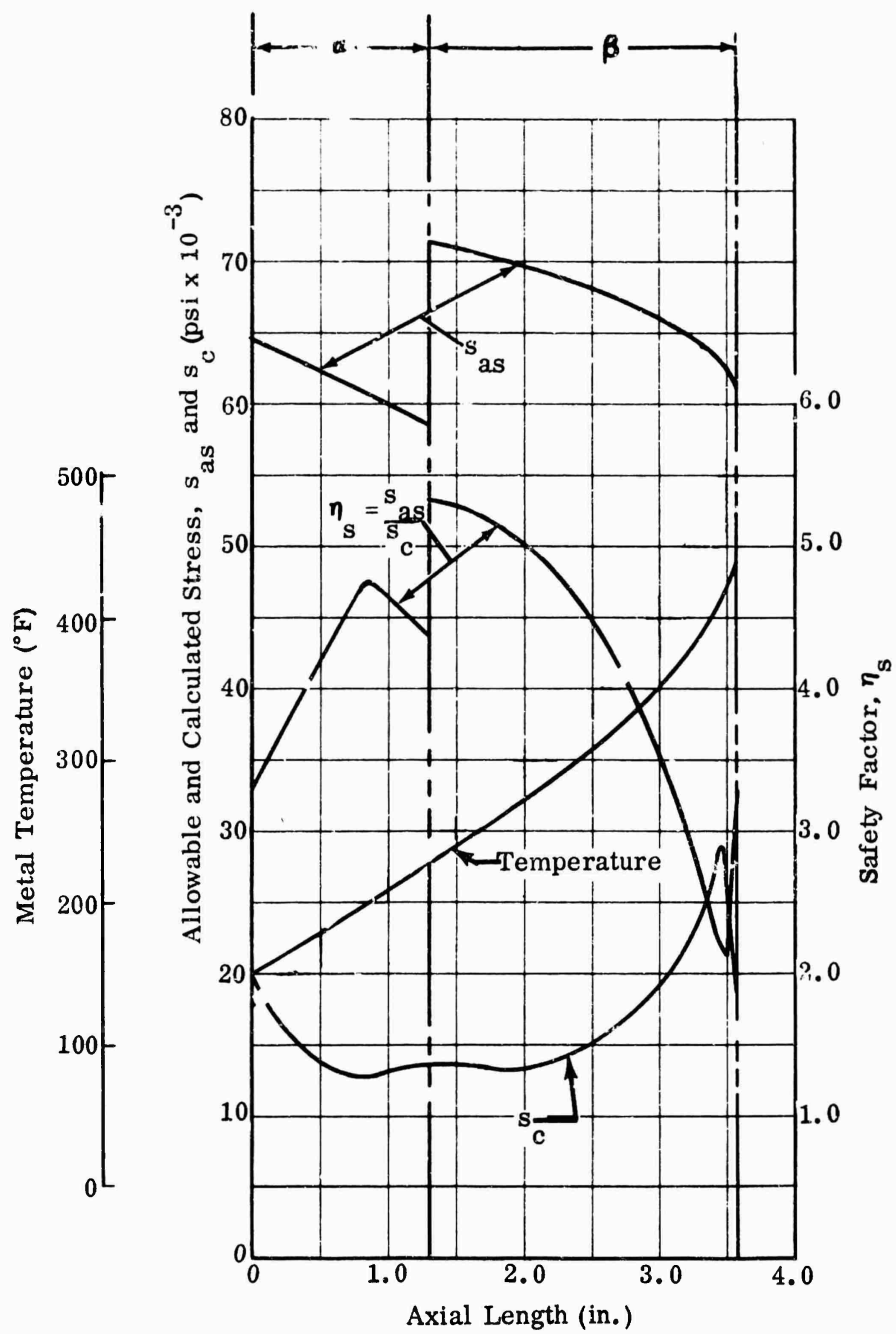
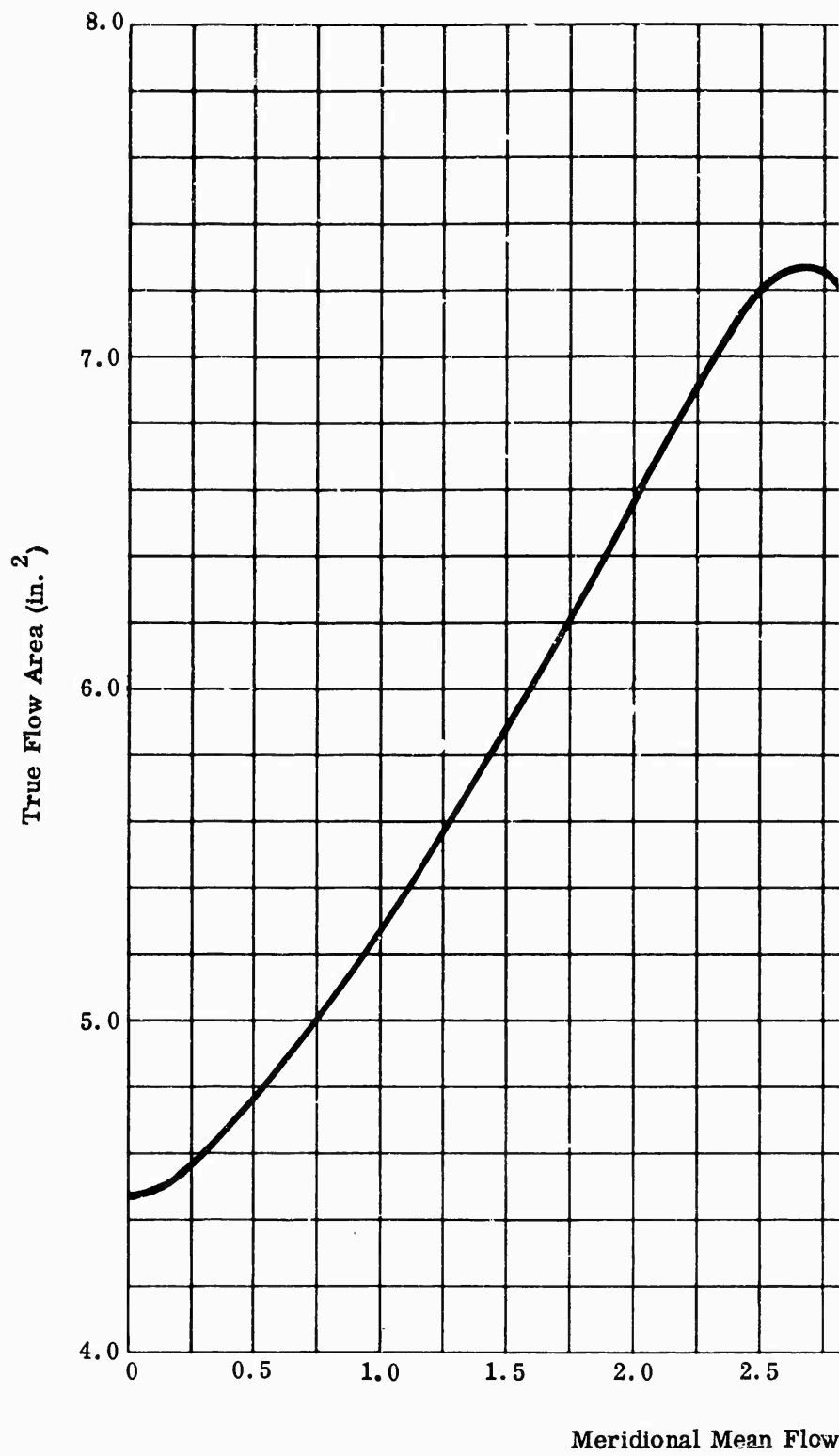


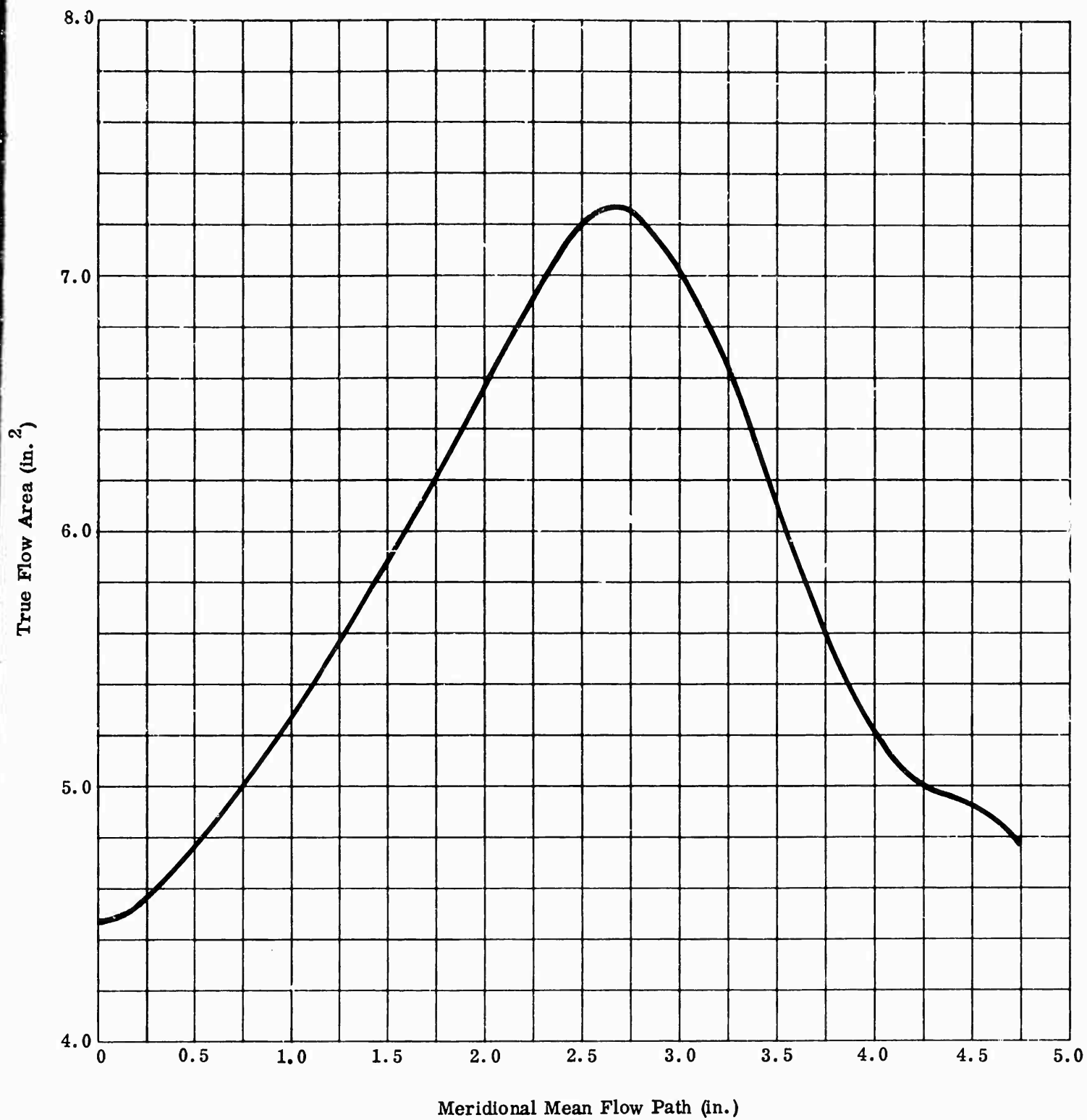
Figure 40. Blade-Root Stress, Temperature, and Safety Factor for RF-1.

Flow Area Calculation											
Sec.	h	r ₁	r ₂	$\frac{A_T}{\pi h (r_1 + r_2)}$	h'	t _t	t _r	$\frac{N}{2} \frac{A_B}{h' (t_t + t_r)}$	$\frac{A'}{A_T - A_B}$	φ	Cos
A	0.789	1.968	1.129	7.8005	0.769	0.045	0.054	0.837	7.0225	50.0	0.0
B	0.790	1.972	1.182	7.8277	0.770	0.043	0.079	1.033	6.7947	48.2	0.0
C	0.790	1.980	1.190	7.8675	0.770	0.038	0.111	1.262	6.6055	44.7	0.0
D	0.783	2.000	1.220	7.9208	0.763	0.035	0.146	1.519	6.4018	37.9	0.0
E	0.770	2.046	1.285	8.0578	0.750	0.032	0.159	1.576	6.4818	31.8	0.0
F	0.747	2.120	1.396	8.2512	0.727	0.030	0.167	1.576	6.6752	25.8	0.0
G	0.708	2.222	1.560	8.4121	0.688	0.028	0.162	1.436	6.9761	19.7	0.0
H	0.653	2.357	1.791	8.5094	0.633	0.026	0.148	1.213	7.2964	13.6	0.0
I	0.563	2.526	2.097	8.1767	0.543	0.026	0.124	0.896	7.2807	7.6	0.0
J	0.455	2.737	2.446	7.4086	0.435	0.025	0.116	0.675	6.7336	1.5	0.0
K	0.346	3.008	2.835	6.3513	0.326	0.025	0.105	0.466	5.8853	0.0	1.0
L	0.268	3.330	3.239	5.5307	0.248	0.025	0.093	0.322	5.2087	0.0	1.0
M	0.243	3.512	3.438	5.3057	0.223	0.025	0.087	0.275	5.0307	0.0	1.0
N	0.226	3.697	3.629	5.2014	0.206	0.025	0.078	0.233	4.9684	0.0	1.0
O	0.194	4.042	3.984	4.8916	0.174	0.025	0.048	0.140	4.7516	0.0	1.0

Figure 41. Impeller Flow Area of RF-1.

A' $(A_T - A_B)$	ϕ	$\cos \phi$	A $A' \cos \phi$
7.0225	50.0	0.64279	4.476
6.7947	48.2	0.66653	4.529
6.6055	44.7	0.71080	4.695
6.4018	37.9	0.78908	5.052
6.4818	31.8	0.84989	5.509
6.6752	25.8	0.90032	6.010
6.9761	19.7	0.94147	6.568
7.2964	13.6	0.97196	7.092
7.2807	7.6	0.99122	7.217
6.7336	1.5	0.99966	6.731
5.8853	0.0	1.000	5.885
5.2087	0.0	1.000	5.209
5.0307	0.0	1.000	5.031
4.9684	0.0	1.000	4.968
4.7516	0.0	1.000	4.752





[illegible]

Figure 42. Disk Calculations for RF-1.

6.6 WORKHORSE IMPELLER ANALYSIS

This impeller is satisfactory for steady-state operation to 50,000 rpm. The intersection of the first mode and eighth order shown at 34,000 rpm on the Campbell diagram, Figure 44, must be avoided for steady-state operation. A complete blade stress survey should be made in the test rig before prolonged aerodynamic tests are performed.

The flow areas were not calculated for this design because the blade configuration was already defined by a prior design.

The calculated minimum safety factors for steady-state operation at 50,000 rpm and for an impeller inlet temperature of 60° F are as follows:

- 1) Blade safety factor is 1.91 to minimum 0.2-percent yield stress including $\pm 12,000$ psi vibratory stress.
- 2) Disk safety factors are 1.86 to minimum 0.2-percent yield stress and 2.08 to minimum ultimate stress.

The calculated minimum safety factors for momentary operation at 60,000 rpm and for an impeller outlet temperature of 60° F are as follows:

- 1) Blade safety factor is 1.73 to minimum 0.2-percent yield stress.
- 2) Disk safety factors are 1.29 to minimum 0.2-percent yield stress and 1.44 to minimum ultimate stress.

The weight of the impeller is 13.51 pounds, and the mass moment of inertia is 0.187 lb-in.-sec².

Figures 43 through 50 present the results of stress and vibration analyses for the workhorse impeller.

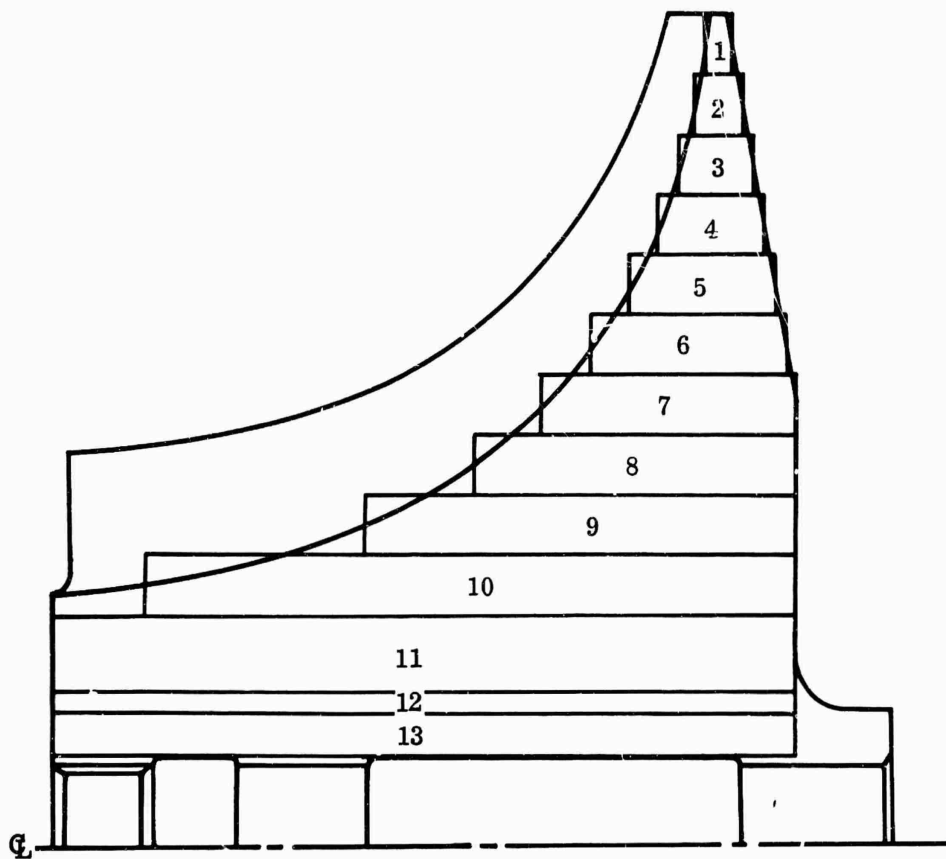


Figure 43. Disk and Blade Profile of Workhorse Impeller.

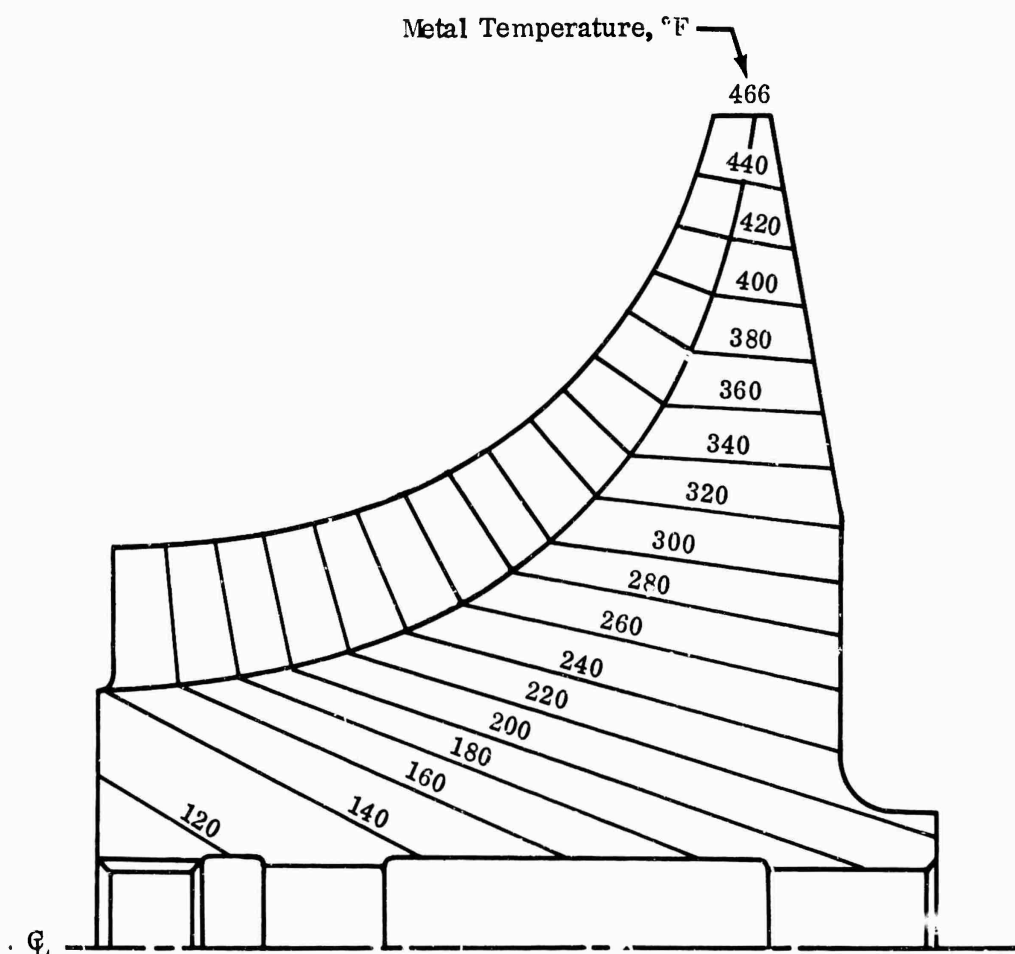


Figure 44. Temperature Distribution of Workhorse Impeller.

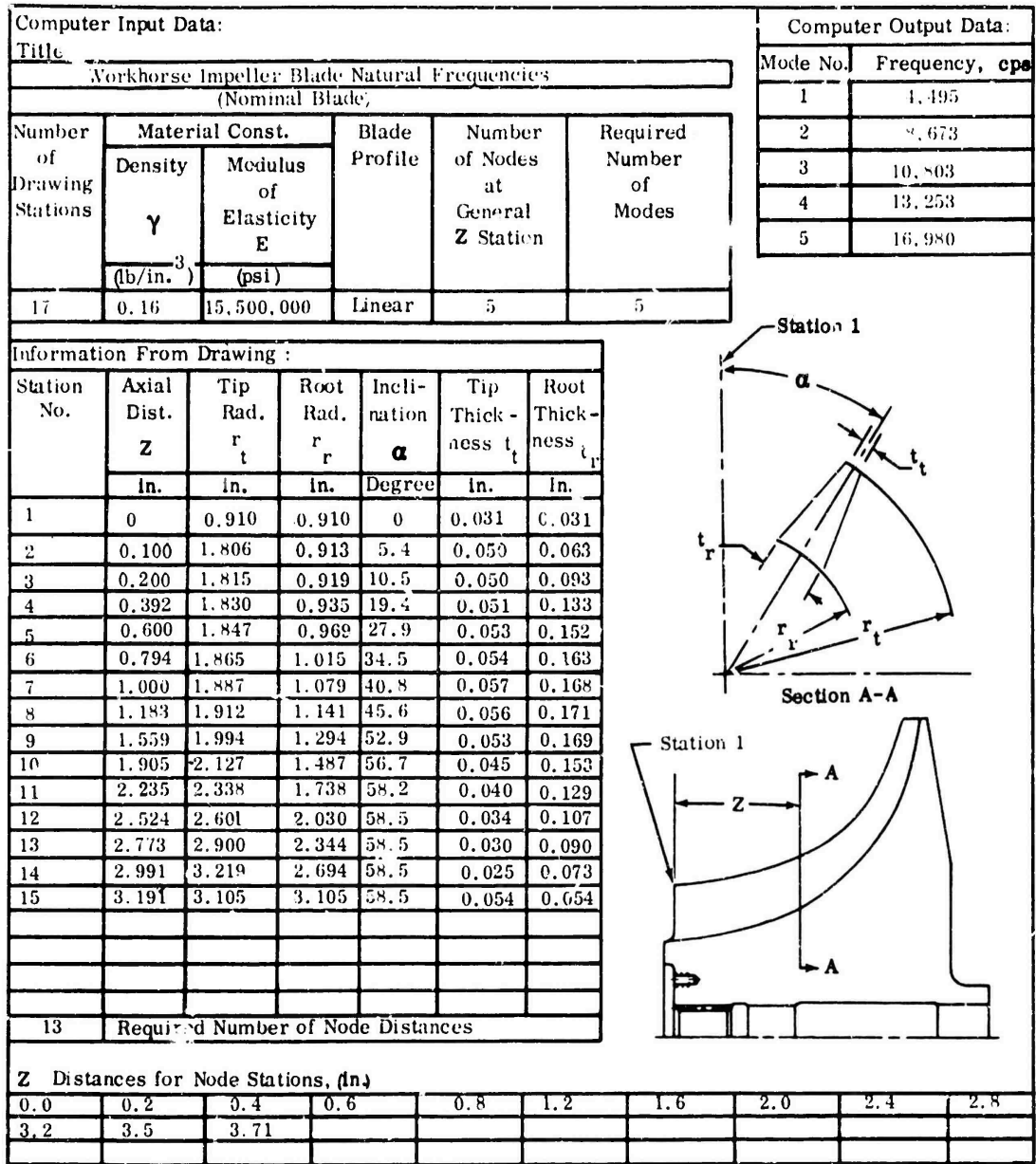


Figure 45. Natural Frequencies of Workhorse Impeller Blades.

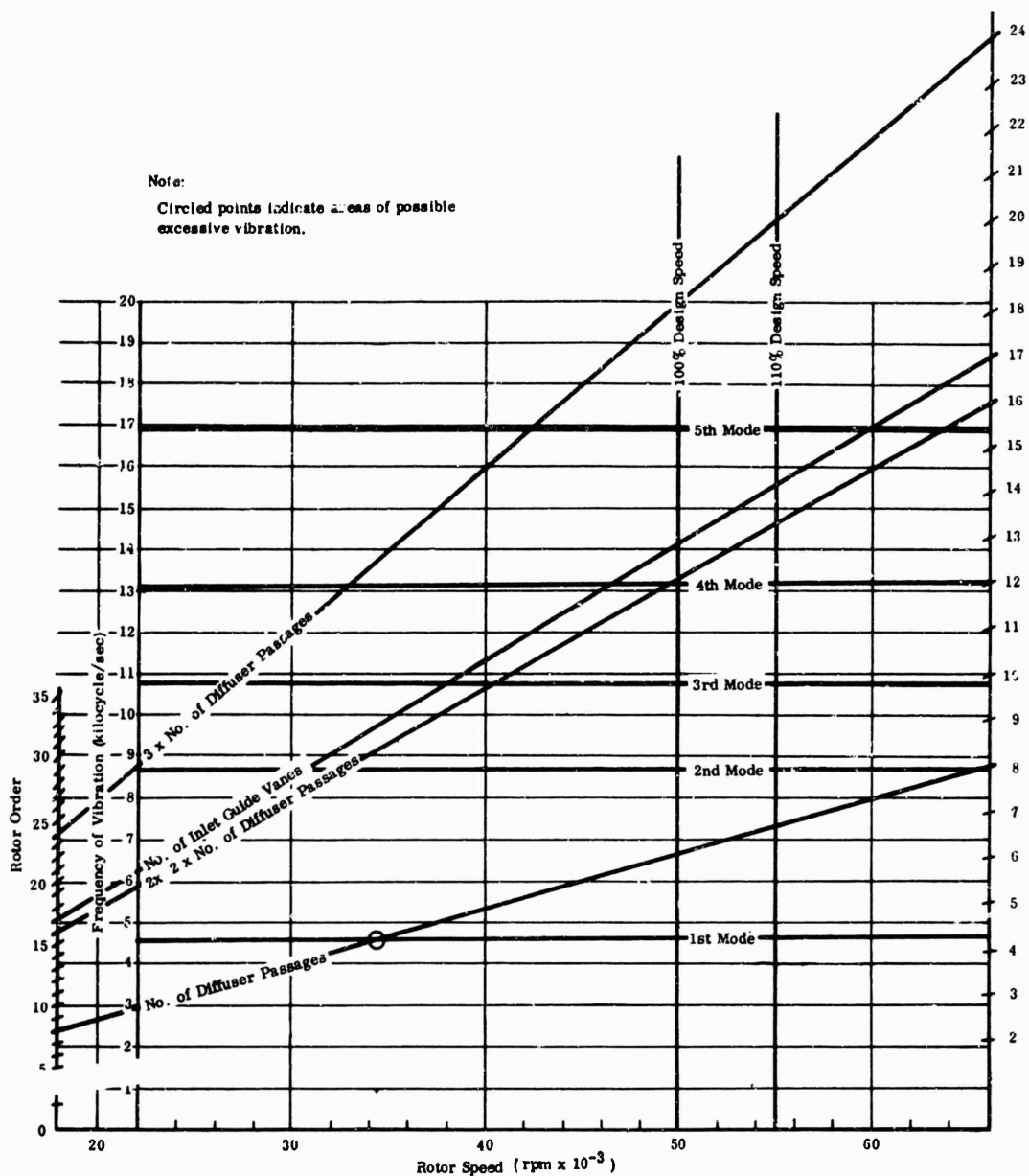


Figure 46. Campbell Diagram for Workhorse Impeller.

Density, $\gamma = 0.160 \text{ lb/in.}^3$

[illegible]

183

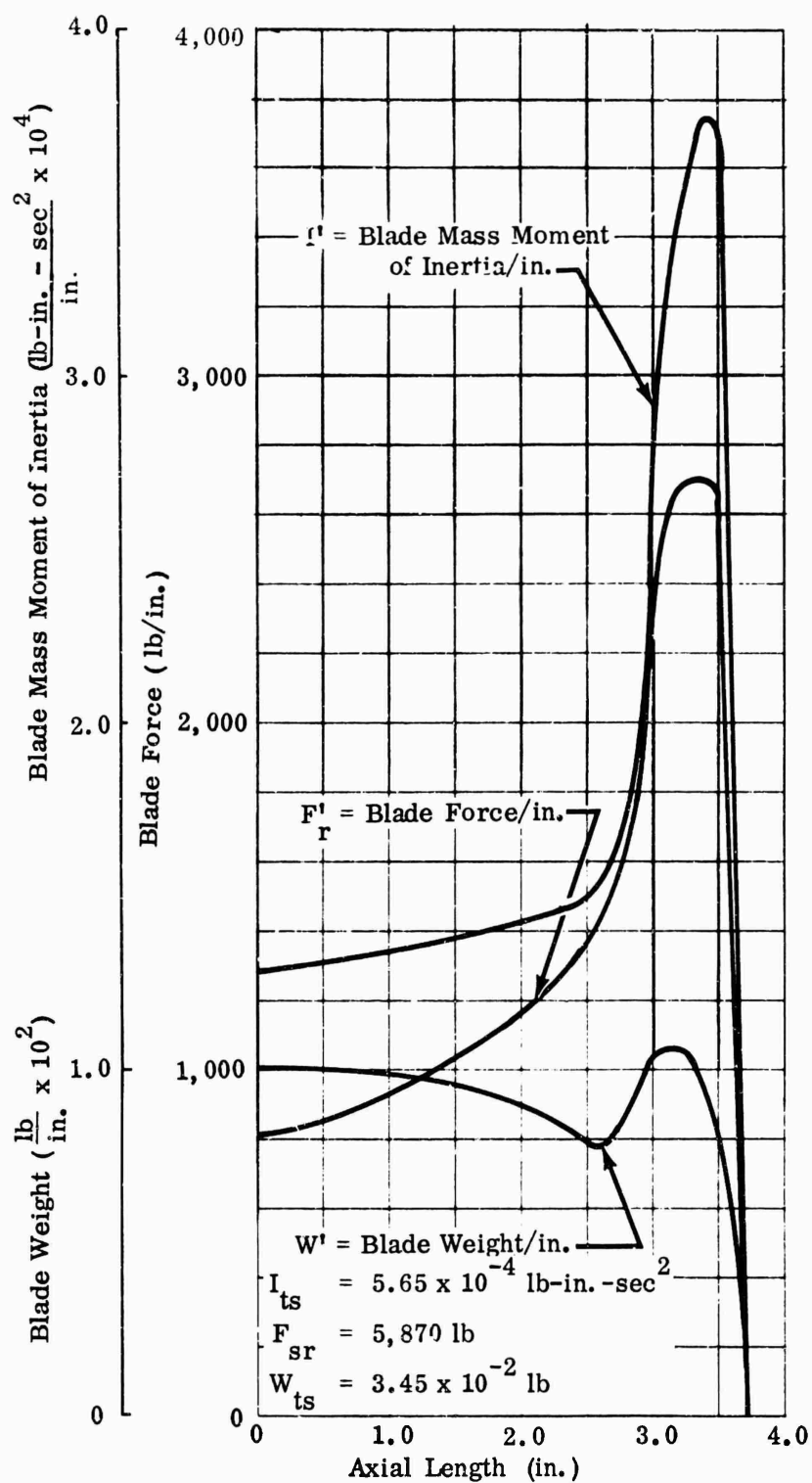


Figure 48. Workhorse Impeller-Blade Force, Weight, and Inertia.

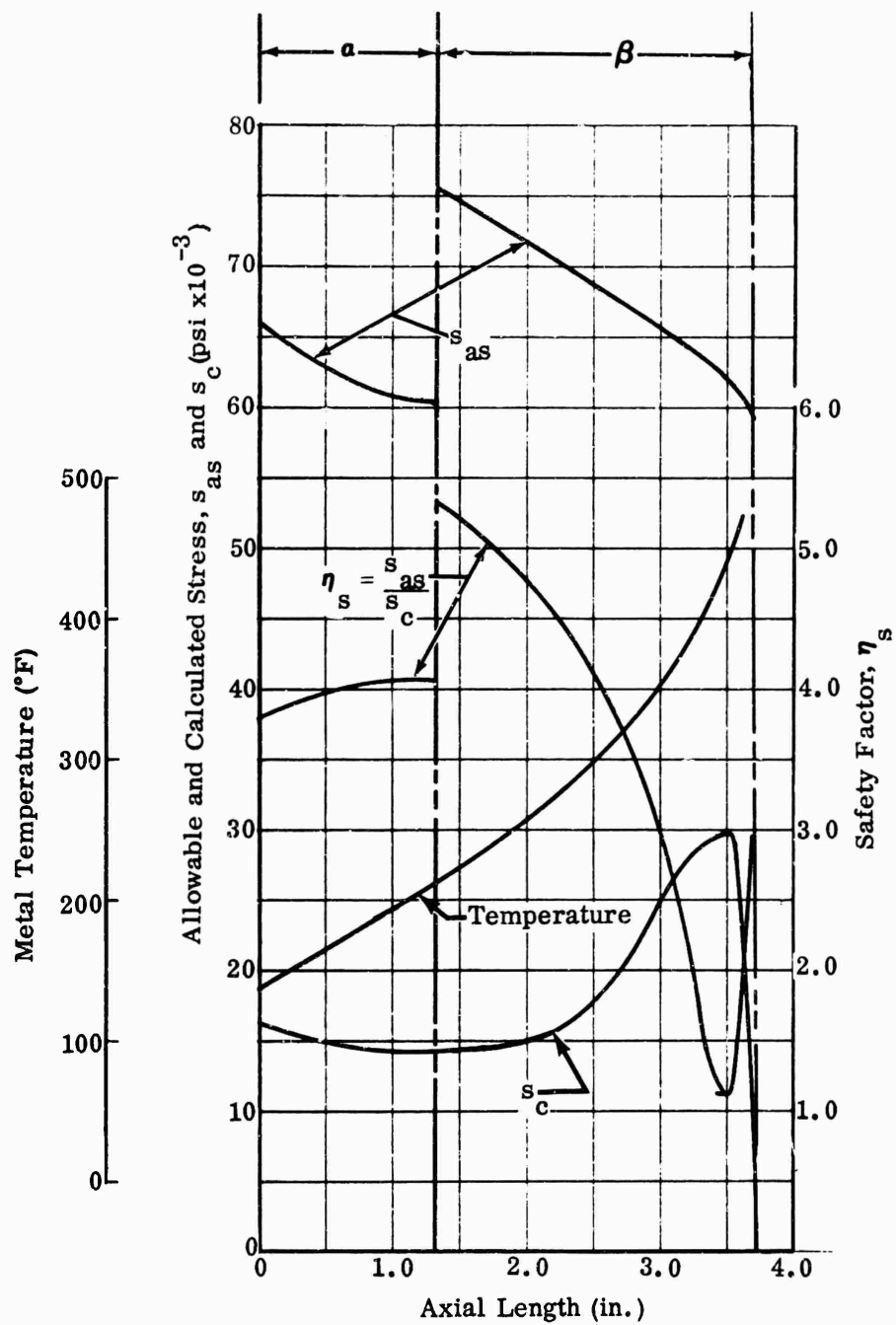


Figure 49. Blade-Root Stress, Temperature, and Safety Factor for Workhorse Impeller.

(U) APPENDIX III

TEST RIG DEVELOPMENT

ABSTRACT

This appendix covers the design development of test rigs required for the Army centrifugal-compressor research program. It provides information relative to methods used in correcting initial operational difficulties encountered with the test sections. The appendix is intended to supplement the discussions given in Section 2.4 in the body of this report.

SYMBOLS

C_c	critical damping coefficient (lb_m/sec)
C_{inner}	inner bearing clearance (in.)
C_{outer}	outer bearing clearance (in.)
C_s	dynamic radial load rating (lb)
c	radial bearing clearance (in.)
c_1	inner bearing-to-journal radial clearance (in.)
c_2	outer bearing-to-journal radial clearance (in.)
D	bearing diameter (in.)
D_i	bearing inner diameter (in.)
D_{mean}	bearing mean diameter (in.), $D_{\text{mean}} = \frac{D_i + D_o}{2}$
D_o	bearing outer diameter (in.)
K_n	spring rate (lb/in.)
L	bearing length (in.)
m	damper mass (lb_m)
N, N_o	journal speed (rps)
N_1	bearing speed (rps)

SYMBOLS (Continued)

n journal bearing attitude,

$$n = \frac{\text{eccentricity}}{\text{radial clearance}}$$

P bearing load (psi)

R_H static radial load (lb)

R_S dynamic radial load (lb)

r, r_1 journal radius (in.)

r_2 outer film radius (in.)

S Sommerfeld number,

$$S = \left(\frac{r}{c} \right)^2 \left(\frac{\mu N}{P} \right)$$

T thrust load (lb)

T_n spring rate $\frac{(\text{lb-sec})}{\text{in.}}$,

$$T_n = \frac{K_n}{\omega_n}$$

W design load (lb)

X, Y imbalance bearing load coefficients

μ absolute viscosity $\left(\frac{\text{lb-sec}}{\text{in}^2} \right)$

ω_n angular velocity $\left(\frac{\text{radians}}{\text{sec}} \right)$

1.0 INTRODUCTION

Two basic test rigs were required to evaluate performance and structural characteristics of the various compressor component configurations. The diffusers were tested in a rig equipped with a workhorse impeller operating at a maximum speed of 55,000 rpm. A second rig was used for evaluation of the impellers at speeds of up to 57,000 rpm. The contractor's concept for compressor rigs was modified to accommodate the diffuser components, and a new rig was designed to accommodate the impeller rotors. This appendix presents the design analyses and subsequent modifications of these test rigs.

2.0 DIFFUSER TEST SECTIONS

The design of the diffuser test rig included provisions for monitoring mechanical operation. The rotor system was an adaptation of an existing rig, but with higher speed requirements (55,000 rpm). Operating temperatures ranged from ambient at the inlet to 750°F at the diffuser exit. The unit was to be operated at various back pressures at a number of constant speed increments of from 33,000 through 55,000 rpm. Instrumentation was to be provided for measurement of static and dynamic pressures and temperatures. A schlieren optical system for evaluating flow patterns near the diffuser vanes was also to be incorporated in the design.

The configuration selected from preliminary studies was a can't-never-rotor system with the shaft passing through the impeller. All bearing supports were flexible to provide versatility in controlling the critical speeds to be encountered. Thrust loads were limited by providing a labyrinth seal at the rear face of the impeller at the tip. The seal was designed to prevent high pressures at the impeller backface.

2.1 BEARING SYSTEM

The rotor system was designed as a stiff shaft assembly supported by 2 hydrodynamic floating-sleeve bearings. A titanium impeller was precision fit to the shaft. In a similar manner, a thrust balance disk was attached to the aft or coupling end of the shaft.

Thrust load was carried in both the forward and aft directions by hydrodynamic-slipper bearings. A damped, resilient support for the forward radial bearing was incorporated during the operational development of the unit to accommodate excessive radial loads due to shaft vibration. A reverse-thrust slipper bearing was also replaced during this period so that the arrangement was capable of carrying both radial and thrust loads in a 3-bearing rotor system.

Hydrodynamic full-floating journal bearings were used to support the rotor system and to provide maximum capacity for radial loads that might result from rotor imbalance or operation near critical speeds. The operating characteristics of the full-floating journal bearing compensate for a number of disadvantages encountered at high speeds with conventional journal bearings. High-speed journal bearings require more clearance than a conventional journal type to induce the proper amount of oil flow. Increased clearance, however, reduces the load carrying capacity of a bearing and increases the tendency for oil-film whirl. The full-floating bearing provides 2 paths through which the oil will flow, which permits operation at an acceptable temperature without increased clearance. Because the forces acting on the inner and outer oil films of the full-floating bearing are in equilibrium, the rotational speed of the bearing may be 25 to 70 percent of the shaft or journal speed and is independent of the Sommerfeld number. The Sommerfeld number, S, defines the operating characteristic of a journal bearing as a function of attitude (n),

where:
$$n = \frac{\text{eccentricity}}{\text{radial clearance}} \quad (166)$$

For a conventional journal bearing:

$$S = \left(\frac{r}{c} \right)^2 \left(\mu \frac{N}{P} \right) = \frac{(2 + n^2) \sqrt{1 - n^2}}{12 \pi^2 n} \quad (167)$$

where:

- S = Sommerfeld number (dimensionless)
- r = journal radius (in.)
- c = radial clearance (in.)
- μ = viscosity, reyns (1 reyn = 68,850 poise)
- N = journal speed (revolutions per second)
- P = bearing load (psi)

The above equation applies to a bearing of infinite length with no end leakage. However, in a full-floating bearing the Sommerfeld number may be used to compare two bearings of the same finite length. The attitude of a full-floating journal bearing is the same as though the journal alone were to rotate at a speed equal to the sum of the journal- and floating-bearing speeds. Therefore, the Sommerfeld number for the inner film of a floating bearing becomes:

$$S = \left(\frac{r_1}{c_1} \right)^2 \frac{\mu (N_o + N_1)}{P} \quad (168)$$

where:

N_o = journal speed (revolutions per second)

N_1 = bearing speed (revolutions per second)

r_1 = journal radius (in.)

c_1 = bearing-to-journal radial clearance (in.)

and for the outer oil film:

$$S_1 = \left(\frac{r_2}{c_2} \right)^2 \left(\frac{\mu N_1}{P_2} \right) \quad (169)$$

where the subscript 2 applies to outer film dimensions.

The bearing analyses are based on the Sommerfeld number for a bearing capable of supporting a 500-pound radial load. A bearing is considered to be lightly loaded when the Sommerfeld number is longer than 0.16, moderately loaded when the Sommerfeld number is between 0.16 and 0.035, and heavily loaded when the Sommerfeld number is less than 0.035. * Sommerfeld numbers for the inner and outer oil film are determined as follows.

*M. C. Shaw and F. Mack, Analysis and Lubrication of Bearings, McGraw-Hill Book Company, Inc., New York, 1949.

Given:

- W = design load = 500 lb
- N_o = journal speed = 50,000 rpm
- S = Sommerfeld No. > 0.16 (lightly loaded bearing)
- r_1 = journal radius = 0.845 in.
- r_2 = bearing outside radius = 1.000 in.
- C_1 = journal to bearing clearance = 0.00125 in.
- C_2 = bearing to retainer clearance = 0.0025 in.
- L = bearing length = 0.80 in.
- μ = absolute viscosity = 3.94×10^{-7} Reyns (MIL-L-7808 oil)

from Figure 51 at $\frac{C_2}{C_1} = 2.0 \quad \frac{N_1}{N_o} = 0.45$

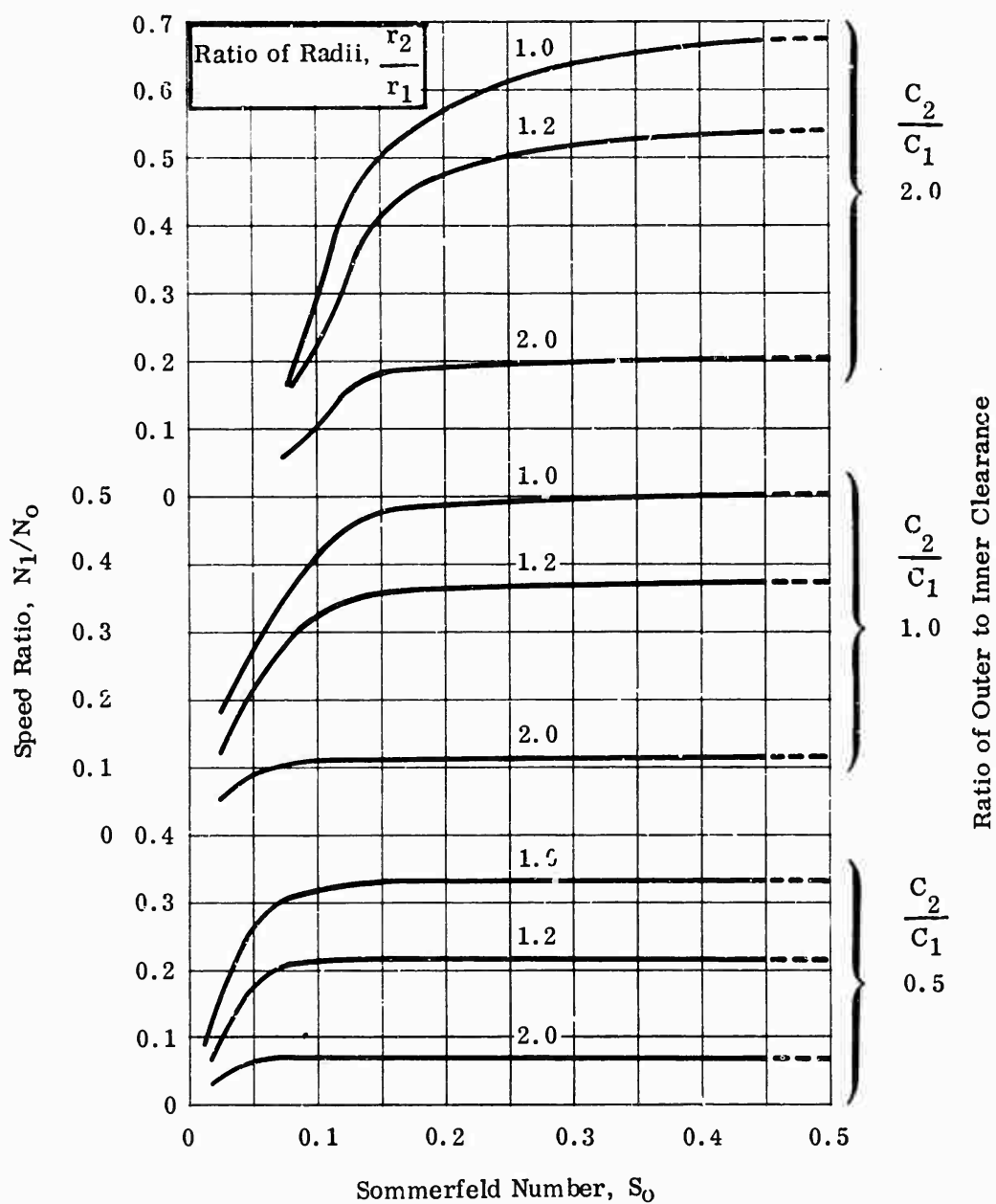
where:

$$N_1 = \text{speed of floating sleeve}$$

For inner film:

$$S_1 = \left(\frac{r_1}{C_1} \right)^2 \left[\frac{\mu (N_o + N_1)}{\frac{60W}{2r_1 L}} \right] \quad (170)$$

$$S_1 = \left(\frac{0.845}{0.00125} \right)^2 \left[\frac{3.94 \times 10^{-7} (50,000 + 22,500)}{\frac{500 \times 60}{(2)(0.8)(0.845)}} \right] = \underline{\underline{0.588}}$$



*See footnote, Page 192.

Figure 51. Variation of Speed Ratio with Sommerfeld Number for Full-Floating Journal Bearing.*

For outer film:

$$S_2 = \left(\frac{r_2}{C_2} \right)^2 \left[\frac{\mu N_1}{60W} \right] = \left(\frac{1.0}{.0025} \right)^2 \left(\frac{(0.394 \times 10^{-6}) (2.25 \times 10^4)}{(500) (60)} \right) = \underline{\underline{0.0755}}$$

The Sommerfeld numbers for the inner and outer films are 0.588 and 0.0755, respectively, with the result that the inner film is lightly loaded and the outer film is moderately loaded. This margin in the oil film loads indicates that the chosen 500-pound radial load was reasonable for the bearing.

2.2 ROTOR DYNAMICS ANALYSIS

The critical speeds of synchronous-whirl modes and the respective mode shapes were determined through use of a mathematical model consisting of 10 mass points and 8 coincident hinged joints with rotational springs. The mathematical model was represented by a linear differential equation. Solution of the equation involved matrix methods and iteration to obtain the eigenvalue for shaft-critical frequencies and the eigenvector for the corresponding mode shapes. Bearing supports were considered to be ideal massless springs. The effect of the gyroscopic-stiffening moment (the difference between gyroscopic moment and rotational inertia) was considered. The bearing supports were simulated by conventional spring constants, K_n (lb/in.), with the radial oil-film stiffness defined as a function of the absolute viscosity of the oil, bearing geometry, and rotor speed by empirical relationship:

$$K_n = \frac{\mu L^3 DN}{6.08 C^3} \quad (171)$$

where:

N = rotor speed (revolutions per second)

μ = absolute viscosity $\left(\frac{\text{lb-sec}}{\text{in.}^2} \right)$

L = bearing length (in.)

D = bearing diameter (in.)

C = total bearing clearance (in.)

When spring rate, K_n , is divided by ω_n , the spring rate can be expressed as a linear function of rotor speed, so that:

$$T_n = \frac{K_n}{\omega_n} \left(\frac{\text{lb-sec}}{\text{in.}} \right) \quad (172)$$

$$T_n \left(\frac{\text{lb-sec}}{\text{in.}} \right) = \frac{K}{\omega_n} \left(\frac{\text{lb/in.}}{\text{rad/sec}} \right) = \frac{\mu L^3 D}{(6.08)C^3 (2\pi)} = \frac{\mu L^3 D}{(38.2)C^3} \quad (173)$$

where:

$$\mu \text{ (at } 210^\circ \text{ F)} = 0.394 \times 10^{-6} \frac{\text{lb-sec}}{\text{in.}^2}$$

$$D_{\text{mean}} = \frac{1.690 + 2.000}{2} = 1.845 \text{ inches}$$

$$C_{\text{inner}} = 1.6895 - 1.6875 = 0.0020 \text{ inch}$$

$$C_{\text{outer}} = 2.0015 - 1.9975 = 0.0040 \text{ inch}$$

$$C_{\text{mean}} = \text{mean radial clearance}$$

$$C_{\text{mean}} = \frac{0.0040 + 0.0020}{2} = 0.0030 \text{ inch}$$

$$L = 0.775 \text{ inch}$$

$$D_i = 1.69 \text{ inches}$$

$$D_o = 2.00 \text{ inches}$$

$$T_n (\text{inner}) = \frac{(0.394 \times 10^{-6}) (0.775)^3 (1.690)}{(6.08) (0.0010)^3 (2 \pi)} = 8.15 \text{ lb-sec/in.}$$

$$T_n (\text{outer}) = \frac{(0.394) (0.466) (2.00 \times 10^{-6})}{(6.08) (0.002)^3 (2 \pi)} = 1.2 \text{ lb-sec/in.}$$

If the inner and outer film stiffnesses are assumed to be 2 springs in series, the overall film stiffness will be:

$$T_n (\text{overall}) = \frac{\left(\frac{1}{T_n \text{ outer}} \right) + \left(\frac{1}{T_n \text{ inner}} \right)}{\left(\frac{1}{T_n \text{ outer}} \right) + \left(\frac{1}{T_n \text{ inner}} \right)} = \frac{(8.15) (1.2)}{(8.15) + (1.2)} \quad (174)$$

$$= 10.45 \text{ lb-sec/in.}$$

Equivalent oil-film stiffness at 46,000 rpm will be:

$$K = T_n \omega_n$$

$$= (10.45) \frac{(46,000) (2 \pi)}{60}$$

$$= 50,400 \text{ lb/in.} \quad (175)$$

The results of the rotor analysis, showing variation in the critical speeds as a function of bearing stiffness, T_n , is presented in Figure 52 with the corresponding mode shapes shown in Figure 53.

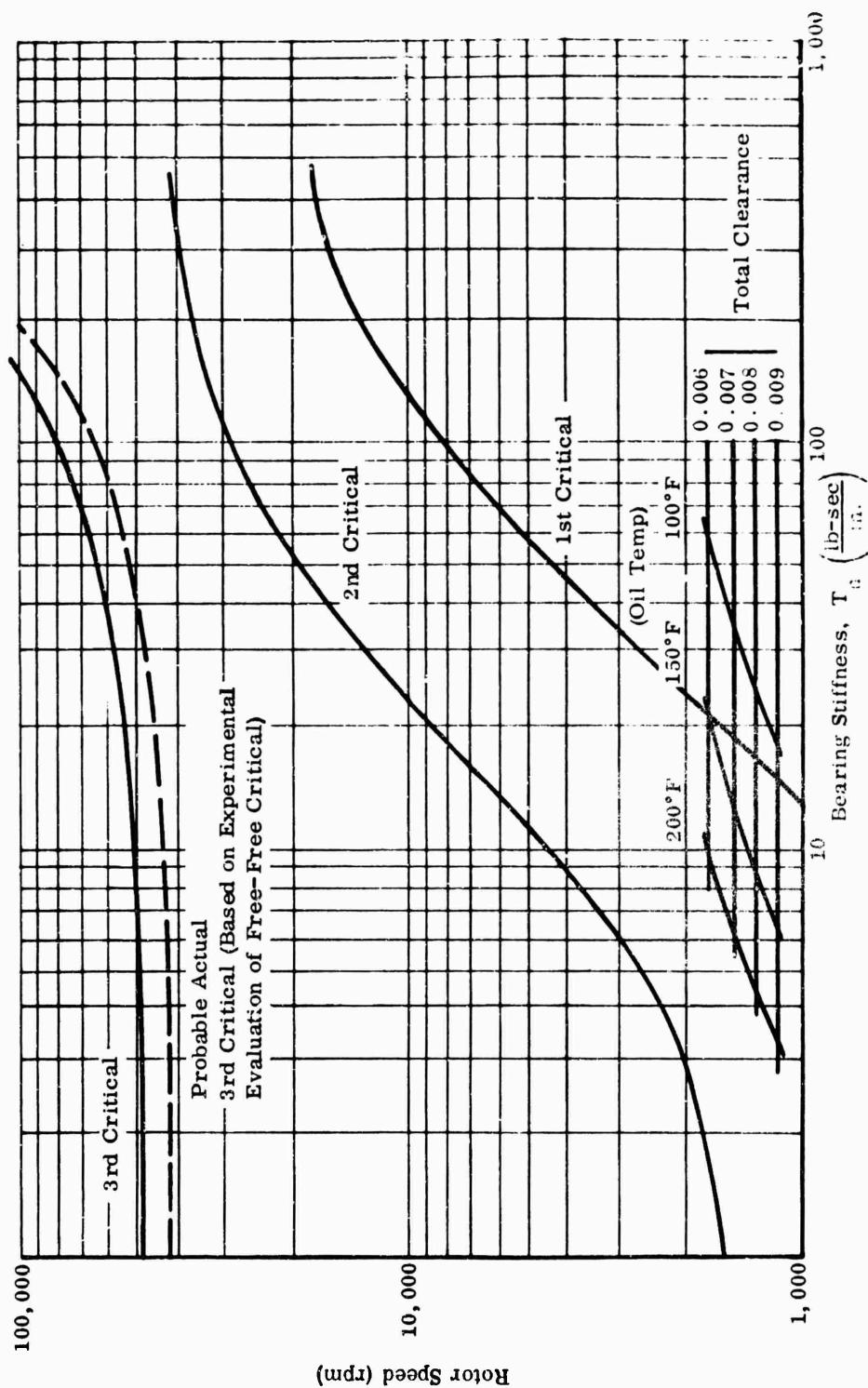
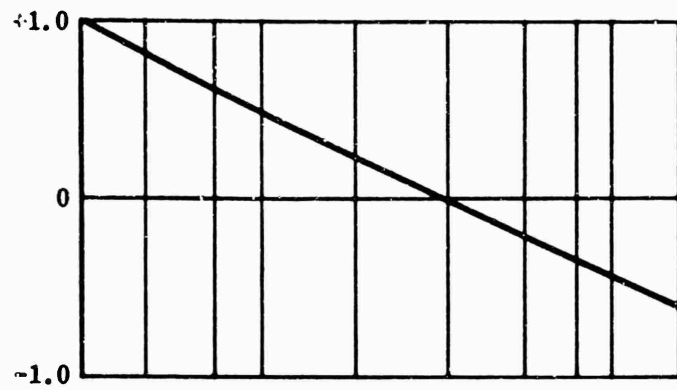
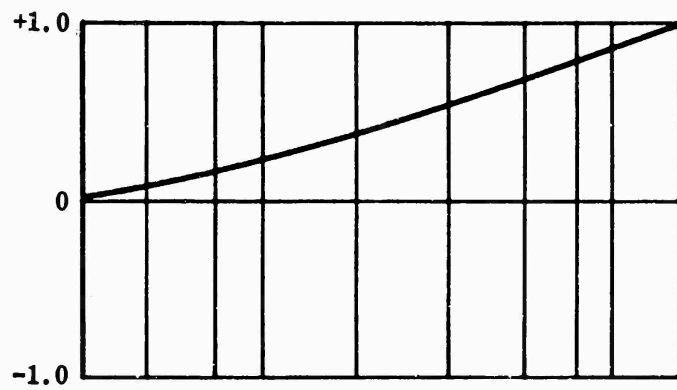


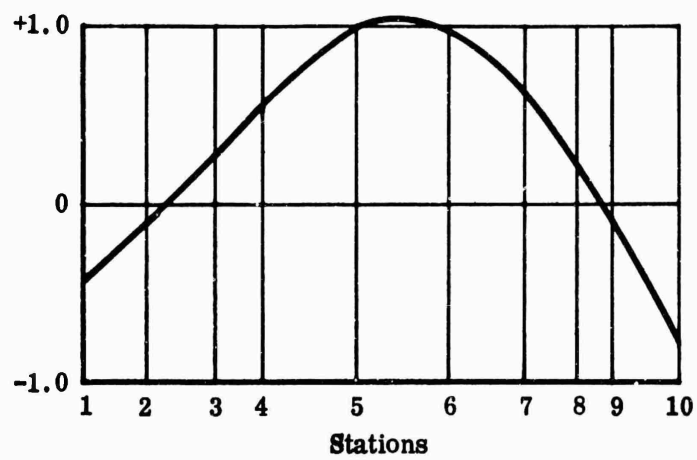
Figure 52. Bearing Stiffness Versus Rotor Speed.



Mode Shape
1st Critical



Mode Shape
2nd Critical



Mode Shape
3rd Critical

$$T_n = 25 \frac{\text{lb-sec}}{\text{in.}}$$

Figure 53. Shaft Mode Shapes.

The first and second critical speeds were noted to be essentially nonbending modes at K values up to 100,000 lb/in. and to be at speeds below 20,000 rpm. Operational experience with a similar rotor system indicated that these modes would not be troublesome, and the shaft displacement resulting from them would be easily accommodated by the clearance of the journal bearings. The third critical, however, was the first bending mode and was noted to occur between 48,000 and 80,000 rpm, depending on the true stiffness of the bearing system (principally the radial stiffness of the oil film). Only limited experimental and analytical data were available to provide an accurate method of determining the fluid-film radial stiffness, since this parameter varies with speed, oil viscosity, temperature, clearance, and rate of oil feed. For a previous turbine rotor design of the contractor, it was noted that the predicted values of critical speeds for comparable journal-bearing systems were approximately 25 percent high when the flexibility of the oil film was neglected. Therefore, with $K = 10^8$ lb/in., it was estimated from Figure 52 that the actual third critical speed would be approximately 67,000 rpm. Since this speed was 22 percent above the maximum design speed, the design was considered to be satisfactory. Subsequent experimental evaluations, however, proved this assumption to be erroneous, with the critical speed actually occurring at approximately 46,000 rpm.

2.3 MODIFICATIONS

The initial mechanical checkout testing revealed a critical-speed condition of the rotor system at 46,000 rpm. Additional testing near the 46,000 rpm speed revealed that the rotor system could not be operated at or above this speed and could not be accelerated through it. A soft-mount bearing design which incorporated an oil-damping system was added. The soft-mount bearing made little change in the critical speed because the bearing stiffness was already below the $K = 10^8$ value originally assumed. However, it did limit the displacement at the resonant condition by damping. The kinetic energy generated by the forced excitation from the rotor imbalance at resonance was dissipated in a damped-bearing-support system.

A flexible bearing support (Figure 54) with spring-loaded disk-type dampers was designed and implemented into the rotor system. This arrangement permitted operation through the critical speed with a minimum change to the rig design.

Testing to evaluate the degree of success attained with the modified bearing support resulted in satisfactory operation throughout the desired range. Analysis of the test data showed 2 new vibration-amplitude peaks at resonant conditions — 1 at 37,000 rpm and the other at 40,000 rpm. The maximum shaft displacements at these resonant speeds were 0.0007 and 0.0005 inch, respectively. However, operation at the previous critical speed of 46,000 rpm was smooth. The new critical speeds were narrow in speed-band width, and the rotor accelerated through them easily.

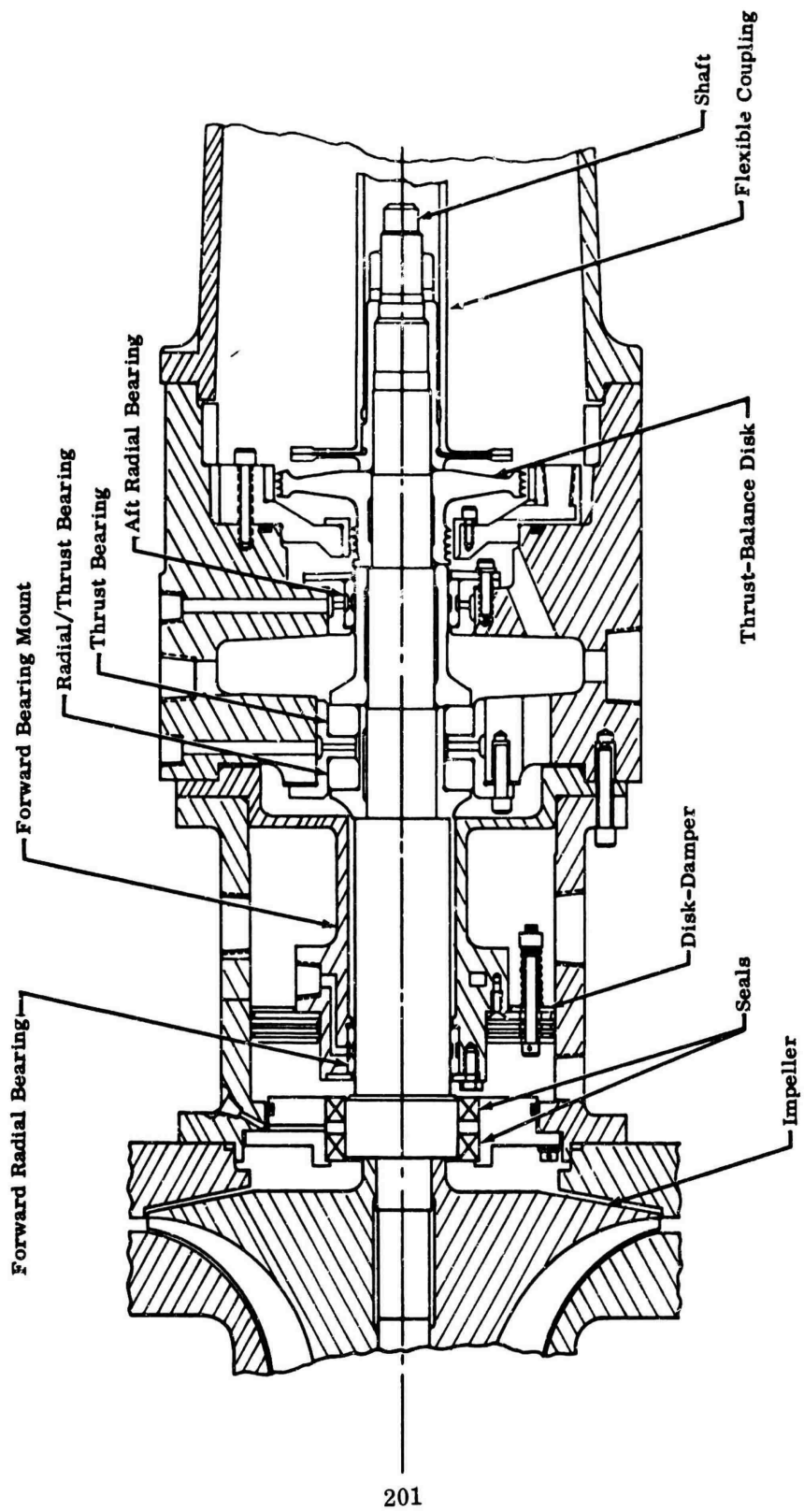


Figure 54. Diffuser Rig Rotor System.

2.4 CONCLUSIONS

It was determined that rig difficulties were caused principally by unpredicted rotor-dynamic characteristics. All bearings were found to be moderately loaded and capable of long-term operation at the design conditions.

Approximately 280 hours of operation under varying speed and surge conditions have been completed successfully with this rig. The rig can be modified readily to accommodate various impellers and compressor systems without appreciably upsetting the existing dynamic characteristics. A smaller mass impeller will very likely increase the current speed limit of 54,000 rpm. A heavier impeller would reduce it in proportion to the $1/2$ power of the mass. With proper maintenance to ensure minimum bearing wear, the system should continue its currently displayed operational capability indefinitely.

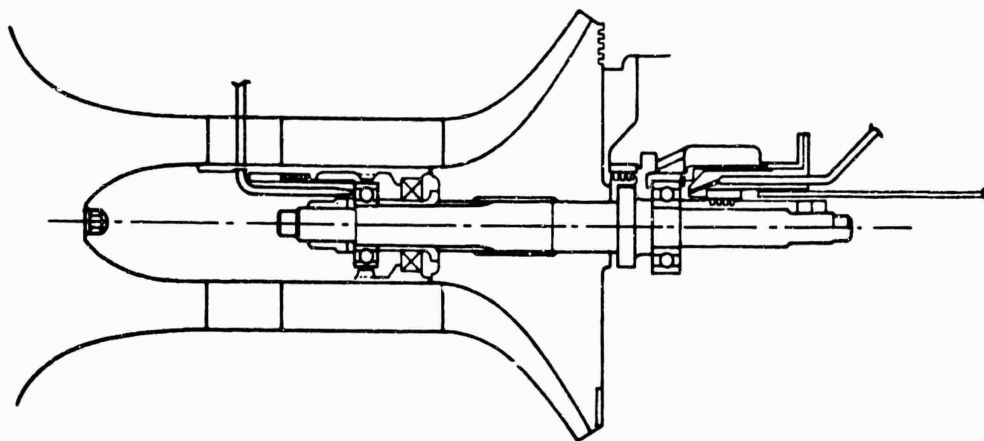
3.0 IMPELLER TEST SECTIONS

Requirements were defined for a test rig capable of accommodating four different impeller configurations of various diameters operating at 2,000 fps tip speed. Three of the impellers were mixed-flow configurations, designated as MF-1, MF-2, and MF-3; and the fourth was a radial-flow unit, designated as RF-1. It was desirable that a single test rig with detachable test sections be provided to reduce fabrication, assembly, and installation time. Three of the impellers (MF-1, MF-3 and RF-1) were required to operate at maximum speeds (10 percent above design speeds) of 63,000, 71,000, and 63,000 rpm. One unit (MF-2) had a maximum speed requirement of 80,000 rpm. The designs consisted of a single housing-collector assembly with a common bearing system for the MF-1, the MF-3, and the RF-1, and with a second bearing system for the high-speed MF-2 unit. A separate turbodrives unit for powering the test sections was provided as a Boeing facility.

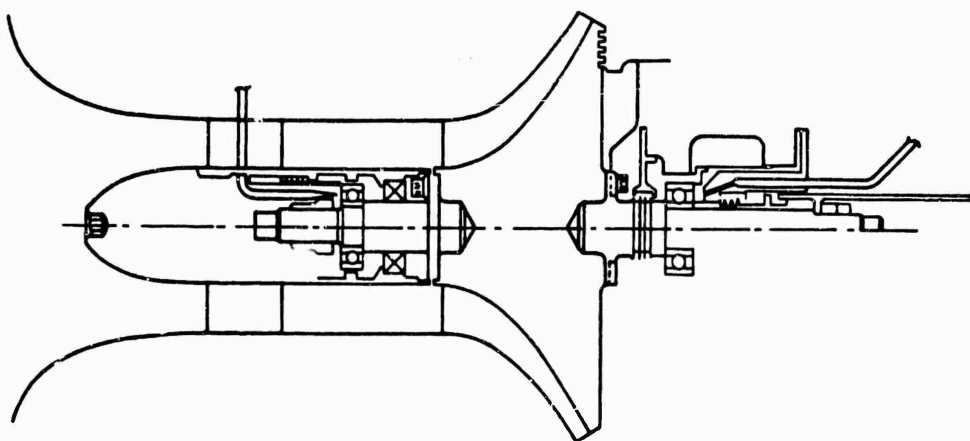
Design analyses were conducted to evaluate three different shaft and housing configurations, as shown in Figure 55. Configuration A consisted of a straddle-mounted bearing system with the impeller mounted on a stub shaft. Configuration C was a cantilevered system with the shaft through the impeller. All bearing supports were flexible to provide versatility in controlling the critical speeds to be encountered. Thrust loads were limited by a labyrinth seal at the rear face of the impeller at the tip.

3.1 BEARING SYSTEM

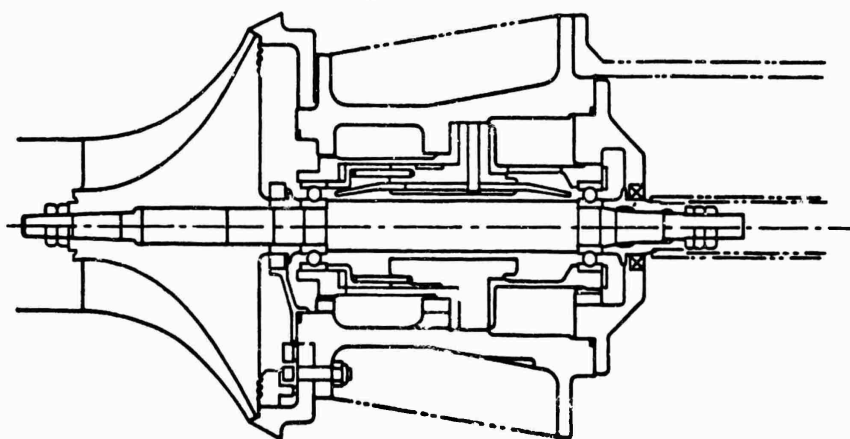
Precision ball bearings, preloaded to reduce axial and radial movement, were selected for the high speed rotors. Bearing sizes of 17 and 20 mm were considered in pairs and combinations to carry the expected radial and thrust loads. Variations in thrust load were expected because of differences in diameters of the



Configuration A



Configuration B



Configuration C

Figure 55 . Impeller Shaft Arrangements.

impellers. It was anticipated that radial loads could be minimized by precision balance of the rotating masses to 0.005 ounce-inch. Design criteria of 500-hour bearing life were established to meet operating requirements. (Design life of 500 hours was projected by bearing manufacturers to 2,500-hour average life.)

Thrust-load calculations showed that a maximum of 60 pounds could be expected at design speed for the MF-1 rotor. A 20 mm bearing most nearly satisfied this design criterion with a projected design life of 500 hours. Maximum radial loads were expected with the MF-2 rotor. Assuming a 0.005 ounce-inch imbalance, a 55-pound radial load was anticipated at 80,000 rpm. A 17 mm bearing met these conditions. Axial loads for the MF-2 rotor were calculated to be approximately 60 pounds, or an equivalent radial load of 147 pounds. Rotating speed limits for a 20 mm bearing, which was capable of carrying the load with a projected design life of 500 hours, were marginal because of the centrifugal load of the balls. A trade between speed limit and bearing life at these loads resulted in selection of the 17 mm bearing for both radial and thrust loads for the MF-2 configuration. The selections, which were based on recommendations of a bearing manufacturer, were high-speed, deep-groove precision bearings with aluminum-phenolic retainers and SAE 52100 chrome steel balls.

The MF-1 and RF-1 sections were designed for a common shaft with 20 mm bearings and the MF-2 and MF-3 rotor for 17 mm bearings. A preload of 40 pounds was specified for each bearing. Air-oil mist lubrication, with MIL-L-7808 synthetic oil being used, was specified, and a positive scavenge system was believed to be unnecessary. Operating temperatures for these bearings were predicted at about 300°F for the design life. Air-oil mist was considered to be adequate to remove the heat generated and to hold bearing temperatures to this limit. A microfog lubrication system was used to provide a feed rate of 4 ounces per hour. The ball-bearing design-life calculation was based on the bearing design data supplied by the bearing manufacturer. An imbalance of 0.005 ounce-inch at 60,000 rpm will produce an unbalance centrifugal force of 32 pounds at the rotor center of gravity. This dynamic load will be 43 pounds at the forward bearing and 11 pounds at the aft bearing. The total thrust load, consisting of a 40-pound bearing preload and a 60-pound impeller thrust, is 100 pounds. The C_s value for the 20 mm bearings (see Figure 56) running at 60,000 rpm is 160.* The equivalent radial load, with the rotor forces shown in Figure 56, is:

$$P = X (R_H + 1.2 R_S) + YT \quad (176)$$

*Engineering Catalog G-3, The Barden Corporation, Danbury, Connecticut, 1962.

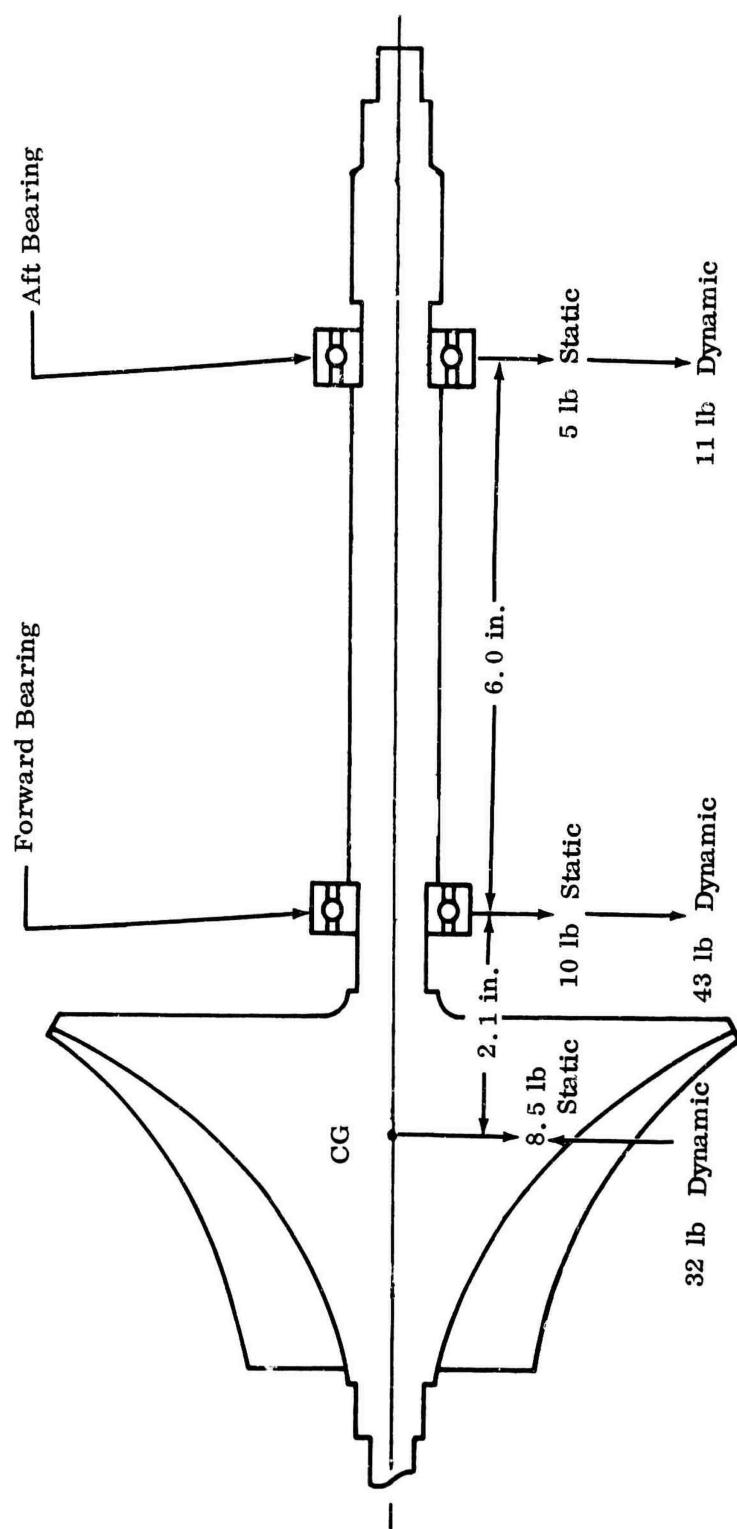


Figure 56. MF-1 Rotor Force Diagram.

where:

C_s	=	dynamic radial load rating, 160 lb
X	=	0.47 for contact angle of 10 degrees
Y	=	1.3 for thrust/ ZD^2 of 228
R_H	=	10-pound static radial load
R_s	=	43-pound dynamic radial load
T	=	100-pound thrust load
P	=	$0.47 (61.5) = 1.3 (100) = 159$ pounds

Bearing design life for the 204 (20 mm diameter) bearing is:

$$\begin{aligned}
 \text{life in hours} &= 500 \left(\frac{C_s}{P} \right)^3 \\
 &= 500 \left(\frac{160}{159} \right)^3 \approx 500 \text{ hours}
 \end{aligned}
 \tag{177}$$

The equivalent average life for the 500-hour bearing design life is 2500 hours. Similarly, the bearing design life for the 203 (17 mm diameter) bearing, with the rotor forces shown in Figure 57, is 280 hours, and the equivalent average bearing life is 1400 hours. The projected test-rig time was only 100 hours.

3.2 ROTOR DYNAMICS ANALYSES

Analyses of the dynamic characteristics of the rotor system with various bearing support stiffnesses were conducted. The cantilevered-shaft configuration shown in Figure 55 was investigated. The resulting first, second, and third critical speeds are shown in Figure 58.

The selected forward and rear bearing-mount spring rates of 10,000 lb/in. permitted operation between the second and third critical speeds, which were 17,000 and 80,000 rpm, respectively.

The typical configuration studied above did not apply directly to the rotor system for the MF-2 impeller, since limiting bearing size to 17 mm precluded use of a shaft with the same diameter and stiffness. An investigation of the effect of shaft

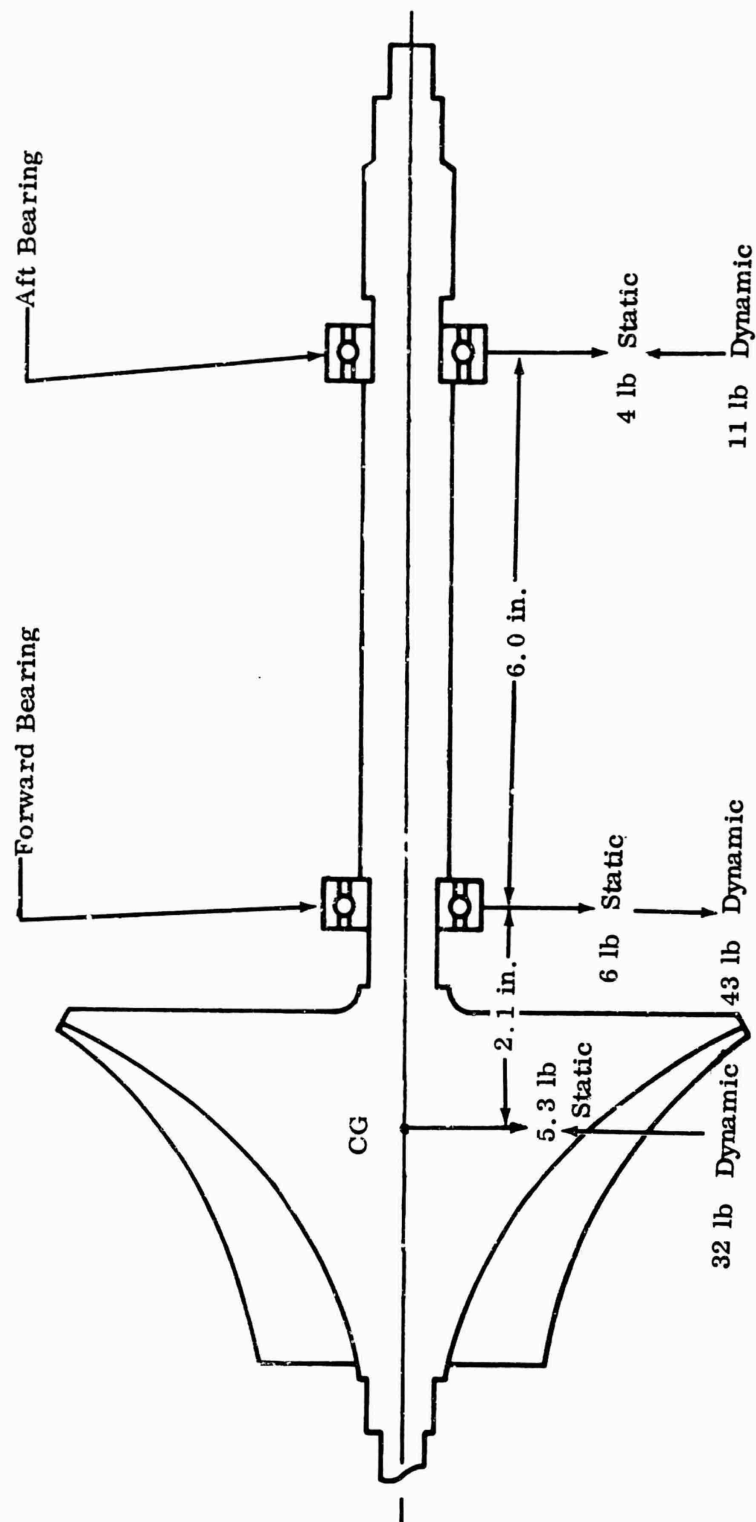


Figure 57. MF-2 Rotor Force Diagram.

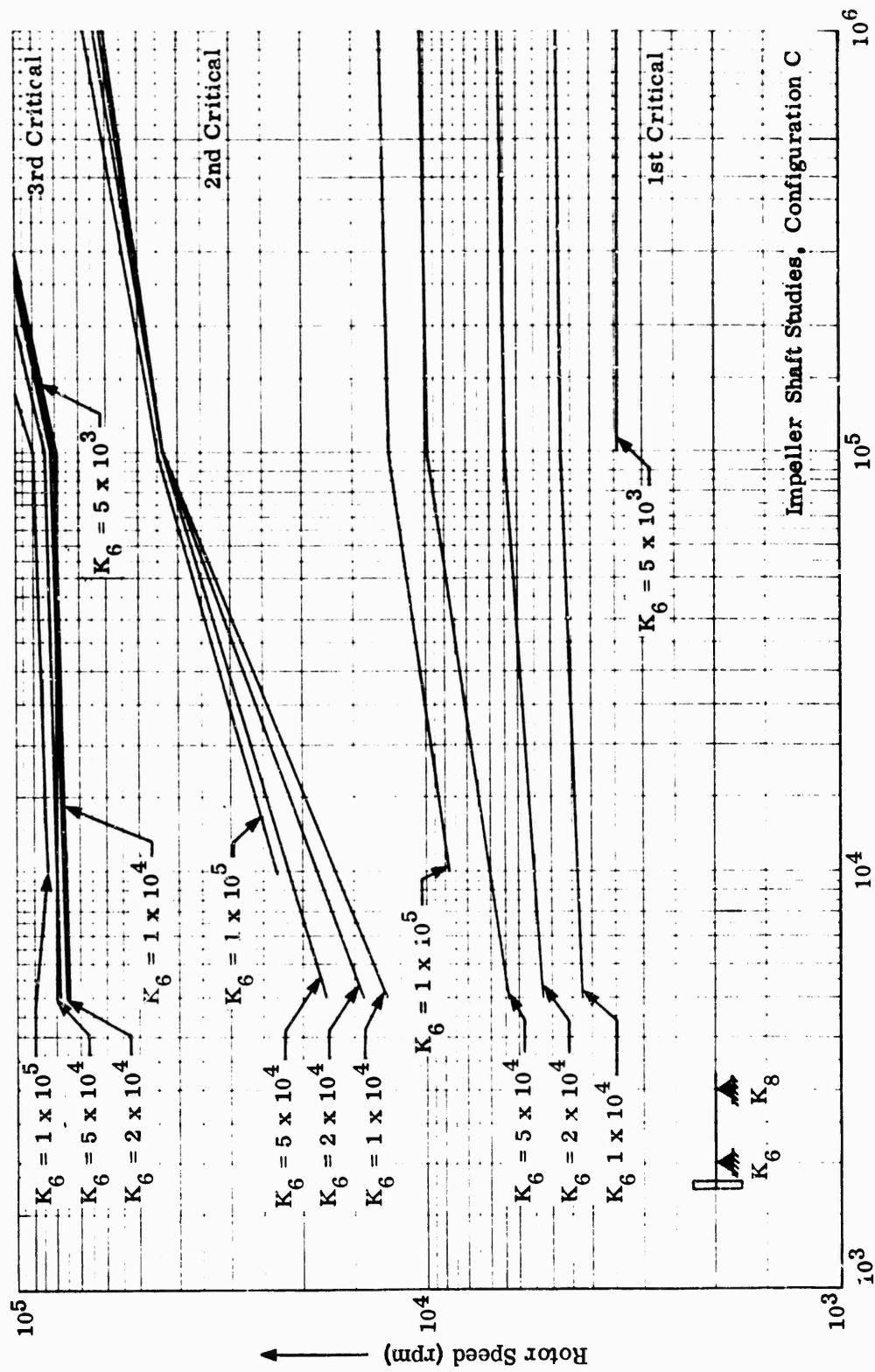


Figure 58. Critical Speed Versus Bearing Stiffness.

diameter and forward bearing stiffness, and assessment of critical speeds as a function of rear bearing stiffness was made. The 17 mm bearing established the shaft diameter to be between 0.65 and 0.80 inch. The first and second criticals presented no problems, but the third and fourth criticals transcended the operating range. The configuration selected was a shaft diameter of 0.70 inch and a bearing stiffness of 10,000 lb/in., projecting the first through fourth criticals at 4,700, 12,999, 36,000 and 102,000 rpm, respectively.

3.3 MODIFICATIONS

A shakedown test to evaluate the structural and operational integrity of each compressor unit was planned.

3.3.1 MF-1 CONFIGURATION

Accelerometers were mounted on the turbodrives and compressor-unit housings to measure the vibration, and thermocouples were installed to monitor bearing outer-race temperatures. The turbodrives were tested to 78,000 rpm as a free turbine with no load. Maximum bearing temperatures of 160°F and vibration levels of 2 g at rotor frequency were recorded at the maximum speed. These conditions were considered to be satisfactory for long-term use of the unit.

The dynamic characteristics of the combined units were initially checked with a dummy impeller, with the mass moment of inertia of the test impeller installed. This allowed operation with a minimum of torsional and thrust loads. With the rotor balanced to within 0.002 ounce-inch, test runs were completed successfully to 63,000 rpm. Resulting vibration levels versus speeds are shown in Figure 59. Maximum bearing temperatures encountered were 300°F. The dummy impeller was removed, and the test impeller was installed for the next phase of the test.

Several mechanical problems were encountered with the test impeller assembly:

- 1) The positive contact bearing seals failed to function above 30,000 rpm due to lack of lubrication from the air-oil-mist system;
- 2) The labyrinth seal at the impeller tip did not provide a sufficient pressure drop to limit the thrust load at the back face of the impeller;
- 3) The air-oil-mist system provided adequate lubrication but failed to remove excessive heat generated in the bearings;
- 4) The splined coupling between the compressor and drive units was considered to be the source of forced excitation to the shaft above that incurred by the imbalance of the rotor system;

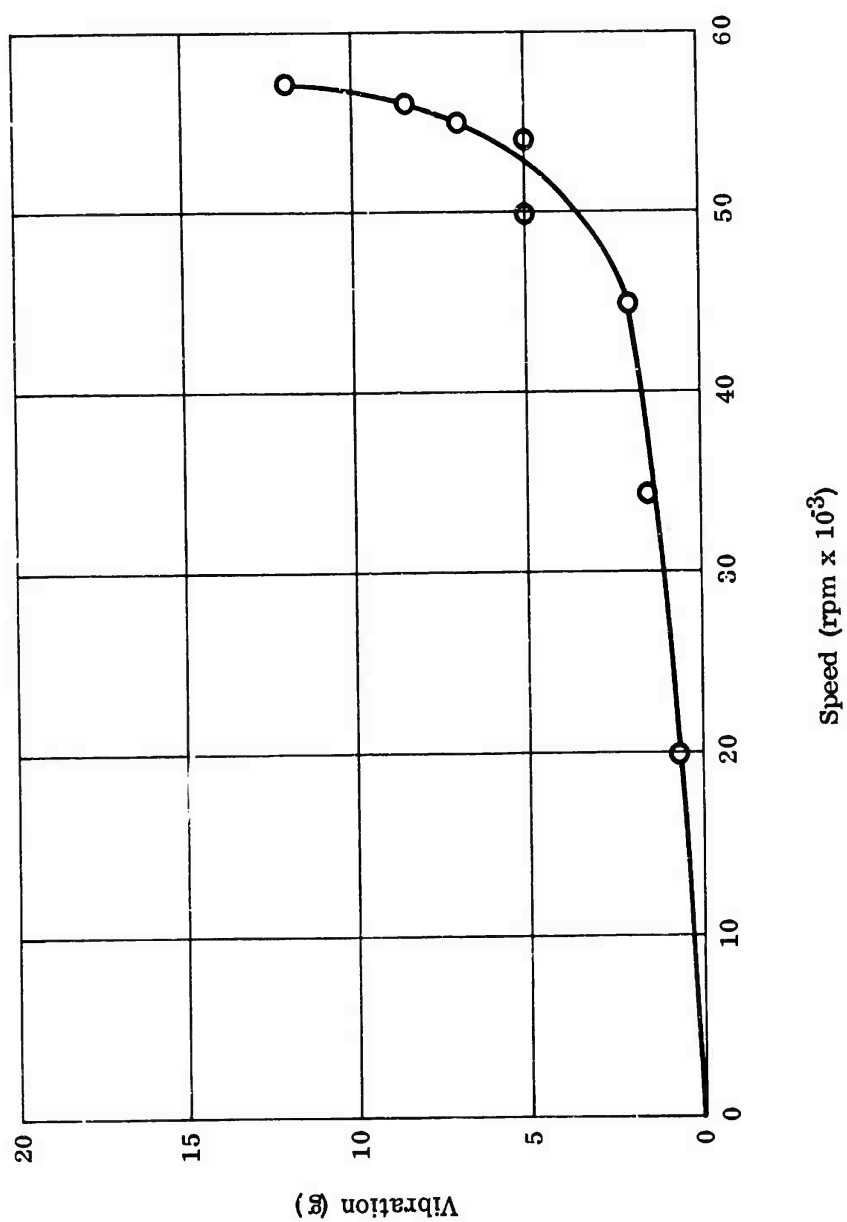


Figure 59. MF-1 Vibration Levels.

- 5) Several instances of contact between the impeller blades and shroud indicated that a change in the clearance between the blade tip and shroud took place with an increase in speed.

Initial evaluations on clearance changes attributed this condition to distortion caused by thermal gradients in the shroud; however, a detailed analysis (Figure 60) revealed that only 40 percent of the distortion was due to thermal growth and 60 percent to elastic growth of the impeller disk. The projected change in clearance as a function of speed was calculated, and further rubs were eliminated by spacing the shroud to allow for the change with speed.

Design modifications were implemented to correct the above problems. Test data indicated that a maximum thrust load of approximately 1700 pounds was produced by the static pressure acting on the back of the impeller disk, which showed that the labyrinth seal at the impeller tip was ineffective. An antithrust disk, with a controlled pressure cavity, was installed at the coupling end of the shaft to balance the thrust and to reduce bearing loads to the capacity of the bearing. The air-oil mist lubrication system was replaced with a jet-spray system. The carbon-seal support was modified to ensure adequate lubrication of the contact surfaces without excessive oil flow into the impeller cavity. This correction reduced bearing operating temperatures from a maximum of 300° to 160°F at the design speeds. The splined coupling was replaced with a flexible-disk frictionless coupling, capable of sustaining a total misalignment of 0.002 inch.

These modifications served to correct the mechanical operating difficulties of the rig and made possible a complete run through the design speed. The dynamic characteristics of the compressor unit with the rotor balanced to within 0.001 ounce-inch were then investigated to check the computed critical speeds.

The level of vibration above 55,000 rpm increased rapidly, which indicated that a rotor- or support-system resonance occurred in the immediate range above this speed. This resonance was not predicted from the initial calculations, which indicated that the third critical would not occur until 80,000 rpm. It was necessary to modify the rotor system to allow operating the test rig at speeds between 55,000 rpm and the design speed. The original design utilized soft bearing mounts similar to these of the diffuser-test-rig modification, but no damping system was used. Therefore the design was modified to incorporate a viscous damper for the bearing mounts.

It was believed that if the clearance between the flexible bearing support and the housing frame were pressurized with lubricating oil, damping effectiveness would increase with frequency. This revision reduced the shaft displacement and bearing loads and allowed safe operation at speeds of up to 59,000 rpm, as shown in Figure 61. At this point the MF-1 rig was considered to be satisfactory.

Curve A, Shroud and Backplate Distortion
 Curve B, Axial Thermal Expansion Differential
 Curve C, Impeller Centrifugal Force Distortion
 Curve D, Dynamic Tip Clearance (sum of A, B, & C)

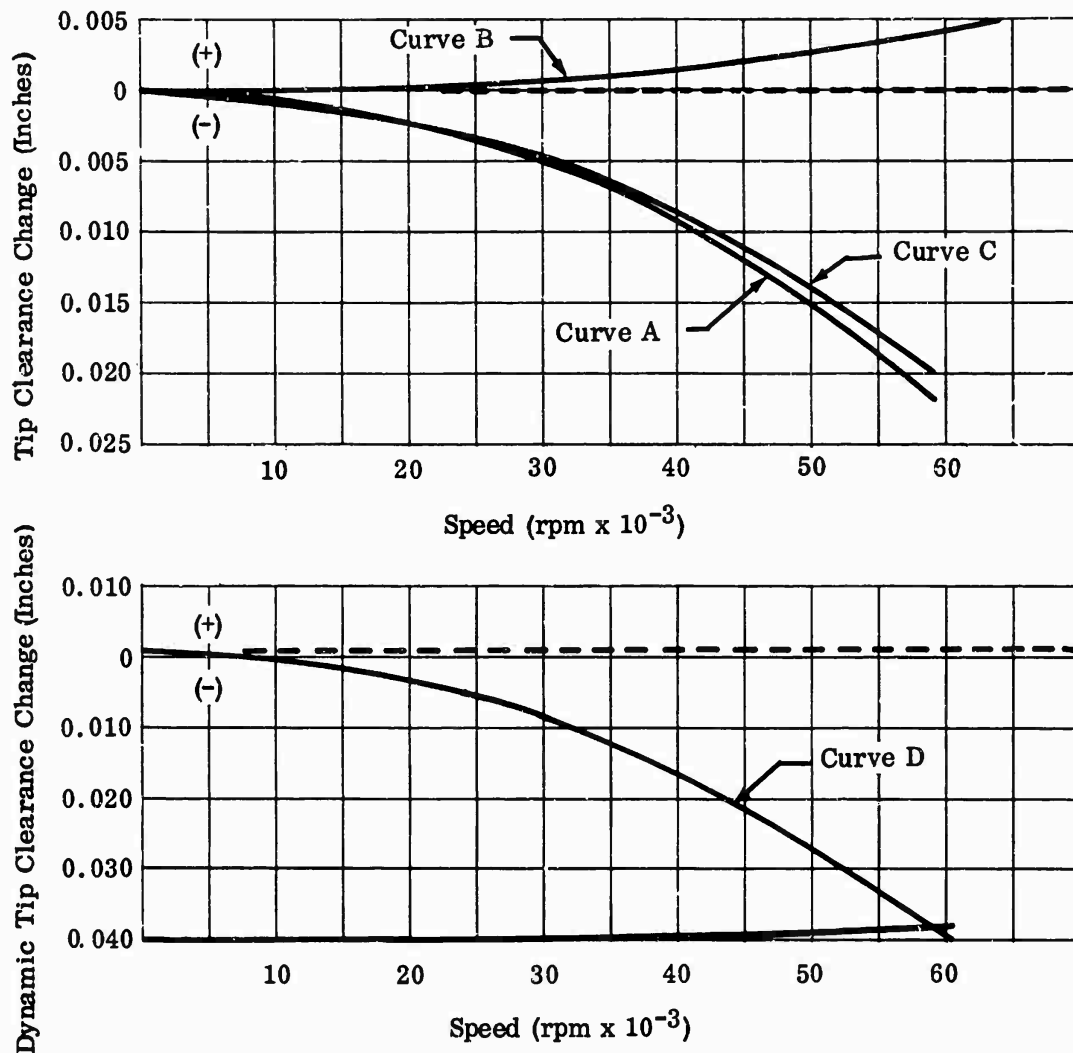


Figure 60. MF-1 Clearance Changes.

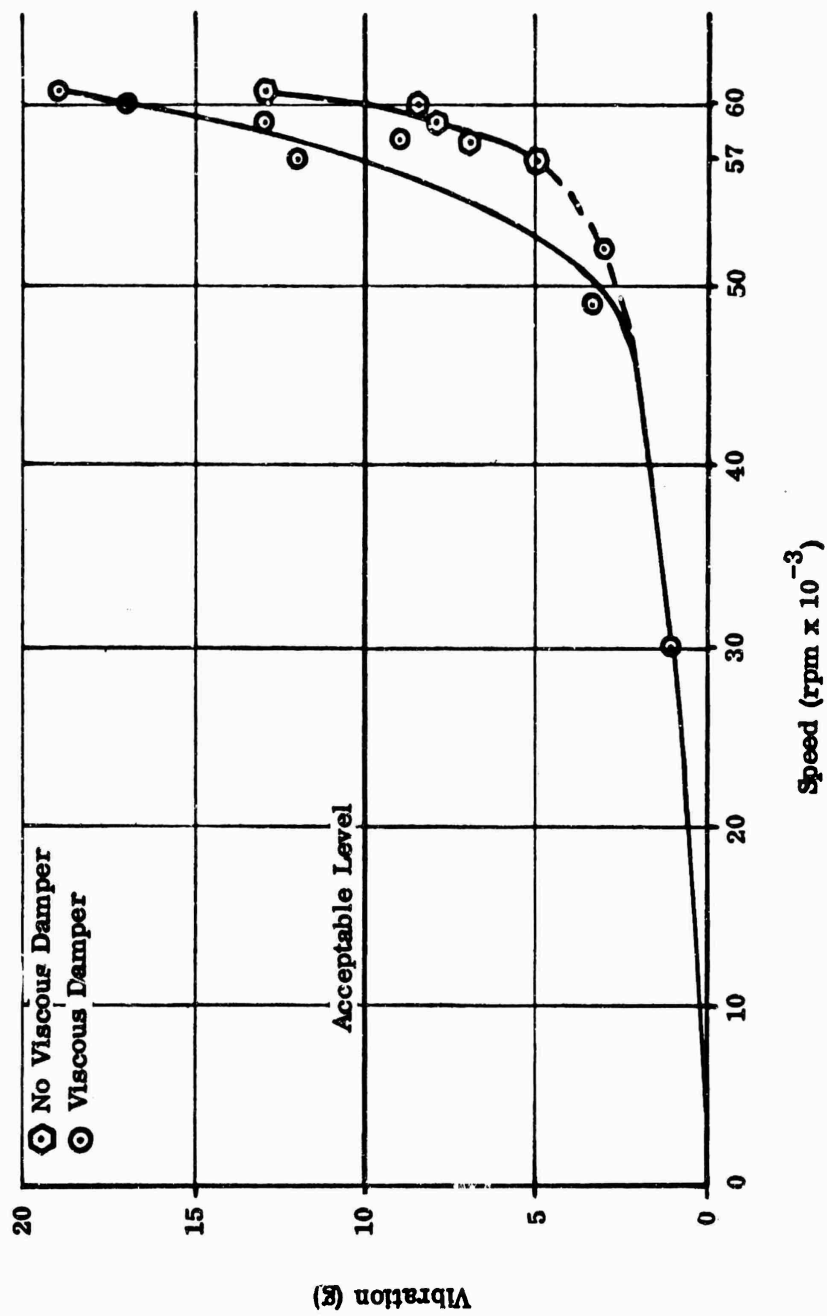


Figure 61. Effects of Viscous Damping.

3.3.2 RF-1 CONFIGURATION

The initial run of the RF-1 was successful at speeds of up to 44,000 rpm as a result of improvements implemented from the MF-1 experience. However, a substantial increase in the vibration level was encountered at speeds above 44,000 rpm. A critical speed was found at 48,000 rpm by accelerating rapidly to 50,000 rpm, at which speed a rub between the impeller and shroud occurred. These dynamic characteristics of the RF-1 rotor assembly were not predicted by the original analysis.

Another preliminary test, similar to the one performed on the MF-1 rig, was planned for the RF-1. Because of the more symmetrical disk shape of the RF-1, its elastic growth at high speeds was less than that encountered with the MF-1. Probes were installed to measure the movement of the related structures and the blade clearances at various speeds. In addition, improved rub sensors were installed to detect contact and to prevent damage to the impeller blades.

Relative to the critical speed, a study was made to evaluate the computer program input parameters. Twenty-eight variations in the input parameters were made in an attempt to correct the previous input variables and to establish improved prediction techniques. The results showed that the best correlation with the test was attained by lumping the large masses and by increasing the number of sections used to define the more flexible part of the shaft. Accordingly, the first, second, and third critical speeds were recalculated for the MF-1 to be 3,239, 8,959, and 56,142, respectively. Additional refinements were made by adjusting the mass in the disk in proportion to the effect of the polar moment of inertia on gyroscopic stiffening.

With the above refinements being made, the critical speeds were recalculated for the RF-1; the results are shown in Table I.

TABLE I
COMPRESSOR CRITICAL SPEEDS

<u>Compressor Unit</u>	<u>Critical Speeds</u>			
	<u>First</u>	<u>Second</u>	<u>Third</u>	<u>Fourth</u>
MF-1	3,239	8,959	56,142	
RF-1	3,262	8,784	48,286	155,440

The third criticals for the MF-1 and RF-1 were within the operating range. Positive resolution of this problem would involve substantial modifications to the rig and rotor hardware. Damping was proved to be only partly effective, since space was not available to provide a damping system with a critical damping factor. Therefore, it was considered that, if each of these units could be balanced for the third mode, the displacement could be reduced to a safe operating level and operation at or through this critical speed would be permitted.

A modal balance technique, as described in Appendix V, was subsequently adopted on the RF-1 unit with rewarding results. An 80-percent reduction in the shaft displacement at the previously determined critical speed was noted without an increase in the displacement at the other speeds. The problem of operating in the critical speed range was therefore resolved without need for further modification of the hardware. The rig was subsequently run up to 59,000 rpm through the third critical without excessive bearing load. Thermal growth of the housing and elastic growth of the rotor disk were compensated by adjusting the shroud position to provide the desired clearance between the impeller blades and the shroud contour at various speeds.

Modal balance of the MF-1 rig was similarly successful. Operation of both impeller sections at speeds of up to 59,000 rpm was demonstrated without further malfunctions.

3.4 CONCLUSIONS

The problems encountered with the impeller test rigs were associated with critical speed, thermal distortion, and elastic deformation. Correlated experimental and analytical evaluations provide an improved technique for predicting dynamics of the rotor system.

The heavy sections used to provide the structure and rotor system housing accommodated the heavy saturation of aerodynamic and rotor dynamics sensors and facilitated fabrication of one-only components with a minimum of tooling. However, temperature gradients across irregularly shaped sections made it difficult to predict the distortion which resulted. Uniform cross sections and flexible structures comparable to the conventional designs used in gas-turbine engine would have provided better assurance of dimensional stability. Accurate prediction of critical speed is largely dependent on previous experimentally confirmed inputs. The correlated experimental and analytical evaluations made with the impeller rig revealed the following specific factors:

- 1) Forced excitation of the rotor system by friction-type couplings, imbalance, and aerodynamic pulsations will prevent operation in the critical-speed range unless compensating factors are provided to minimize or dissipate the energy being generated. Damping can be effective if the geometry and design speed make it possible to provide a damper with critical damping coefficient (C_c) where $C_c = 2 m \omega_n$. Modal balance was proven to be most effective for operation at or near a shaft critical speed. With the forced excitation caused by built-in imbalance, counteracted by an equal and opposite imbalance at the point of maximum shaft deflection, the exciting force in the rotor is held to a minimum and results in smooth operation at or near resonance. The method is especially effective if some damping can be provided, since it is possible to attain critical balance only for specific modes of vibration. The process was relatively simple for the subject rotor but would become increasingly more complex if compensation for additional modes of vibration were necessary.
- 2) The magnitudes of thermal distortions and elastic deformations, due to the dynamic behavior of a rotor system, are difficult to predict accurately. Experimental systems which are designed to accommodate rotors with minimum shroud clearances should be equipped with proximity probes for continuous monitoring of the clearances.

- 3) High-speed antifriction bearing systems should be designed with spray- or jet-lubrication system. Air-oil-mist systems may not remove the heat generated in the bearings at high speed. Although bearings are designed for operation at up to 300°F, the design life is substantially reduced by dimensional changes which will alter the bearing design clearances and will result in operation at various contact angles.

(U) APPENDIX IV

SPIN-PIT TESTING

ABSTRACT

Research impellers tested by the contractor for the Army compressor research program were proof-spun in a high-speed spin pit before assembly in the aerodynamic test rig. This appendix describes the high-speed spin-pit facility and discusses its operation. General recommendations are made that should contribute to a successful high-speed spin-pit operation.

1.0 BACKGROUND AND INTRODUCTION

The impellers associated with the Army centrifugal-compressor research program were designed for high blade-tip speed (2000 feet per second compared to 1600 feet per second in previous contractor applications). In minimizing the risk of damage to the aerodynamic test rig, proof of material integrity was important. This was accomplished by running the impellers overspeed in the spin pit. The RF-1 and MF-1, as well as a workhorse impeller used for diffuser research, were successfully proof-spun. The MF-2 impeller was damaged in the spin pit because of a combined failure in a bent drive quill shaft, a severely scored bearing race in the drive turbine, and a broken test-rotor arbor.

2.0 BOEING SPIN-PIT FACILITY

The Boeing spin pit has a design maximum speed of 100,000 rpm and can accommodate rotors up to 16 inches in diameter or 17 inches in length. The chamber was constructed of armor plate with a replaceable 4-inch-thick hardwood inner liner. The test rotor was positioned with the rotational axis vertical and was suspended from the air-drive turbine on a long, slender quill shaft. Figure 62 is a photograph of the spin-pit facility.

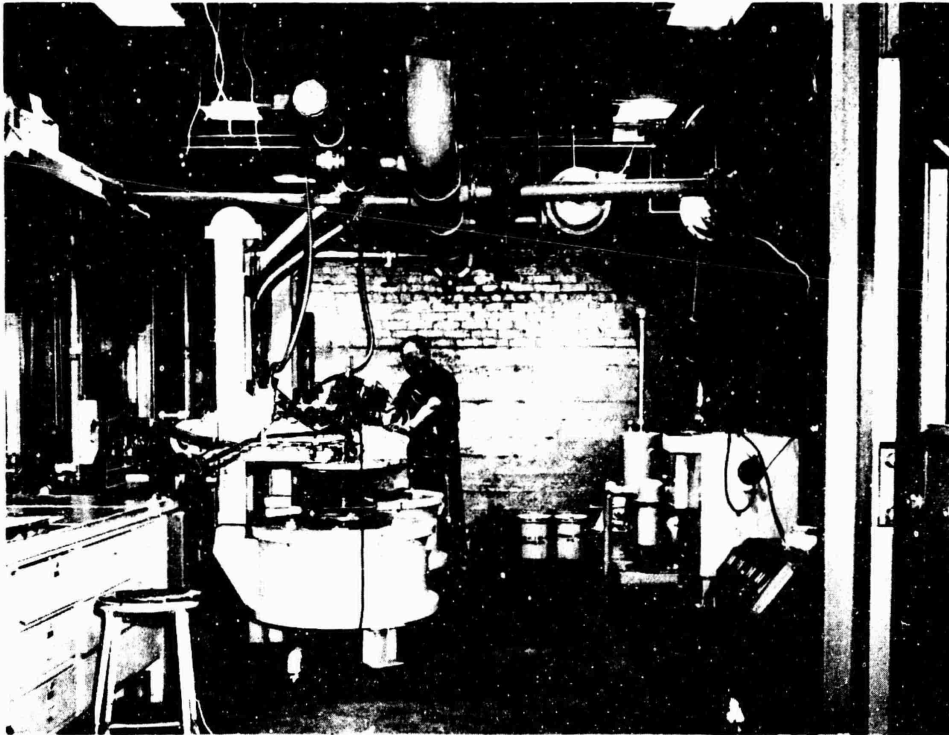


Figure 62. Spin-Pit Facility.

Figure 63 is a cross section of the drive system with the MF-2 impeller installed. The ends of the quill shaft were attached with shear pins to the test-rotor arbor and to the drive-turbine shaft. Snubber bushings with approximately 0.005-inch diametric clearance were provided to contain the quill shaft. This arrangement was intended to permit the test rotor to rotate about its own mass center and to isolate it from the drive turbine if a test-rotor failure occurred. In such an event, shearing of the pins would allow the lower end of the test-rotor arbor to drop into the bearing-mounted catch cup, while gyrations of the upper end of the arbor would be limited by the clearance between the arbor and the upper catch ring.

The drive turbine was mounted on preloaded ball bearings, which were oil-mist lubricated. Devices for controlling, indicating, and recording speed were used.

Proof-spinning was accomplished by bringing the impeller up to speed as rapidly as possible. For this application, the drive-turbine bearing selections were based on short-operating-life considerations. Operating limits of the spin pit are as follows:

- 1) Rotor-shaft displacement, 0.010 inch;
- 2) Bearing temperature, 250°F;
- 3) Lubrication, one drop oil per 10 seconds (gravity feed);
- 4) Spin-pit vacuum, 0.5 inch Hg;
- 5) Spin-pit temperature, 1800°F;
- 6) Speed limit, 100,000 rpm.

The test-rotor assembly on the arbor had to be balanced within 0.001 ounce-inch about the axis on which it will spin in the pit.

3.0 IMPELLER SPIN TESTS

The first 3 impellers proof-spun in this program were the RF-1, the MF-1, and the diffuser-test-rig workhorse impeller. Proof-spinning of these impellers was accomplished satisfactorily. However, an instability was encountered when an attempt to proof-spin impeller MF-2 was made.

Of the impellers proof-spun, including the impeller of the T50-BO-10 engine, the MF-2 had the lowest equivalent diameter length.

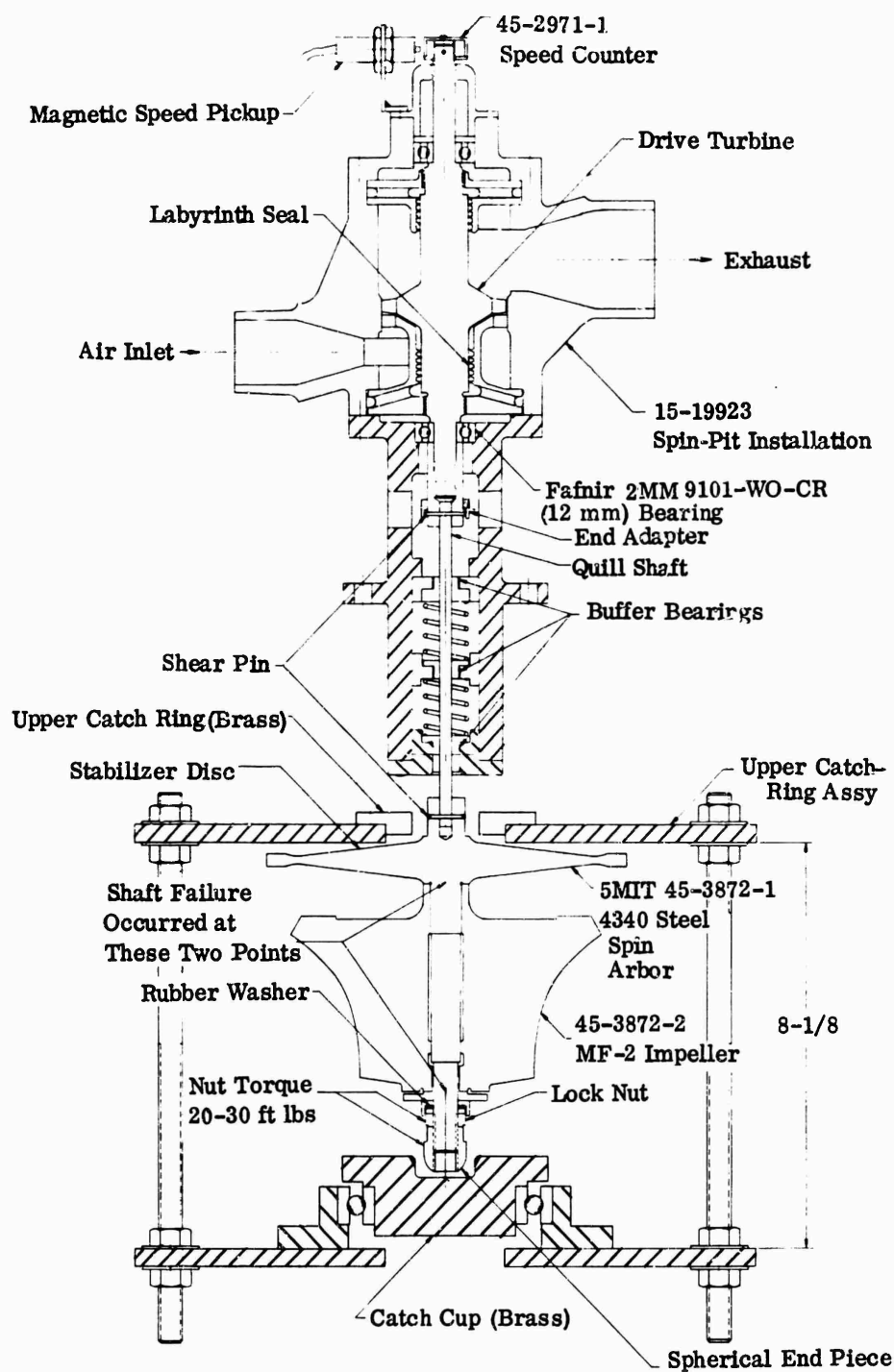


Figure 63. MF-2 Impeller (Spin-Pit Installation).

<u>Impeller</u>	<u>D/L</u>
T-50	3.55
MF-1	3.10
RF-1	2.85
MF-2	2.22

Den Hartog* states that as the D/L ratio approaches the theoretical minimum stable ratio of 1.1, varying degrees of instability may be encountered. In this case, an impeller may be excited readily by extraneous forces such as residual imbalance, rubbing of the quill-shaft bushings, or turbine bearing-induced vibrations. A rotor that has an unfavorable D/L ratio will tend to seek another axis of rotation when spun.

To increase the D/L ratio, a stabilizer disk was added (Figure 63). This raised the equivalent D/L ratio to 3.33.

4.0 DISCUSSION

The instability in the test-rotor assembly could have been triggered by a number of conditions, singly or in combination, as described in the following sections.

4.1 RESIDUAL IMBALANCE

The assembly was balanced to an accuracy of 0.0005 ounce-inch, which was adequate. However, if a misalignment or eccentricity existed in the counterbore where the drive quill was attached, unstable operation could occur with the resulting imbalance. The accompanying forces vary in amplitude as a function of the square of the speed.

The final balancing correction of the impeller and stabilizing disk assembly was made in 2 planes normal to the rotational axis (i.e., at the impeller inlet end and at the stabilizer disk). Because the imbalance to be corrected did not lie in either of these planes, the correction produced force couples between the actual imbalance and the 2 correction planes which increased in magnitude as a function of the square of the speed.

If the hub connection between impeller and stabilizing disk were sufficiently flexible, it was expected that these 2 main elements of the assembly could be

*J.P. Den Hartog, Mechanical Vibrations, McGraw Hill Book Co., New York, 1956.

deflected from the axis of rotation. This effect was minimized by balancing the impeller and the disk individually before final assembly and balancing.

4.2 IMPELLER-TO-SHAFT FIT

The spin arbor was sized to provide 0.0002-inch diametrical interference in the impeller bore at both ends to ensure positive alignment on center. Analysis of the deflection in the impeller bore due to centrifugal force at 66,000 rpm showed that the lower (inlet) end would increase in diameter by 0.0009 inch allowing 0.0007-inch diametrical or 0.00035-inch radial clearance. The diameter of the hub extension at the upper end contracts 0.0005 inch, which increases the effective diametrical interference to 0.0007 inch. While the interference occurring at the upper end would tend to hold the impeller centered, the clearance at the lower end could have permitted a radial shift, with a possible resultant force (imbalance) of 58 pounds at 66,000 rpm.

4.3 AXIAL CLAMPING LOAD

The axial clamping load of the impeller on the arbor could tend to deter a radial shift, such as that indicated above, or it could force the shift in one direction as a result of squareness tolerance between the nut and the impeller clamping surface. An analysis of the arbor stretch (due to retainer nut torque) versus axial contraction of the impeller-hub dimension (due to centrifugal load) showed a clamping load of approximately 3100 pounds at 66,000 rpm, compared to an initial load of 5640 pounds.

4.4 EXTRANEOUS EXCITATIONS

A high-speed rotating system such as the MF-2 in the spin pit could have been excited by various external vibrations or cyclic loads. Those excitations most likely to have affected the system are:

- 1) Residual imbalance in the drive-turbine rotor and quill shaft;
- 2) Dynamic action in the drive-turbine bearings, including motion of ball bearings and cages relative to the races, which could have been affected by axial preload and radial clearance in the bearings;
- 3) Dynamic behavior of the drive quill in the buffer bearings. If the rotor system encountered a dry rub while whirling in a backward, nonsynchronous fashion, the whirl could have become self-excited and would have been catastrophic.

This combination was subjected to a spin test, and it sustained a failure at 65,940 rpm as indicated by the speed recording reproduced in Figure 64. The

speed trace showed essentially constant acceleration of the drive turbine up to the point of failure, then 400 rpm drop in speed followed by a rapid acceleration to the overspeed cutoff point of 71,000 rpm.

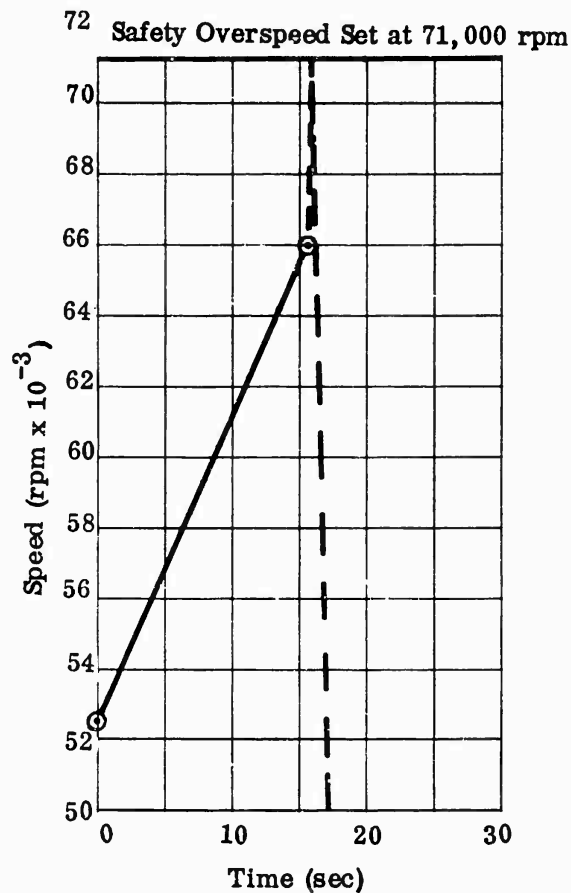


Figure 64. MF-2 Impeller (Spin-Pit Speed Record).

Post-test examination of the parts revealed the following points.

- 1) The drive quill shaft was bent at the lower end, indicating a substantial lateral displacement of the test-rotor arbor (Figure 65). Both pins had sheared. The bent quill shaft had worn the bushings oversize and there had been relative rotation between the quill and the drive-turbine shafts after the quill shaft was bent.
- 2) The inner race of the lower bearing in the drive turbine was severely scored, indicating a heavy side load similar to imbalance (Figure 66). The phenolic

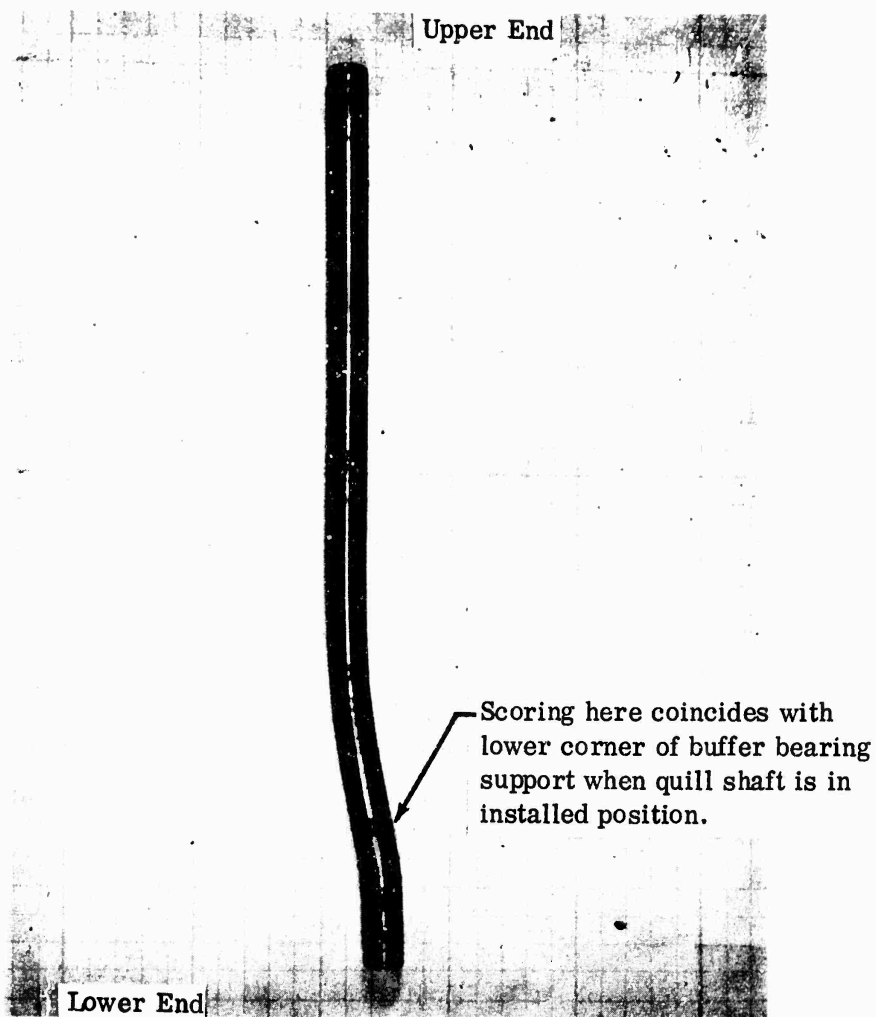


Figure 65. Spin-Pit Drive Quill Shaft After Attempted Proof Spin of Impeller MF-2.



**Figure 66. Spin-Pit Drive Turbine Lower Bearing After
Attempted Proof Spin of Impeller MF-2.**

cage and the balls in the outer race of the bearing were relatively undamaged, indicating that the load which damaged the inner race did not persist for any substantial interval.

- 3) The spin-test arbor was broken in 2 places, at the upper and the lower side of the impeller. The impeller sustained blade damage from random contact with the walls of the chamber (Figures 67 and 68). Examination of the fractured arbor ends in the impeller (Figures 69 and 70) indicated that the arbor had broken at the upper end first, then was pulled downward about 0.060 inch as the lower end of the arbor broke off. Closer scrutiny of the score marks in Figure 69 shows that the impeller was probably rotating faster than the stabilizing disk as the 2 pieces separated. The probable sequence of events in the failure was as follows:
 - a) The rotor and arbor assembly lost stability at 65,940 rpm, causing lateral movement of the spin-arbor axis and bending of the quill shaft.
 - b) The quill shaft jammed in its buffer bearings, momentarily causing an excessive rotating radial load on the lower drive-turbine bearing.
 - c) The shear pins then failed, permitting the turbine to accelerate relative to the quill shaft and allowing the impeller to drop into the catch cup.
 - d) The upper hub of the arbor was not constrained by the upper catch ring. (There were no marks on the upper hub to indicate contact with the upper catch ring. It was concluded that the ring must have been positioned too high to be effective.)
 - e) With no restraint at the upper end, the impeller with the stabilizing disk tumbled in the spin chamber, breaking the arbor in 2 places as described above.



Figure 67. Impeller MF-2 After Attempted Proof Spin.

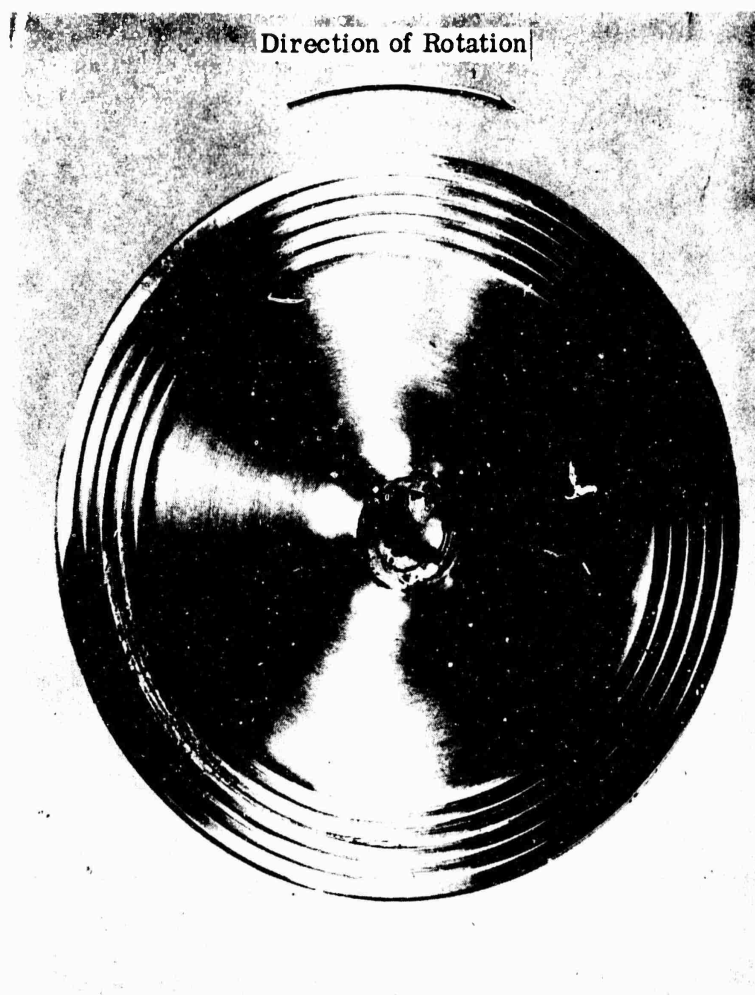


Figure 68. Upper (Rear) Face of Impeller MF-2
After Attempted Proof Spin.

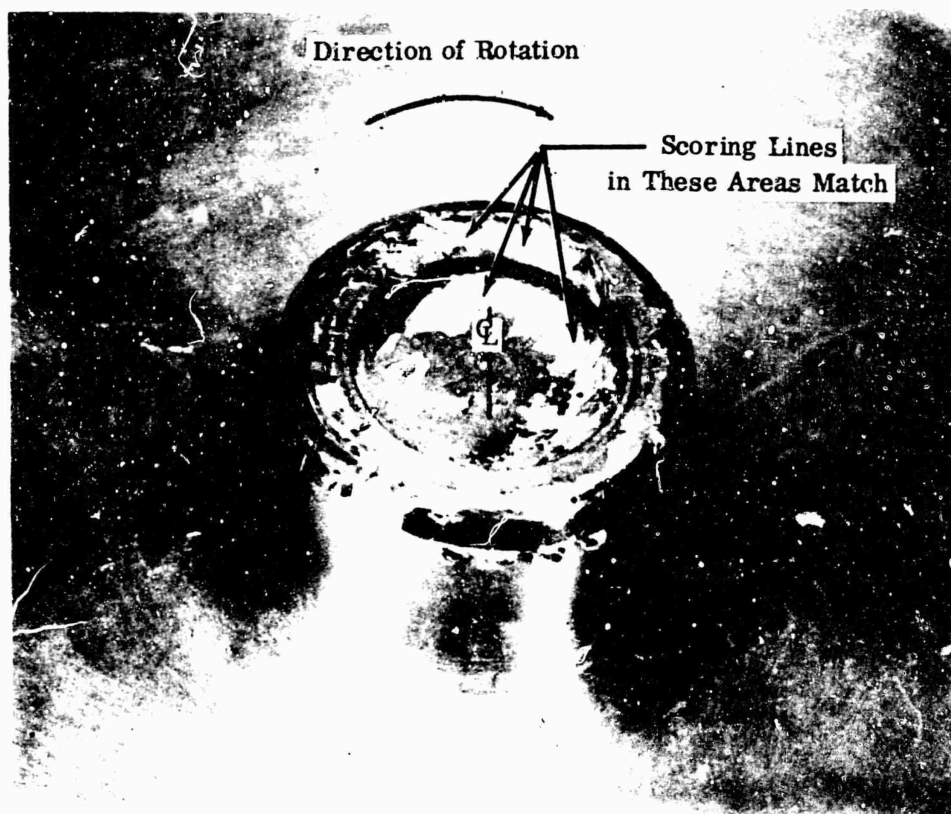


Figure 69. Broken Arbor at the Upper End of Impeller MF-2
After Attempted Proof Spin.



Figure 70. Broken Arbor at the Lower End of
Impeller MF-2 After Attempted Proof Spin.

5.0 CONCLUSIONS AND RECOMMENDATIONS

Of the considerations discussed above, indications were that a radial shift of the MF-2 impeller on the spin arbor was the most likely explanation for the sudden instability that caused failure. As the rotor accelerated, the gradual reduction in axial clamping load, accompanied by increasing internal force couples, could have permitted the shift, possibly triggered by a cyclic vibration transmitted from the drive quill shaft on the drive turbine, or both.

The following recommendations should ensure successful high-speed spin-pit operation:

- 1) Consult with a reliable bearing manufacturer in the selection, installation, and operation of drive-turbine bearings;
- 2) Dynamically balance the drive turbine and the spin-pit-test rotor to less than 0.001 ounce-inch;
- 3) If the spin-pit-test rotor is comprised of more than 1 disk or wheel, dynamically balance the separate parts before assembly, and then dynamically balance the assembly;
- 4) If the rotative speed is such that the bore fit of the spin-pit-test rotor will be lost due to centrifugal load, provide for holding the rotor on center;
- 5) When the axial length of the test rotor permits, undercut the spin arbor to reduce the tensile spring rate, thus minimizing the variation of axial clamping load with speed.

(U) APPENDIX V

MODAL BALANCE

ABSTRACT

This appendix presents the balancing method used to reduce the vibration amplitude of the first shaft-flexure mode. This technique is commonly known as modal balancing and is useful if excessive vibrations are encountered when accelerating rotating machinery through a shaft critical speed.

SYMBOLS

A_1	displacement amplitude
CW	calibration weight
M_1	modal balance weight
θ_1	phase angle (degrees)
ϕ	phase angle (degrees)
W	base speed (rpm)

1.0 GENERAL INFORMATION

Static and dynamic balancing operations of a rotor system will result in smooth operation at speeds below the first shaft-bending critical (the third shaft critical for soft-mounted bearings). The balance corrections are made in 2 planes, regardless of how the imbalance is distributed. As the rotational speed of the shaft is increased, elastic deflections due to centrifugal forces occur and the condition of balance is upset. The changes in balance caused by these deflections can become large and prohibit running at certain speeds. The forces caused by the eccentricity of the shaft and the resultant forces for particular shapes of elastic deflections can be determined. As a result, small correcting masses which introduce imbalance (static and dynamic) can produce vibration-free operation at all speeds. This process of counterbalancing a dynamically unstable rotor system is termed modal balancing.

The process of modal balancing was experimentally tried when the MF-1 rotor system was discovered to be operating at a critical speed. The success of the first application of this technique led to modal balancing the RF-1 rotor system to improve its acceleration through the shaft critical speed.

The basic theory of modal balance technique shows that a rotor assembly can be balanced (i.e., made to operate through a critical speed with little or no vibration amplitude) by the addition of small weights to the shaft.* The number of weights and corresponding planes of application required equals the number of shaft-vibration modes in the operating range. Most shafts can be designed to operate below the third critical; thus only 1 plane is required for the correction weight. For high-order criticals, the modal balance method becomes increasingly difficult because it is necessary to position the correction weights in such a manner that their combination will balance but that it will not excite other criticals as the speed is advanced through the operating range. The discussion here will be limited to the first critical-speed modal balance solution.

The first mode of vibration is excited by an inherent imbalance due to manufacturing tolerances of the rotor assembly. In this mode, the shaft will bend in a plane that passes through the axial centerline of the rotor assembly. As long as the rotor remains assembled, this bending plane will remain at the same phase angle on the shaft. To modal balance the rotor, a compensating, small imbalance weight is used. This weight is placed in the bending plane, but at 180 degrees out of phase with the initial bend (Figure 71). The weight can be positioned arbitrarily along the shaft. Thus, this small weight counteracts the original imbalance that caused the large amplitudes at the critical speed. The added weight also produces equal but opposite forces and cancels the bending.

*Jon Parkinson, Critical Speed Vibration-Modal Balance, SAE Paper 928A, October 1964.

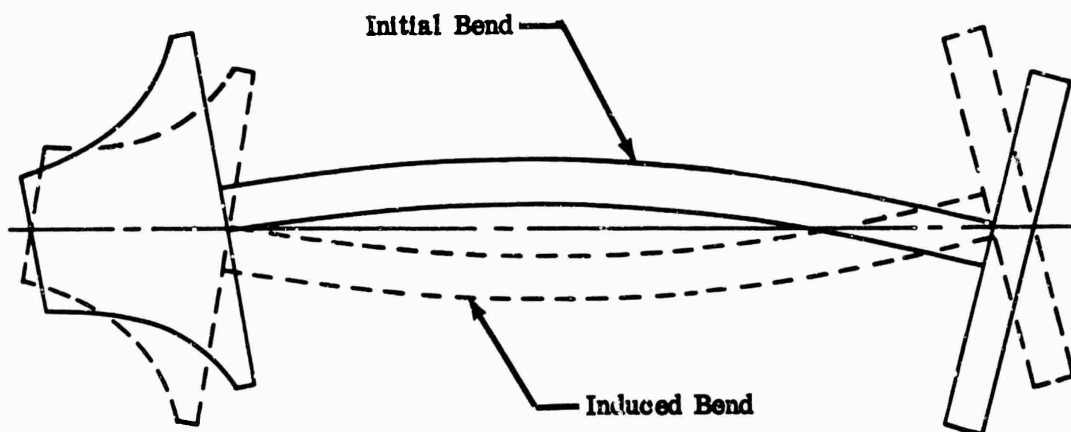


Figure 71. Shaft-Bending Schematic.

2.0 INSTRUMENTATION

The modal balance technique required running the rotor assembly in the rig near the critical speed. Therefore, instrumentation for monitoring the shaft deflection was provided. Electronic induction-type proximity probes had proved to be accurate and reliable for measuring shaft displacement at high rpm during previous tests and were used for these runs. A typical probe of this type is shown in Figure 72, and its installation is shown in Figure 73. The probe was installed in a threaded screw to allow setting the head at various distances from the shaft for the purpose of calibration. This probe was connected to an oscillograph paper recorder for a permanent data record.

3.0 PROCEDURE

Two different methods of modal balancing are presented and were used for different test-rig modal balance operations. The results were identical for either procedure. One procedure uses a trial and error solution of placing the weights while the other uses a single trial and an analytical solution.

3.1 TRIAL AND ERROR METHOD

The trial and error balance operation is a fast and simple procedure. The first operation is to establish definitely that the vibration problem is due to the first shaft-bending critical. This can be done by analysis or by experimental measurement with shaft proximity probes. These investigations also give a fair indication of the rpm at which the critical occurs. A base speed was next established just below the critical speed at which the rig will operate safely while the modal balance operation is performed. This speed was selected at approximately

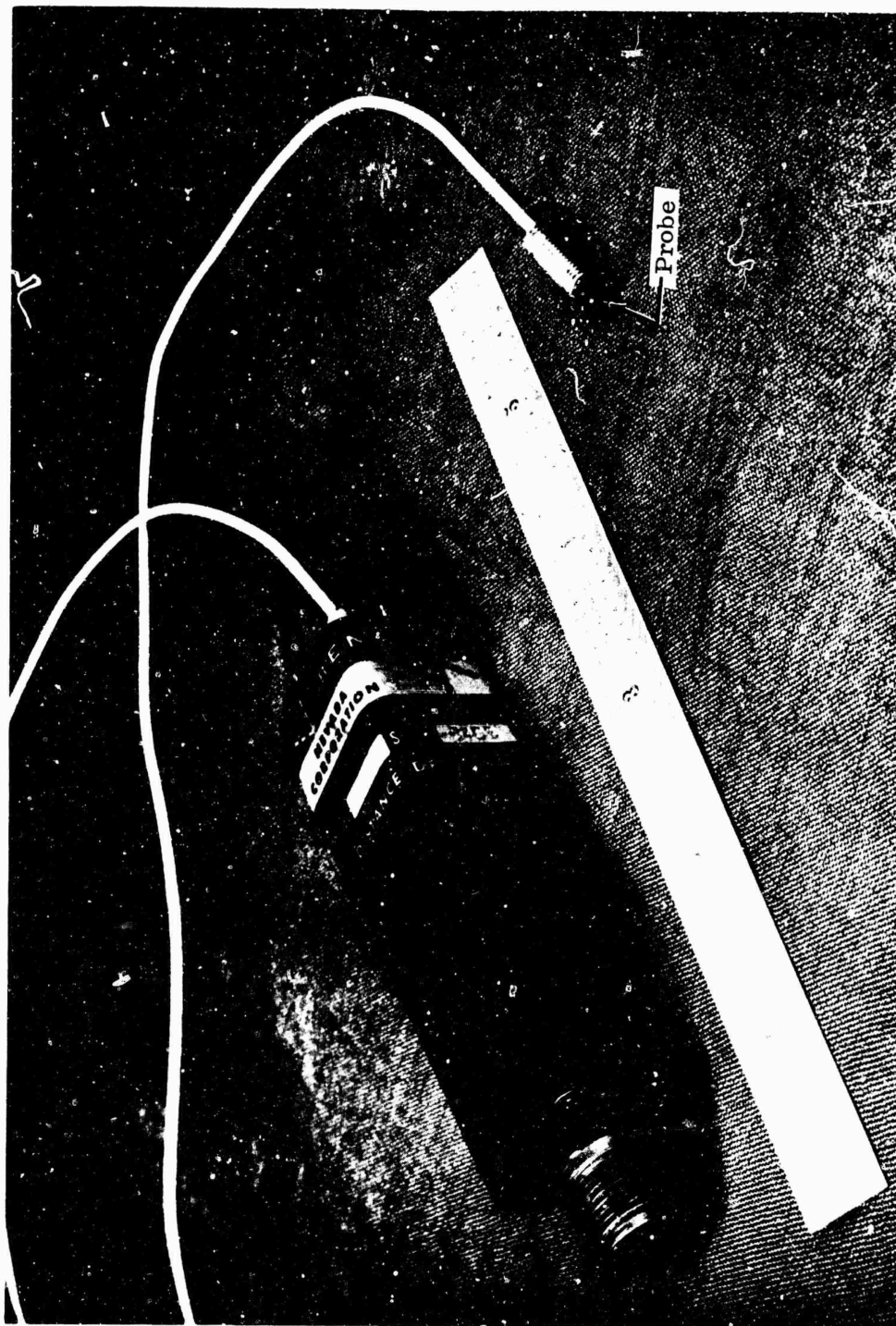


Figure 72. Proximity Probe.

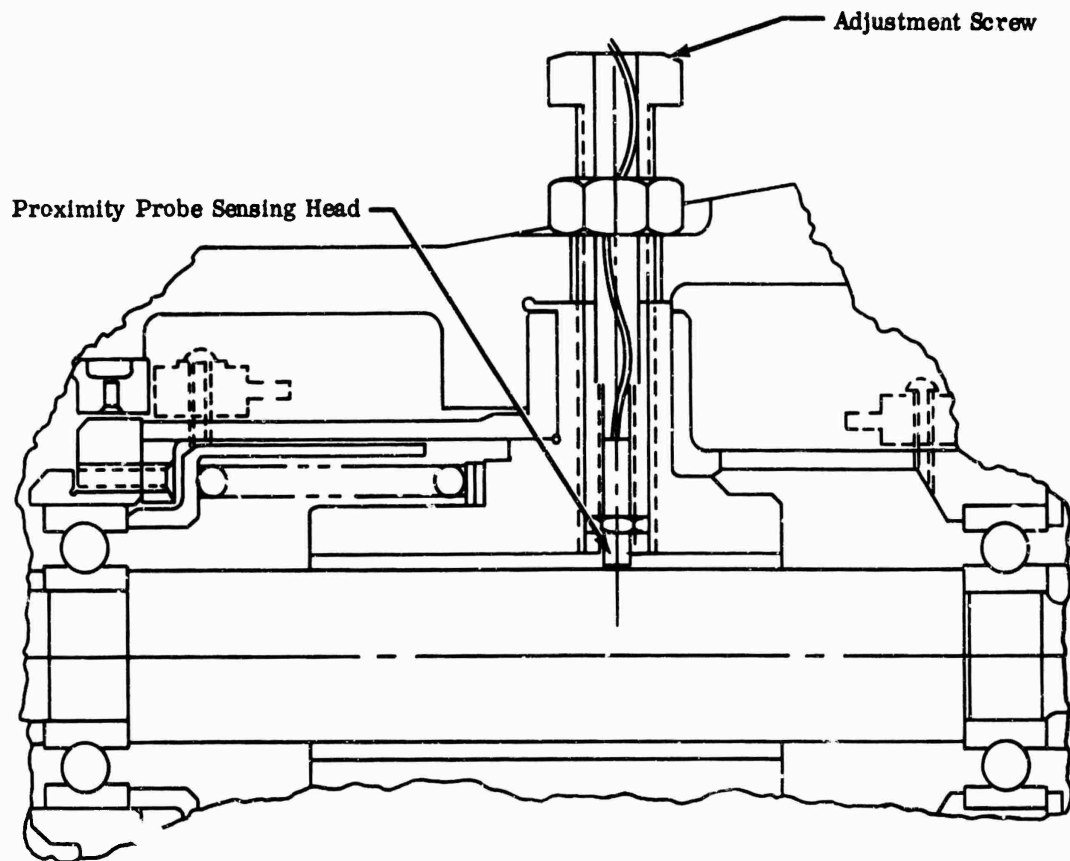


Figure 73. Proximity-Probe Installation.

10 percent below the critical speed. At this rpm, the base displacement of the shaft was plotted as shown in Figure 74. A small imbalance weight (Figure 75) was installed at the forward end of the impeller shaft, Figure 76. The angular location on the shaft for the imbalance weight was chosen to coincide with the angular location of maximum displacement. The test rig was then rerun at the same base speed with the weight attached. The shaft amplitude was recorded, and this value was plotted at the 0-degree phase angle (see Figure 74). The same imbalance weight then was rotated 90 degrees, and the test was repeated at the base speed. The shaft amplitude was again recorded and plotted. This process was repeated with the imbalance weight rotated 180 and 270 degrees. The resultant data were plotted and the points were connected by a sinusoidal curve. The desired phase angle for the imbalance weight was the point of minimum amplitude. With the correct phase angle known, the amount of im-

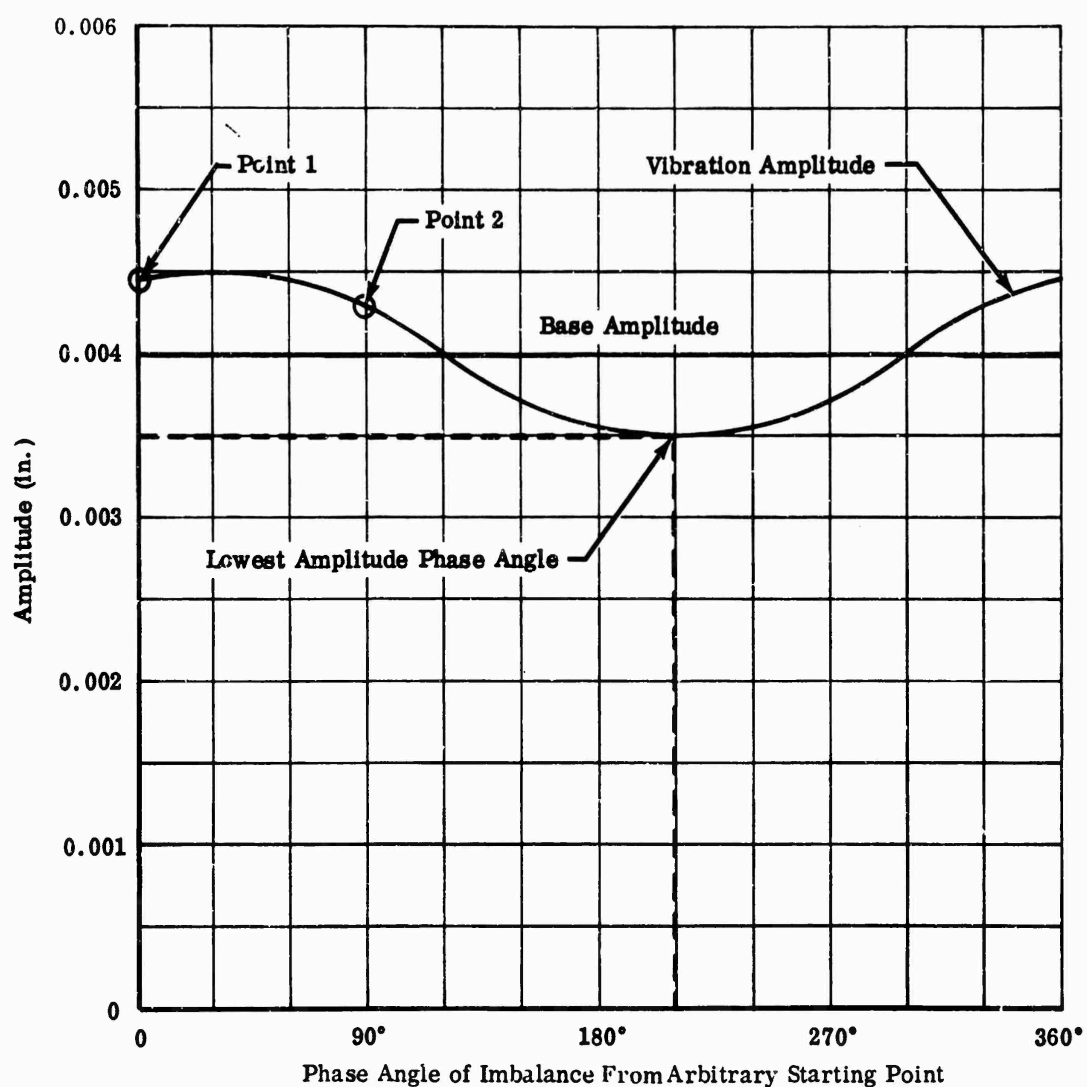


Figure 74. Amplitude-Phase Relationship.

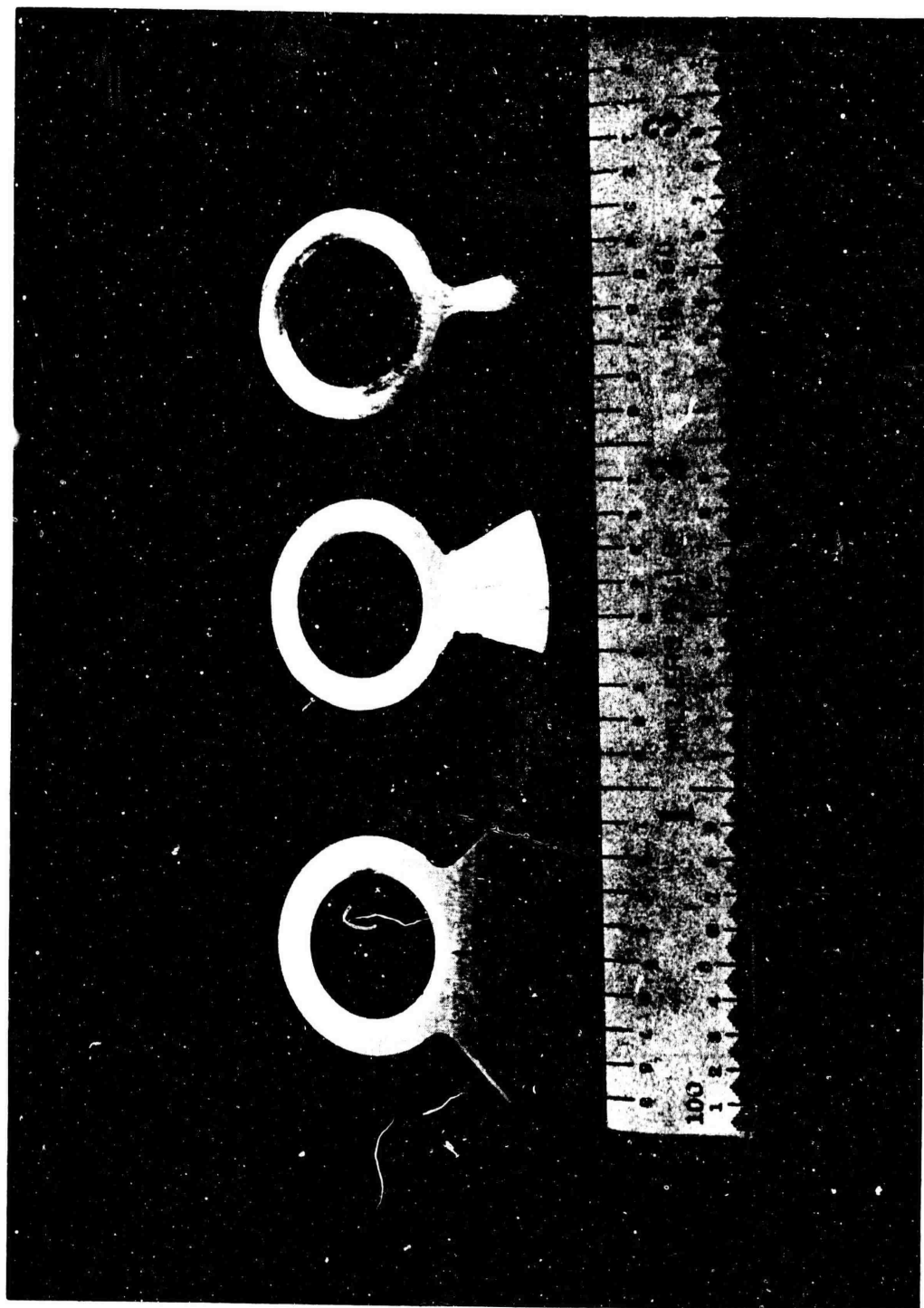


Figure 75. Typical Modal-Balance Weights.



Figure 76. Impeller With Modal-Balance Weight.

balance was varied at this angle until the amplitude at the base speed was a minimum. The rig then was able to accelerate through the critical speed safely.

This method was used on the impeller test rig with the MF-1 impeller. The design speed of the rig was 57,000 rpm. To run this speed, it was necessary to accelerate through the first shaft-bending mode critical speed (48,000 rpm). Near this speed the shaft-vibration amplitude was 0.007 inch, peak-to-peak. This amplitude would have imposed a high bearing load while accelerating through the critical speed. The base speed was set at 43,000 rpm, and the base amplitude of 0.004 inch peak-to-peak was observed. After the modal balance procedure was performed, the amplitude was less than 0.001 inch peak-to-peak. The rig was then able to operate safely through the 48,000 rpm critical speed at less than 0.002 inch peak-to-peak vibration amplitude.

3.2 ANALYTICAL METHOD

The analytical method required additional instrumentation to that which was available for the initial trial and error method of modal balancing the impeller test rig with the MF-1 impeller. The analytical solution was vectorial: it required measurement of the shaft-displacement amplitude and displacement phase relative to a fixed reference on the shaft. The simplest method was to notch the shaft in the area of the displacement pickup and to display the signal on an oscilloscope. Figure 77 is a sketch of a typical oscilloscope recording.

A base speed (ω) was established as in the previous trial and error solution. It was necessary to repeat the speed accurately because of a 180-degree shift in the phase angle (Figure 78) as the rotor passes through the critical speed. An initial plot of the displacement amplitude (A_1) and phase angle (θ_1) was made on polar coordinates (Figure 79) for the rotor system at the base speed. A known calibration weight (CW) was installed, and the resultant displacement amplitude (A_2) and phase angle (θ_2) were measured at the base speed (ω_1). These values were plotted (Figure 79), and the correct modal balance weight (M_1) and phase angle (ϕ) were computed by vector subtraction.

$$\left| M_1 \right| = \frac{\left| A_1 \right|}{\left| AB \right|} CW_1 \quad (178)$$

Vector AB (Figure 79) was the vector due to the calibration weight (CW_1), and ϕ was the location of M_1 from the position of CW_1 .

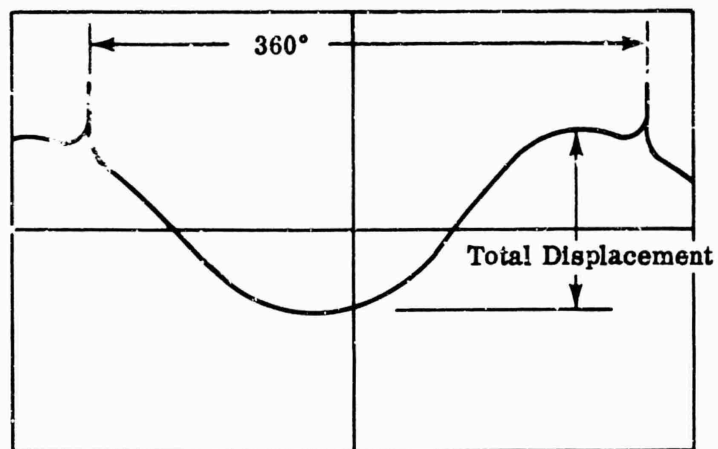


Figure 77. Shaft-Displacement Sketch.

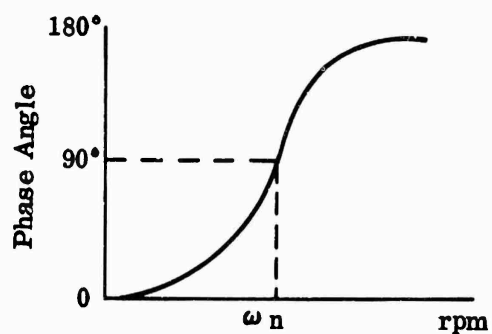


Figure 78. Phase Angle Versus Rotational Speed.

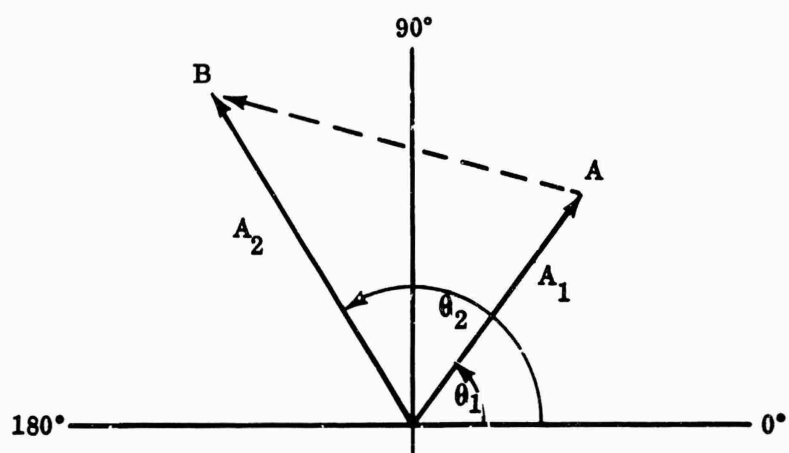


Figure 79. Shaft-Displacement Diagram.

VIBRATORY-STRESS TEST OF WORKHORSE IMPELLER

ABSTRACT

This report covers the vibratory-stress test of a titanium impeller. The objectives were to corroborate calculated blade natural frequencies and to determine whether conditions existed which would prevent operation of the compressor in any area required for performance tests. Results are presented in terms of blade natural frequencies and stresses at the various speeds.

SYMBOLS

a	peak-to-peak amplitude (in.)
c	gage calibration factor (psi/in.)
f	frequency (cps)
K	gage factor
K'	gage factor sensitivity compensation
N	rotor speed (rps)
n	number of oscillations per time period (cycles)
P _S	static-pressure tap, wall
P _R	total-pressure rake
P _T	total-pressure probe, fixed
P _{Tφ}	total-pressure probe, directional
R _L	lead resistance (ohm)
R _S	shunt resistance (ohm)
R _{g'}	strain gage resistance after installation (ohm)
T	temperature probe, unshielded
T _{SH}	temperature probe, shielded
T _T	total-temperature probe, stagnation
t	time period (sec)

1.0 SUMMARY

The test was considered to be successful in that all major objectives were met. The blade frequencies determined from this test were compared with the predicted values. Differences between predicted and test frequencies were generally within 500 cps. Therefore, the speeds at which these critical vibrations actually occurred necessitated correcting the predicted Campbell diagram. With this small change in the Campbell diagram, there were only minor restrictions for operation in the test rig. Vibratory-stress levels in nearly all regions were below the allowable of $\pm 20,000$ psi. As expected, the vibratory stresses in surge exceeded the design allowable for about half of the speed range. However, the levels of steady stress and metal temperature provided enough margin to permit operation in all regions along the surge line except in the range of from 39,000 to 41,500 rpm. This range must be avoided entirely for steady-state operation at reduced-flow conditions. In addition, the accumulated number of surges in the speed ranges between 49,200 and 50,100 rpm, and between 51,500 and 55,000 rpm, must be limited to 30 with the surge-relief valve in operation. The inlet guide vane angles do not affect the vibratory-stress level.

2.0 DISCUSSION

The purpose of this test was to determine the natural frequencies and vibratory-stress levels of the workhorse impeller under varying conditions of compressor operation. In addition, the investigation was directed toward establishing all critical vibration conditions to be used as an operating guide in future performance testing of this impeller. The testing was to be accomplished by use of a strain-gage instrumented impeller running under the same environmental conditions that would be encountered during performance testing.

2.1 RIG COMPONENTS AND INSTRUMENTATION EQUIPMENT

The following special equipment was used for the test:

- 1) Inlet guide vane assembly;
- 2) Diffuser islands;
- 3) Eight strain gages (1/8 inch);
- 4) One 8-channel water-cooled slip-ring assembly;
- 5) Bridge completion and signal conditioning equipment;
- 6) One frequency-modulated tape recorder and support equipment;

7) Three light-beam-type oscillographs.

All strain gages on the impeller had a gage factor of 1.99 ± 3 percent. The strain gages had been used previously on impellers and axial compressors.

2.2 PROCEDURE

Extension lead wires were attached to the strain gages before they were cemented on the impeller. The leads were No. 32 AWG solid conductors with baked-on enamel insulation. Leads were attached to the strain gages by first removing about 0.25 inch of insulation from the lead ends. The ends were twisted together with the strain-gage leads, and the lead ends were then fused by using a heli-arc-welding process.

A preliminary test specimen of titanium was prepared to verify the strain-gage installation procedure before instrumenting the impeller. Strain gages were mounted on the specimen to test the cement in shear and tension under actual centrifugal loads and temperatures. Preparation of titanium for strain-gage installation required careful evaluation of the chemicals used. The common degreaser, trichloroethylene, could not be used because of halogenation. However, the standard metal conditioners and neutralizer solutions supplied by most strain-gage manufacturers could be used where the temperature of the titanium parts was less than 700° F. Beyond 700° F, titanium is subject to hydrogen embrittlement.

For the impeller-stress test, the impeller surface was degreased by soaking the areas to be instrumented in Dow Chemical Company 19AC E-Z Strip, followed by repeated washings in household ammonia. The surface was then sanded lightly and washed with metal-conditioner and neutralizer solutions. Because titanium oxidizes rapidly, a base coat of cement about 0.001-inch thick was applied to the areas on which the strain gages and lead wires were to be placed. The surface protection was sufficient for cementing the strain gages. The cement used was Budd Company GA-60 2-part epoxy. Curing of the cement took 5 hours at 350° F.

Because only dynamic strain-gage data were required, potentiometric circuitry was used. A 1200-ohm ballast resistor was used in series with each 120-ohm strain gage, and the outputs were capacitively coupled to the amplifiers.

2.2.1 BENCH TEST

Resistance of the strain gages after installation (R_g') and strain-gage and lead-wire resistance ($R_g' + R_L$) were measured to the nearest 0.1 ohm. Gage-factor sensitivity compensations (K') were computed by:

$$K' = \frac{R_g'}{R_g' + R_L} (K) \quad (179)$$

where:

K is the gage-factor nominal value specified by the manufacturer.

Strain gages were calibrated with resistors using:

$$\text{Strain (microinches/inch)} = \frac{R_g' + R_L}{(R_g' + R_L + R_s)} (K') \quad (180)$$

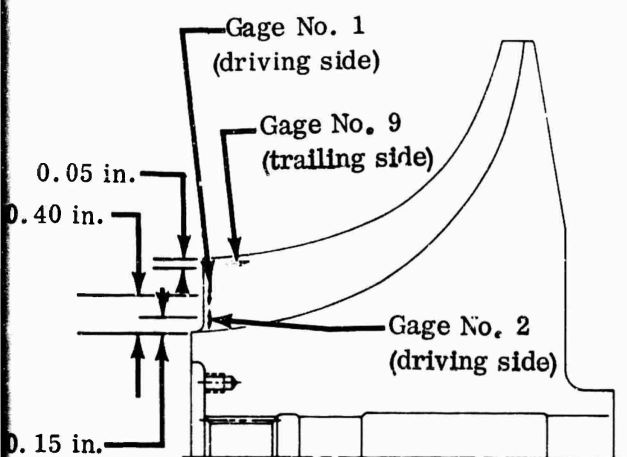
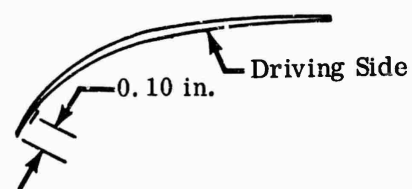
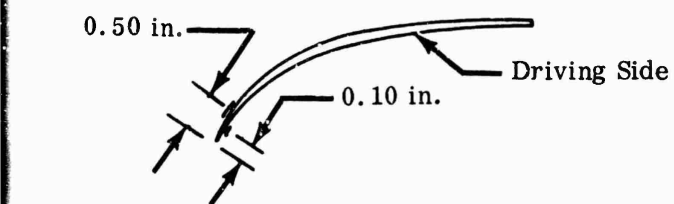
where:

R_s is the calibration shunt resistance.

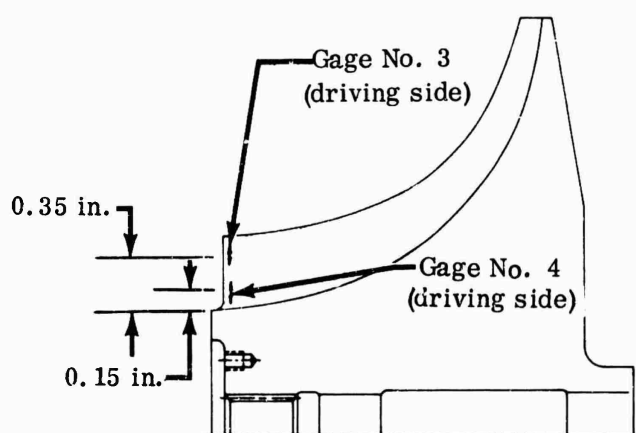
Gage-factor sensitivity compensation for temperature was not necessary because the metal temperature was below 300° F in the areas where strain gages were installed; strain gages were not necessary in the higher temperature regions near the impeller tip because of the shorter, stiffer blade sections in this region.

A bench test of the impeller blades was made to determine natural frequencies and areas of maximum stress that corresponded to each of the first 3 modes of vibration. The frequencies were determined first with the use of an electromechanical excitor and were rechecked with a pulsed-air rig (siren) by reading the output frequency of the strain gages attached at critical areas of the blades (Figure 80). The strain signals read from these gages were recorded on magnetic tape and on an oscillograph for subsequent data reduction.

The recording system was calibrated for frequency response throughout the test range, and correction factors were computed for each recorded blade natural frequency. The strain signals were corrected and were compared to each other to obtain the relation between the amplitude and strain-gage location on each instrumented blade. These bench-test data were then used to correct the analytically predicted frequencies on the Campbell diagram. In addition, regions of maximum stress were identified for each of the first 3 modes. This information was used to select the locations of strain gages to be used in the compressor-rig test. The gages were located where the greatest number of modes could be read



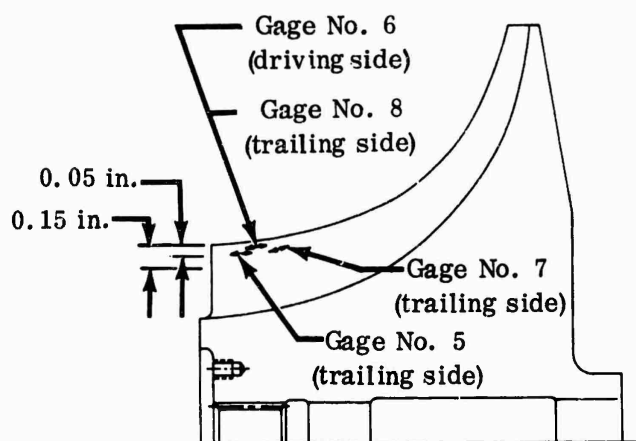
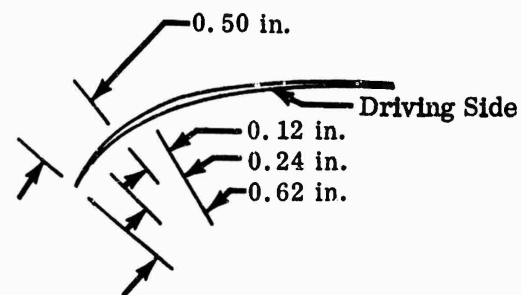
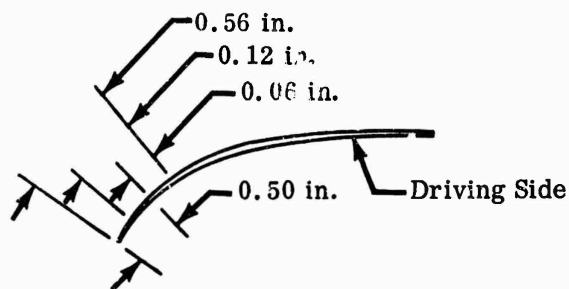
A. Blade No. 1.



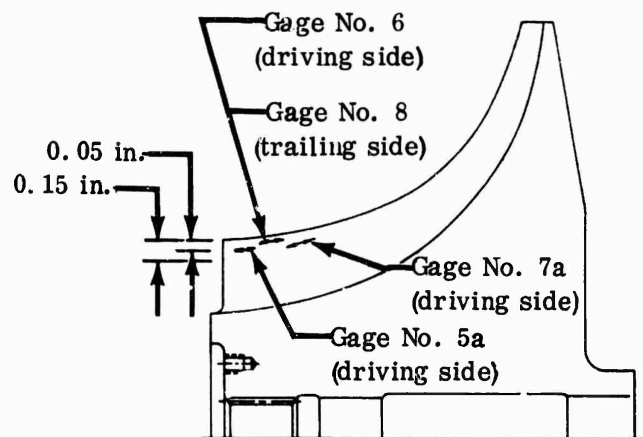
B. Blade No. 6.

No Scale

Figure 30. Bench-Test Strain-Gage Locations.



C. Blade No. 13.



D. Blade No. 13.
(alternate instrumentation)

from each gage and were not necessarily at points of maximum stress. The results of these preliminary tests are given in Figures 81 through 83.

2.2.2 COMPRESSOR-RIG TEST

The impeller was tested in a compressor test rig in which the turbodrives unit was independent of the impeller test section; thus, maximum flexibility was permitted in selecting airflow rate versus compressor pressure ratio throughout the operating range. The test setup and data sensors are shown in Figure 84.

A slip-ring connector assembly was fabricated, and the receptacle was designed to shrink-fit within the impeller hub face. The connector-assembly plug was mounted directly on the slip-ring flexible-drive shaft. Two threaded studs held the plug-receptacle assembly together — 16 female pins were installed on the impeller receptacle and 8 male pins on the slip-ring plug. The pin-pattern design enabled repositioning of the slip-ring connector (180 degrees with respect to the impeller) so that a different set of pins could be mated if desired. This design permitted installing twice the number of strain gages that could be handled by an 8-ring system and increased its utility.

The slip-ring assembly was cradled in an enclosed support duct at the diffuser-rig inlet. The duct was tapered to prevent airflow restrictions, and the core of the duct, which supports the slip ring, was held in place by 4 thin vanes. Two of the vanes carried cooling water and instrumentation leads to the slip-ring assembly.

The typical test procedure was as follows:

- 1) The rig was brought up to design speed with the flow valve in the full-flow position;
- 2) The magnetic tape recorder and oscillograph were started;
- 3) The flow valve was closed slowly until surge while the rotor speed was held constant;
- 4) Repeat 2) and 3) at 500 rpm decrements from the design speed of 50,000 rpm to 25,000 rpm.

Cycle duration was approximately 1 minute for each of the first 63 runs. The test was rerun at speeds offset from the first series by 250 rpm to collect additional data. This second test included runs in the 50,000 to 55,000 rpm range. The inlet guide vane setting was 0 degrees for all runs except at 35,000 and 50,000 rpm, where the guide vanes were varied from +40° to -20° with the impeller operating at the knee of the constant-speed line. Positive angle is defined as moving the vane trailing edge in the direction of rotor rotation.

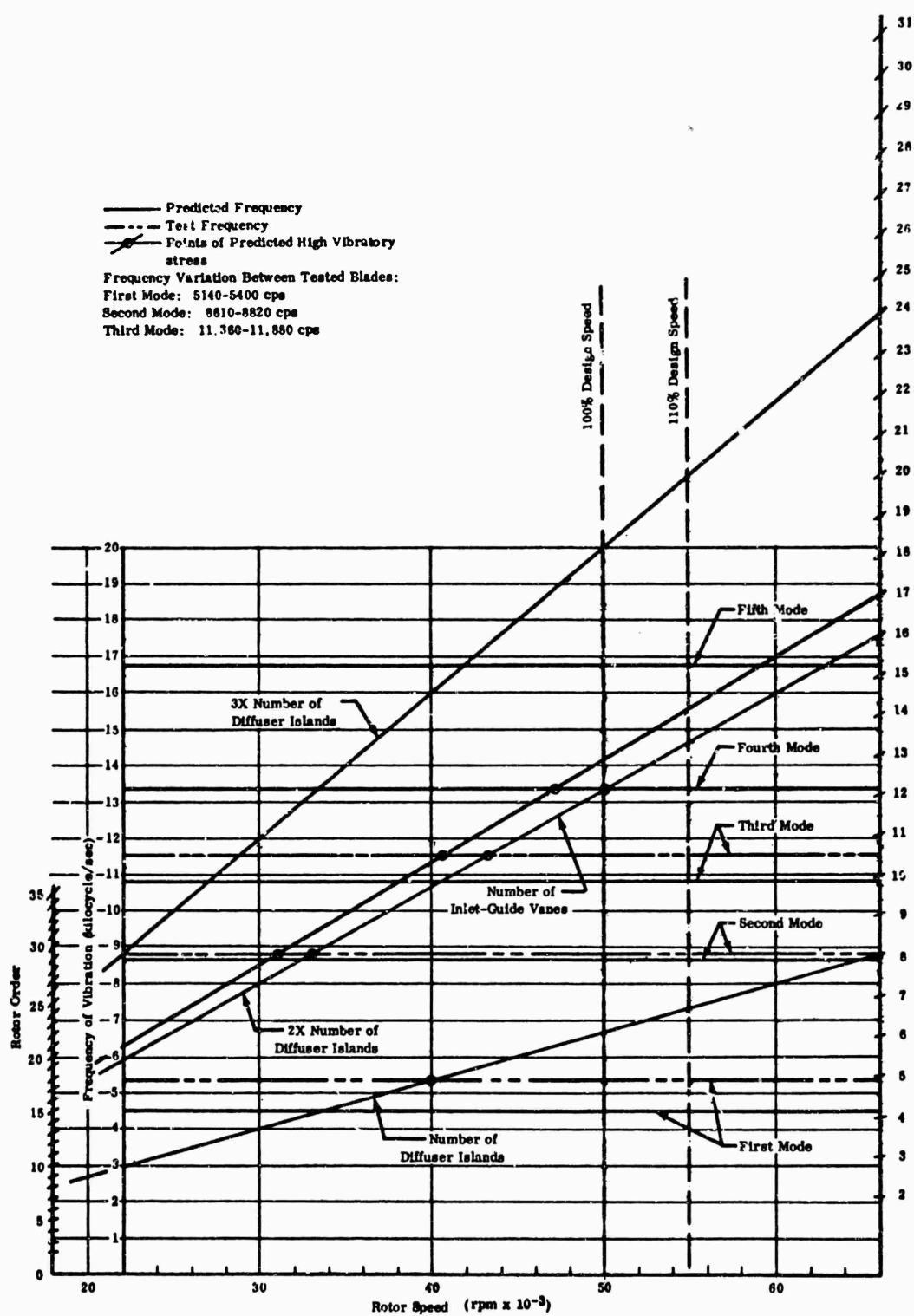


Figure 81. Campbell Diagram.

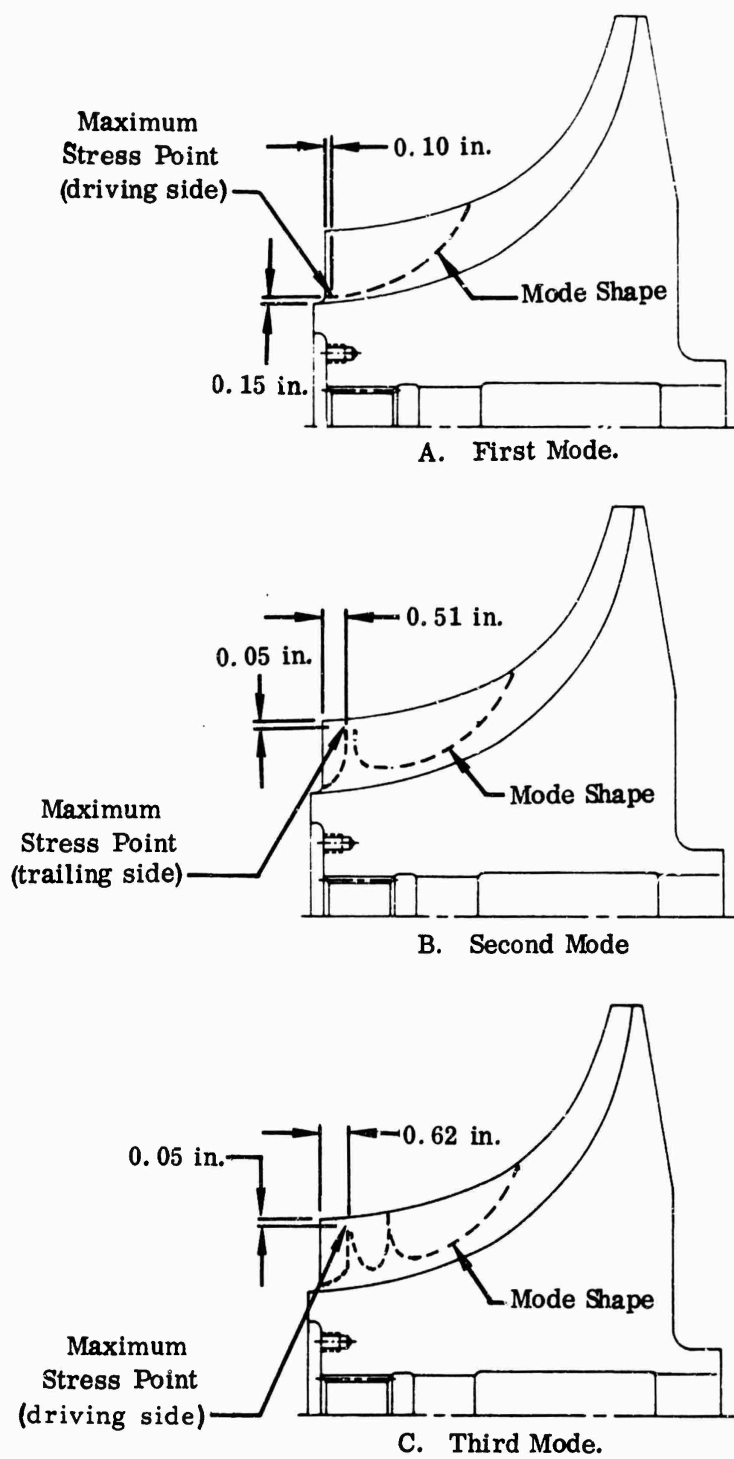


Figure 82. Maximum Vibratory-Stress Points.

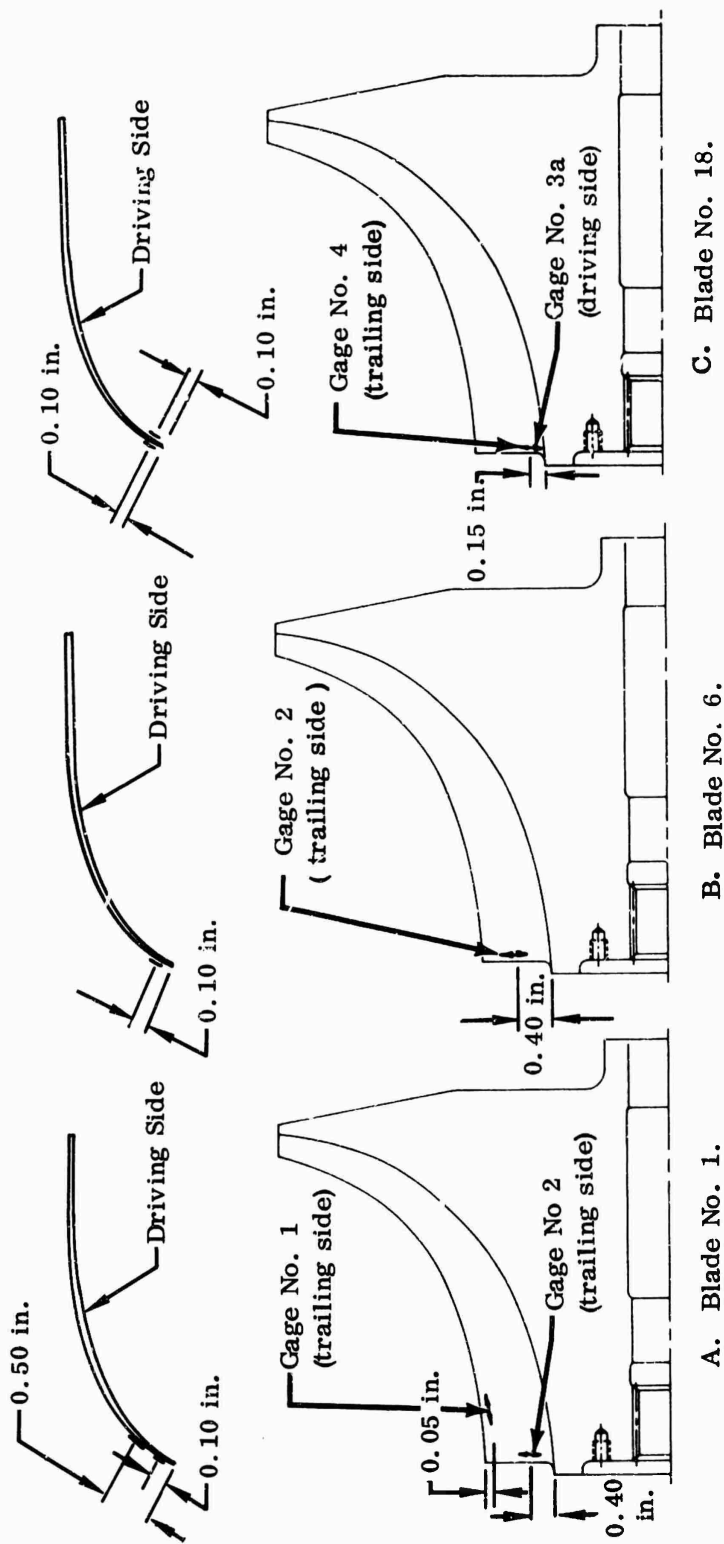


Figure 83. Rig-Test Strain-Gage Locations.

Symbols:

- P_S - Static Pressure Tap, Wall
- P_T - Total Pressure Probe, Fixed
- P_R - Total Pressure Rake
- T - Temperature Probe, Unshielded
- T_T - Total Temperature Probe (stagnation)
- T_{SH} - Temperature Probe, Shielded
- $P_{T\phi}$ - Total Pressure Probe, Directional

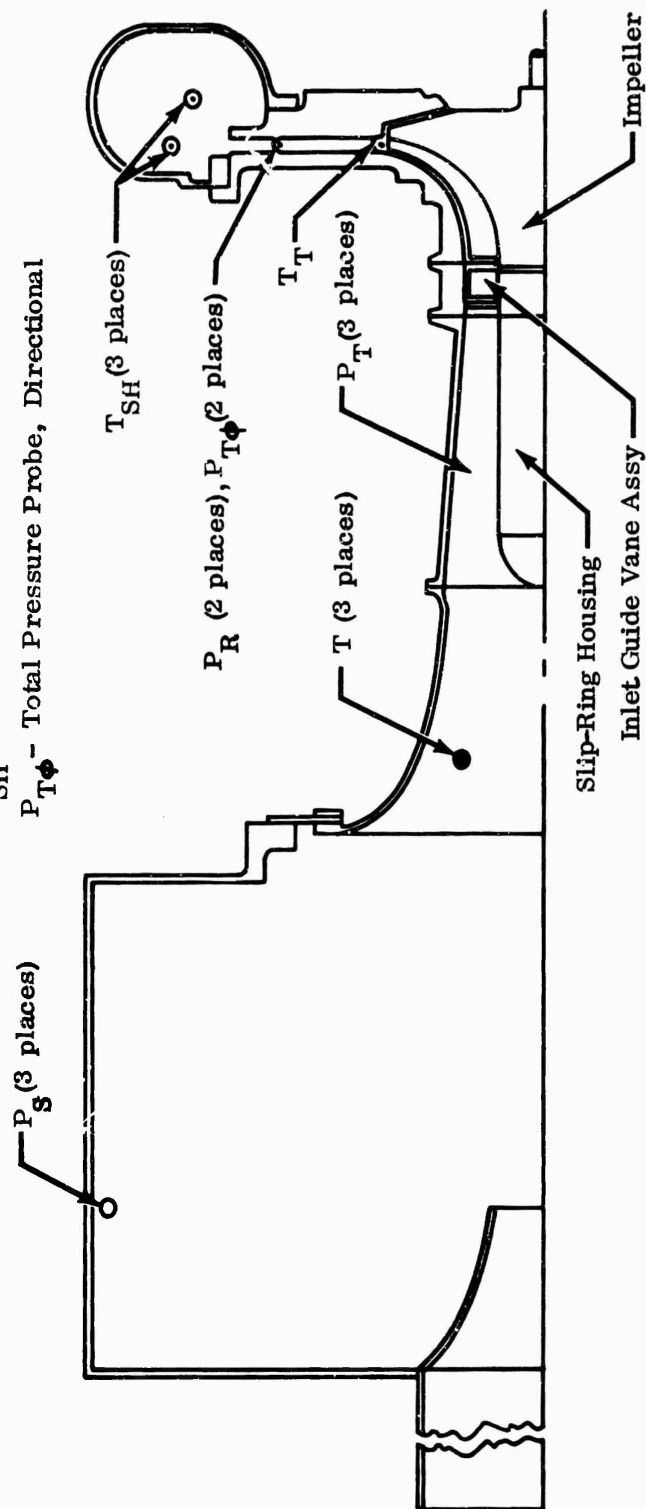


Figure 84. Test Equipment Instrumentation.

After the first 5 runs, 3 strain channels were found to be inoperative. The malfunctioning channels affected signals from gages 1a, 3, and 4. However, backup (and redundant) instrumentation was incorporated in the buildup as a safeguard against such an occurrence.

From run No. 6 and on, 5 strain signals and 1 rotor-speed signal were recorded on the magnetic tape. Simultaneously, signals were recorded for inlet-duct temperature, collector temperature, impeller-exit pressure, inlet pressure, flow-nozzle pressure, and rotor speed on the oscillograph. The magnetic-tape recording was synchronized with the oscillograph by picking up a prerecorded binary-coded time signal from the tape and by recording it simultaneously on the oscillograph. This technique allowed comparison of instantaneous aerodynamic data with strain data.

The strain recordings for the entire test were reproduced on an oscillograph with a low paper speed to produce a condensed version of the data so that resonances could be scanned easily. Each trace that showed a resonance was checked with the calibration values for that channel to determine if the indicated stress exceeded ± 4000 psi (vibratory stresses below ± 4000 psi were considered negligible). All resonance points with indicated vibratory stresses greater than ± 4000 psi were identified on the tape; with a speed reduction of 8:1, they were reproduced on the oscillograph at a paper speed of 100 inches per second. This method of expanding the data allowed frequency resolution of vibratory signals to over 30,000 cps.

Resonances to be studied were selectively chosen at a level of $\pm 7,300$ psi and were analyzed in detail for frequency, amplitude, and excitation orders, as shown in Figure 85.

Vibratory stresses at the surge point were considered separately from the vibratory stresses at steady-state conditions. The surge stresses were analyzed in the same manner as the steady-state vibratory stresses, but were plotted against rpm on a scale adjacent to the compressor map. This method for displaying the surge stresses allows simultaneous comparison with the surge line on the compressor map.

2.3 RESULTS

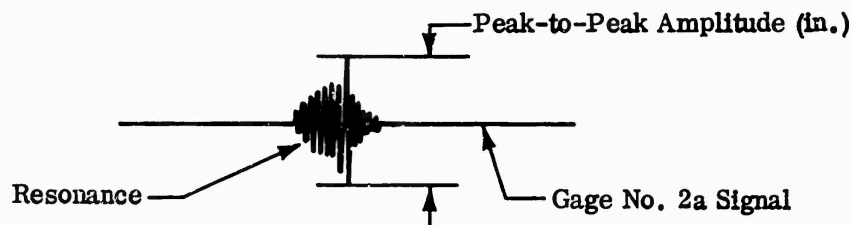
An example of a typical expanded oscillograph trace is shown in Figure 86. It shows run number, binary-location number, the numbers of the recorded strain-gage signals, and the rpm. In addition, any significant strain signal is marked with the indicated vibratory-stress level (i.e., the stress level measured from the trace without correction for system-frequency response or gage location), the frequency, and the rotor-speed order.

Sample

Calibration Factor for Gage No. 2a:
 $\pm 10,000$ psi/in. Peak-to-Peak Amplitude

Sample

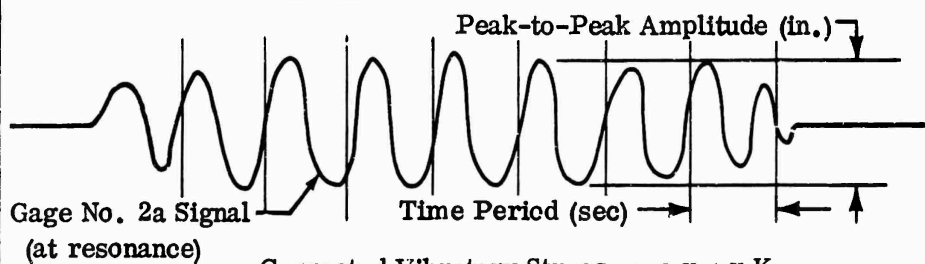
Frequency Response and Gage Location Correction for Gage No. 2a:
 $K = 2.0$ (for First Mode of Vibration)



$$\begin{aligned}\text{Indicated Vibratory Stress} &= a \times c \\ &= \pm a \times 10,000 \text{ psi;} \end{aligned}$$

where a = Peak-to-Peak Amplitude (in.)
 c = Gage No. 2a Calibration Factor (\pm psi/in.)

A. Condensed Oscillograph Trace.



$$\begin{aligned}\text{Corrected Vibratory Stress} &= a \times c \times K \\ &= \pm a \times 20,000 \text{ psi,} \end{aligned}$$

where a and c are as above
 $K = 2.0$

Frequency = n/t ; where n = Number of Oscillations Per Time Period (cycles)

t = Time Period (sec)

Order = $\frac{f}{N}$; where f = Frequency (cps)
 N = Rotor Speed (rps)

B. Expanded Oscillograph Trace.

Figure 85. Data Reduction Method.

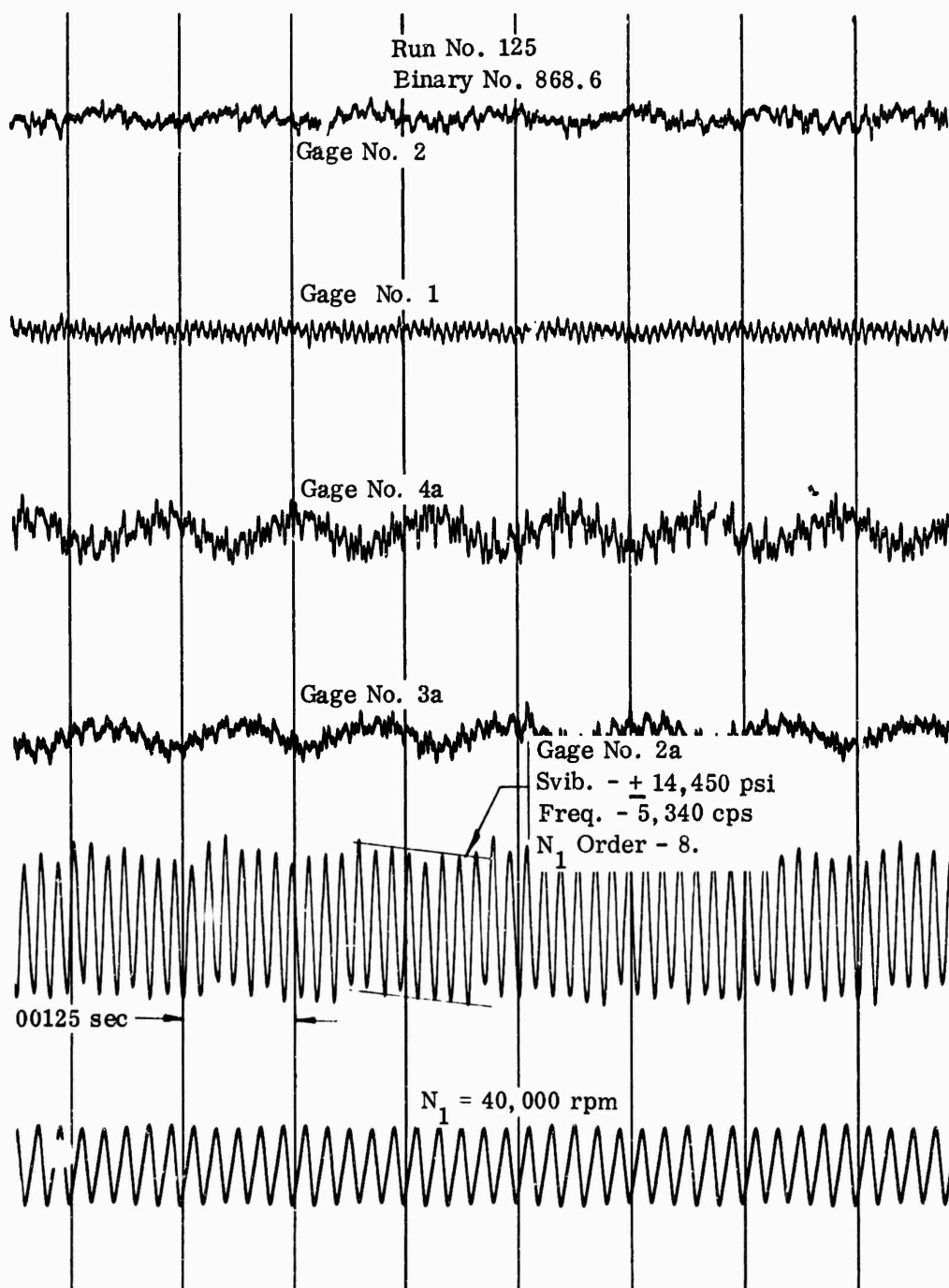


Figure 86. Expanded Oscillograph Trace.

The frequencies determined during the test varied slightly from the predicted frequencies, but the first mode showed the maximum deviation (18 percent high). The second mode showed the least deviation (2.3 percent high). The frequency spread of the tested blades was not more than ± 3 percent from the mean frequency for a given mode. This information is shown on the Campbell diagram in Figure 81.

All indicated vibratory stresses (outside of surge) in excess of ± 7300 psi appear on the Campbell diagram in corrected form in Figure 87. One point below this stress level is plotted (± 7000 psi resonance point at the 9th mode and the 34th order). The point is unique because of its unusually high frequency at the upper limit of the speed range. It should be noted that all major disturbances are related to the number of inlet guide vanes or diffuser islands.

Vibratory stresses occurring at surge are identified on the stress map in Figure 88 and correspond to the surge line shown in the adjacent compressor map. Those stresses occurring during a rapid approach to surge are marked as triangles on the stress map. Because the surge vibratory-stress levels through much of the speed range are above $\pm 20,000$ psi, consideration of temperature and centrifugal stress at a given speed was used to obtain the allowable vibratory-stress level from a Goodman diagram. Vibratory stress from the Goodman diagram was divided by 2 to obtain the allowable and was plotted on the stress map (shaded). Only 3 areas in the speed range exceeded the limit. One critical area (Area A) for steady-state operation is marked on the compressor map between 39,000 and 41,500 rpm. The maximum recorded stress in this range is marked for reference at the pressure ratio and weight flow where it occurred. Other highly stressed rpm ranges are between 49,200 and 50,100 rpm, and between 51,500 and 55,000 rpm. In these 2 ranges, all high stresses occur in surge (Figure 88).

At the test speeds of 35,000 and 50,000 rpm, no variation in stress level was observed when the inlet guide vane angles were changed.

3.0 CONCLUSIONS

The test was considered to have met all of its objectives. Natural frequencies and associated stress levels were determined during actual rig testing, and an operating map was prepared.

The actual and predicted frequencies did not coincide as close as had been shown in previous tests using aluminum impellers. However, this test was the first with titanium, and this new experience should form a basis for improved predictions. The reasons for the deviation were not explored beyond the scope of this test.

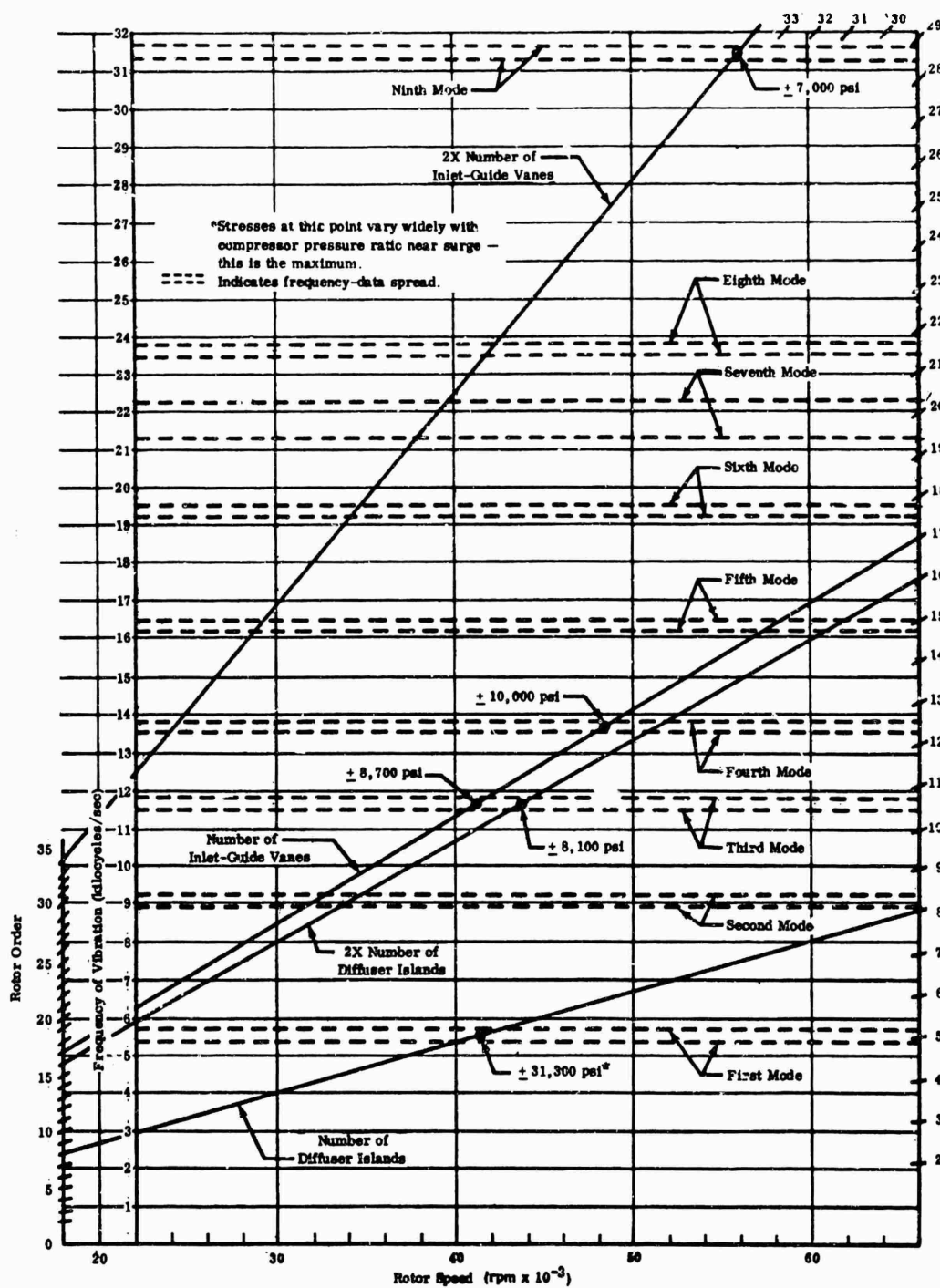


Figure 87. Campbell Diagram.

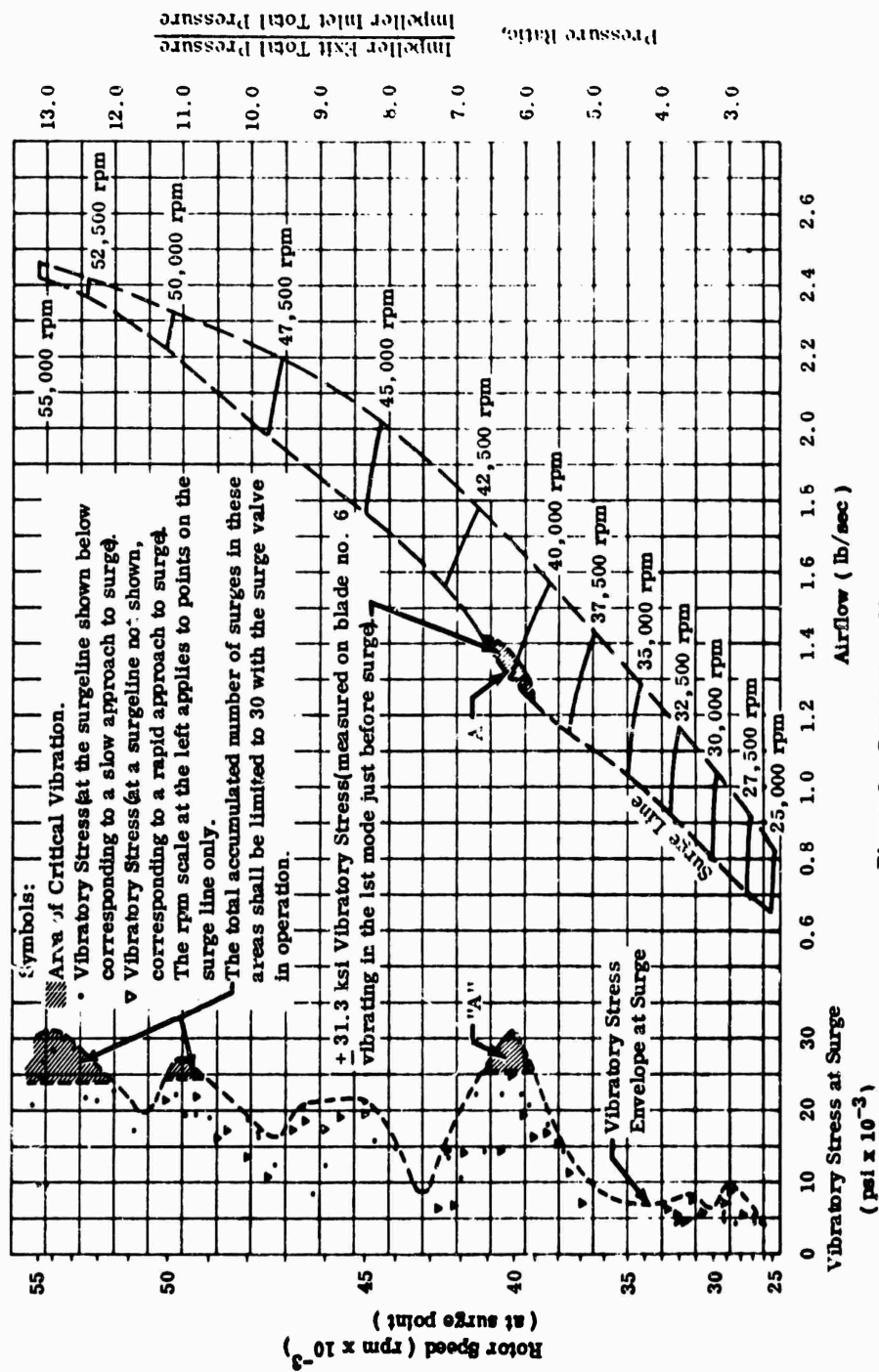


Figure 9. Compressor Map

Figure 88. Compressor Map.

The impeller should not be operated for prolonged periods near the surge region between 39,000 and 41,500 rpm. In the speed ranges of from 49,200 to 50,100 rpm and from 51,500 to 55,000 rpm, the total number of surges should be limited to 30 (surge is defined as one audible pop). The surge-relief valve should be in operation at all times. By limiting the number of surges, the total number of cycles at the high stress levels will not become excessive.

Because the inlet guide vane angle did not affect the stress level, guide vane use is not restricted.

(U) APPENDIX VII

WAKE INTERACTION EFFECTS AND PERFORMANCE CHARACTERISTICS
OF STAGNATION-TYPE THERMOCOUPLE

ABSTRACT

This appendix presents the results of a study sponsored by the contractor aimed at (1) Determining the wake interaction on the accuracy of the thermocouple measurements near the rim of a high-speed, separated-flow rotor; and (2) Estimating the performance characteristics of a stagnation-type thermocouple probe. The studies were based on temperature measurements taken during centrifugal-compressor research programs. The purpose was to resolve differences in temperature measured between the impeller tip and the collector. A complete mathematical treatment of effects on a typical probe is presented.

The work was conducted by Robert J. Moffat (Associate Professor of Mechanical Engineering, Stanford University) with assistance from Dr. Robert C. Dean (Creare, Incorporated, Hanover, New Hampshire).

SYMBOLS

- A = apparent overall recovery factor of the probe, including the effects of internal conduction but with no losses to the walls by conduction or by radiation
- A_i = area of the control volume at the impeller exit (in.^2 or ft^2)
- A_o = area of the control volume at the outer diameter (in.^2 or ft^2)
- C_p = coefficient of specific heat at constant pressure ($\text{Btu/lbm} - ^\circ\text{F}$)
- D = diameter (inches or feet)
- E = error introduced by heat transfer from thermocouple
- f_1 = the fraction of one blade period during which the probe is exposed to the jet-fluid portion of the blade spacing
- g_c = gravitational constant (32.17 ft/sec^2)
- h = heat-transfer coefficient ($\text{Btu/hr-ft}^2 - ^\circ\text{F}$)
- h_1 = average heat-transfer coefficient between jet fluid and thermocouple ($\text{Btu/lb-ft}^2 - ^\circ\text{F}$)
- h_2 = average heat-transfer coefficient between the wake fluid and thermocouple ($\text{Btu/lb-ft}^2 - ^\circ\text{F}$)
- J = mechanical equivalent of heat ($778 \text{ ft} - \text{lb/Btu}$)
- k = thermal conductivity ($\text{Btu/hr-ft}^2 - ^\circ\text{F/ft}$)
- L = characteristic length (feet or inches)
- N_{nu} = Nusselt number
- P_j = static pressure of the jet (psia)
- P_w = static pressure of the wake (psia)

SYMBOLS (Continued)

R	= radius (inches or feet)
Re	= Reynolds number
T	= temperature ($^{\circ}R$)
T_m	= average system temperature ($^{\circ}R$)
\overline{T}	= average temperature ($^{\circ}R$)
$\overline{T}_{f,p}$	= average temperature of fluid swept past the probe position ($^{\circ}R$)
\overline{T}_1	= average static temperature of the jet fluid ($^{\circ}R$)
\overline{T}_2	= average static temperature of the wake fluid ($^{\circ}R$)
V	= fluid velocity (fps)
α	= thermal diffusivity of the solid, $k/\rho C_p$ (ft^2/hr)
α_B	= recovery factor of the base, referenced to free stream
α_j	= recovery factor of the junction, referenced to local condition
α_s	= recovery factor of the shield, referenced to free stream
ϵ	= emmissivity
ϵ_s	= surface-temperature variation
ϵ_G	= gas-temperature variation
$\rho_1 V_1$	= average mass velocity of the jet fluid with respect to the stationary probe
$\rho_2 V_2$	= average mass velocity of the wake fluid with respect to the stationary probe
σ	= Stefan-Boltzmann constant (0.1713×10^{-8} Btu/hr-ft ² - $^{\circ}R^4$)
τ	= time (hour)

SYMBOLS (Continued)

τ_o = period of disturbance (hour)

Subscripts

a = adiabatic

abs = absolute component

B = base

c = heat transfer by convection

f = fluid

j = thermocouple junction

M = mean

o = stagnation conditions

P = junction-shield combination

r = heat transfer by radiation

rel = relative component

s = thermocouple shield

w = wall

1 = jet

2 = wake

∞ = free-stream conditions

1.0 SUMMARY, CONCLUSIONS, AND OUTLINE OF ANALYSIS

1.1 SUMMARY

Thermocouple probes placed near the rim of a compressor rotor operating in the jet-wake mode may be seriously in error with respect to the true bulk-fluid temperature of the fluid leaving the compressor. For a typical case, considered in this report, the error is between 45° and 60°F.

The error is caused by the fact that the wake fluid affects the thermocouple temperature, but not the temperature of the through-flow fluid, and it is assumed that the wake is more or less permanently attached to the rotor. Redesign of the probes can in no way affect this behavior.

If the wake fluid is hotter than the jet fluid, then the thermocouple will read high. The amount of the error will depend on the jet-wake width ratio, the jet-wake radial-velocity ratio, and the difference in temperatures of the jet and the wake.

Experimental results from compressor tests at Boeing support the trends deduced from this analysis.

1.2 RECOMMENDATIONS AND CONCLUSIONS

- 1) Thermocouple probes should not be installed close to the rim of the rotor.
- 2) Schlieren studies suggest that the flow is steady and well mixed at a radius ratio of 1.06 for typical cases, and thermocouples should be located no nearer than 1.06 radius ratio from the rim.
- 3) The error may be on the order of 50°F for typical cases, and cannot be reduced by modifying the probe geometry. The error may be calculated, although much of the input for this equation can only be estimated.

1.3 OUTLINE OF ANALYSIS

The steady-state recovery factor of the contractor's temperature probe is first calculated based on its geometry. The effects of the fluctuating-velocity field on this probe are then investigated, using conventional heat-transfer relationships. It is shown that the thermocouple assumes a quasi-steady state when the fluctuations are of compressor frequency. The relationship to gas temperature is then developed by using low-velocity heat-transfer relations. Introduction of the adiabatic wall temperature as the effective gas temperature for heat transfer in a

high-velocity environment allows the low-velocity results to be used directly and rigorously in the high-velocity case. The effect of the wake-fluid temperature on the thermocouple temperature is then determined, as is the effect of the wake-fluid temperature on the temperature of the fluid leaving the compressor. Comparison of the two reveals that the probe is always affected by the wake-fluid temperature, while the discharge-fluid temperature is only affected by the wake fluid when there is an appreciable radial velocity in the wake region. Thus the temperature sensed by the probe cannot reflect the temperature which is significant in evaluating the compressor performance.

2.0 STEADY-STATE PROBE BEHAVIOR

The behavior of the thermocouple probe must be understood under steady-flow conditions before the unsteady problem can be discussed reasonably.

The following represents an estimate of the performance of the probe (see Figure 89) based on its geometry and on the characteristics of its components: cylinders parallel to and perpendicular to the flow. The probe-analysis procedure is straightforward. Any uncertainty in the final result is the result of estimating (rather than calculating) the conduction relationships which govern the behavior. These links were estimated (based on approximate calculations of Reynolds numbers) and the data of Figure 9* were used.

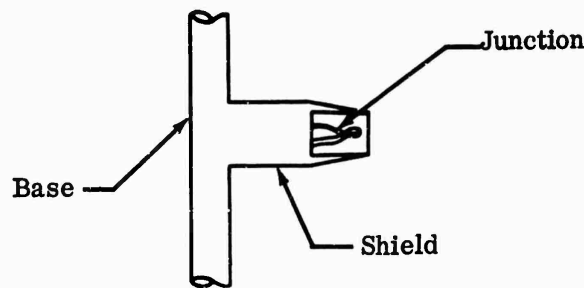


Figure 89. Sketch of Temperature Probe.

*R. J. Moffat, "Gas Temperature Measurement," Temperature, Its Measurement and Control in Science and Industry. Vol. 3, Part 2, 1962, p. 553.

The junction is 0.063/0.058 inch long, measured to the weld bead. It should be noted that the twisted-wire junction is not well suited to this type of probe design, since the effective thermocouple junction will be at the location of the first point of electrical contact and thus may be very close to the base of the apparent junction. Such an accidental junction would greatly increase the susceptibility to conduction errors and cause the probe to read lower than its design capabilities.

The wire diameter is not specified, but it is reasonable to suppose that it is between 0.010 and 0.013 inch, in keeping with general commercial practice in the 0.0625 swaged MgO thermocouple stock. The junction is between 4.6 and 6.3 wire diameters long (assuming no accidental junctions closer to the base than the weld bead).

The shield-bleed slots have a total area of 0.00151 square inch, and the shield-entrance area is 0.00247 square inch. At the entrance plane, then, the air velocity is approximately 0.6 times the free-stream velocity just ahead of the probe (behind the shock, if one exists).

The thermocouple junction is assumed to have a recovery factor of 0.86, similar to that of a tent-type or steeple junction. While twisted junctions may have slightly lower recovery factors, the assumption greatly simplifies the analysis.

The following notation will be used:

$T_{j,a}$	=	junction temperature with no conduction or radiation loss
T_s	=	shield temperature
T_o	=	gas-stream stagnation temperature
V	=	velocity at the junction location (inside the shield)
V_∞	=	velocity of the free-stream gas
α_j	=	recovery factor of the junction, referenced to local condition
α_s	=	recovery factor of the shield, referenced to free stream
α_B	=	recovery factor of the base, referenced to free stream
α_p	=	apparent recovery factor of the junction-shield combination; no conduction or radiation losses
A	=	apparent overall-recovery factor of the probe, including the effects of internal conduction, but with no losses to the walls by conduction or by radiation

The adiabatic junction temperature can be written as:

$$T_{j,a} = T_o - (1 - \alpha_j) \frac{V^2}{2g_c J C_p} \quad (181)$$

In terms of the apparent recovery factor of the junction-shield combination,

$$T_{j,a} = T_o - (1 - \alpha_P) \frac{V_\infty^2}{2g_c J C_p} \quad (182)$$

The relationship between the junction-recovery factor and that of the junction-shield combination is:

$$\alpha_P = 1 - (1 - \alpha_j) \left(\frac{V}{V_\infty} \right)^2 \quad (183)$$

The analysis has so far dealt only with adiabatic systems. The junction does, in fact, lose heat by conduction to the shield, and the shield loses heat, in turn, to the base. Even if the base were sufficiently long so that there was no heat transfer to the duct walls by conduction, the internal conduction problem would persist, and would link the junction temperature to that of the base. The base, being a cylinder in cross-flow, has a much lower recovery factor than the junction-shield combination, about 0.75 compared to 0.92. This internal-conduction link is one of the chief problems in the design of accurate probes.

Assuming no conduction to the walls, the base temperature is:

$$T_B = T_o - (1 - \alpha_B) \frac{V_\infty^2}{2g_c J C_p} \quad (184)$$

The shield, taken alone as a cylinder parallel to flow, has a recovery factor of about 0.85. The conduction link between the shield and base is estimated (Figure 9)* to be 0.25 for the purposes of illustrating the analysis. A more accurate calculation does not seem warranted for this study. The shield temperature is thus given by:

$$T_s \cong T_{s,a} - 0.25 (T_{s,a} - T_B) \quad (185)$$

The adiabatic shield temperature is:

$$T_{s,a} = T_o - (1 - \alpha_s) \frac{V_\infty^2}{2 g_c J C_p} \quad (186)$$

The base temperature, assuming no conduction to the walls, is:

$$T_B = T_o - (1 - \alpha_B) \frac{V_\infty^2}{2 g_c J C_p} \quad (187)$$

Combining these relationships yields:

$$T_s \cong T_o - (1 - \alpha_s) \frac{V_\infty^2}{2 g_c J C_p} - 0.25 (\alpha_s - \alpha_B) \frac{V_\infty^2}{2 g_c J C_p} \quad (188)$$

$$T_s \cong T_o - (1 - 0.75 \alpha_s - 0.25 \alpha_B) \frac{V_\infty^2}{2 g_c J C_p} \quad (189)$$

*(See footnote, page 272.)

The junction-recovery factor is quite near that of the shield, and will be taken to be exactly equal, for convenience. The adiabatic junction temperature can be written:

$$T_{j,a} = T_o - \left[(1 - \alpha_j) \left(\frac{V}{V_\infty} \right)^2 \right] \frac{V_\infty^2}{2 g_c J C_p} \quad (190)$$

The conduction link between the junction and the shield is estimated to be 0.20*, and is used to determine the actual junction temperature from the adiabatic junction temperature and that of the shield.

$$T_j \cong T_{j,a} - 0.2 (T_{j,a} - T_s) \quad (191)$$

$$T_j \cong T_o - \left\{ \left[1 - \alpha_j \right] \left(\frac{V}{V_\infty} \right)^2 \frac{V_\infty^2}{2 g_c J C_p} + 0.2 \left[\left([1 - 0.75 \alpha_s - 0.25 \alpha_B] - (1 - \alpha_j) \left(\frac{V}{V_\infty} \right)^2 \right) \frac{V_\infty^2}{2 g_c J C_p} \right] \right\} \quad (192)$$

$$T_j \cong T_o - \left\{ 0.8 (1 - \alpha_j) \left(\frac{V}{V_\infty} \right)^2 + 0.2 (1 - 0.75 \alpha_s - 0.25 \alpha_B) \right\} \frac{V_\infty^2}{2 g_c J C_p} \quad (193)$$

*(See footnote, page 272.)

Define an overall-probe factor, A , by the following equation:

$$T_j = T_o - (1 - A) \frac{V_\infty^2}{2 g_c J C_p} \quad (194)$$

The factor, A , can be evaluated from:

$$A = 1 - \left\{ 0.8 (1 - \alpha_j) \left(\frac{V}{V_\infty} \right)^2 + 0.2 (1 - 0.75 \alpha_s - 0.25 \alpha_B) \right\} \quad (195)$$

Substituting the values assumed for the present probe yields:

$$\begin{aligned} \alpha_B &= 0.75 \\ \alpha_s &= 0.85 \\ \alpha_j &= 0.85 \\ \frac{V}{V_\infty} &= 0.60 \\ \text{and } A &= 0.928 \end{aligned} \quad (196)$$

As the velocity of the gas in the main stream goes down, the conduction links between the shield and the base, and between the junction and the shield, become more important in determining the performance of the probe. This is the natural result of decreasing the convective-heat input at the surface while maintaining the same conduction path through the solid.

At approximately 30 percent of design flow the conduction links will have nearly doubled, and the value of the factor (A) is given by:

$$A = 1 - \left\{ 0.6 (1 - \alpha_j) \left(\frac{V}{V_\infty} \right)^2 + 0.4 (1 - 0.5 \alpha_s - 0.5 \alpha_B) \right\} = 0.88 \quad (197)$$

Note that the component-recovery factors of the assembly are not changed; only the conduction links are affected.

At extremely low flows, conduction will dominate, and if the base is large enough to act as a heat sink, the factor (A) will approach the recovery factor of the base:

$$A \longrightarrow 0.75 \qquad (198)$$

The variation in the overall-probe-recovery factor, A , is shown qualitatively on the sketch in Figure 90.

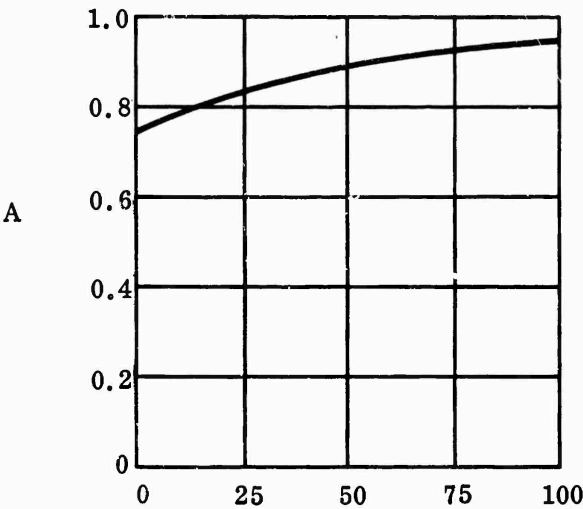


Figure 90. Variation in Overall Probe-Recovery Factor.

This probe performance map is predicated on zero heat transfer to the duct walls by conduction or radiation, and serves only to describe the recovery-factor aspects of the probe design.

The relationship between the probe indicated temperature (T_j) and true gas-stream stagnation temperature must also account for the effects of conduction and radiation to the walls.

The radiation effect can be estimated by using a linearized radiation-heat-transfer coefficient, defined by:

$$h_r \triangleq 4 \sigma \epsilon T_m^3 \quad (199)$$

where: σ = Stefan-Boltzmann constant, $0.1713 \times 10^{-8} \text{ Btu/hr-ft}^2\text{-}^\circ\text{R}^4$
 ϵ = emissivity (estimated at 0.75)
 T_m = average system temperature ($^\circ\text{R}$)

The radiation causes the shield temperature to go down. The junction then radiates and conducts to the shield, attaining a new stable temperature.

$$T_s - T_{s,a} = \frac{h_r}{h_c} (T_s - T_w) \quad (200)$$

If the errors are assumed to be small, then $(T_s - T_w) \cong (T_{s,c} - T_w)$ and the radiation problem can be written:

$$\frac{T_s - T_{s,a}}{T_{s,a} - T_w} = \frac{h_r}{h_c} \quad (201)$$

The heat-transfer coefficient, h_c , can be evaluated from the Reynolds number, based on shield diameter ($Re = 50,000$) (using Figure 3 of the reference by extrapolation).* The value of the Nusselt number is found to be $\cong 130$. The values of h_r and h_c are then (for $T_m = 1200^\circ\text{R}$):

$$h_r = 4 \sigma \epsilon T_m^3 = 7.34$$

$$h_c = \frac{N_{nu} (kf)}{D} = 748$$

*(See footnote, page 272.)

The radiation of the shield is then:

$$\frac{T_s - T_{s,a}}{T_{s,a} - T_w} \approx 0.01 \quad (202)$$

For each 100°F difference between the wall temperature and the adiabatic shield temperature, the shield temperature will drop about 1°F.

The junction is linked to the shield, both by radiation and by conduction. Conduction is by far the stronger link, estimated to be 0.25 for the present problem. The junction temperature will drop 0.25° for each 100°F wall-temperature depression.

The wall conduction effect is also related to the difference between the shield temperature and the wall temperature. Assuming a passage 5 inch wide, with the probe centered, the shield can be approximated by a fin having an effective immersion of 4 diameters (2 diameters in the base and 2 diameters in the shield itself). Using the previously determined value of h_c in the conduction-error equation (Equation 3 of the reference*) yields:

$$\frac{T_s - T_{s,a}}{T_{s,a} - T_w} = \frac{1}{\cosh \left\{ \frac{L}{D} \sqrt{\frac{4 h_c}{k_s}} D \right\}} = 0.01 \quad (203)$$

The effects of conduction and radiation are of approximately equal importance, each resulting in about 0.25°F drop in probe indicated temperature per 100°F wall-temperature depression.

As the free-stream airflow goes down, the conduction and radiation errors will increase.

*(See footnote, page 272.)

The probe performance is summarized as:

$$\begin{array}{rcl}
 A & = & 0.928 \\
 \frac{E_r + E_c}{\Delta T_w} & = & 0.50/100
 \end{array}
 \left. \vphantom{\begin{array}{rcl} A & = & 0.928 \\ \frac{E_r + E_c}{\Delta T_w} & = & 0.50/100 \end{array}} \right\} \text{Design Point}$$

$$\begin{array}{rcl}
 A & = & 0.88 \\
 \frac{E_r + E_c}{\Delta T_w} & = & 1.00/100
 \end{array}
 \left. \vphantom{\begin{array}{rcl} A & = & 0.88 \\ \frac{E_r + E_c}{\Delta T_w} & = & 1.00/100 \end{array}} \right\} \text{30-Percent Flow}$$

2.1 CONCLUSIONS

The performance of the adiabatic probe can be described in terms of a single probe-performance factor, A , which serves to define the adiabatic junction temperature of the probe. This value will be used in the high-velocity heat-transfer analysis in Section 3.0 of this appendix.

The probe, at design-flow conditions, is essentially adiabatic, having losses of less than $0.5^\circ/100^\circ\text{F}$. The treatment of the probe as an adiabatic body is justified.

2.2 RECOMMENDATIONS

The performance of the probe would be considerably improved if the junction were made longer, up to 10-15 wire diameters, and if it were of the tent or steeple type, instead of the present twisted junction. The shield, of course, should also be extended in length. Bleed holes drilled in the shield at the base of the junction (area ratio set for $V/V_\infty = 0.5$) would then be recommended in place of the milled bleed slots.

3.0 EQUILIBRIUM TEMPERATURE OF AN ISOLATED PROBE IN A HIGH-FREQUENCY INTERMITTENT FLOW

It will first be shown that the frequencies encountered in testing of radial-flow compressors are sufficiently high that only negligible fluctuating components are induced in the thermocouple temperature. The quasi-steady thermocouple-equilibrium temperature will then be determined as a function of the jet-wake area, velocity, and temperature ratios using incompressible-flow heat-transfer relationships. The solution to the heat-transfer problem is then expressed for compressible-flow conditions by substitution of stagnation temperature for static temperature in each of the heat-transfer-rate equations.

3.1 THE EFFECT OF HIGH-FREQUENCY/FLUCTUATIONS

When a solid body is immersed in a fluid whose temperature is cyclically varying with time, the surface temperature of the solid varies cyclically also, and at the same frequency as the disturbances in the fluid temperature. The amplitude of the surface-temperature disturbance is less than that of the fluid temperature, as a result of the resistance to heat transfer in the boundary layer between the fluid and the surface. This reduction is calculable by the following:

Let the fluid temperature oscillate about its average temperature according to:

$$T_f = \bar{T}_f + \epsilon_G \cos \left(\frac{2 \pi \tau}{\tau_0} \right) \quad (204)$$

A nonsinusoidal variation can be resolved, by a Fourier analysis, into a sum of sinusoidal terms (each term follows the above description).

Then the surface temperature oscillates about the same mean temperature with an amplitude less than that of the fluid temperature. The ratio given by Eckert and Drake* is:

*E. R. G. Eckert and R. M. Drake, Heat and Mass Transfer, McGraw-Hill Book Co., New York, 1959, pp. 103-107.

$$\frac{\epsilon_s}{\epsilon_G} = \frac{1}{\left(1 + 2 \sqrt{\frac{\pi k^2}{\alpha \tau_0 h^2}} + 2 \frac{\pi k^2}{\alpha \tau_0 h}\right)^{1/2}} \quad (205)$$

where:

- k = thermal conductivity of the solid, Btu/hr-ft²-°F/ft
- τ_0 = period of the disturbance (hour)
- α = thermal diffusivity of the solid, k/ρ c
- h = heat-transfer coefficient (Btu/hr-ft²-°F)

Taking typical properties for thermocouple materials,

- k = 16 Btu/hr-ft²-°F/ft
- α = 0.50 ft²/hr
- h = 1160 Btu/hr-ft²-°F (using velocity inside probe as 400 fps and wire diameter as 0.012 inch)*

Considering a 15-blade rotor at 20,000 rpm,

$$\tau_0 = 5.5 \times 10^{-8} \text{ hr}$$

The amplitude ratio is thus found to be:

$$\frac{\epsilon_s}{\epsilon_G} = 0.0048$$

Estimates of the jet-wake temperature differences (from the contractor's compressor-test data, see Table II) indicate that it can be equal to or less than 66°F for a typical installation. The surface-temperature variation is thus seen to be:

$$\epsilon_s = 0.88^\circ\text{F}$$

*(See footnote, page 282.)

The thermocouple may be assumed to produce an output based on the average temperature of its cross section (radial nonuniformity in temperature will cause radially flowing electrical currents), which will further reduce the amplitude, since the fluctuation observed at the surface will be attenuated more and more at increasing depths beneath the surface. This attenuation can also be calculated, by methods given in the reference.* Using the values listed above shows that the disturbance would be reduced to less than 1 percent of its surface value at the centerline of a wire size of 0.012 inch in diameter. The decline is more rapid than a linear variation with radius.

TABLE II	
COMPRESSOR DATA FOR THE GENERAL TEST CASE OF THE WORKHORSE IMPELLER SUPPLIED BY THE CONTRACTOR	
<u>Jet</u>	<u>Wake</u>
$P_j = P_w$	$P_w = P_j$
$T_j = 777^{\circ}\text{R (static)}$	$T_w = 850^{\circ}\text{R (static)}$
$T_{j\text{rel}} = 850^{\circ}\text{R (total)}$	$T_{w\text{rel}} = 850^{\circ}\text{R (total, assume } V_R = 0)$
$T_{j\text{abs}} = 1127^{\circ}\text{R (total)}$	$T_{w\text{abs}} = 1175^{\circ}\text{R (total)}$
$V_{j\text{abs}} = 2050 \text{ fps}$	$V_{w\text{abs}} = 2000 \text{ fps}$
$V_{j\text{rel}} = 931 \text{ fps}$	$V_{w\text{rel}} = 0$
Discharge angle, rel.= 10 degrees	Discharge angle, rel.= 0 degrees

As an approximation, the average temperature across the section might be taken to be constant to within 0.4°F. This 0.4°F fluctuation would be evidenced by an A. C. component of the thermocouple output, at a frequency of 5000 cps. Most thermocouple-recording systems would not be capable of interpreting this component.

*(See footnote, page 282.)

The thermocouple will be considered to indicate a quasi-steady temperature equal to the mean temperature under the above conditions; i.e., constant h and equal duration of the positive and negative half-cycles of the temperature fluctuation.

A problem arises when conditions are such that the values of h are not the same on the positive and negative half-cycles. The problem is then one of determining the relationship between the mean temperature of the thermocouple and the mean temperature of the fluid. It is apparent that the heat-transfer coefficient acts as a weight factor in determining the mean temperature of the thermocouples. This effect can cause the thermocouple to establish a mean temperature, which is different from the time averaged fluid temperature.

In the specific case considered in this report, another problem arises; i.e., that of defining the mean temperature of the fluid. When a thermocouple is installed very close to the tip of a rotor operating in the jet-wake mode, the thermocouple is alternately exposed to jet fluid and to wake fluid, and it assumes an average temperature based on these two components. However, if the wake fluid does not leave the rotor, but is simply carried around with it, then that fluid is not part of the through-flow fluid of the compressor, and its temperature should not be permitted to affect the temperature of the thermocouple. This problem will be treated in more detail in Section 4.0.

3.2 THE LOW-VELOCITY HEAT-TRANSFER PROBLEM — ENERGY-BALANCE RELATIONS

- $\overline{T}_{f,p}$ = average temperature of fluid swept past the probe position
- T_j = temperature of thermocouple junction (indicated temperature)
- \overline{T}_1 = average static temperature of the jet fluid
- \overline{h}_1 = average heat-transfer coefficient between jet fluid and thermocouple
- \overline{T}_2 = average static temperature of wake fluid
- \overline{h}_2 = average heat-transfer coefficient between the wake fluid and the thermocouple
- $\rho_1 V_1$ = average mass velocity of the jet fluid with respect to the stationary probe

$\rho_2 V_2$ = average mass velocity of the wake fluid with respect to the stationary probe

f_1 = the fraction of one blade period during which the probe is exposed to the jet-fluid portion of the blade spacing

Applying an energy balance to the isolated probe over the duration of one cycle of the gas flow (assuming no heat transfer by conduction or by radiation) yields:

$$\bar{h}_1 (\bar{T}_1 - T_j) f_1 = \bar{h}_2 (T_j - \bar{T}_2) (1 - f_1) \quad (206)$$

Solving for T_j yields:

$$T_j = \frac{\bar{T}_1 + \frac{\bar{h}_2}{\bar{h}_1} \left(\frac{1 - f_1}{f_1} \right) \bar{T}_2}{1 + \frac{\bar{h}_2}{\bar{h}_1} \left(\frac{1 - f_1}{f_1} \right)} \quad (207)$$

An expression describing the average temperature of the fluid passing the stationary probe will now be presented, in terms of the absolute velocities of the jet and wake regions:

$$\bar{T}_{f,p} = \frac{\rho_1 \bar{V}_1 f_1 C_p \bar{T}_1 + \rho_2 \bar{V}_2 (1 - f_1) C_p \bar{T}_2}{C_p [\rho_1 \bar{V}_1 f_1 + \rho_2 \bar{V}_2 (1 - f_1)]} \quad (208)$$

Based on data from Table II for a typical case, the absolute velocity of the jet fluid might be taken as 2050 fps, while that of the wake, having no slip relative to the rotor (but also no radial component), might at the same time be on the order of 2000 fps. Estimating the temperatures of the jet and wake, considering the wake to exchange heat with the rotor and equilibrate at jet-relative-stagnation temperature (rotor recovery factor of unity), indicates that the wake would

probably be hotter than the jet. Estimates from the table were, specifically, T_j (static) = 777°R and T_w (static) = 845°R. Under the assumption, then, of uniform static pressure around the periphery of the rotor, the jet-wake mass-velocity ratio (based on absolute velocity) is unity, within 11 percent:

$$\frac{\rho_1 V_1}{\rho_2 V_2} = \frac{2050 \times 845}{2000 \times 777} = 1.112$$

Thus the average temperature of the fluid swept past the stationary probe can be approximated by:

$$\bar{T}_{f,p} = f_1 \bar{T}_1 + (1 - f_1) \bar{T}_2 \quad (209)$$

The relationship of the probe temperature to the mean fluid temperature at the probe position is given by:

$$T_j - \bar{T}_{f,p} = \left(\frac{1}{1 + \frac{\bar{h}_2}{\bar{h}_1} \left(\frac{1-f_1}{f_1} \right)} - f_1 \right) \bar{T}_1 + \left\{ \frac{\frac{\bar{h}_2}{\bar{h}_1} \left(\frac{1-f_1}{f_1} \right)}{1 + \frac{\bar{h}_2}{\bar{h}_1} \left(\frac{1-f_1}{f_1} \right)} - (1-f_1) \right\} \bar{T}_2 \quad (210)$$

Some special cases can be examined to illustrate the behavior described by the above equation:

- 1) When $\bar{h}_1 = \bar{h}_2$, $T_j = \bar{T}_{f,p}$ for all values of f_1 ;
- 2) When $f_1 = 0.5$, the probe temperature will be unbalanced toward that of the jet fluid when \bar{h}_1 exceeds \bar{h}_2 and toward the wake temperature when \bar{h}_2 exceeds \bar{h}_1 .

Examination of the special case (2) shows clearly that the heat-transfer coefficient acts as a weight factor by which the thermocouple determines its equilibrium temperature in terms of the jet and wake temperatures. The true mass-flow-averaged temperature of the gas stream is determined by using the individual

mass velocities as weight factors; in the present case, these are equal. When the heat-transfer coefficients are not in the same ratio as the mass velocities, the thermocouple cannot make a true-average interpretation of the gas temperature. In the most general case (unequal mass velocities in the two streams) the heat-transfer coefficients will not be equal. The heat-transfer coefficients vary, in general, either with the square root of the mass velocity (laminar heat transfer) or with the fifth root (turbulent heat transfer). It can also be seen from Equation 210 that the jet-wake fraction is of importance in determining the measurement error $(T_j - \bar{T}_{f,p})$ whenever the heat-transfer coefficients are not equal.

It is also important to recognize that the average temperature of the fluid swept past the probe may not be the proper temperature to use in evaluating compressor performance. In the simplest model of the jet-wake mode of operation, the wake can be thought of as a rigid body rotating with the rotor. If the probe is mounted close to the rotor, it will be affected by the wake-fluid temperature as the wakes are swept by the probe. The wake fluid, however, does not leave the rotor, under this simplest model, and its temperature should not be allowed to affect the reading of the probe. It would be more pertinent, under this simple model, to compare the thermocouple temperature to the temperature of the jet fluid alone, since that is the fluid which actually leaves the rotor. This comparison is given by the following relationship:

$$T_j - \bar{T}_1 = - \frac{\frac{\bar{h}_2}{\bar{h}_1} \left(\frac{1 - f_1}{f_1} \right)}{1 + \frac{\bar{h}_2}{\bar{h}_1} \left(\frac{1 - f_1}{f_1} \right)} (\bar{T}_1 - \bar{T}_2) \quad (211)$$

Note that the thermocouple cannot correctly indicate jet-fluid temperature unless the heat transfer to the wake is zero.

When the heat-transfer coefficients are equal, Equation 211 reduces to:

$$\bar{T}_j - \bar{T}_1 = - (1 - f_1) (\bar{T}_1 - \bar{T}_2) \quad (212)$$

3.3 ESTIMATE OF THE JET- AND WAKE-FLOW CONDITIONS AFFECTING THE TEMPERATURE-MEASURING PROBLEM

It must be borne in mind, in considering the values of Table II, that they are estimates based on plausible models of the fluid-rotor interaction. They do not have the certainty of experimental data, but serve only to provide estimators of the problems discussed in this report. Nor is it felt worthwhile to conduct experiments solely for the purpose of improving these estimates unless there is a considerable amount of data already gathered which might be reinterpreted based on this analysis. Wake-temperature profiles could be measured by instrumenting a special rotor, as could the jet-wake width ratio, but the experiments would be time-consuming and costly.

As will later be brought out, a more effective way of avoiding the errors described in this report is simply to relocate the thermocouples so they are no longer affected by the wake region.

3.4 THE EFFECT OF VELOCITY FLUCTUATIONS ON THE HEAT-TRANSFER COEFFICIENT

The heat-transfer coefficient is not sensitive to velocity alone, but is also sensitive to the mass velocity, ρV , as it occurs in the Reynolds number of the probe-flow situation. From the estimates provided, it can be seen that while the velocities and densities of the jet and wake are not respectively equal, it is true that the mass velocities are equal to within 11 percent. This point was previously demonstrated. Thus the Reynolds numbers of the 2 flow regimes are equal within 1 order of magnitude. Steady-state heat-transfer literature and experiments both suggest that this is a sufficient condition for the heat-transfer coefficients to be substantially equal (h varying either with the square root or the fifth root of the Reynolds number). On the assumption that pulsating flows at steady Reynolds numbers yield the same results as steady flows, then the heat-transfer coefficients in the 2 flow regimes would remain the same within 1.25 percent.

Since probe-to-probe variations in heat-transfer coefficient may be on the order of 5 percent, and since experiments indicate an uncertainty of 5-10 percent in repeating heat-transfer data under supposedly identical, steady-state conditions, it does not appear warranted to try to account for variations on the order of 1.25 percent.

3.5 THE EFFECT OF FLUCTUATIONS IN THE ANGLE OF INCIDENCE OF THE STREAM

The angle of incidence of the air stream on the probe will fluctuate ± 12.5 degrees about the mean, as the jet and wake regions pass the probe.

A probe of the type under consideration will typically have a yaw plateau of ± 15 degrees for a 1-percent drop-off in recovery factor, or a 2-percent drop-off in heat-transfer coefficient.

Comparing the above figures indicates that there should be no significant effects due to the fluctuating angle of incidence, providing that the probe is aligned with the mean-incidence angle.

3.6 THE HIGH-VELOCITY HEAT-TRANSFER PROBLEM

High- and low-velocity heat transfer differ chiefly due to the shear-work dissipation in the boundary layer. This causes even an adiabatic wall to achieve a temperature different than the gas-stream temperature. In fluids whose Prandtl number is unity, the adiabatic wall temperature is equal to the stagnation temperature of the free-stream fluid. For air ($Pr = 0.68$), the adiabatic wall temperature is usually referred to by means of the recovery factor, referenced to the stagnation state of the free stream. It is this phenomenon of boundary-layer-shear work which is responsible for the recovery factors of 0.86 and 0.75 used in Section 1.0 of this appendix for cylinders parallel and perpendicular to the flow.

It is apparent that the temperature potential for heat transfer in a high-velocity flow should be based on the difference between the actual wall temperature and the adiabatic wall temperature.

In many respects it is more useful to think of the adiabatic wall temperature as the effective gas temperature. This is the temperature which an adiabatic system will reach when immersed in the stream. It must be borne in mind, however, that this effective gas temperature is not a property of the gas stream only, but of the system of a particular body immersed in the stream (recall that cylinders parallel and perpendicular to the stream see different effective gas temperatures even though they are in the same stream).

With the substitution of the effective gas temperature for the actual gas temperature, the high-velocity heat-transfer problem can be handled by the low-velocity results; the same Reynolds number dependent relationships which determined the heat-transfer coefficient for the low-velocity, high-density problem can be used.

To convert the low-velocity results of Section 2.1 to high-velocity information it is only necessary to make the following substitutions for T_1 and T_2 :

$$T_1 = T_{o,1} - (1 - A) \frac{V_1^2}{2g_c J C_p} \quad (213)$$

$$T_2 = T_{o,2} - (1 - A) \frac{V_2^2}{2g_c J C_p} \quad (214)$$

$T_{o,1}$ is the stagnation temperature of the jet flow; $T_{o,2}$ is the stagnation temperature of the wake flow; and A is the overall probe recovery factor described in Section 2.

Thus Equation 210 becomes:

$$T_j = \left(T_{f,o} - [1-A] \frac{V^2}{2g_c J C_p} \right) \left\{ \frac{1}{1 + \frac{h_2}{h_1} \left(\frac{1-f_1}{f_1} \right)} - f_1 \right\} \left\{ T_{o,1} - [1-A] \frac{V_{\infty,1}^2}{2g_c J C_p} \right\} + \left[- \frac{\frac{h_2}{h_1} \left(\frac{1-f_1}{f_1} \right)}{1 + \frac{h_2}{h_1} \left(\frac{1-f_1}{f_1} \right)} - [1-f_1] \right] \left(T_{o,2} - [1-A] \frac{V_{\infty,2}^2}{2g_c J C_p} \right) \quad (215)$$

and Equation 211 becomes:

$$T_j - \left(T_{1,o} - [1-A] \frac{V_1^2}{2g_c J C_p} \right) = \left\{ - \frac{\frac{h_2}{h_1} \left(\frac{1-f_1}{f_1} \right)}{1 + \frac{h_2}{h_1} \left(\frac{1-f_1}{f_1} \right)} \right\} \left\{ \left(T_{o,1} - [1-A] \frac{V_1^2}{2g_c J C_p} \right) - \left(T_{o,2} - [1-A] \frac{V_2^2}{2g_c J C_p} \right) \right\} \quad (216)$$

3.7 SIMPLIFICATIONS BASED ON $h_1 = h_2$ AND $\rho_1 V_1 = \rho_2 V_2$

Sections 3.3 and 3.4 produced the information that the above assumptions are reasonable (probably within 1 or 2 percent). Thus, Equations 210 and 212 can be used.

Equation 210 (comparison of T_j with average fluid temperature, $h_1 = h_2$):

$$T_j = T_{f,o} - (1 - A) \frac{V^2}{2g_c J C_p} \quad (217)$$

Equation 212 (comparison of T_j with jet-fluid temperature, $h_1 = h_2$):

$$T_j - \left(T_{o,1} - [1 - A] \frac{V_1^2}{2g_c J C_p} \right) = - (1 - f_1) (T_{o,1} - T_{o,2}) \quad (218)$$

4.0 THE EFFECT OF WAKE-FLUID ENTRAINMENT AND PROBE POSITION

The mass-flow-averaged total temperature is defined as that which should be used in determining the efficiency of the compressor. The first question which might be asked is: Where should the thermocouple be placed so as to measure this

temperature? The answer is, obviously, that it should be far enough away from the rotor so that the fluid has been well mixed and has established a uniform temperature. R. C. Dean, commenting on the draft of this appendix, says:

"The mixing outside the impeller apparently takes place in a very small distance; i.e., a radius ratio around 1.05..... In experimental work the total-temperature probe may be placed very close to the tip of the impeller so that in estimating errors, it would probably be best to assume that it is at the tip, before mixing occurs. High-speed schlieren movies have shown no significant unsteadiness of the flow at the leading edge of the vaned diffusers which lie in a radius ratio of 1.06. One obvious means for avoiding these temperature errors due to fluctuating flow would be to place the probe at radius ratios greater than 1.05....."

The second question which might be asked is: Can the thermodynamically significant temperature be measured by a probe close to the rotor? To answer this, one must propose a model of the flow near the rotor.

Consider the simplest model, where the wake fluid forms a rigid, radially extending node of fluid (at rest with respect to the rotor). When the probe is close to the rotor, it is swept by these nodes as they rotate, and the thermocouple seeks some temperature between that of the jet fluid and that of the wake fluid. If the heat-transfer coefficients in the 2 regions are equal, and it has been shown that they are for practical purposes, the thermocouple will read the average temperature of the jet and wake fluids. Is this the thermodynamically significant temperature? No, because the wake fluid does not leave the rotor under this simplest model (only the jet fluid leaves the rotor); therefore, the thermodynamically significant temperature is the temperature of the fluid leaving the rotor (the jet fluid only). The relationship between the thermocouple temperature and the jet-fluid temperature is given by Equations 211 or 212.

It seems apparent that the wake-fluid region cannot be exactly at rest with respect to the rotor. When the wake fluid has a radial-velocity component, some of the wake fluid will be mixed with the jet fluid in determining the thermodynamically significant temperature. An energy balance, performed on an annular-control volume around the rotor, can be used to describe the mixed-mean temperature of the discharge fluid in terms of the entering flows of jet and wake fluids and to describe their individual temperatures.

The thermocouple temperature will be relatively unaffected by small changes in the radial-velocity component of the wake region; whether or not the wake fluid leaves the compressor, it is still swept past the thermocouple and affects the temperature of the thermocouple.

The probe temperature, close to the rotor, is given by Equation 207. In high velocity form,

$$T_j = \frac{T_{o,1} - (1-A) \frac{V_1^2}{2g_c J C_p} + \left(\frac{1-f_1}{f_1} \right) \left[T_{o,2} - (1-A) \frac{V_2^2}{2g_c J C_p} \right]}{1 + \left(\frac{1-f_1}{f_1} \right)} \quad (219)$$

For purposes of this analysis, the difference in velocities of the jet and wake will be ignored. The differences are about 11 percent; the term is then squared (21 percent) and multiplied by $(1-A)$, where A is about 0.928. Therefore, the error is about 1.4 percent of the kinetic temperature. This is on the same order as the uncertainties in the value of A . Under this simplification, the kinetic temperature terms can be combined, yielding:

$$T_j = \frac{T_{o,1} + \left(\frac{1-f_1}{f_1} \right) T_{o,2}}{1 + \frac{1-f_1}{f_1}} - (1-A) \frac{V^2}{2g_c J C_p} \quad (220)$$

With the thermocouple-indicated temperature described in terms of the jet-wake conditions at the tip diameter of the rotor, the mixed-mean fluid temperature actually leaving the rotor can be determined.

Consider an annular-control volume around the rotor, extending radially outward far enough to permit the assertion that the fluid leaving the control volume is at a uniform temperature given by $T_{M,o}$ (stagnation temperature, mixed-mean discharge) (see Figure 91).

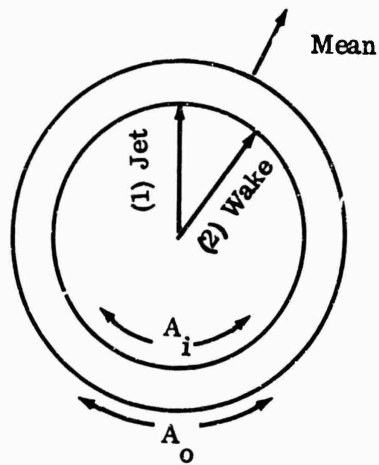


Figure 91. Annular-Control Volume (Jet and Wake).

Fluid entering from the jet region (1) carries with it energy in the amount:

$$\text{Jet Contribution: } \rho_1 V_{R,1} f_1 A_i C_p T_{o,1}$$

For fluid entering from the wake region (2):

$$\text{Wake Contribution: } \rho_2 V_{R,2} f_2 A_i C_p T_{o,2}$$

The mixed-mean fluid temperature at the outer diameter of the control volume is defined to account for all of the energy inputs:

$$\rho_M V_{R,M} A_o C_p T_{o,M} \quad (221)$$

The control volume is also subject to the Conservation of Matter Principle, which relates the mean radial velocity at the outer diameter to the inner-diameter conditions:

$$\rho_1 V_{R,1} f_1 A_i + \rho_2 V_{R,2} (1-f_1) A_i = \rho_M V_{R,M} A_o \quad (222)$$

If the control volume is shrunk to zero radial width (instantaneous mixing) and the fluid density is assumed uniform, then:

$$f_1 V_{R,2} + (1 - f_1) V_{R,2} = V_{R,M} \quad (223)$$

Applying the Conservation of Energy Principle to Equations 220 through 222 and assuming no heat transfer from the gas to the compressor case yields:

$$\rho_M V_{R,M} A_o C_p T_{o,M} = \rho_1 V_{R,1} f_1 A_i T_{1,0} + \rho_2 V_{R,2} (1 - f_1) A_i C_p T_{o,2} \quad (224)$$

Introducing the same simplification used in Equation 223 yields:

$$V_{R,M} T_{o,M} = f_1 V_{R,1} T_{o,1} + (1 - f_1) V_{R,2} T_{o,2} \quad (225)$$

Substituting Equation 223 into Equation 225,

$$T_{o,M} = \frac{f_1 V_{R,1} T_{o,1} + (1 - f_1) V_{R,2} T_{o,2}}{f_1 V_{R,1} + (1 - f_1) V_{R,2}} \quad (226)$$

Dividing through by $f_1 V_{R,1}$ yields:

$$T_{o,M} = \frac{T_{o,1} + \left(\frac{1 - f_1}{f_1} \right) \left(\frac{V_{R,2}}{V_{R,1}} \right) T_{o,2}}{1 + \left(\frac{1 - f_1}{f_1} \right) \frac{V_{R,2}}{V_{R,1}}} \quad (227)$$

Equations 227 and 220 combine to present:

$$T_j - T_{o,M} = - \frac{\left(\frac{1-f_1}{f_1}\right) \left(1 - \frac{V_{R,2}}{V_{R,1}}\right) (T_{o,1} - T_{o,2})}{\left(1 + \frac{1-f_1}{f_1}\right) \left(1 + \left(\frac{1-f_1}{f_1}\right) \left(\frac{V_{R,2}}{V_{R,1}}\right)\right)} - (1-A) \frac{V^2}{2g_c J C_p} \quad (228)$$

Two special cases may be considered:

- 1) If $V_{R,2} = 0$, then $T_{o,M} = T_{o,1}$, and the high-velocity form of Equation 212 is:

$$T_j - T_{o,1} = - (1 - f_1) (T_{o,1} - T_{o,2}) - (1 - A) \frac{V^2}{2g_c J C_p} \quad (229)$$

- 2) If $V_{R,2} = V_{R,1}$ the high-velocity form of Equation 210 for equal heat-transfer coefficients is determined, since $T_{o,M} = T_{f,p,o}$ in that case (mixed-mean stagnation temperature at the probe location).

$$T_j - T_{o,1} = - (1 - A) (T_{\text{kinetic}}) = - (1 - A) \frac{V^2}{2g_c J C_p} \quad (230)$$

It would appear that Equation 228 provides the most flexible and general form for considering the problem of measuring the bulk temperature of the discharge fluid, using a thermocouple located close enough to the rotor to be affected by the wake temperature.

Equation 228 will be used to estimate effects, based on estimates of f_1 and $V_{R,2}/V_{R,1}$ shown in the table.

Take:

$$f_1 = 0.25$$

$$\frac{V_{R,2}}{V_{R,1}} = 0; 0.15 \text{ (estimated to be 0 based on the impeller model)}$$

Then, taking $A = 0.928$ (typically), we have

$$T_j - T_{o,M} = -0.75 (T_{o,1} - T_{o,2}) - 0.072 \left(\frac{V^2}{2g_c J C_p} \right) \text{ for the case of } \frac{V_{R,2}}{V_{R,1}} = 0 \quad (231)$$

$$T_j - T_{o,M} = -0.44 (T_{o,1} - T_{o,2}) - 0.072 \left(\frac{V^2}{2g_c J C_p} \right) \text{ for } \frac{V_{R,2}}{V_{R,1}} = 0.15 \quad (232)$$

If the wake and jet stagnation temperatures differ by as much as 50° to 70°F, as has been estimated, and if the other estimates of jet width and radial-velocity ratios are correct, then a probe mounted close to the rotor will be reading between 45° and 60°F higher than the value it would have read had it been placed far enough from the rotor to sense the mixed-fluid condition.

From the way in which this mixing error is introduced, by sensing the temperature of fluid which does not actually leave the system, it can be seen that the effect is exaggerated by low radial velocities in the wake and goes to zero when the wake fluid has the same radial velocity as the jet. In this case, all of the fluid sensed by the probe influences the temperature of the fluid leaving the system.

Contractor's note:

Significant differences have been observed in the past between collector temperature (at the end of the compressor) and that measured at the rim of the impeller. Part of this difference has been ascribed to heat transfer, but not all of it (nor even the largest fraction of it) can be accounted for in that way. Thus the effects predicted by this analysis seem to be borne out by experience in testing compressors.

INSTRUMENTATION RESEARCH

ABSTRACT

This appendix describes instrumentation research conducted in 1966 by the contractor in support of other engine and component development programs. Specifically investigated were methods of measuring (1) blade-to-shroud running clearance, (2) total pressure in the presence of unsteady flow fields, (3) torque at rotational speeds up to 60,000 rpm, and (4) total temperature utilizing miniature probes.

A system was evaluated that would measure blade-to-shroud running clearance with an accuracy of ± 0.002 inch. An analysis of existing typical total-pressure-measuring installations indicated that no errors were being introduced due to the unsteady flow fields encountered. Several methods of torque measurement were investigated, but all required major modifications to the test rigs. A calibration facility was constructed to determine temperature-recovery ratio of existing miniature total-temperature probes.

The above research was conducted in a company-funded program.

SYMBOLS

B	= shape factor
D	= probe internal diameter (feet)
f	= minimum frequency for which probe will give true average readings
f_m	= minimum permissible square wave frequency (cps)
L	= probe tube length (feet)
P	= pressure (psia)
P_f	= fluctuation pulse amplitude (psia)
P^*	= root-mean-square average pressure (psia)
\bar{P}	= true average pressure (psia)
S	= pulse duration period (sec)
T	= time period between pulses (sec)
ν	= kinematic viscosity (ft-sec)
ρ	= mass density of fluid (lbm/ft ³)

1.0 INTRODUCTION

1.1 OBJECTIVE

The objective of the research program was to investigate instrumentation hardware and application techniques to provide an accurate definition of performance characteristics of turbine engines and components.

The instrumentation technology developed has application to several of the contractor's engine and component development programs, such as the T50-BO-10 improvement and the Army centrifugal-compressor research program.

1.2 SCOPE

The research was divided into 4 parts:

- 1) Blade-to-shroud running clearance measurement;
- 2) The influence of unsteady flow fields on total-pressure measurement;
- 3) Torque measurement at high rotational speeds;
- 4) More accurate measurement of total temperature in diffuser passages.

2.0 MEASUREMENT OF BLADE-TO-SHROUD RUNNING CLEARANCE

2.1 GOALS

A monitor of impeller blade-to-shroud clearance during rig operation is necessary in order to avoid mechanical rub of the impeller and shroud as they expand thermally and distort under centrifugal forces. In addition, a knowledge of clearance allows clearance losses to be calculated, which contributes to a more accurate definition of performance. The measurement accuracy goal was 10 percent of the clearance. An operating range of 0 to 0.060 inch and an ability to withstand temperatures up to 700°F were necessary.

2.2 RESEARCH AND DEVELOPMENT EFFORT

Specifications of several commercially available distance measuring systems were studied. Two systems were selected for evaluation: the gated-beam proximity detection and sensing system and the eddy-current clearance detection system.

2.2.1 GATED-BEAM PROXIMITY DETECTION AND SENSING SYSTEM

System Description

The proximity detection and sensing system was procured on a 3-month lease. The system was received by the contractor on 11 April 1966.

This system is basically a gated-beam detector, a circuit commonly employed in later generation television receivers. The circuit provides an output which is a function of the difference in frequency between 2 parallel resonant circuits. These circuits are designed to operate at a frequency between 10 and 14 MHz, providing an essentially flat response to changes in capacitance occurring between 0 and 1 MHz.

In this system, shown schematically in Figure 92, the sensor and its capacitance to its surroundings comprise one of the resonant circuits, while a conventional inductor and capacitor make up the reference circuit. Variation in the capacitance between the sensor and its surroundings changes the operating frequency of the active (sensor) circuit. This difference in frequency causes a change in output of the gated-beam tube. The output of this tube is amplified in several stages and is indicated on a panel meter or on an oscilloscope.

System Evaluation

Initial checkout and evaluation of the system indicated that successful operation demanded that calibration be carried out with the sensor installed in the actual hardware to be measured.

The sensor assembly was mounted in the diffuser-rig frontplate, which in turn was clamped to the work table of a layout-drilling machine. The impeller was mounted on a spare balancing arbor and chucked in the machine spindle. The parts were aligned and checked for concentricity between the impeller and plate. The initial attempt was made to obtain a static calibration, that is, with a blade positioned over the sensor. It soon became obvious that the short-term drift of the system electronics was great enough to cause nearly a ± 10 -percent uncertainty in the calibration. Static calibration attempts were abandoned; however, satisfactory calibrations were obtained by measuring the alternating component of the system output while driving the impeller at 1500 rpm.

The calibrations thus obtained were satisfactory from a standpoint of short-term repeatability; however, long-term drift remained a problem. Long-term drift is estimated to be ± 10 -percent full scale per day.

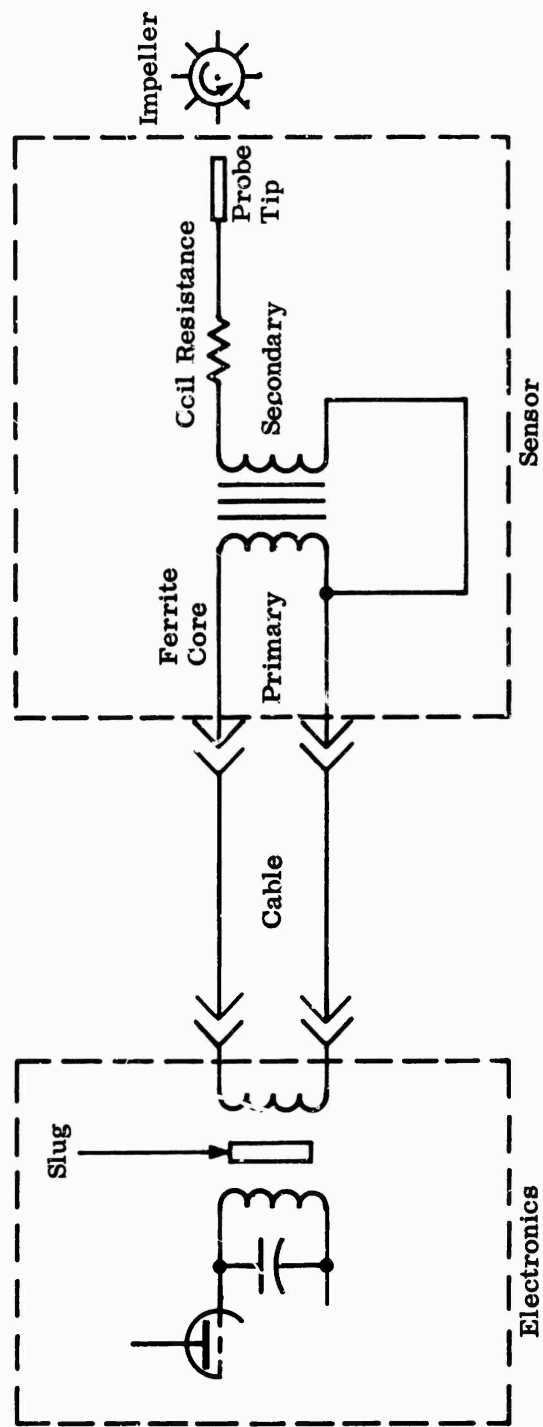


Figure 92. Gated-Beam Proximity Detection System (Schematic Diagram).

The calibrated system was immediately moved to the test rig where elapsed time for assembly and installation was about 1.5 hours. This delay was tolerable for long-term drift. Measurements taken during rig operation soon led to the conclusion that the temperature change of the probe during operation was causing excessive signal drift.

Several checks were made with the sensor in the operating position, while monitoring the temperature of the probe body. It was observed that an increase in sensor body temperature of 60°F caused the system output to decrease to zero, equivalent to 100-percent drift. An attempt was made to cool the sensor by surrounding it with a simple shroud and directing an air blast at it. This proved to be insufficient cooling. The sensor body temperature still increased approximately 25°F during the run, causing an estimated 30-percent error in system output. Analysis of these results indicated that the error primarily was a result of the change in resistance of the sensor inductor.

It was obvious that means of protecting the sensor from the high temperatures encountered in the compressor test rigs was necessary. A flush-mounted, water-cooled mounting adapter, Figure 93, was designed and built. First attempts to calibrate the sensor-adapter assembly revealed several shortcomings:

- 1) The area of the adapter center conductor was 0.0002 square inch (0.016-inch diameter). This was too small an area and resulted in a small change in capacitance when an impeller blade was moved under the sensor.
- 2) The attempt to build the adapter with a flush center conductor (no protrusion into the diffuser passage) resulted in excessive stray capacitance to the surrounding frontplate surface. This lowered the self-resonant frequency of the sensor assembly below the capability of the electronics.
- 3) The method of insulating the center conductor of the adapter resulted in destruction of the sensor when disassembly was attempted.

The following changes were incorporated in the reassembly of the adapter with a new sensor:

- 1) The adapter center-conductor area was increased to 0.003 square inch (0.062-inch diameter) to increase the capacitance change when an impeller blade moved past the sensor. A loss in blade shape definition resulted from this configuration. It was believed that this loss had no effect on the application of the system to the immediate task.

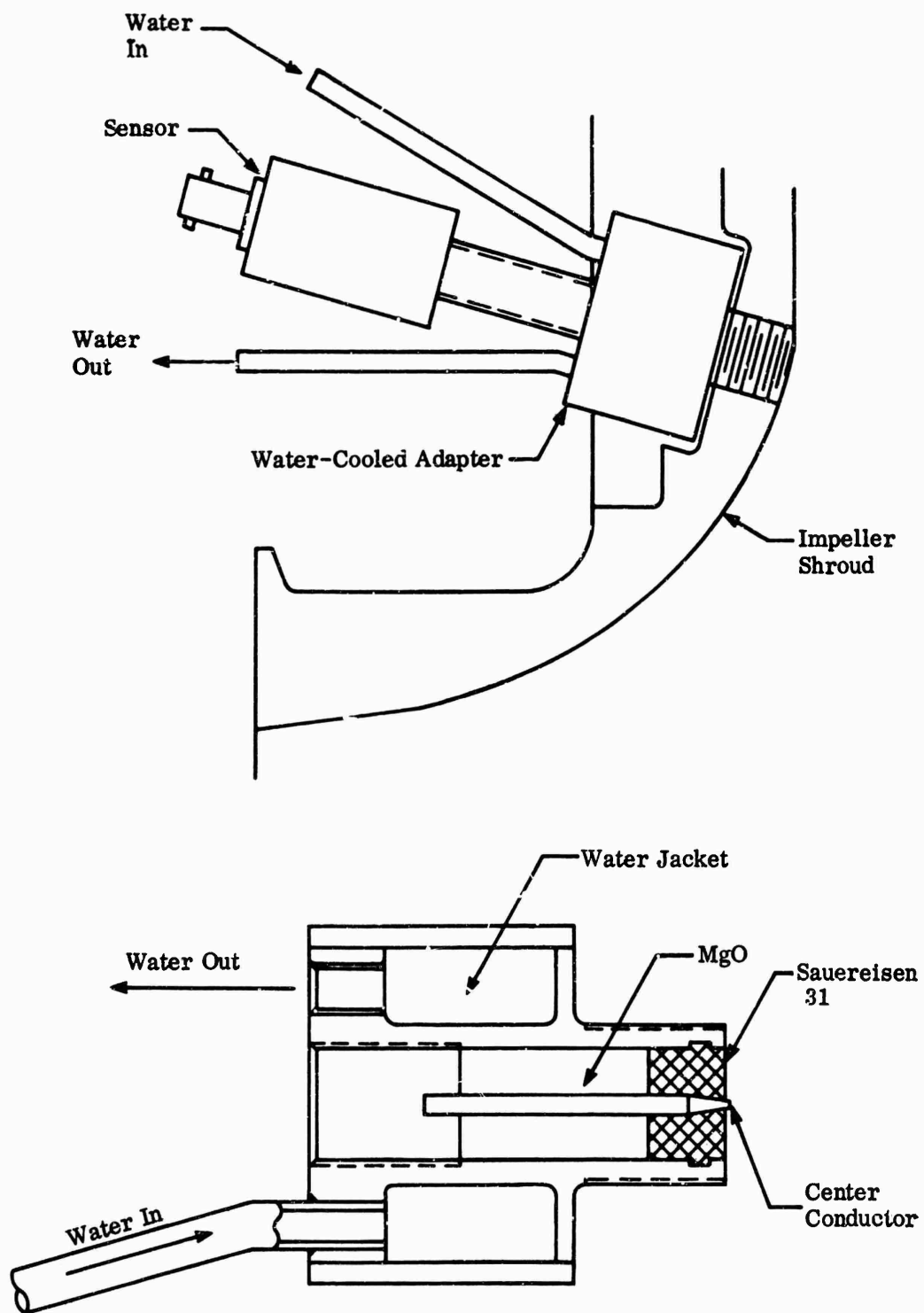


Figure 3. Detail of Water-Cooled Sensor Adapter.

- 2) The adapter center conductor was allowed to stand approximately 0.050 inch salient of the rig frontplate when installed. This was later decreased to bring the protrusion below the point that would cause it to be the first point to rub if running clearance decreased to the minimum. This decrease in protrusion left the center conductor approximately 0.022 inch salient of the frontplate. This change decreased the stray capacitance to the point that the self-resonant frequency of the sensor assembly was raised to 10.5 MHz: well within the operating range of electronics.
- 3) The annular space between the adapter body and its center conductor was packed with an hydrous magnesium oxide (MgO) to within 0.2 inch of full. A thin layer of Sauereisen No. 31 cement was laid over the MgO and cured at approximately 250°F for 8 hours. The cement was trimmed away from the center conductor to further minimize stray capacitance. Chipping or grinding away the thin cement layer should permit easy disassembly with little risk of damage to the sensor proper.

Proposed Improvements

It was proposed to surround the sensor completely with a water jacket; however, the center conductor was still the most direct path of heat transfer between the diffuser passage and the sensor inductor. Any attempt to cool the center conductor would almost certainly increase the leakage capacitance.

Some improvement was possible by a redesign of the electronics. The possibility of making the reference oscillator circuit into a compensating dummy sensor was an avenue of improvement which could be explored by the system manufacturer.

System Application

Contact with 2 other companies who have had experience with probes of this type disclosed that 1 company had rejected the system as unworkable. The other company is employing a gated-beam detector system for obtaining qualitative information on rotor behavior. No attempt was being made to obtain static displacement information.

Conclusions

This application of the capacitance-type proximity-measurement system was limited mainly by its sensitivity to temperature. The possibility of holding the sensor at a constant temperature was remote. A means of introducing temperature compensation into the electronics appeared to be the only workable way to

overcome temperature sensitivity. Design of the electronics, including manufacturing and testing, to evaluate means of temperature compensation will necessitate an extensive development effort. The system was not usable in its present stage of development for the intended purpose, i.e., measurement of clearance between a high-speed rotor and its surroundings at elevated temperatures. The system is usable for observing qualitative dynamic behavior of a high-speed rotor.

2.2.2 THE EDDY-CURRENT CLEARANCE-DETECTION SYSTEM

System Description

A turbine blade-tip clearance monitor system was acquired by the contractor, on a temporary loan basis, for evaluation in the compressor test rigs.

The system arrived on 11 July 1966, and consisted of a calibration fixture, a chassis of electronics, a modified oscilloscope with calibrated bezel, cables, and two water-cooled transducers. The system operating principle was based on an eddy-current sensitive transducer. The transducer consisted of a coil of fine wire, usually wound in pancake form and mounted on the probe tip. A high-frequency current is passed through the coil, and the resultant magnetic field induces eddy currents in a nearby conducting body (in this case, the impeller blade). A. C. loading of the coil, by the secondary magnetic field created by these eddy currents, causes the coil impedance to vary, depending on the proximity of the coil to the surface under observation. The system electronics senses this impedance change and provides readout.

Previous correspondence and discussion with instrumentation personnel of another company indicated that the system had been used successfully over a measurement and temperature range similar to the contractor's requirements, but with turbine wheels with more blades and operating at lower rotational speeds than the contractor's test rigs.

System Evaluation

One of the water-cooled transducers was installed in the KF-1 test rig impeller shroud. The shroud was set up in a layout-drilling machine with the impeller mounted on an arbor and chucked in the machine spindle. The static calibration thus obtained indicated excellent linearity and repeatability. Warm air from a hair dryer was used to check the temperature sensitivity of the transducer. The heat did not affect the calibration.

The impeller and shroud were then installed in the RF-1 test rig. The results of runs in the RF-1 test rig are shown in Figures 94 and 95. A total of 18 actuated-rub-sensor probes were used during the test for comparative data. Data were taken at 30,000 rpm through 57,000 rpm. Several minutes were allowed at each speed for the hardware to stabilize thermally.

Conclusions

The eddy-current system is relatively easy to set up, holds its calibration well, and is not affected by the temperatures involved in the compressor test rigs. The eddy-current-type transducers require a large (0.75-inch-diameter) mounting hole.

The data indicate that the actuated probe is not repeatable enough for use as a calibration reference. However, the repeatability band of the eddy current probe data was ± 5 percent of the impeller-shroud clearance in the tests run. No test data were obtained at clearances below about 0.028 inch. It is felt from the data taken that the long-term system measurement uncertainty would be about ± 0.002 inch. Therefore, at clearances above 0.020 inch, the accuracy goal of 10 percent of the gap was attained.

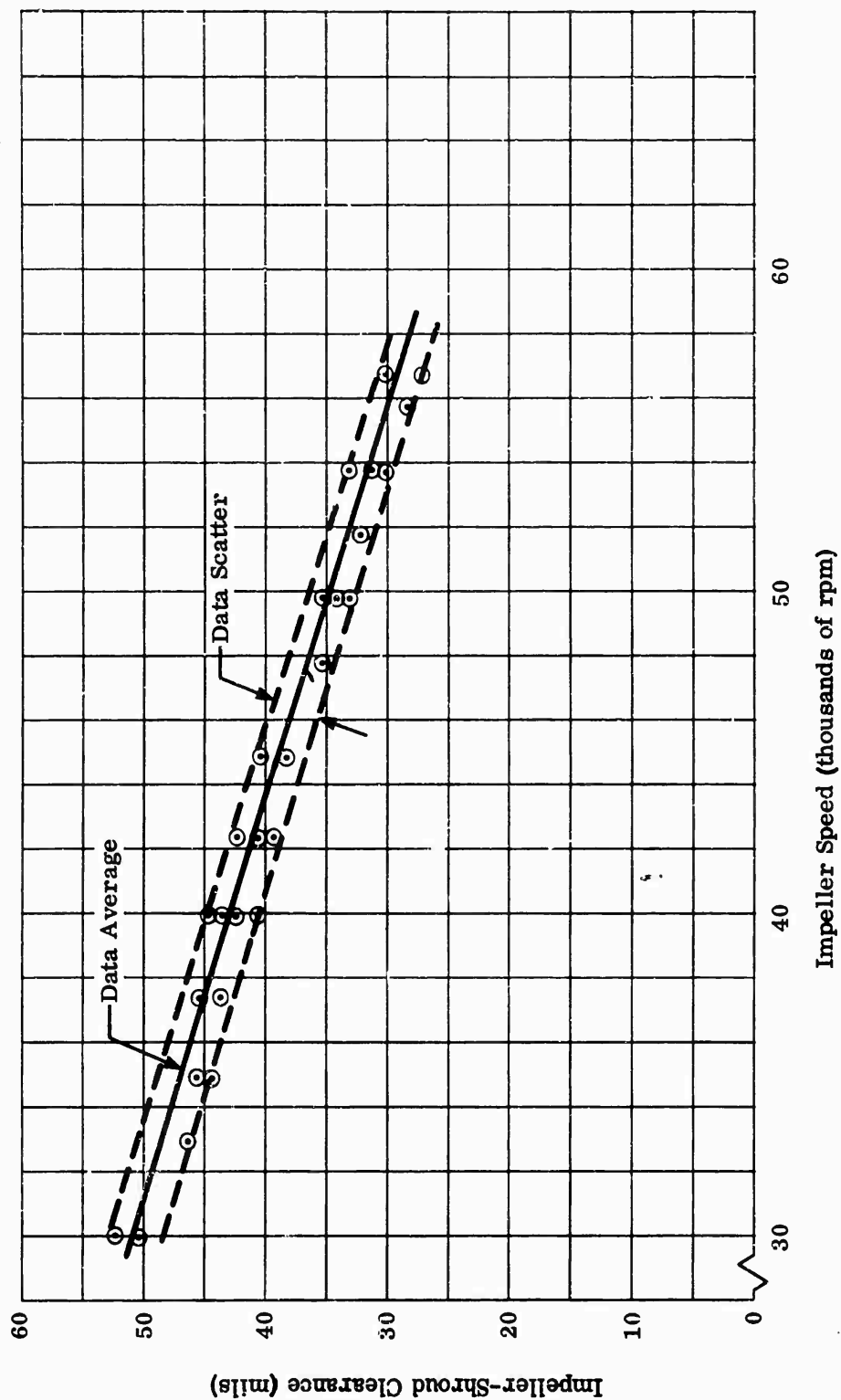


Figure 94. Eddy-Current Clearance-Probe Data.

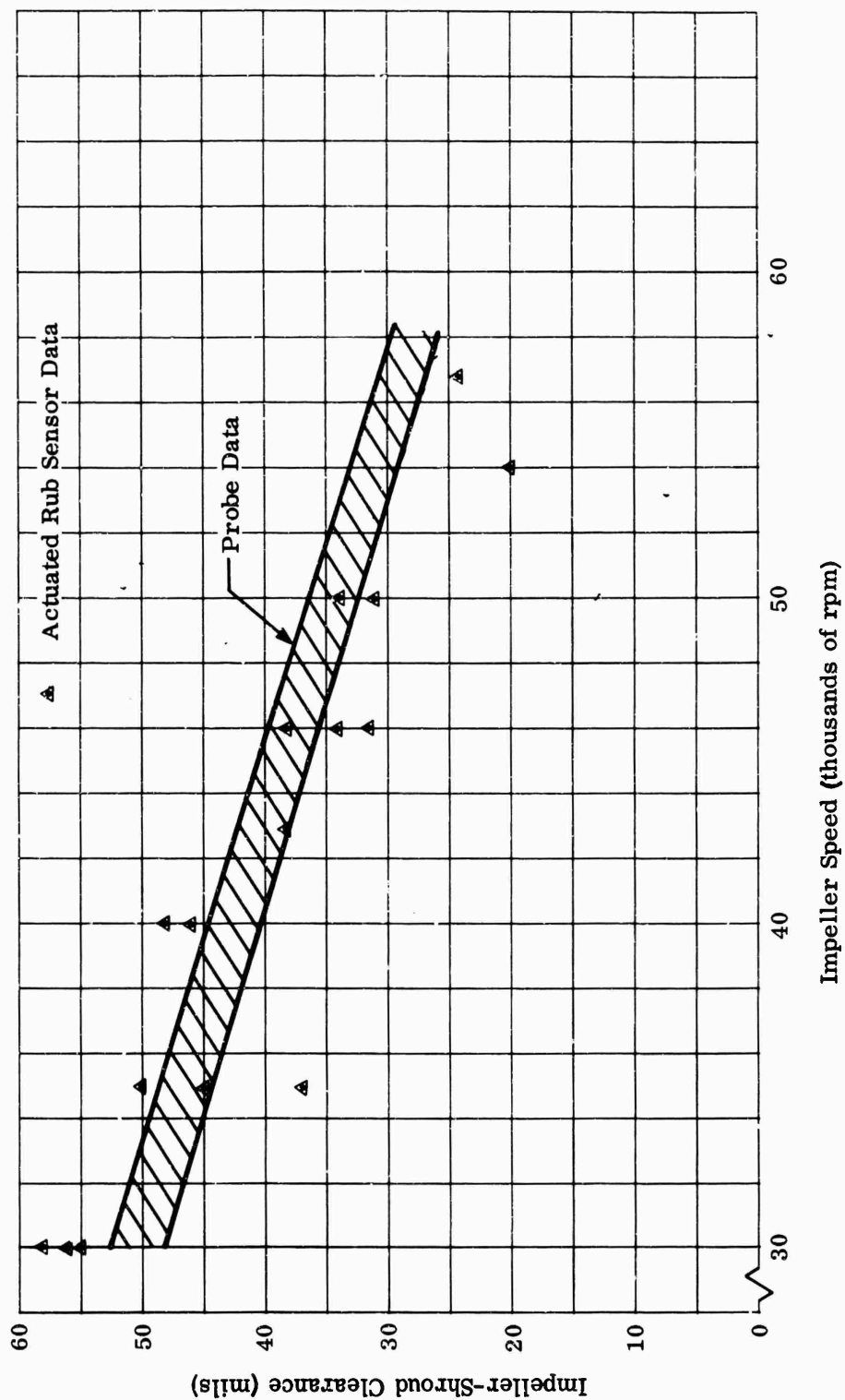


Figure 95. Actuated Rub Sensor Data and Eddy-Current Clearance-Probe Data.

3.0 MEASUREMENT OF TOTAL PRESSURE IN THE PRESENCE OF UNSTEADY FLOW

3.1 GOALS

Pressure fluctuations generated by the motion of impeller blades are superimposed on the stream total pressure in compressor diffuser passages.

A study was made to determine if true average total pressure could be measured with pitot probes and venturi-shrouded (Kiel) probes under these fluctuating conditions. Of particular interest was a determination of the performance of total-pressure-measuring systems in current test use.

3.2 RESEARCH EFFORT

Considerable information was already available; therefore, the study was confined to a literature survey and the compilation of a bibliography covering the general subject of pressure measurement in the presence of fluctuating flow.

3.2.1 FINDINGS

In general, the authors of all the entries in the bibliography, References 1 to 25 inclusive, agree that in turbulent or pulsed flow, total-pressure probes and their associated receiver and sensor systems (i.e., manometer, bourdon tubes, or transducers, along with their interconnecting tubing) will tend to give readings lying between true average and root-mean average. The difference between true average and root-mean average can be as much as 15 percent of the fluctuation pulse amplitude, depending upon wave shape.

Considering the rectangular wave of Figure 96 and the following equations, derived from Reference 14,

$$(P + P_f - P^*)^{1/2} S = (P^* - P)^{1/2} (T - S)$$

$$P + P_f - P^* = (P^* - P) \left(\frac{T - S}{S} \right)^2$$

$$P^* = P + P_f \left(\frac{(S/T)^2}{(S/T)^2 + (1 - S/T)^2} \right) \quad (233)$$

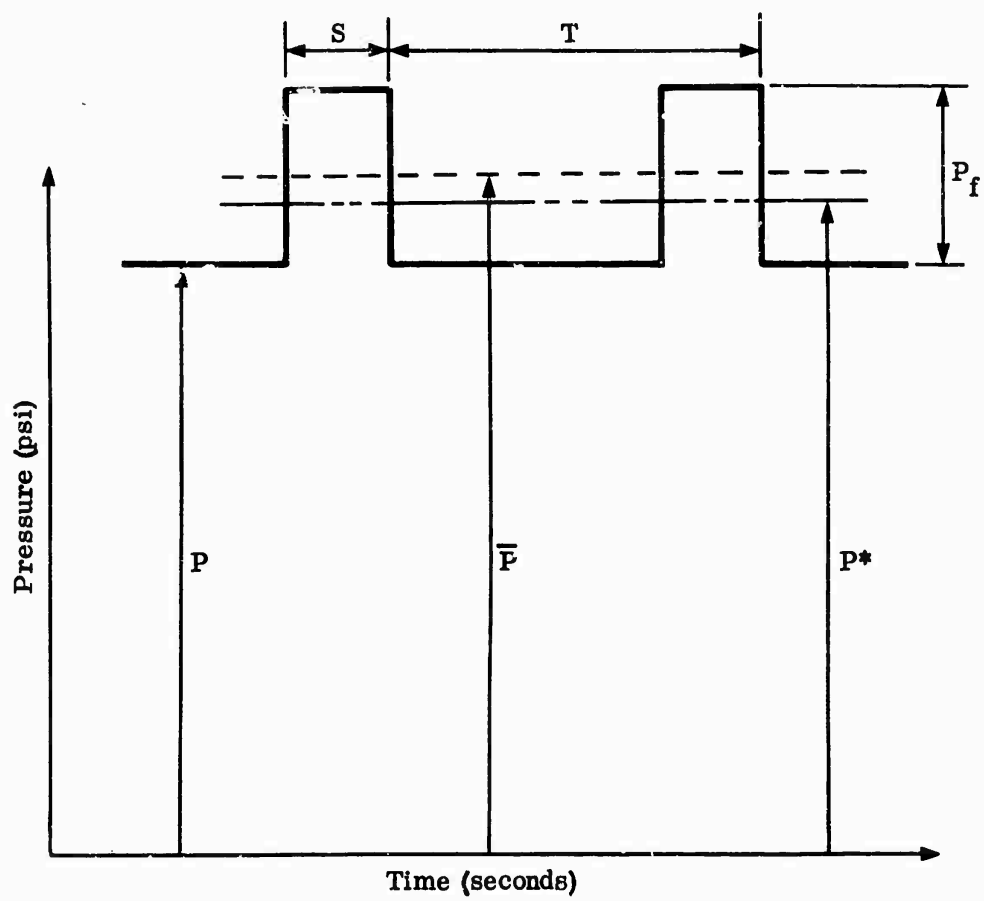


Figure 96. Rectangular-Wave Pressure Pulsation.

$$\bar{P} = \frac{P T + P_f S}{T} = P + P_f \frac{S}{T} \quad (234)$$

Combining equations 233 and 234:

$$\frac{\bar{P} - P^*}{P_f} = \frac{S}{T} - \frac{(S/T)^2}{(S/T)^2 + (1 - S/T)^2} \quad (235)$$

where:

- P = pressure, psi
- P* = root-mean-square average pressure, psi
- \bar{P} = true average pressure, psi
- P_f = fluctuation pulse amplitude, psi
- S = pulse duration period, sec
- T = time period between pulses, sec

It is clear that the shape of the pulse, S, will affect the difference between true average and root-mean average pressures. Figure 97 shows that when the wave is truly symmetrical, i.e., when S is 50 percent of the period T, there is no difference in these average pressures. The maximum difference is 15 percent, when S is 25 percent of period T.

Reference 14 discusses 3 ways in which nonlinearity may arise and cause pressure readings to be different from true average pressures. First, unsymmetrical ends of the probe may cause unsymmetrical losses, depending on flow direction in the probe. The authors conclude that this effect is small and, further, that it can be eliminated by making the aft end of the probe be empty abruptly into a chamber whose diameter is large compared with the probe diameter, essentially duplicating the total pressure probe tip configuration. Second, compressibility may result in higher density in the probe during inflow than outflow, or vice versa. Reference 16 reports that compressibility can account for a deviation from true average of up to 2 percent of pulsation amplitude depending upon wave form, 2 percent being a likely occurrence at low frequencies.

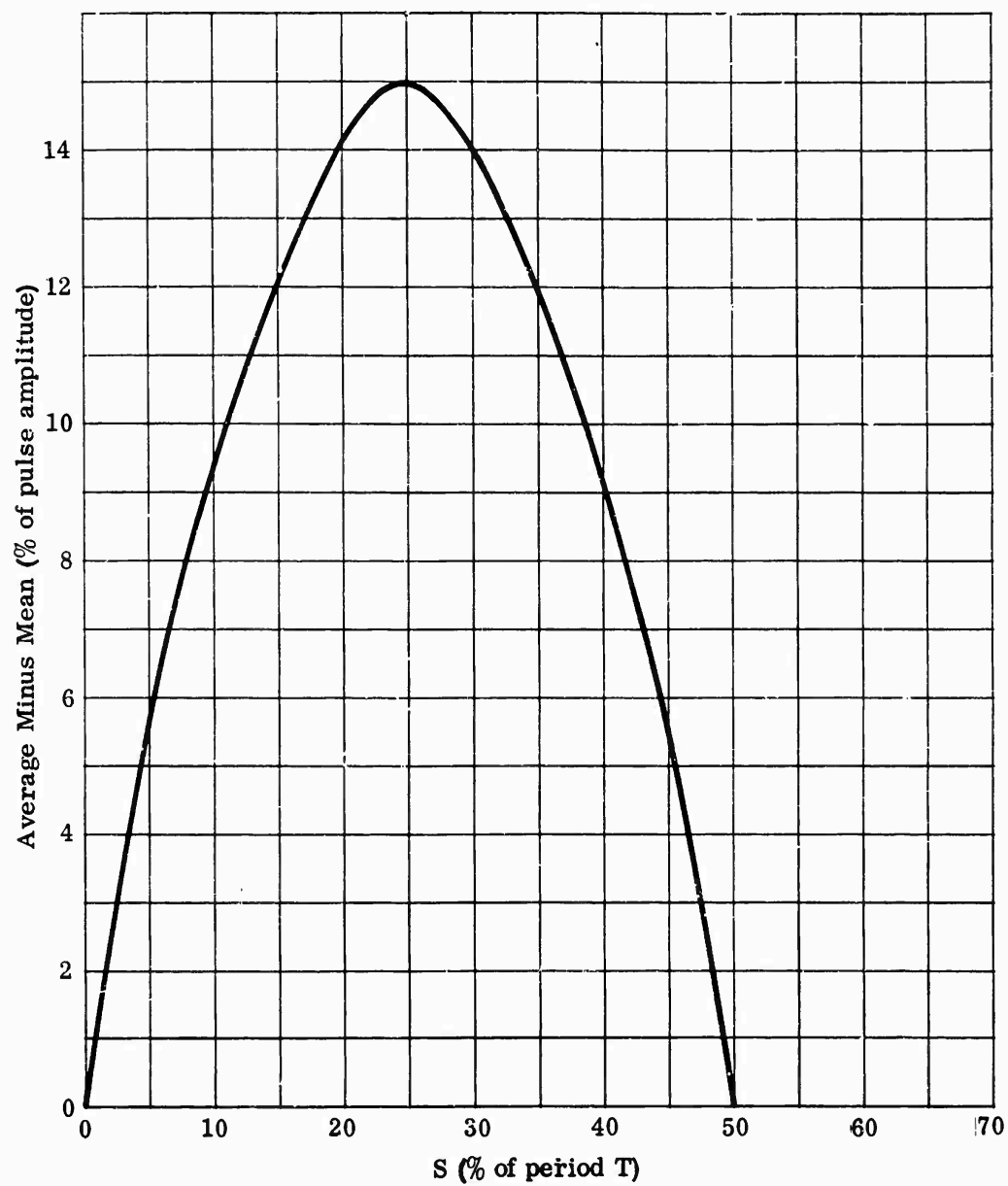


Figure 97. Effect of Pressure Pulse Shape on Root-Mean Balance Pressure.

This deviation diminishes at higher frequencies (several thousand Hz) where the flow inside the probe is very small. Third, turbulent flow in the probe can cause deviations from true average pressure up to a theoretical maximum of 15 percent of the pulse amplitude for an unsymmetrical rectangular wave.

Pertinent to the turbulent flow problem, Reference 14 discusses fluid dynamic analyses, supporting laboratory experiments, and compressor impeller-blade wake tests. Two equations were derived for relating probe dimensions to conditions which produce laminar flow in the probe hole. One equation gives the maximum permissible pressure fluctuation amplitude at low frequencies, and the other, which is reproduced below, gives the minimum permissible square-wave frequency.

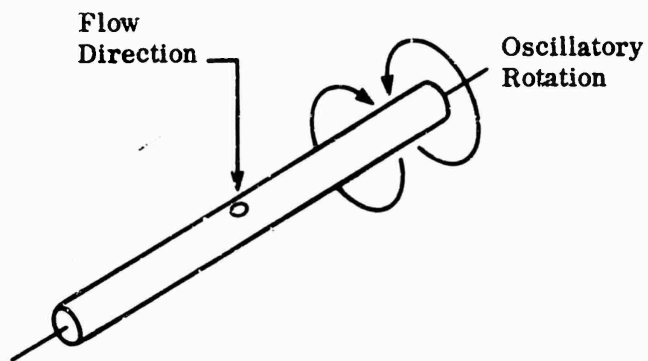
$$f_m = \left[\left(\frac{P_f}{\rho L} \right)^3 \frac{\nu}{D^5} (0.317)^4 \right]^{1/7} \left[\frac{S/T (1 - S/T) \left[\frac{(S/T)^2 + (1 - S/T)^2}{(S/T)^{8/7} + (1 - S/T)^{8/7}} \right]}{1} \right]^{4/7} \quad (236)$$

where:

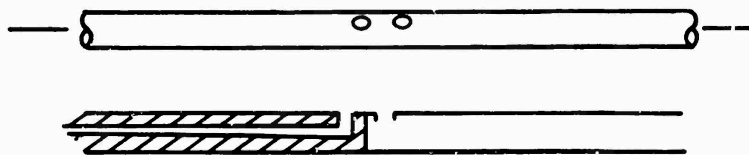
- D = probe internal diameter, ft
- f_m = minimum permissible square-wave frequency
- L = probe tube length, ft
- ρ = mass density of fluid, lb-mass/(foot)³
- ν = kinematic viscosity, ft-sec

This equation was derived by solving simultaneously the classic textbook equation for incipient turbulent flow in a tube with an equation derived for maximum theoretical nonviscous inertial flow per pulsation cycle.

Laboratory experiments on pressure probes, as shown in Figure 98a, were subjected to a known steady flow. To simulate modulated pressure, the probe was rotated ± 90 degrees at rates up to 400 Hz. Probes with various internal geometries were compared with each other.



98a. Oscillatory Probe.



98b. Stationary Probe.

Figure 98. Pressure Probes Tested.

A similar stationary probe (Figure 98b), having 2 sensing holes close together, was placed in the fluctuating airstream behind a rotating axial-flow-compressor blade row. Fluctuating frequencies of up to 3,300 Hz were thus studied. Hot-wire anemometers were used to determine instantaneous flow direction and pressure wave form.

As predicted by the equation above, pressure readings of probes were affected by probe-hole geometry. Probes with holes opening directly into a cavity gave readings which closely matched root-mean average pressure. Probes with long small-gage holes tended to give true average pressure readings. True average pressure was read when probe length, probe-hole gage, fluctuation amplitude, and fluctuation frequency were in accord with the limits set by the equation.

The equation for the minimum permissible square-wave frequency was solved with a set of conditions applicable to the contractor's compressor tests.

Rewriting Equation 235:

$$f = \left[\left(\frac{P_f}{\rho L} \right)^3 \frac{\nu}{D^5} (0.317)^4 \right]^{1/7} (B) \quad (237)$$

where: B = shape factor

$$= \left[S/T (1 - S/T) \frac{[(S/T)^2 + (1 - S/T)^2]^{4/7}}{(S/T)^{8/7} + (1 - S/T)^{8/7}} \right] \quad (238)$$

Typical Test Conditions:

Assume:

Probe Length L = 0.5 foot

Probe Diameter D = 0.01 inch = 0.00083 foot

Density ρ = 0.0141 lb mass/(foot)³
(air at 1060°R and 340 in. Hg Abs)

Kinematic Viscosity $\nu = 0.0000485 \text{ ft-sec}$

(air at 1000°R and 340 in. Hg Abs)

Pulse Ratio S/T = 0.25 (worst case per Figure 6)

Assume Pressure Amplitude $P_f = 20 \text{ psi}$

Calculations:

Solve for f = minimum frequency for which probe will give true average readings under conditions stated

$$B = \left[\frac{S/T (1 - S/T) \left[\frac{(S/T)^2 + (1 - S/T)^2}{(S/T)^{8/7} + (1 - S/T)^{8/7}} \right]^{4/7}}{1} \right] = 0.155$$

$$f = \left\{ \left[\frac{(20)(144)}{(.0141)(0.50)} \right]^3 \frac{0.0000485}{(0.00083)^5} (0.317)^4 \right\} \times 0.155$$

$$f = 790 \text{ cycles/sec}$$

The results indicate that roughly 800 Hz is the minimum frequency for which inertial effects dominate in limiting flow inside the probe. Above this frequency, flow is laminar, the condition required for obtaining true average pressure. Fluctuation frequencies caused by impeller-blade motion in the contractor's compressor tests range between 10,000 Hz and 23,000 Hz.

3.2.2 CONCLUSIONS

In pulsating flow, deviations of indicated pressure from true average pressure are caused chiefly by a combination of turbulent flow inside the probe and asymmetrical wave shape. If the pulsation frequency is high enough for a particular pulsation amplitude and set of probe dimensions, inertia prevents the air inside the probe from reaching velocities which cause turbulence. At pulsation amplitudes of 5 or 10 psi, frequencies generated in the contractor's compressor tests by motion of impeller blades are much higher than the highest frequency

which can cause turbulent flow inside currently used total-pressure probes. Although no measurements have been made by the contractor of pressure fluctuations occurring at the impeller exit, it is felt that fluctuation amplitudes of 5 to 10 psi are possible. Literature surveys indicate that mixing is quite complete within a radius ratio of 1.02 to 1.05. Therefore, fluctuation amplitudes become less significant as the pressure-probe location is moved downstream. Total-pressure probes are typically located at a radius ratio of 1.02 to 1.025 in the contractor's compressor tests.

A worst-case calculation for the contractor's tests, assuming a pressure pulsation amplitude of 20 psi, showed that typical operating frequencies were 12 to 35 times higher than the frequency at which the probe indicated that pressure would be expected to deviate from the true average pressure. Therefore, for the conditions stated, true average total pressure is obtained with current probe design.

4.0 MEASUREMENT OF TORQUE AT ROTATIONAL SPEEDS TO 60,000 RPM

Accurate means of measuring torque in engine and component research and development programs is desirable for performance evaluations. Torque measurement allows a better determination of work done than measurement of temperature differences alone. A measurement of turbodrive torque on the compressor test rigs would be useful as a cross-check on work absorbed by the compressor (usually determined by measurement of inlet and outlet temperatures).

4.1 RESEARCH EFFORT

Several methods of torque measurement were studied. Primary considerations were high accuracy, ability to operate at speeds up to 60,000 rpm, and adaptability to compressor test rigs without major rig modification.

Four of the methods studied showed promise upon initial examination. These methods were:

- 1) Variable Reluctance (noncontacting);
- 2) Electronic Vernier (noncontacting);
- 3) Strain Gage (contacting);
- 4) Optical Torquemeter (noncontacting).

4.1.1 VARIABLE RELUCTANCE (NONCONTACTING)

This method of torque measurement makes use of the Vallari effect. In a cylindrical shaft under pure torsion, the principal stress lines are 45-degree helices around the axis, 1 for tension and the other for compression. These are also the directions of maximum and opposite permeability changes for a shaft of magnetostrictive material.

Devices utilizing this effect have been built and are commercially available. These devices are accurate within ± 2 percent, if shaft runout and radial vibration are held to within acceptable limits. Radial shaft displacements measured on compressor test rigs have been as great as 0.005 inch peak-to-peak. The combined effects of a large pole piece to shaft air gap necessitated by this radial displacement and the lightly stressed shafts used in the test rigs would result in an output signal smaller than the minimum required for acceptable resolution and accuracy. Further study of the system was not warranted in view of the required rig changes.

4.1.2 ELECTRONIC VERNIER (NONCONTACTING)

This method of torque measurement uses two toothed wheels or other pulse generating devices mounted along the shaft and separated, as far as possible, within limitations of space and shaft dynamics. The 2 pulse generators produce a different number of pulses per revolution. The 2 frequencies are heterodyned and the resultant frequency is analyzed by means of servomechanism techniques. This method requires dynamic calibration. Space and shaft length limitations preclude the use of this method without major modification to the compressor test rigs.

4.1.3 STRAIN GAGE (CONTACTING)

The strain gage method is probably the most desirable method from the standpoint of accuracy and ease of calibration. Liquid-cooled sliprings of the type presently used by the contractor could be used for picking the signal off the shaft. However, the high rotational speeds involved require the use of a hollow shaft with the strain gages mounted on the inner surface. For satisfactory signal strength, the shaft would have to be highly stressed under operating conditions. To be usable over a moderately wide range of speed and load conditions, the shaft would have a low safety factor at maximum load. In addition, some loss in axial stiffness could be expected. This method also was considered unsatisfactory, since major rig modification would be necessary.

4.1.4 OPTICAL TORQUEMETER (NONCONTACTING)

An optical torquemeter was under development prior to the establishment of this research program. The system consisted of a torque shaft with a system of optics and associated servomechanisms to provide readout of torsional displacement. The principal factors that motivated the prototype design and development were the projected accuracy and ability to calibrate the system statically.

In mid-1966, it was considered inadvisable to continue evaluation and development of the optical torquemeter. The torque shaft and coupling showed intolerable hysteresis (0.7 to 5 percent). In addition, the design configuration initially was intended for use in measuring turbine-power output and was not adaptable to the compressor test rigs. The principle, however, showed promise. Further development of this system could lead to a satisfactory high-speed, noncontacting-type, torque-measuring device.

4.2 CONCLUSIONS

Of the 4 methods investigated, only the variable reluctance method appeared usable, but only with major compressor test-rig modifications. This method required a shaft operating highly stressed and with very small radial displacement. The shafts used in compressor test rigs did not meet these requirements.

5.0 ACCURATE MEASUREMENT OF TOTAL TEMPERATURE IN COMPRESSOR DIFFUSER PASSAGES

Due to the small (0.25 inch) width of the diffuser passage in the compressor test rigs, probes installed to measure diffuser gas temperature were very small. In addition, probe immersion was low enough that conduction errors could be expected. It was felt that a check on probe temperature recovery was necessary, since the probes were smaller than previously reported upon in the literature and since individual probes differed somewhat due to the difficulty of fabricating and assembling small pieces.

5.1 RESEARCH EFFORT

To validate the accuracy in total-temperature measurements, the possible sources of probe error were investigated:

- 1) Uncertainty of probe total-temperature recovery;
- 2) Conduction errors due to the short immersion lengths made necessary by rig hardware;
- 3) Radiation errors;
- 4) Thermocouple wire calibration.

5.1.1 PROBE RECOVERY

A test facility (Figure 99) was fabricated for the determination of total-temperature-probe recovery ratio. The facility consisted of a supersonic duct with test stations located along its length. A controlled flow of compressed air was supplied through a heat exchanger to the test section. Calibration was accomplished by insertion of the probe under test into one of the various test stations along the length of the duct. Airflow was established; Mach number was determined from pressure data, and probe indicated temperature was measured. This procedure was repeated as the probe was inserted in each of the nine test stations along the duct. Reference air total temperature was measured in a plenum upstream of the duct. From these data, temperature recovery versus Mach number characteristics of a particular probe were established. The duct was capable of calibration over the range of Mach 0.2 to 1.35 at temperatures from ambient to 700°F.

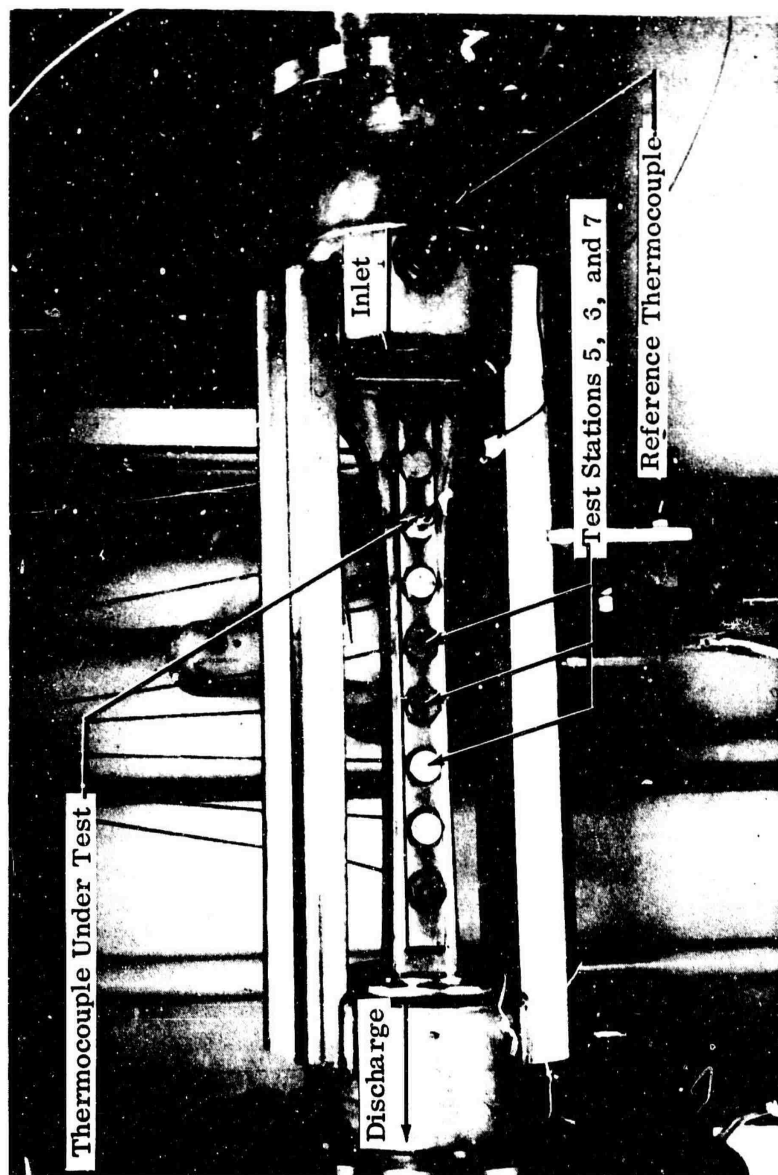


Figure 99. Supersonic Duct (Temperature-Recovery Calibration Facility).

The duct was checked with a 24-gage bare-wire thermocouple probe built per Reference 26 (Figure 100a). The test results compared favorably with data reported in Reference 26 up to Mach 0.9. A scatter of 1 percent recovery-ratio data was noted in the Mach 1.0 to 1.35 range (Figure 100b).

Three of the slotted-shield total-temperature probes (Figure 101), typical of those used in the compressor development program, were calibrated in the duct. Test results (Figure 102) indicate that the true recovery ratio agreed within $\pm 1/4$ percent with the assumed ratio (0.995) used in previous data reduction. This uncertainty in recovery ratio is equivalent to a $\pm 2.3^\circ\text{F}$ uncertainty in total temperature at 700°F . The variation in probe recovery ratio as a function of pitch angle is also shown in Figure 102.

Several of the miniature (0.032 inch in diameter) total-temperature probes were calibrated (Figure 103). A probe of this type was used to measure temperature profile in the diffuser passage. In the Mach number range of 1.0 to 1.35, a maximum uncertainty in recovery ratio equivalent to 4.1°F at 700°F was obtained. Due to the extremely small size of this type probe, construction tolerances contributed to the scatter in recovery data.

5.1.2 CONDUCTION ERRORS

Several methods have been devised and used in the compressor development program to minimize conduction errors in gas temperature measurements. Testing done by the contractor indicated that a minimum insertion of 25 times the thermocouple probe outside diameter was desirable in order to reduce the conduction error to 2 percent of the difference between gas temperature and probe base (wall) temperature at Mach 0.25 and less. As gas velocity increases, immersion requirements become less (Reference 27).

When space was available, immersion of 25 diameters was accomplished with no problems. In the diffuser passage, however, a thermocouple probe mounting tower (Figure 104) was devised such that the effective exposure to gas temperature met the required minimum.

5.1.3 RADIATION ERRORS

A literature study indicated that with the hardware and the temperatures involved in the compressor program, radiation errors were not significant. A bare-wire probe in the collector would have a radiation error of only about 3°F if the gas and wall temperatures differed by 100°F (Reference 28), which is unlikely. The

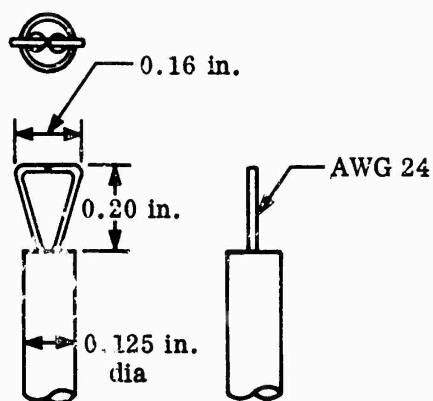


Figure 100a. Thermocouple Probe Built (per Reference 26).

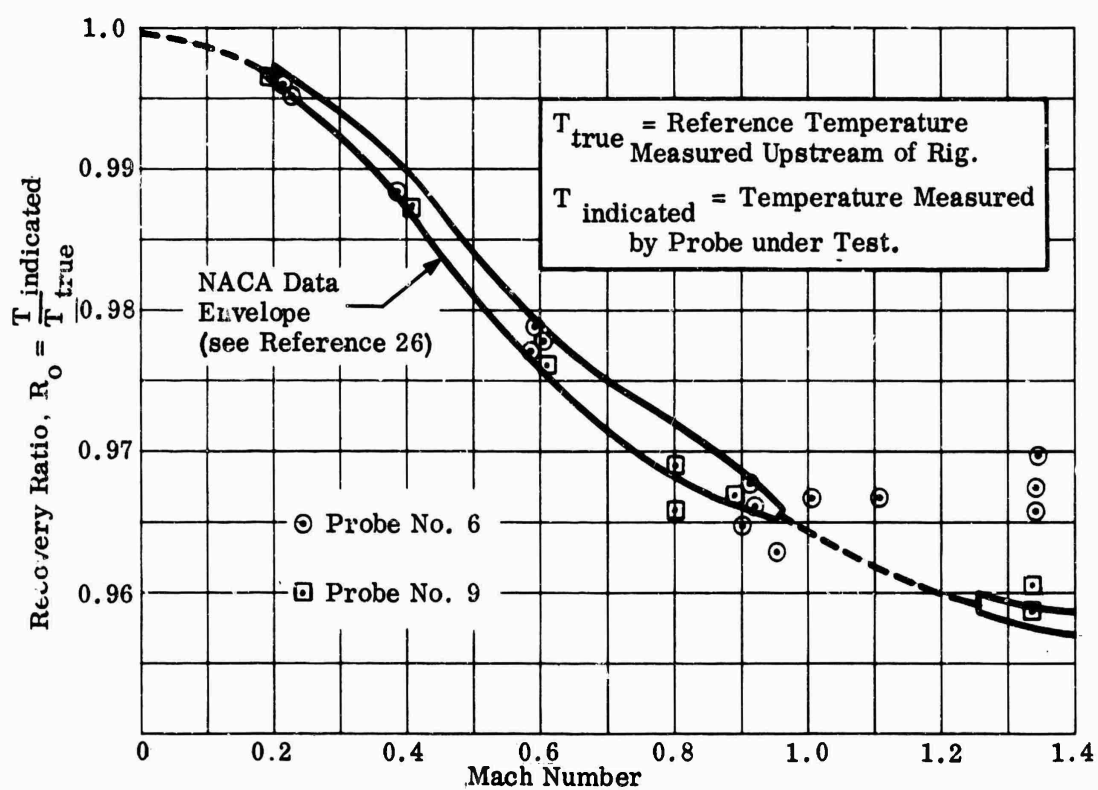


Figure 100b. Temperature Recoveries.

Figure 100. Temperature Recovery Data.

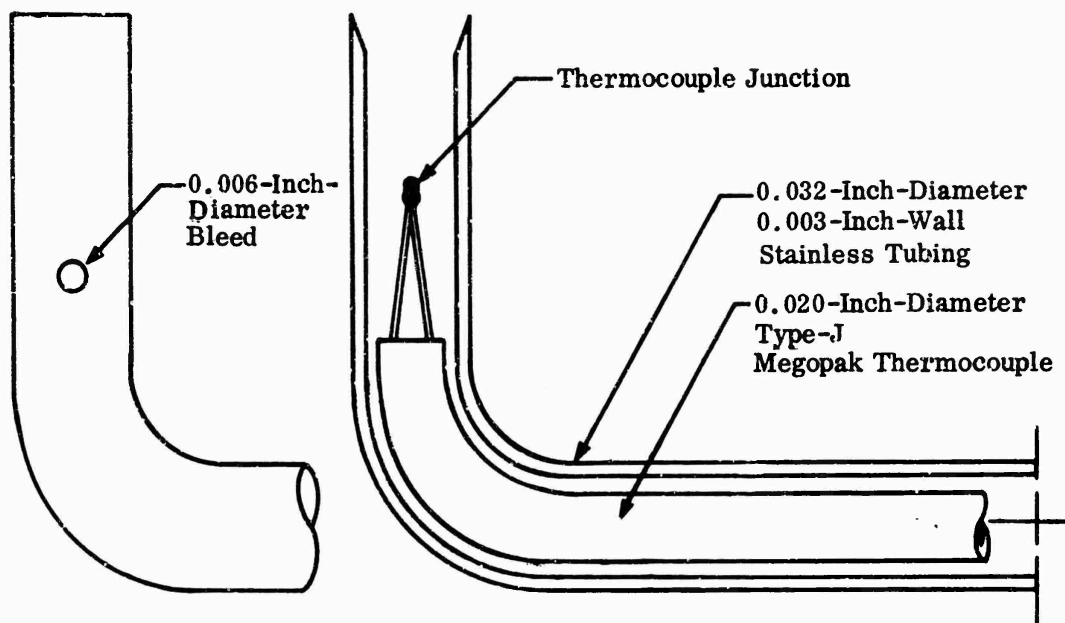


Figure 101a. Miniature Total-Temperature Probe.

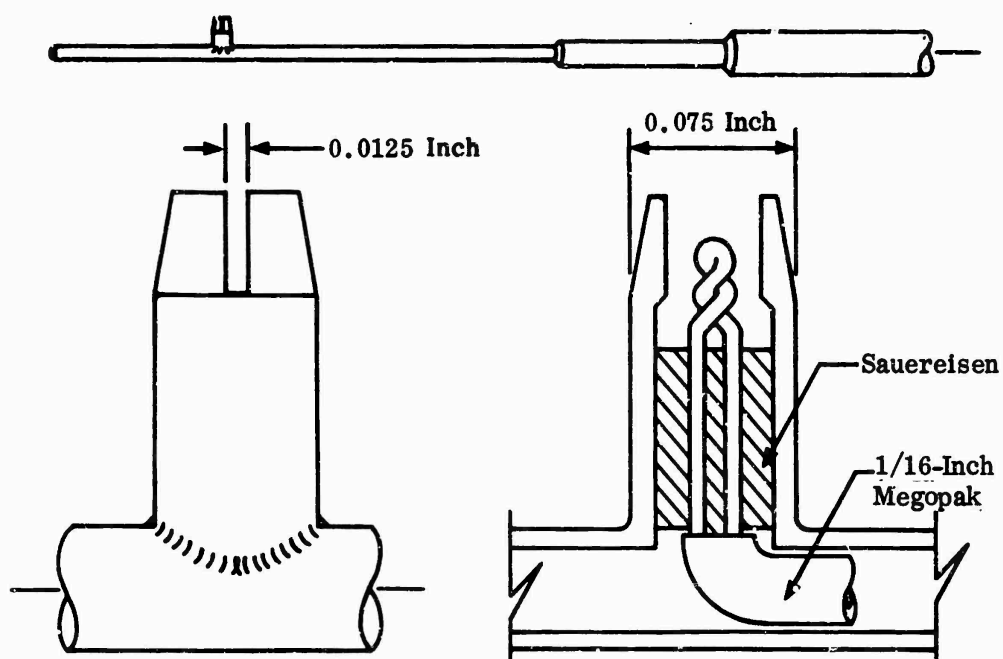


Figure 101b. Slotted-Shield Probe.

Figure 101. Temperature Probes.

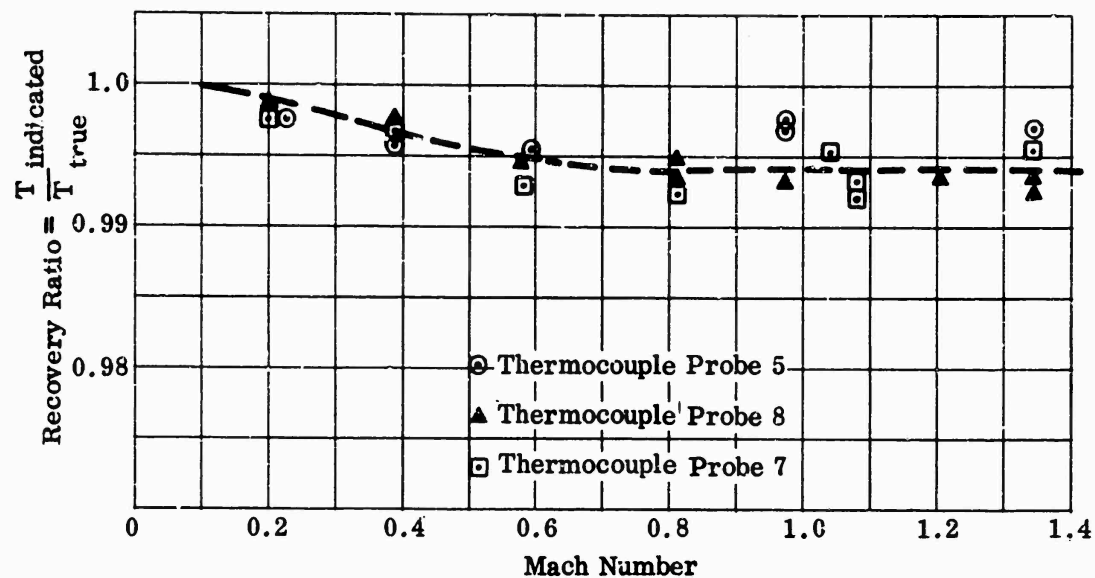


Figure 102a. Temperature-Recovery Ratio Versus Mach Number.

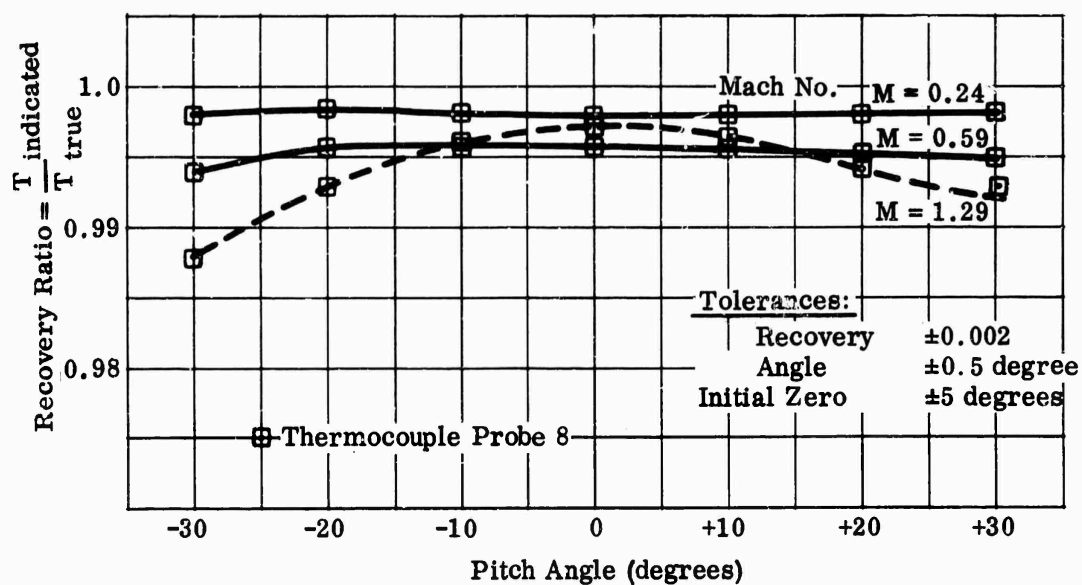


Figure 102b. Temperature-Recovery Ratio Versus Pitch Angle.

Figure 102. Slotted-Shield Total-Temperature-Probe Data.

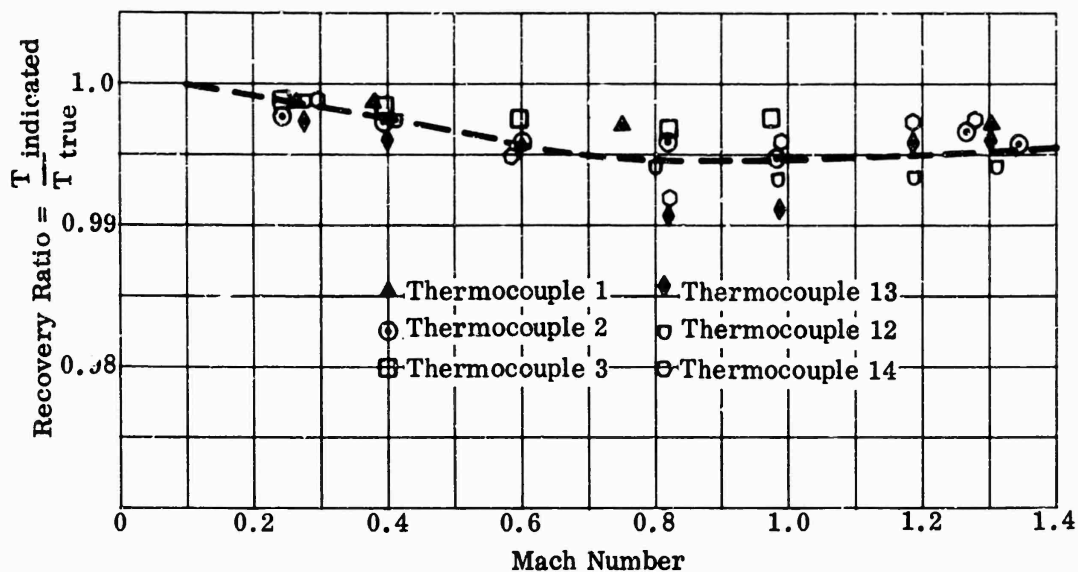


Figure 103a. Temperature-Recovery Ratio Versus Mach Number.

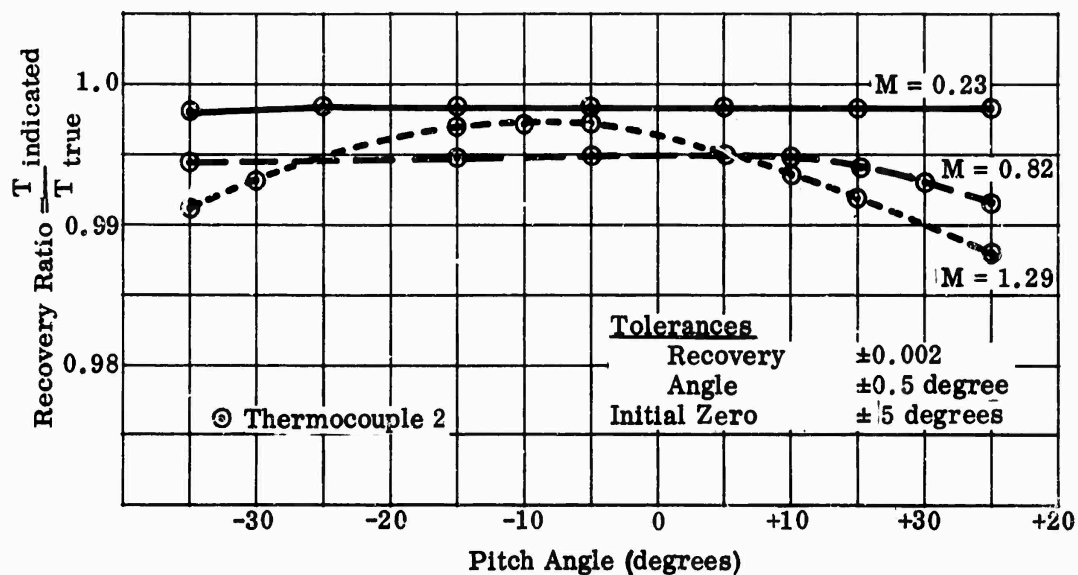


Figure 103b. Temperature-Recovery Ratio Versus Pitch Angle.

Figure 103. Miniature Total-Temperature-Probe Data.

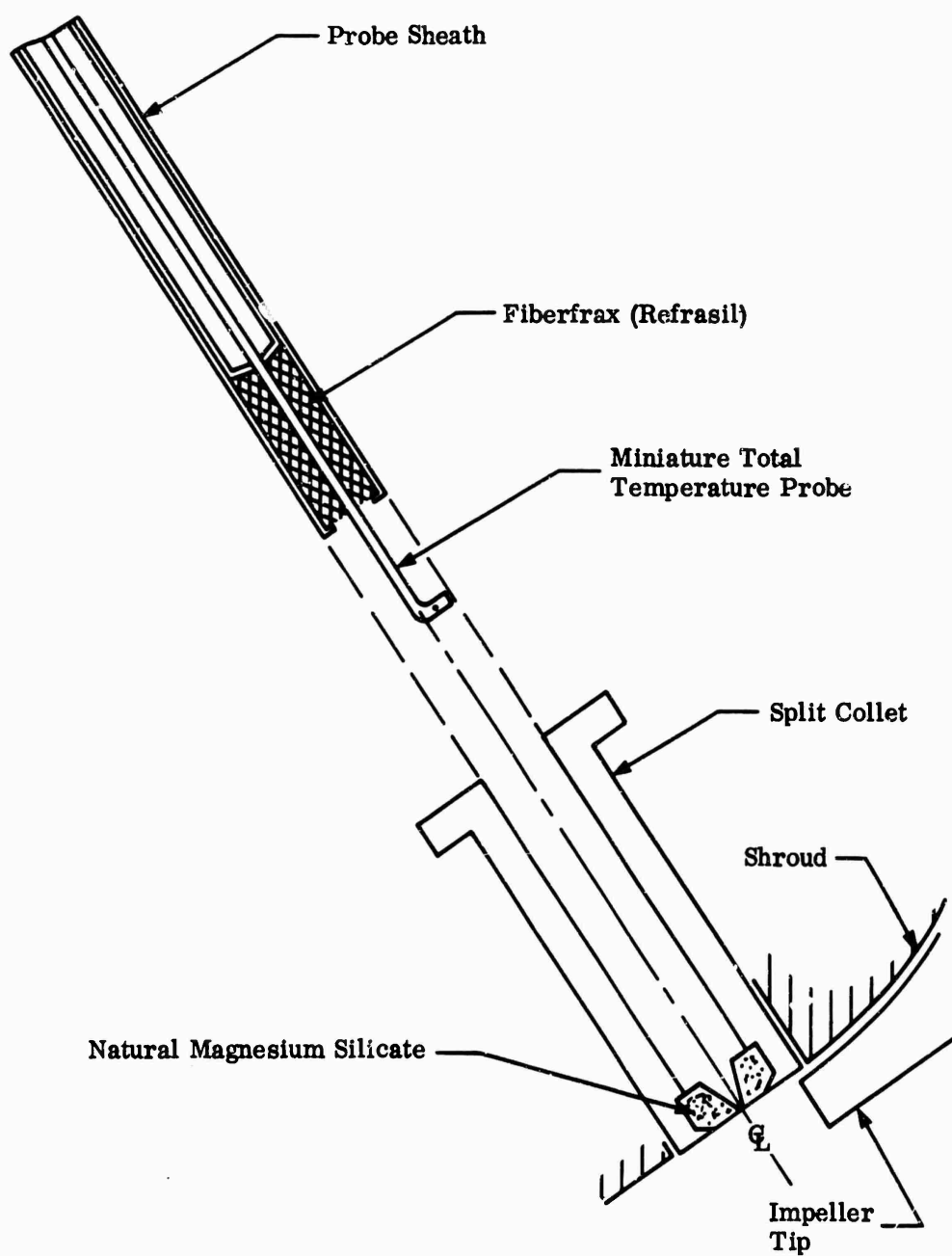


Figure 104. Total-Temperature-Probe Mounting Tower.

total-temperature probes used had 1 shield which reduced the radiation error by approximately two-thirds (Reference 29).

5.1.4 THERMOCOUPLE WIRE CALIBRATION

All thermocouple probes were fabricated from premium grade iron-constantan type-J wire. In addition, thermocouple probes used in test work were calibrated by the Pyrometrics Laboratory of the contractor. Calibration error, at or near observed points, was quoted as $\pm 0.5^\circ\text{F}$ over the temperature range of 500° to 700°F .

5.2 CONCLUSIONS

Utilizing the slotted-shield total-temperature probes, a measurement uncertainty of $\pm 3.5^\circ\text{F}$ was determined for the diffuser passage, provided that conduction errors were minimized.

The miniature total-temperature probes were very difficult to fabricate due to small size of the pieces of material involved. In addition, the probes tested showed a greater spread in recovery data than the slotted-shield type, and an overall measurement uncertainty of $\pm 5.5^\circ\text{F}$ was determined.

A study of the data taken indicated that a probe can be designed that has a nearly constant recovery ratio over the flow range involved in diffuser passages. Design would involve an increase in the thermocouple junction length exposed to the gas. The data indicated that a short, stubby junction effects a dip in the recovery ratio between Mach 0.6 and 1.0. Probe numbers 1, 2, and 3 (Figure 103) were built with long thermocouple junctions. Probes 13 and 14 had very short, stubby junctions. Probe 12 had a medium length junction. It can be seen from the recovery data, Figure 103, that probes 1, 2, and 3 had a more constant recovery factor as the Mach number changed than probes 12, 13, and 14.

(U) REFERENCES

1. Bailey, N. P., Pulsating Air Velocity Measurement, Transactions of the ASME, May 1939.
2. Bietler, S. R., The Effect of Pulsations on Orifice Meters, Transactions of the ASME, May 1939.
3. Bietler, S. R., Lindahl, E. J., and McNichols, Developments in the Measuring of Pulsating Flows with Inferential-Heat Meters, Transactions of the ASME, May 1943.
4. Bruer, L. J. F., and DeHann, R. E., "Total-Head Measurements in Fluctuating Flows", Journal of Applied Mathematics and Physics (ZAMP), Vol. IXb (1958, p. 162).
5. Corcos, G. M., Pressure Measurements in Unsteady Flows, ASME Symposium on Measurement in Unsteady Flow, Worcester, Massachusetts, May 1962, T15-19-1962, pp. 15-21.
6. Corcos, G. M., Pressure Measurements in Unsteady Flows, University of California, Institute of Engineering Research, Report Series No. 183, Issue No. 1 (Jan. 1962).
7. Delio, G. J., Schwent, G. V., and Cesaro, R. S., Transient Behavior of Lumped Constants System for Sensing Gas Pressures, NACA TN 1988, 1949.
8. Earles, S. W., and Zarek, J. M., Use of Sharpe-Edged Orifices for Metering Pulsating Flow, Institute of Mechanical Engineers, Proceedings, Vol. 177, No. 37, 1963, pp. 997-1024.
9. Goldstein, S., A Note on the Measurement of Total Head and Static Pressure in a Turbulent Stream, Proceedings of the Royal Society of London, Series A, Vol. 155, No. 886 (July 1936), pp. 570-575.
10. Hubbard, P. G., Interpretation of Data and Response of Probes in Unsteady Flow, ASME Symposium on Measurement of Unsteady Flow, Worcester, Massachusetts, May 21-23, 1962, pp. 3-8, T15-19-1962.
11. Iberall, A. S., Attenuation of Oscillatory Pressures in Instrument Lines, National Bureau of Standards Research Paper RP2115, Vol. 45, 1950.

REFERENCES (Continued)

12. Johnson, R. C., Averaging of Periodic Pressure Pulsations by a Total-Pressure Probe, NACA TN 3568, Lewis Flight Propulsion Laboratory, Cleveland, Ohio, October 1955.
13. Kastner, L. J., and Williams, T. J., Pulsating Flow Measurement by Viscous Meters, with Particular Reference to the Air Supply of Internal-Combustion Engines, Proceedings of the Institute of Mechanical Engineers, Vol. 169, Number 26, 1955.
14. Kronauer, R. E., and Grant, H. P., Pressure Probe Response in Fluctuating Flow, Proceedings of the 2nd U. S. National Congress of Applied Mechanics, 1954.
15. Kuelte, A. M., and Dryden, H. L., Effect of Turbulence in Wind Tunnel Measurements, NACA TR 342, 1929.
16. Nesbitt, M. V., The Measurement of True Mean Pressures and Mach Numbers in Oscillatory Flow, Memo No. M. 180 British N.G.T.E., March 1953.
17. Rose, W. G., Corrections to Average Measurements in Unsteady Flow, ASME Symposium on Measurement in Unsteady Flow, Worcester, Massachusetts, May 1962, pp. 85-89, T15-19-1962.
18. Sparks, C. R., Pulsation Effects on Flow Metering of Compressible and Non-Compressible Fluids, Annual Symposium on Instrumentation for Process Industries, 17th Proceeding, 1962, pp. 42-46.
19. Strasberg, M., Measurements of the Static and Total-Head Pressures in a Turbulent Wake, Boeing Turbine Division library file No. ST 81, December 1963.
20. Taback, I., The Response of Pressure Measuring System to Oscillating Pressures, NACA TN 1819 (February 1949).
21. Ury, J. F., "Pulsation Errors of Rotameters", Israel Journal of Technology, Vol. 1., No. 1, July 1963, pp. 19-31.
22. Walshe, D. E. and Garner, H. C., Usefulness of Various Pressure Probes in Fluctuating Low-Speed Flow, Aeronautical Research Council, A.R.C. 21, 714, February 1960.

REFERENCES (Continued)

23. Weidemann, Hans, Inertia of Dynamic Pressure Arrays, NACA TM 998, July 1940.
24. Wildhack, W. A., Pressure Drop in Tubing in Aircraft Instrument Installations, NACA TN 593, February 1937.
25. Williams, T. J., Pulsation Errors in Manometer Gages, ASME paper 55-A-92, January 1955.
26. Stickney, T. M., Recovery and Time Response Characteristics of Six Thermocouple Probes in Subsonic and Supersonic Flow, NACA TN 3455, Figure 4a, July 1955.
27. Moffat, R. J., Gas Temperature Measurement, GMR-329, pp. 19-23.
28. Glawe, Simmons, and Stickney, Radiation and Recovery Corrections and Time Constants of Several Chromel-Alumel Thermocouple Probes in High-Temperature, High-Velocity Gas Streams, NACA Tech. Note 3766, p. 4.
29. Moffat, R. J., Gas Temperature Measurement, GMR-329, p. 28.

(U) APPENDIX IX

COMPUTER PRINTOUT OF DIFFUSER
DATA — STATIC PRESSURES

SUMMARY

This appendix contains the static-pressure measurements on the sidewalls of the diffuser in the vaneless space, the semivaneless space, and the channels for the 8-vane-island diffuser configurations that were tested. Only the data necessary for analysis are presented.

Since this appendix supplements the data of Section 6, the line number, which locates the test point on the speed line, is given to facilitate cross referencing. Line 3 is near surge airflow and Line 7 is near maximum airflow as shown in Figure 105. The data are presented in tabular form and the location of each pressure tap with respect to the vanes is shown in Figures 106 through 114. The sketch shows the basic DI-1 configuration in all cases. The dashed lines show the surfaces that deviated from the DI-1 configuration.

The pressures given are in psia and are not corrected to a standard day. The δ correction is listed for each test on the respective computer printout. The speed given is corrected ($N/\sqrt{\theta}$) in rpm, and airflows are corrected ($W\sqrt{\theta/\delta}$) in pounds per second. Inlet guide vane (IGV) settings are in degrees, and throat areas are given in percent of design throat area.

Some taps were covered by the diffuser islands when vane configurations were changed. Although these measurements were recorded, and shown on the printout, their location is not shown on the figures. These pressures should be disregarded.

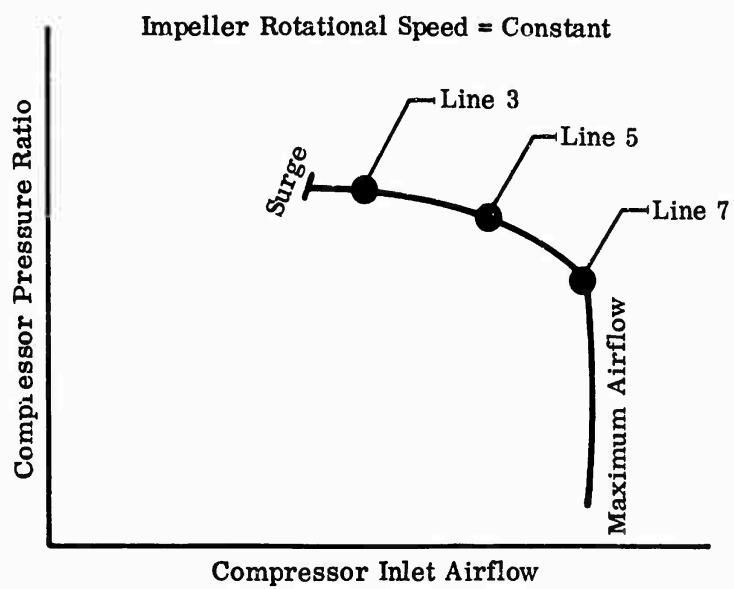


Figure 105. Test Points.

TEST NO. 3306 F SPEED = 50000 AIR FLOW = 2.36
IGV = 0 THROAT AREA = 100% RADIUS RATIO = 1.10
LINE NO. 5 $\delta = 1.000$

ALL PRESSURES ARE IN PSIA

[illegible]

TEST NO. 3339	SPEED = 50000	AIR FLOW = 2.45
IGV = REMOVED	THRUST AREA = 100%	RADIUS RATIO = 1.06
LINE NO. 3	$\delta = 0.989$	

ALL PRESSURES ARE IN PSIA

[illegible]

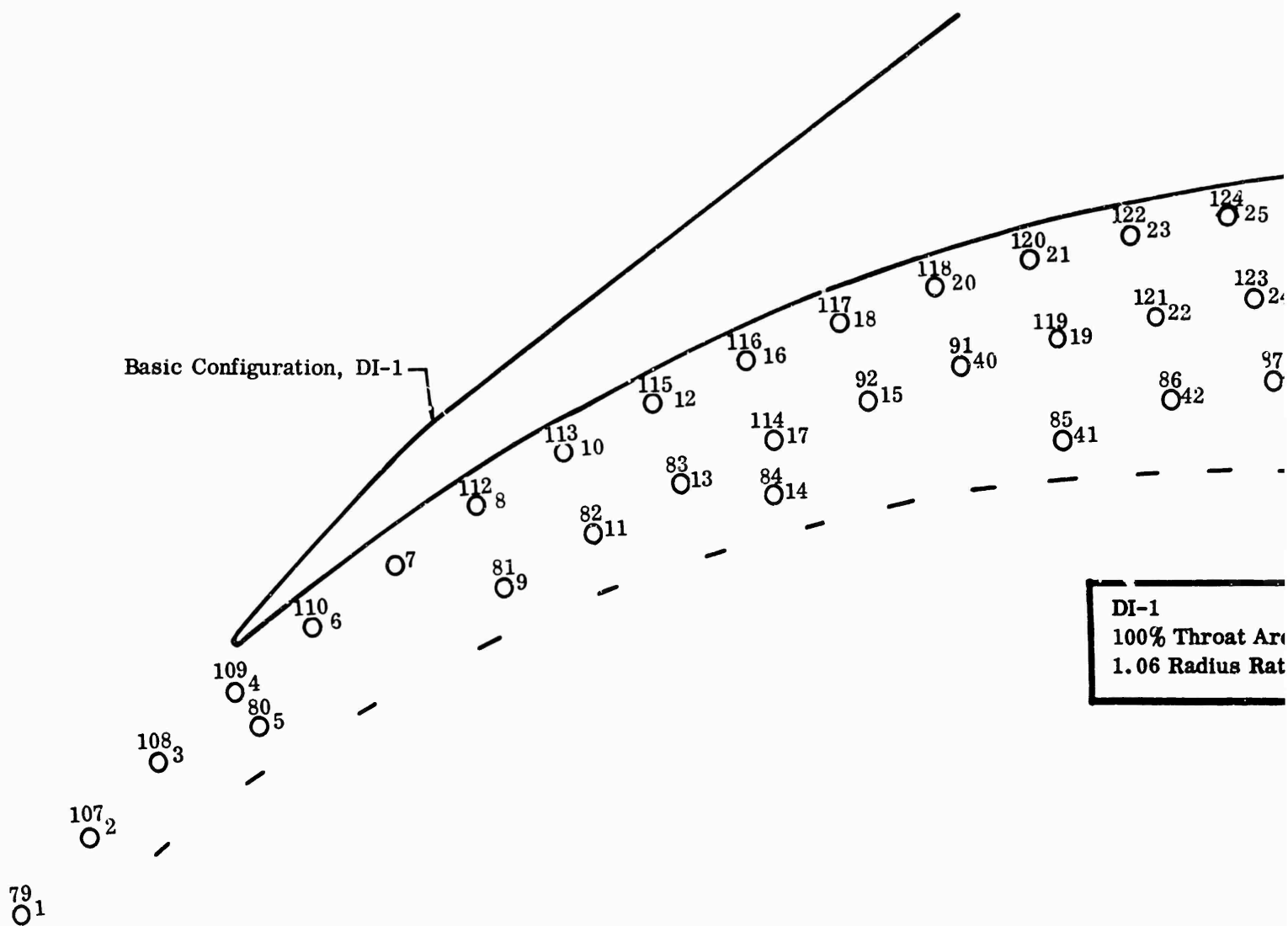
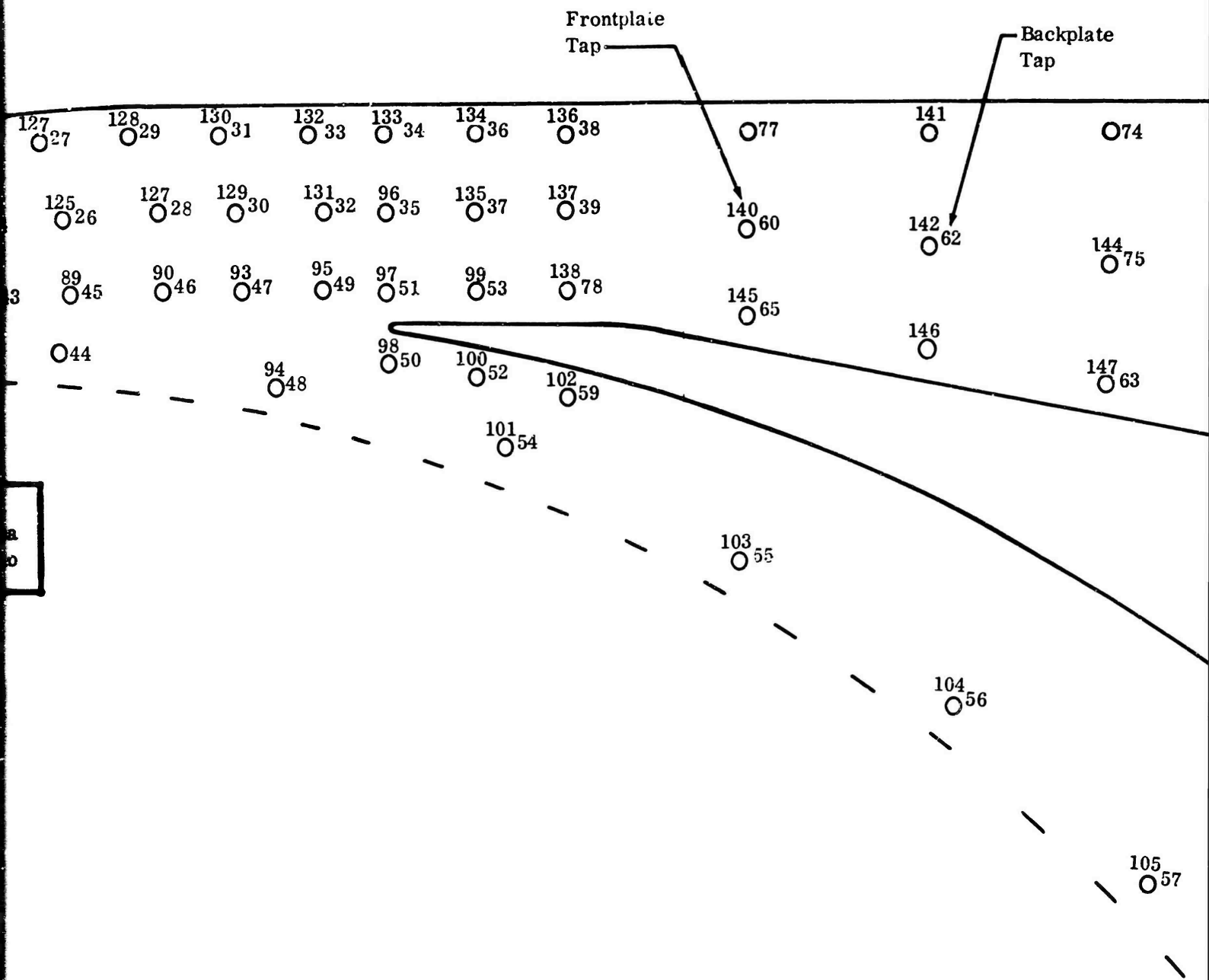
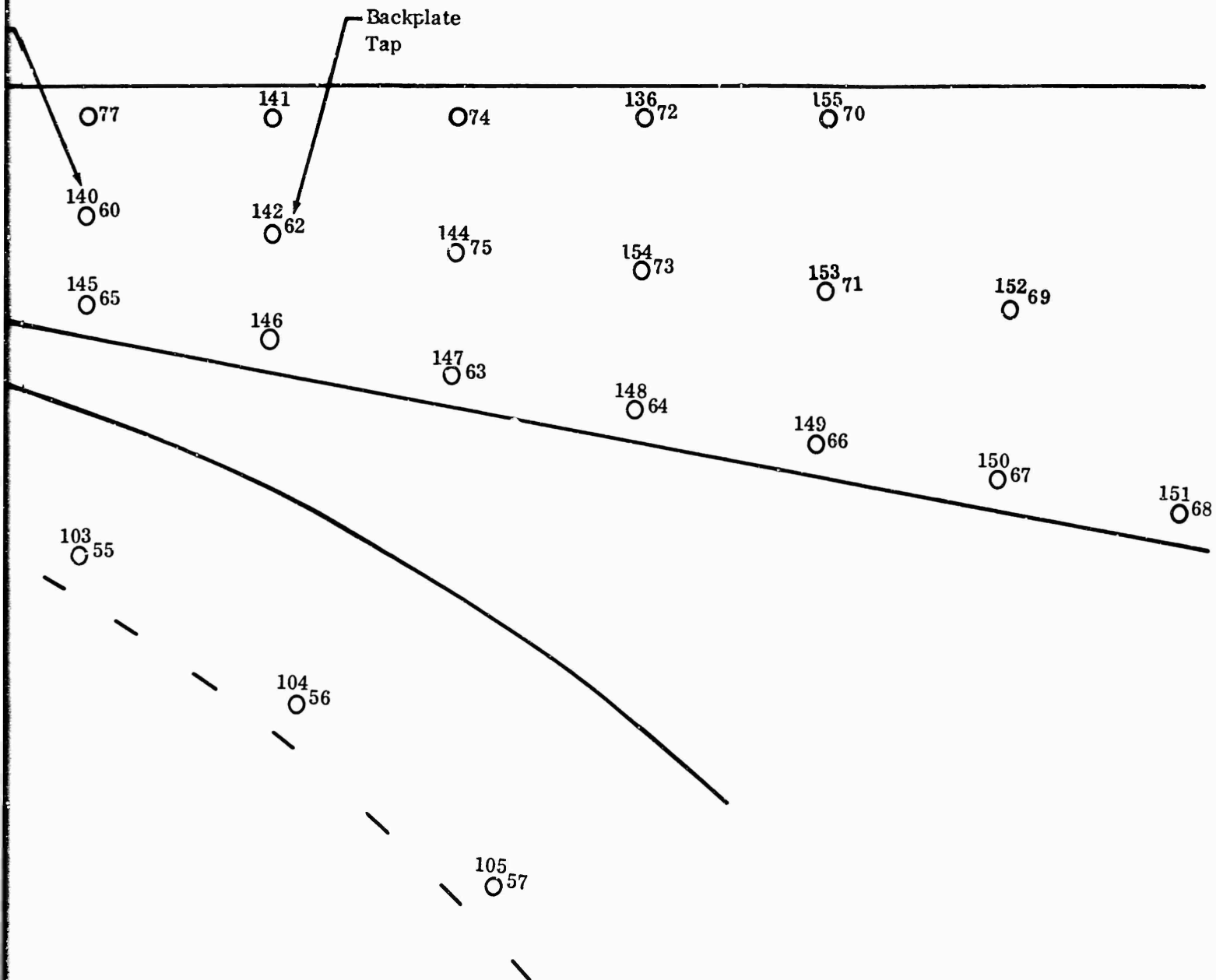


Figure 106. Diffuser Static-Pressure Instrumentation, DI-1.





TEST NO. 3309 F SPEED = 5000 AIR FLOW = 2.48
IGV = 0 THROAT AREA = 100' RADIUS RATIO = 1.10
LINE NO. 3 $\delta = 0.998$

ALL PRESSURES ARE IN PSIA

TAP NO.	STATIC PRESSURE	TAP NO.	STATIC PRESSURE	TAP NO.	STATIC PRESSURE	TAP NO.	STATIC PRESSURE	TAP NO.	STATIC PRESSURE	TAP NO.	STATIC PRESSURE
1	66.3	2	66.5	3	66.5	4	67.2	5	63.9	6	66.2
7	64.3	8	73.4	9	68.8	10	66.1	11	60.4	12	67.8
13	64.7	14	62.8	15	67.4	16	71.6	17	66.1	18	71.8
19	70.3	20	72.8	21	74.6	22	71.6	23	75.7	24	72.1
25	77.2	26	22.8	27	76.6	28	76.2	29	80.3	30	74.7
31	79.2	32	75.3	33	80.2	34	77.8	35	73.9	36	72.6
37	69.5	38	80.7	39	81.8	40	68.6	41	64.2	42	65.5
43	67.5	44	64.8	45	67.1	46	0.0	47	71.5	48	69.9
48	65.5	49	70.8	50	65.1	51	68.9	52	62.7	53	66.5
54	63.2	55	55.4	56	64.7	57	64.7	58	64.7	59	76.9
60	89.5	62	95.7	63	109.0	64	115.5	65	88.8	66	119.1
67	120.6	68	123.1	69	121.6	70	120.8	71	119.0	72	37.1
73	114.7	74	47.7	75	107.8	77	90.4	78	0.0	79	83.9
79	66.8	80	62.4	81	72.5	82	49.8	83	64.2	84	32.2
85	64.2	86	66.7	87	69.1	88	23.3	89	0.0	90	77.0
91	70.0	92	67.7	93	73.0	94	65.8	95	0.0	96	0.0
97	71.7	98	68.8	99	0.0	99	71.1	100	67.9	102	78.6
104	0.0	105	64.7	106	65.1	107	66.6	108	66.5	109	23.1
110	67.5	112	76.1	113	0.0	114	38.4	115	70.2	116	73.2
117	73.6	118	75.2	119	71.3	120	75.6	121	73.0	122	79.1
123	75.3	124	79.6	125	74.1	126	69.1	127	78.7	128	80.8
129	77.1	130	79.5	132	82.1	133	79.6	134	74.9	135	72.7
136	77.9	137	0.0	140	90.7	141	95.6	142	97.9	144	108.5
145	92.0	146	97.0	147	109.4	148	115.5	149	119.5	150	122.7
151	123.4	152	122.1	153	119.2	154	115.6	155	120.1	156	115.3
157	125.7	158	126.2	159	126.4	160	126.2				

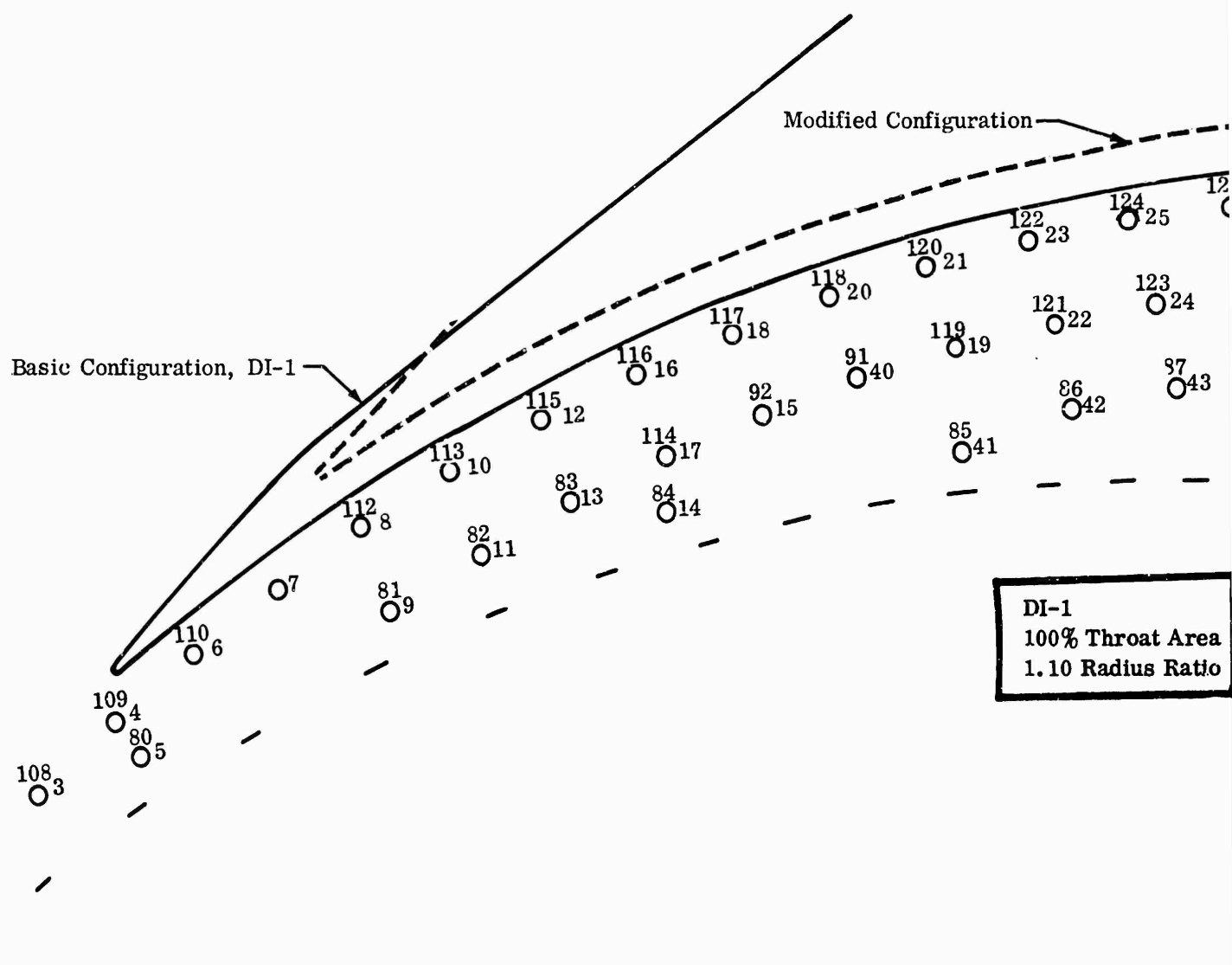


Figure 107. Diffuser Static-Pressure Instrumentation, DI-1.

Backplate
Tap

140
○₆₀

142
○₆₂

144
○₇₅

154
○₇₃

153
○₇₁

152
○₆₉

145
○₆₅

146
○

147
○₆₃

148
○₆₄

149
○₆₆

150
○₆₇

151
○₆₈

103
○₅₅

104
○₅₆

105
○₅₇

TEST NO. 3309 G SPEED = 50000 AIR FLOW = 2.48
IGV = 0 THROAT AREA = 125 % RADIUS RATIO = 1.06
LINE NO. 5 $\delta = 1.00$

ALL PRESSURES ARE IN PSIA

TAP NO.	STATIC PRESSURE	TAP NO.	STATIC PRESSURE	TAP NO.	STATIC PRESSURE	TAP NO.	STATIC PRESSURE	TAP NO.	STATIC PRESSURE
1	53.4	2	55.0	3	55.2	4	75.3	5	64.8
7	48.9	8	52.1	9	48.5	10	56.8	11	53.3
13	56.0	14	52.5	15	56.7	16	60.3	17	53.4
19	57.7	20	60.6	21	62.0	22	59.6	23	63.5
25	65.6	26	22.3	27	64.5	28	64.7	29	67.6
31	72.1	32	80.6	33	79.8	34	86.8	35	86.8
37	90.0	38	91.9	39	90.4	40	56.3	41	51.6
43	56.4	44	54.2	45	57.1	46	0.0	47	59.1
48	67.2	49	80.0	50	68.5	51	89.9	52	47.5
54	43.7	55	53.9	56	55.0	57	54.5	58	59.6
60	95.6	62	101.4	63	105.1	64	107.1	65	96.0
67	109.2	68	107.7	69	111.4	70	110.1	71	109.9
73	107.8	74	105.4	75	105.2	77	96.8	78	0.0
79	53.7	80	64.4	81	47.3	82	44.8	83	54.9
85	51.6	86	54.5	87	57.5	88	21.3	89	0.0
91	57.4	92	55.5	93	68.0	94	65.6	95	0.0
97	90.4	98	69.9	99	0.0	99	92.3	100	48.3
104	0.0	105	54.5	106	59.0	107	55.0	108	54.8
110	46.7	112	52.0	113	0.0	114	32.3	115	61.6
117	61.4	118	62.4	119	58.3	120	63.0	121	60.3
123	63.3	124	67.5	125	61.9	126	54.3	127	66.2
129	72.2	130	72.1	132	80.9	133	86.9	134	90.7
136	92.1	137	0.0	140	96.2	141	102.0	142	102.5
145	96.7	146	101.9	147	104.7	148	104.1	149	107.1
151	111.3	152	111.5	153	110.0	154	108.2	155	110.1
157	114.4	158	114.8	159	115.1	160	115.0		

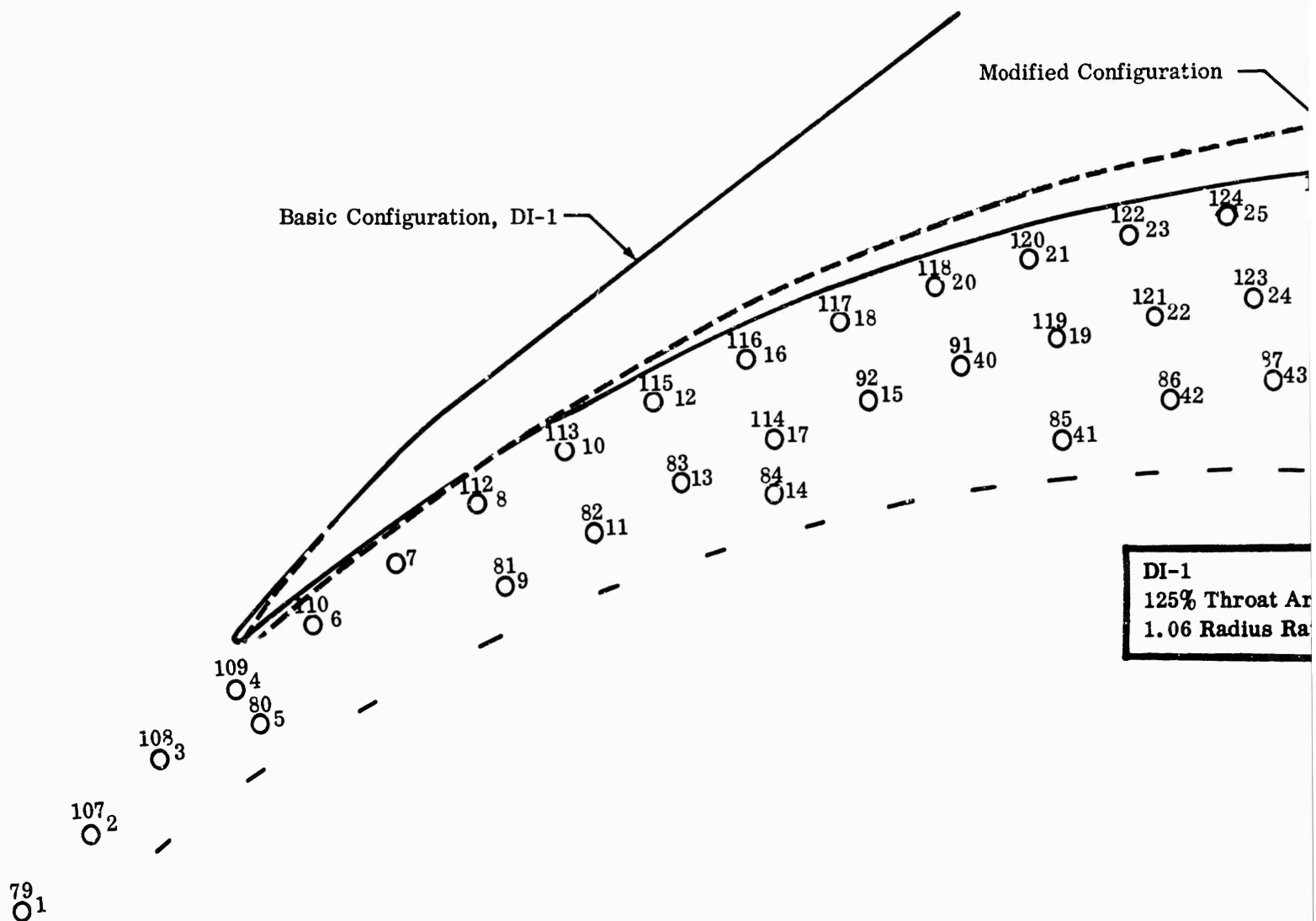
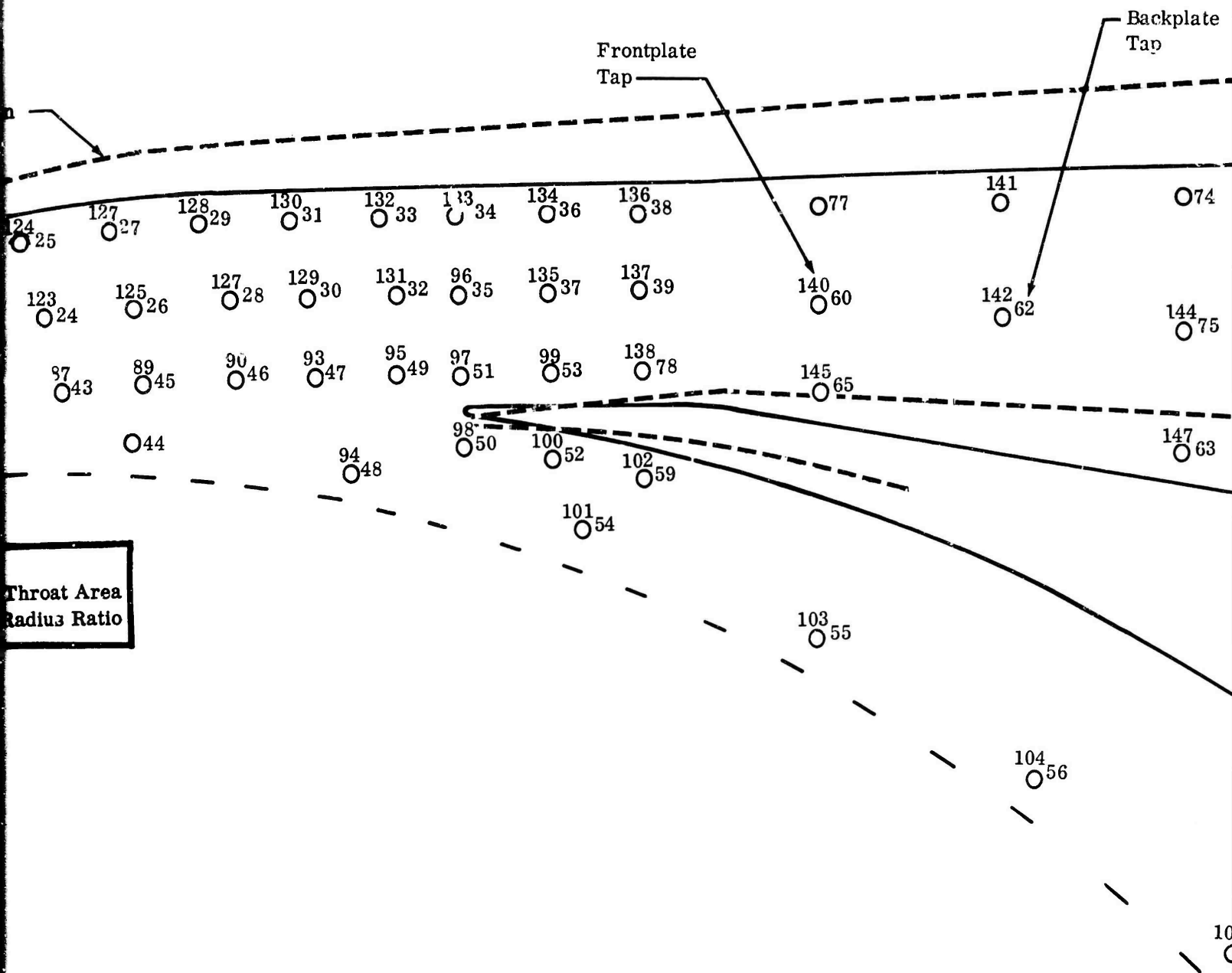
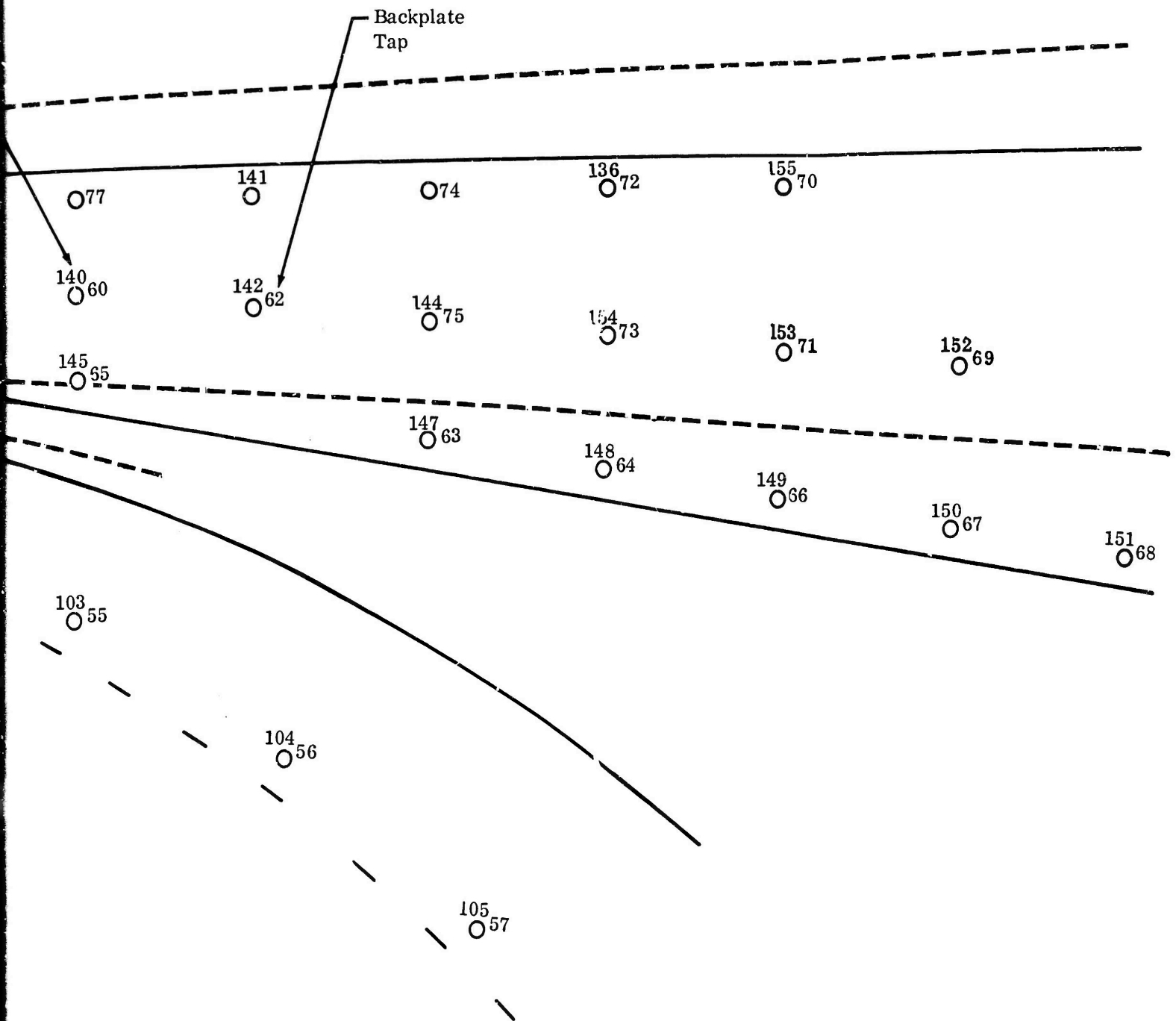


Figure 108. Diffuser Static-Pressure Instrumentation, DI-1.





TEST NO. 3334	SPEED = 50000	AIR FLOW = 2.35
IGV = REMOVED	THRGT AREA = 100 %	RADIUS RATIO = 1.06
LINE NO. 3	$\delta = 0.990$	

ALL PRESSURES ARE IN PSIA

[illegible]

TEST NO. 3334	SPEED = 50000	AIR FLOW = 2.41
IGV = REMOVED	THROAT AREA = 100 TM	RADIUS RATIO = 1.06
LINE NO. 5	$\delta = 0.990$	

ALL PRESSURES ARE IN PSIA

[illegible]

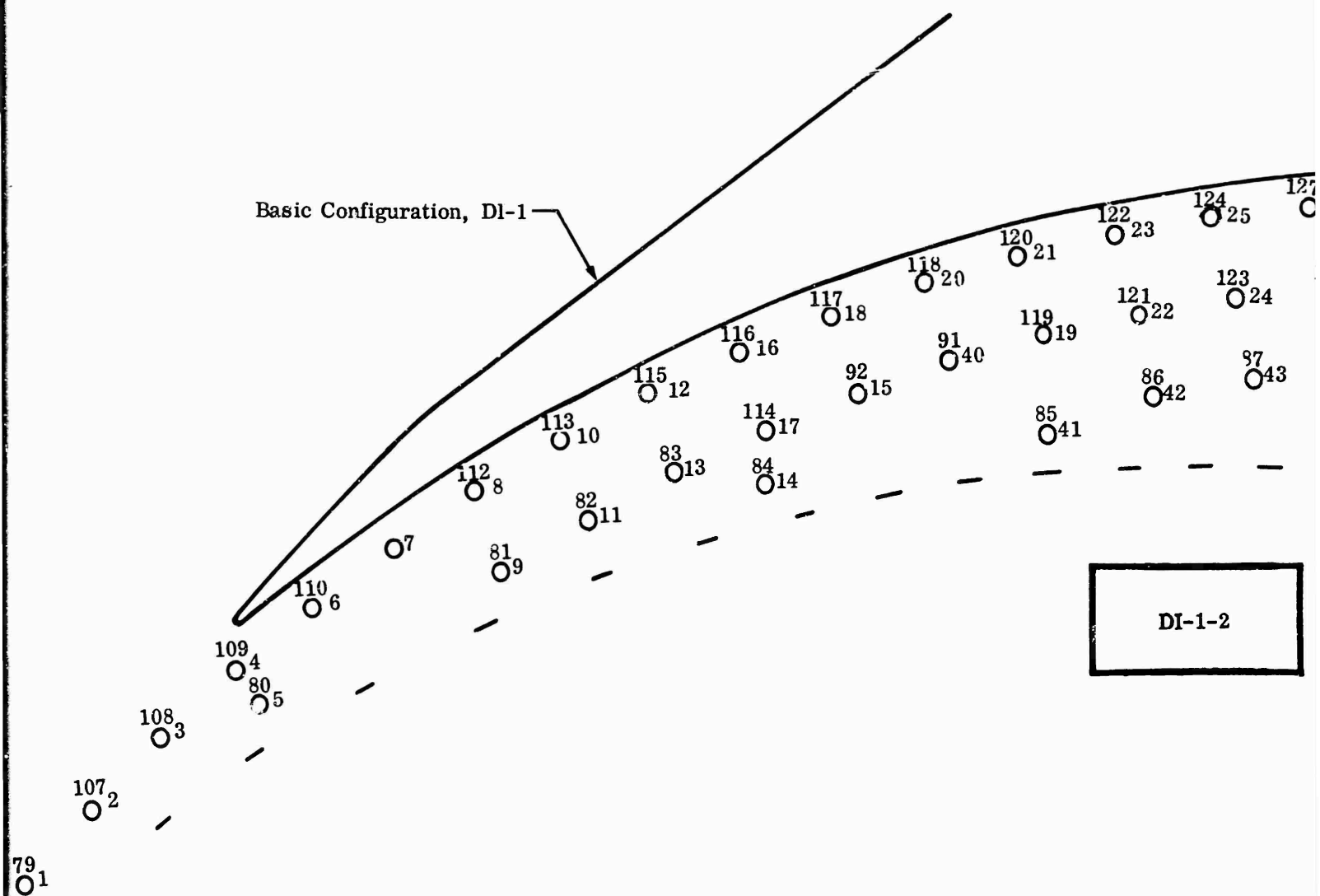
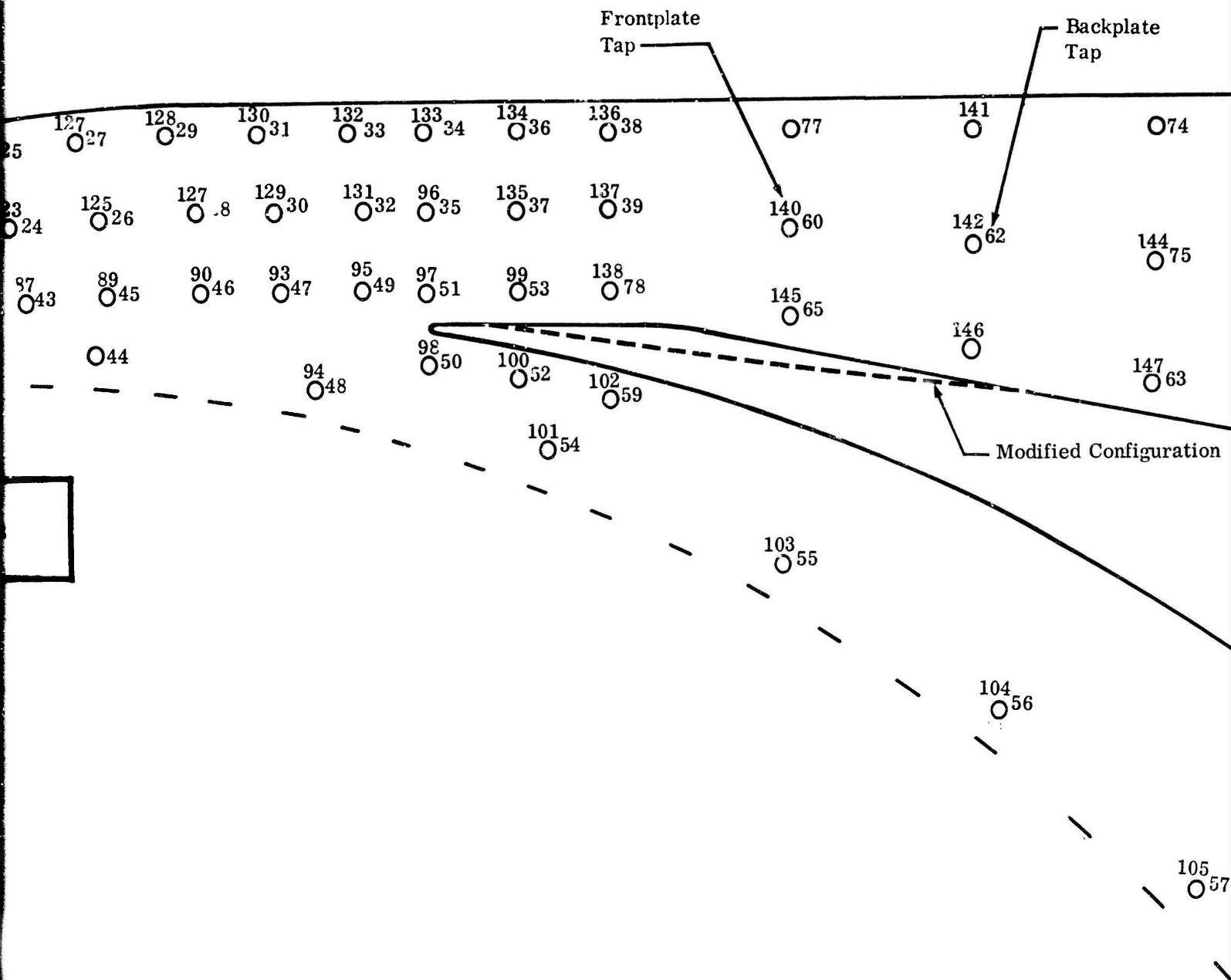
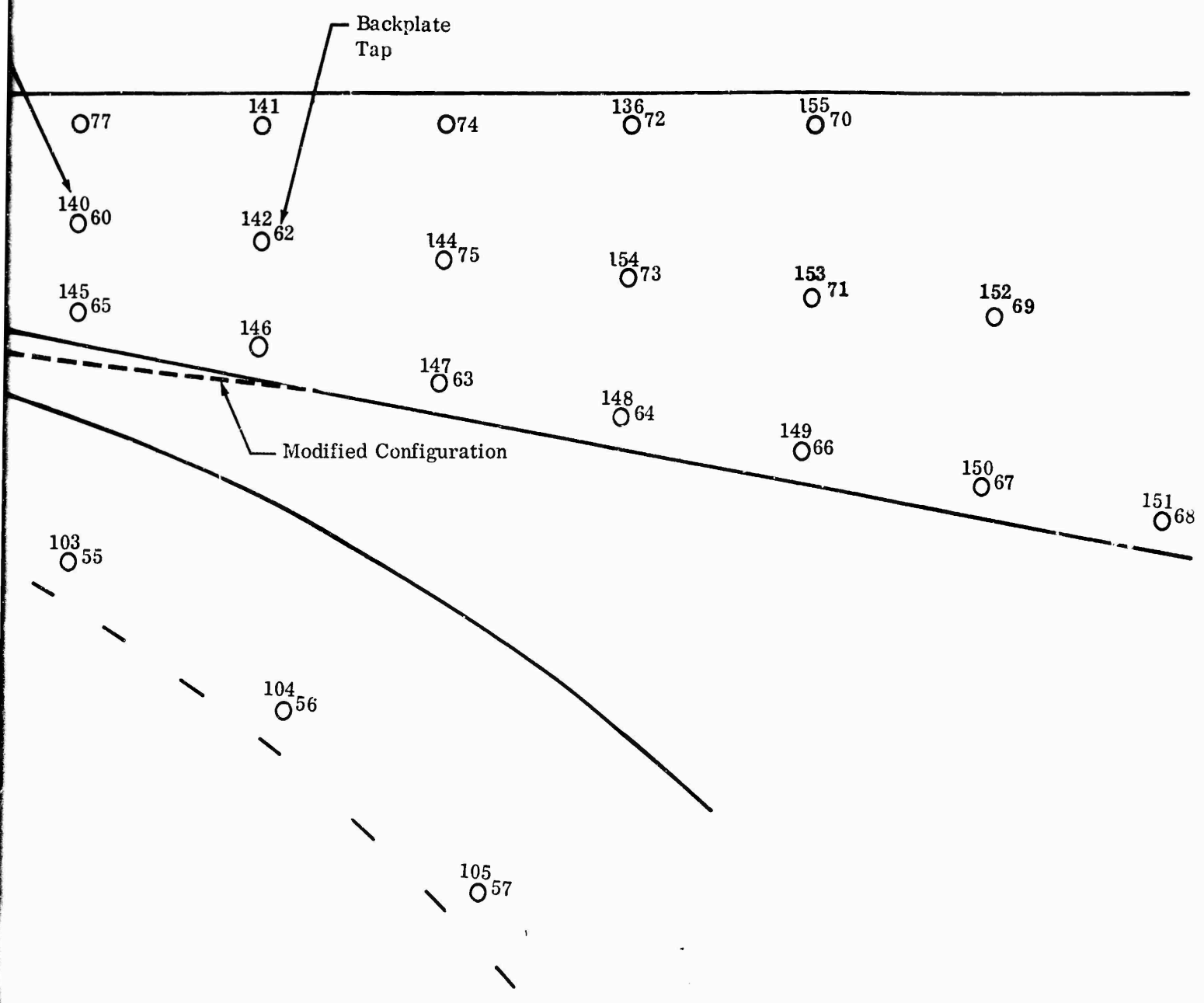


Figure 109. Diffuser Static-Pressure Instrumentation, DI-1-2.





TEST NO. 3340	SPEED = 50000	AIR FLOW = 2.43
IGV = REMOVED	THROAT AREA = 100%	RADIUS RATIO = 1.06
LINE NO. 3	$\delta = 0.990$	

ALL PRESSURES ARE IN PSIA

TAP NO.	STATIC PRESSURE	TAP NO.	STATIC PRESSURE	TAP NO.	STATIC PRESSURE	TAP NO.	STATIC PRESSURE	TAP NO.	STATIC PRESSURE	TAP NO.	STATIC PRESSURE	TAP NO.	STATIC PRESSURE
2	66.2	3	64.5	4	62.5	5	62.0	6	79.6	7	72.6		
8	71.3	9	63.9	10	71.2	11	66.5	13	66.5	15	67.6		
17	61.6	19	70.1	20	73.0	21	75.3	24	74.3	25	79.9		
27	80.3	28	75.2	29	82.0	31	77.9	32	65.5	33	68.8		
34	68.8	35	95.0	35	67.1	36	88.2	37	87.4	38	97.6		
39	95.6	40	68.4	41	63.9	42	66.4	43	69.2	44	71.5		
45	72.1	46	70.5	47	67.4	48	63.0	49	63.7	50	68.2		
51	72.0	52	67.3	53	83.8	54	63.1	55	64.2	56	66.9		
57	64.2	58	63.7	59	67.5	60	104.0	62	114.2	63	120.3		
64	124.3	65	105.3	66	126.3	68	126.7	69	128.1	70	126.3		
71	126.7	72	124.1	73	124.3	74	120.0	75	120.6	77	107.5		
78	95.4	84	68.1	115	0.0	118	72.3	122	94.8	127	74.2		
156	0.0	157	130.0	158	130.6	159	130.8	160	130.7				

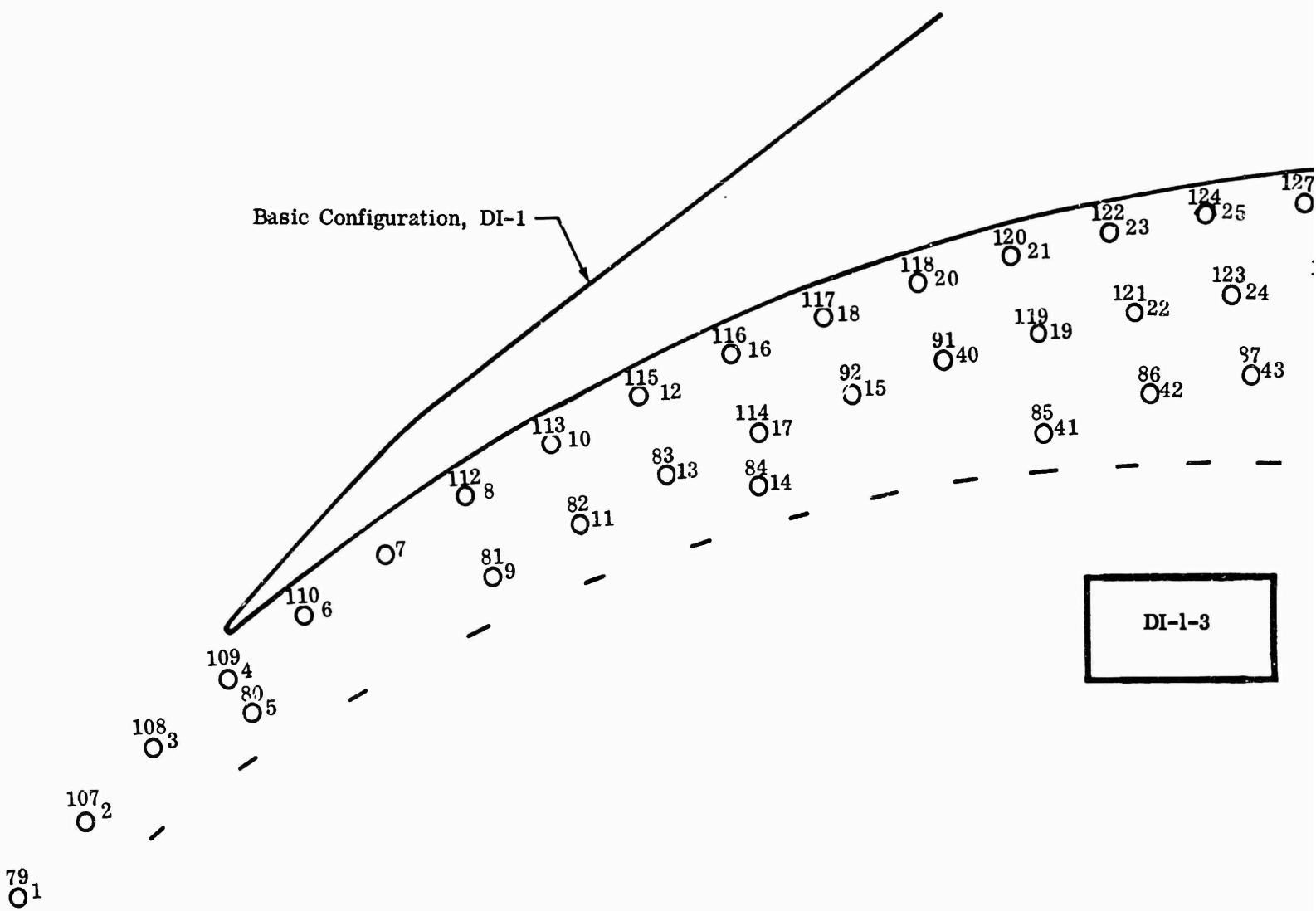
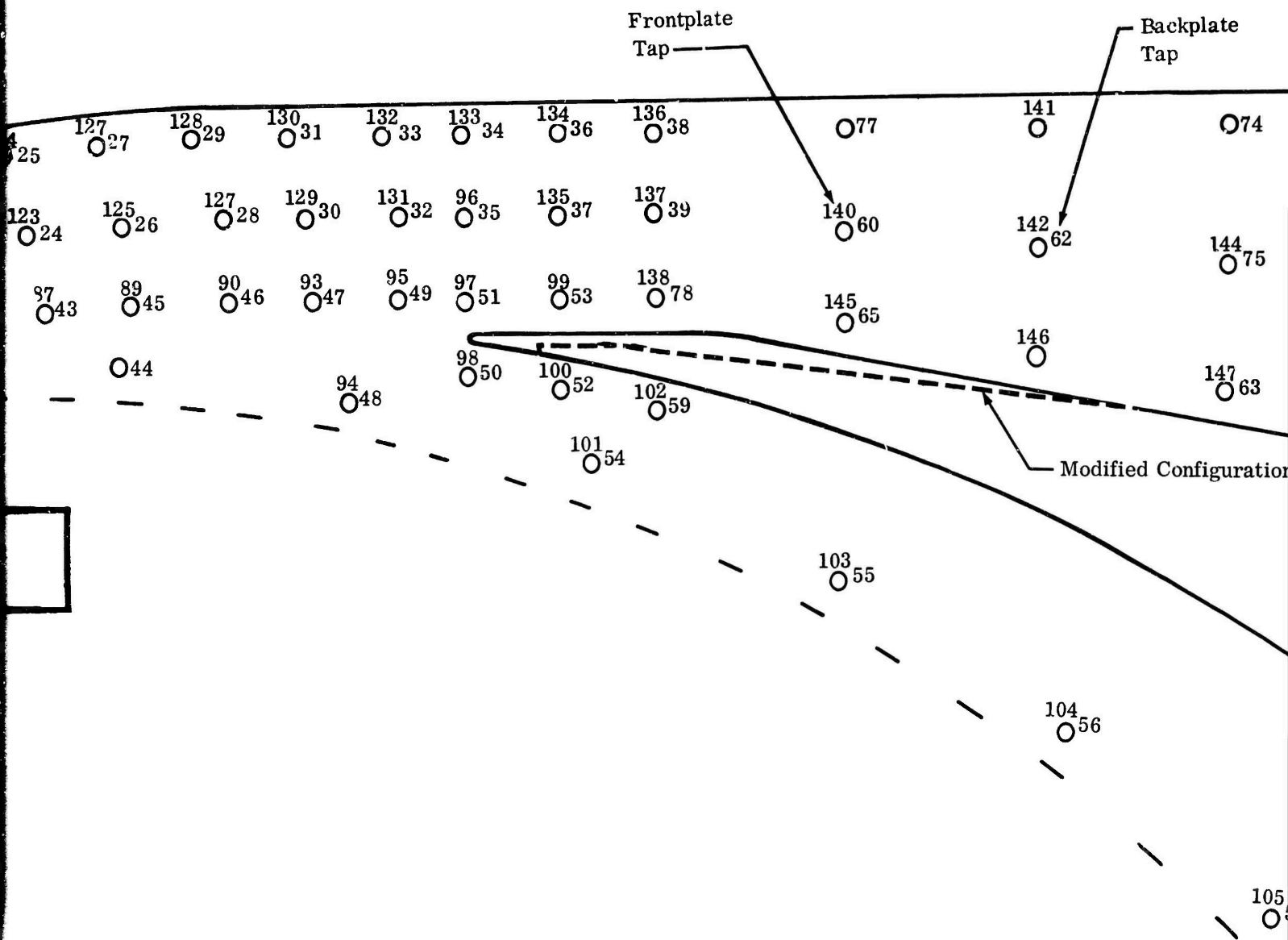
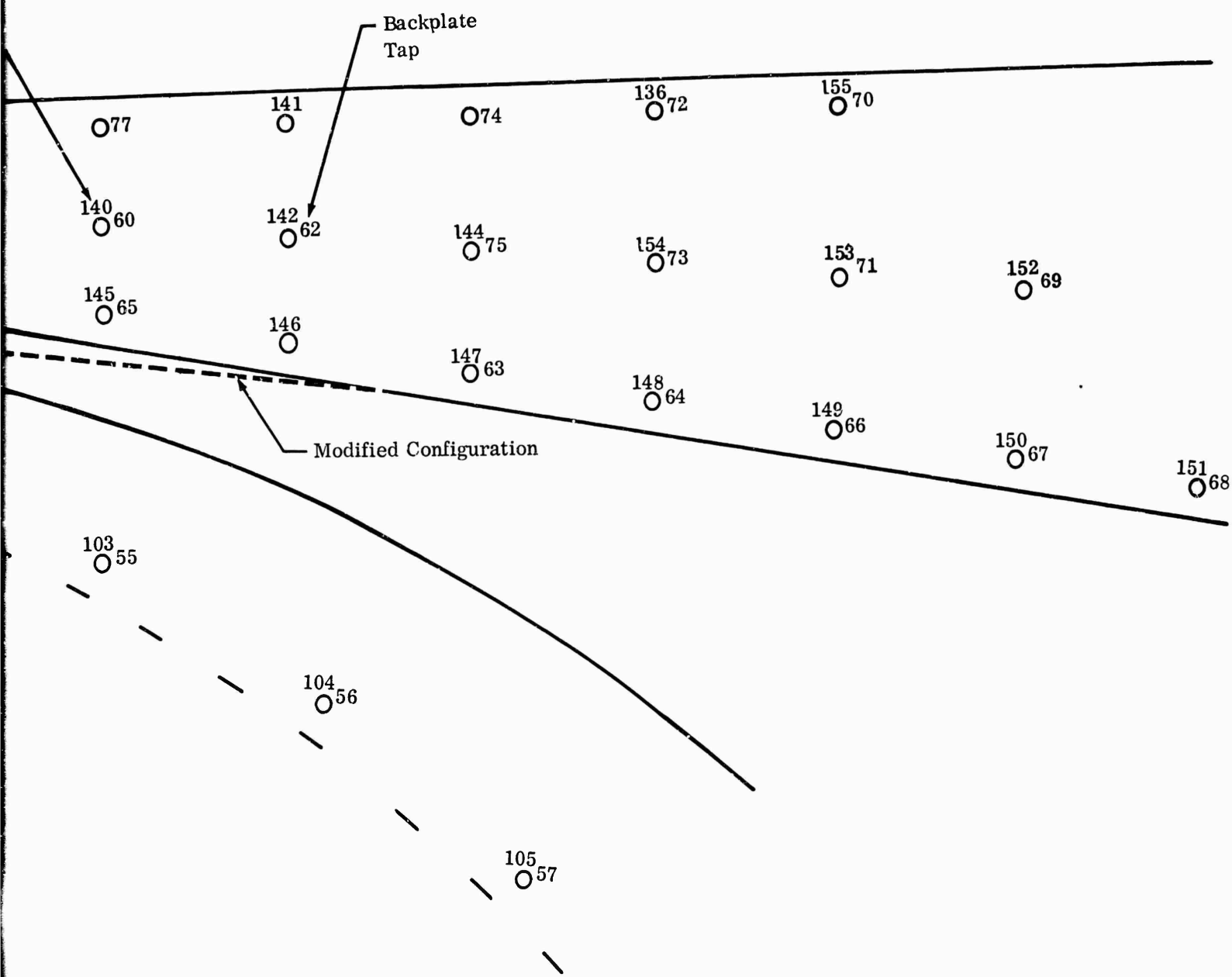


Figure 110. Diffuser Static-Pressure Instrumentation, DI-1-3.





TEST NO. 3310A	SPEED = 50000	AIR FLOW = 2.38
IGV = 0	THROAT AREA = 100%	RADIUS RATIO = 1.06
LINE NO. 3.1	$\delta = 0.997$	

ALL PRESSURES ARE IN PSIA

TAP NO.	STATIC PRESSURE	TAP NO.	STATIC PRESSURE	TAP NO.	STATIC PRESSURE	TAP NO.	STATIC PRESSURE	TAP NO.	STATIC PRESSURE	TAP NO.	STATIC PRESSURE
1	64.6	2	62.7	3	59.3	4	77.0	5	70.9	6	61.9
7	65.0	8	70.7	9	64.0	10	70.9	11	65.3	12	70.8
13	64.5	14	61.5	15	65.0	16	69.4	17	61.2	18	69.1
19	70.1	20	73.8	21	76.0	22	72.0	23	77.3	24	71.7
25	78.1	26	20.4	27	77.6	28	68.5	29	70.9	30	0.0
31	67.2	32	62.9	33	62.3	34	84.8	35	87.0	36	91.8
37	91.1	38	95.1	39	92.9	40	67.0	41	63.2	42	65.5
43	66.9	44	62.3	45	67.5	45	0.0	46	64.9	47	60.6
48	57.3	49	71.4	50	78.0	51	91.2	52	62.9	53	90.9
54	60.1	55	61.9	56	0.0	57	65.1	58	72.1	59	62.4
60	104.2	62	113.2	63	117.4	64	120.4	65	105.2	66	123.1
67	124.8	68	126.1	69	126.3	70	124.5	71	124.7	72	122.3
73	122.3	74	118.7	75	118.8	77	105.4	77	0.0	78	91.2
79	65.0	80	65.0	81	64.9	82	56.2	83	64.4	84	29.4
85	62.7	86	66.9	87	68.3	88	23.4	89	0.0	90	87.6
91	68.1	92	64.9	93	63.9	94	56.7	95	0.0	96	0.0
97	90.4	98	80.7	99	0.0	99	92.9	100	64.6	102	65.9
104	62.2	105	65.0	106	72.5	107	63.3	108	59.8	109	35.4
110	62.5	112	70.9	113	0.0	114	39.4	115	73.2	116	72.2
117	73.0	118	76.0	119	71.2	120	76.8	121	73.3	122	80.0
123	75.1	124	80.1	125	74.6	126	66.7	127	71.4	128	74.2
129	65.4	130	66.9	132	64.0	133	83.0	134	92.3	135	93.0
136	95.3	137	0.0	140	105.0	141	113.6	142	114.7	144	119.5
145	105.3	146	113.4	147	118.4	148	120.3	149	122.0	150	124.7
151	126.0	152	126.4	153	124.9	154	122.8	155	124.7	156	122.4
157	128.9	158	129.3	159	129.4	160	129.5				

TEST NO. 331CA

RADIUS RATIO = 1.06

THROAT AREA = 100%

$$\delta = 1.00$$

ALL PRESSURES ARE IN PSIA

[illegible]

TEST NO. 3320 SPEED = 50000 AIR FLOW = 2.23
IGV = 0 THROAT AREA = 100 % RADIUS RATIO = 1.06
LINE NO. 3 $\delta = 0.990$

ALL PRESSURES ARE IN PSIA

[illegible]

TEST NO. 3331	SPEED = 50000	AIR FLOW = 2.41
IGV = REMOVED	THROAT AREA = 100%	RADIUS RATIO = 1.06
LINE NO. 3	$\delta \approx 1.003$	

ALL PRESSURES ARE IN PSIA

TAP NO.	STATIC PRESSURE	TAP NO.	STATIC PRESSURE	TAP NO.	STATIC PRESSURE	TAP NO.	STATIC PRESSURE	TAP NO.	STATIC PRESSURE	TAP NO.	STATIC PRESSURE	TAP NO.	STATIC PRESSURE	TAP NO.	STATIC PRESSURE	TAP NO.	STATIC PRESSURE	TAP NO.	STATIC PRESSURE	TAP NO.	STATIC PRESSURE	TAP NO.	STATIC PRESSURE	TAP NO.	STATIC PRESSURE	TAP NO.	STATIC PRESSURE	TAP NO.	STATIC PRESSURE	TAP NO.	STATIC PRESSURE	TAP NO.	STATIC PRESSURE	TAP NO.	STATIC PRESSURE	TAP NO.	STATIC PRESSURE	TAP NO.	STATIC PRESSURE	TAP NO.	STATIC PRESSURE	TAP NO.	STATIC PRESSURE	TAP NO.	STATIC PRESSURE	TAP NO.	STATIC PRESSURE	TAP NO.	STATIC PRESSURE	TAP NO.	STATIC PRESSURE	TAP NO.	STATIC PRESSURE	TAP NO.	STATIC PRESSURE	TAP NO.	STATIC PRESSURE	TAP NO.	STATIC PRESSURE	TAP NO.	STATIC PRESSURE	TAP NO.	STATIC PRESSURE	TAP NO.	STATIC PRESSURE	TAP NO.	STATIC PRESSURE	TAP NO.	STATIC PRESSURE	TAP NO.	STATIC PRESSURE	TAP NO.	STATIC PRESSURE	TAP NO.	STATIC PRESSURE	TAP NO.	STATIC PRESSURE	TAP NO.	STATIC PRESSURE	TAP NO.	STATIC PRESSURE	TAP NO.	STATIC PRESSURE	TAP NO.	STATIC PRESSURE	TAP NO.	STATIC PRESSURE	TAP NO.	STATIC PRESSURE	TAP NO.	STATIC PRESSURE	TAP NO.	STATIC PRESSURE	TAP NO.	STATIC PRESSURE	TAP NO.	STATIC PRESSURE	TAP NO.	STATIC PRESSURE	TAP NO.	STATIC PRESSURE	TAP NO.	STATIC PRESSURE	TAP NO.	STATIC PRESSURE	TAP NO.	STATIC PRESSURE	TAP NO.	STATIC PRESSURE	TAP NO.	STATIC PRESSURE	TAP NO.	STATIC PRESSURE	TAP NO.	STATIC PRESSURE	TAP NO.	STATIC PRESSURE	TAP NO.	STATIC PRESSURE	TAP NO.	STATIC PRESSURE	TAP NO.	STATIC PRESSURE	TAP NO.	STATIC PRESSURE	TAP NO.	STATIC PRESSURE	TAP NO.	STATIC PRESSURE	TAP NO.	STATIC PRESSURE	TAP NO.	STATIC PRESSURE	TAP NO.	STATIC PRESSURE	TAP NO.	STATIC PRESSURE	TAP NO.	STATIC PRESSURE	TAP NO.	STATIC PRESSURE	TAP NO.	STATIC PRESSURE	TAP NO.	STATIC PRESSURE	TAP NO.	STATIC PRESSURE	TAP NO.	STATIC PRESSURE	TAP NO.	STATIC PRESSURE	TAP NO.	STATIC PRESSURE	TAP NO.	STATIC PRESSURE	TAP NO.	STATIC PRESSURE	TAP NO.	STATIC PRESSURE	TAP NO.	STATIC PRESSURE	TAP NO.	STATIC PRESSURE	TAP NO.	STATIC PRESSURE	TAP NO.	STATIC PRESSURE	TAP NO.	STATIC PRESSURE	TAP NO.	STATIC PRESSURE	TAP NO.	STATIC PRESSURE	TAP NO.	STATIC PRESSURE	TAP NO.	STATIC PRESSURE	TAP NO.	STATIC PRESSURE	TAP NO.	STATIC PRESSURE	TAP NO.	STATIC PRESSURE	TAP NO.	STATIC PRESSURE	TAP NO.	STATIC PRESSURE	TAP NO.	STATIC PRESSURE	TAP NO.	STATIC PRESSURE	TAP NO.	STATIC PRESSURE	TAP NO.	STATIC PRESSURE	TAP NO.	STATIC PRESSURE	TAP NO.	STATIC PRESSURE	TAP NO.	STATIC PRESSURE	TAP NO.	STATIC PRESSURE	TAP NO.	STATIC PRESSURE	TAP NO.	STATIC PRESSURE	TAP NO.	STATIC PRESSURE	TAP NO.	STATIC PRESSURE	TAP NO.	STATIC PRESSURE	TAP NO.	STATIC PRESSURE	TAP NO.	STATIC PRESSURE	TAP NO.	STATIC PRESSURE	TAP NO.	STATIC PRESSURE	TAP NO.	STATIC PRESSURE	TAP NO.	STATIC PRESSURE	TAP NO.	STATIC PRESSURE	TAP NO.	STATIC PRESSURE	TAP NO.	STATIC PRESSURE	TAP NO.	STATIC PRESSURE	TAP NO.	STATIC PRESSURE	TAP NO.	STATIC PRESSURE	TAP NO.	STATIC PRESSURE	TAP NO.	STATIC PRESSURE	TAP NO.	STATIC PRESSURE	TAP NO.	STATIC PRESSURE	TAP NO.	STATIC PRESSURE	TAP NO.	STATIC PRESSURE	TAP NO.	STATIC PRESSURE	TAP NO.	STATIC PRESSURE	TAP NO.	STATIC PRESSURE	TAP NO.	STATIC PRESSURE	TAP NO.	STATIC PRESSURE	TAP NO.	STATIC PRESSURE	TAP NO.	STATIC PRESSURE	TAP NO.	STATIC PRESSURE	TAP NO.	STATIC PRESSURE	TAP NO.	STATIC PRESSURE	TAP NO.	STATIC PRESSURE	TAP NO.	STATIC PRESSURE	TAP NO.	STATIC PRESSURE	TAP NO.	STATIC PRESSURE	TAP NO.	STATIC PRESSURE	TAP NO.	STATIC PRESSURE	TAP NO.	STATIC PRESSURE	TAP NO.	STATIC PRESSURE	TAP NO.	STATIC PRESSURE	TAP NO.	STATIC PRESSURE	TAP NO.	STATIC PRESSURE	TAP NO.	STATIC PRESSURE	TAP NO.	STATIC PRESSURE	TAP NO.	STATIC PRESSURE	TAP NO.	STATIC PRESSURE	TAP NO.	STATIC PRESSURE	TAP NO.	STATIC PRESSURE	TAP NO.	STATIC PRESSURE	TAP NO.	STATIC PRESSURE	TAP NO.	STATIC PRESSURE	TAP NO.	STATIC PRESSURE	TAP NO.	STATIC PRESSURE	TAP NO.	STATIC PRESSURE	TAP NO.	STATIC PRESSURE	TAP NO.	STATIC PRESSURE	TAP NO.	STATIC PRESSURE	TAP NO.	STATIC PRESSURE	TAP NO.	STATIC PRESSURE	TAP NO.	STATIC PRESSURE	TAP NO.	STATIC PRESSURE	TAP NO.	STATIC PRESSURE	TAP NO.	STATIC PRESSURE	TAP NO.	STATIC PRESSURE	TAP NO.	STATIC PRESSURE	TAP NO.	STATIC PRESSURE	TAP NO.	STATIC PRESSURE	TAP NO.	STATIC PRESSURE	TAP NO.	STATIC PRESSURE	TAP NO.	STATIC PRESSURE	TAP NO.	STATIC PRESSURE	TAP NO.	STATIC PRESSURE	TAP NO.	STATIC PRESSURE	TAP NO.	STATIC PRESSURE	TAP NO.	STATIC PRESSURE	TAP NO.	STATIC PRESSURE	TAP NO.	STATIC PRESSURE	TAP NO.	STATIC PRESSURE	TAP NO.	STATIC PRESSURE	TAP NO.	STATIC PRESSURE	TAP NO.	STATIC PRESSURE	TAP NO.	STATIC PRESSURE	TAP NO.	STATIC PRESSURE	TAP NO.	STATIC PRESSURE	TAP NO.	STATIC PRESSURE	TAP NO.	STATIC PRESSURE	TAP NO.	STATIC PRESSURE	TAP NO.	STATIC PRESSURE	TAP NO.	STATIC PRESSURE	TAP NO.	STATIC PRESSURE	TAP NO.	STATIC PRESSURE	TAP NO.	STATIC PRESSURE	TAP NO.	STATIC PRESSURE	TAP NO.	STATIC PRESSURE	TAP NO.	STATIC PRESSURE	TAP NO.	STATIC PRESSURE	TAP NO.	STATIC PRESSURE	TAP NO.	STATIC PRESSURE	TAP NO.	STATIC PRESSURE	TAP NO.	STATIC PRESSURE	TAP NO.	STATIC PRESSURE	TAP NO.	STATIC PRESSURE	TAP NO.	STATIC PRESSURE	TAP NO.	STATIC PRESSURE	TAP NO.	STATIC PRESSURE	TAP NO.	STATIC PRESSURE	TAP NO.	STATIC PRESSURE	TAP NO.	STATIC PRESSURE	TAP NO.	STATIC PRESSURE	TAP NO.	STATIC PRESSURE	TAP NO.	STATIC PRESSURE	TAP NO.	STATIC PRESSURE	TAP NO.	STATIC PRESSURE	TAP NO.	STATIC PRESSURE	TAP NO.	STATIC PRESSURE	TAP NO.	STATIC PRESSURE	TAP NO.	STATIC PRESSURE	TAP NO.	STATIC PRESSURE	TAP NO.	STATIC PRESSURE	TAP NO.	STATIC PRESSURE	TAP NO.	STATIC PRESSURE	TAP NO.	STATIC PRESSURE	TAP NO.	STATIC PRESSURE	TAP NO.	STATIC PRESSURE	TAP NO.	STATIC PRESSURE	TAP NO.	STATIC PRESSURE	TAP NO.	STATIC PRESSURE	TAP NO.	STATIC PRESSURE	TAP NO.	STATIC PRESSURE	TAP NO.	STATIC PRESSURE	TAP NO.	STATIC PRESSURE	TAP NO.	STATIC PRESSURE	TAP NO.	STATIC PRESSURE	TAP NO.	STATIC PRESSURE	TAP NO.	STATIC PRESSURE	TAP NO.	STATIC PRESSURE	TAP NO.	STATIC PRESSURE	TAP NO.	STATIC PRESSURE	TAP NO.	STATIC PRESSURE	TAP NO.	STATIC PRESSURE	TAP NO.	STATIC PRESSURE	TAP NO.	STATIC PRESSURE	TAP NO.	STATIC PRESSURE	TAP NO.	STATIC PRESSURE	TAP NO.	STATIC PRESSURE	TAP NO.	STATIC PRESSURE	TAP NO.	STATIC PRESSURE	TAP NO.	STATIC PRESSURE	TAP NO.	STATIC PRESSURE	TAP NO.	STATIC PRESSURE	TAP NO.	STATIC PRESSURE	TAP NO.	STATIC PRESSURE	TAP NO.	STATIC PRESSURE	TAP NO.	STATIC PRESSURE	TAP NO.	STATIC PRESSURE	TAP NO.	STATIC PRESSURE	TAP NO.	STATIC PRESSURE	TAP NO.	STATIC PRESSURE	TAP NO.	STATIC PRESSURE	TAP NO.	STATIC PRESSURE	TAP NO.	STATIC PRESSURE	TAP NO.	STATIC PRESSURE	TAP NO.	STATIC PRESSURE	TAP NO.	STATIC PRESSURE	TAP NO.	STATIC PRESSURE	TAP NO.	STATIC PRESSURE	TAP NO.	STATIC PRESSURE	TAP NO.	STATIC PRESSURE	TAP NO.	STATIC PRESSURE	TAP NO.	STATIC PRESSURE	TAP NO.	STATIC PRESSURE	TAP NO.	STATIC PRESSURE	TAP NO.	STATIC PRESSURE	TAP NO.	STATIC PRESSURE	TAP NO.	STATIC PRESSURE	TAP NO.	STATIC PRESSURE	TAP NO.	STATIC PRESSURE	TAP NO.	STATIC PRESSURE	TAP NO.	STATIC PRESSURE	TAP NO.	STATIC PRESSURE	TAP NO.	STATIC PRESSURE	TAP NO.	STATIC PRESSURE	TAP NO.	STATIC PRESSURE	TAP NO.	STATIC PRESSURE	TAP NO.	STATIC PRESSURE	TAP NO.	STATIC PRESSURE	TAP NO.	STATIC PRESSURE	TAP NO.	STATIC PRESSURE	TAP NO.	STATIC PRESSURE	TAP NO.	STATIC PRESSURE	TAP NO.	STATIC PRESSURE	TAP NO.	STATIC PRESSURE	TAP NO.	STATIC PRESSURE	TAP NO.	STATIC PRESSURE	TAP NO.	STATIC PRESSURE	TAP NO.	STATIC PRESSURE	TAP NO.	STATIC PRESSURE	TAP NO.	STATIC PRESSURE	TAP NO.	STATIC PRESSURE	TAP NO.	STATIC PRESSURE	TAP NO.	STATIC PRESSURE	TAP NO.	STATIC PRESSURE	TAP NO.	STATIC PRESSURE	TAP NO.	STATIC PRESSURE	TAP NO.	STATIC PRESSURE	TAP NO.	STATIC PRESSURE	TAP NO.	STATIC PRESSURE	TAP NO.	STATIC PRESSURE	TAP NO.	STATIC PRESSURE	TAP NO.	STATIC PRESSURE	TAP NO.	STATIC PRESSURE	TAP NO.	STATIC PRESSURE	TAP NO.	STATIC PRESSURE	TAP NO.	STATIC PRESSURE	TAP NO.	STATIC PRESSURE	TAP NO.	STATIC PRESSURE
---------	-----------------	---------	-----------------	---------	-----------------	---------	-----------------	---------	-----------------	---------	-----------------	---------	-----------------	---------	-----------------	---------	-----------------	---------	-----------------	---------	-----------------	---------	-----------------	---------	-----------------	---------	-----------------	---------	-----------------	---------	-----------------	---------	-----------------	---------	-----------------	---------	-----------------	---------	-----------------	---------	-----------------	---------	-----------------	---------	-----------------	---------	-----------------	---------	-----------------	---------	-----------------	---------	-----------------	---------	-----------------	---------	-----------------	---------	-----------------	---------	-----------------	---------	-----------------	---------	-----------------	---------	-----------------	---------	-----------------	---------	-----------------	---------	-----------------	---------	-----------------	---------	-----------------	---------	-----------------	---------	-----------------	---------	-----------------	---------	-----------------	---------	-----------------	---------	-----------------	---------	-----------------	---------	-----------------	---------	-----------------	---------	-----------------	---------	-----------------	---------	-----------------	---------	-----------------	---------	-----------------	---------	-----------------	---------	-----------------	---------	-----------------	---------	-----------------	---------	-----------------	---------	-----------------	---------	-----------------	---------	-----------------	---------	-----------------	---------	-----------------	---------	-----------------	---------	-----------------	---------	-----------------	---------	-----------------	---------	-----------------	---------	-----------------	---------	-----------------	---------	-----------------	---------	-----------------	---------	-----------------	---------	-----------------	---------	-----------------	---------	-----------------	---------	-----------------	---------	-----------------	---------	-----------------	---------	-----------------	---------	-----------------	---------	-----------------	---------	-----------------	---------	-----------------	---------	-----------------	---------	-----------------	---------	-----------------	---------	-----------------	---------	-----------------	---------	-----------------	---------	-----------------	---------	-----------------	---------	-----------------	---------	-----------------	---------	-----------------	---------	-----------------	---------	-----------------	---------	-----------------	---------	-----------------	---------	-----------------	---------	-----------------	---------	-----------------	---------	-----------------	---------	-----------------	---------	-----------------	---------	-----------------	---------	-----------------	---------	-----------------	---------	-----------------	---------	-----------------	---------	-----------------	---------	-----------------	---------	-----------------	---------	-----------------	---------	-----------------	---------	-----------------	---------	-----------------	---------	-----------------	---------	-----------------	---------	-----------------	---------	-----------------	---------	-----------------	---------	-----------------	---------	-----------------	---------	-----------------	---------	-----------------	---------	-----------------	---------	-----------------	---------	-----------------	---------	-----------------	---------	-----------------	---------	-----------------	---------	-----------------	---------	-----------------	---------	-----------------	---------	-----------------	---------	-----------------	---------	-----------------	---------	-----------------	---------	-----------------	---------	-----------------	---------	-----------------	---------	-----------------	---------	-----------------	---------	-----------------	---------	-----------------	---------	-----------------	---------	-----------------	---------	-----------------	---------	-----------------	---------	-----------------	---------	-----------------	---------	-----------------	---------	-----------------	---------	-----------------	---------	-----------------	---------	-----------------	---------	-----------------	---------	-----------------	---------	-----------------	---------	-----------------	---------	-----------------	---------	-----------------	---------	-----------------	---------	-----------------	---------	-----------------	---------	-----------------	---------	-----------------	---------	-----------------	---------	-----------------	---------	-----------------	---------	-----------------	---------	-----------------	---------	-----------------	---------	-----------------	---------	-----------------	---------	-----------------	---------	-----------------	---------	-----------------	---------	-----------------	---------	-----------------	---------	-----------------	---------	-----------------	---------	-----------------	---------	-----------------	---------	-----------------	---------	-----------------	---------	-----------------	---------	-----------------	---------	-----------------	---------	-----------------	---------	-----------------	---------	-----------------	---------	-----------------	---------	-----------------	---------	-----------------	---------	-----------------	---------	-----------------	---------	-----------------	---------	-----------------	---------	-----------------	---------	-----------------	---------	-----------------	---------	-----------------	---------	-----------------	---------	-----------------	---------	-----------------	---------	-----------------	---------	-----------------	---------	-----------------	---------	-----------------	---------	-----------------	---------	-----------------	---------	-----------------	---------	-----------------	---------	-----------------	---------	-----------------	---------	-----------------	---------	-----------------	---------	-----------------	---------	-----------------	---------	-----------------	---------	-----------------	---------	-----------------	---------	-----------------	---------	-----------------	---------	-----------------	---------	-----------------	---------	-----------------	---------	-----------------	---------	-----------------	---------	-----------------	---------	-----------------	---------	-----------------	---------	-----------------	---------	-----------------	---------	-----------------	---------	-----------------	---------	-----------------	---------	-----------------	---------	-----------------	---------	-----------------	---------	-----------------	---------	-----------------	---------	-----------------	---------	-----------------	---------	-----------------	---------	-----------------	---------	-----------------	---------	-----------------	---------	-----------------	---------	-----------------	---------	-----------------	---------	-----------------	---------	-----------------	---------	-----------------	---------	-----------------	---------	-----------------	---------	-----------------	---------	-----------------	---------	-----------------	---------	-----------------	---------	-----------------	---------	-----------------	---------	-----------------	---------	-----------------	---------	-----------------	---------	-----------------	---------	-----------------	---------	-----------------	---------	-----------------	---------	-----------------	---------	-----------------	---------	-----------------	---------	-----------------	---------	-----------------	---------	-----------------	---------	-----------------	---------	-----------------	---------	-----------------	---------	-----------------	---------	-----------------	---------	-----------------	---------	-----------------	---------	-----------------	---------	-----------------	---------	-----------------	---------	-----------------	---------	-----------------	---------	-----------------	---------	-----------------	---------	-----------------	---------	-----------------	---------	-----------------	---------	-----------------	---------	-----------------	---------	-----------------	---------	-----------------	---------	-----------------	---------	-----------------	---------	-----------------	---------	-----------------	---------	-----------------	---------	-----------------	---------	-----------------	---------	-----------------	---------	-----------------	---------	-----------------	---------	-----------------	---------	-----------------	---------	-----------------	---------	-----------------	---------	-----------------	---------	-----------------	---------	-----------------	---------	-----------------	---------	-----------------	---------	-----------------	---------	-----------------	---------	-----------------

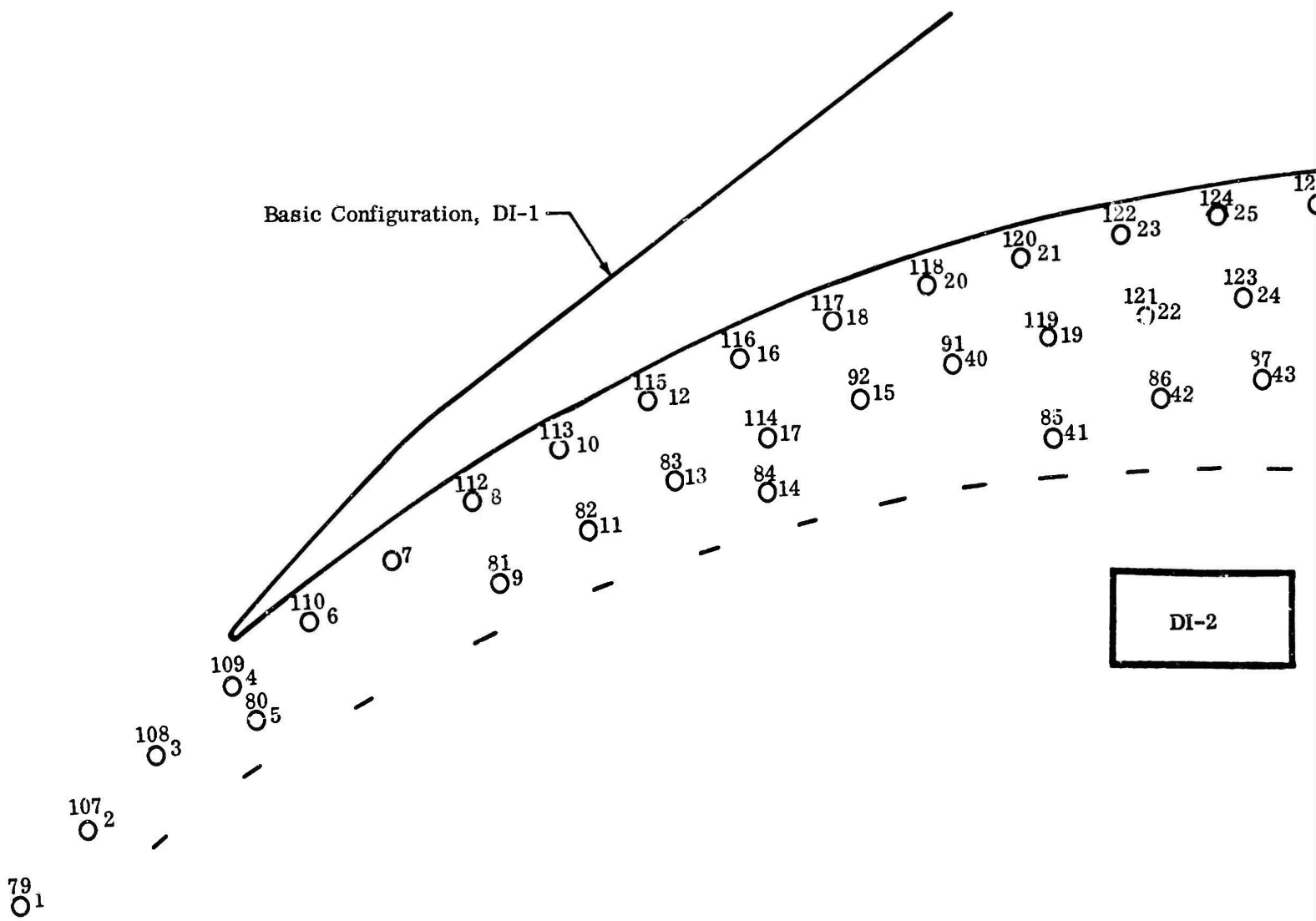
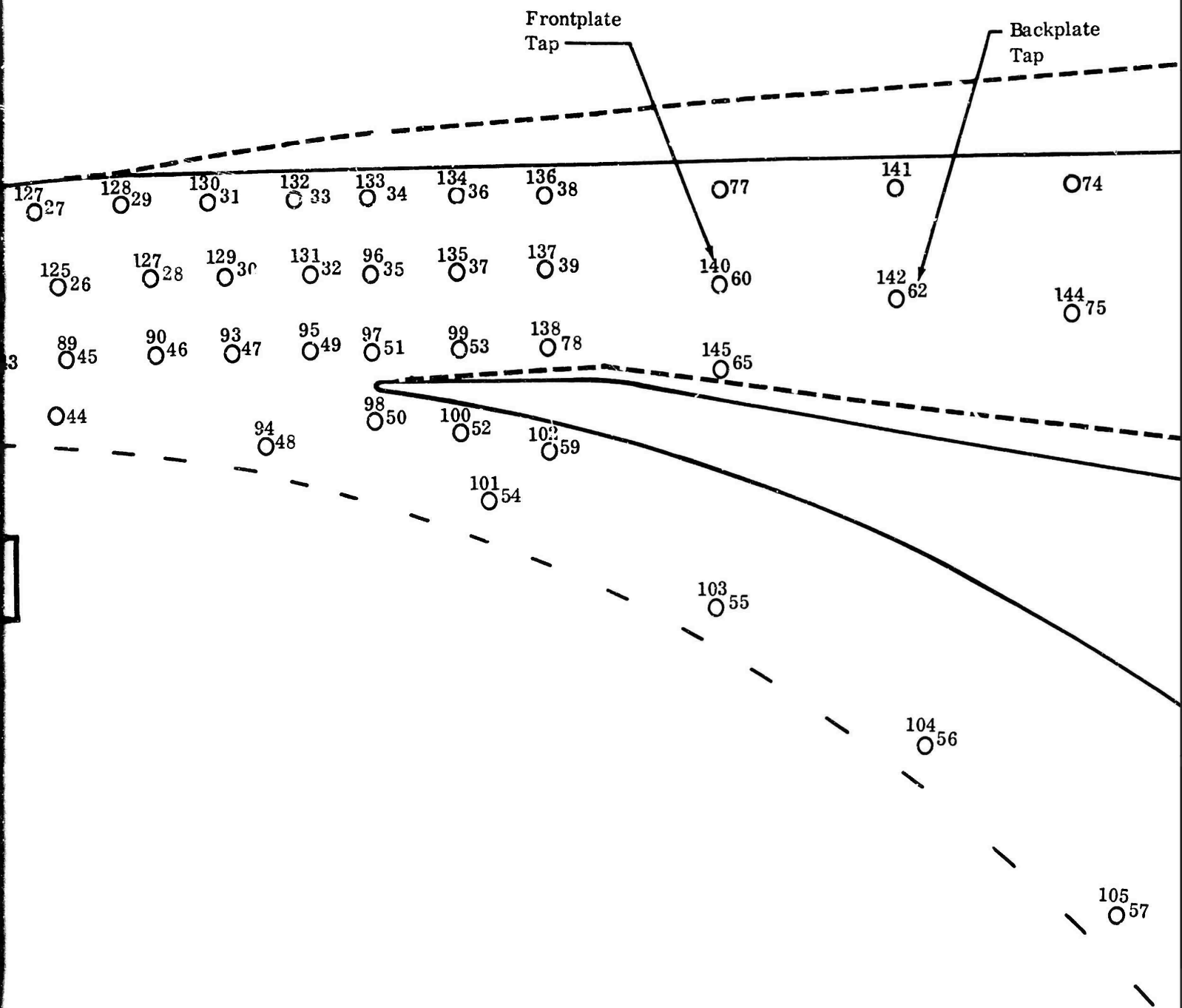
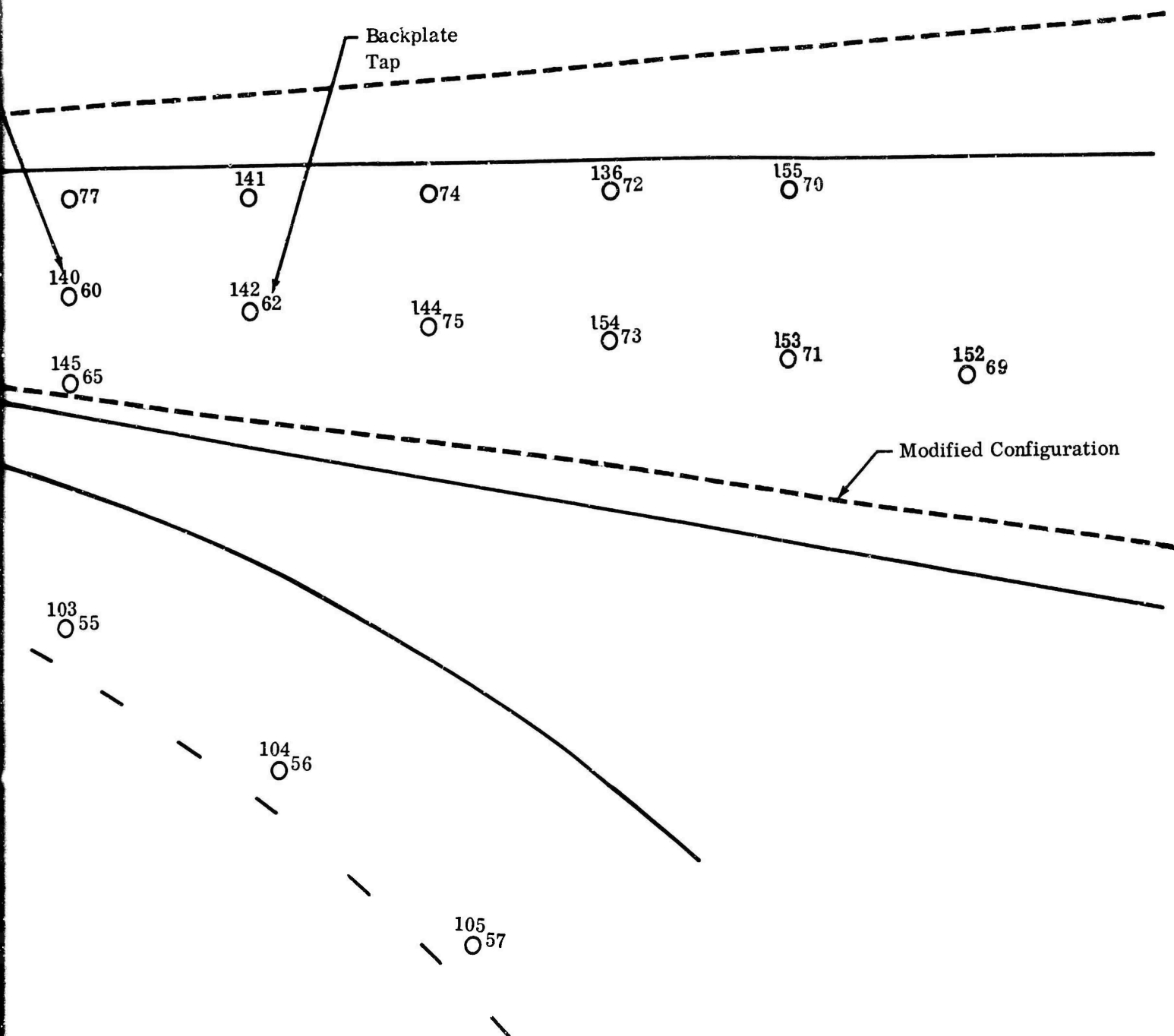


Figure 111. Diffuser Static-Pressure Instrumentation, DI-2.





TEST NO. 3338
SPEED = 50000
AIR FLOW = 2.48
IGV = REMOVED
THRUST AREA = 100 %
RADIUS RATIO = 1.06
LINE NO. 5
 $\delta = 0.989$

ALL PRESSURES ARE IN PSIA

[illegible]

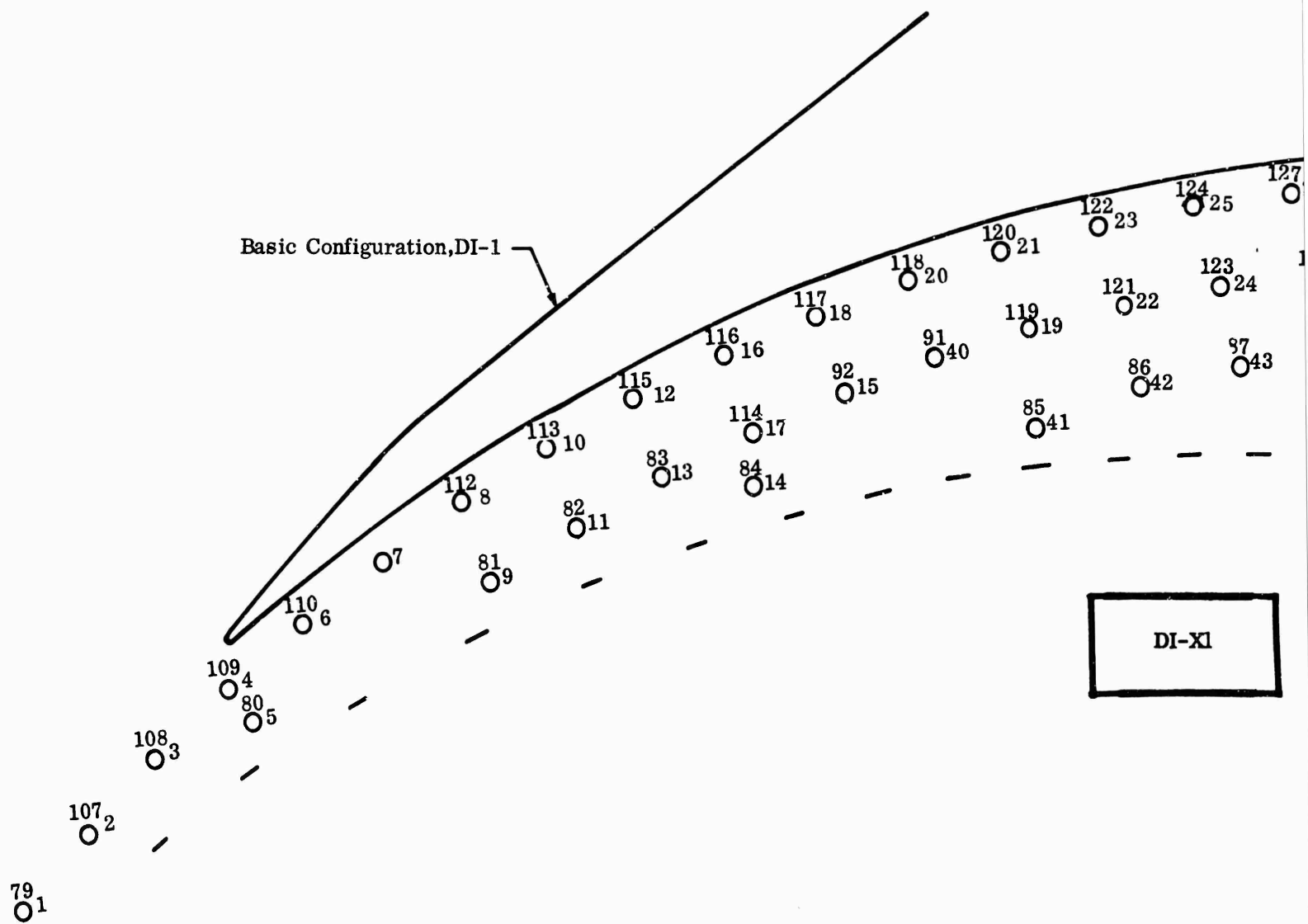
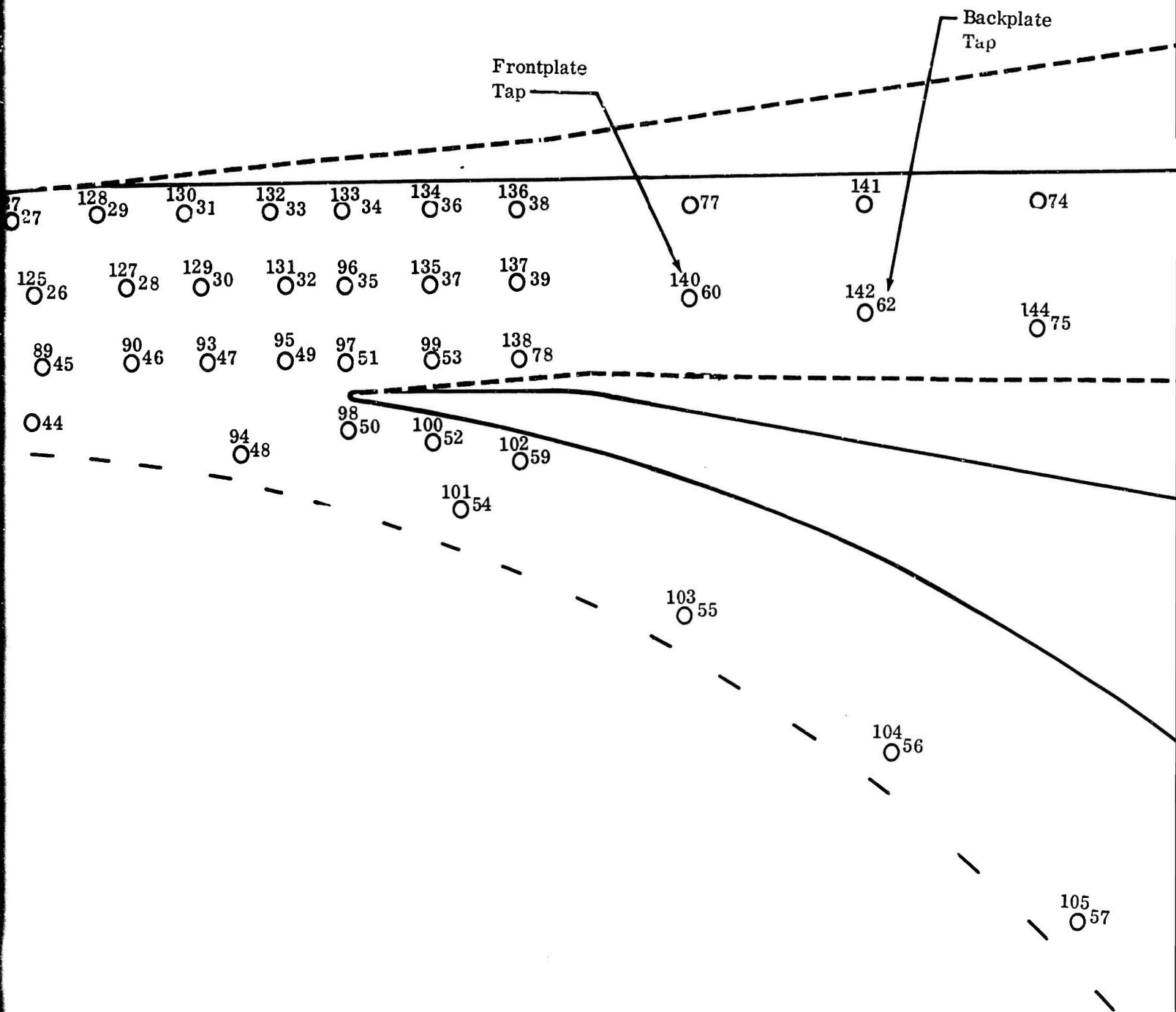
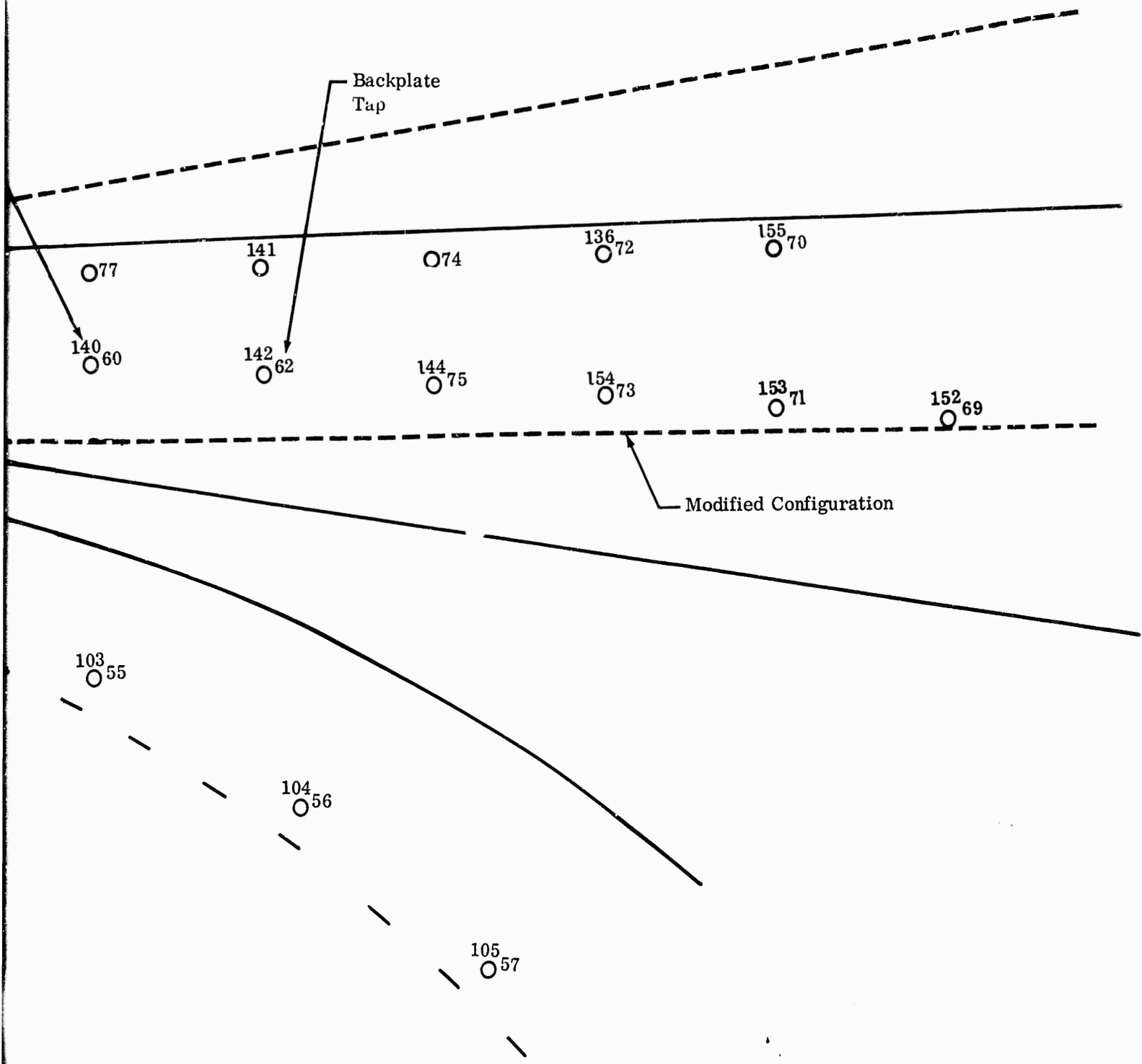


Figure 112. Diffuser Static-Pressure Instrumentation, DI-X1.





ALL PRESSURES ARE IN PSIA

369

TEST NO. 3333	SPEED =	AIR FLOW = 2.50
IGV = REMOVED	THROAT AREA = 100%	RADIUS RATIO = 1.06
LINE NO. 3	$\delta = 0.997$	

ALL PRESSURES ARE IN PSIA

[illegible]

TEST NO. 3326 SPEED = 50000 AIR FLOW = 2.50
IGV = REMOVED THROAT AREA = 100% RADIUS RATIO = 1.06
LINE NO. 3 $\delta = 0.990$

ALL PRESSURES ARE IN PSIA

TAP NO.	STATIC PRESSURE	TAP NO.	STATIC PRESSURE	TAP NO.	STATIC PRESSURE	TAP NO.	STATIC PRESSURE	TAP NO.	STATIC PRESSURE	TAP NO.	STATIC PRESSURE	TAP NO.	STATIC PRESSURE
1	58.1	2	60.8	3	53.9	4	61.5	5	61.9	6	64.7		
7	65.4	8	67.6	9	55.5	10	64.8	11	59.8	12	64.9		
13	61.0	15	62.7	16	66.9	17	56.1	19	63.3	20	65.9		
21	57.7	22	65.4	23	66.5	24	66.6	25	71.5	27	71.5		
28	67.4	29	42.5	30	58.2	31	67.1	32	51.7	33	54.6		
34	79.2	35	79.6	36	83.0	37	83.1	38	83.3	39	83.6		
40	61.6	41	58.0	42	58.8	43	60.8	44	64.7	45	65.3		
46	63.6	47	59.9	48	56.5	49	55.8	50	0.0	51	82.9		
52	59.1	53	83.1	54	61.0	55	62.0	56	61.1	57	58.9		
58	61.1	59	58.3	60	97.7	62	107.2	63	112.7	64	116.1		
65	99.0	66	117.5	67	118.9	68	120.4	69	120.0	70	118.3		
71	118.5	72	116.4	73	116.0	74	112.3	75	112.8	77	98.9		
78	82.8	79	0.0	80	0.0	81	0.0	83	0.0	86	0.0		
87	0.0	90	0.0	91	0.0	92	0.0	93	0.0	95	0.0		
96	0.0	97	0.0	98	0.0	99	0.0	100	0.0	102	0.0		
104	0.0	105	0.0	106	0.0	107	0.0	108	0.0	110	0.0		
112	0.0	115	0.0	116	0.0	117	0.0	118	66.2	118	0.0		
119	0.0	120	0.0	121	0.0	122	0.0	123	0.0	124	0.0		
125	0.0	127	0.0	128	0.0	129	0.0	131	0.0	132	0.0		
134	0.0	135	0.0	136	0.0	138	0.0	139	0.0	140	0.0		
142	0.0	144	0.0	146	0.0	147	0.0	148	0.0	149	0.0		
150	0.0	151	0.0	152	0.0	153	0.0	154	0.0	155	0.0		
156	0.0	157	123.0	158	123.8	159	124.4	160	124.4				

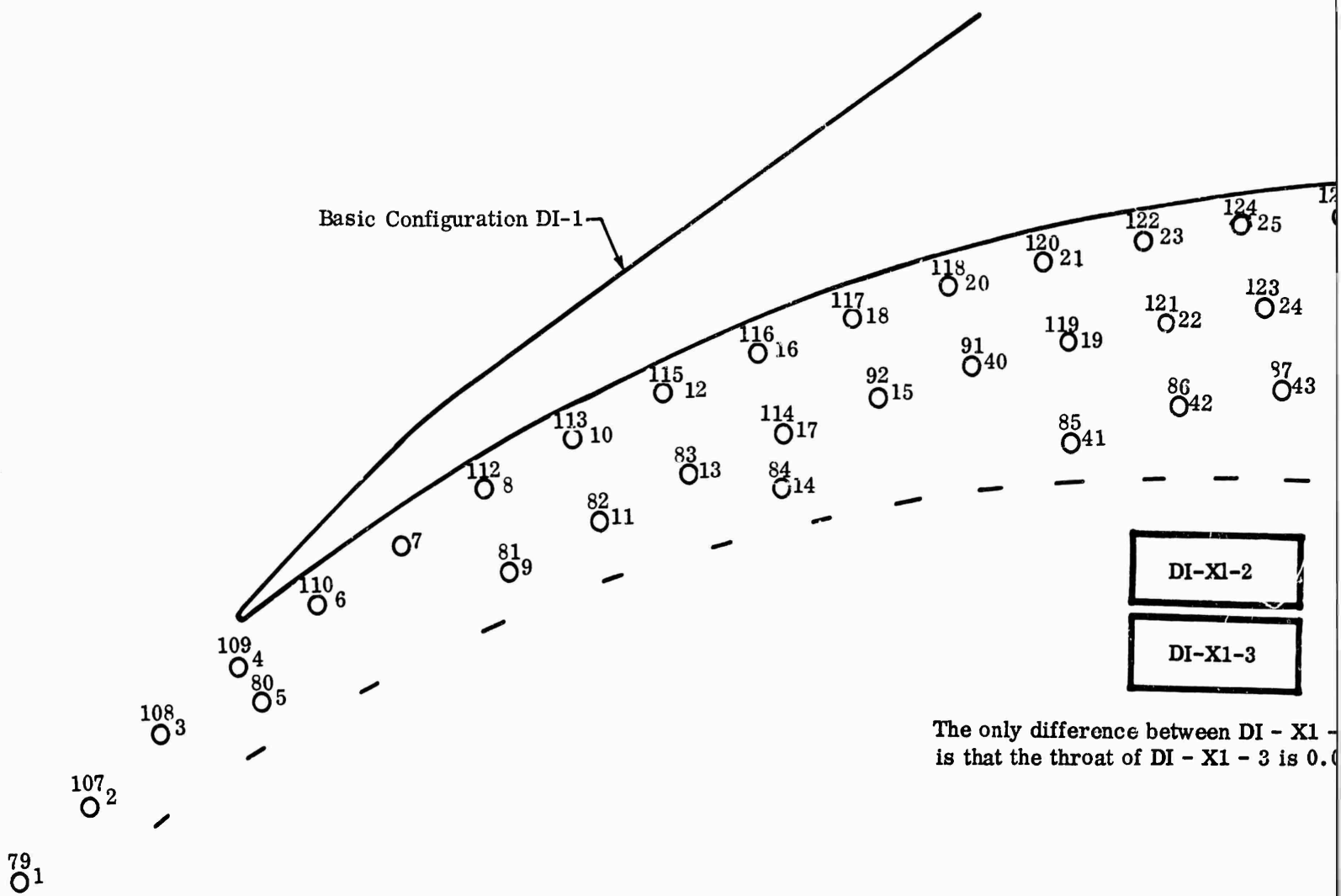
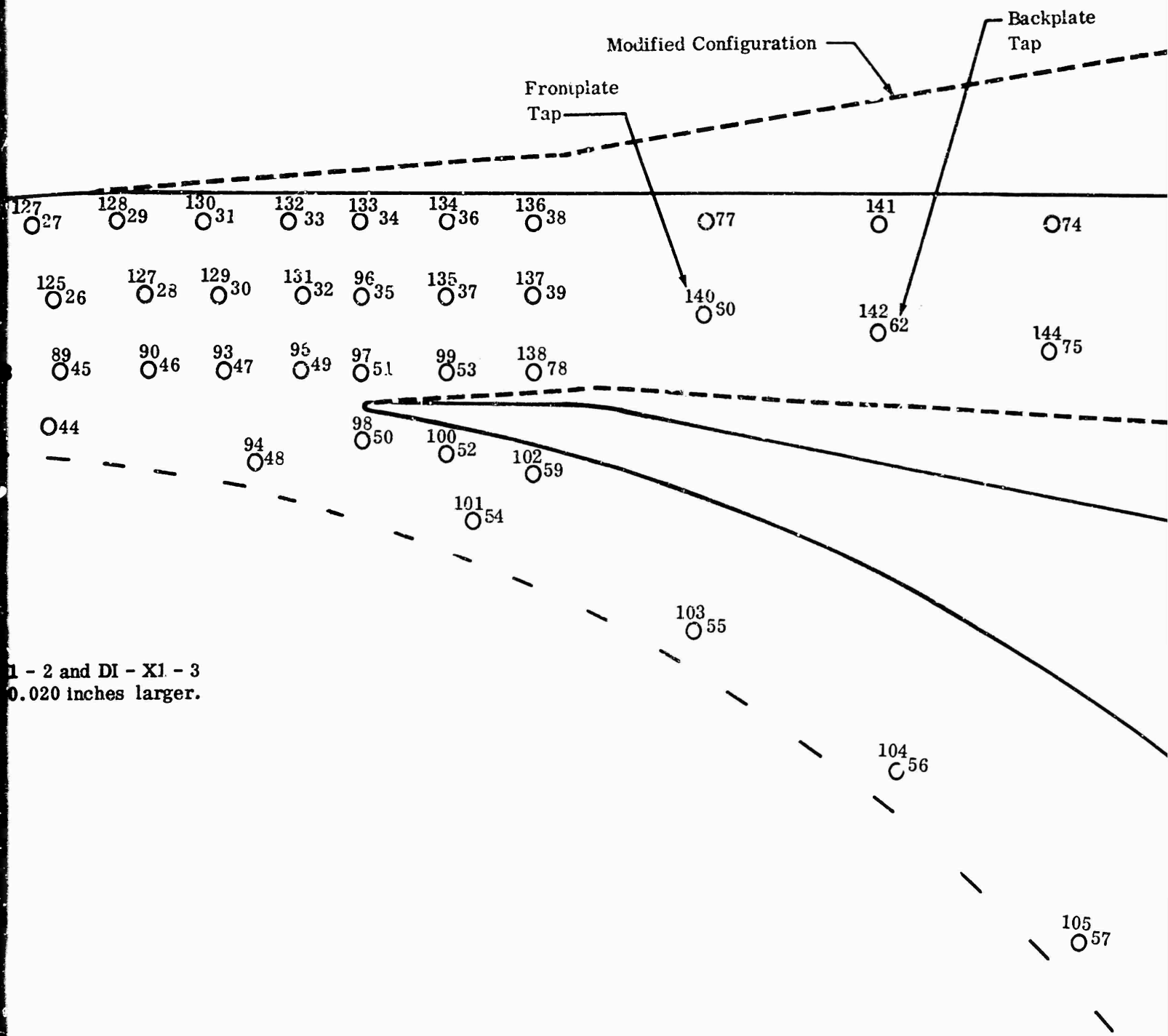
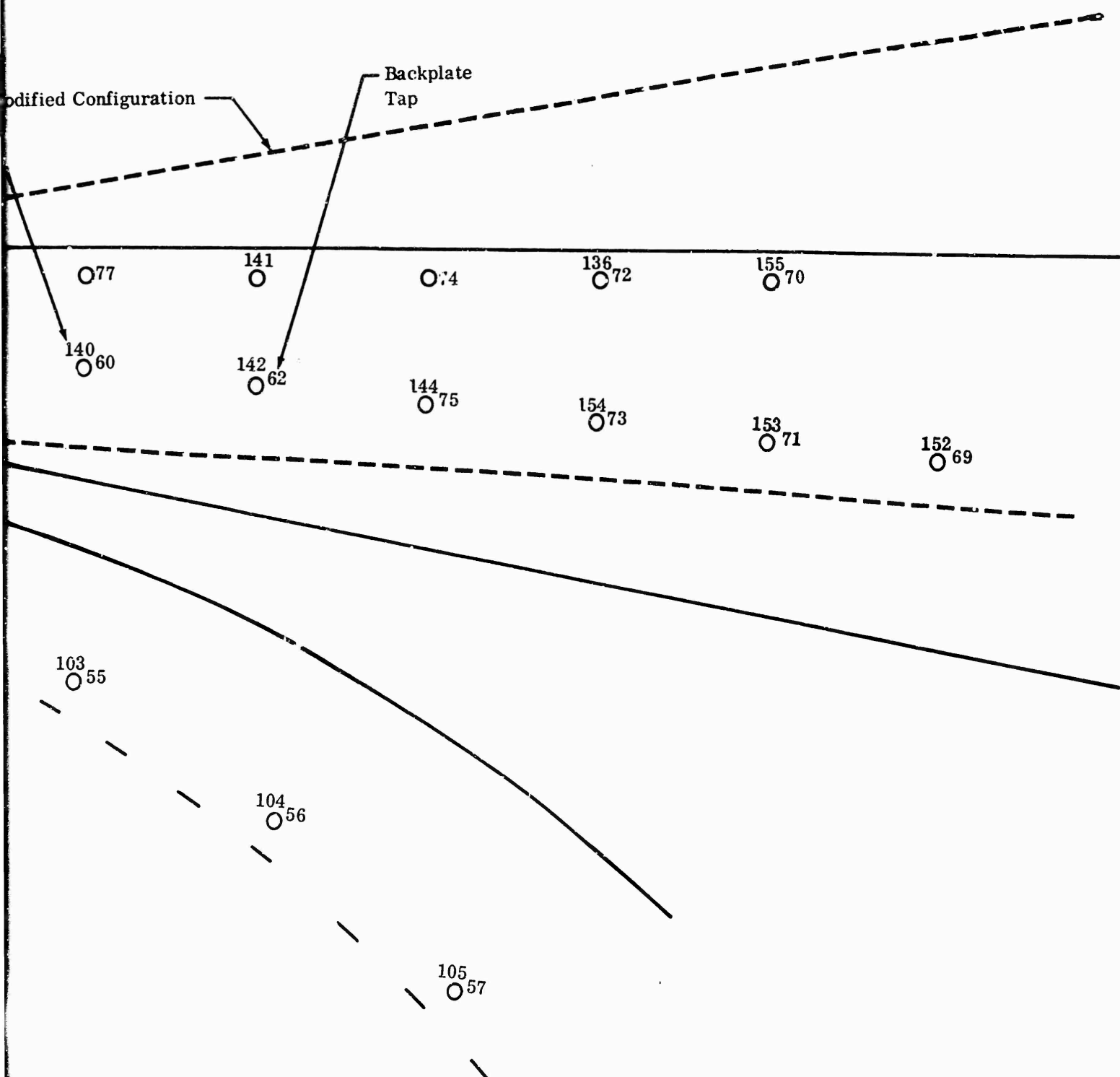


Figure 113. Diffuser Static-Pressure Instrumentation, DI-X1-2 and DI-X1-3.



Modified Configuration

Backplate
Tap



TEST NO. 3327	SPEED = 50000	AIR FLOW = 2.51
IGV = REMOVED	THROAT AREA = 100 %	RADIUS RATIO = 1.06
LINE NO. 3	$\delta = 0.985$	

ALL PRESSURES ARE IN PSIA

TAP NO.	STATIC PRESSURE	TAP NO.	STATIC PRESSURE	TAP NO.	STATIC PRESSURE	TAP NO.	STATIC PRESSURE	TAP NO.	STATIC PRESSURE	TAP NO.	STATIC PRESSURE	TAP NO.	STATIC PRESSURE	TAP NO.	STATIC PRESSURE	TAP NO.	STATIC PRESSURE	TAP NO.	STATIC PRESSURE	TAP NO.	STATIC PRESSURE	TAP NO.	STATIC PRESSURE	TAP NO.	STATIC PRESSURE	TAP NO.	STATIC PRESSURE	TAP NO.	STATIC PRESSURE	TAP NO.	STATIC PRESSURE	TAP NO.	STATIC PRESSURE	TAP NO.	STATIC PRESSURE	TAP NO.	STATIC PRESSURE	TAP NO.	STATIC PRESSURE	TAP NO.	STATIC PRESSURE	TAP NO.	STATIC PRESSURE	TAP NO.	STATIC PRESSURE	TAP NO.	STATIC PRESSURE	TAP NO.	STATIC PRESSURE	TAP NO.	STATIC PRESSURE	TAP NO.	STATIC PRESSURE	TAP NO.	STATIC PRESSURE	TAP NO.	STATIC PRESSURE	TAP NO.	STATIC PRESSURE	TAP NO.	STATIC PRESSURE	TAP NO.	STATIC PRESSURE	TAP NO.	STATIC PRESSURE	TAP NO.	STATIC PRESSURE	TAP NO.	STATIC PRESSURE	TAP NO.	STATIC PRESSURE	TAP NO.	STATIC PRESSURE	TAP NO.	STATIC PRESSURE	TAP NO.	STATIC PRESSURE	TAP NO.	STATIC PRESSURE	TAP NO.	STATIC PRESSURE	TAP NO.	STATIC PRESSURE	TAP NO.	STATIC PRESSURE	TAP NO.	STATIC PRESSURE	TAP NO.	STATIC PRESSURE	TAP NO.	STATIC PRESSURE	TAP NO.	STATIC PRESSURE	TAP NO.	STATIC PRESSURE	TAP NO.	STATIC PRESSURE	TAP NO.	STATIC PRESSURE	TAP NO.	STATIC PRESSURE	TAP NO.	STATIC PRESSURE	TAP NO.	STATIC PRESSURE	TAP NO.	STATIC PRESSURE	TAP NO.	STATIC PRESSURE	TAP NO.	STATIC PRESSURE	TAP NO.	STATIC PRESSURE	TAP NO.	STATIC PRESSURE	TAP NO.	STATIC PRESSURE	TAP NO.	STATIC PRESSURE	TAP NO.	STATIC PRESSURE	TAP NO.	STATIC PRESSURE	TAP NO.	STATIC PRESSURE	TAP NO.	STATIC PRESSURE	TAP NO.	STATIC PRESSURE	TAP NO.	STATIC PRESSURE	TAP NO.	STATIC PRESSURE	TAP NO.	STATIC PRESSURE	TAP NO.	STATIC PRESSURE	TAP NO.	STATIC PRESSURE	TAP NO.	STATIC PRESSURE	TAP NO.	STATIC PRESSURE	TAP NO.	STATIC PRESSURE	TAP NO.	STATIC PRESSURE	TAP NO.	STATIC PRESSURE	TAP NO.	STATIC PRESSURE	TAP NO.	STATIC PRESSURE	TAP NO.	STATIC PRESSURE	TAP NO.	STATIC PRESSURE	TAP NO.	STATIC PRESSURE	TAP NO.	STATIC PRESSURE	TAP NO.	STATIC PRESSURE	TAP NO.	STATIC PRESSURE	TAP NO.	STATIC PRESSURE	TAP NO.	STATIC PRESSURE	TAP NO.	STATIC PRESSURE	TAP NO.	STATIC PRESSURE	TAP NO.	STATIC PRESSURE	TAP NO.	STATIC PRESSURE	TAP NO.	STATIC PRESSURE	TAP NO.	STATIC PRESSURE	TAP NO.	STATIC PRESSURE	TAP NO.	STATIC PRESSURE	TAP NO.	STATIC PRESSURE	TAP NO.	STATIC PRESSURE	TAP NO.	STATIC PRESSURE	TAP NO.	STATIC PRESSURE	TAP NO.	STATIC PRESSURE	TAP NO.	STATIC PRESSURE	TAP NO.	STATIC PRESSURE	TAP NO.	STATIC PRESSURE	TAP NO.	STATIC PRESSURE	TAP NO.	STATIC PRESSURE	TAP NO.	STATIC PRESSURE	TAP NO.	STATIC PRESSURE	TAP NO.	STATIC PRESSURE	TAP NO.	STATIC PRESSURE	TAP NO.	STATIC PRESSURE	TAP NO.	STATIC PRESSURE	TAP NO.	STATIC PRESSURE	TAP NO.	STATIC PRESSURE	TAP NO.	STATIC PRESSURE	TAP NO.	STATIC PRESSURE	TAP NO.	STATIC PRESSURE	TAP NO.	STATIC PRESSURE	TAP NO.	STATIC PRESSURE	TAP NO.	STATIC PRESSURE	TAP NO.	STATIC PRESSURE	TAP NO.	STATIC PRESSURE	TAP NO.	STATIC PRESSURE	TAP NO.	STATIC PRESSURE	TAP NO.	STATIC PRESSURE	TAP NO.	STATIC PRESSURE	TAP NO.	STATIC PRESSURE	TAP NO.	STATIC PRESSURE	TAP NO.	STATIC PRESSURE	TAP NO.	STATIC PRESSURE	TAP NO.	STATIC PRESSURE	TAP NO.	STATIC PRESSURE	TAP NO.	STATIC PRESSURE	TAP NO.	STATIC PRESSURE	TAP NO.	STATIC PRESSURE	TAP NO.	STATIC PRESSURE	TAP NO.	STATIC PRESSURE	TAP NO.	STATIC PRESSURE	TAP NO.	STATIC PRESSURE	TAP NO.	STATIC PRESSURE	TAP NO.	STATIC PRESSURE	TAP NO.	STATIC PRESSURE	TAP NO.	STATIC PRESSURE	TAP NO.	STATIC PRESSURE	TAP NO.	STATIC PRESSURE	TAP NO.	STATIC PRESSURE	TAP NO.	STATIC PRESSURE	TAP NO.	STATIC PRESSURE	TAP NO.	STATIC PRESSURE	TAP NO.	STATIC PRESSURE	TAP NO.	STATIC PRESSURE	TAP NO.	STATIC PRESSURE	TAP NO.	STATIC PRESSURE	TAP NO.	STATIC PRESSURE	TAP NO.	STATIC PRESSURE	TAP NO.	STATIC PRESSURE	TAP NO.	STATIC PRESSURE	TAP NO.	STATIC PRESSURE	TAP NO.	STATIC PRESSURE	TAP NO.	STATIC PRESSURE	TAP NO.	STATIC PRESSURE	TAP NO.	STATIC PRESSURE	TAP NO.	STATIC PRESSURE	TAP NO.	STATIC PRESSURE	TAP NO.	STATIC PRESSURE	TAP NO.	STATIC PRESSURE	TAP NO.	STATIC PRESSURE	TAP NO.	STATIC PRESSURE	TAP NO.	STATIC PRESSURE	TAP NO.	STATIC PRESSURE	TAP NO.	STATIC PRESSURE	TAP NO.	STATIC PRESSURE	TAP NO.	STATIC PRESSURE	TAP NO.	STATIC PRESSURE	TAP NO.	STATIC PRESSURE	TAP NO.	STATIC PRESSURE	TAP NO.	STATIC PRESSURE	TAP NO.	STATIC PRESSURE	TAP NO.	STATIC PRESSURE	TAP NO.	STATIC PRESSURE	TAP NO.	STATIC PRESSURE	TAP NO.	STATIC PRESSURE	TAP NO.	STATIC PRESSURE	TAP NO.	STATIC PRESSURE	TAP NO.	STATIC PRESSURE	TAP NO.	STATIC PRESSURE	TAP NO.	STATIC PRESSURE	TAP NO.	STATIC PRESSURE	TAP NO.	STATIC PRESSURE	TAP NO.	STATIC PRESSURE	TAP NO.	STATIC PRESSURE	TAP NO.	STATIC PRESSURE	TAP NO.	STATIC PRESSURE	TAP NO.	STATIC PRESSURE	TAP NO.	STATIC PRESSURE	TAP NO.	STATIC PRESSURE	TAP NO.	STATIC PRESSURE	TAP NO.	STATIC PRESSURE	TAP NO.	STATIC PRESSURE	TAP NO.	STATIC PRESSURE	TAP NO.	STATIC PRESSURE	TAP NO.	STATIC PRESSURE	TAP NO.	STATIC PRESSURE	TAP NO.	STATIC PRESSURE	TAP NO.	STATIC PRESSURE	TAP NO.	STATIC PRESSURE	TAP NO.	STATIC PRESSURE	TAP NO.	STATIC PRESSURE	TAP NO.	STATIC PRESSURE	TAP NO.	STATIC PRESSURE	TAP NO.	STATIC PRESSURE	TAP NO.	STATIC PRESSURE	TAP NO.	STATIC PRESSURE	TAP NO.	STATIC PRESSURE	TAP NO.	STATIC PRESSURE	TAP NO.	STATIC PRESSURE	TAP NO.	STATIC PRESSURE	TAP NO.	STATIC PRESSURE	TAP NO.	STATIC PRESSURE	TAP NO.	STATIC PRESSURE	TAP NO.	STATIC PRESSURE	TAP NO.	STATIC PRESSURE	TAP NO.	STATIC PRESSURE	TAP NO.	STATIC PRESSURE	TAP NO.	STATIC PRESSURE	TAP NO.	STATIC PRESSURE	TAP NO.	STATIC PRESSURE	TAP NO.	STATIC PRESSURE	TAP NO.	STATIC PRESSURE	TAP NO.	STATIC PRESSURE	TAP NO.	STATIC PRESSURE	TAP NO.	STATIC PRESSURE	TAP NO.	STATIC PRESSURE	TAP NO.	STATIC PRESSURE	TAP NO.	STATIC PRESSURE	TAP NO.	STATIC PRESSURE	TAP NO.	STATIC PRESSURE	TAP NO.	STATIC PRESSURE	TAP NO.	STATIC PRESSURE	TAP NO.	STATIC PRESSURE	TAP NO.	STATIC PRESSURE	TAP NO.	STATIC PRESSURE	TAP NO.	STATIC PRESSURE	TAP NO.	STATIC PRESSURE	TAP NO.	STATIC PRESSURE	TAP NO.	STATIC PRESSURE	TAP NO.	STATIC PRESSURE	TAP NO.	STATIC PRESSURE	TAP NO.	STATIC PRESSURE	TAP NO.	STATIC PRESSURE	TAP NO.	STATIC PRESSURE	TAP NO.	STATIC PRESSURE	TAP NO.	STATIC PRESSURE	TAP NO.	STATIC PRESSURE	TAP NO.	STATIC PRESSURE	TAP NO.	STATIC PRESSURE	TAP NO.	STATIC PRESSURE	TAP NO.	STATIC PRESSURE	TAP NO.	STATIC PRESSURE	TAP NO.	STATIC PRESSURE	TAP NO.	STATIC PRESSURE	TAP NO.	STATIC PRESSURE	TAP NO.	STATIC PRESSURE	TAP NO.	STATIC PRESSURE	TAP NO.	STATIC PRESSURE	TAP NO.	STATIC PRESSURE	TAP NO.	STATIC PRESSURE	TAP NO.	STATIC PRESSURE	TAP NO.	STATIC PRESSURE	TAP NO.	STATIC PRESSURE	TAP NO.	STATIC PRESSURE	TAP NO.	STATIC PRESSURE	TAP NO.	STATIC PRESSURE	TAP NO.	STATIC PRESSURE	TAP NO.	STATIC PRESSURE	TAP NO.	STATIC PRESSURE	TAP NO.	STATIC PRESSURE	TAP NO.	STATIC PRESSURE	TAP NO.	STATIC PRESSURE	TAP NO.	STATIC PRESSURE	TAP NO.	STATIC PRESSURE	TAP NO.	STATIC PRESSURE	TAP NO.	STATIC PRESSURE	TAP NO.	STATIC PRESSURE	TAP NO.	STATIC PRESSURE	TAP NO.	STATIC PRESSURE	TAP NO.	STATIC PRESSURE	TAP NO.	STATIC PRESSURE	TAP NO.	STATIC PRESSURE	TAP NO.	STATIC PRESSURE	TAP NO.	STATIC PRESSURE	TAP NO.	STATIC PRESSURE	TAP NO.	STATIC PRESSURE	TAP NO.	STATIC PRESSURE	TAP NO.	STATIC PRESSURE	TAP NO.	STATIC PRESSURE	TAP NO.	STATIC PRESSURE	TAP NO.	STATIC PRESSURE	TAP NO.	STATIC PRESSURE	TAP NO.	STATIC PRESSURE	TAP NO.	STATIC PRESSURE	TAP NO.	STATIC PRESSURE	TAP NO.	STATIC PRESSURE	TAP NO.	STATIC PRESSURE	TAP NO.	STATIC PRESSURE	TAP NO.	STATIC PRESSURE	TAP NO.	STATIC PRESSURE	TAP NO.	STATIC PRESSURE	TAP NO.	STATIC PRESSURE	TAP NO.	STATIC PRESSURE	TAP NO.</
---------	-----------------	---------	-----------------	---------	-----------------	---------	-----------------	---------	-----------------	---------	-----------------	---------	-----------------	---------	-----------------	---------	-----------------	---------	-----------------	---------	-----------------	---------	-----------------	---------	-----------------	---------	-----------------	---------	-----------------	---------	-----------------	---------	-----------------	---------	-----------------	---------	-----------------	---------	-----------------	---------	-----------------	---------	-----------------	---------	-----------------	---------	-----------------	---------	-----------------	---------	-----------------	---------	-----------------	---------	-----------------	---------	-----------------	---------	-----------------	---------	-----------------	---------	-----------------	---------	-----------------	---------	-----------------	---------	-----------------	---------	-----------------	---------	-----------------	---------	-----------------	---------	-----------------	---------	-----------------	---------	-----------------	---------	-----------------	---------	-----------------	---------	-----------------	---------	-----------------	---------	-----------------	---------	-----------------	---------	-----------------	---------	-----------------	---------	-----------------	---------	-----------------	---------	-----------------	---------	-----------------	---------	-----------------	---------	-----------------	---------	-----------------	---------	-----------------	---------	-----------------	---------	-----------------	---------	-----------------	---------	-----------------	---------	-----------------	---------	-----------------	---------	-----------------	---------	-----------------	---------	-----------------	---------	-----------------	---------	-----------------	---------	-----------------	---------	-----------------	---------	-----------------	---------	-----------------	---------	-----------------	---------	-----------------	---------	-----------------	---------	-----------------	---------	-----------------	---------	-----------------	---------	-----------------	---------	-----------------	---------	-----------------	---------	-----------------	---------	-----------------	---------	-----------------	---------	-----------------	---------	-----------------	---------	-----------------	---------	-----------------	---------	-----------------	---------	-----------------	---------	-----------------	---------	-----------------	---------	-----------------	---------	-----------------	---------	-----------------	---------	-----------------	---------	-----------------	---------	-----------------	---------	-----------------	---------	-----------------	---------	-----------------	---------	-----------------	---------	-----------------	---------	-----------------	---------	-----------------	---------	-----------------	---------	-----------------	---------	-----------------	---------	-----------------	---------	-----------------	---------	-----------------	---------	-----------------	---------	-----------------	---------	-----------------	---------	-----------------	---------	-----------------	---------	-----------------	---------	-----------------	---------	-----------------	---------	-----------------	---------	-----------------	---------	-----------------	---------	-----------------	---------	-----------------	---------	-----------------	---------	-----------------	---------	-----------------	---------	-----------------	---------	-----------------	---------	-----------------	---------	-----------------	---------	-----------------	---------	-----------------	---------	-----------------	---------	-----------------	---------	-----------------	---------	-----------------	---------	-----------------	---------	-----------------	---------	-----------------	---------	-----------------	---------	-----------------	---------	-----------------	---------	-----------------	---------	-----------------	---------	-----------------	---------	-----------------	---------	-----------------	---------	-----------------	---------	-----------------	---------	-----------------	---------	-----------------	---------	-----------------	---------	-----------------	---------	-----------------	---------	-----------------	---------	-----------------	---------	-----------------	---------	-----------------	---------	-----------------	---------	-----------------	---------	-----------------	---------	-----------------	---------	-----------------	---------	-----------------	---------	-----------------	---------	-----------------	---------	-----------------	---------	-----------------	---------	-----------------	---------	-----------------	---------	-----------------	---------	-----------------	---------	-----------------	---------	-----------------	---------	-----------------	---------	-----------------	---------	-----------------	---------	-----------------	---------	-----------------	---------	-----------------	---------	-----------------	---------	-----------------	---------	-----------------	---------	-----------------	---------	-----------------	---------	-----------------	---------	-----------------	---------	-----------------	---------	-----------------	---------	-----------------	---------	-----------------	---------	-----------------	---------	-----------------	---------	-----------------	---------	-----------------	---------	-----------------	---------	-----------------	---------	-----------------	---------	-----------------	---------	-----------------	---------	-----------------	---------	-----------------	---------	-----------------	---------	-----------------	---------	-----------------	---------	-----------------	---------	-----------------	---------	-----------------	---------	-----------------	---------	-----------------	---------	-----------------	---------	-----------------	---------	-----------------	---------	-----------------	---------	-----------------	---------	-----------------	---------	-----------------	---------	-----------------	---------	-----------------	---------	-----------------	---------	-----------------	---------	-----------------	---------	-----------------	---------	-----------------	---------	-----------------	---------	-----------------	---------	-----------------	---------	-----------------	---------	-----------------	---------	-----------------	---------	-----------------	---------	-----------------	---------	-----------------	---------	-----------------	---------	-----------------	---------	-----------------	---------	-----------------	---------	-----------------	---------	-----------------	---------	-----------------	---------	-----------------	---------	-----------------	---------	-----------------	---------	-----------------	---------	-----------------	---------	-----------------	---------	-----------------	---------	-----------------	---------	-----------------	---------	-----------------	---------	-----------------	---------	-----------------	---------	-----------------	---------	-----------------	---------	-----------------	---------	-----------------	---------	-----------------	---------	-----------------	---------	-----------------	---------	-----------------	---------	-----------------	---------	-----------------	---------	-----------------	---------	-----------------	---------	-----------------	---------	-----------------	---------	-----------------	---------	-----------------	---------	-----------------	---------	-----------------	---------	-----------------	---------	-----------------	---------	-----------------	---------	-----------------	---------	-----------------	---------	-----------------	---------	-----------------	---------	-----------------	---------	-----------------	---------	-----------------	---------	-----------------	---------	-----------------	---------	-----------------	---------	-----------------	---------	-----------------	---------	-----------------	---------	-----------------	---------	-----------------	---------	-----------------	---------	-----------------	---------	-----------------	---------	-----------------	---------	-----------------	---------	-----------------	---------	-----------------	---------	-----------------	---------	-----------------	---------	-----------------	---------	-----------------	---------	-----------------	---------	-----------------	---------	-----------------	---------	-----------------	---------	-----------------	---------	-----------------	---------	-----------------	-----------

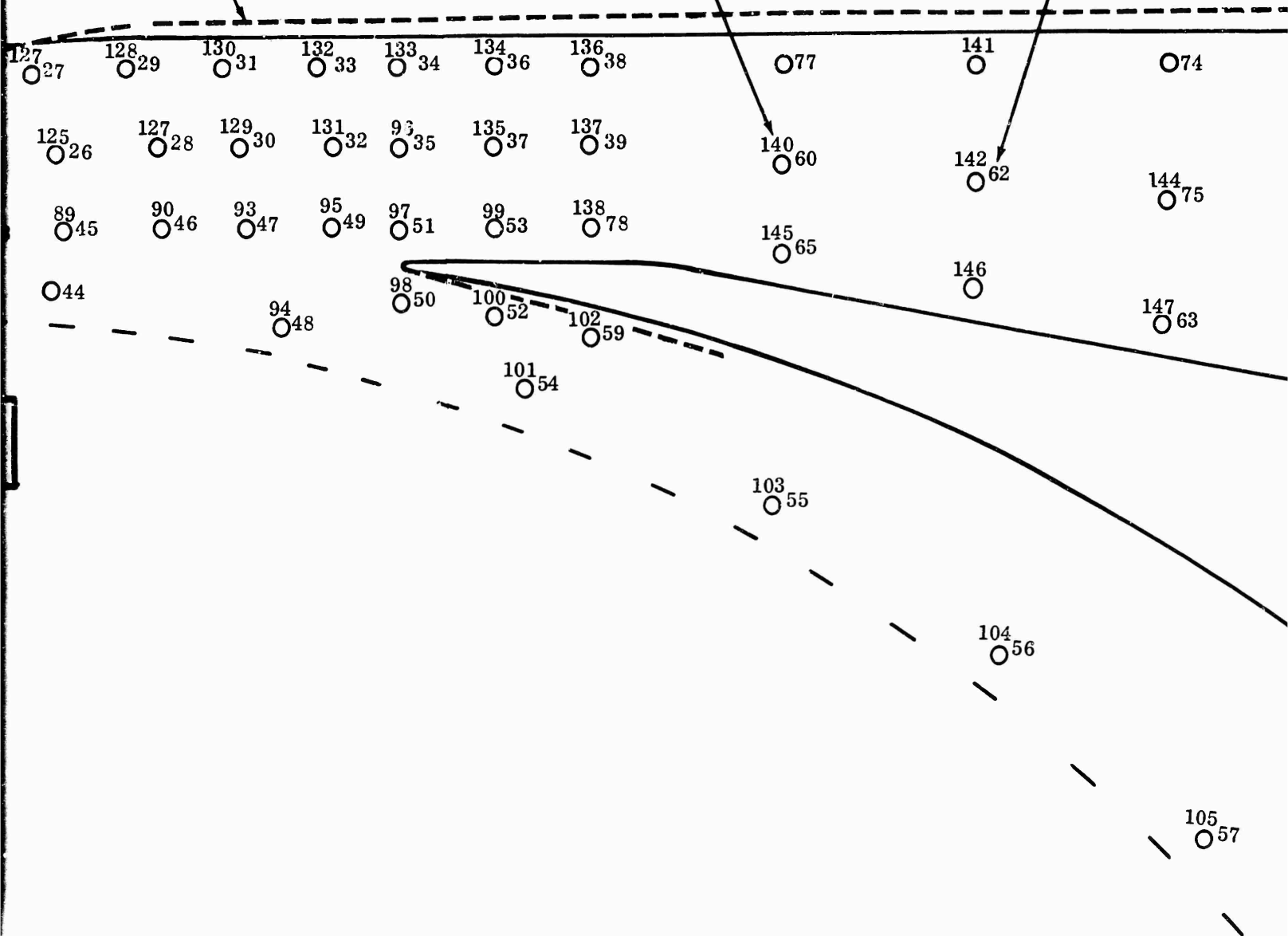
TEST NO. 3332 SPEED = 50000 AIR FLOW = 2.46
IGV = REMOVED THROAT AREA = 100% RADIUS RATIO = 1.06
LINE NO. 3 $\delta = 1.00$

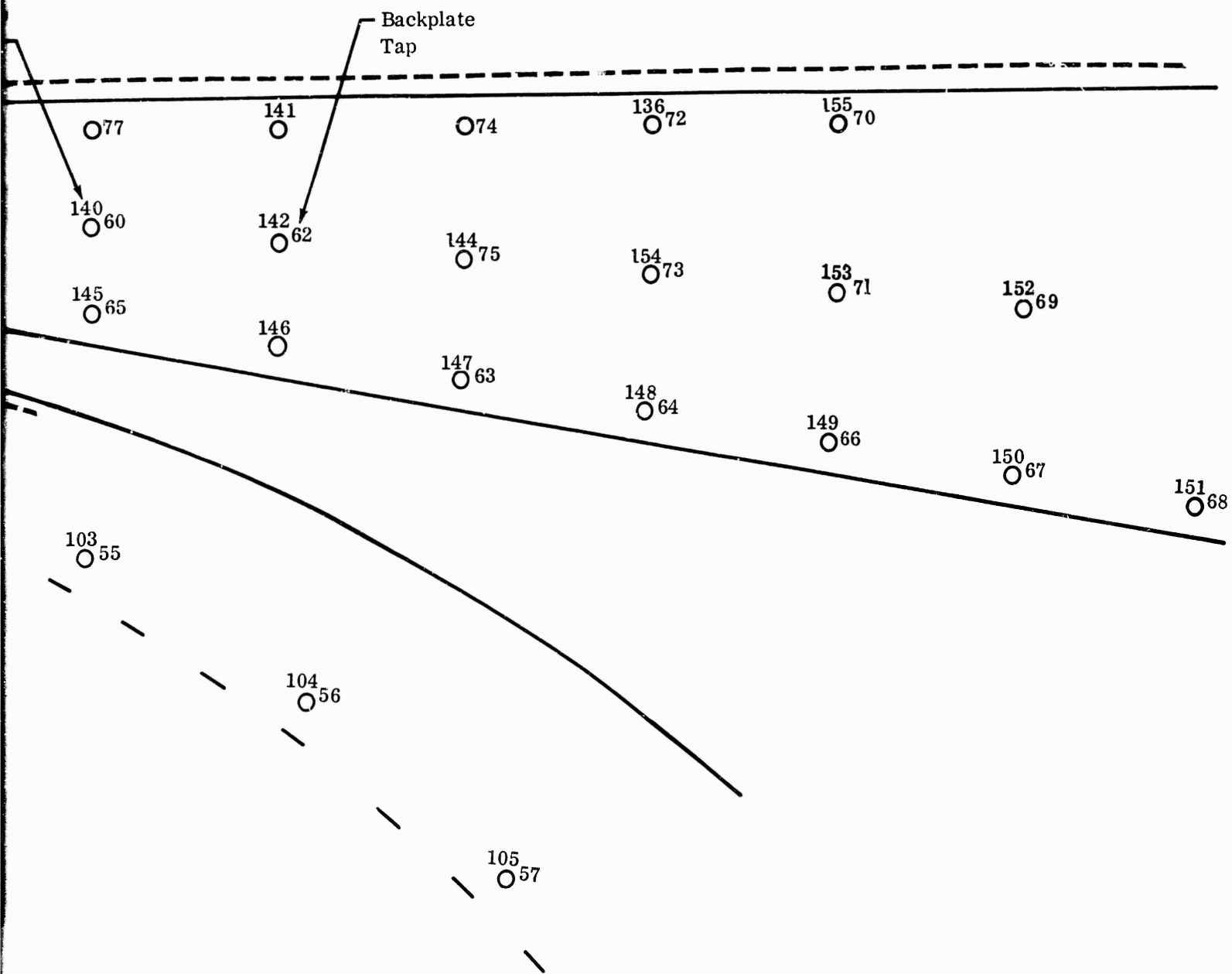
[illegible]

Fixed Configuration

Frontplate
Tap

Backplate
Tap





CONFIDENTIAL

(C) APPENDIX X (U)

SCHLIEREN PHOTOGRAPHS (U)

ABSTRACT (U)

This appendix presents information on the calibration of the schlieren unit and the information obtained from the photographs. The unit was developed on a company-sponsored research program by the contractor to study diffusers for centrifugal compressors. Flow patterns for the diffusers were photographed, and a discussion of results is given in Section 7.0 of the body of this report.

CONFIDENTIAL

CONFIDENTIAL

1.0 OBJECTIVES

Schlieren photographs were obtained for the basic research diffusers in the compressor test rig. The objectives were to:

- 1) Determine whether flow at the diffuser throat entrance is steady or pulsating and relate the flow conditions to position of the impeller blades;
- 2) Determine shock strength and variations in shock pattern as the compressor back pressure changes (flow changes) at a constant impeller rotational speed;
- 3) Determine variation in shock-strength pattern with impeller rotational speed change;
- 4) Compare flow-pattern, shock-strength, and shock-pattern variations for the three diffuser designs.

2.0 METHOD

The schlieren unit was calibrated to obtain photographs at desired impeller blade positions (see Figure 1). Impeller movement was effectively stopped every 4 degrees (within an arc of 16 degrees), with an instantaneous light source of 1-microsecond duration. The light source for the schlieren photographs was triggered by an indexed pointer on the shaft, which actuated a magnetic proximity pickup on a stationary support. A variable time-delay device in the circuit between the light and the magnetic pickup permitted the photographs to be obtained at the desired impeller-blade position. The time-delay calibration was obtained by removing the impeller front housing and photographing the impeller at various settings (see Figure 116). Time-delay values for the desired rotational speeds and impeller-blade position are given in Table III. Schlieren photographs were obtained by opening the camera lens and energizing the circuit between the magnetic proximity pickup and light source. An automatic reset circuit prevented multiple exposures by allowing only one light source trigger impulse per frame.

Tests were run at several operating conditions for the selected impeller rotational speeds. These operating conditions are shown in Figure 117 and were selected to be near surge (Line 3), near full flow (Line 7), and midway between the extremes (Line 5).

CONFIDENTIAL

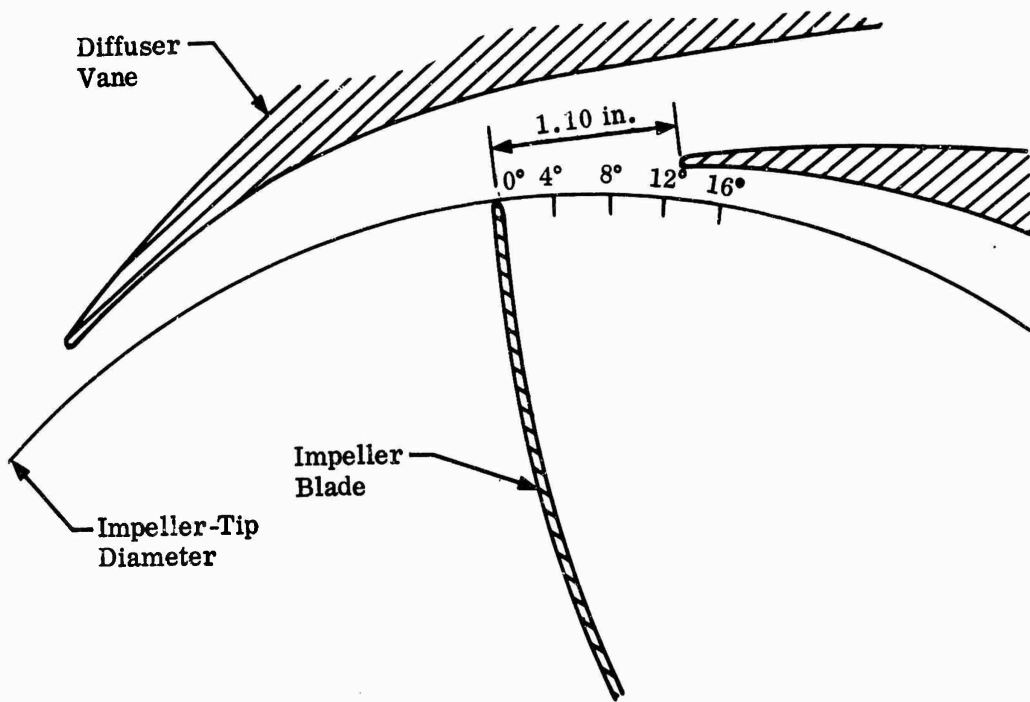
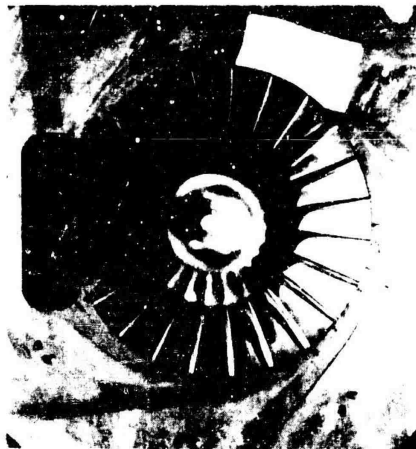


Figure 115. Impeller-Blade Positions for Schlieren Photographs.

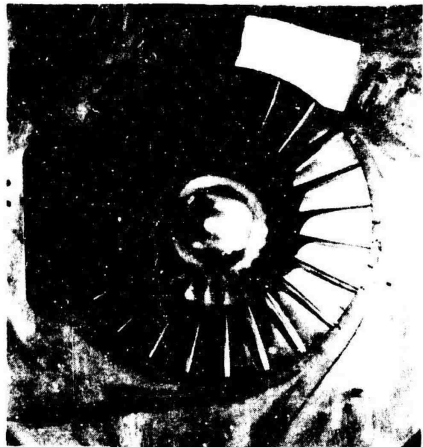
CONFIDENTIAL



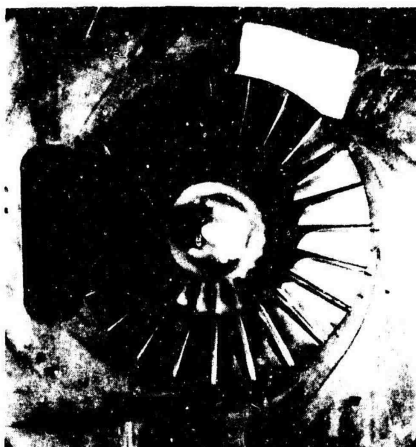
0 Degrees



4 Degrees



8 Degrees



12 Degrees



16 Degrees

Figure 116. (C) Time-Delay Calibration. (U)

CONFIDENTIAL

CONFIDENTIAL

TABLE III					
TIME DELAY IN MICROSECONDS					
Impeller Rotational Speed (rpm)	Impeller-Blade Position (degrees)				
	0	4	8	12	16
30,000	66.7	88.9	111.1	133.3	155.5
31,000	64.5	86.1	107.5	129.0	150.5
32,000	62.5	83.3	104.2	125.0	145.8
33,000	60.6	80.8	101.0	121.2	141.3
34,000	58.8	78.5	98.0	117.6	137.2
35,000	57.1	76.2	95.2	114.2	133.3
36,000	55.5	74.2	92.6	111.1	129.6
37,000	54.1	72.2	90.1	108.1	126.1
38,000	52.7	70.2	87.7	105.3	122.8
39,000	51.2	68.3	85.5	102.5	119.6
40,000	50.0	66.7	83.3	100.0	116.6
41,000	48.8	65.1	81.3	97.6	113.8
42,000	47.7	63.5	79.3	95.3	111.1
43,000	46.5	62.0	77.5	93.0	108.5
44,000	45.4	60.7	75.7	90.9	106.0
45,000	44.4	59.3	74.0	88.8	103.7
46,000	43.4	57.9	72.4	87.0	101.4
47,000	42.6	56.7	70.9	85.2	99.2
48,000	41.7	55.5	69.4	83.3	97.2
49,000	40.8	54.4	68.0	81.7	95.2
50,000	40.0	53.3	66.7	80.0	93.3

CONFIDENTIAL

CONFIDENTIAL

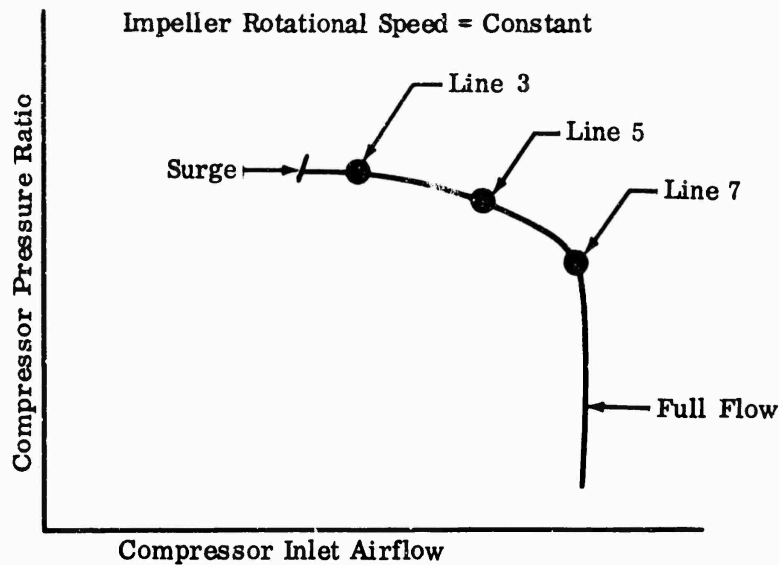


Figure 117. Test Points.

3.0 RESULTS

In light of the objectives, schlieren photographs of the basic diffuser models, showing blade positions, shock locations, and test points, are listed below.

- 1) Figures 118 through 122 show that the flow is steady and does not pulsate at the throat inlet.
- 2) Figures 122 through 124 show the variation of shock strength and pattern as compressor back pressure changes at a constant impeller rotational speed.
- 3) Figures 125 through 131 show the variation of shock strength and pattern as the impeller rotational speed changes.
- 4) Comparisons of flow patterns, shock strength, and shock patterns of the three diffuser designs are shown in the following figures:

Figures 125 through 131, Diffuser Design DI-1;

Figures 118 through 124 and 132 through 137, Diffuser Design DI-2;

CONFIDENTIAL

Figures 138 through 142, Diffuser Design DI-3;

Figure 143, modification to Diffuser Design DI-1 (DI-1-2);

Figure 144, modification to Diffuser Design DI-2 (DI-X1);

Figure 145, modification to Diffuser Design DI-2 (DI-X1-2).

The diffuser modifications are described in Section 7.0 of the body of the report.

What appears as an isolated airfoil in Figure 131 and Figures 143 through 145 is a permanent etching of the glass caused by prior testing with the 16-channel (DI-3) diffuser.

A photograph of the schlieren unit provided by the contractor for this program is given in Figure 146. The test setup is shown schematically in Figure 147.

CONFIDENTIAL

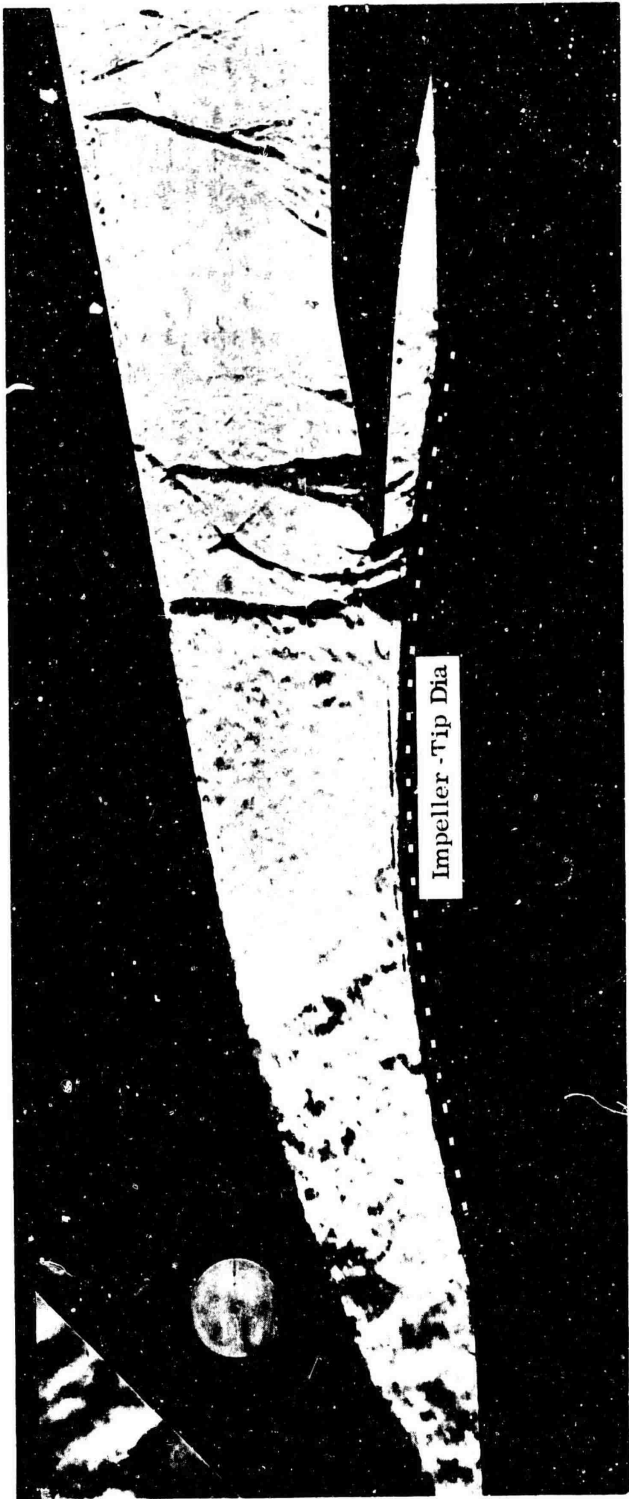


Figure 118. Schlieren Photograph of DI-2 (Test Number 3312, Impeller Position = 16 Degrees, Impeller Speed = 46,000 rpm, Data Point 5).

CONFIDENTIAL



Figure 119. Schlieren Photograph of DI-2 (Test Number 3312, Impeller Position = 12 Degrees, Impeller Speed = 46,000 rpm, Data Point 5).

CONFIDENTIAL

CONFIDENTIAL

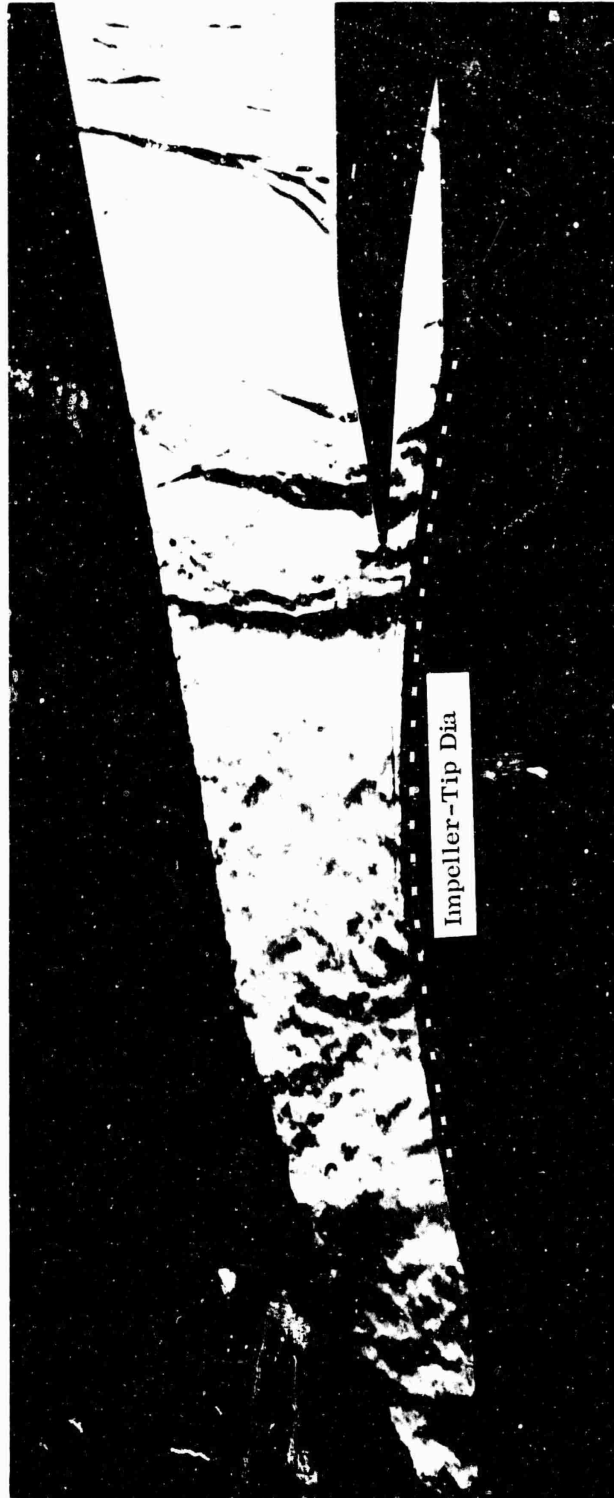


Figure 120. Schlieren Photograph of DI-2 (Test Number 3312, Impeller Position = 8 Degrees, Impeller Speed = 46,000 rpm, Data Point 5).

CONFIDENTIAL



Figure 121. Schlieren Photograph of DI-2 (Test Number 5312, Impeller Position = 4 Degrees, Impeller Speed = 46,000 rpm, Data Point 5).

CONFIDENTIAL

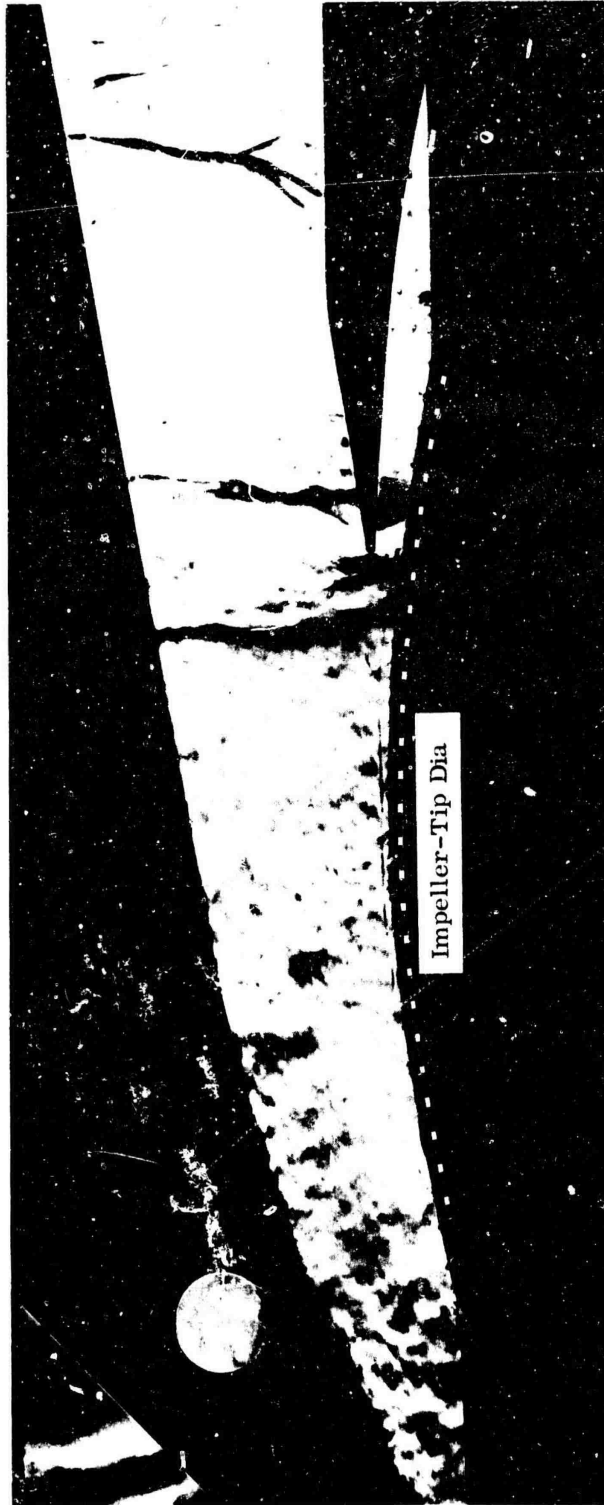


Figure 122. Schlieren Photograph of DI-2 (Test Number 3312, Impeller Position = 0 Degrees, Impeller Speed = 46,000 rpm, Data Point 5).

CONFIDENTIAL



Figure 123. Schlieren Photograph of DI-2 (Test Number 3312, Impeller Speed = 46,000 rpm, Data Point 3).

CONFIDENTIAL

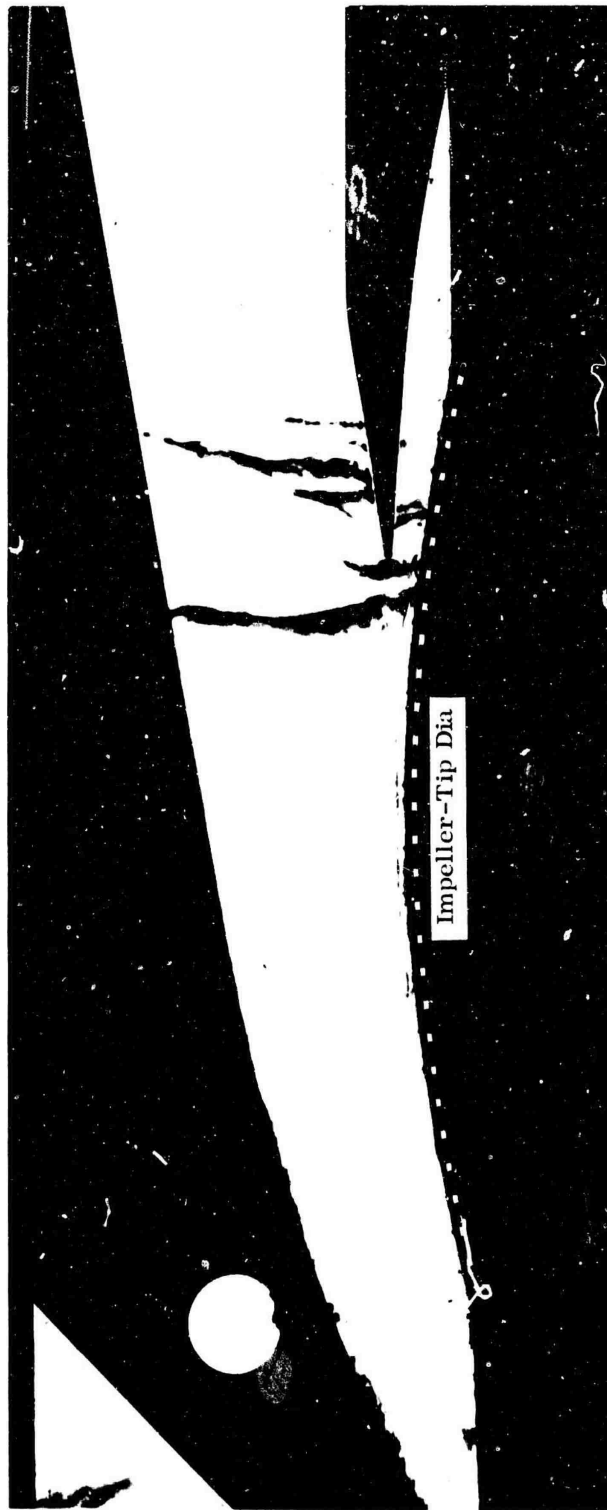


Figure 124. Schlieren Photograph of DI-2 (Test Number 3312, Impeller Speed = 46,000 rpm, Data Point 7).

CONFIDENTIAL

CONFIDENTIAL

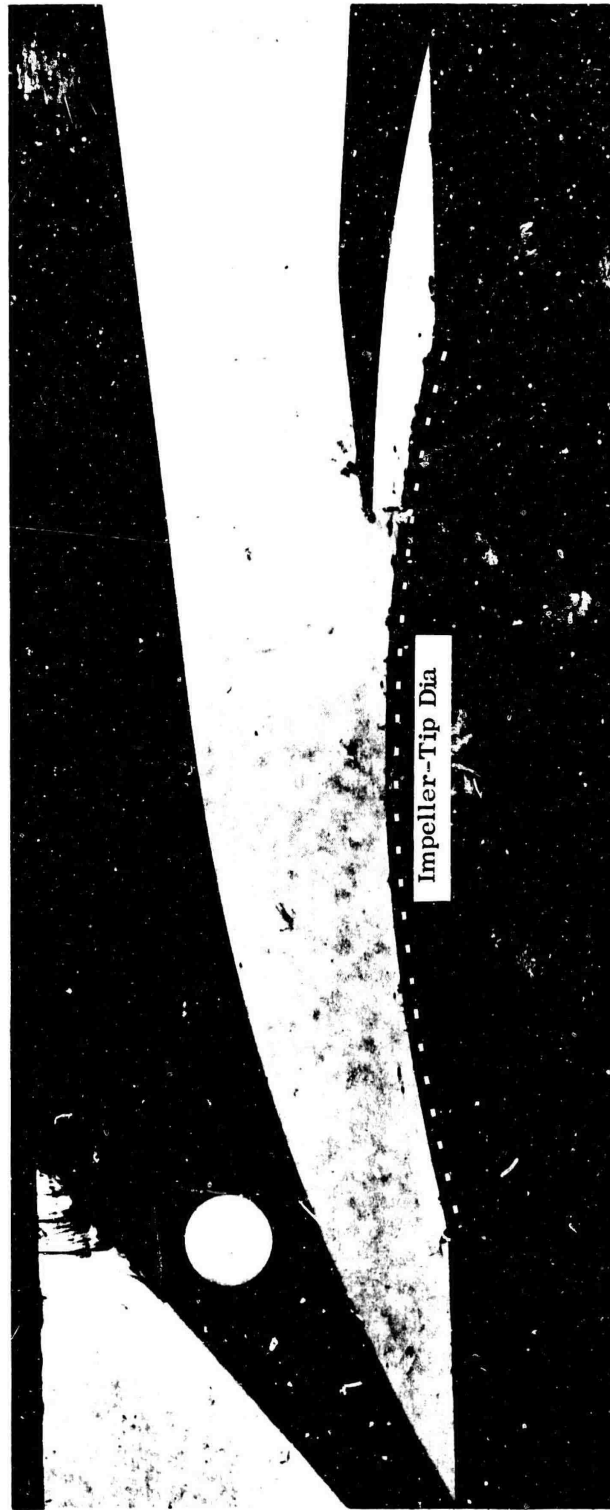


Figure 125. Schlieren Photograph of DI-1 (Test Number 3311, Impeller Speed = 15,000 rpm, Data Point 5).

CONFIDENTIAL

CONFIDENTIAL

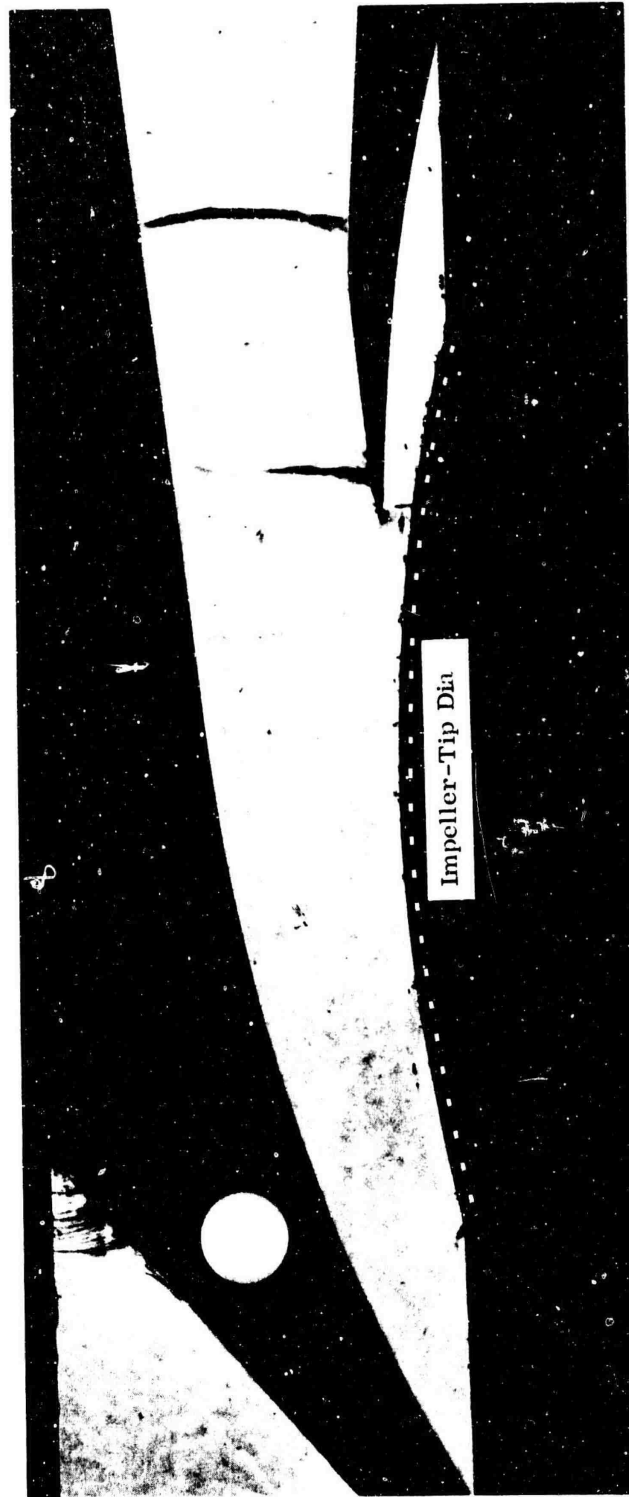


Figure 126. Schlieren Photograph of DI-1 (Test Number 3311, Impeller Speed = 20,000 rpm, Data Point 5).

CONFIDENTIAL



Figure 127. Schlieren Photograph of DI-1 (Test Number 3311, Impeller Speed = 25,000 rpm, Data Point 5).

CONFIDENTIAL



Figure 128. Schlieren Photograph of DI-1 (Test Number 3311, Impeller Speed = 30,000 rpm, Data Point 5).

CONFIDENTIAL

CONFIDENTIAL



Figure 129. Schlieren Photograph of DI-1 (Test Number 3311, Impeller Speed = 35,000 rpm, Data Point 5).

CONFIDENTIAL

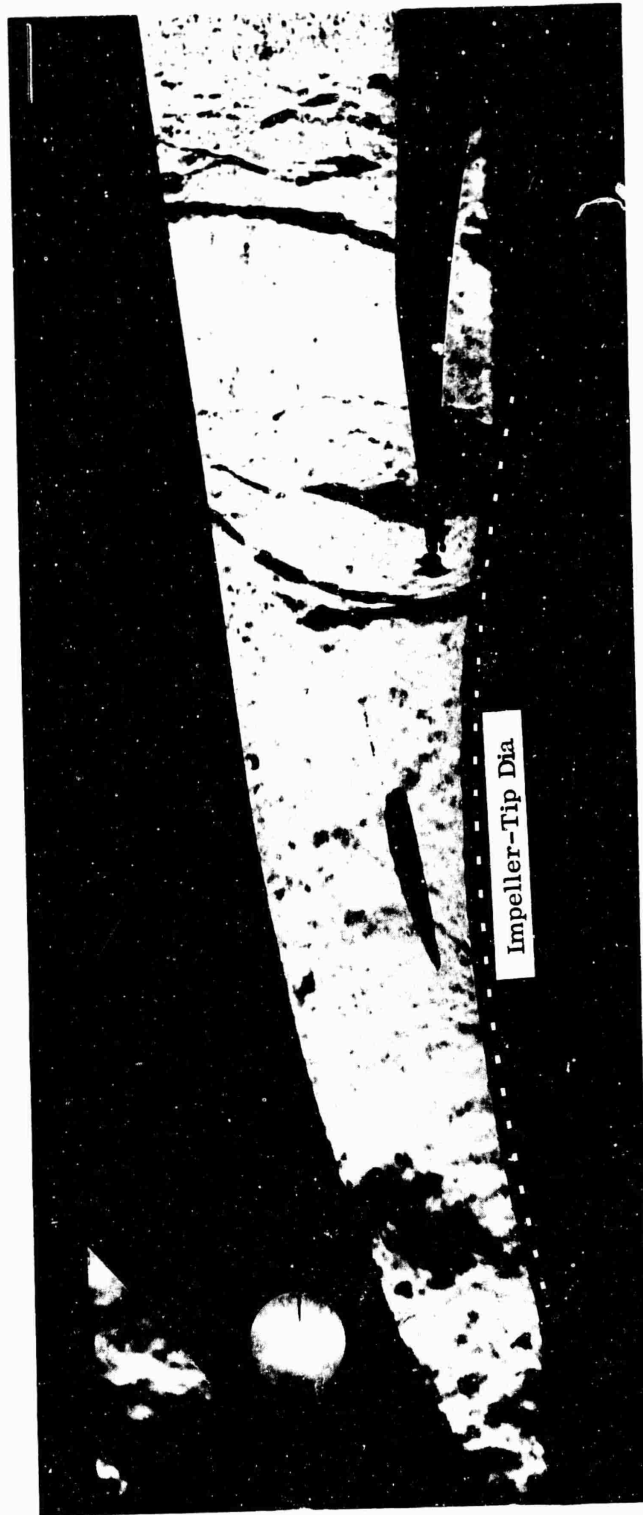
CONFIDENTIAL



Figure 130. Schlieren Photograph of DI-1 (Test Number 3311, Impeller Speed = 46,000 rpm, Data Point 5).

CONFIDENTIAL

CONFIDENTIAL



Schlieren Photograph of DI-1 (Test Number 3317, Impeller Speed
= 50,000 rpm, Data Point 5).

Figure 131.

CONFIDENTIAL

CONFIDENTIAL

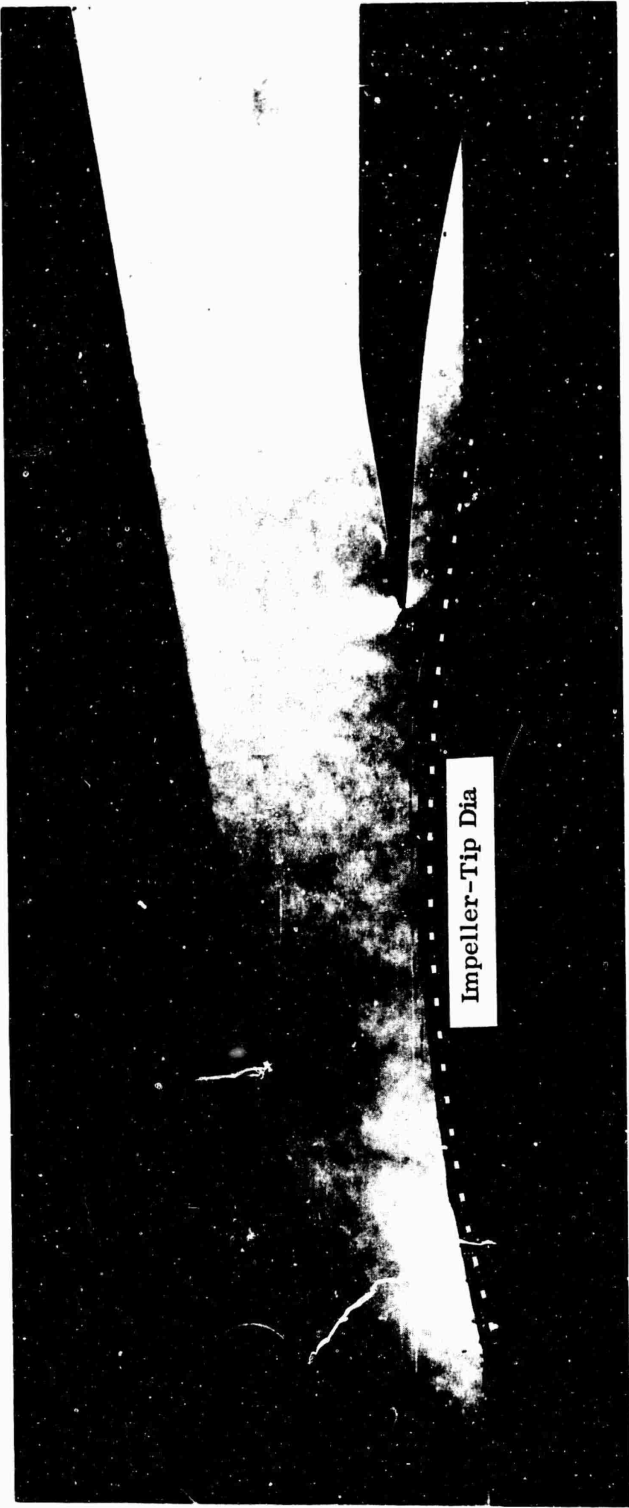


Figure 132. Schlieren Photograph of DI-2 (Test Number 3312, Impeller Speed = 20,000 rpm, Data Point 5).

CONFIDENTIAL

CONFIDENTIAL

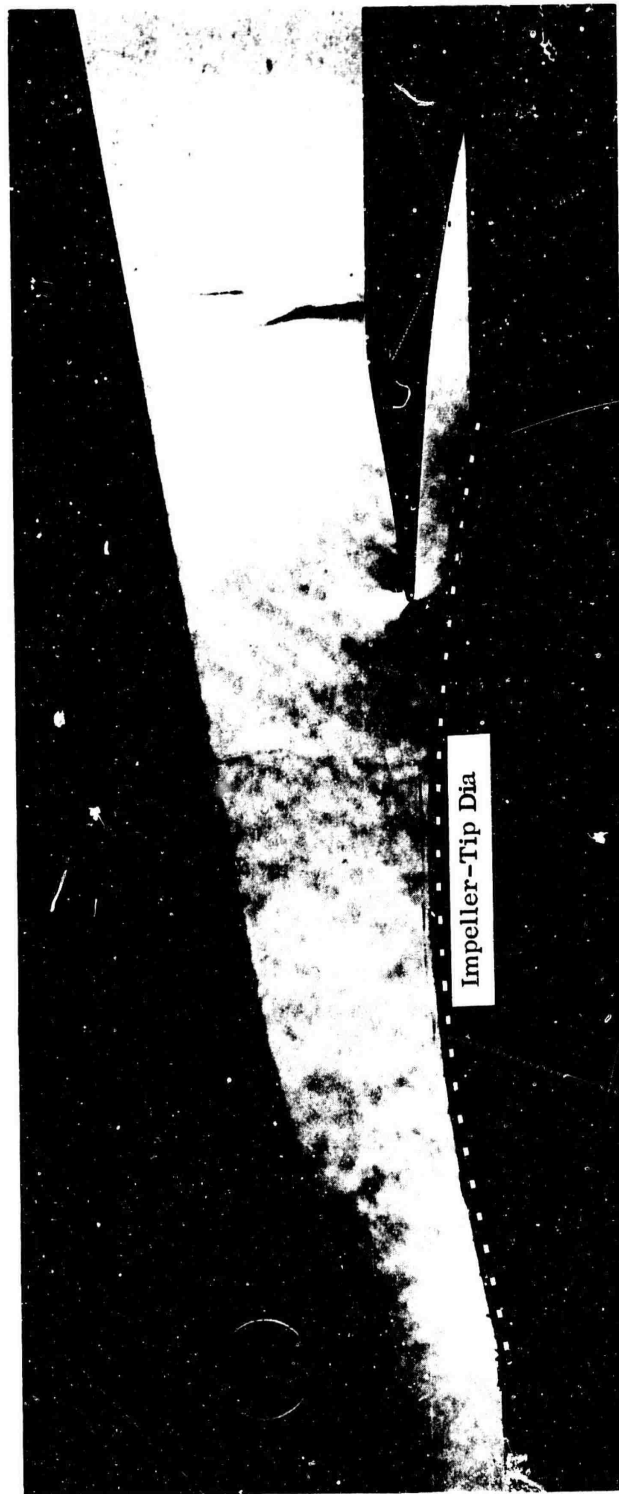


Figure 133. Schlieren Photograph of DI-2 (Test Number 3312, Impeller Speed = 25, 000 rpm, Data Point 5).

CONFIDENTIAL



Figure 134. Schlieren Photograph of DI-2 (Test Number 3312, Impeller Speed = 30,000 rpm, Data Point 5).

CONFIDENTIAL

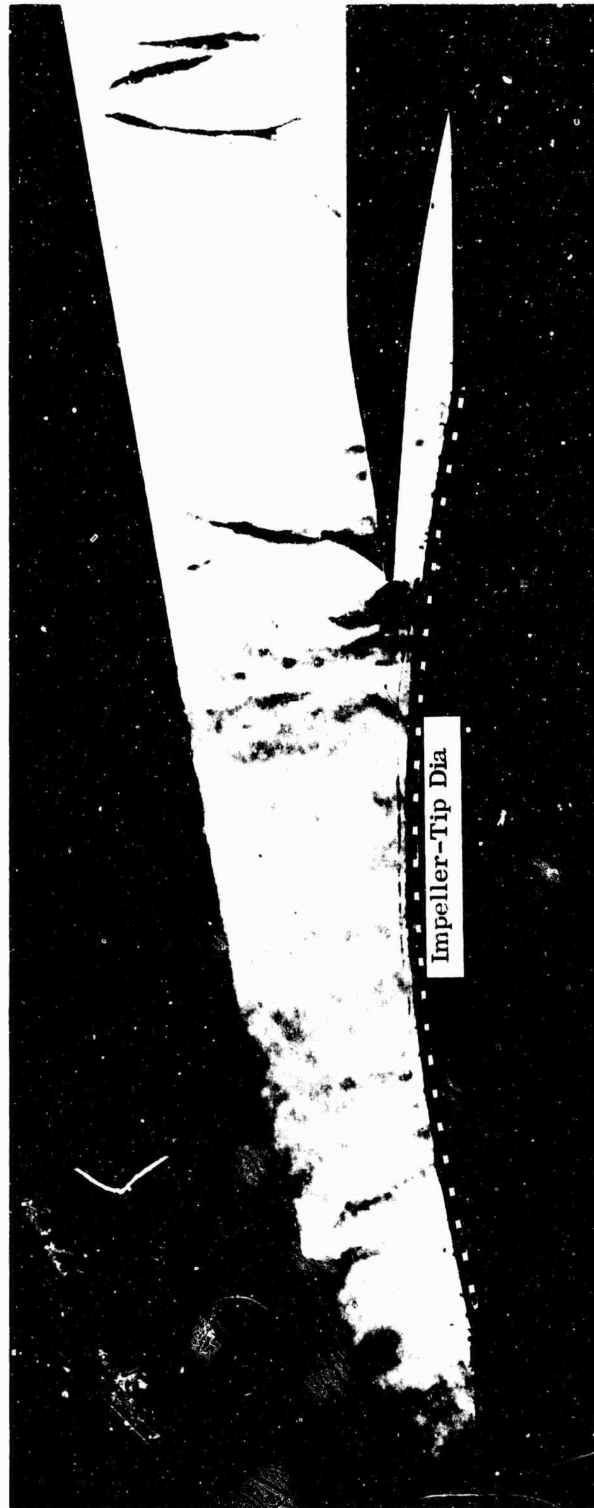


Figure 135. Schlieren Photograph of DI-2 (Test Number 3312, Impeller Speed = 35,000 rpm, Data Point 5).

CONFIDENTIAL

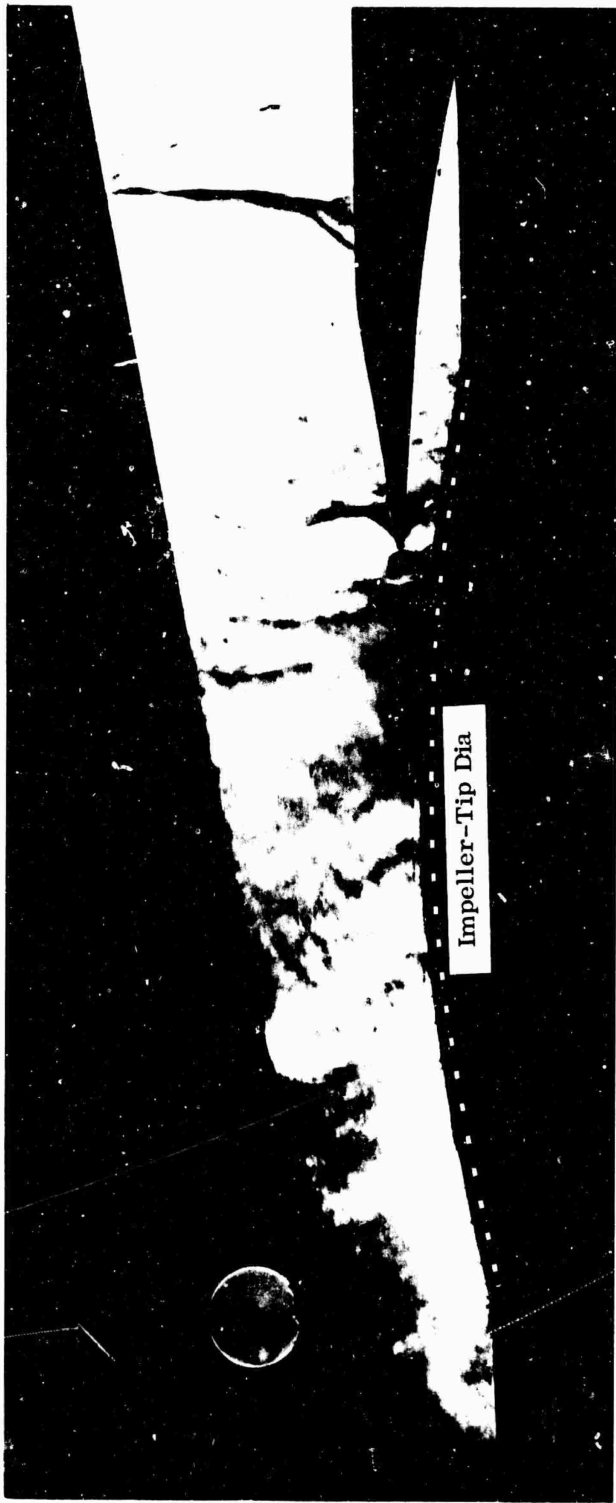


Figure 136. Schlieren Photograph of DI-2 (Test Number 3312, Impeller Speed = 39,000 rpm, Data Point 5).

CONFIDENTIAL

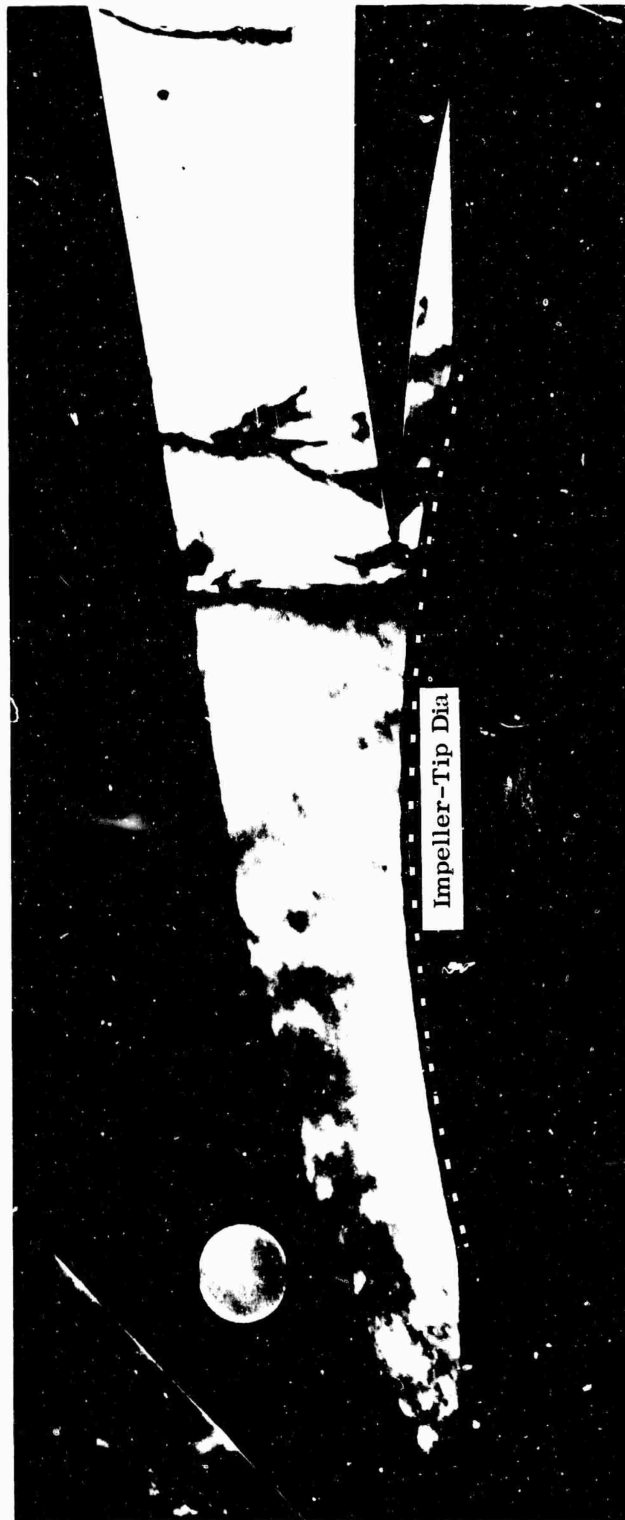


Figure 137. Schlieren Photograph of LI-2 (Test Number 3313, Impeller Speed = 46,000 rpm, Data Point 5).

CONFIDENTIAL

CONFIDENTIAL

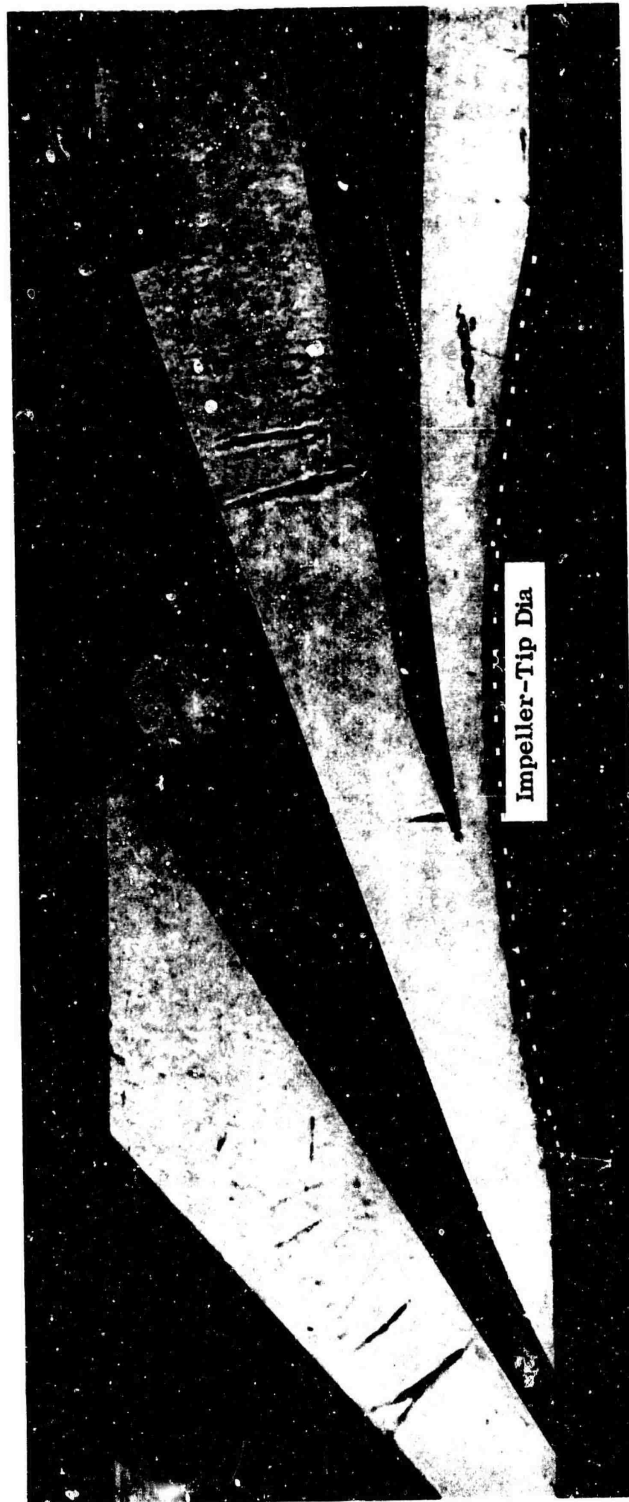


Figure 138. Schlieren Photograph of DI-3 (Test Number 3314, Impeller Speed = 25,000 rpm).

CONFIDENTIAL

CONFIDENTIAL

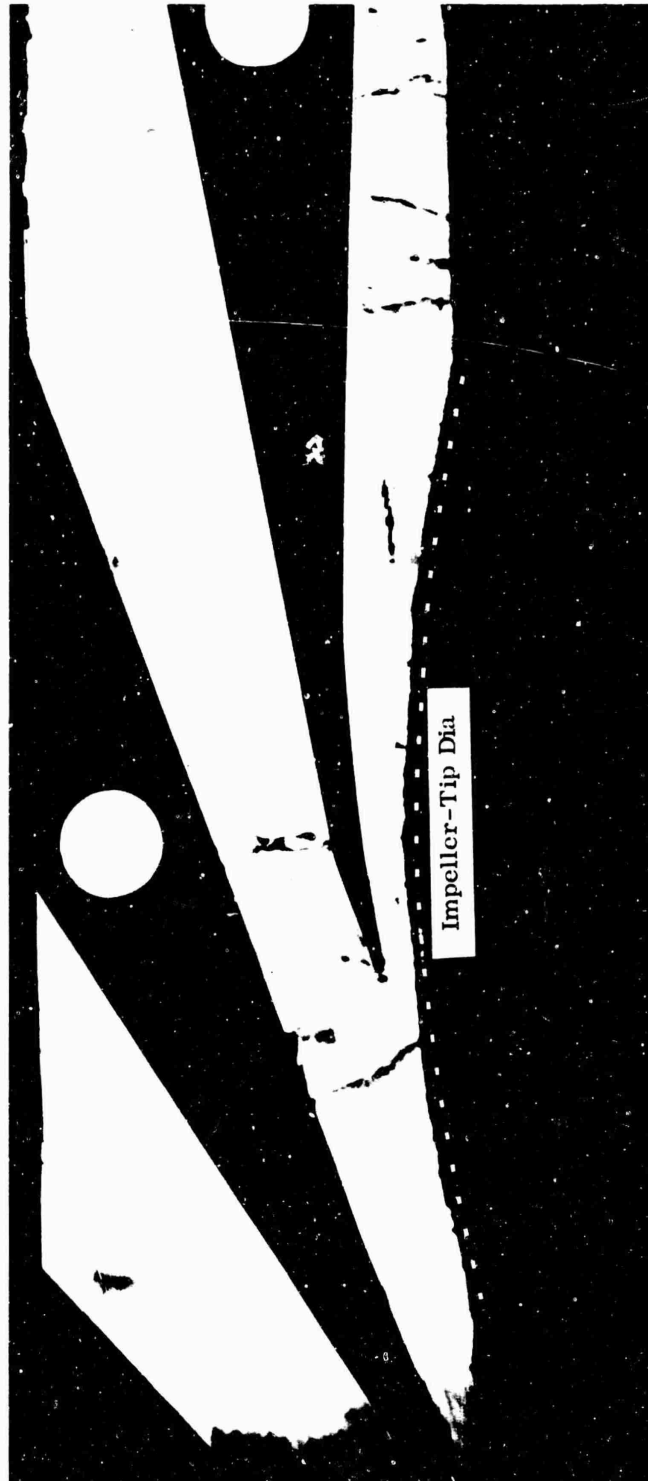


Figure 139. Schlieren Photograph of DI-3 (Test Number 3314, Impeller Speed = 46,000 rpm, Data Point 2).

CONFIDENTIAL

CONFIDENTIAL



Figure 140. Schlieren Photograph of DI-3 (Test Number 3314, Impeller Speed = 46,000 rpm, Data Point 3).

CONFIDENTIAL

CONFIDENTIAL



Figure 141. Schlieren Photograph of DI-3 (Test Number 3314, Impeller Speed = 46,000 rpm, Data Point 5).

CONFIDENTIAL

CONFIDENTIAL



Schlieren Photograph of DI-3 (Test Number 3314, Impeller
Speed = 46,000 rpm, Data Point 7).

Figure 142.

CONFIDENTIAL

CONFIDENTIAL

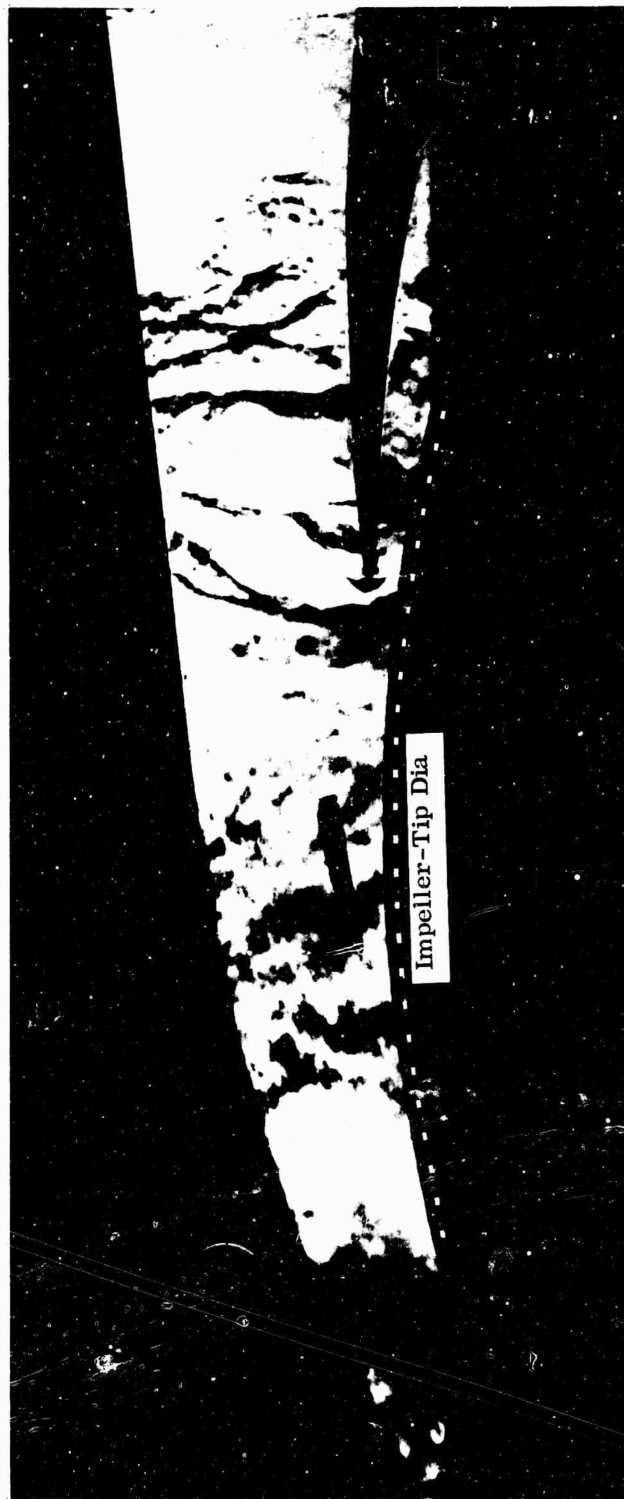


Figure 143. Schlieren Photograph of DI-1-2 (Test Number 3319, Impeller Speed = 50,000 rpm, Data Point 5).

CONFIDENTIAL

CONFIDENTIAL



Figure 144. Schlieren Photograph of DI-X1 (Test Number 3315, Impeller Speed = 50,000 rpm, Data Point 5).

CONFIDENTIAL

CONFIDENTIAL

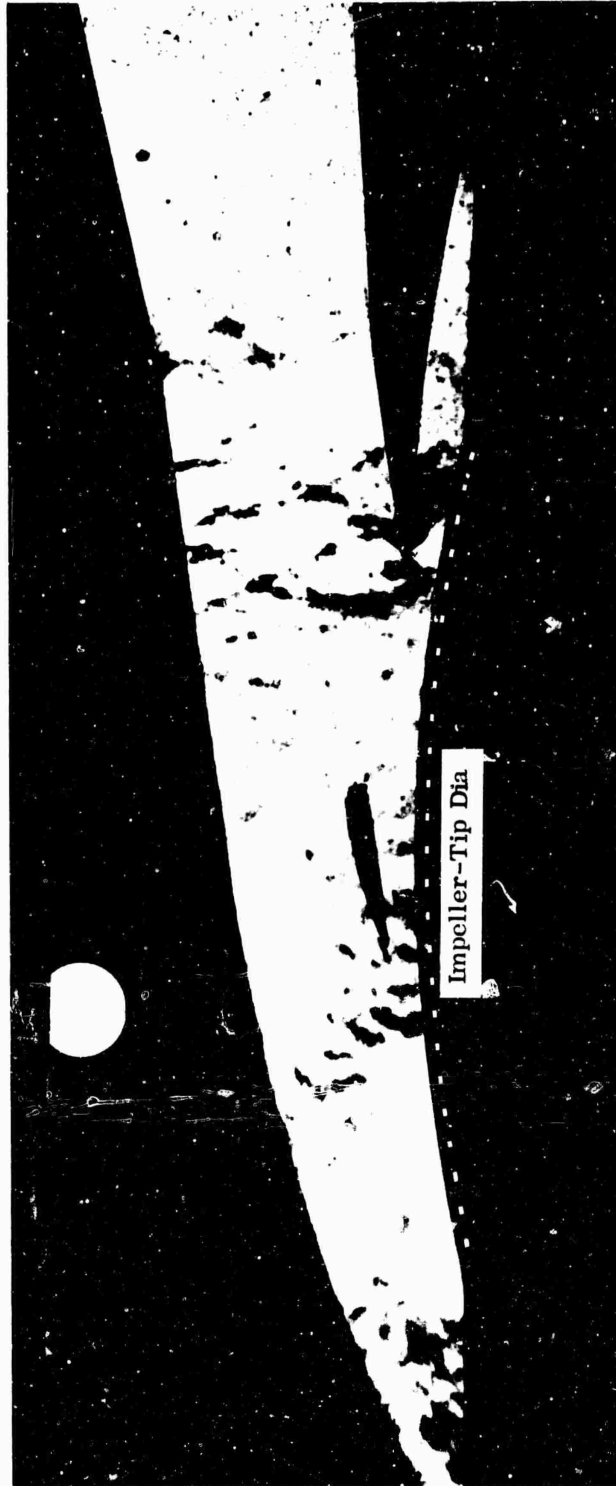


Figure 145. Schlieren Photograph of DI-X1-2 (Test Number 3318, Impeller Speed = 50,000 rpm, Data Point 5).

CONFIDENTIAL

CONFIDENTIAL

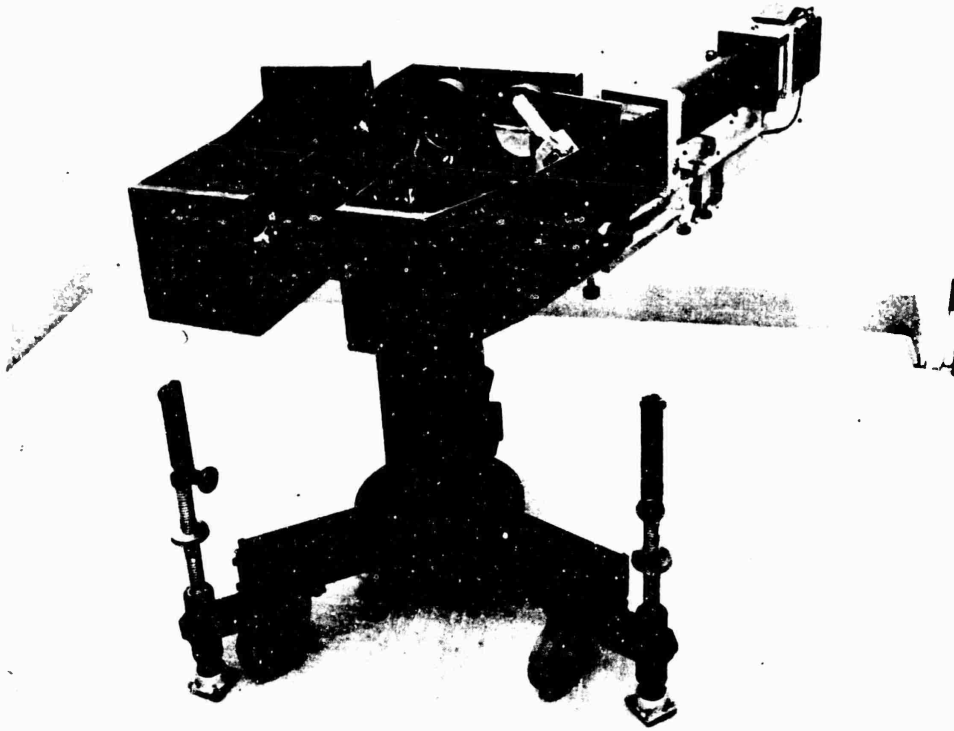


Figure 146. Schlieren Unit.

CONFIDENTIAL

CONFIDENTIAL

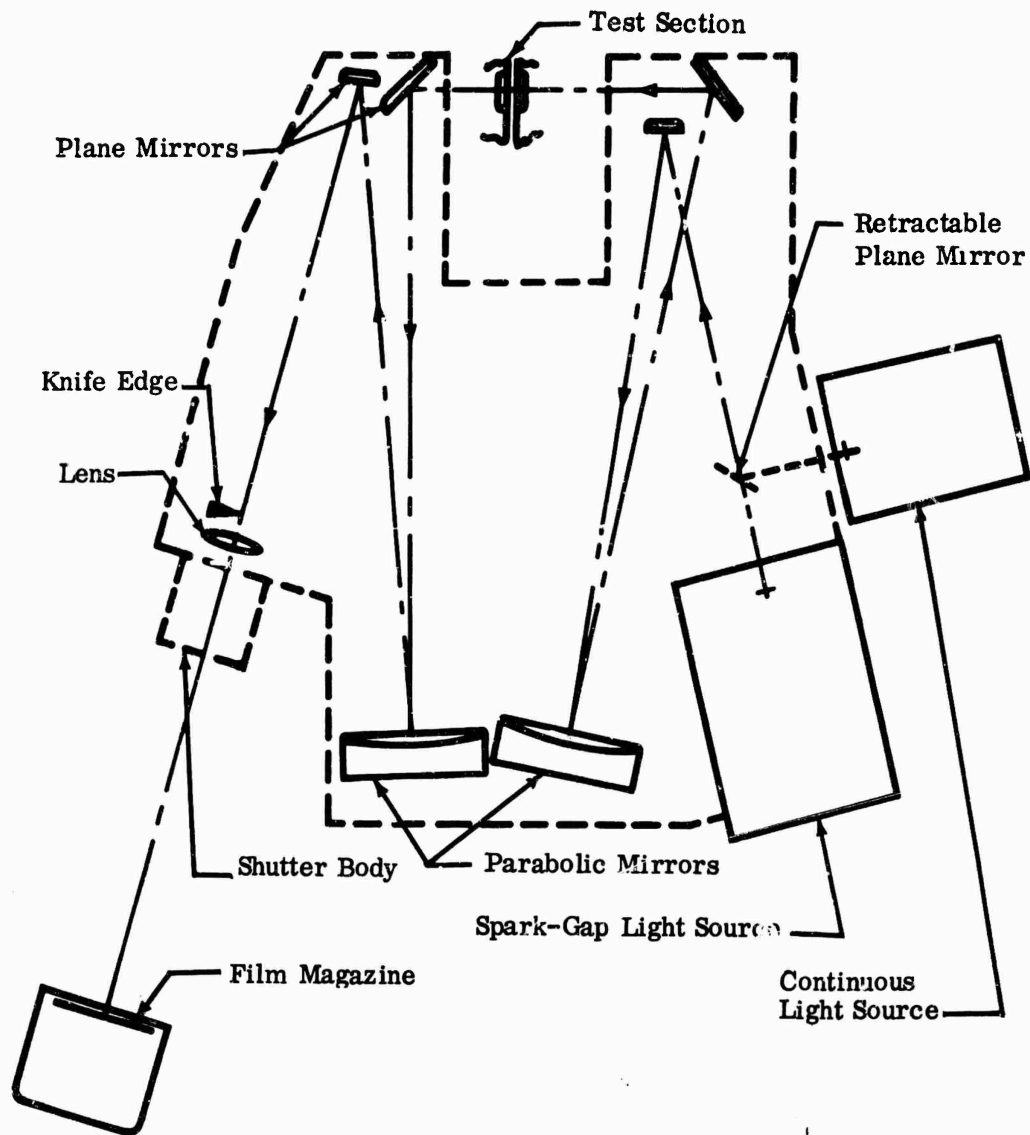


Figure 147. Schlieren Schematic Diagram.

CONFIDENTIAL

(U) APPENDIX XI

INLET-MACH-NUMBER EFFECTS ON SUBSONIC
DIFFUSER PERFORMANCE

ABSTRACT

The following literature survey and data correlation by R. M. Halleen and J. P. Johnston were accomplished by Creare, Incorporated, under a separate contract to The Boeing Company.

The survey results show the design technologies available from the literature on high subsonic diffusers that have stable boundary-layer and uniform conditions at the inlet; they also show various geometric limitations.

SYMBOLS

$\frac{A}{A}$	= area ratio
B_1	= ratio of inlet boundary-layer blockage area to the inlet cross-sectional area (see Reference 11)
C_p	= pressure-recovery coefficient — $(P_2 - P_1)/\bar{q}_1$
C_p^*	= locus of maximum pressure-recovery coefficient at prescribed nondimensional length (see Reference 11)
C_p^{**}	= locus of maximum pressure-recovery coefficient at prescribed area ratio (see Reference 11)
L	= axial length
M	= Mach number
N	= nondimensional axial length: L/R_1 for conical; L/W_1 (two-dimensional); $2L/W$ for square (three-dimensional); $L/(R_o - R_i)$ for annular diffusers
P_1	= inlet static pressure
P_2	= exit static pressure
\bar{q}	= mass-averaged dynamic pressure
R_1	= radius
u	= velocity parallel to wall
W	= width
y	= perpendicular distance from wall

1.0 LITERATURE SURVEYS OF SUBSONIC DIFFUSERS

Extensive literature surveys on subsonic diffuser performance and other characteristics are available, and some additional experimental studies on diffusers have been reported recently. These studies, with few exceptions, deal essentially with incompressible fluid flow. Design procedures have been developed for particular classes of diffusers. Some experimental information is available that indicates trends in the effect of inlet Mach number on diffuser performance, but generally this information is not satisfactorily correlated. Suggested correlations are given subsequently in terms of limitations and modifications to the incompressible-fluid design procedures.











Three references list the major diffuser studies published through 1963 (see References 4, 7, and 9). Two references on design procedure are available (References 9 and 11). A survey of diffuser literature published since 1963 applicable to the present work on diffuser design procedures was also completed. The significant work heretofore unreported by the previous surveys is found in References 7, 11, and 12. Table IV summarizes the reference data and symbols used in this study.

2.0 EVALUATION OF INLET-MACH-NUMBER EFFECTS

Inlet Mach number is not an important performance parameter when the Mach number is below the range of 0.20 to 0.30. Such performance can be predicted by using incompressible-fluid design procedures (see References 9 and 11). For inlet Mach numbers in excess of 0.20 to 0.30, diffuser performance variation as a function of inlet Mach number can be categorized into three different groups. The typical variation of the pressure-recovery coefficient, C_p , for each group is shown in Figure 148.

When the geometry of the diffusers studied at high subsonic inlet Mach number is plotted on the incompressible flow-regime map (see Figure 150), performance-variation classification — Groups A, B, and C — correlates with the geometric classification of the flow map. All diffusers exhibiting the Group A performance variation characteristic lie to the right of and below the appropriate line of appreciable stall. Those with the characteristic of Group B lie between the line of appreciable stall and Line B-B, and the only diffuser referenced with the characteristic of Group C lies to the left of Line B-B.

This correlation was true in all cases where a normal inlet boundary-layer velocity profile was obtained or could be anticipated. When a separating type of profile occurred at the inlet (Reference 10), Group B variation occurred, whereas the geometry predicts Group A behavior (see Figure 149).

TABLE IV					
REFERENCE DATA AND SYMBOLS					
Investigator	References	Symbols for Figures 3, 4, 5	$\frac{A}{A}$	N	B_1
<u>Conical Diffusers</u>					
Johnston	5		4.0	15.25	0.008 (est)
			4.0	5.39	-
			4.0	3.17	-
Copp	2		2.0	4.72	0.012
			2.0	4.72	0.056
Little & Wilbur	6		2.0	2.10	0.038
			2.0	3.92	0.016
			2.0	3.92	0.049
			2.0	4.02	0.007
Scherrer & Anderson	10		2.0	4.02	0.038
			1.96	4.30	0.004
			1.96	4.30	0.020
			1.96	6.40	0.004
<u>Annular Diffusers</u>					
Johnston	5		4.0	18.5	0.040 to 0.045 (est)
			3.39	10.8	0.028 to 0.033 (est)
Nelson & Popp	8		1.75	23.2	0.015
			1.75	12.9	0.015
<u>Two-Dimensional Diffusers</u>					
Woollett	13		3.0	12.0	-
			3.0	5.5	-
Young & Green	14		4.0	21.6	0.030 (est)
			4.0	16.2	0.030 (est)
			4.0	10.8	0.030 (est)
			4.0	8.1	0.030 (est)
Friedlich	15		4.0	5.4	0.030 (est)
			4.0	17.1	-
			3.0	11.4	-
Friedlich (Square & Three-Dimensional)	15		2.0	5.7	-
			4.0	22.9	-
			3.0	16.8	-
			2.0	9.5	-

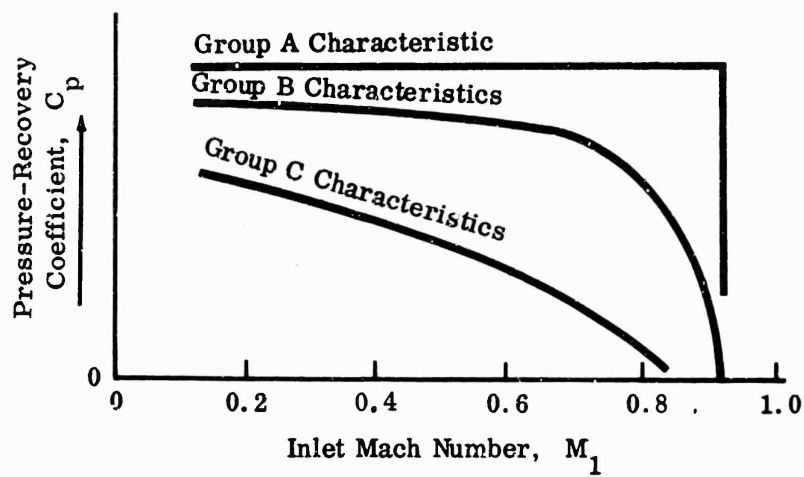


Figure 148. Typical Variation of Pressure-Recovery Coefficient Versus Inlet Mach Number.

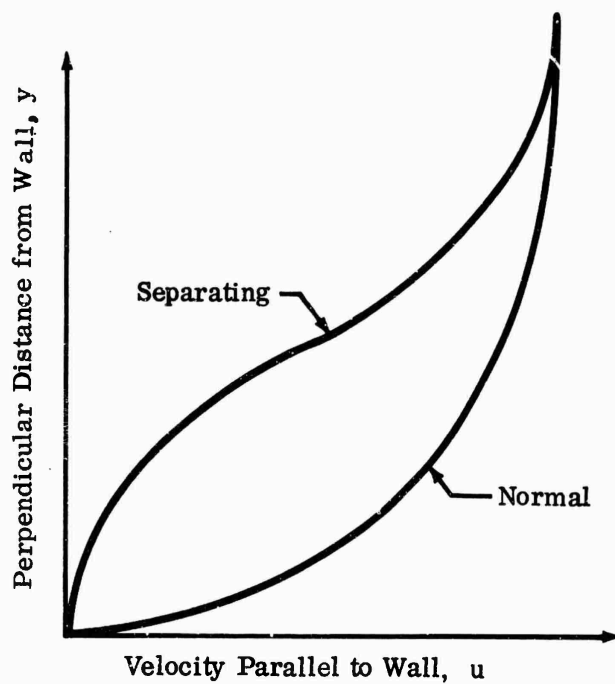


Figure 149. Velocity Profiles of Normal and Separating Boundary Layers.

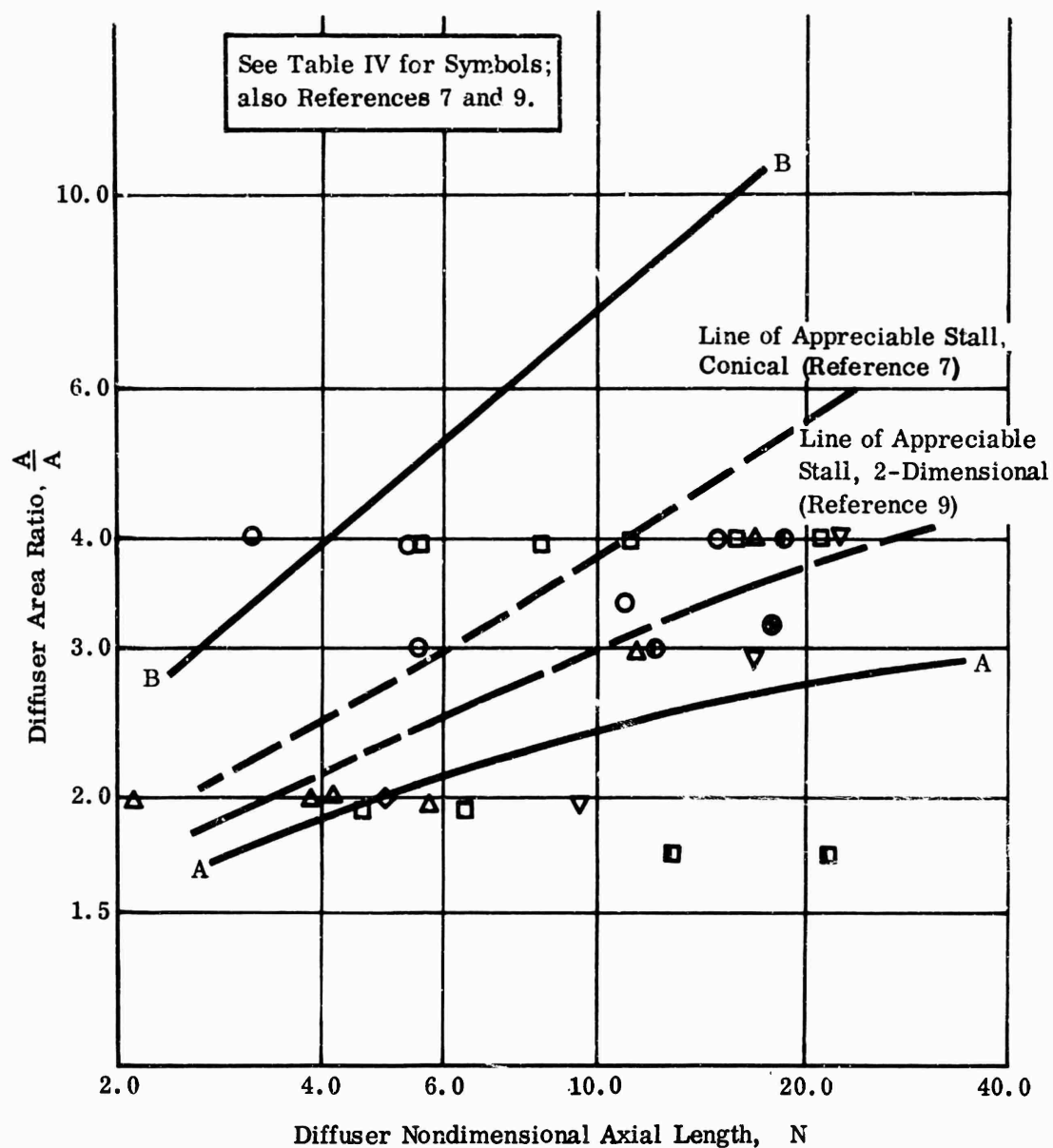


Figure 150. Flow-Regime Map.

The line of appreciable stall is different for conical diffusers from the 2-dimensional case, and Line B-B is from the 2-dimensional data only. Flow-regime information does not exist for the annular case, but the various data correlate on the basis of annular diffuser structure — either 2-dimensional or conical.

A further correlation was attempted using the system geometry and the pressure-recovery coefficients, C_p^* and C_p^{**} , from the incompressible data. Figure 151 shows that no apparent correlation is available for subsonic diffusers from the given data.

2.1 EFFECT OF INLET MACH NUMBER ON GROUP A DIFFUSERS

Data indicate that the performance of diffusers in this classification is unaffected, or even slightly improved, by increasing inlet Mach number until some critical value is attained. At the critical value, the performance decreases almost instantaneously to zero. This behavior is generally attributed to the absence of local shocks until the critical value, or choking condition, is reached at the inlet, where local shocks at the inlet cause flow separation and associated stalled flow from the inlet through the diffuser.

The critical inlet Mach number is a direct function of the inlet blockage ratio, B_1 . A relation that correlates the available data for Group A diffusers is a straight line, shown in Figure 152. The scatter in the data is due principally to the several methods used in determining the inlet Mach number. The data have not been correlated by a standard method; thus, variation in these values would be expected.

The performance of Group A diffusers below critical Mach numbers can be predicted satisfactorily using a technique similar to that given in References 9 and 11. The analytical procedure would be to consider the core flow on a 1-dimensional compressible basis and the boundary layer on an incompressible basis.

2.2 EFFECT OF INLET MACH NUMBER ON GROUP B DIFFUSERS

Data show that the performance of this group of diffusers is affected adversely by increasing inlet Mach number. The form of the effect is such that the C_p change is relatively small (less than 20 percent) for low Mach numbers (0.2 to 0.6), but decreases more rapidly toward zero in the higher Mach number range. There is no well-defined critical inlet Mach number, as with the Group A diffusers. Insufficient data also prevent correlating the value of inlet Mach number where this parameter will have a major effect on diffuser performance.

See Table IV for Symbols;
also Reference 11.

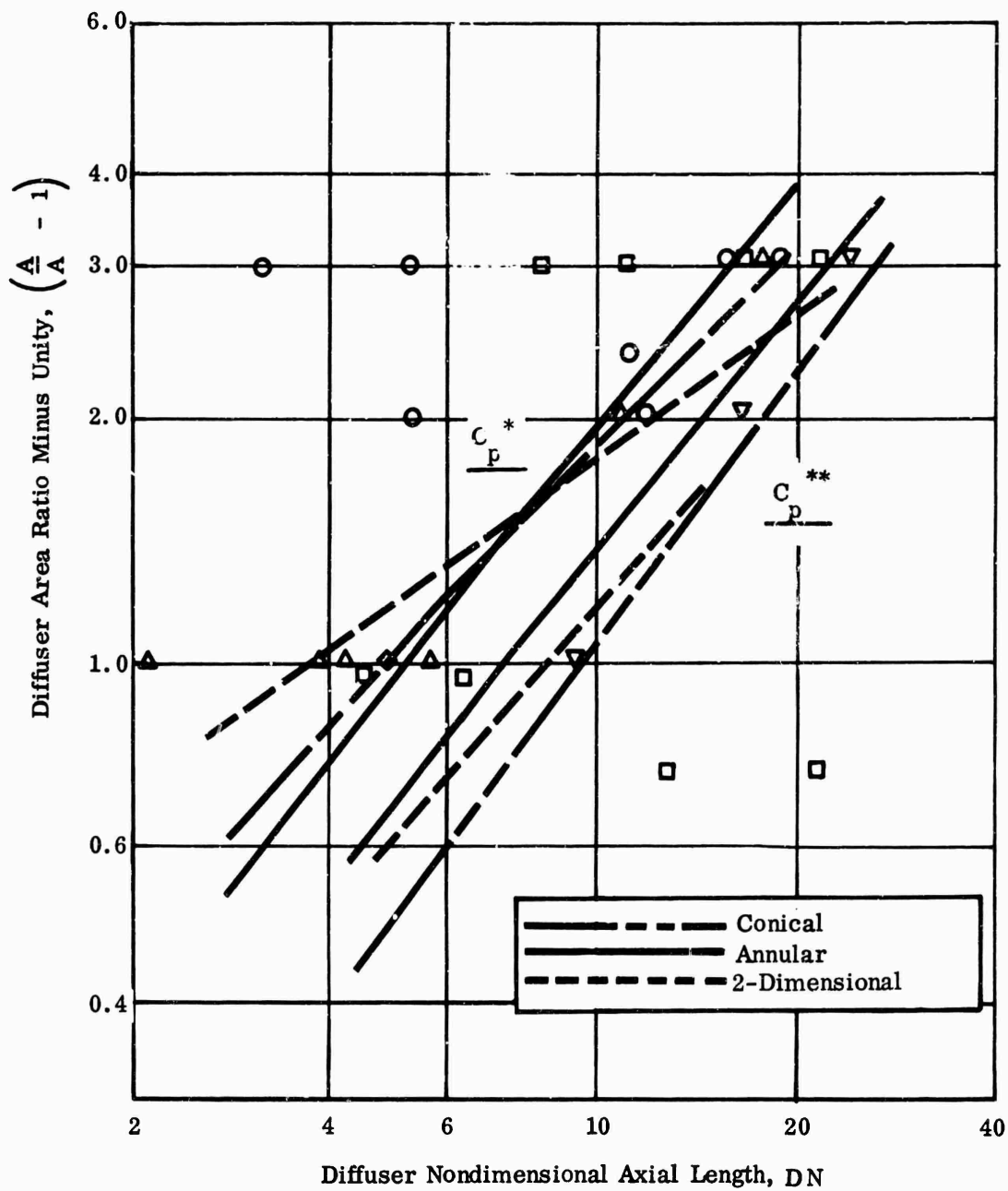


Figure 151. Locus of Maximum Pressure Recovery Versus System Geometry.

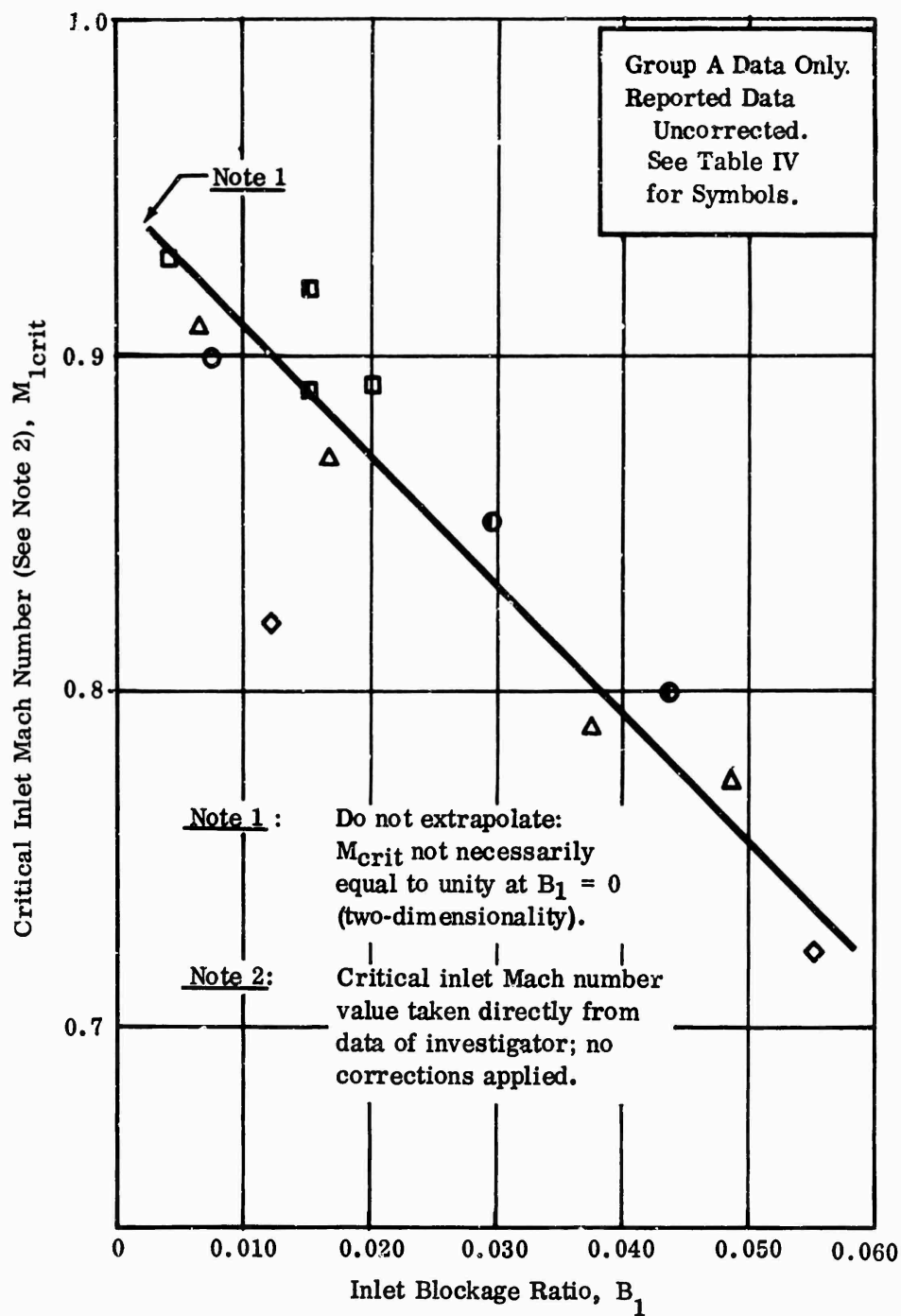


Figure 152. Critical Inlet Mach Number Versus Inlet Blockage Ratio.

Performance, within 20 percent, should be predicted for Group B diffusers with inlet Mach numbers less than 0.6 when a similar scheme to that given for Group A units is used.

2.3 EFFECT OF INLET MACH NUMBER ON GROUP C DIFFUSERS

The performance of this group of diffusers is continuously affected by variation in the inlet Mach number. Major performance reductions are found for small increases in the inlet Mach number over the entire spectrum. No predictive schemes are available for the incompressible case. The only available guides to performance-prediction information for this group of diffusers, and also those of Group B, for high inlet Mach numbers are the correlations given in Reference 4. Caution should be exercised when using these results, as no attempt was made to separate effects, other than inlet Mach number, from the correlation. An example of this can be found in the correlation given in Figure 18 of Reference 4 for critical Mach number as a function of inlet blockage. The resultant correlation, which is more complicated than that shown in Figure 152, was developed by using data from both Group A and B diffusers for curve-fitting.

3.0 SUMMARY

- 1) The performance variation of subsonic diffusers due to inlet Mach number effects can be classified into 3 groups: A, B, and C.
- 2) Performance variation classifications correlate directly with the diffuser geometry in the incompressible-flow regimes.
- 3) The critical inlet Mach number for Group A diffusers is primarily a function of inlet blockage.
- 4) Prediction of the effect of inlet Mach number on performance can be made for Group A diffusers, but no analytical procedure exists for predicting the critical inlet Mach number.
- 5) The classification and correlations found are valid for normal inlet boundary-layer velocity profiles, but partial evidence indicates that these results may have to be modified for separating profiles.

REFERENCES

1. Cockrell, D.J., Diamond, M.J., and Jones, G.D., "The Diffuser Inlet Flow Parameter," Journal of Royal Aeronautical Society, Vol. 69, 1965, pp. 350-2.
2. Copp, M.R., Effects of Inlet Wall Contour On the Pressure Recovery of a 10° 10-Inch-Inlet-Diameter Conical Diffuser, NACA RM L51E11a, 1951.
3. Emmons, H.W., The Theoretical Flow of a Frictionless, Adiabatic, Perfect Gas Inside of a Two-Dimensional Hyperbolic Nozzle, NACA TN 1003, 1946.
4. Henry, J.R., Wood, C.C., and Wilbur, S.W., Summary of Subsonic-Diffuser Data, NACA RM L56F05, 1956, Released 1963.
5. Johnston, J.P., Summary of Results of Tests on Short, Conical Diffusers with Flow Control Inserts; as of June 1, 1959, Ingersoll-Rand Company, Philipsburg, N.J., Technical Note No. 71.
6. Little, B.H., Jr., and Wilbur, S.W., Performance and Boundary-Layer Data from 12° and 23° Conical Diffusers of Area Ratio 2.0 at Mach Numbers up to Choking and Reynolds Numbers up to 7.5×10^6 , NACA Report 1201, 1954.
7. McDonald, A.T., and Fox, R.W., Incompressible Flow in Conical Diffusers Purdue Research Foundation, Lafayette, Indiana, Project No. 3684, Technical Report No. 1, September 1964.
8. Nelson, W.J., and Popp, E.G., Performance Characteristics of Two 6° and Two 12° Diffusers at High Flow Rates, NACA RM L9H09, 1949.
9. Reneau, L.R., Johnston, J.P., and Kline, S.J., Performance and Design of Straight, Two-Dimensional Diffusers, Stanford University, Stanford, California, Thermosciences Division Report No. PD-8, September 1964.
10. Scherrer, R., and Anderson, W.E., Preliminary Investigation of a Family of Diffusers Designed for Near Sonic Inlet Velocities, NACA TN 3668, 1956.
11. Sovran, G., and Klomp, E.D., Experimentally Determined Optimum Geometries for Rectilinear Diffusers with Rectangular, Conical, or Annular Cross-Section, General Motors Research Laboratories Publication GMR-511, November 1965.

REFERENCES (Continued)

12. Stratford, B.S., and Tubbs, H., "Maximum Pressure Rise Attainable in Subsonic Diffusers," J. Roy. Aero. Soc., Vol 69, No. 652, April 1965, pp. 275-8.
13. Woollett, R.R., Preliminary Investigation of Short Two-Dimensional Subsonic Diffusers, NACA RM E56C02, 1956.
14. Young, A.D., and Green, G.L., Tests of High-Speed Flow in Diffusers of Rectangular Cross-Section, A.R.C.R. & M. No. 2201, 1944.
15. Friedlich, S., Performance Characteristics of Plane Wall Diffuser and Some New Concepts of Diffuser Flow Mechanisms, M.S. Thesis, University of Washington, 1959.

STRAIGHT DIFFUSER PERFORMANCE AT HIGH INLET
MACH NUMBERS

ABSTRACT

This test series by Peter W. Runstadler, Jr. was accomplished by Creare, Incorporated, under a separate contract to The Boeing Company.

Measurements have been made of the pressure recovery of straight-wall diffusers with inlet Mach numbers between 0.3 and choking. Two aspect ratios are studied: 5.7 and 0.25. For the 5.7 aspect ratio diffusers, blockages of 0.01 to 0.15 for $L/W = 15$ and 0.04 for $L/W = 10$ at choking conditions are reported. For the 0.25 aspect ratio diffusers, blockages range between 0.03 and 0.17 at choking conditions for $L/W = 15$. Divergence angles, 2θ , from 4 to 12 degrees are covered for both aspect ratios.

There is no critical subsonic inlet Mach number at which a sharp drop in pressure recovery occurs. Evidence in the published literature has previously indicated such a critical subsonic inlet Mach number. There is a severe drop in performance in supercritical flow when the shock Mach number in the diffusing passage exceeds approximately 1.1 to 1.2.

Variation of pressure recovery with inlet Mach number in the subsonic range is observed as a function of divergence angle and blockage.

A significant difference exists between the present data at high inlet Mach numbers and previous data at low Mach numbers to rule out the use of low Mach number data in the design of high inlet Mach number diffusers.

The present data show maximum pressure recovery at a divergence angle of 10 degrees for all blockages up to 0.17 with a diffuser aspect ratio of 0.25, L/W of 15, and inlet Mach number of 1. For an aspect ratio of 5.7, the data indicate maximum pressure recovery for a divergence angle of 6 degrees.

SYMBOLS

AR	= aspect ratio
A_t	= $A_{\text{geometric}}$ = throat geometrical area
A_{flow}	= one-dimensional-flow area
B	= boundary-layer blockage = boundary-layer displacement area/geometrical area of throat
C_p	= diffuser pressure-recovery coefficient = $\frac{P_{\text{exit}} - P_{\text{throat}}}{P_o - P_{\text{throat}}}$
D_H	= hydraulic diameter = $\frac{4A_t}{P_T}$
L	= diffuser wall length (centerline distance from throat to exit)
m	= mass flow rate
M	= inlet Mach number on centerline
P	= static pressure
P_o	= stagnation pressure at diffuser inlet (throat) on centerline
P_T	= wetted perimeter
R_e	= Reynolds number
\bar{U}	= mean velocity = $\frac{m}{\rho A_t}$
W	= diffuser throat width
2θ	= diffuser divergence angle
ϕ	= $1 - B$
ρ	= density
ν	= kinematic viscosity

SYMBOLS (Continued)

Subscripts

- throat - diffuser throat
- exit - diffuser exit
- choke - choking conditions at diffuser throat

1.0 INTRODUCTION

A substantial body of data exists in the published literature on the performance of straight-wall diffusers at low inlet Mach numbers. Reneau* has surveyed these data. Diffuser performance (usually in the form of pressure recovery (C_p)) is correlated as a function of divergence angle (2θ), wall length-to-throat-width ratio (L/W), and inlet flow blockage ratio (B). (Reneau reports data in terms of $2\delta^*/W$, which is equivalent to blockage (B) as defined in this report.) There is relatively little information on diffuser performance at high inlet Mach numbers, i.e., $M > 0.2$ to 0.3 . The design of efficient diffusers for high-speed centrifugal compressors depends upon this information.

Halleen and Johnston (Appendix XI) recently surveyed available published data on the performance of straight diffusers at high inlet Mach numbers. They were able to conclude the following:

- 1) The variation in pressure recovery (C_p) of subsonic diffusers due to inlet Mach number effects can be classified into 3 groups: A, B, and C. The typical variation of pressure recovery for each group is shown in Figure 153.
- 2) Performance variation in each classification correlates directly with diffuser geometry — the correlation is in agreement with the incompressible flow-regime map of Figure 154.
- 3) Group A diffusers (conical or 2-dimensional), which are at divergence angles below the line of appreciable stall (conical or 2-dimensional, respectively), exhibit the characteristic of a critical Mach number above which the relatively constant recovery of the diffuser up to this Mach number suffers a drastic drop. This critical Mach number is a function of inlet blockage ratio (B), as shown in Figure 155.
- 4) Arguments for the existence of a critical Mach number for Group A diffusers can be presented (see Appendix XI), but no analytical procedure exists for predicting the critical inlet Mach number.
- 5) The classifications and correlations are valid for normal inlet boundary-layer velocity profiles, but partial evidence indicates that these results may have to be modified for separating types of velocity profiles.

*L. R. Reneau, et al, Performance and Design of Straight Two-Dimensional Diffuser, Report PD-8, Thermosciences Division, Department of Mechanical Engineering, Stanford University, Stanford, California, September 1964.

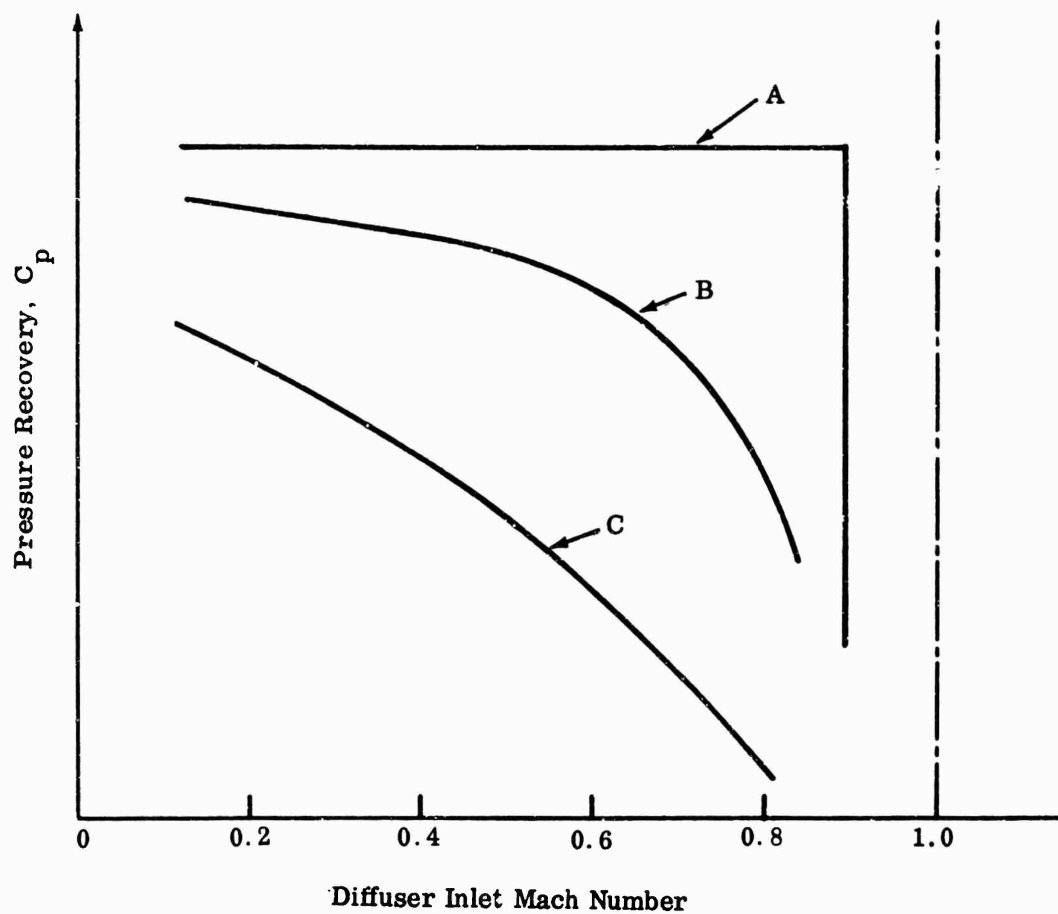


Figure 153. Characteristic Grouping of Diffuser Data, (C_p Versus Inlet Mach Number at Fixed Geometry).

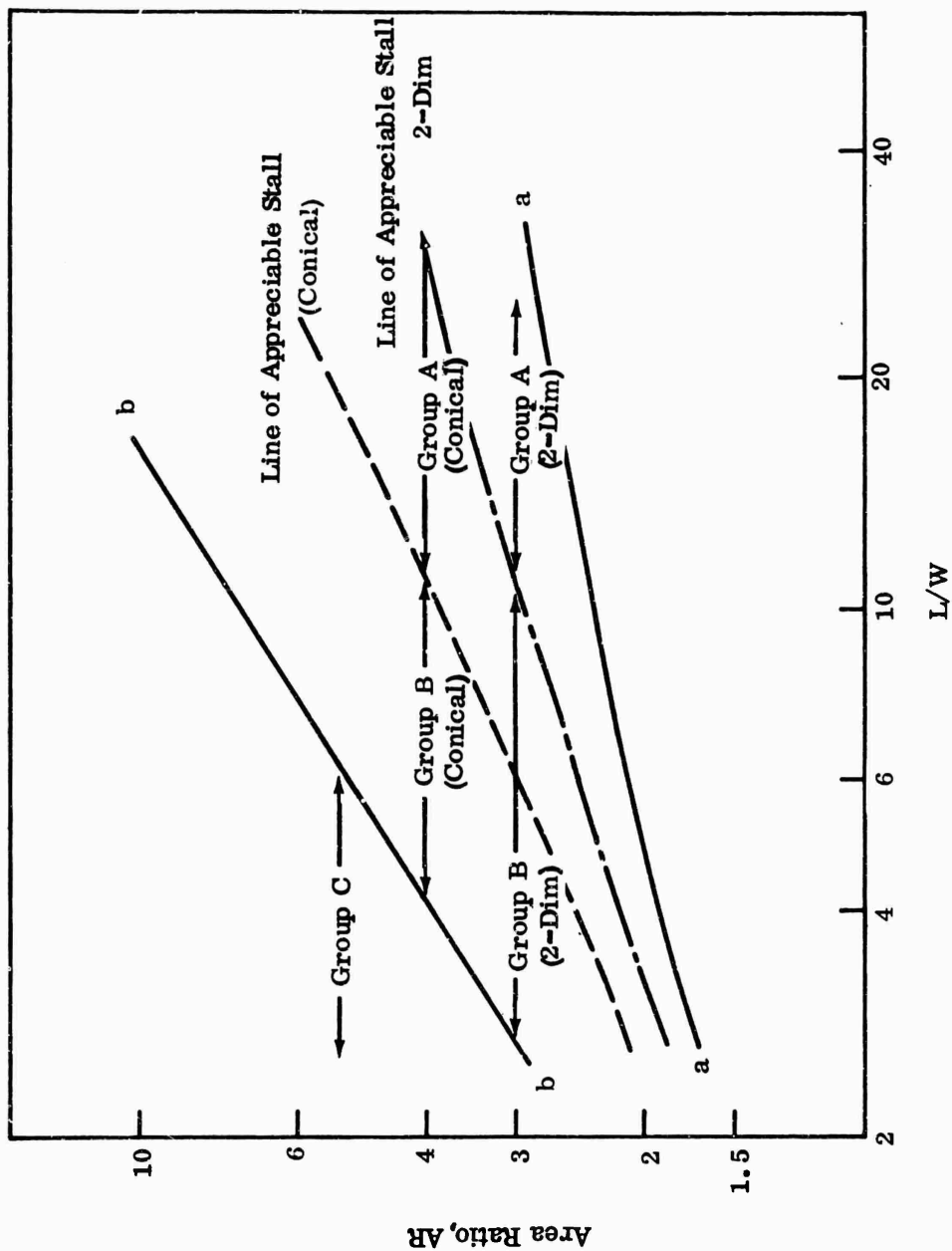


Figure 154. Flow-Regime Map, Inlet Mach Number Group Classification.

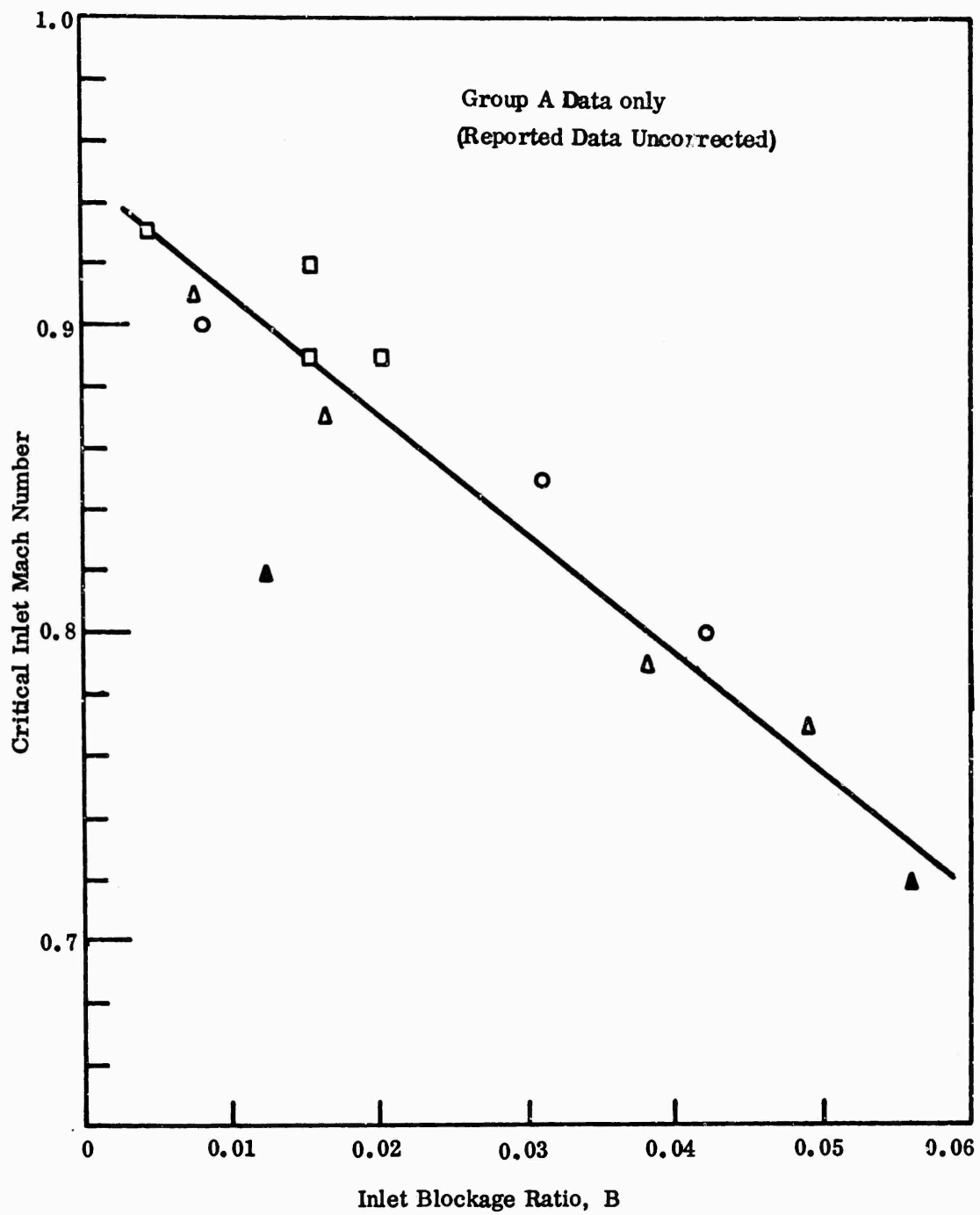


Figure 155. Critical Inlet Mach Number Versus Blockage Ratio.

The aspect ratio, divergence angle, and length-to-width ratio of diffusers for centrifugal compressors yield diffuser geometries which fall largely under the group A classification of Halleen and Johnston. Thus, these diffusers should suffer relatively poor performance at high inlet Mach numbers compared to the performance at low Mach numbers, if conclusions 1, 2, and 3 are correct. However, experimental data on high speed compressors, from the contractor's diffuser research, show that good diffuser performance is obtained, even though throat Mach numbers are higher than the critical values reported in Appendix XI. Two reasons for this discrepancy appear possible:

- 1) The critical Mach number at subsonic inlet conditions as shown in previously available evidence is not correct*; or
- 2) A critical Mach number does exist, producing a region of very poor diffuser performance, but this is then followed by a gain in performance at higher Mach numbers; i.e., the C_p versus inlet Mach number characteristic has a "dip" at some high inlet Mach number.

The present work was undertaken (1) to resolve which, if either, of these is correct, and (2) to provide design criteria for high inlet Mach number diffusers with parameters within the range of interest for high-speed centrifugal-compressor applications.

The experimental procedures are considered first, and are followed by a discussion of the results, and major conclusions.

2.0 EXPERIMENTAL PROCEDURE

The pressure recovery for the straight-wall, 2-dimensional diffuser geometry can be correlated on 5 independent parameters:

- 1) Divergence angle (2θ);
- 2) Diffuser length-to-throat-width ratio (L/W);
- 3) Aspect ratio (AR);
- 4) Flow blockage at the diffuser throat (B);
- 5) Inlet throat Mach number (M_t).

*H. Pearson, J. B. Holiday, S. F. Smith, "A Theology of the Cylindrical Ejector Supersonic Propelling Nozzle," Journal of the Royal Aeronautical Society, 62, 746, 1958.

Design criteria for predicting optimum diffuser performance require a diffuser performance map (C_p) as a function of these 5 variables. The variables were chosen to cover areas of interest to the centrifugal-compressor, vane-island diffuser.

2.1 GEOMETRICAL PARAMETERS

The geometrical configurations of the diffuser and diffuser inlets are shown in Figures 156 through 160. The diffuser test section consists of a series of nozzle blocks and diffuser blocks sandwiched between parallel side plates. The interchangeable nozzle blocks permit the use of different throat lengths preceding the diffuser passage; this allows a range of blockage values to be obtained for a fixed diffuser geometry. Likewise, the different diffuser blocks cover the range of diffuser angles for fixed aspect ratio and length-to-width ratio.

The assembly is bolted together and sealed with RTV sealant. The test section is connected with flanges (Figures 156 and 157) to 4-inch pipe upstream and downstream of the test section. The throat width and diffuser angle are accurately set (< 0.5 percent) with gage blocks at the throat and diffuser exit. The diffuser and throat passages are maintained clean of any residue RTV sealant, etc. The flow exits into the gage space at the end of the diffuser and then into the 4-inch pipe. The exit static pressure is measured in the 4-inch pipe downstream of the diffuser. The difference between the diffuser exit static pressure and the downstream static pressure was less than 0.5 percent.

For convenience of presentation, the tests are divided into two groups; tests with a 5.7 aspect ratio and tests with an 0.25 aspect ratio.

The 5.7 aspect ratio test section had side plates, nozzle, and diffuser blocks of aluminum. The 0.25 aspect ratio test section had one side plate made of 1-inch-thick Lucite, permitting visual observation of the flow. Early in the 0.25 aspect ratio studies it was observed that an oil and water emulsion visible in the flow appeared to produce erratic pressure measurements at the diffuser inlet. (The effect might be caused by any one of a number of factors: an effective increase in the throat blockage caused by water and oil in the flow, a change in sonic velocity as a result of 2-phase flow, the possibility of condensation shock effects, etc.) Since the water and oil came from the compressor supplying air to the test section, 2 centrifugal separators were installed upstream of the test section to assist in reducing the amount of oil and water in the flow. The 0.25 aspect ratio data were only taken when the flow by visual observation was substantially clear of oil and water mist. We suspect that the 5.7 aspect ratio tests (conducted prior to the 0.25 aspect ratio studies) may have had substantial amounts of oil and water vapor in the flow; however, time did not permit these tests to be repeated to determine the possible influence of any mist conditions on the pressure recovery.

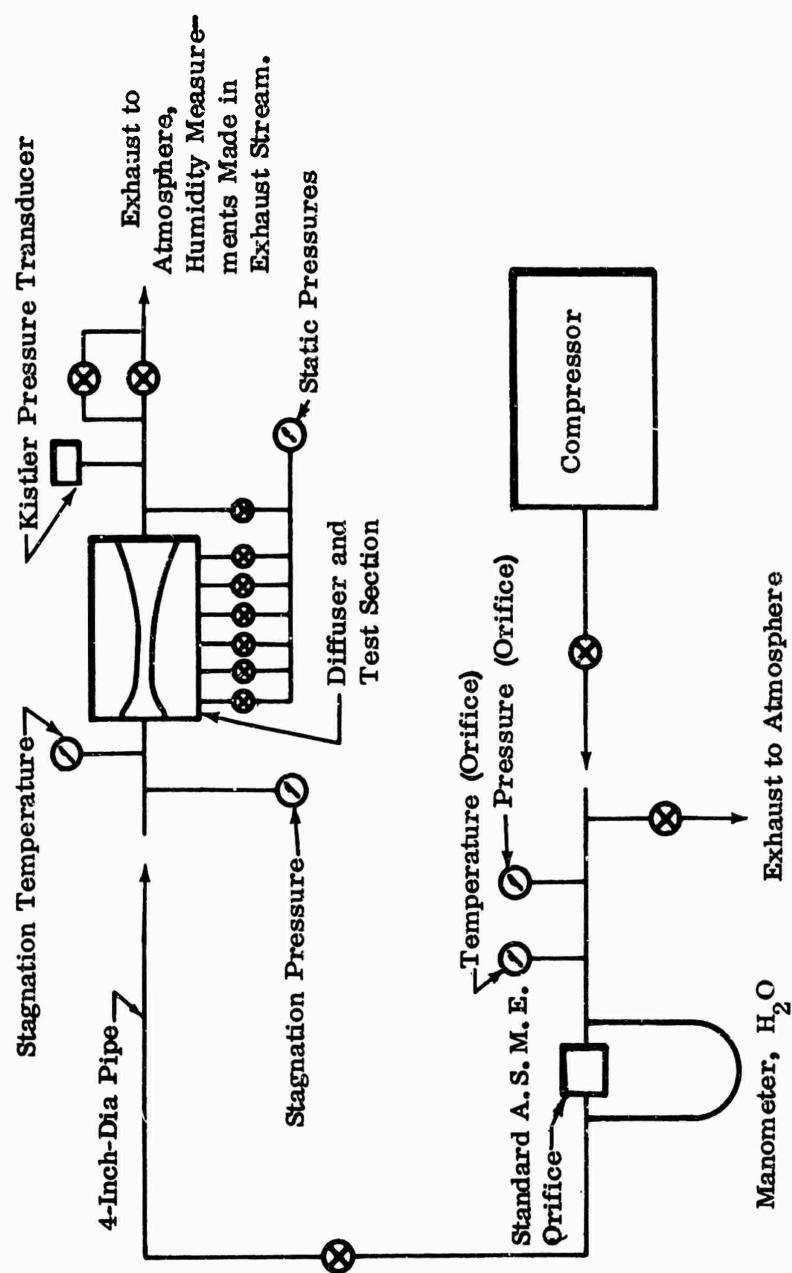


Figure 156. Flow Arrangement and Measurement Techniques.

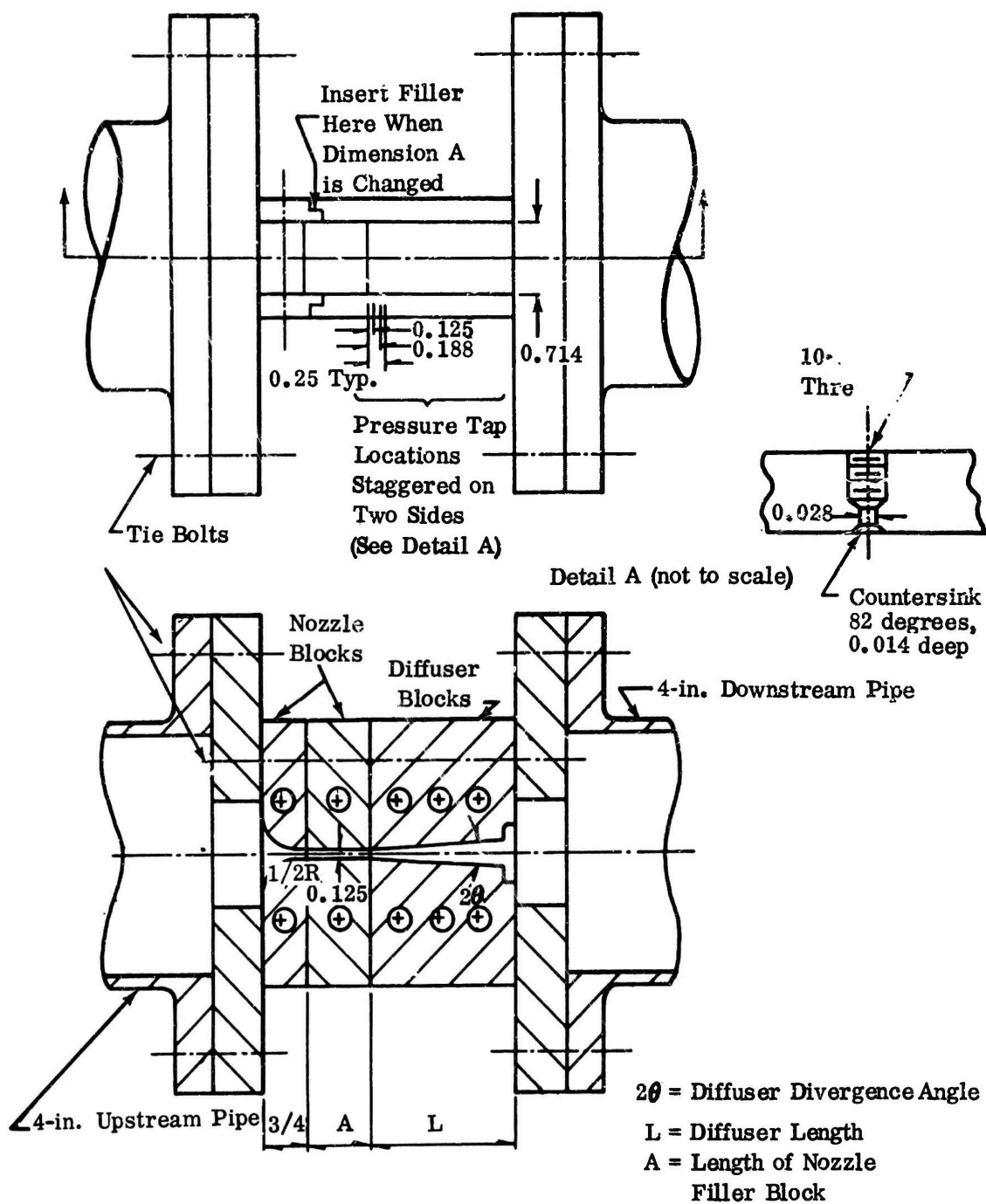


Figure 157. Diffuser Test Section (5.7 Aspect Ratio).

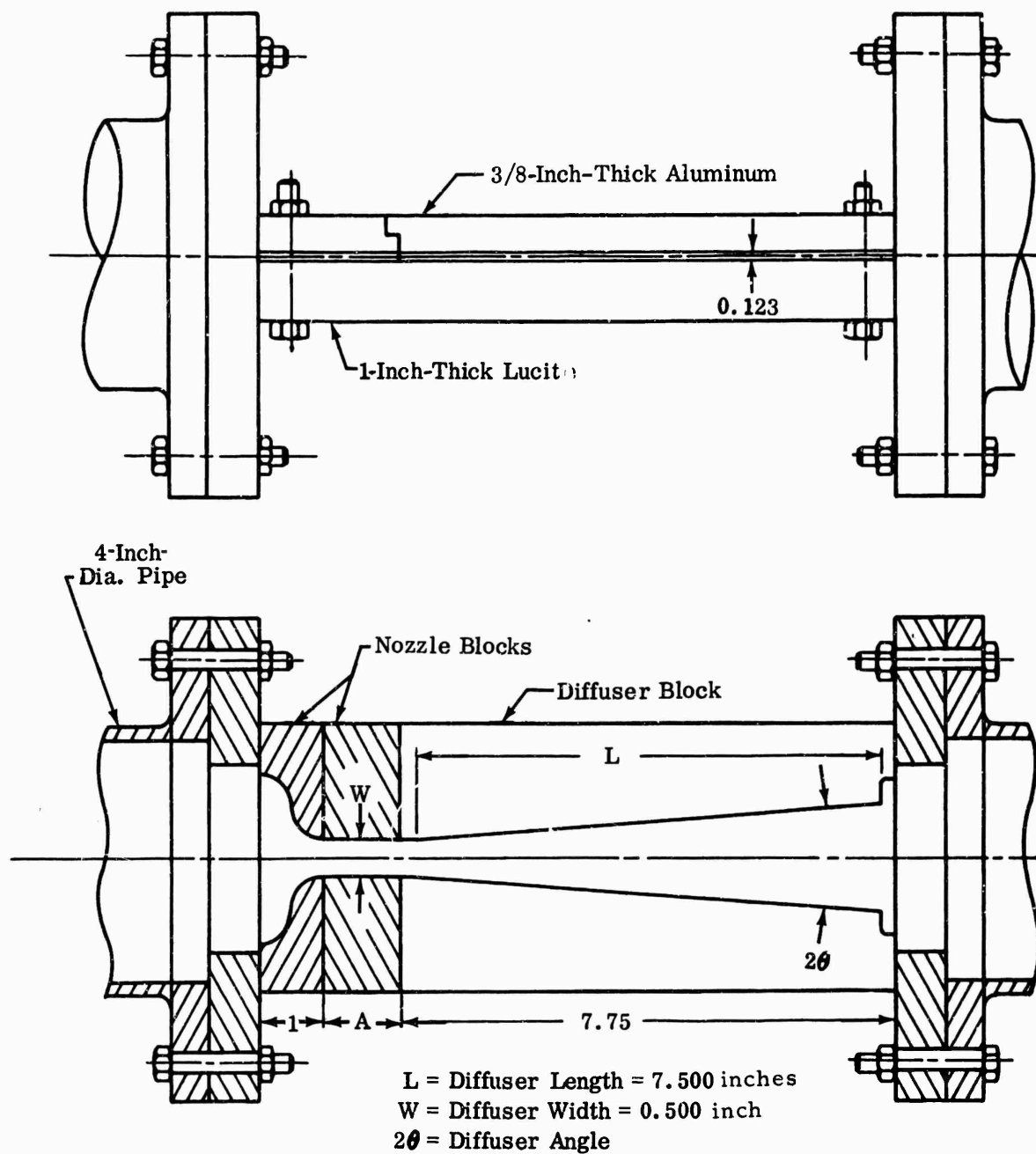
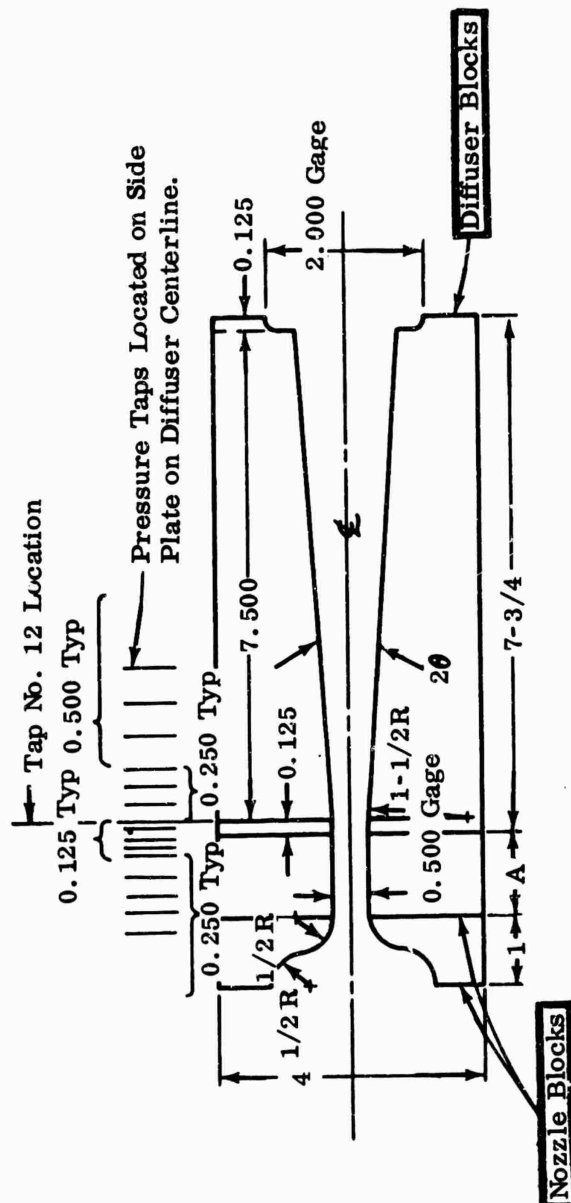


Figure 159. Diffuser Test Section (0.25 Aspect Ratio).



Depth of Blocks = 0.128 Inch
Material: 2024 Aluminum

2θ	=	4.0°	$\pm 0.1^\circ$	A	=	0	Tolerances:
	=	6.0°	$\pm 0.1^\circ$		=	0.500	All Fractional Dimensions $\pm 1/64$ inch
	=	8.0°	$\pm 0.1^\circ$		=	1.500	All Decimal Dimensions ± 0.005 inch
	=	10.0°	$\pm 0.1^\circ$		=	3.500	All Gage Dimensions ± 0.0005 inch
	=	12.0°	$\pm 0.1^\circ$				

Figure 160. Nozzle and Diffuser Block Geometry¹ (0.25 Aspect Ratio Tests, $L/W = 15$).

2.1.1 GEOMETRICAL PARAMETERS, 5.7 ASPECT RATIO

A throat width of 0.125 inch and throat depth of 0.714 inch gave a 5.7 aspect ratio diffuser.

Sets of diffuser blocks provided symmetrical divergence angles (2θ) of 4, 6, 8, 10, and 12 degrees.

Four nozzle blocks gave inlet throat length-to-diffuser-width ratios of 3, 11, 19, and 35.

Two sets of diffuser blocks provided diffuser length-to-width ratios:

$$L/W = 15, 10$$

2.1.2 GEOMETRICAL PARAMETERS, 0.25 ASPECT RATIO

The throat depth of 0.125 inch and throat width of 0.500 inch provided an aspect ratio of 0.25.

Divergence angles covered:

$$2\theta = 4^\circ, 6^\circ, 8^\circ, 10^\circ, 12^\circ$$

Inlet nozzle blocks provided inlet throat-length-to-throat-width ratios of 0.25, 1.25, 2.25, 4.25, 7.25.

A single diffuser wall length was used giving a $L/W = 15$.

2.2 FLOW PARAMETERS

Stagnation pressure (~ 95 psia) and temperature ($\sim 125^\circ\text{F}$) provided a throat Reynolds number (Reynolds number based on throat hydraulic diameter (D_H) = $\frac{4A_t}{P_T}$ and mean flow velocity \overline{U}) of about 6×10^5 at choking conditions for both aspect ratios.

For the largest inlet throat length to diffuser width at 10, this Reynolds number is equivalent to a throat length Reynolds number

$$\left(Re_{L_{throat}} = \frac{\bar{U} L_{throat}}{\nu} \right) \text{ of approximately } 1.2 \times 10^7.$$

2.3 FLOW MEASUREMENTS

A schematic of the flow arrangement and instrumentation is shown in Figure 156. Static-pressure taps are located along the centerline of the inlet and diffuser blocks (Figures 157 and 160). The mass-flow rate was measured with a standard ASME orifice meter, upstream of the test section. Stagnation pressure and temperatures upstream of the diffuser and static pressure in the pipe downstream of the diffuser were also measured.

The inlet Mach number is defined in terms of the centerline Mach number, i. e.,

- 1) The potential core flow Mach number, if the throat passage is sufficiently short that the sidewall boundary layers have not met in the center of the throat passage at the entrance to the diffuser;
- 2) The centerline Mach number, in the case where the sidewall boundary layers have met.

In either case, it is the maximum Mach number of the flow at the diffuser inlet which is used, and not an averaged inlet Mach number obtained from averaging the stagnation pressure across the throat flow. The throat flow is thus treated as a boundary-layer flow where the centerline conditions correspond to the core flow outside the boundary layers.

An equivalent flow area is calculated based on these centerline conditions. This flow area is the area required to pass a 1-dimensional flow with the measured values of stagnation pressure and temperature.

The blockage is the difference between the geometric throat area and the equivalent 1-dimensional flow area. The blockage is expressed in terms of the blockage ratio (B):

$$B = 1 - \phi = \frac{A_{\text{geometric}} - A_{\text{flow}}}{A_{\text{geometric}}} \quad (239)$$

where:

$$\phi = \frac{A_{\text{flow}}}{A_{\text{geometric}}} \quad (240)$$

When the throat length is sufficiently short to permit a potential core to exist at the diffuser inlet, the use of stagnation conditions upstream of the throat in the 4-inch pipe can be used for calculation of the Mach number and blockage. When the throat is long and the sidewall boundary layers have merged at the throat centerline, it is necessary to measure the throat stagnation pressure at the entrance to the diffuser. A total-pressure probe of 0.040 outside diameter was inserted from downstream along the centerline of the diffuser to the throat location, and total-pressure measurements were made with the 1.5- and 3.5-inch throats in the 0.25 aspect ratio diffuser, Figure 161. For all throat lengths up to 1.5 inch, the total-pressure drop in the throat passage is negligible (0.4 psi out of 95 psia for the 1.5-inch throat). For the 3.5-inch-throat tests, the stagnation pressure at the throat centerline was determined from the measured upstream stagnation pressure and Figure 161.

For the short throat passage lengths (1.5 inches or less) there is a potential core flow at the end of the throat passage; the static-pressure distribution through the diffuser throat should be given by the 1-dimensional isentropic compressible flow relations, since the wall pressure is imposed by the core flow. With choking flow, the ratio of static pressure to upstream total pressure should be 0.528 at the end of the inlet passage (throat). Figures 162 and 163 show the measured static-pressure distributions for $2\theta = 6$ degrees and $L_{\text{throat}} = 0$ and 1.5 inches, respectively (0.25 aspect ratio). If the above remarks are correct, the throat with choking flow is located along the inlet passage where the pressure ratio is 0.528. For the subsonic flow distributions, the throat can be located where the static pressure is minimum. (With the 1/8-inch spacing between pressure taps in the throat region, there is actually $\pm 1/8$ -inch uncertainty in the location of the minimum pressure in the subsonic distributions). Fitting curves to the measured data (Figures 162 and 163) gives good agreement between the throat location, as determined from the subsonic distributions and the 0.528-pressure-ratio location. The static pressure at the throat (with choking flow) has been obtained by using the measured upstream stagnation pressure and the 0.528-critical-pressure ratio.

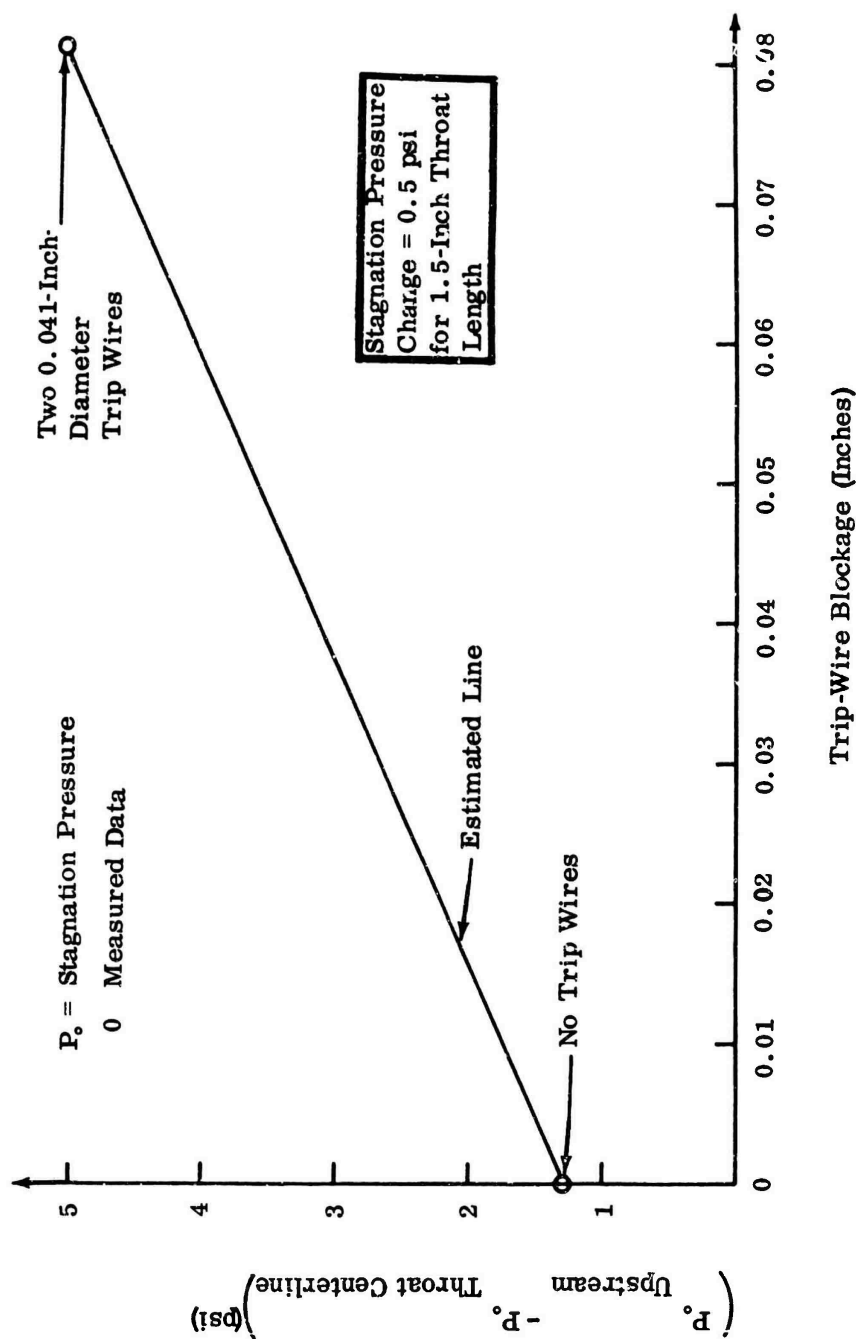


Figure 161. Centerline Stagnation Pressure Change (3.5-Inch-Long Throat).

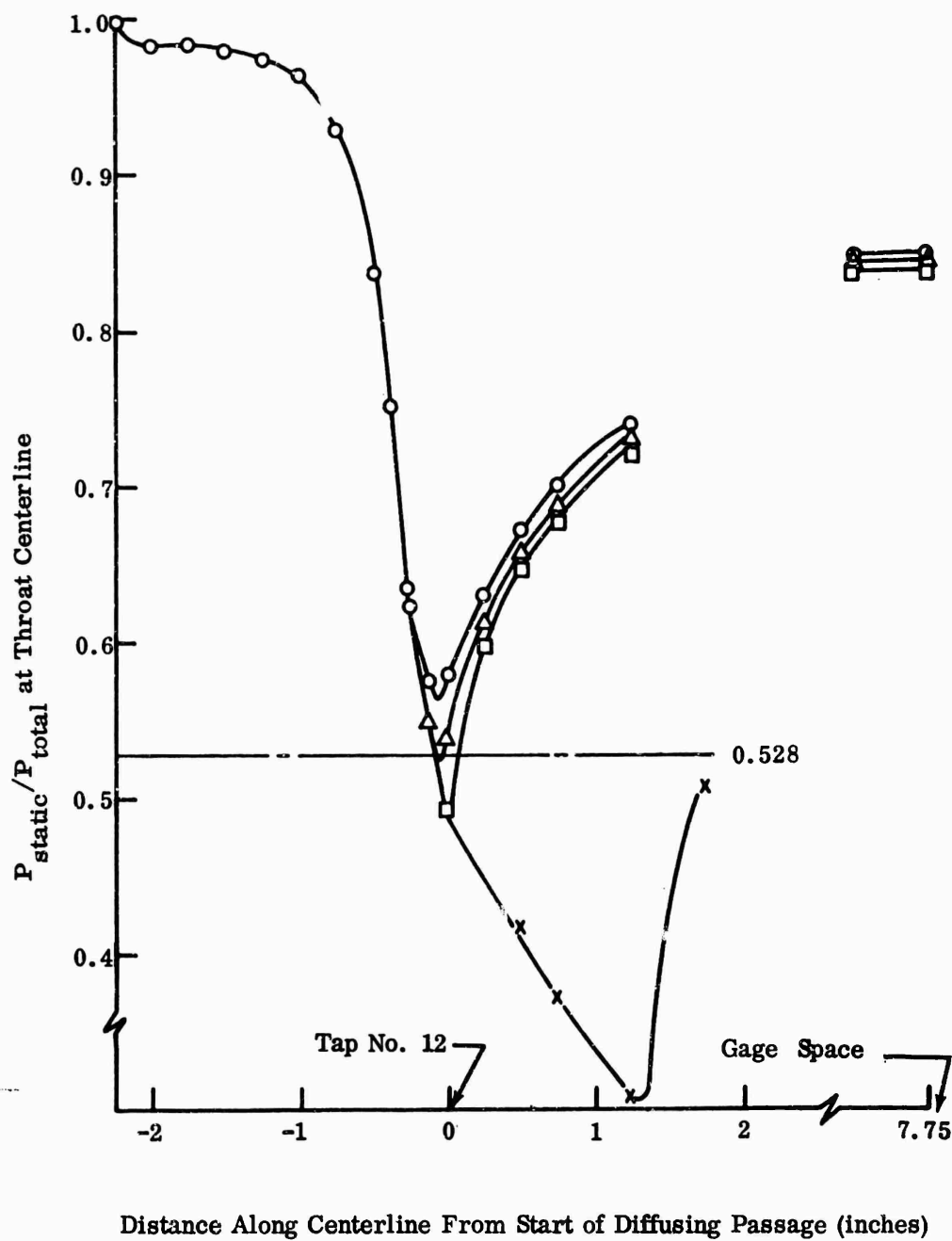


Figure 162. Straight Diffuser Performance (Pressure Ratio Versus Axial Distance For Various Backpressures, 0.25 Aspect Ratio, $2\theta = 6^\circ$, $L_{\text{throat}} = 0.125$ Inch).

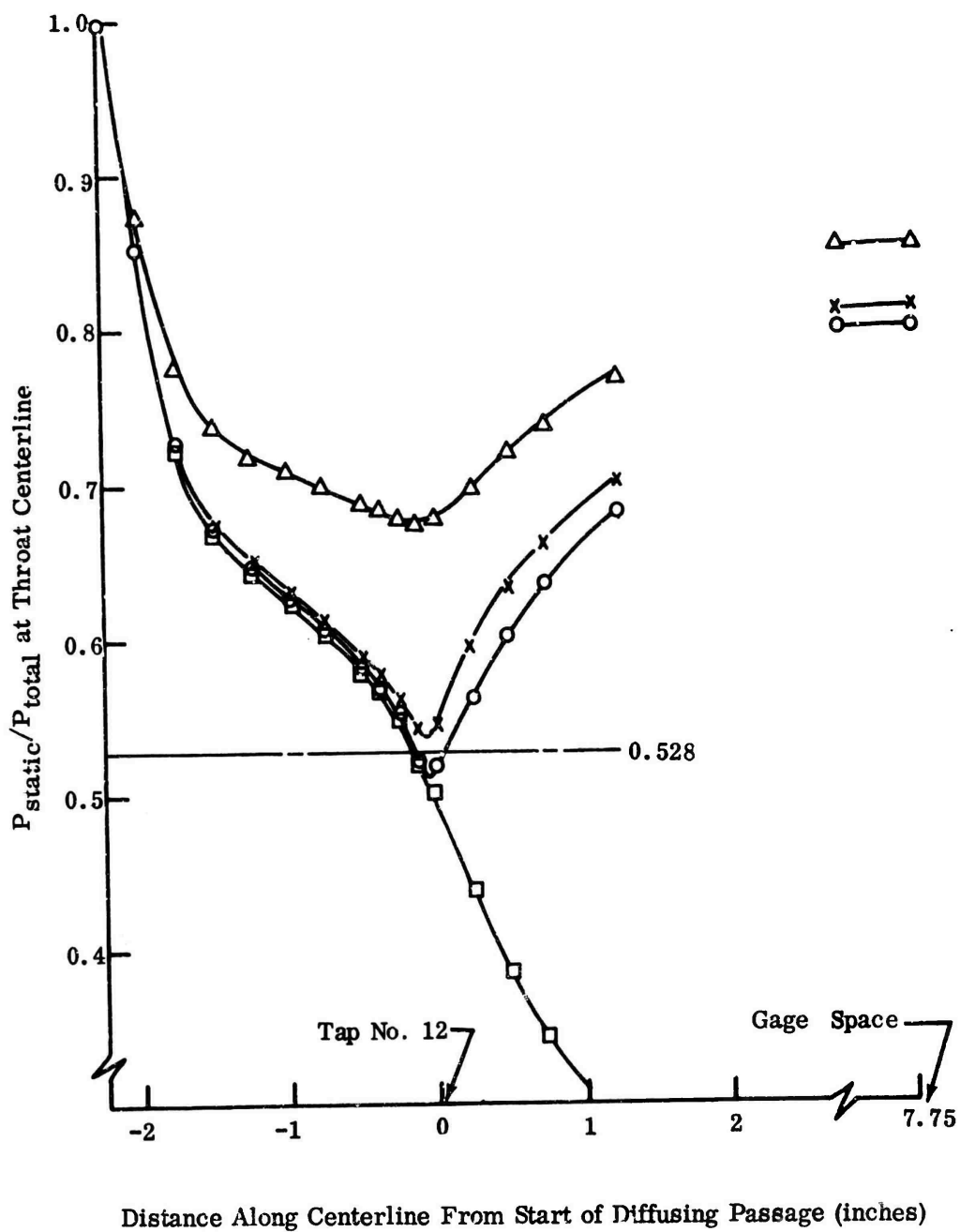


Figure 163. Straight Diffuser Performance (Pressure Ratio Versus Axial Distance For Various Backpressures, 0.25 Aspect Ratio, $2\theta = 6^\circ$, $L_{throat} = 1.625$ Inch.

In the tests with the 3.5-inch throat length, the boundary layers merge before the end of the inlet passage. In these tests, the static pressure at the diffuser inlet (for choking flow) has been found by using the 0.528 critical-pressure ratio and the stagnation pressure measured at the throat (obtained from Figure 161). The flow is thus treated as a 1-dimensional Fanno line flow, with a choking stagnation pressure equal to the measured stagnation pressure at the throat centerline. Static-pressure measurements for $2\theta = 6$ degrees and $L_{throat} = 3.5$ inches are shown in Figure 164. The throat location, as determined by the 0.528-critical-pressure ratio, is $1/4$ to $3/8$ inch upstream of the location determined from the subsonic distributions. The reasons for this are not entirely clear. The 1-dimensional Fanno calculation should be based upon the proper average stagnation pressure across the throat flow. We have used the centerline, or maximum stagnation pressure, at the diffuser inlet. We have not made measurements to determine the variation in stagnation pressure across the flow, although the high Reynolds number turbulent flow should provide an average stagnation pressure not too much different from the centerline value. Furthermore, a 1-dimensional analysis is only an approximation to the actual flow situation, which in this case is a 3-dimensional developing pipe flow. There has been discussion in recent literature by Pearson, et al,* of the true behavior of compound compressible flows, i.e., compound flows with fluid streams having different stagnation conditions. The passage boundary-layer flow is in actuality such a compound flow, with each streamtube in the boundary layer having a different stagnation pressure, and it does appear possible that alterations in throat location may be possible with this type of passage flow. Further work, however, needs to be done to clarify the behavior of choked flows, which at the same time have significant blockage effects caused by subsonic boundary layers. We have chosen to use the 0.528-critical-pressure ratio to determine the throat static pressure in the 3.5-inch-throat tests. Until a clearer understanding of the behavior of such choked flows with relatively large blockages is obtained, the uncertainty of the pressure-recovery values calculated with the 0.528-critical-pressure ratio for the 3.5-inch-throat data will be open to question. (For example, C_p calculated with the 0.528 pressure ratio yields a value $C_p = 0.52$, while a pressure ratio of 0.475 yields $C_p = 0.54$, a difference of 4 percent. The minimum throat pressure ratio corresponding to choking conditions is apparently 0.475, Figure 164). Note that values lower than 0.528-critical-pressure ratio would produce higher pressure recoveries.

The pressure recovery C_p is calculated from

$$C_p = \frac{P_{exit} - P_{throat}}{P_{stagnation throat} - P_{throat}} \quad (241)$$

*(See footnote, page 436.)

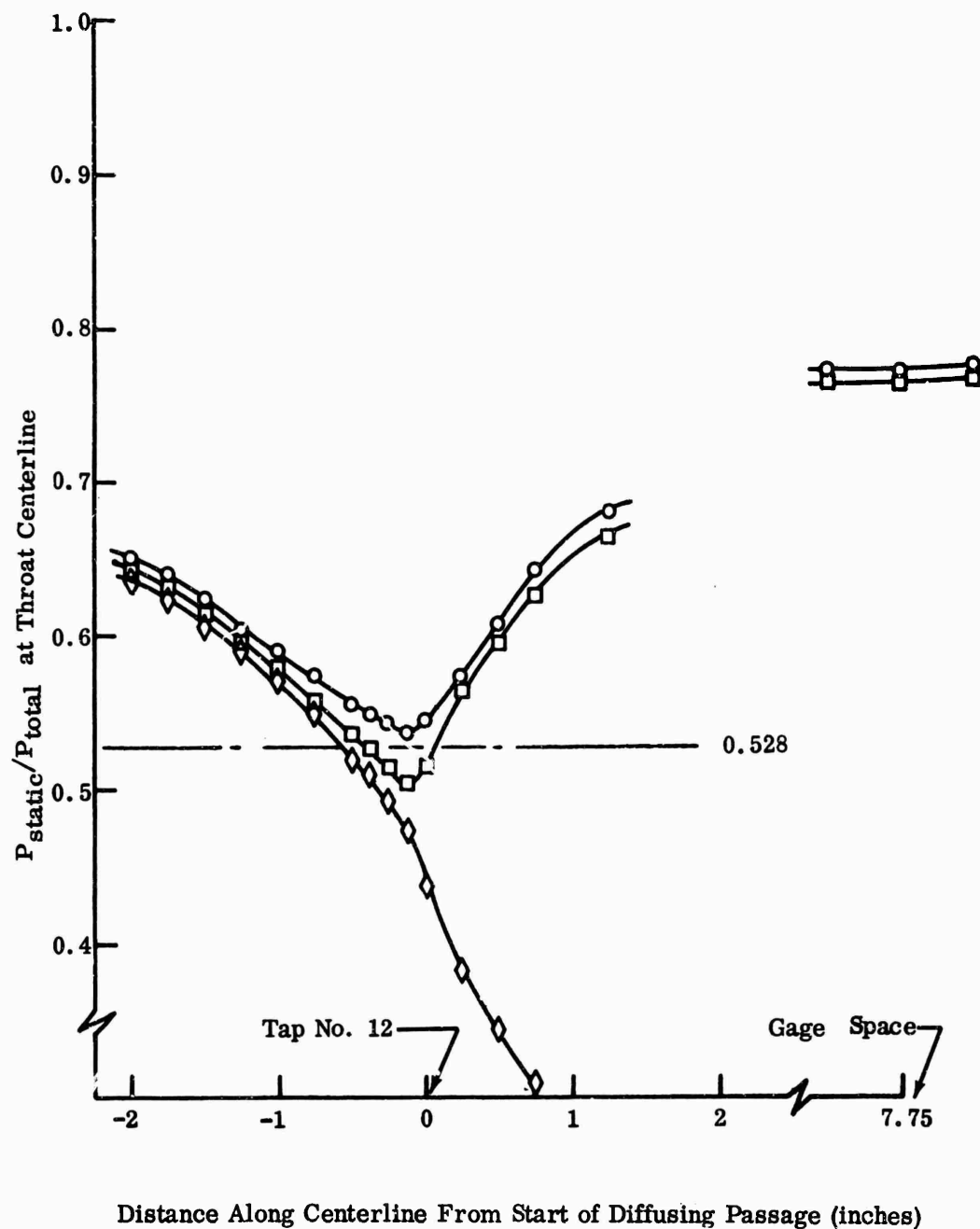


Figure 164. Straight Diffuser Performance (Pressure Ratio Versus Axial Distance For Various Backpressures, 0.25 Aspect Ratio, $2\theta = 6^\circ$, $L_{\text{throat}} = 3.5$ Inches).

The data for each test were reduced to the form of Figure 164, pressure ratio versus axial location, and the pressure recovery as a function of Mach number was determined from these plots using the above expression; i.e.,

$$C_p = \frac{\frac{P_{\text{exit}}}{P_o} - \frac{P_{\text{throat}}}{P_o}}{1 - \frac{P_{\text{throat}}}{P_o}} \quad (242)$$

where:

$$P_o = P_{\text{stagnation throat}}$$

To obtain large values of blockage, some 3.5-inch-throat tests were also made with 0.040-inch-diameter trips glued to the upper and lower nozzle blocks at the entrance to the throat passage. These tests were only run for the 0.25 aspect ratio diffuser.

A pressure transducer was used early in the measurements on the 5.7 aspect ratio diffuser to measure the frequency and amplitude of pressure fluctuations near the throat and in the pipe at the exit of the diffuser. The transducer was coupled closely enough to the flow so that it measured the actual pressure fluctuations with good fidelity. No appreciable difference was noticed between the measurements observed near the throat and in the exit of the diffuser. Some effect on frequency and amplitude of pressure fluctuations was observed as a function of inlet Mach number (increasing amplitude and frequency with increasing Mach number). The transducer was not used for the 0.25 aspect ratio tests.

In the 5.7 aspect ratio studies, the uncertainty in determining pressure recovery was approximately 10 percent for low Mach numbers (Mach numbers approximately equal to 0.3), reducing to approximately 4 percent near choke conditions. For the 0.25 aspect ratio tests, the uncertainty in pressure recovery near choking is approximately ± 2 percent. These uncertainty calculations and the uncertainty in determining Mach number, 2θ , and L/W are given in Section 5.

2.4 FLOW UNSTEADINESS

In all tests, pressure measurements were fairly steady (± 0.5 percent), although some rather large, unsteady fluctuations were sometimes observed (± 1.0 to 1.5 percent). Reasonably long pressure lines were used to reduce the amplitude of observed fluctuations. In practically all of the 5.7 aspect ratio tests, rather large fluctuations in flow rate (manometer reading) were observed at or near choking flow; the manometer reading would fluctuate about some readings (± 1.5 percent), then quickly drop in magnitude (-15 percent) and quickly recover to the same random unsteadiness as before the drop.

3.0 RESULTS AND DISCUSSION

There are 2 sets of data at high inlet Mach numbers; the 2 sets of present data at aspect ratios of 5.7 and 0.25 , and the collection of low Mach number data reported by Reneau for large aspect ratios from which conclusions may be drawn about the performance of straight-wall diffusers. The data are most usefully presented in the form of contour plots (usually with C_p as a parameter, i.e., a contour plot with C_p appearing as the elevation) from which conditions for obtaining maximum pressure recovery can be graphically seen.

Reneau reports sufficient data to present such contour plots. The data are given in the form of area ratio versus inlet throat-length-to-diffuser-width ratio, with contours of constant pressure recovery (for fixed values of blockage, aspect ratio, and low Mach numbers). From such contour maps (in this case for low inlet Mach numbers) a ridge of maximum pressure recovery can be seen. Along this ridge optimum diffuser performance can be obtained.

The present high inlet Mach number data are insufficient to present the results of diffuser performance in the form given by Reneau. The present data have been obtained at essentially only a single throat-length-to-width ratio ($L/W = 15$). However, the range of blockage used in the present tests makes other forms of presentation appropriate. Performance maps will be presented in 2 forms which permit the easiest grasp of the significance of the data:

- 1) In the form of pressure recovery versus divergence angle with blockage as parameter; or
- 2) In the form of blockage versus divergence angle with pressure recovery as parameter.

The data of Reneau are compared in these same forms from cross-plots. Some data at $L/W = 10$ for the 5.7 aspect ratio studies were also obtained. However, the extent of these data is really insufficient for meaningful conclusions to be made.

3.1 C_p VERSUS INLET MACH NUMBER

For the 5.7 aspect ratio studies, diffuser performance was measured over a wide range of subsonic inlet Mach numbers. Over this range of inlet Mach numbers, pressure recovery correlates on diffuser divergence angle 2θ , as follows:

- 1) At small divergence angles ($2\theta = 4$ degrees) with low blockage ratios ($B_{choke} = 0.05$), the pressure recovery rises with increasing Mach number; a variation of 25 to 30 percent between Mach number = 0.3 and choking conditions at $L/W = 10$.
- 2) At large angles ($2\theta = 12$ degrees) and low blockage ratios ($B_{choke} = 0.05$), the recovery falls with increasing Mach numbers; a variation of 15 percent between Mach number 0.3 and choking conditions at $L/W = 10$.
- 3) For intermediate angles and for all angles at higher blockage ratios (data for $B_{choke} = 0.14$), the performance remains relatively constant from Mach number = 0.3 to choking.

The interpretation of these trends is subject to the uncertainty in the data discussed earlier; 10 percent (or six to seven points in recovery) at Mach number = 0.3, decreasing to 4 percent (or two to three points in recovery) at choking.

Insufficient data are available at $L/W = 15$ to draw the same conclusions for the 0.25 and 5.7 aspect ratio tests.

The following results are apparent from an examination of these data (Figures 165 through 173):

- 1) For the present range of parameters, no critical subsonic inlet Mach number exists in the sense of the conclusions reached in Appendix XI.
- 2) There is no clear-cut classification, on the basis of performance versus inlet Mach number characteristic, of groupings of diffuser characteristics such as A, B, and C predicated in Appendix XI. The range of the diffuser parameters on the flow-regime map covers the regions common to Groups A and B (Figure 154).
- 3) Diffuser performance does not suffer a drastic drop until supercritical flow conditions are reached. Performance drops abruptly when the Mach number immediately ahead of the shock in the diffuser passage reaches a value of approximately 1.1 to 1.2. The performance probably suffers

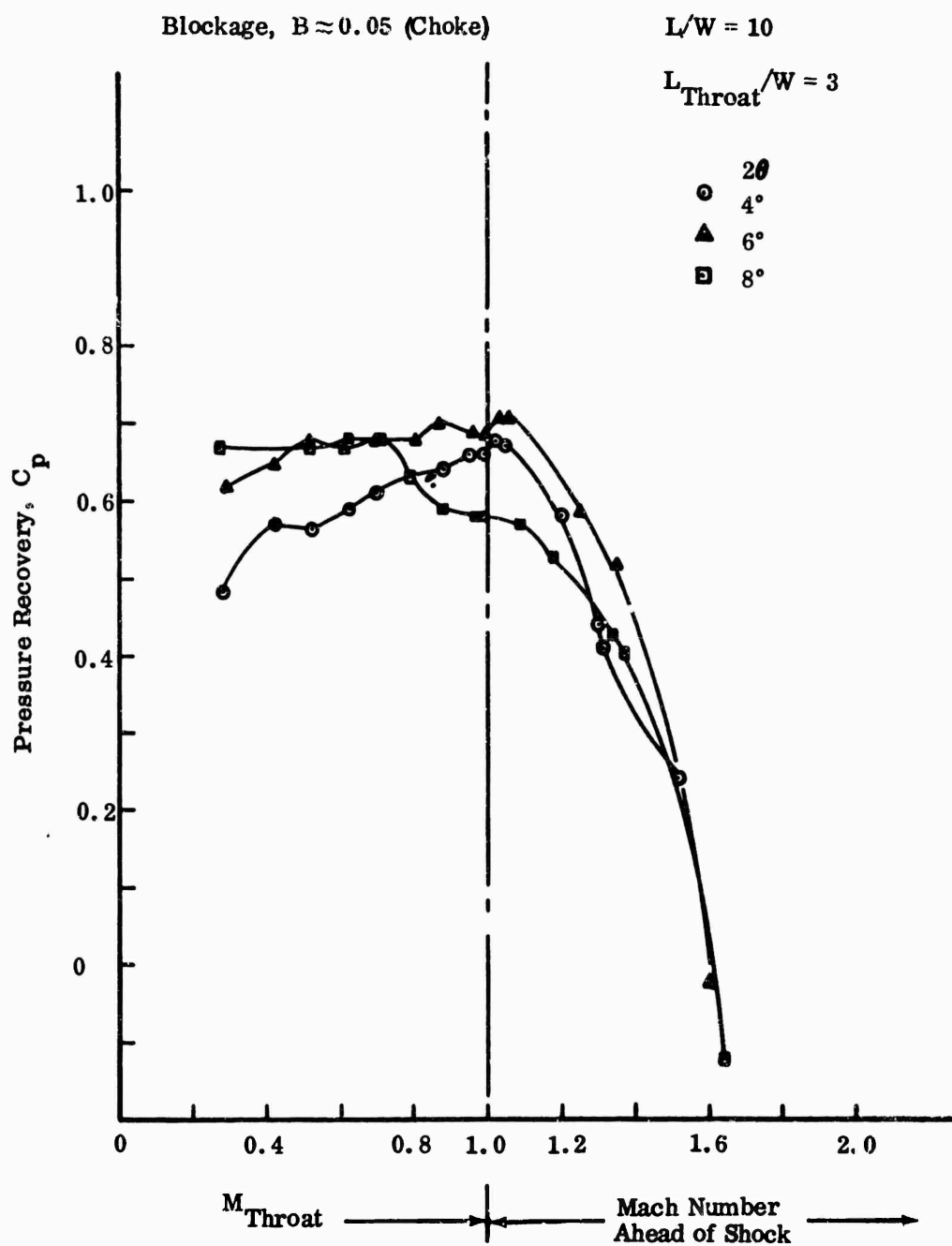


Figure 165. Straight Diffuser Performance (C_p Versus Mach Number).

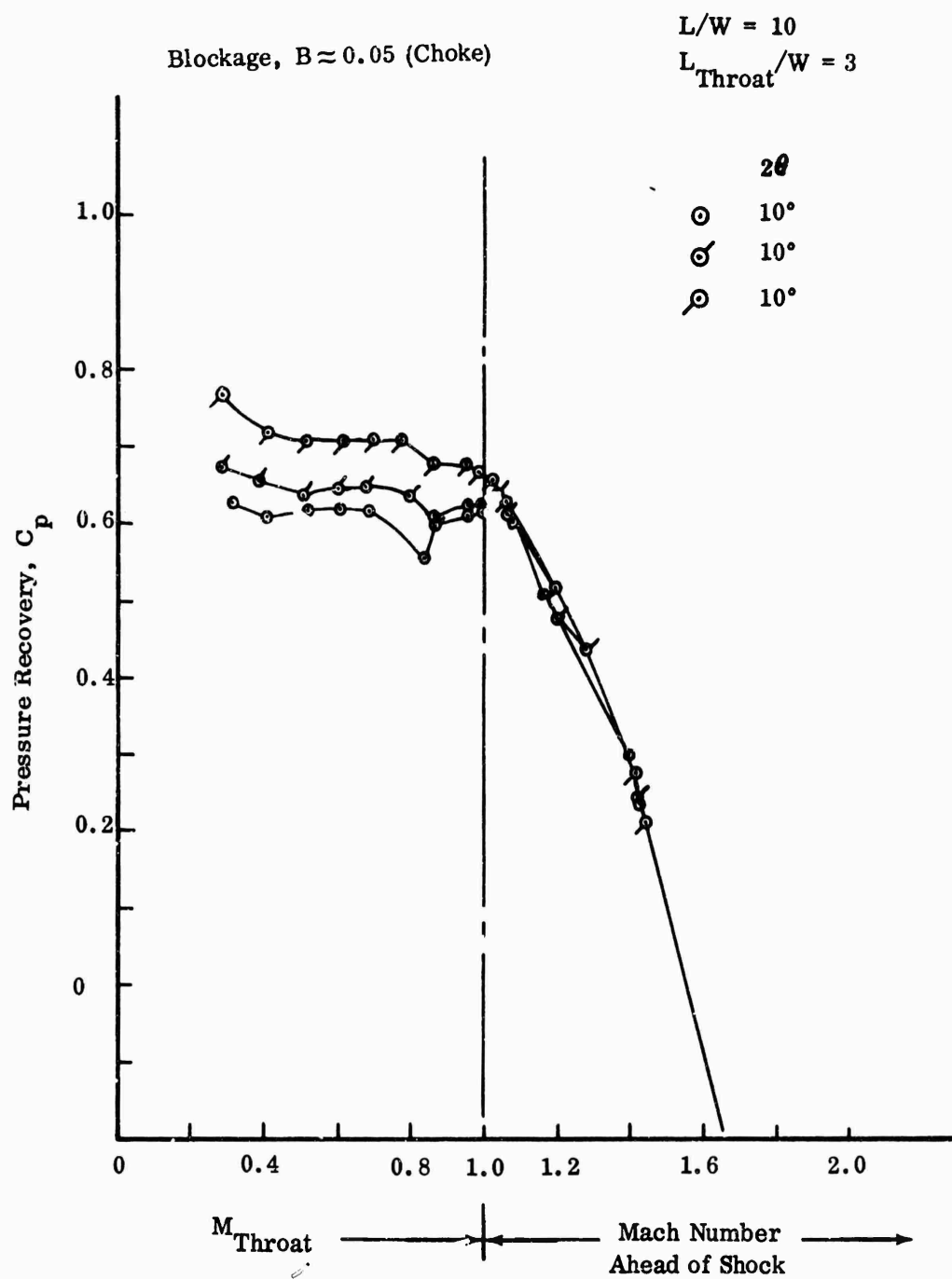


Figure 166. Straight Diffuser Performance (C_p Versus Mach Number).

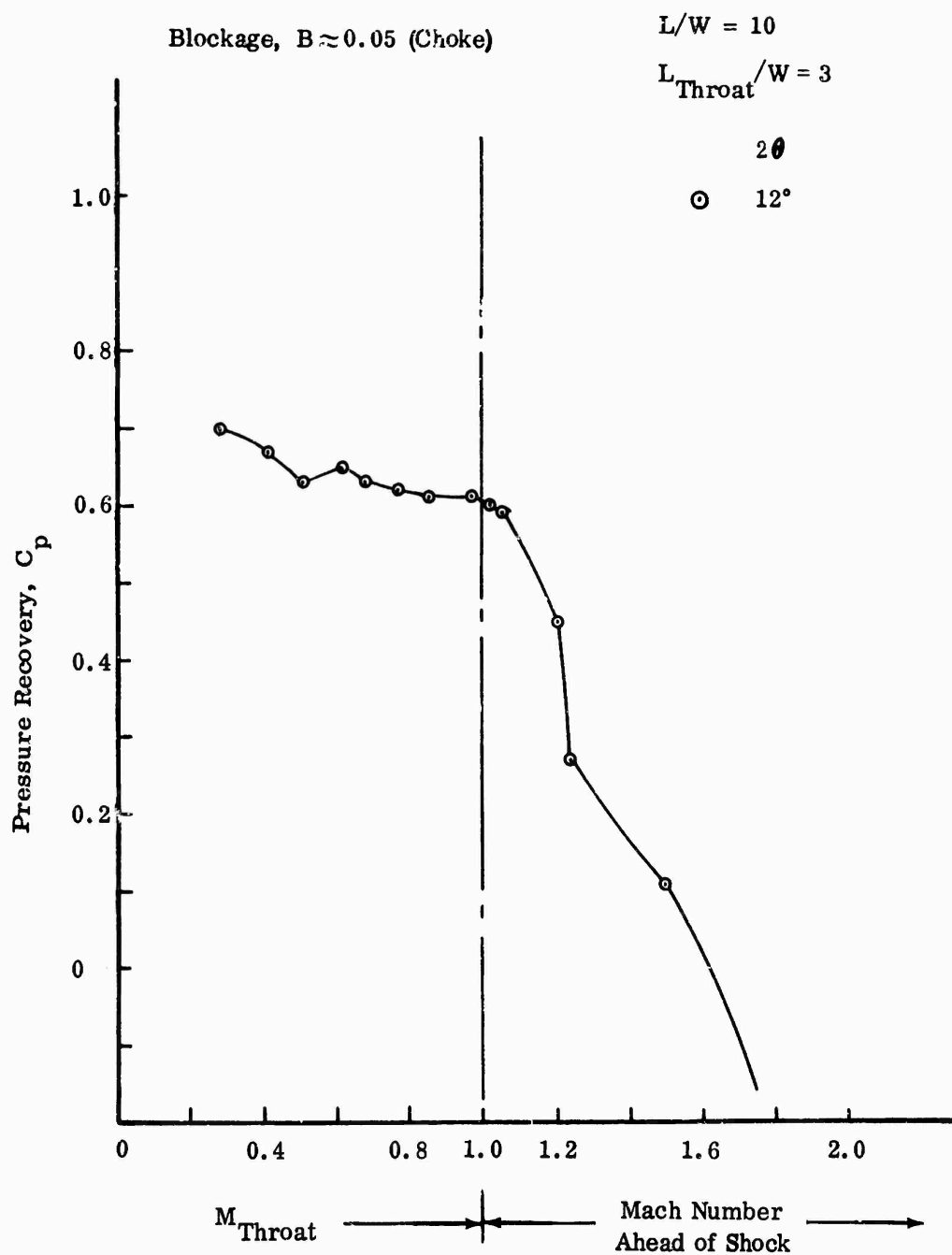


Figure 167. Straight Diffuser Performance (C_p Versus Mach Number).

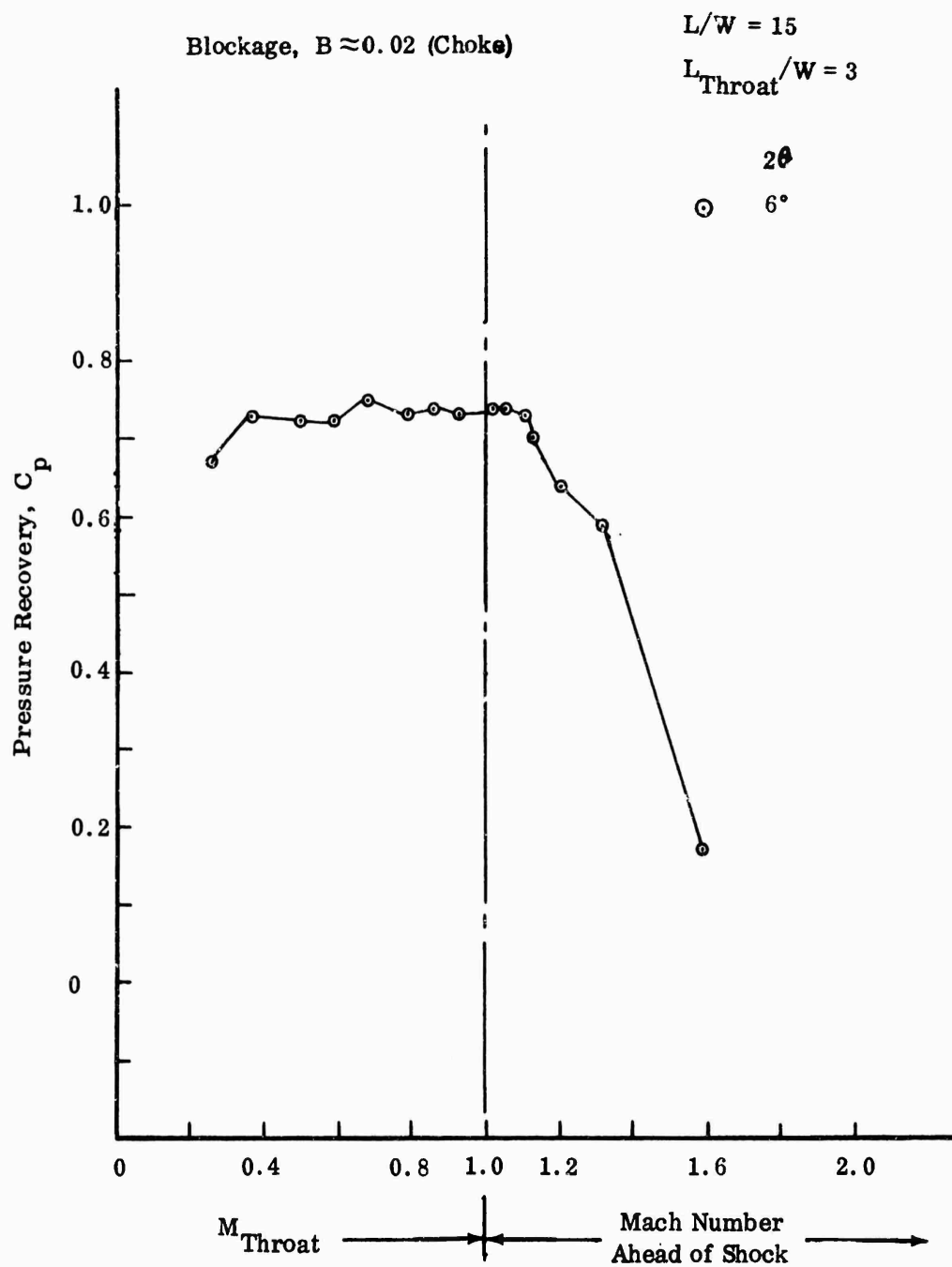


Figure 168. Straight Diffuser Performance (C_p Versus Mach Number).

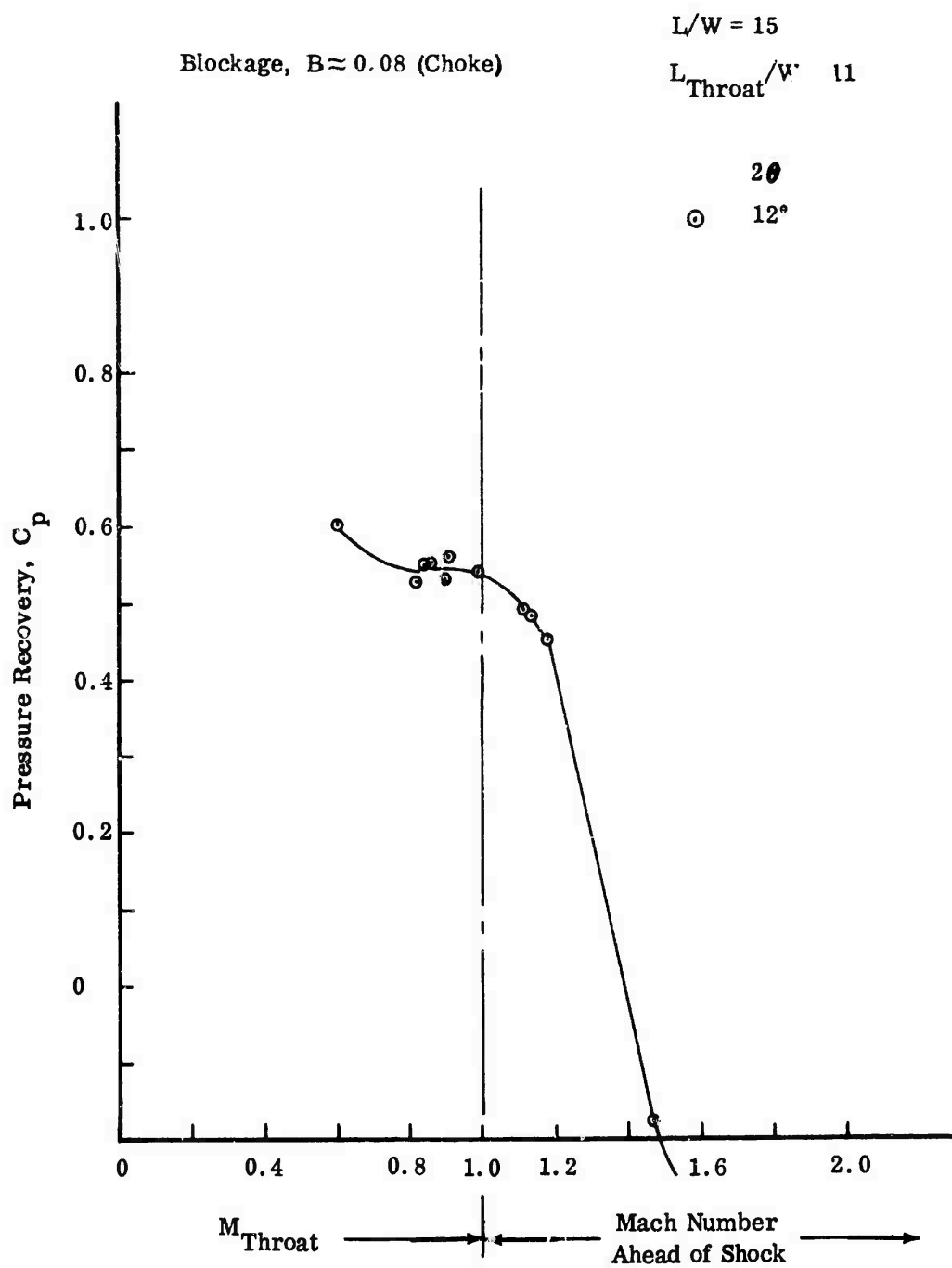


Figure 169. Straight Diffuser Performance (C_p Versus Mach Number).

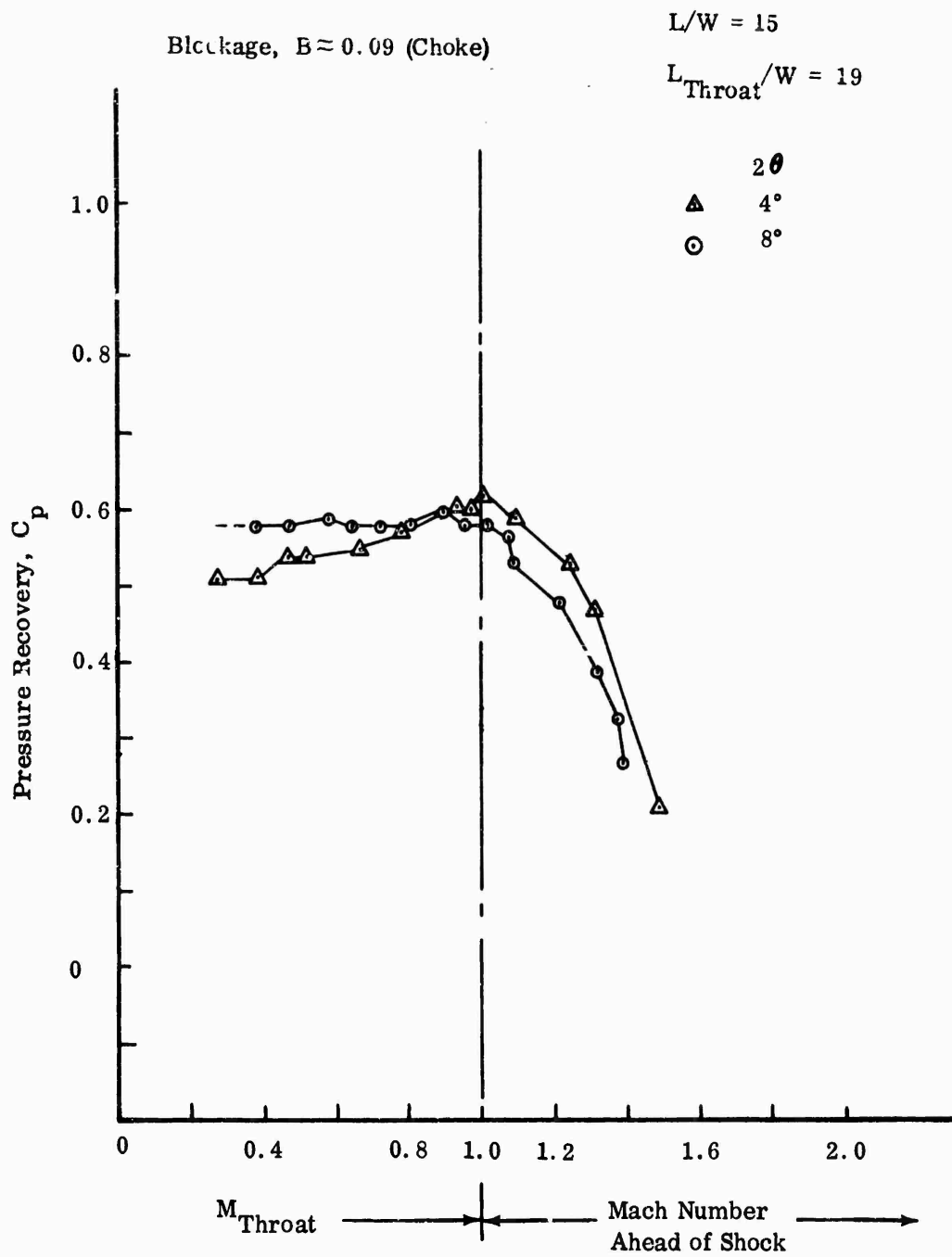


Figure 170. Straight Diffuser Performance (C_p Versus Mach Number).

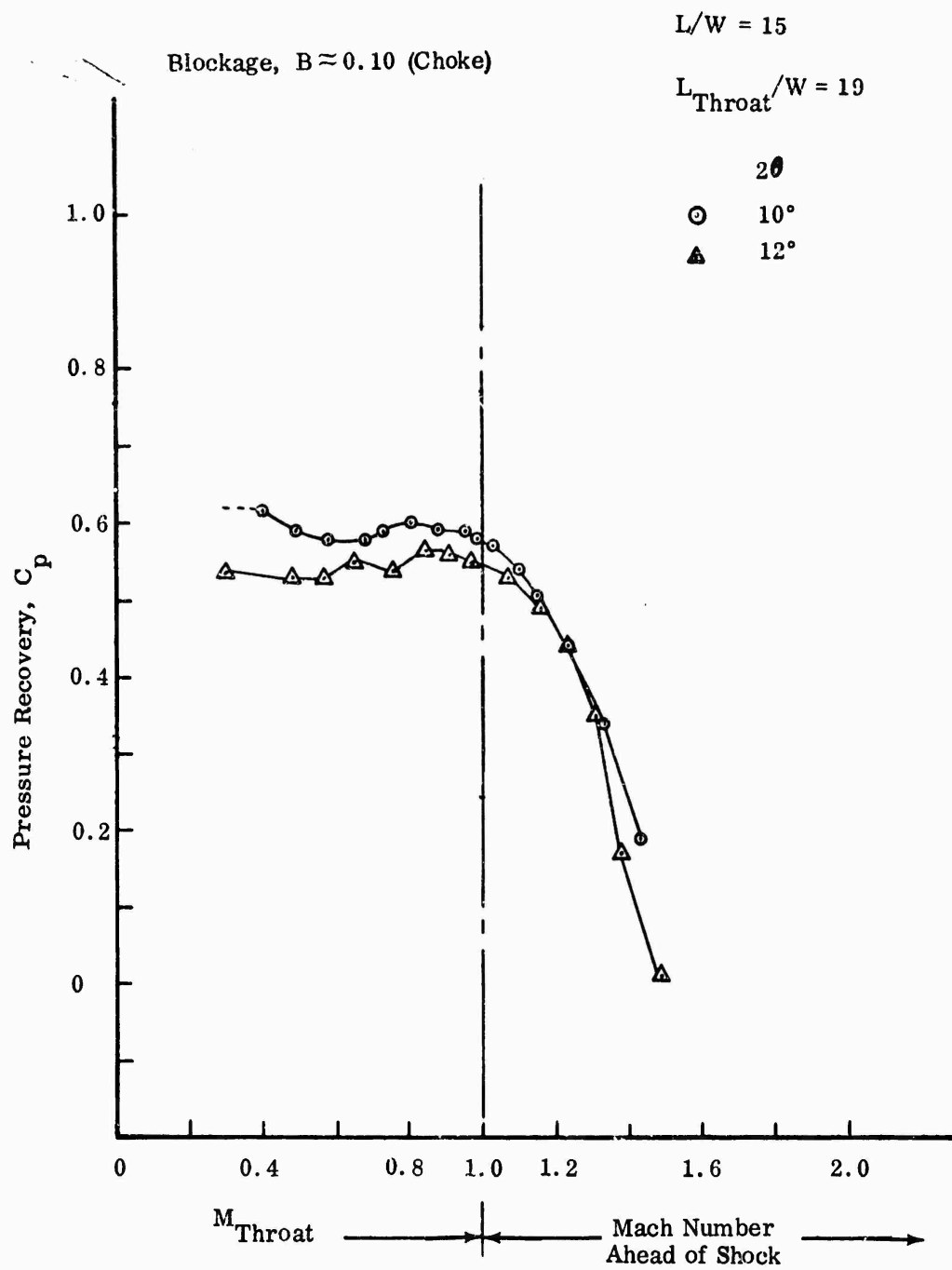


Figure 171. Straight Diffuser Performance (C_p Versus Mach Number).

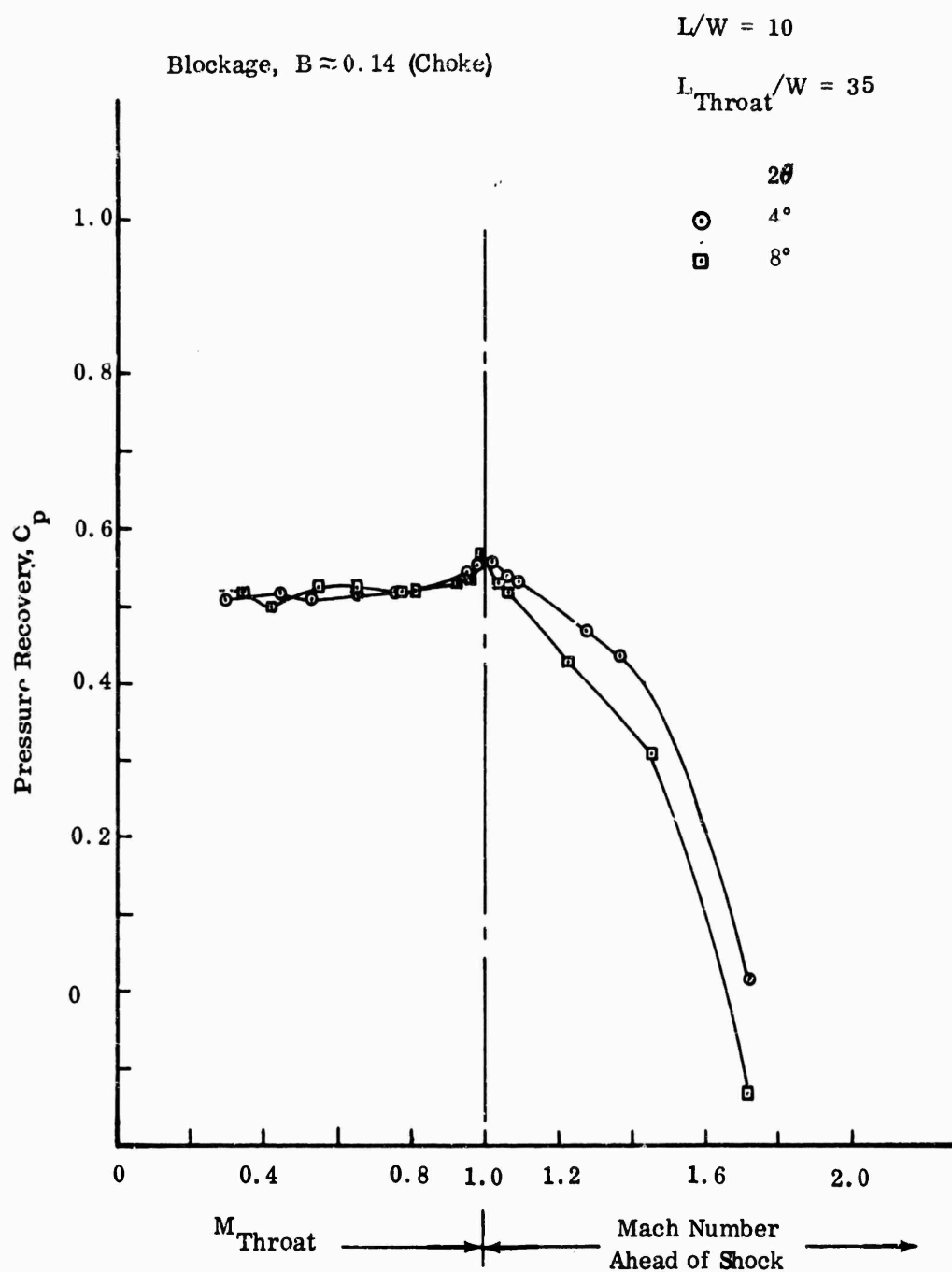


Figure 172. Straight Diffuser Performance (C_p Versus Mach Number).

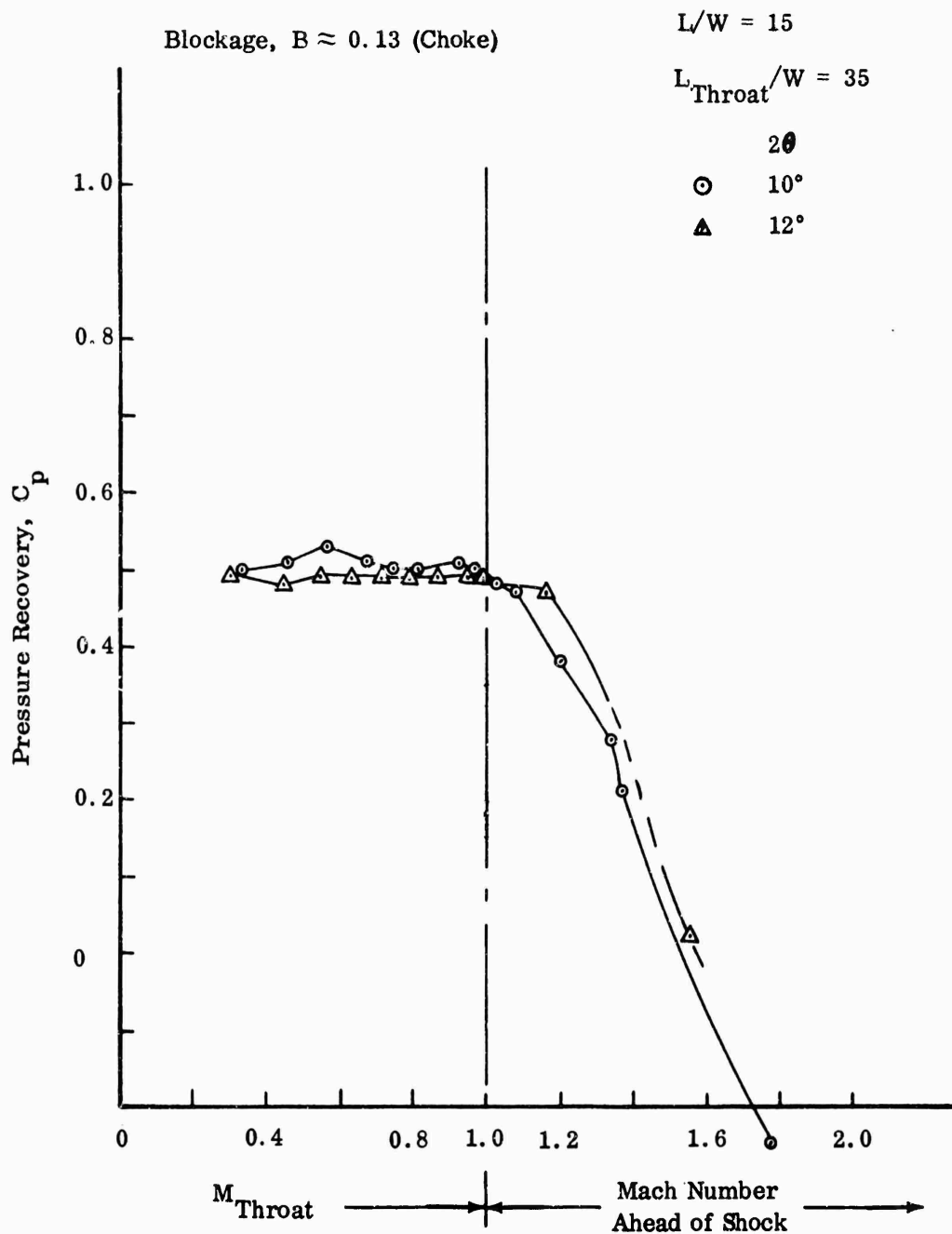


Figure 173. Straight Diffuser Performance (C_p Versus Mach Number).

beyond this point largely because of shock-induced boundary-layer separation, resulting in separated flow throughout the diffuser.

- 4) Data at low Mach numbers agree with the data of Reneau* ($M < 0.2$), if consideration is made of the rather large uncertainty (approximately 6 to 7 points in performance) in the present data. The data taken at low Mach numbers have this large uncertainty because of the large uncertainty in the pressure readings compared to the pressure difference terms appearing in the expression for the pressure coefficient at these low Mach numbers (see Section 5.0).

These tests show that for the range of diffuser parameters tested, the major conclusions reached in Appendix XI are not correct, at least regarding the Group A characteristics, and that in most cases good performance is maintained over the entire range of subsonic inlet Mach numbers.

3.2 C_p SUPERCRITICAL FLOW CONDITIONS

Supercritical flow conditions are defined as all diffuser back pressure conditions at which choking ($M_{\text{throat}} = 1.0$) is maintained at the diffuser throat. In all cases of supercritical conditions, a sudden decrease in recovery is observed when a shock stands in the diffuser with a Mach number immediately upstream of the shock of approximately 1.1 to 1.2. Fair performance can be expected, even at supercritical conditions, if a normal shock in the diffuser is weak enough such that the stagnation-pressure loss through the shock is small and the static-pressure rise across the shock is small enough not to induce separation of the wall boundary layers. Based on an analysis of Stodola's data ** and the results of the present studies, a choked diffuser will produce recovery (approximately the same as its recovery at incipient choking) as long as the shock Mach number in the diffusing passage is less than 1.1 to 1.2. Above a shock Mach number of this value, a precipitous drop in recovery occurs. For optimum performance of a fixed geometry diffuser under supercritical flow conditions, a diffuser should be operated at a back pressure as close to $P_{\text{exit}} = P_{\text{exit choke}}$ as possible.

3.3 COMPARISON OF PRESENT DATA WITH LOW MACH NUMBER DATA OF RENEAU — C_p VERSUS 2θ

The present data are compared with the low Mach number data of Reneau* in Figures 174 through 176 (C_p versus 2θ).

*(See footnote, page 432.)

**A. Stodola, and L.C. Loewenstein, Steam and Gas Turbines, Vol. 1, pp 82-105; Peter Smith, New York, 1945.

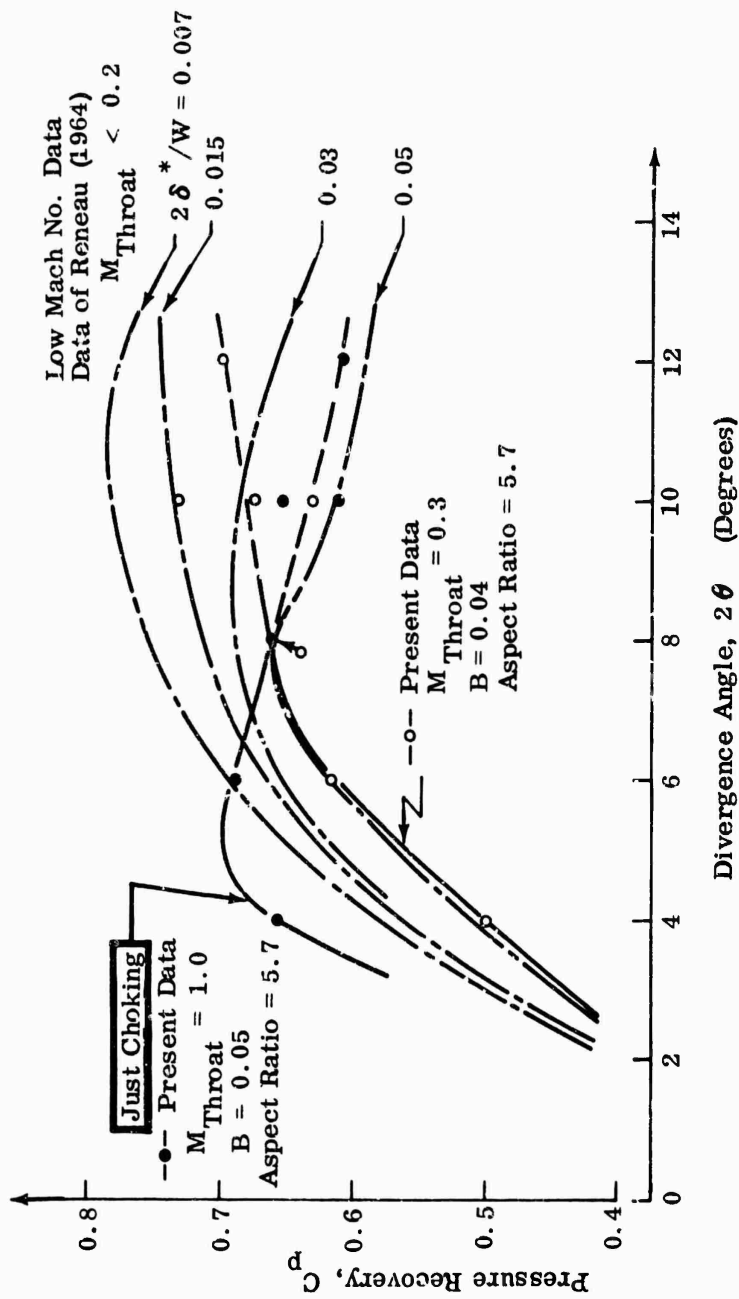


Figure 174. Straight Diffuser Performance (Pressure Recovery Versus Divergence Angle, $L/W = 10$).

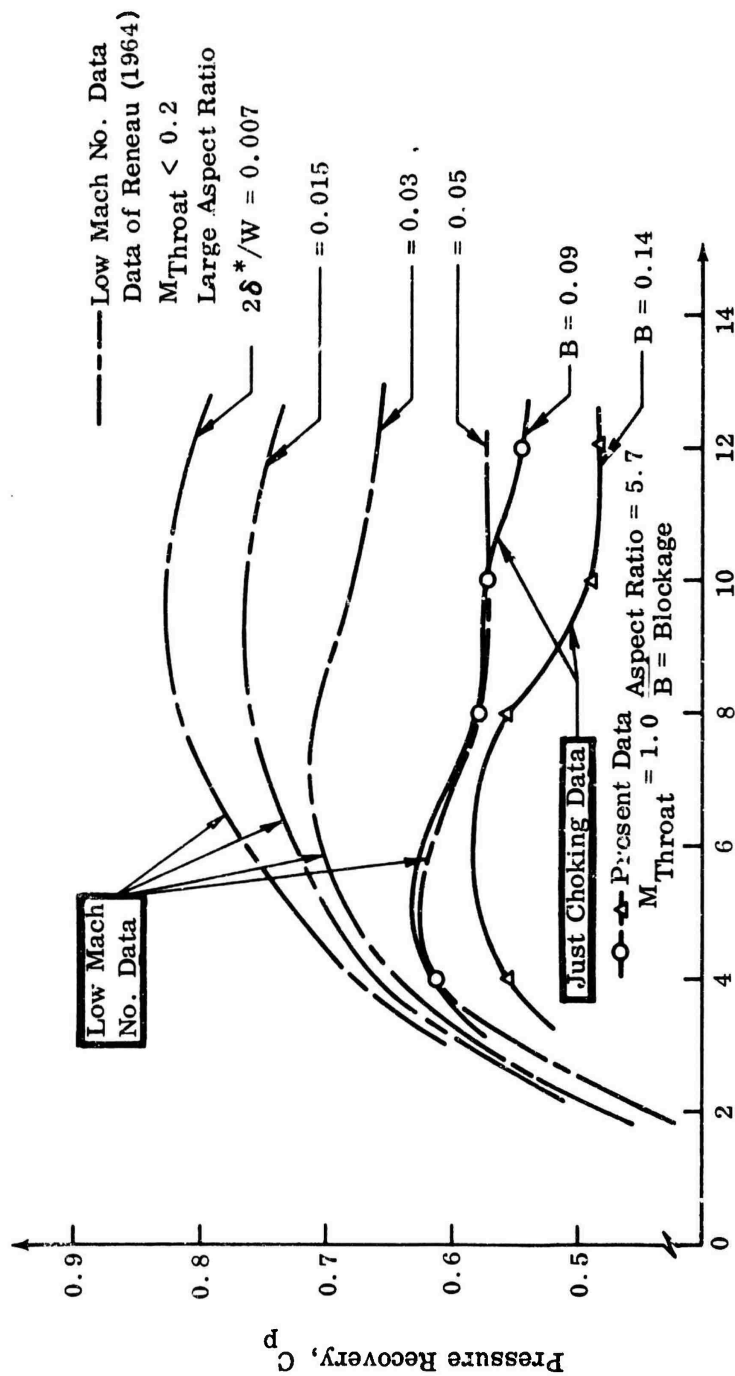


Figure 175. Straight Diffuser Performance (Pressure Recovery Versus Divergence Angle, $L/W = 15$).

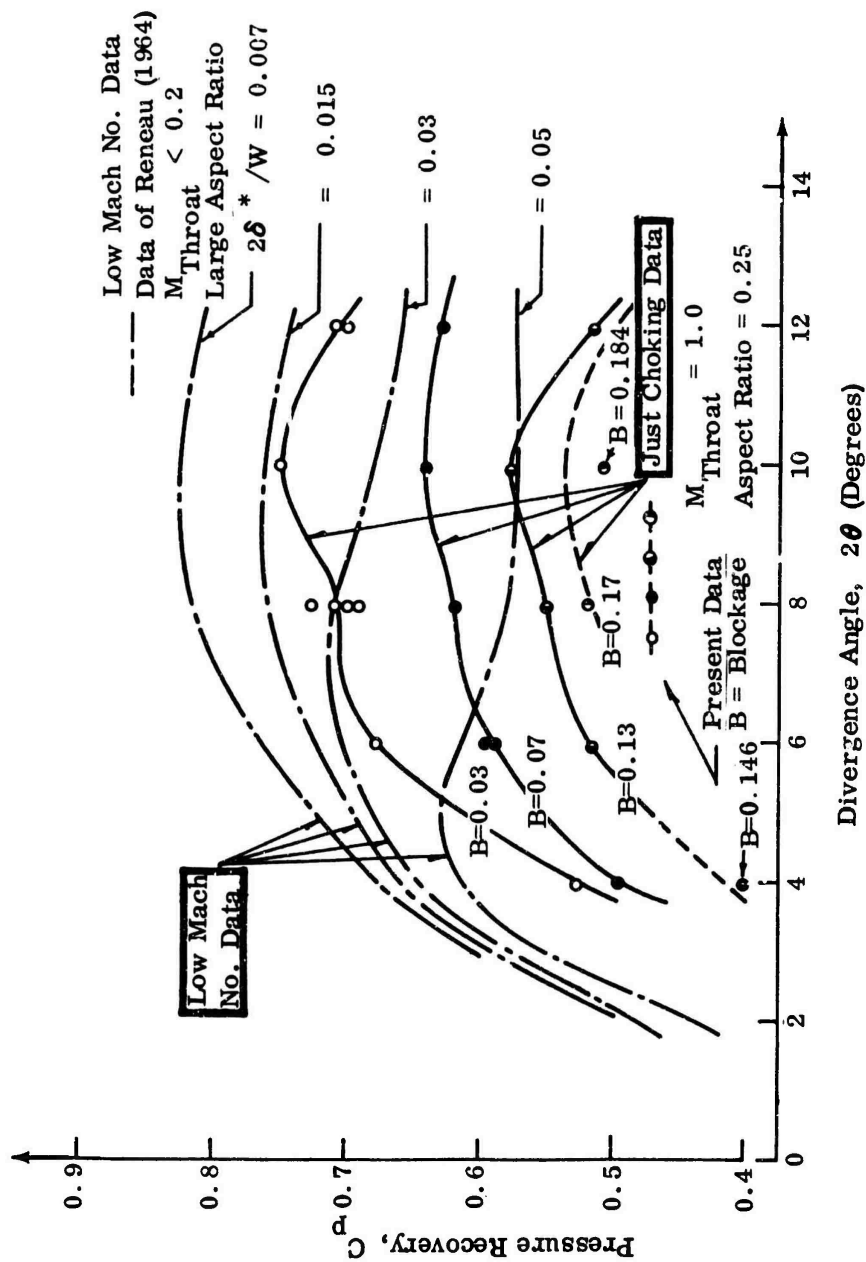


Figure 176. Straight Diffuser Performance (Pressure Recovery Versus Divergence Angle, $L/W = 15$).

Reneau reports his data to be valid for Mach numbers less than 0.2 to 0.3. Data are reported by Reneau only for blockage ratios less than 0.05. For $L/W = 10$, only one set of data has been taken at low blockage ratios ($B = 0.04$) and low Mach numbers (Mach number = 0.3) in the present studies. Within the certainty of the data at this low Mach number, there is agreement between the data of Reneau and the present data except at the higher divergence angles; the present data do not show as early a drop-off in performance with increasing divergence angle at constant blockage as reported by Reneau. The data continue to rise for a 2θ of 8 degrees.

The data for throat Mach number = 1 and blockage $B = 0.05$ ($L/W = 10$, aspect ratio = 5.7) show a significant alteration in C_p versus 2θ from that reported for low Mach number flow. Higher values of pressure recovery are obtained at the lower divergence angles studied ($2\theta = 4$ and 6 degrees), while approximately the same pressure recovery is obtained at higher divergence angles. A change in the pressure-recovery characteristic between low inlet Mach numbers and high inlet Mach numbers is observed in all of the data.

For $L/W = 15$, $M = 1.0$, aspect ratio = 5.7 (Figure 175), all of the present data are at larger values of blockage than covered by Reneau except for one point at $2\theta = 6$ degrees and $B = 0.04$. This 6-degree point agrees with the data of Reneau.

The principal conclusion is that it is not reliable to predict high inlet Mach number performance on the basis of low inlet Mach number data. On the basis of the pressure recovery versus inlet Mach number characteristic results discussed in 3.1, an extrapolation may be made from low inlet Mach number data. However, such extrapolation of data would not be expected to be highly reliable.

3.4 C_p VERSUS B AND ASPECT RATIO AT HIGH INLET MACH NUMBERS

Whereas a survey of low inlet Mach number performance was made for the 5.7 aspect ratio studies, the 0.25 aspect ratio studies only measured pressure recovery at or near choking conditions.

A sufficient amount of data to formulate design criteria at high inlet Mach numbers is only available for $L/W = 15$. Of these data, the more complete set is available for the 0.25 aspect ratio diffuser: C_p data for blockages of 0.03, 0.07, 0.09, and 0.17 at just choking conditions. For the 5.7 aspect ratio diffuser, data are available only for blockages of 0.09 and 0.14 at just choking conditions. The data, in the form of C_p versus 2θ as a function of blockage, are presented for the 0.25 aspect ratio diffuser in Figure 176 and the 5.7 aspect ratio diffuser in Figure 175. These figures represent a composite of these sets of data overlaid on the $L/W = 15$ data of Reneau (large aspect ratio, Mach number less than 0.2). From these data, 3 important conclusions may be drawn:

- 1) The 2 sets of data for large aspect ratio (aspect ratio = 5.7 and data of Reneau) exhibit the same trend in pressure recovery with divergence angle and blockage: a rapidly rising pressure recovery at low angles (with a peak pressure recovery at some angle which is a function of blockage) followed by a gently falling recovery at large 2θ . However, there is a marked shift in the pressure-recovery characteristic (C_p versus 2θ) between the low inlet and high inlet Mach number data; at high inlet Mach numbers, increasing blockage produces higher recovery for a given angle than at low inlet Mach numbers.
- 2) Entirely different characteristics (C_p versus 2θ) are obtained with low aspect ratios than with high aspect ratios.
- 3) In spite of the fact that diffuser performance is reasonably well behaved over the entire range of subsonic inlet Mach numbers, i.e., no critical Mach numbers above which performance suffers a drastic decline (Section 3.1), high inlet Mach number data cannot be predicted using low inlet Mach number characteristics. At high inlet Mach numbers there is a drastic alteration in performance characteristics with diffuser aspect ratio. Although data are not available for low Mach number diffusers, the same effect of aspect ratio may hold for low Mach number diffuser performance.

The performance data at $L/W = 15$ as a function of blockage and divergence angle 2θ (Figures 175, 176, 177, and 179) for high inlet Mach number show the following characteristics:

- 1) For the 0.25 aspect ratio diffuser, a ridge of maximum recovery exists at a divergence angle 2θ of 10 degrees and recovery decreases with increasing blockage. The functional relationship between pressure recovery and blockage, for aspect ratio 0.25, $2\theta = 10$ degrees, and $L/W = 15$, with just choking flow, is shown in Figure 179.
- 2) For an aspect ratio of 5.7, a ridge of maximum pressure recovery at just choking flow occurs at a divergence angle $2\theta \approx 6$ degrees (Figure 175). Leaky pressure taps invalidated data for $B = 0.02$ at $2\theta = 4, 8, 10$, and 12 degrees, and data for $2\theta = 6$ degrees at $B = 0.09$ and 0.14. Time has not permitted a recheck of these points.

The trend of pressure recovery with blockage and divergence angle is also conveniently seen on contour maps with pressure recovery as a function of blockage and divergence angle, 2θ . The just choking inlet Mach number data are presented in this form for $L/W = 15$ and 10 and for the two aspect ratios 0.25 and 5.7 in Figures 177 and 178. Also indicated on these plots are cross-plots of the low Mach number data of Reneau.

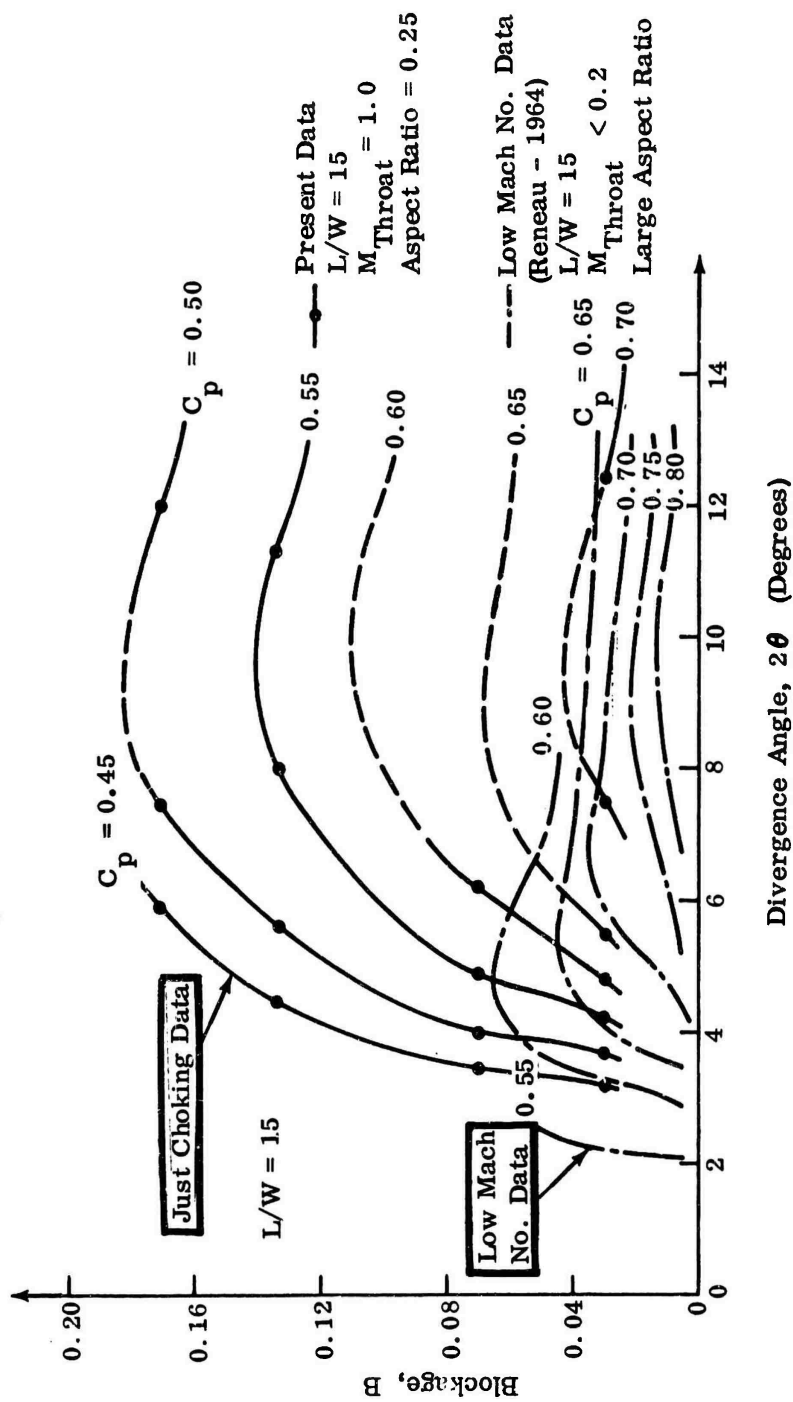


Figure 177. Straight Diffuser Performance (Blockage Versus Divergence Angle With Pressure Recovery as Parameter).

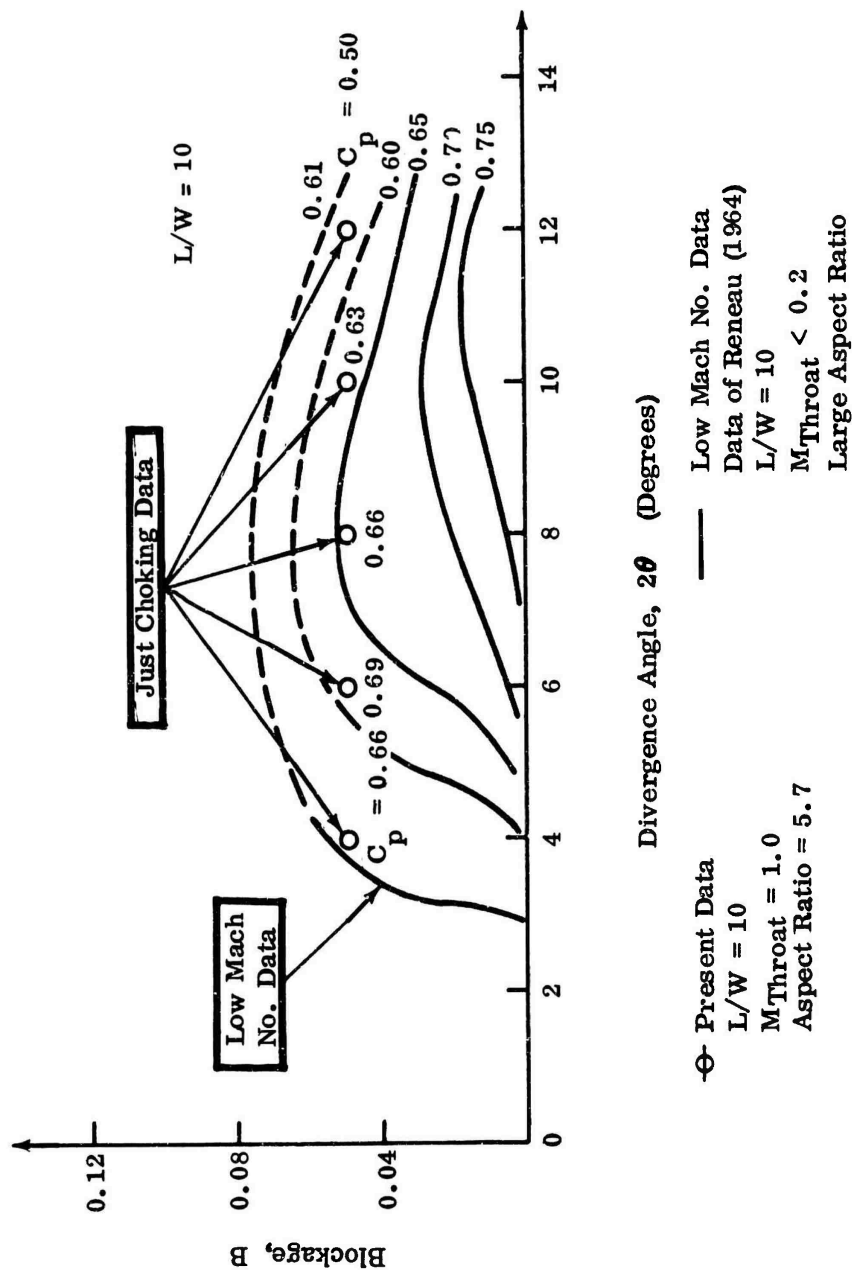


Figure 178. Straight Diffuser Performance (Blockage Versus Divergence Angle With Pressure Recovery as Parameter).

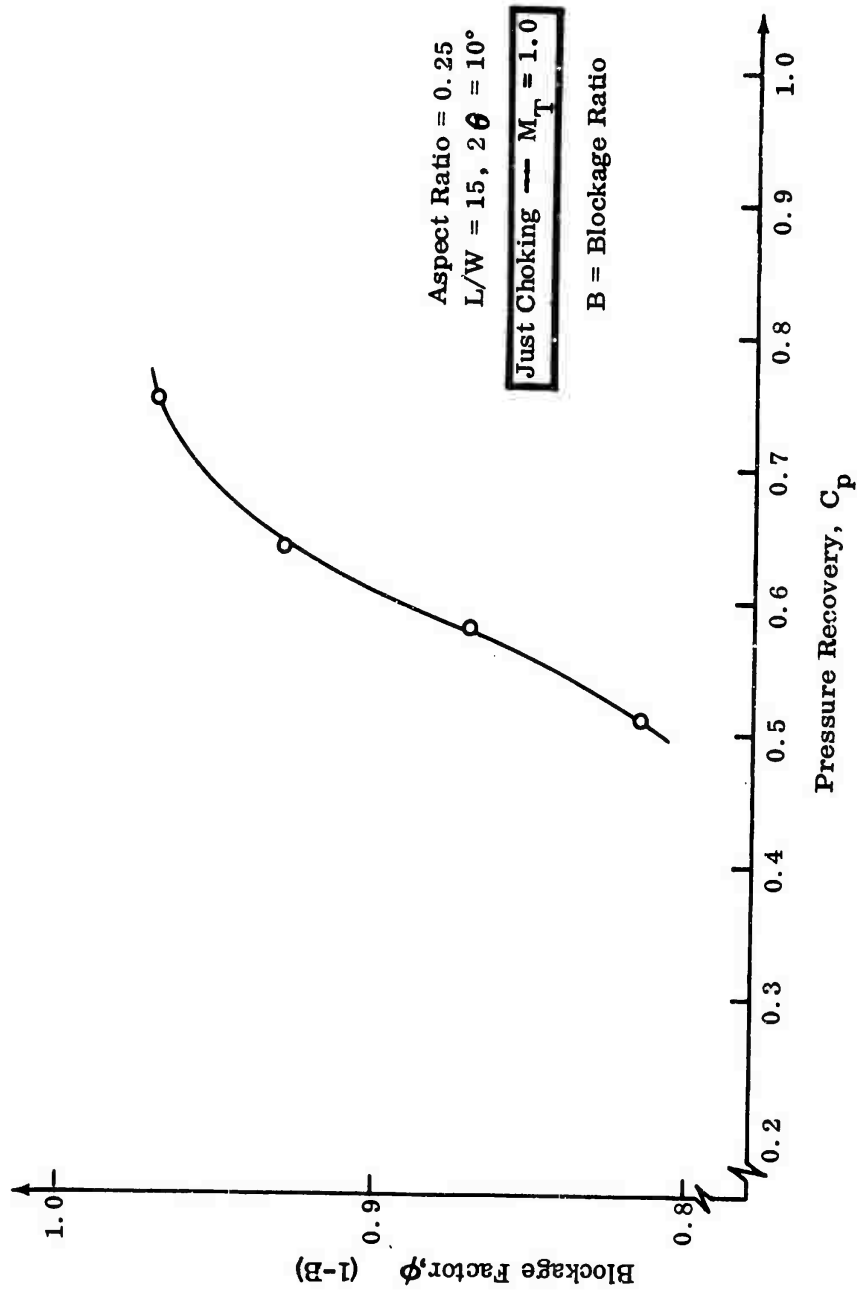


Figure 179. Straight Diffuser Performance.

4.0 RECOMMENDATIONS

Further studies are desirable to:

- 1) Extend diffuser performance maps at high inlet Mach number over a wider range of L/W and aspect ratio;
- 2) Extend the present data to low inlet Mach numbers.

4.1 HIGH MACH NUMBER DIFFUSER MAP

In order to map diffuser performance adequately at high inlet Mach numbers, a larger range of geometrical variables (L/W and aspect ratio) is needed. The present high Mach number data for $L/W = 15$ do not permit the selection of an optimum design at other values of L/W .

The large change in C_p characteristics, as a function of aspect ratio, suggests the importance of further studies to determine the optimum aspect ratio, other variables being fixed.

The selection of the optimum diffuser, i.e., the selection of optimum C_p from maps of C_p as a function of B and 2θ for a range of L/W and aspect ratio, is required for the development of optimum diffuser designs. The development of diffuser performance maps, i.e., C_p as a function of

- 1) 2θ ;
- 2) L/W ;
- 3) aspect ratio;
- 4) throat blockage;
- 5) inlet Mach number;

involves a lengthy experimental program. It is recommended that further investigations of diffuser performance maps be pursued. Immediate studies should be concentrated on L/W ratios surrounding $L/W = 15$, e.g., $L/W = 10$ and 20 , and for aspect ratios between 0.25 and 5.7 , e.g., 1.0 .

4.2 LOW MACH NUMBER DATA

As a further cross-check on the data reported here and by Reneau, it may be desirable to repeat and extend data to lower inlet Mach numbers. If such data are taken, more sensitive gages (such as mercury or water manometers instead of

bourdon tube gages, as used in the present study) should be used to obtain more accurate data.

4.3 RESOLVING UNSTEADY CHARACTER OF MASS FLOW RATE

It may be desirable to determine if the shedding of stalled fluid from upstream of the diffuser throat was responsible for large fluctuations in mass flow rate observed in the 5.7 aspect ratio diffuser tests. A single test of a redesigned inlet geometry to eliminate any possible shedding of stalled fluid should determine the effect on measured C_p of any flow unsteadiness (if produced by the shedding of stalled fluid from upstream). If the elimination of flow unsteadiness produces an alteration in C_p , then the 5.7 aspect ratio data should be repeated.

4.4 INLET BOUNDARY-LAYER VELOCITY PROFILE

The shape of the inlet boundary-layer velocity profile producing a given value of blockage may have an important influence on the magnitude of the pressure recovery. The present tests have not made a systematic study of this parameter which may be important in the design of high-speed machines. Future work should survey the importance of this parameter.

5.0 UNCERTAINTY ANALYSIS

1) BLOCKAGE —B

$$\text{At choking, } \dot{m} = \frac{0.532}{\sqrt{T_o}} P_o A_{\text{flow}} \quad (243)$$

$$(\text{at choking conditions } P_{\text{throat}} = 0.528 P_o)$$

$$\text{Hence, } A_{\text{flow}} = \frac{\dot{m} \sqrt{T_o}}{0.532 P_o}$$

$$\text{or } \frac{A_{\text{flow}}}{A_{\text{geometric}}} = \frac{\dot{m} \sqrt{T_o}}{0.532 P_o A_{\text{geometric}}}$$

$$\text{Blockage } B = \frac{A_{\text{flow}} - A_{\text{geometric}}}{A_{\text{geometric}}} = 1 - \frac{A_{\text{geometric}} - A_{\text{flow}}}{A_{\text{geometric}}} = 1 - \phi \quad (239)$$

$$\text{where: } P_o = \text{psia}$$

$$T_o = ^\circ\text{R}$$

UNCLASSIFIED

$$A = \text{in.}^2$$

$$\text{From orifice reading, } \dot{m} = \frac{k \sqrt{H P_1}}{T_1} \quad (244)$$

where: H = manometer reading = in. H_2O

P_1 = orifice pressure = psia

T_1 = orifice temperature = °R

$$\begin{aligned} \frac{\Delta B}{B} = \frac{\Delta \phi}{\phi} = & \left[\left(\frac{1}{2} \frac{\Delta H}{H} \right)^2 + \left(\frac{1}{2} \frac{\Delta P_1}{P_1} \right)^2 + \left(\frac{1}{2} \frac{\Delta T_o}{T_o} \right)^2 \right. \\ & \left. + \left(\frac{1}{2} \frac{\Delta T_1}{T_1} \right)^2 + \left(\frac{\Delta P_o}{P_o} \right)^2 \right]^{1/2} \quad (245) \end{aligned}$$

For $L_{\text{throat}} = 0, 1.5, 3.5$ inches

$$T_o = 600^\circ R$$

$$\Delta T_o = T_1 = 1^\circ R$$

$$P_o = P_1 = 95 \text{ psia}$$

$$\Delta P_o = P_1 = 0.2 \text{ psia}$$

$$H = 30 \text{ in. } H_2O$$

$$\Delta H = 0.07$$

$$\frac{\Delta B}{B} = 0.0039 = \pm 0.4\%$$

UNCLASSIFIED

UNCLASSIFIED

Blockage values at subsonic conditions are calculated in a similar fashion except that account is taken of the 1-dimensional A_{flow} due to subsonic flow, i.e.,

$$\dot{m} = k \frac{P_o}{\sqrt{T_o}} f(M) A_{\text{flow}} \quad \text{where: } f(M) \text{ is a function of Mach number.}^*$$

2) L/W

$$L = 1.865$$

$$\Delta L = 0.001$$

$$W = 0.125$$

$$\Delta W = 0.001$$

$$\begin{aligned} \frac{\Delta L/W}{L/W} &= \left[\left(\frac{\Delta L}{L} \right)^2 + \left(\frac{\Delta W}{W} \right)^2 \right]^{1/2} = \left[\left(\frac{0.001}{1.865} \right)^2 + \left(\frac{0.001}{0.125} \right)^2 \right]^{1/2} \\ &= [(0.000536)^2 + (0.008)^2]^{1/2} = 0.008 = .8\% \text{ (maximum)} \end{aligned} \quad (246)$$

3) 2θ

$$2\theta = 4, 6, 8, 10, 12 \text{ degrees } \pm 0.1 \text{ degree}$$

$$\frac{\Delta 2\theta}{2\theta} = \frac{0.10}{4} = 0.025 = 2.5\% \text{ (maximum)}$$

*A. H. Shapiro, The Dynamics and Thermodynamics of Compressible Fluid Flow, Vol. I, The Ronald Press Company, New York, 1953, p. 84.

UNCLASSIFIED

UNCLASSIFIED

4) PRESSURE RECOVERY — C_p

$$C_p = \frac{\frac{P_{\text{exit}}}{P_o} - \frac{P_{\text{throat}}}{P_o}}{1 - \frac{P_{\text{throat}}}{P_o}} = \frac{x}{y} \quad (242)$$

$$\frac{\Delta x}{x} = \left[\left(\frac{\Delta P_{\text{exit}}}{P_{\text{exit}} - P_{\text{throat}}} \right)^2 + \left(\frac{\Delta P_{\text{throat}}}{P_{\text{exit}} - P_{\text{throat}}} \right)^2 \right]^{1/2} \quad (247)$$

$$\frac{\Delta y}{y} = \left[\left(\frac{\Delta P_o}{P_o - P_{\text{throat}}} \right)^2 + \left(\frac{\Delta P_{\text{throat}}}{P_o - P_{\text{throat}}} \right)^2 \right]^{1/2} \quad (248)$$

$$\frac{\Delta C_p}{C_p} = \left[\left(\frac{\Delta x}{x} \right)^2 + \left(\frac{\Delta y}{y} \right)^2 \right]^{1/2} \quad (249)$$

a) Low Inlet Mach Number ($M \approx 0.2$)

(Aspect ratio = 5.7, $L_{\text{throat}} = 0$, $L/W = 15$, $2\theta = 4$ degrees)

P_{exit}	=	72 psig	ΔP_{exit}	=	0.1 psi
P_{throat}	=	70 psig	ΔP_{throat}	=	0.1 psi
P_o	=	75 psig	ΔP_o	=	0.2 psi

$$\frac{\Delta x}{x} \approx \frac{\Delta y}{y} \approx 0.07$$

$$\frac{\Delta C_p}{C_p} = \left[2 \times 50 \times 10^{-4} \right]^{1/2} = 0.1 = \pm 10\%$$

UNCLASSIFIED

UNCLASSIFIED

03715 UNCLASSIFIED

b) High Inlet Mach Number ($M = 1.0$)

(Aspect ratio = 5.7, $L_{\text{throat}} = 0$, $L/W = 15$, $2\theta = 4$ degrees)

$$P_{\text{exit}} = 60 \text{ psig} \quad \Delta P_{\text{exit}} = 0.2 \text{ psi}$$

$$P_{\text{throat}} = 33 \text{ psig} \quad \Delta P_{\text{throat}} = 0.4 \text{ psi}$$

$$P_o = 75 \text{ psig} \quad \Delta P_o = 0.2 \text{ psi}$$

$$\frac{\Delta x}{x} = 0.016$$

$$\frac{\Delta y}{y} = 0.0105$$

$$\frac{\Delta C_p}{C_p} \approx 0.02 = \pm 2\%$$

The above examples of the uncertainty in C_p represent typical examples of test data from these studies. The uncertainty odds in the basic quantities appearing in these estimates is 20:1. Particular tests may have slightly lower or higher uncertainty, depending upon the differences in values of $P_{\text{exit}} - P_{\text{throat}}$ and $P_o - P_{\text{throat}}$.

6.0 CONCLUSIONS

This study has demonstrated that:

- 1) Performance in terms of C_p as a function of inlet Mach number does not show a critical subsonic inlet Mach number above which performance suffers a drastic drop.
- 2) Performance of supercritical flow diffusers is approximately the same as diffusers on the verge of choking, if the shock Mach number is about 1.1 to 1.2 or less.
- 3) The range of present data covers both group A and B diffusers, previously deduced in Appendix XI to depend upon flow-regime behavior based on their available evidence. No such groupings are apparent in the present data.

037122A JOMU

UNCLASSIFIED

UNCLASSIFIED

- 4) There is a strong dependence of diffuser pressure recovery C_p on diffuser aspect ratio. For given blockage and L/W ($L/W = 15$), maximum pressure recovery occurs at $2\theta = 10$ degrees for an aspect ratio of 0.25 and at $2\theta = 6$ degrees for an aspect ratio of 5.7.

For given values of blockage, higher recovery appears to occur for the larger aspect ratios. This conclusion may not be valid for all values of blockage and aspect ratios, however.

- 5) In all cases, pressure recovery C_p declines with increasing blockage for fixed values of divergence angle 2θ , L/W , and inlet Mach number.
- 6) Pressure recovery variation with inlet Mach number appears to be correlated with divergence angle 2θ and blockage ratio B . At low values of blockage ($B = 0.04$), C_p increases with increasing Mach number at small divergence angles ($2\theta = 4$ degrees). C_p decreases with increasing Mach number at large divergence angles ($2\theta = 12$ degrees). At large values of blockage ($B = 0.15$), C_p is relatively constant with inlet Mach number for divergence angles 2θ from 4 degrees to 12 degrees.
- 7) The appearance in the published literature of a critical Mach number for a group of A classification of diffusers is perhaps a miscalculation of true inlet Mach number by other investigators. The reasons for this may be:
- a) Many pressure taps are needed near the throat to determine inlet Mach number, because of the large gradient of static pressure at high subsonic Mach numbers;
 - b) The adjustment of diffuser back pressure (and hence setting of throat Mach number) near choking conditions is very sensitive; the mass flow hardly changes as diffuser back pressure is varied;
 - c) Other investigators have often used throat pressure taps on curved walls. Wall curvature can produce a false indication of true throat Mach number (the Mach number probably appearing higher than actual). Also, wall curvature in some cases could produce strongly 2-dimensional flows. In this case the throat Mach number would not be uniform and the meaning of obtaining Mach number = 1.0 would not be too clear.
- 8) The accurate determination of throat stagnation pressure at large values of blockage is necessary to the accurate measurement of pressure recovery in this type of study.

UNCLASSIFIED

UNCLASSIFIED

Unclassified

Security Classification

DOCUMENT CONTROL DATA - R&D		
(Security classification of title, body of abstract and indexing annotation must be entered when the overall report is classified)		
1. ORIGINATING ACTIVITY (Corporate author)		2a. SECURITY CLASSIFICATION
The Boeing Company Seattle, Washington		UNCLASSIFIED
		2b. GROUP
3. REPORT TITLE		
Element Design and Development of Small Centrifugal Compressor (U) - Volume II		
4. DESCRIPTIVE NOTES (Type of report and inclusive dates)		
5. AUTHOR(S) (Last name, first name, initial)		
Welliver, A. D. Acurio, J.		
6. REPORT DATE	7a. TOTAL NO. OF PAGES	7b. NO. OF REFS
August 1967	500	44
8a. CONTRACT OR GRANT NO.		9a. ORIGINATOR'S REPORT NUMBER(S)
DA 44-177-AMC-173(T)		USAAVLABS Technical Report 67-30
b. PROJECT NO.		9b. OTHER REPORT NO(S) (Any other numbers that may be assigned this report)
Task 1M121401D14413		D4-3434
10. AVAILABILITY/LIMITATION NOTICES		
In addition to security requirements which apply to this document and must be met, each transmittal outside the agencies of the US Government must have prior approval of US Army Aviation Materiel Laboratories, Fort Eustis, Virginia 23604.		
11. SUPPLEMENTARY NOTES		12. SPONSORING MILITARY ACTIVITY
		US Army Aviation Materiel Laboratories Fort Eustis, Virginia
13. ABSTRACT		
<p>Contained in this document are appendixes to a report on a research program involving the advancement of single-stage centrifugal compressor technology to attain high pressure ratio (10:1) at a usable efficiency. The main elements, namely, the impeller and the diffuser, were designed, tested, and developed as elements; the results are analyzed and described.</p> <p>An analysis of the loss of flow through the impeller passage and conditions contributing to early flow separation are discussed as well as suggestions for their prevention. The flow behavior in the vaneless and semivaneless areas and in the channel passage was evaluated from pressure data and schlieric photographs.</p>		

DD FORM 1 JAN 64 1473

Unclassified

Security Classification

14. KEY WORDS	LINK A		LINK B		LINK C	
	ROLE	WT	ROLE	WT	ROLE	WT
<p>Compressor:</p> <p>Single-Stage</p> <p>Centrifugal</p> <p>High-Pressure-Ratio</p>						

INSTRUCTIONS

1. ORIGINATING ACTIVITY: Enter the name and address of the contractor, subcontractor, grantee, Department of Defense activity or other organization (*corporate author*) issuing the report.

2a. REPORT SECURITY CLASSIFICATION: Enter the overall security classification of the report. Indicate whether "Restricted Data" is included. Marking is to be in accordance with appropriate security regulations.

2b. GROUP: Automatic downgrading is specified in DoD Directive 5200.10 and Armed Forces Industrial Manual. Enter the group number. Also, when applicable, show that optional markings have been used for Group 3 and Group 4 as authorized.

3. REPORT TITLE: Enter the complete report title in all capital letters. Titles in all cases should be unclassified. If a meaningful title cannot be selected without classification, show title classification in all capitals in parentheses immediately following the title.

4. DESCRIPTIVE NOTES: If appropriate, enter the type of report, e.g., interim, progress, summary, annual, or final. Give the inclusive dates when a specific reporting period is covered.

5. AUTHOR(S): Enter the name(s) of author(s) as shown on or in the report. Enter last name, first name, middle initial. If military, show rank and branch of service. The name of the principal author is an absolute minimum requirement.

6. REPORT DATE: Enter the date of the report as day, month, year, or month, year. If more than one date appears on the report, use date of publication.

7a. TOTAL NUMBER OF PAGES: The total page count should follow normal pagination procedures, i.e., enter the number of pages containing information.

7b. NUMBER OF REFERENCES: Enter the total number of references cited in the report.

8a. CONTRACT OR GRANT NUMBER: If appropriate, enter the applicable number of the contract or grant under which the report was written.

8b, 8c, & 8d. PROJECT NUMBER: Enter the appropriate military department identification, such as project number, subproject number, system numbers, task number, etc.

9a. ORIGINATOR'S REPORT NUMBER(S): Enter the official report number by which the document will be identified and controlled by the originating activity. This number must be unique to this report.

9b. OTHER REPORT NUMBER(S): If the report has been assigned any other report numbers (*either by the originator or by the sponsor*), also enter this number(s).

10. AVAILABILITY/LIMITATION NOTICES: Enter any limitations on further dissemination of the report, other than those imposed by security classification, using standard statements such as:

(1) "Qualified requesters may obtain copies of this report from DDC."

(2) "Foreign announcement and dissemination of this report by DDC is not authorized."

(3) "U. S. Government agencies may obtain copies of this report directly from DDC. Other qualified DDC users shall request through _____."

(4) "U. S. military agencies may obtain copies of this report directly from DDC. Other qualified users shall request through _____."

(5) "All distribution of this report is controlled. Qualified DDC users shall request through _____."

If the report has been furnished to the Office of Technical Services, Department of Commerce, for sale to the public, indicate this fact and enter the price, if known.

11. SUPPLEMENTARY NOTES: Use for additional explanatory notes.

12. SPONSORING MILITARY ACTIVITY: Enter the name of the departmental project office or laboratory sponsoring (*paying for*) the research and development. Include address.

13. ABSTRACT: Enter an abstract giving a brief and factual summary of the document indicative of the report, even though it may also appear elsewhere in the body of the technical report. If additional space is required, a continuation sheet shall be attached.

It is highly desirable that the abstract of classified reports be unclassified. Each paragraph of the abstract shall end with an indication of the military security classification of the information in the paragraph, represented as (TS), (S), (C), or (U).

There is no limitation on the length of the abstract. However, the suggested length is from 150 to 225 words.

14. KEY WORDS: Key words are technically meaningful terms or short phrases that characterize a report and may be used as index entries for cataloging the report. Key words must be selected so that no security classification is required. Identifiers, such as equipment model designation, trade name, military project code name, geographic location, may be used as key words but will be followed by an indication of technical context. The assignment of links, rules, and weights is optional.